



# Kent Academic Repository

**Gough, Rosemarie Elizabeth (2019) *Interaction of Talin with Proteins Containing LD-Motifs*. Doctor of Philosophy (PhD) thesis, University of Kent, University of Kent.**

## Downloaded from

<https://kar.kent.ac.uk/74305/> The University of Kent's Academic Repository KAR

## The version of record is available from

## This document version

UNSPECIFIED

## DOI for this version

## Licence for this version

CC BY-ND (Attribution-NoDerivatives)

## Additional information

## Versions of research works

### Versions of Record

If this version is the version of record, it is the same as the published version available on the publisher's web site. Cite as the published version.

### Author Accepted Manuscripts

If this document is identified as the Author Accepted Manuscript it is the version after peer review but before type setting, copy editing or publisher branding. Cite as Surname, Initial. (Year) 'Title of article'. To be published in *Title of Journal*, Volume and issue numbers [peer-reviewed accepted version]. Available at: DOI or URL (Accessed: date).

## Enquiries

If you have questions about this document contact [ResearchSupport@kent.ac.uk](mailto:ResearchSupport@kent.ac.uk). Please include the URL of the record in KAR. If you believe that your, or a third party's rights have been compromised through this document please see our [Take Down policy](https://www.kent.ac.uk/guides/kar-the-kent-academic-repository#policies) (available from <https://www.kent.ac.uk/guides/kar-the-kent-academic-repository#policies>).

# Interaction of Talin with Proteins Containing LD-Motifs

---

**Rosemarie Elizabeth Gough**

A thesis submitted for degree of doctor of philosophy

Department of Biosciences

The University of Kent

2018

Success is stumbling from failure to failure with no loss of enthusiasm

*Sir Winston Churchill*

## **Declaration**

No part of this thesis has been submitted in support of an application for any degree or other qualification of the University of Kent, or any other University or Institution of learning.

Rosemarie Elizabeth Gough

**Date: 05 June 2019**



## Acknowledgements

I would like to start by thanking my supervisor Dr Ben Goult for the opportunity to study for this PhD and his guidance throughout the project. Also to all the Goult members past and present: Karen Baker, Austin Whitewood, Alana Cowell, Regina Khan, William Castle and Abhi Singh with a big thank you to Marie Anderson who gave me invaluable support and was always available for a cup of tea! A further thank you to all the members of the MADCAP groups including the Geeves, Mulvihull and Kad labs.

I want to also say a thank you to Chris Toseland and everyone from the Toseland lab for making the lab a fun environment to work in. I have to give a special thank you to Ália dos Santos with whom I started my PhD journey and I honestly am not sure I would have finished it without her! Thank you for pulling me through the tough days and making a more sophisticated cultured human being out of me!

I give thanks to Gary Thompson for help with NMR analysis and setting up experiments (thank you for coming in late at night when the machine decided to play up!)

A further thank you to our collaborators from Anna Akhmanovas group at the Utrecht University and to Martin Humphries group at the University of Manchester.

I need to say the biggest thank you to my family; my dad, mum and sister Hana. As well as my boyfriend Connor, who have all supported me tirelessly through my journey and have given me so much support and encouragement even when I haven't always believed in myself. Connor I know you believe you deserve an authorship for your help but I think the printer must have run out of ink on that page.....

# Table of Contents

Chapter 1.	Foreword .....	xv
1.1	Research contributions .....	xvi
1.1.1	Publications .....	xvi
1.1.2	Poster and presentations .....	xvi
1.2	Abstract .....	xvii
1.3	Abbreviations .....	xix
Chapter 2.	Introduction.....	1
2.1	Cell Migration .....	2
2.2	Cell adhesion Molecules.....	2
2.2.1	Selectins.....	3
2.2.2	Cadherins.....	4
2.3	Integrins.....	4
2.3.1	Integrin Structure .....	5
2.3.2	The extracellular matrix .....	7
2.3.3	Integrin activation .....	7
2.4	Different adhesive structures.....	9
2.4.1	Nascent adhesions.....	10
2.4.2	Focal complexes and focal adhesions .....	11
2.4.3	Fibrillar adhesions .....	11
2.4.4	Podosomes .....	11
2.5	Talin .....	12
2.5.1	Talin Isoforms .....	13
2.5.2	The talin head .....	15
2.5.3	The talin rod .....	17
2.6	Talin rod interactions within adhesions .....	20
2.6.1	Actin.....	20

2.6.2	Vinculin .....	21
2.6.3	Integrin .....	22
2.6.4	Talin-moesin .....	23
2.6.5	Talin-alpha synemin could provide a link to intermediate filaments.....	23
2.6.6	Talin binds LD-motifs .....	23
2.7	Layers of talin autoinhibition and mechano-sensing properties .....	27
2.8	Talin in disease .....	29
2.9	Talin post-translational modifications.....	30
2.9.1	Objectives of work.....	34
Chapter 3.	Materials and methods .....	36
3.1	Materials.....	37
3.1.1	Chemicals.....	37
3.1.2	Buffers .....	37
3.1.3	Hardware and apparatus.....	38
3.1.4	Plasmids.....	40
3.2	General microbiology techniques .....	43
3.2.1	Bacteria strains used .....	43
3.2.2	Making competent cells .....	43
3.2.3	Making agar plates .....	43
3.2.4	Transformation.....	43
3.2.5	Plasmid DNA isolation from bacterial cells .....	44
3.3	Protein purification methods .....	44
3.3.1	Making a glycerol stock .....	44
3.3.2	Inoculating a liquid bacterial culture.....	44
3.3.3	Protein expression.....	45
3.3.4	Cell lysis by sonication .....	45
3.3.5	Protein purification by immobilized metal affinity chromatography .....	45
3.3.6	Buffer exchange.....	46

3.3.7	TEV cleavage.....	46
3.3.8	Ion exchange chromatography.....	46
3.3.9	Protein concentration estimation .....	47
3.3.10	SDS-PAGE gels .....	47
3.4	Biochemical methods.....	48
3.4.1	Differential scanning fluorimetry .....	48
3.4.2	Fluorescence polarisation .....	49
3.4.3	Nuclear magnetic resonance- NMR .....	52
3.4.4	X-Ray crystallography .....	55
3.4.5	Actin co-sedimentation assay .....	55
3.4.6	<i>In vitro</i> kinase assay.....	56
3.4.7	Identification of talin phosphorylation sites by mass spectrometry.....	57
3.4.8	Cell culture techniques.....	58
Chapter 4.	Identifying and characterising the interaction between talin and KANK.....	59
4.1	Introduction.....	60
4.1.1	Microtubules .....	60
4.1.2	Microtubules are found to localise to focal adhesions .....	61
4.1.3	Microtubules are stabilised at the cell edge through the cortical microtubule stabilising complex .....	63
4.1.4	KANK protein family .....	64
4.1.5	Identifying talin as a KANK binding protein.....	66
4.1.6	Identifying the region of KANK involved in interaction talin.....	67
4.2	Results .....	69
4.2.1	Designing KANK1 KN domain peptide .....	69
4.2.2	Determining the region of talin involved in the talin:KANK interaction .....	73
4.2.3	Chemical shift mapping of talin1 R7R8 domain with KANK peptide.....	73
4.2.4	Chemical shift mapping of talin1 R7 domain with KANK peptide .....	76
4.2.5	Structural characterisation of the talin:KANK complex .....	81

4.2.6	Designing KANK mutations to perturb talin:KANK1 interaction .....	82
4.2.7	Biochemically characterisation of the KANK1_4A mutant .....	84
4.2.8	Designing talin1 R7 mutants to perturb the talin: KANK1 interaction.....	88
4.2.9	Validating the structural integrity of the talin1 R7R8 mutants.....	92
4.2.10	Measuring the binding affinity of KANK1 to the talin mutants.....	93
4.2.11	Investigating talin binding to different KANK isoforms.....	101
4.2.12	Does the binding of KANK to talin R7 increase thermal stability? .....	104
4.2.13	Can KANK influence the interaction between talin and actin?.....	106
4.3	Testing the physiological role of KANK mutants in a cellular context.....	108
4.3.1	Characterisation of KANK1_4A mutant in mammalian cells.....	108
4.3.2	Characterisation of talin1 G1404L mutant in mammalian cells.....	111
4.3.3	How does mislocalisation of KANK1 due to perturbed talin1:KANK1 binding affect other CMSC components?.....	115
4.3.4	Disruption of talin1:KANK1 leads to microtubules plus-end disorganisation at the cell periphery.....	118
4.4	Conclusion .....	120
4.4.1	Does talin nucleate CMSC assembly?.....	120
4.4.2	Why is KANK kept at the rim of focal adhesions? .....	121
4.4.3	KANK proteins in disease.....	123
4.4.4	Expression of KANK family members .....	123
4.4.5	Why do humans have four KANK isoforms? .....	124
4.4.6	What is the role of the talin:KANK interaction in organisms? .....	126
Chapter 5.	Defining an LD talin-binding motif.....	129
5.1	Introduction.....	130
5.1.1	What are Leucine-Aspartic acid motifs .....	130
5.1.2	Leucine-Aspartate binding domains (LDBDs) .....	132
5.1.3	Talin can bind LD-motifs.....	133
5.1.4	Searching for additional non-paxillin LD-motifs.....	136

5.2	Results .....	136
5.2.1	Designing a search query to identify novel LD talin-binding motif (LD-TBM) containing proteins .....	137
5.2.2	Searching for LD talin-binding motifs .....	138
5.2.3	Validating the potential LD talin-binding motifs .....	140
5.2.4	Determining if the LD talin-binding motifs bind talin.....	148
5.3	Discussion.....	152
5.3.1	Identifying future talin binding partners.....	152
5.3.2	LD-motifs can bind to multiple LDBDs.....	153
5.3.3	Talin LDBD specificity .....	154
Chapter 6.	Identifying and characterising the interaction between talin and CDK1 .....	159
6.1	Introduction.....	160
6.1.1	The cell cycle .....	160
6.1.2	Cyclin Dependent Kinases .....	161
6.1.3	Cyclin-dependent kinase activation .....	162
6.1.4	CDK1 Phosphorylation.....	164
6.1.5	Cell adhesions regulated by CDK1.....	167
6.2	Results .....	169
6.2.1	Determination of the CDK1 binding site(s) on talin .....	169
6.2.2	Chemical shift mapping of the CDK1 binding site on talin1 R7R8.....	171
6.2.3	Chemical shift mapping of the CDK1 binding site on talin R8.....	172
6.2.4	Biochemical comparison of DLC1 and CDK1 binding talin1 R8 .....	175
6.2.5	Designing a CDK1 mutant to disrupt the talin:CDK1 interaction .....	178
6.2.6	Structural characterization of the talin:CDK1 complex.....	182
6.2.7	Designing a talin mutant to perturb CDK1:talin binding.....	184
6.2.8	Testing of designed talin mutants to perturb CDK1 binding.....	191
6.2.9	Is the talin mutant 'VDKD' specific to perturbing the talin:CDK1 Interaction?.....	193
6.2.10	Can CDK1:Cyclin:talin form a complex? .....	195

6.2.11	How does talin affect CDK1 kinase activity? .....	197
6.2.12	Talin phosphorylation by CDK1 is cyclin specific .....	198
6.2.13	Mass spectrometry-based phosphosite mapping of talin phosphorylation .....	202
6.2.14	Isoform differences in CDK1 talin phosphorylation .....	205
6.2.15	Biochemically characterising the CDK1 phosphorylation site on talin1 R7R8 .....	210
6.2.16	Biochemically characterising CDK1 phosphorylation site on talin2 R7R8 .....	213
6.2.17	Does CDK1 localise to adhesions .....	215
6.2.18	Characterisation of CDK1_2A mutant in mammalian cells .....	217
6.3	Conclusion .....	219
6.3.1	What is targeting CDK1 to adhesions? .....	219
6.3.2	Why is talin phosphorylated by CDK1? .....	220
6.4	Does CKS1 binding talin regulate the talin:CDK1 interaction? .....	222
6.4.1	Could other members of the CDK family bind to talin? .....	224
Chapter 7.	Conclusions .....	229
7.1	Summary .....	230
7.2	Potential Limitations .....	232
7.3	Future Directions .....	232
Chapter 8.	References .....	234
Chapter 9.	Appendix .....	256

## Table of Figures

FIGURE 2.1: TYPES OF CELL ADHESION MOLECULES (CAMs) .....	3
FIGURE 2.2: INTEGRIN SUBUNIT PAIRINGS.....	5
FIGURE 2.3: STRUCTURE OF INTEGRINS.....	6
FIGURE 2.4: ACTIVATION STATE OF INTEGRINS .....	8
FIGURE 2.5: TALIN-INDUCED INTEGRIN ACTIVATION.....	9
FIGURE 2.6: LOCATION OF CELL-MATRIX ADHESIONS ACROSS A CELL.....	10
FIGURE 2.7: TALIN DOMAIN STRUCTURE AND CONSERVATION.....	12
FIGURE 2.8: TALIN2 SPLICE VARIANTS.....	14
FIGURE 2.9: TALIN1 FERM DOMAIN INTERACTING WITH THE MEMBRANE.....	17
FIGURE 2.10: TALIN R7R8 DOMAIN STRUCTURE .....	19
FIGURE 2.11: ACTIN BINDING SITES ACROSS TALIN .....	21
FIGURE 2.12: LAYERS OF AUTOINHIBITION IN TALIN .....	22
FIGURE 2.13: LD LIGAND BINDING TO TALIN ROD DOMAIN.....	25
FIGURE 2.14: DOMAIN STRUCTURE OF TALIN1 SHOWING THE LOCATION OF LIGAND BINDING SITES .....	26
FIGURE 2.15: DIFFERENT BINDING SITES ON TALIN REVEALED UNDER FORCE .....	28
FIGURE 2.16: TALIN IN A COSTAMERE .....	30
FIGURE 3.1: FLUORESCENCE POLARISATION .....	49
FIGURE 3.2: DIFFERENCES IN TROSY AND HSQC EXPERIMENTS .....	54
FIGURE 4.1: THE STRUCTURE OF MICROTUBULES AND THE CYCLE OF GROWING AND SHRINKING .....	61
FIGURE 4.2: THE CORTICAL MICROTUBULE STABILISING COMPLEX.....	64
FIGURE 4.3 SECONDARY STRUCTURE OF KANK FAMILY PROTEINS .....	65
FIGURE 4.4: GFP-TALIN1 AND GFP-KANK1 PROTEOMIC DATA SETS. ....	66
FIGURE 4.5: KANK1 KN DOMAIN IS RESPONSIBLE FOR LOCALISATION TO FOCAL ADHESIONS ..	68
FIGURE 4.6: CONSERVATION ALIGNMENT OF KANK1 TO DESIGN A KANK PEPTIDE.....	70
FIGURE 4.7: TALIN1 R8 DOMAIN IS LD RECOGNITION BOX .....	71
FIGURE 4.8: BIOCHEMICAL CHARACTERISATION OF KANK BINDING TO TALIN .....	72
FIGURE 4.9: $^1\text{H}^{15}\text{N}$ HSQC CORRELATION BETWEEN THE PROTON AND THE NITROGEN ATOM ...	74
FIGURE 4.10: $^{15}\text{N}$ TROSY NMR TITRATION TALIN1 R7R8 AND KANK1 30-68C PEPTIDE.....	75
FIGURE 4.11: $^{15}\text{N}$ HSQC NMR TITRATION TALIN1 R7 AND KANK1 30-68C PEPTIDE .....	77
FIGURE 4.12: CHEMICAL SHIFT MAPPING OF TALIN1 R7R8 AND KANK1 42-68C .....	79
FIGURE 4.13: CHEMICAL SHIFT MAPPING OF THE KANK1 BINDING SURFACE ON TALIN1 R7 .....	80



<b>FIGURE 4.14: STRUCTURAL MODEL OF THE TALIN1 R7R8: KANK1 INTERACTION</b> .....	82
<b>FIGURE 4.15: STRUCTURAL REVIEW KANK_4A MUTANT</b> .....	83
<b>FIGURE 4.16: KANK_4A MUTANT PERTURBS BINDING TO TALIN</b> .....	84
<b>FIGURE 4.17: KANK_4A MUTANT PERTURBS BINDING TO TALIN1 R7R8</b> .....	86
<b>FIGURE 4.18: KANK_4A MUTANT PERTURBS BINDING TO TALIN1 R7</b> .....	87
<b>FIGURE 4.19: STRUCTURAL ANALYSIS OF TALIN1 R7 TO DESIGN TALIN MUTANTS TO PERTURB KANK INTERACTION</b> .....	89
<b>FIGURE 4.20: STRUCTURAL ANALYSIS OF DESIGNED TALIN MUTANTS TO PERTURB KANK INTERACTION</b> .....	91
<b>FIGURE 4.21: THERMAL STABILITY OF TALIN R7R8 MUTANTS</b> .....	93
<b>FIGURE 4.22: TALIN R7R8 MUTANTS BINDING TO TALIN</b> .....	94
<b>FIGURE 4.23: <sup>15</sup>N TROSY SPECTRA OF THE R7R8 TALIN MUTANTS</b> .....	95
<b>FIGURE 4.24: TALIN G1404L MUTANT PERTURBS BINDING TO TALIN R7</b> .....	97
<b>FIGURE 4.25: <sup>15</sup>N HSQC SPECTRA OF THE TALIN R7 MUTANTS</b> .....	98
<b>FIGURE 4.26: TALIN R7 MUTANTS PERTURB BINDING TO KANK1</b> .....	100
<b>FIGURE 4.27: KANK KN DOMAIN ALIGNMENT</b> .....	101
<b>FIGURE 4.28: CHARACTERISING THE KANK1 KN DOMAIN BOUNDARY</b> .....	102
<b>FIGURE 4.29: CHARACTERISING KANK ISOFORMS 1-4 BINDING TO TALIN1 R7R8 AND TALIN2 R7R8</b> .....	103
<b>FIGURE 4.30: KANK EFFECTS STABILITY OF TALIN HELIX</b> .....	105
<b>FIGURE 4.31: TALIN1:KANK1 INTERACTION INCREASES ACTINS AFFINITY TO TALIN ACTIN BINDING SITE 2</b> .....	107
<b>FIGURE 4.32: CHARACTERISATION OF KANK LOCALISATION IN MAMMALIAN CELLS</b> .....	110
<b>FIGURE 4.33: G1404L TALIN1 MUTANT DOES NOT AFFECT TALINS ABILITY TO FORM FOCAL ADHESIONS</b> .....	112
<b>FIGURE 4.34: CHARACTERISATION OF THE TALIN1 G1404L MUTANT IN CELLS</b> .....	114
<b>FIGURE 4.35: KANK1 MUTANTS AFFECT ON CMSC COMPONENTS CLUSTERING AROUND FOCAL ADHESIONS</b> .....	116
<b>FIGURE 4.36: TALIN G1404L MUTANT STOPS CLUSTERING OF CMSC COMPONENTS TO FOCAL ADHESIONS</b> .....	117
<b>FIGURE 4.37: DISRUPTION OF THE TALIN:KANK INTERACTION DISORDERS MICROTUBULE PLUS END ORGANIZATION AT THE CELL PERIPHERY</b> .....	119
<b>FIGURE 4.38: TALIN NUCLEATES CMSC ASSEMBLY BY INITIATING A SEEDING COMPLEX WITH KANK1</b> .....	121

<b>FIGURE 4.39: TALIN:KANK INTERACTION IS REQUIRED FOR KANK TO BE RECRUITED TO FOCAL ADHESIONS RIM.</b> .....	122
<b>FIGURE 4.40: HUMAN KANK ISOFORMS COILED COIL ALIGNMENT</b> .....	125
<b>FIGURE 4.41: SINGLE NUCLEOTIDE POLYMORPHISMS FOUND IN THE KANK BINDING SITE ON TALIN R7</b> .....	128
<b>FIGURE 5.1: PAXILLIN DOMAIN STRUCTURE AND KNOWN BINDING PARTNERS.</b> .....	131
<b>FIGURE 5.2: LD-MOTIF BINDING TO AN LDBD</b> .....	133
<b>FIGURE 5.3: TALIN R8 DOMAIN IS AN LD BINDING DOMAIN</b> .....	134
<b>FIGURE 5.4: SEQUENCE ALIGNMENT OF KNOWN OF LD TALIN-BINDING MOTIFS</b> .....	137
<b>FIGURE 5.5: PROSITE SOFTWARE USED TO IDENTIFY LD TALIN-BINDING MOTIFS</b> .....	140
<b>FIGURE 5.6: SEPTIN ISOFORMS DOMAIN STRUCTURE AND SUBGROUPS</b> .....	141
<b>FIGURE 5.7: STRUCTURAL EVALUATION OF SEPTIN2 159-174 PEPTIDE</b> .....	143
<b>FIGURE 5.8: STRUCTURAL EVALUATION OF CDK1 206-223 PEPTIDE</b> .....	145
<b>FIGURE 5.9: STRUCTURAL EVALUATION OF CDK1 283-297 PEPTIDE</b> .....	147
<b>FIGURE 5.10: THE TALIN ROD DIVIDED INTO FOUR BIG FRAGMENTS</b> .....	149
<b>FIGURE 5.11: BIOCHEMICAL CHARACTERISATION OF LD TALIN-BINDING MOTIFS TO TALIN ROD FRAGMENTS</b> .....	150
<b>FIGURE 5.12: BIOCHEMICAL CHARACTERISATION OF CDK1 206-223 PEPTIDE</b> .....	151
<b>FIGURE 5.13: SEQUENCE ALIGNMENT AND EVALUATION OF LD TALIN-BINDING MOTIFS</b> .....	152
<b>FIGURE 5.14: TALIN R8 DOMAIN STRUCTURE IN RELATION TO THE TALIN TAIL</b> .....	155
<b>FIGURE 5.15: TALIN AUTOINHIBITION</b> .....	156
<b>FIGURE 5.16: TALIN R7R8 POST-TRANSLATIONAL MODIFICATIONS</b> .....	158
<b>FIGURE 6.1: THE CELL CYCLE</b> .....	161
<b>FIGURE 6.2: CDKS AND CORRESPONDING CYCLINS</b> .....	162
<b>FIGURE 6.3: LEVELS OF CYCLIN AND CDK COMPLEXES IN THE DIFFERENT PHASES OF THE CELL CYCLE</b> .....	163
<b>FIGURE 6.4: CELL ADHESIONS RETRACT BEFORE ENTRY INTO MITOSIS</b> .....	164
<b>FIGURE 6.5: STRUCTURE OF CDK2</b> .....	165
<b>FIGURE 6.6: MECHANISM OF PHOSPHORYLATION</b> .....	166
<b>FIGURE 6.7: ADHESION AREA IS DEPENDENT ON THE CELL CYCLE PHASE</b> .....	168
<b>FIGURE 6.8: BIOCHEMICAL CHARACTERISATION OF CDK1 BINDING TO TALIN</b> .....	170
<b>FIGURE 6.9: <sup>15</sup>N TROSY NMR TITRATION TALIN1 R7R8 AND CDK1 206-223C PEPTIDE</b> .....	171
<b>FIGURE 6.10: <sup>15</sup>N HSQC NMR TITRATION OF TALIN1 R8 AND CDK1 206-223C PEPTIDE</b> .....	173
<b>FIGURE 6.11: CHEMICAL SHIFT MAPPING OF TALIN1 R8 AND CDK1 206-223C</b> .....	174

FIGURE 6.12: BINDING OF DLC1 AND CDK1 TO TALIN1 R7R8 .....	175
FIGURE 6.13: <sup>15</sup> N TROSY SPECTRA SHOWING DLC1 AND CDK1 BINDING TO TALIN1 R7R8 .....	177
FIGURE 6.14: DESIGN OF ACDK1_2A MUTANT TO PERTURB TALIN:CDK1 INTERACTION .....	179
FIGURE 6.15: NMR TROSY OF THE CDK1_2A MUTANT ON BINDING TO TALIN R7R8 .....	180
FIGURE 6.16: NMR HSQC OF THE CDK1_2A MUTANT AFFECT ON BINDING TO TALIN R8 .....	181
FIGURE 6.17: CRYSTALLIZATION TRIALS OF TALIN1 R7R8 AND CDK1 206-223C PEPTIDE .....	182
FIGURE 6.18: STRUCTURAL MODEL OF TALIN1 R7R8:CDK1 206-223 .....	183
FIGURE 6.19: LD SPECIFICITY BETWEEN TALIN R8 LIGANDS: DLC1, RIAM AND CDK1 .....	185
FIGURE 6.20: IDENTIFYING IF CDK1 TRP228 AND GLU230 RESIDUES ARE IMPORTANT FOR TALIN BINDING .....	187
FIGURE 6.21: DESIGNING A TALIN R8 MUTANT TO PERTURB CDK1 BINDING.....	189
FIGURE 6.22: DETERMINING IF THE DESIGNED TALIN R7R8 MUTANTS PERTURB CDK1 BINDING .....	192
FIGURE 6.23: DETERMINING THE BINDING AFFINITY FOR DLC1, RIAM AND CDK1 AGAINST THE TALIN1 R7R8 VDKD MUTATION. ....	194
FIGURE 6.24: STRUCTURAL MODEL OF TALIN1 R7R8:CDK2:CYCLINA2 .....	196
FIGURE 6.25: CDK1 KINASE ACTIVITY IS NOT AFFECTED BY TALIN BINDING .....	198
FIGURE 6.26: TALIN R7R8 IS PHOSPHORYLATED BY CDK1-CYCLINA2 .....	200
FIGURE 6.27: IMMUNOBLOTS CONFIRMING TALIN R7R8 IS PHOSPHORYLATED BY CDK1-CYCLINA2 .....	201
FIGURE 6.28: PHOSPHOSITE MAPPING OF TALIN1 R7R8 .....	203
FIGURE 6.29: PHOSPHOSITE MAPPING OF TALIN2 R7R8 PHOSPHORYLATION SITE .....	205
FIGURE 6.30: ALIGNMENT HIGHLIGHTING THE TALIN1 PHOSPHORYLATION SITE BY CDK1:CYCLINA2 .....	207
FIGURE 6.31: ALIGNMENT HIGHLIGHTING THE TALIN2 PHOSPHORYLATION SITE BY CDK1:CYCLINA2 .....	209
FIGURE 6.32: TALIN1 CDK1 PHOSPHORYLATION SITE S1589 .....	211
FIGURE 6.33: TALIN1 SER1589 BINDING AFFINITY TO DLC1, KANK1 AND CDK1 .....	212
FIGURE 6.34: TALIN2 CDK1 PHOSPHORYLATION SITE S1489 .....	214
FIGURE 6.35: LOCALISATION OF GFP-CDK1 IN THE CELL .....	216
FIGURE 6.36: CDK1_2A MUTANT PREVENTS TALIN BINDING .....	218
FIGURE 6.37: TALIN2 PHOSHOMUTATION MAY PRETURB ACTIN BINDING .....	222
FIGURE 6.38: TALIN AND CKS1 BIDNING SITES ON CDK1 .....	223
FIGURE 6.39 SEQUENCE ALIGNMENT OF HUMAN CDK ISOFORMS .....	225

<b>FIGURE 6.40: SEQUENCE ALIGNMENT OF LD-TBM ACROSS THE CDK ISOFORMS .....</b>	<b>226</b>
<b>FIGURE 6.41 STRUCTURAL OF HUMAN CDK11A.....</b>	<b>227</b>
<b>FIGURE 6.42 STRUCTURAL ALIGNMENT OF HUMAN CDK1 AND CDK2 AND CDK3.....</b>	<b>228</b>
<b>FIGURE 7.1: THE TALIN KANK INTERACTION LINKS FA WITH CMSC .....</b>	<b>230</b>

## Table of Tables

TABLE 1: POST-TRANSLATIONAL MODIFICATIONS IN TALIN ISOFORMS.....	33
TABLE 2: CHEMICAL REAGENTS.....	37
TABLE 3: BUFFER COMPOSITIONS.....	38
TABLE 4: LABORATORY EQUIPMENT .....	39
TABLE 5: PLASMIDS.....	42
TABLE 6: GEL CONTENTS.....	48
TABLE 7: PEPTIDE SEQUENCES .....	51
TABLE 8: PRIMARY AND SECONDARY ANTIBODIES.....	57
TABLE 9: EXPRESSION LEVELS OF KANK1,2,3 AND 4 GENES.....	124

## List of Equations

EQUATION 1: ONE SITE BINDING EQUATION FOR FLUORESCENCE POLARISATION .....	50
EQUATION 2: WEIGHTED COMBINATION OF AMIDE SECONDARY SHIFTS.....	78

# Chapter 1. Foreword

---

## **1.1 Research contributions**

### **1.1.1 Publications**

Gough RE, Goult BT. (2018) The tale of two talins – two isoforms to fine-tune integrin signalling. *FEBS Letters* 592(12):2108-2125

Bouchet BP, Gough RE, van de Willige D, Ammon Y-C, Post H, Jacquemet G, Altelaar AFM, Heck AJR, Goult BT\* and Akhmanova A\*. (2016) Talin-KANK1 interaction controls the cortical microtubule stabilizing complexes to focal adhesions. *eLife* 5:18124

### **1.1.2 Poster and presentations**

Poster Presentation at The Royal Society Forces in Cancer: interdisciplinary approaches in tumour mechanobiology (2018) Meeting held in London.

“Identifying and characterising LD- motif binding sites in the mechanosensitive protein talin”  
RE Gough and BT Goult.

Oral Presentation at The Science Faculty Research Festival- Science and Health (2017) Meeting held in Medway Campus University of Kent.

“Mechanical Regulation of the Cell Cycle” RE Gough, M Jones, MJ Humphries and BT Goult.

Poster Presentation at The Cell Adhesion Society: The force is awake: integrins and beyond (2016) Meeting held in London.

“Talin-KANK1 interaction controls the recruitment of cortical microtubule stabilising complexes to focal adhesions” RE Gough, BP Bouchet, A Akhmanova and BT Goult.

## 1.2 Abstract

Talin is a 250 kDa cytoplasmic protein that activates integrins and provides a link to cytoskeletal actin, thus producing the necessary force to stabilise adhesions. Talin is classically defined as an integrin-activator, but here we show that talin also couples adhesion assemblies to cortical microtubules via the Cortical Microtubule Stabilising Complex (CMSC) and plays a role in the mechano-regulation of the cell cycle.

Cross talk between cortical microtubules and focal adhesions (FA) plays a critical role in cell polarity and migration. Microtubules regulate the turnover of adhesions and, equally, FAs help capture and stabilise microtubules in their vicinity. The molecular basis for this mechanism was unknown and remained a key question within the field.

Here, I describe biochemical and biophysical evidence that the interaction between KANK and talin is the crucial link between the macromolecular assemblies FAs and CMSC. Fluorescence polarisation (FP) and Nuclear Magnetic Resonance (NMR) data show that the conserved KN domain in KANK1 binds to the talin rod domain R7 via a LD talin-binding motif. Through the design of point mutants in both the KANK1 KN domain and talin R7 domain this interaction could be perturbed. Our data show that the KANK1 KN domain binds to talin through a helix addition mechanism. Immunofluorescence work in HeLa cells corroborates our findings on the importance of this interaction, and that a single talin point mutation (G1404L) is enough to abrogate the association of FAs with the CMSC and, in turn, disrupts microtubule dynamics at the cell edge. The discovery of KANK1 as a binding partner of talin provides the missing link for how microtubules are targeted to FAs.

The talin:KANK interaction gave a new insight on LD talin-binding motifs and allowed us to develop a novel pipeline for identifying talin-binding partners. After designing a LD talin-binding search motif, we identified cyclin dependent kinase1 (CDK1) as a talin-binding protein. CDK1 is the master regulator of the cell cycle, helping to drive cells from G2 phase into mitosis. Using similar biochemical and biophysical techniques I characterise the interaction between talin and CDK1. FP and NMR show that CDK1 binds to the talin R8 domain via helices 32 and 33 and based on structural modelling, we propose that this interaction also occurs through helix addition.

Biochemical data combined with phosphoproteomics shows that the CDK1-cyclinA complex phosphorylates talin1 and talin2 isoforms at two unique sites (Ser1589 in talin1 and Ser1489 in talin2). Interestingly, in talin2 this novel phosphorylation site is in the talin actin-binding site (ABS2). We postulate that this could be a mechanism to regulate the coupling/uncoupling of actin to talin. Talin phosphorylation could perturb actin binding, thus reducing tension across the



adhesions and leading to their disassembly. This interaction gives an insight into how adhesions and the cell cycle are entwined and poses many questions regarding how adhesion formation and disassembly regulates or occurs within the cell cycle.

My thesis describes the discovery of two novel talin-binding partners KANK and CDK1 which reveals talin is a crucial player in both coupling FAs to microtubules and gives new evidence into how adhesions can be involved in the regulation of the cell cycle.

## 1.3 Abbreviations

ABS	Actin Binding Site
Amp	Ampicillin antibiotic
BSA	Bovine Serum Albumin
CAMs	Cell Adhesion Molecules
CD	Circular dichroism
CDK1	Cyclin Dependent Kinase
DD	Dimerization Domain
dH <sub>2</sub> O	distilled water
DLC1	Deleted Liver Cancer 1
DNA	Deoxyribonucleic acid
DTT	Dithiothreitol
ECM	Extracellular Matrix
FA	Focal Adhesions
FAK	Focal Adhesion Kinase
FERM	4.1 protein, erzin, radixin, moesin
HSQC	Heteronuclear single quantum spectroscopy
IBS	Integrin Binding Site
IF	Intermediate Filament
IPTG	Isopropyl- $\beta$ -D- thiogalactopyronoside
Kan	Kanamycin Antibiotic
KANK	Kidney Ankyrin Repeat-containing protein
LD	Leucine Aspartate
LDBD	Leucine Aspartate Binding Domain

MS	Mass Spectrometry
MT	Microtubules
NaCl	Sodium Chloride
NMR	Nuclear Magnetic Resonance
PBS	Phosphate Buffered Saline
PCR	Polymerised Chain reaction
PFA	Paraformaldehyde
PI	Isoelectric Point
PIP2	Phosphatidylinositol 4,5- biphosphate
PIP3	Phosphatidylinositol 3,4,5- triphosphate
PTM	Post Translational Modifications
RIAM	Rap1-interacting adapter molecule
RPM	Rotations per minute
SNP	Single Nucleotide Polymorphisms
TROSY	Traverse relaxation optimised spectroscopy
TBS	Talin Binding site
LD-TBM	Leucine-Aspartate- talin binding motif
TEV	Tobacco Etch Virus
TLN1	Talin1 gene
TLN2	Talin2 gene
VBS	Vinculin Binding Site

# Chapter 2. Introduction

---

## 2.1 Cell Migration

Multicellular organisms are organised through tightly co-ordinated cell-cell and cell-matrix interactions. Cells are continually sensing their extracellular environment, identifying different biochemical and biophysical properties and translating this information into a broad range of biological outputs including: cell migration, cell proliferation and cell differentiation.

Cell migration is vital for all eukaryotic life and is essential for embryonic development, tissue formation, immune responses and wound healing (Case and Waterman, 2015). When misregulated cell migration can cause huge damage to organisms including: tumour formation and metastasis, chronic inflammatory diseases and vascular disease (Carmona-Fontaine, Matthews and Mayor, 2008). For a cell to dictate direction of movement and co-ordinate with surrounding cells it needs to have a defined leading edge (front) and a rear end (back). This is achieved through cell polarity, which gives the cell an asymmetric organisation of cellular components, vital for cell co-ordination, shape, structure and function (Case and Waterman, 2015).

Additionally, all migrating cells need to apply force to generate traction against their immediate surroundings. The actin cytoskeleton is one of the major sources of internally generated force that enables the cell to regulate shape and drive migration (Pollard and Cooper, 2009). For actin to be able to transmit force to the outside of the cell, the force must first be transmitted through the cellular membrane. This can occur through specific cell surface receptors known as cell adhesion molecules (CAMs). CAMs can bind to the extracellular matrix (ECM) or to other cells and generate the traction needed to help the cell move. Fully understanding which proteins are involved in the regulation of this process would aid in the development of novel therapeutic cancer treatments, transplant methods and the manufacturing of artificial tissues.

## 2.2 Cell adhesion Molecules

CAMs are divided into five main groups: integrins, selectins, cadherins, mucins and immunoglobulin superfamily as seen in **FIGURE 2.1** (Lodish 2016). Selectins, cadherins, mucins and immunoglobulins can form cell-cell interactions, whereas integrins provide a link between cells and the ECM.

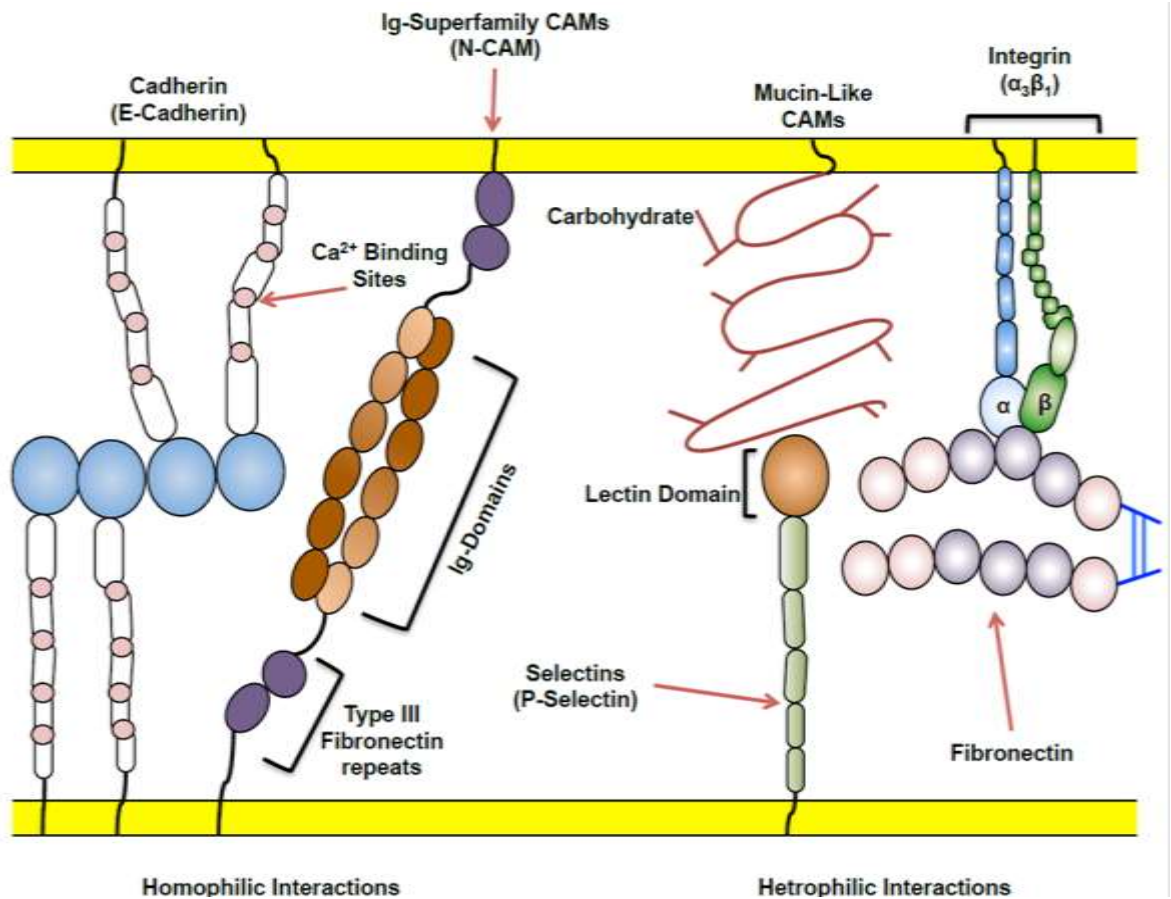


**FIGURE 2.1: TYPES OF CELL ADHESION MOLECULES (CAMS)**

Diagram representing the five classes of CAMs in cell-cell and cell-matrix adhesions; cadherins, integrins, Ig-superfamily, selectins and Mucins. The CAMs are separated into homophilic interactions and heterophilic interactions. Figure based from: (Lodish *et al.*, 2000)

### 2.2.1 Selectins

Selectins, are a family of three structurally and functionally related adhesion molecules: L-selectins, P-selectins and E-selectins. P-selectins are primarily found on platelets and leukocytes, E-selectins are expressed on endothelial cells and L-selectins are present on leukocytes, monocytes, neutrophils and eosinophils (Bou-Gharios and de Crombrughe, 2008). All selectins have a common domain structure consisting of an important N-terminal  $\text{Ca}^{2+}$  dependent lectin domain (see **FIGURE 2.1**), which is integral for selectins function (Ley, 2001). The selectin family are adhesion molecules that facilitate the binding of cell-cell interactions; they specialise in capturing leukocytes from the blood stream and attach them to the vessel wall. This contact between the leukocyte and the vessel wall allows the process known as leukocyte rolling to take place. This process occurs in a cascade –like fashion whereby the leukocyte cell is captured and rolls along the cell membrane before it slows down enough to extravasate from the blood vessel into the tissue (Ley, 2001).

## 2.2.2 Cadherins

Cadherins are a large family of adhesion receptors that are defined by the inclusion of the extracellular cadherin (EC) domains and the requirement of  $\text{Ca}^{2+}$  for their activity (Morishita and Yagi, 2007). The number of EC domains can vary dependent on the isoform, they form  $\text{Ca}^{2+}$  dependent linkages with other cadherin EC domains forming a cell-cell interaction (Helfrich *et al.*, 2008). The cadherin receptors can be categorised into four groups: classical cadherins, protocadherins, unconventional cadherins and desmosomal cadherin's.

Classical cadherin's include E-cadherin, P-cadherin and N-cadherin that all have a similar structure with five EC domains, a transmembrane region and intracellular C-terminal domain. The cytoplasmic tail can interact with  $\beta$ -catenin which forms a link to the actin cytoskeleton. This interaction with actin allows tension and contractility to be transferred to the adjoining cell which can drive cell re-arrangement at both a local and a tissue level (Lecuit and Yap, 2015).

## 2.3 Integrins

Integrins are expressed in all metazoan species and are formed of two subunits:  $\alpha$  and  $\beta$ . Integrins were first discovered in 1986 and were named on the basis they could integrate the intracellular and extracellular environments of a cell (Tamkun *et al.*, 1986). Humans have 18  $\alpha$  and 8  $\beta$  integrin subunits that can form 24  $\alpha\beta$  heterodimeric pairs of integrin shown in **FIGURE 2.2** (Campbell and Humphries, 2011). Integrins are expressed in nearly all cell types and different cell types express different combinations of integrins; each integrin has distinct patterns in cell-types and tissue expression helping to support cell-matrix and cell-cell attachment.

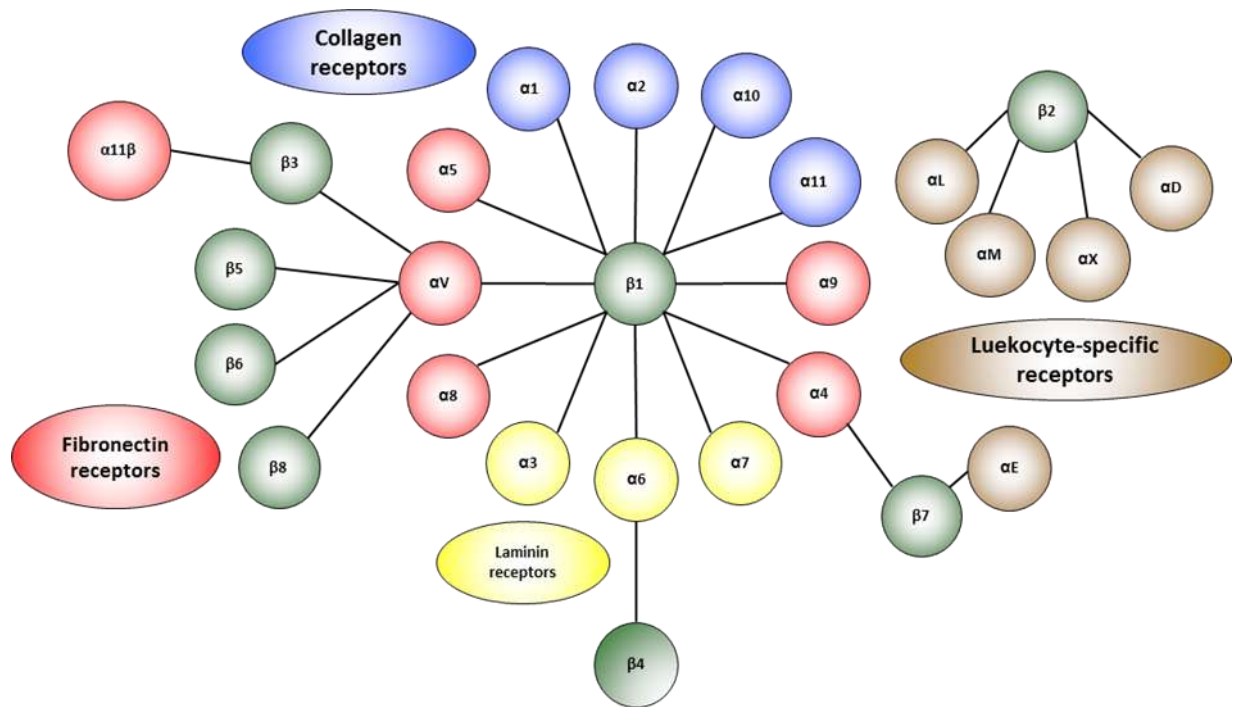


**FIGURE 2.2: INTEGRIN SUBUNIT PAIRINGS**

A schematic of all integrin  $\alpha$  and  $\beta$  subunits illustrating the pairings they can make in humans and categorised into the ECM component they can interact with. Figure based from (Lal, 2009).

### 2.3.1 Integrin Structure

$\alpha$  integrins comprise around 1000 amino acid residues whereas  $\beta$  integrins are composed of around 750 amino acids (Hynes, 2002). Both subunits contain an ectodomain, a single transmembrane region and an intracellular domain as shown in **FIGURE 2.3**.

$\alpha$  integrin ectodomains are composed of four, or five, domains depending on the  $\alpha$  integrin subtype, whereas  $\beta$  integrin ectodomain is split into several domains which have flexible linker regions joining them. Both  $\alpha$  and  $\beta$  integrins have a single transmembrane region (TM), these regions are highly conserved and link to a short cytoplasmic tail of around 25-50 amino acids. The cytoplasmic tails appear to be flexible until bound to a ligand (Campbell and Humphries, 2011). Integrin tails are important for the communication between the cell and the ECM; they form 'hub' interactions with a number of cellular proteins which is especially important for inside-out activation of the integrins (Wegener and Campbell, 2008), see **section 2.3.3**.

The cytoplasmic tails of  $\beta$  integrins have two Asp-Pro-x-Tyr (NPxY) motifs- where x is any amino acid, which are important for the binding of many proteins including talin and kindlin. As shown in **FIGURE 2.3B**, the two NPxY motifs are defined as proximal and distal regions and these



sequences are found in all  $\beta$  integrins (Wegener and Campbell, 2008).  $\alpha$  integrins also have a common sequence found in all isoforms, the GFFKR motif (shown in **FIGURE 2.3B**), which has been found important for binding both sharnin and the mammary-derived growth inhibitor (MDGI) (Li *et al.*, 2014). Sharnin and MDGI are both inhibitors of integrin activation and are needed to keep the integrin in an inactive state (Rantala *et al.*, 2011).

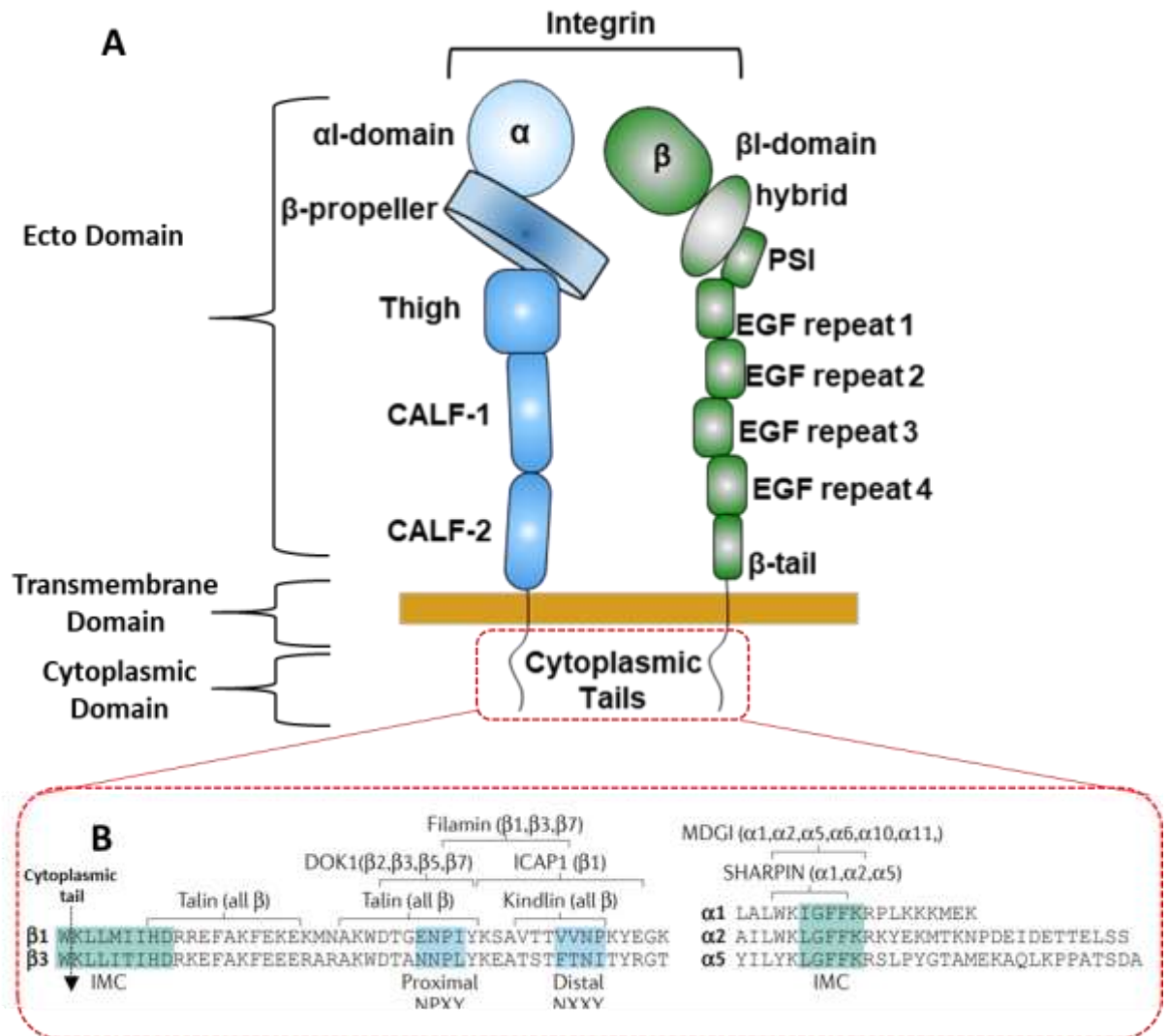


**FIGURE 2.3: STRUCTURE OF INTEGRINS**

(A). There is variation in integrin ecto domain structure and this represents a schematic of the domains present in integrin  $\alpha_4\beta_1$ . (B) The cytoplasmic tail region of integrins, the NPXY motifs on  $\beta$  integrin tails are highlighted in blue and the binding regions for several integrin activators and their specific integrin subtype are indicted, this image is adapted from: (Bouvard *et al.*, 2013).

### 2.3.2 The extracellular matrix

The ECM is a non-cellular component that is found in all tissues and organs and provides a scaffolding network for surrounding cells (Frantz, Stewart and Weaver, 2010). The ECM is made up of three main components: proteoglycans including, keratin sulphate and heparan sulphate; insoluble collagen fibres (which provide strength) and soluble multi-adhesive ECM proteins such as fibronectin and lamin (Frantz, Stewart and Weaver, 2010).

Although the ECM is primarily made up of the same components, all tissues have a unique ECM composition and topology which is determined during embryonic development through various cellular components such as fibroblast cells (which secrete all major precursors for the ECM). The difference in ECM composition is a major element in what gives different tissues and organs their mechanical and biochemical properties. The composition is tightly regulated to maintain stability of tissue and organ physiology. In diseases such as cancer the ECM becomes disordered and unregulated, often stiffer and more fibrous which leads to the promotion of cell migration and cancer metastasis. Abnormalities in the ECM can also lead to tumour-associated angiogenesis which in turn gives tumour cells their own microenvironment and facilitates further spreading (Lu, Weaver and Werb, 2012).

### 2.3.3 Integrin activation

Integrins receptors link the actin cytoskeleton to the ECM which allows the cell to generate traction an important feature for cell shape, adhesion and migration (Calderwood *et al.*, 1999). One important and reversible mechanism for regulating integrin adhesions comes through the regulation of integrins activation state. Integrins fluctuate between states of high affinity ('active' conformation) whereby it can interact with the ECM (see **FIGURE 2.4** and a state of low affinity ('closed' conformation) where it is unable to make interaction with the ECM (Calderwood, 2004). The state of affinity can be controlled by intracellular signals (in a process known as 'inside-out' activation) binding to the integrin cytoplasmic tails, these interactions induce conformational changes in the integrin extracellular domains that can result in integrins having a higher affinity for the ECM (Calderwood *et al.*, 1999).

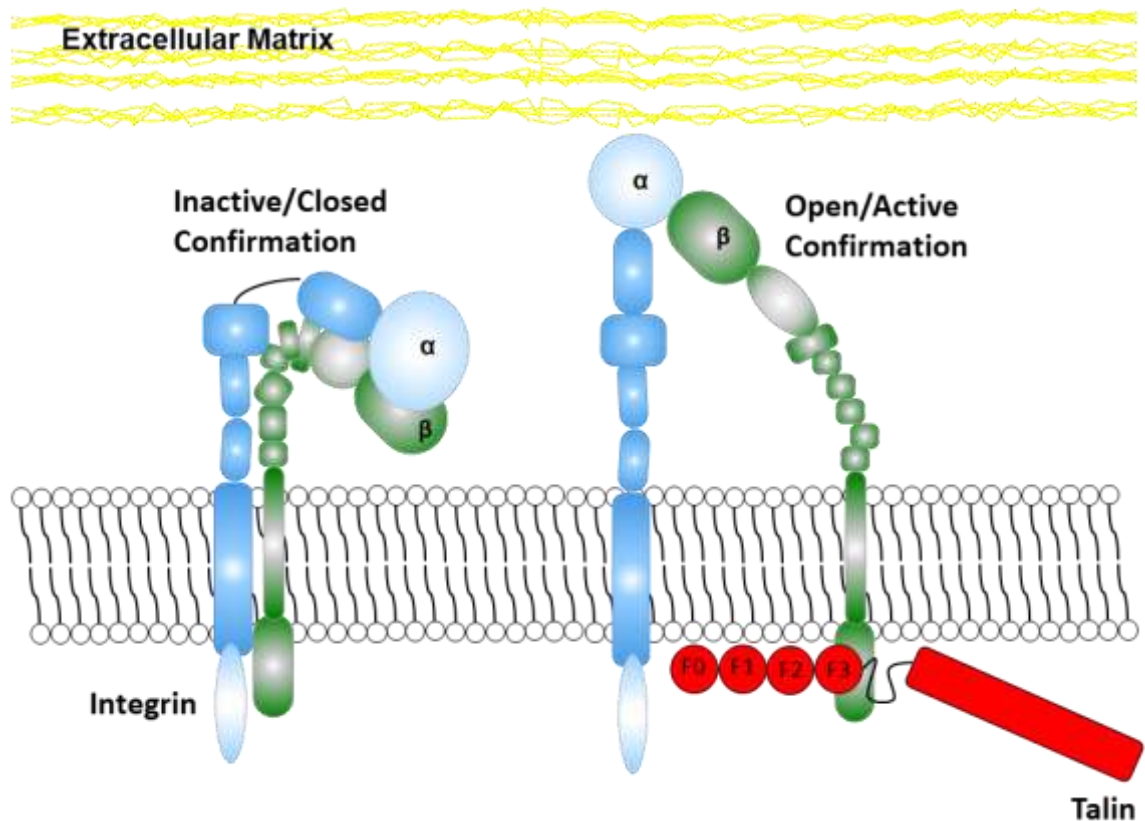


**FIGURE 2.4: ACTIVATION STATE OF INTEGRINS**

Schematic diagram illustrating the integrin affinity states. Integrins fluctuate between states of low affinity where they are in a ‘closed’ conformation (left) and a high affinity ‘active’ conformation (right). Talin binding the  $\beta$  integrin tail induces conformational changes in the integrin extracellular domains that can result in integrins having a higher affinity for the ECM.

The cell has to ensure that the integrin is in an ‘active’ conformation only when required otherwise, adhesions to the ECM could occur in unwanted places leading to problems such as blood clots and cell metastasis (Ganguly *et al.*, 2013). Integrins use a network of dynamic interactions known as the integrin adhesion complex (IAC) to mediate their activation state. The complexity of the IACs has been highlighted in analysis of the ‘integrin adhesome’ where mass spectrometry of multiple integrin adhesion complexes revealed a network of >240 proteins are involved in integrin regulation (Horton *et al.*, 2016; Ronen Zaidel-Bar, 2007).

Further analysis of the integrin adhesome indicated that there is a consensus adhesome of around 60 proteins that all centre around four different centred around four ‘axes’ comprising ILK-PINCH-kindlin, FAK-paxillin, talin-vinculin and  $\alpha$ -actinin-zyxin-VASP (Horton *et al.*, 2016).

In all of the different ‘axes’ of the IAC it appears that the adapter protein talin is linked in some way. Talin is a cytoplasmic adapter protein that is vital to integrin activation; talin can bind to the highly conserved proximal NPxY motif in the  $\beta$  integrin tail via the talin FERM F3 domain

(Calderwood *et al.*, 2002). This interaction between talin and integrin disrupts a salt bridge interaction between the integrin  $\alpha$   $\beta$  tails, which holds the two tails in close proximity keeping the integrin in a low affinity state (Calderwood, 2004). Talin F3 still with the  $\beta$  integrin bound forms electrostatic interactions with lipid groups in the membrane (as shown in **FIGURE 2.5**) which leads to conformational change in the positioning of the talin-integrin complex and results in the separation of the  $\alpha$   $\beta$  integrin tails and activates the integrin.

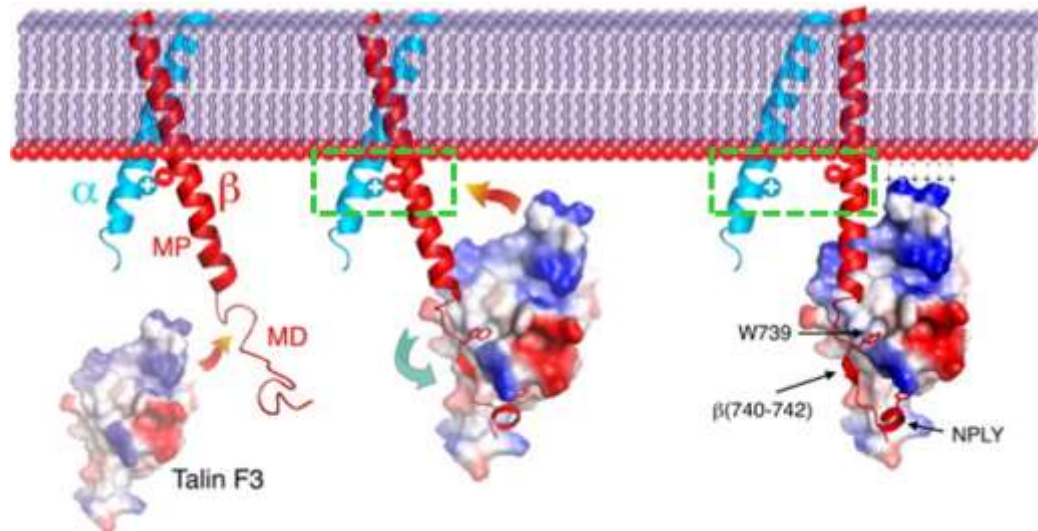


**FIGURE 2.5: TALIN-INDUCED INTEGRIN ACTIVATION**

Structural representation of the talin F3 domain binding to the membrane distal region of the  $\beta$  integrin tail. Talin F3 subsequently, engages with the membrane proximal region of the  $\beta$  integrin which leads to the disruption of the putative integrin salt bridge highlighted by green box. Talin can then make electrostatic contacts with the lipid head groups in the membrane, this results in the change of positioning of the  $\beta$  integrin tail and forces apart the  $\alpha$   $\beta$  integrin tails and activates the integrin. Figure adapted from (Goksoy *et al.*, 2008)

## 2.4 Different adhesive structures

IACs form distinct adhesive structures which include: focal adhesion complexes, nascent adhesions, focal adhesions, fibrillar adhesions and podosomes. These adhesive structures can be categorised by their distinctive structures and play different roles in cell migration, shape and adhesion as shown in **FIGURE 2.6**.

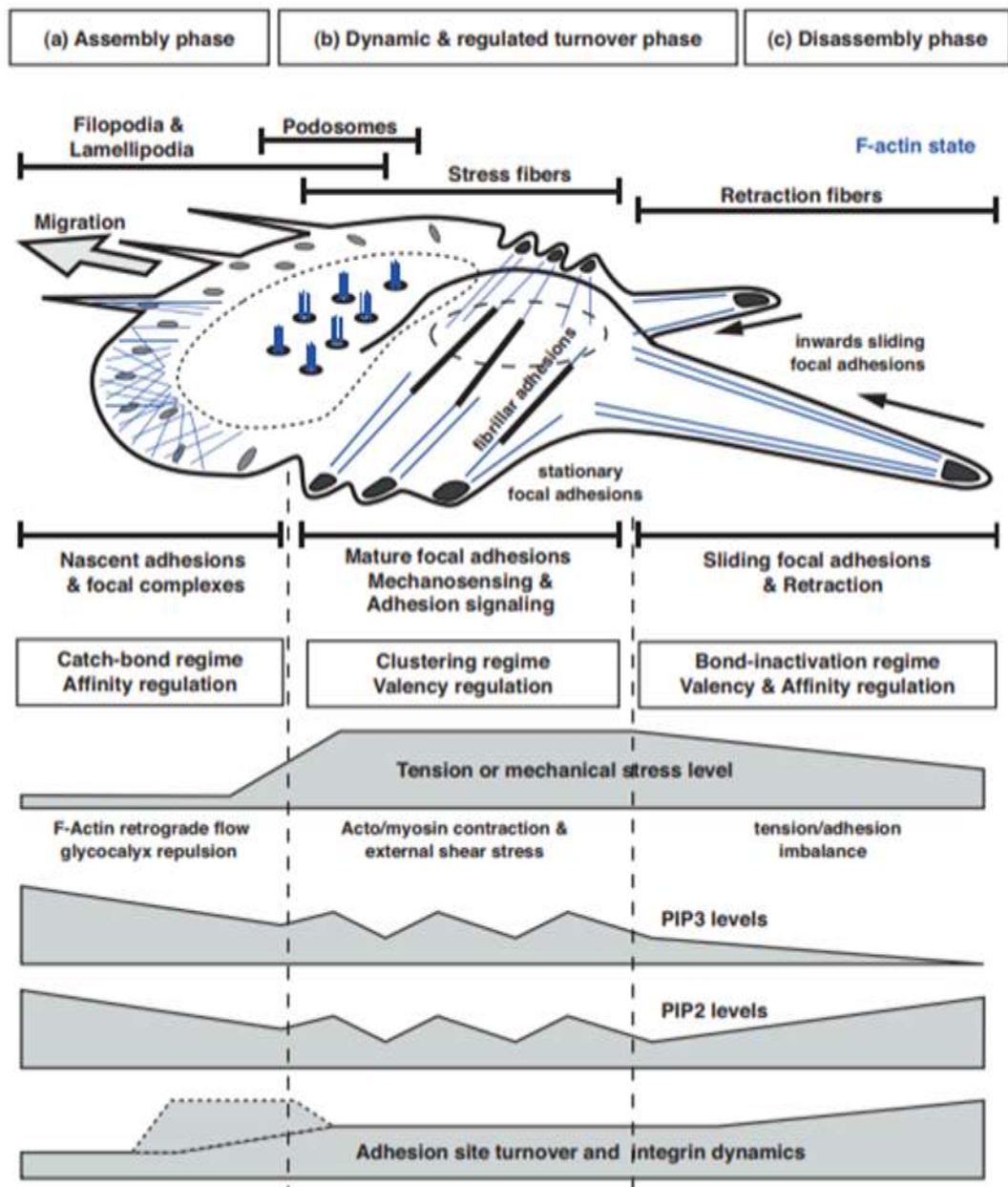


**FIGURE 2.6: LOCATION OF CELL-MATRIX ADHESIONS ACROSS A CELL**

Diagram highlighting where the different cell-ECM adhesion types are located across a migrating cell. The diagram also highlights the levels of tension the adhesions are under and the adhesion turnover rate. Figure from (Wehrle-Haller, 2012).

### 2.4.1 Nascent adhesions

Nascent adhesions are found to assemble under filopodia and lamellipodia protrusions (Ridley *et al.*, 2003); they are the smallest type of integrin adhesion and typically assemble in milliseconds. Nascent adhesions provide crucial links between the integrin and actin cytoskeleton through the interaction of integrin:talín:actin. The addition of actin allows nascent adhesions to transition to focal adhesions (FAs) a more stable adhesion.

## 2.4.2 Focal complexes and focal adhesions

FAs and focal complexes arise from nascent adhesions and are larger measuring around 1  $\mu\text{M}$  in size (Anderson, Owens and Naylor, 2014). In FAs talin is a crucial player in coupling integrins to the actin cytoskeleton, as the force increases across the adhesion (through binding of actin) talin domains can unfold revealing vinculin binding sites. These unfolded domains allow vinculin to bind which re-enforces talin in a stretched confirmation and prevents the talin domains from re-folding (Yao *et al.*, 2014). Additionally, vinculin binding to talin is thought to activate vinculin as it out-competes the interaction between the vinculin head and tail (associated with auto-inhibited vinculin). This addition of vinculin binding talin promotes a formation of stronger actin linkage and assembles and more stable adhesion.

## 2.4.3 Fibrillar adhesions

Fibrillar adhesions are located away from the leading edge and near to the nucleus and vary in size, ranging from 1  $\mu\text{M}$  to 10  $\mu\text{M}$  in diameter (Anderson, Owens and Naylor, 2014). Fibrillar adhesions develop from mature FAs and are characterised through the inclusion of the protein tensin which cross links actin cables to fibronectin fibrils located in the ECM (Huveneers and Danen, 2009). Fibrillar adhesions can be distinguished from FAs as they are not attached to stress fibres which prevents them from dis-assembling when force across the adhesion is relaxed (Zamir *et al.*, 2000).

## 2.4.4 Podosomes

Podosomes are found at the lamellopodia (see **FIGURE 2.6**) and differ structurally from the other adhesive structures. Structurally, the most distinguishing feature of podosomes is their two part organisational design; they have a dense F-actin core that is surrounded by a ring structure of adhesion proteins such as talin, vinculin and integrins (Linder and Kopp, 2005). The actin-rich core is not found in any of the other cell-matrix adhesion types and consequently actin regulation proteins exert a major influence on the podosome-type contacts. Podosomes are typically found in macrophages, dendritic cells and osteoclasts. However, they are also found in a number of other cell type including endothelial cells and smooth muscle as they play a large role in matrix degradation (Linder and Kopp, 2005).



## 2.5 Talin

A key protein found in all of the cell-matrix adhesion types is the adapter protein talin. Talin is a large 270 kDa adapter protein that was first discovered in 1983 as a component of FAs and ruffling membranes (Burrige and Connell, 1983). Talin is comprised of an N-terminal FERM domain (head) attached to a C-terminal rod domain by an unstructured linker (as shown in **FIGURE 2.7**). The rod domain encompasses 13 alpha helical bundles, each comprised of either four or five helices (Goult, Zacharchenko, *et al.*, 2013).

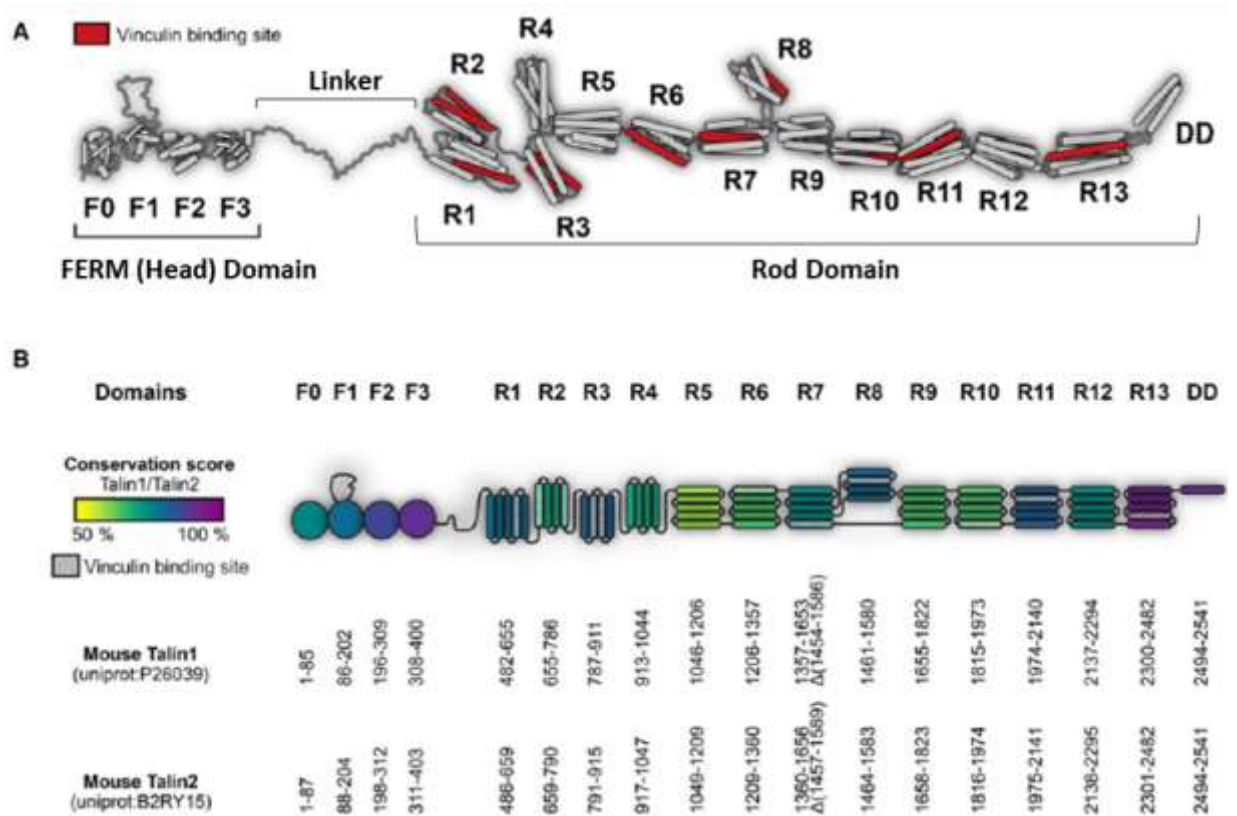


**FIGURE 2.7: TALIN DOMAIN STRUCTURE AND CONSERVATION**

(A) Structural model of talin showing highlighting the different domains, vinculin sites are detailed in red across the protein. (B) Schematic representation of the talin domain structures coloured by sequence identity between the two isoforms. The domain boundaries are given for mouse talin1 (UniProt: P26039) and talin2 (UniProt: B2RY15). Figure adapted from (Gough and Goult, 2018).

Talin is one of the key elements in integrin activation and provides the link between integrins and actin cytoskeleton (Shattil, Kim and Ginsberg, 2010). The interaction between integrin-talin-actin forms the basis of a nascent adhesion allowing the recruitment of numerous other FA and signalling molecules, to form a more stable adhesion (Calderwood, Campbell and Critchley, 2013).

Furthermore, talin is a mechanosensing protein, with its 13 alpha helical rod domains capable of undergoing force-dependent conformational transitions that can modulate binding interactions with mechanosensitive ligands (del Rio *et al.*, 2009; Goult, Zacharchenko, *et al.*, 2013; Yao *et al.*, 2014, 2016; Yan *et al.*, 2015). Until the work presented here in this thesis and the subsequent publications (Bouchet *et al.*, 2016; Sun *et al.*, 2016) it was not known that talin also has a pivotal role in linking adhesions to cortical microtubule stabilising complexes, through its interaction with the KANK family of proteins (see **chapter 4**).

## **2.5.1 Talin Isoforms**

There are two isoforms of talin; talin1 and talin2 which share an identical domain structure and have a 74% amino acid sequence identity (shown in **FIGURE 2.7B**). In vertebrates, the isoforms are encoded by two different genes, *TLN1* and *TLN2*, both of which have highly conserved intron and exon boundaries (Monkley, Pritchard and Critchley, 2001; Senetar, Moncman and McCann, 2007). The genes are located on different chromosomes; *TLN1* is located on Ch9 and *TLN2* is located on Ch15, furthermore, *TLN2* (190 Kb) is a larger gene than *TLN1* (30 Kb) due to larger introns.

### **2.5.1.1 Talin2**

*TLN2* has been shown to have multiple splice variants which lead to multiple talin2 isoforms as shown in **FIGURE 2.8** (Debrand *et al.*, 2009). These talin2 isoforms still currently have no known function but the expression of the different splice variants is interesting. The shorter isoforms (lacking the N-terminal FERM domain) are found to be expressed in the brain, kidneys and testes which raises the prospect that they are not involved in integrin binding and may serve other functions (Debrand *et al.*, 2009). Furthermore, it was found that if a talin1 fragment (the same as the short C-terminal testes specific talin2 isoform) was expressed in cells depleted of talin1 then this was sufficient to rescue cell cycle progression suggesting a potential role in cellular signalling (Himmel *et al.*, 2009; Wang, Ballestrem and Streuli, 2011).



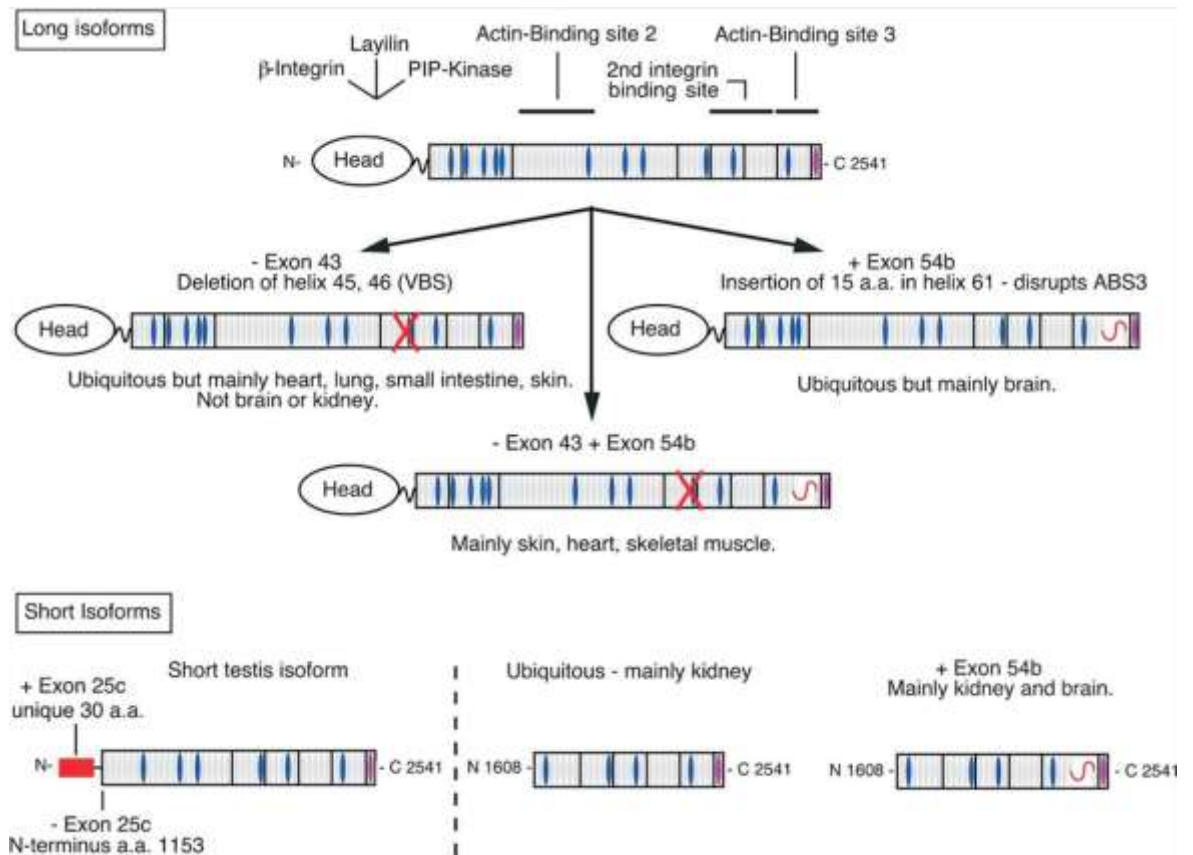


**FIGURE 2.8: TALIN2 SPLICE VARIANTS**

Schematic diagram displaying the main talin2 isoforms that arise due to alternative splicing. Vinculin binding sites are highlighted in blue and red crosses indicate the vinculin binding regions that have been deleted due to exon skipping. At the top of the diagram the longer talin2 isoforms are shown and at the bottom the shorter talin2 isoforms, that are lacking the FERM domain. Figure taken from: (Debrand *et al.*, 2009).

*TLN2* is the ancestral gene, and through early duplication in the chordate lineage it led to the emergence of talin 1 (Senetar and McCann, 2005). Interestingly, over evolution the talin domain structure has not changed, even since the talin2 duplication in the chordates lineage that lead to the emergence of talin1; the sequence length has remained the same (talin1 2541aa and talin2 2540aa). This is quite an unusual finding compared to other large multi-domain proteins such as; filamin, titin and spectrin of which all have varied in length over evolution (Higgins *et al.*, 1994; Baines, 2010; Light *et al.*, 2012). This unvarying domain structure gives compelling evidence that every domain within talin has an important functional role.

Independent functions of the two isoforms within cells have not yet been fully understood but it has been found that tissue expression and cellular localisation varies significantly between both isoforms. Talin2 expression is more variable than talin1 and unlike talin1, it has not been found to be expressed in all cell types for example, there is no expressed talin2 in endothelial cells (Kopp *et al.*, 2014).

*al.*, 2010; Monkley *et al.*, 2011). There is however, high expression of talin2 in heart muscle, kidneys and the cerebral cortex of the brain (Manso *et al.*, 2013).

### 2.5.1.2 Talin1

Talin1 on the other hand, is expressed in nearly all tissues and is believed to be ‘the more essential talin isoform’. *TLN1-knockout* mice embryos are not viable and mice die due to arrested gastrulation, indicating that talin1 is essential for early development (Monkley *et al.*, 2000). In contrast a *TLN2-knockout* is not lethal at embryonic stages and instead, mice were viable and fertile expressing only mild dystrophic phenotypes with small variations in mouse pups reaching adulthood (Debrand *et al.*, 2012). Evidence does show that talin2 can rescue the cell’s phenotype, following the loss of talin1 after embryonic development. In fact, in embryonic fibroblasts cells (MEFs) of *TLN1-knockout* mice, *TLN2* expression is rapidly up-regulated, to compensate for the loss of talin1 and resulting phenotype (Zhang *et al.*, 2008). Similarly, a *knockout* of both talin isoforms entirely destroys cell-ECM adhesions, highlighting the essential role that talin plays in integrin adhesions (Manso *et al.*, 2017).

In fibroblasts both isoforms localise to FAs with talin1 being directly recruited to the cells leading edge via RIAM, the RAP1 effector (Rap1-interacting adapter molecule) (Lee *et al.*, 2009; Lagarrigue *et al.*, 2015). The mechanism that recruits talin2 to the leading edge is not yet understood. Talin2 is known to bind RIAM although this is thought to cause aggregates to form throughout the cell which have been found to overtime co-localise to fibrillar adhesions. Fibrillar adhesions are found in the centre of the cell (see **FIGURE 2.6**) and localisation of talin2 to fibrillar adhesions could suggest that it is involved in fibronectin assembly or possibly invadopodia formation (Singh, Carraher and Schwarzbauer, 2010; Qi *et al.*, 2016). Recently it was found that talin2 was essential for generating the traction force needed to allow invadopodia-mediated matrix degradation which is required for invadopodia formation (Qi *et al.*, 2016).

## 2.5.2 The talin head

Both talin isoforms have a N-terminal head domain (as shown **FIGURE 2.9**); this is formed from an atypical FERM (4.1 protein, ezrin, radixin, moesin) domain containing four sub-domains: F0-F3. The talin FERM domain is classed as atypical as it comprises of four subdomains rather than three (F1-F3) and also because of the linear structure it takes compared to the more commonly found clover leaf shape of other FERM domain proteins (Elliott *et al.*, 2010).

The FERM domain is essential for talin to bind and activate integrin; the talin F3 domain binds to the  $\beta$ -integrin tail via interaction with the membrane proximal NPXY motif (Calderwood *et al.*, 1999). This interaction with talin breaks the electrostatic interaction holding the two integrin tails ( $\alpha$  and  $\beta$ ) together, converting integrin to an active conformation (Vinogradova *et al.*, 2002).

Isolated Talin F3 can bind to  $\beta$ -integrin tails however, it is fairly ineffective at activating integrins due to the need of the other talin sub-domains to form an effective 'integrin activation lock' and hold the integrin in the active, high-affinity conformation (Bouaouina, Lad and Calderwood, 2008). The other sub-domains help to promote this 'integrin activation lock' through the formation of interactions with phosphoinositides such as PtdIns(4,5) $P_2$  (PIP2) at the cell membrane. The F2 sub-domain has a basic patch on the membrane interacting surface which promotes interaction with the membrane helping stabilise the talin-integrin interaction (Anthis *et al.*, 2009; Saltel *et al.*, 2009; Franceschi *et al.*, 2017). Additionally, the F1 sub-domain contains a large unstructured loop insertion, which can interact with PIP2 which is essential for integrin activation (Goult *et al.*, 2010). The F3 domain itself has also been shown to form electrostatic contacts with the membrane when bound to the  $\beta$ -integrin tail (Vinogradova *et al.*, 2002) and together the electrostatic interactions from the talin sub-domains and the membrane provide the force on the integrin needed to help stabilise the integrin-activated state.

In addition to integrin binding the talin head can also bind PIP kinase gamma (de Pereda *et al.*, 2005) through interaction with the F3 sub-domain. PIP kinase gamma is required to produce PIP2 at the membrane which is needed to promote integrin activation (Legate *et al.*, 2011). The F3 sub-domain can also bind a host of other ligands including: RIAM (Yang *et al.*, 2014), FAK (Lawson *et al.*, 2012), T-Cell Lymphoma Invasion And Metastasis 1 (TIAM) (Wang *et al.*, 2012) and G-protein subunit *Galpha13* ( $G\alpha13$ ) (Schiemer *et al.*, 2016).

Both talin isoforms have three actin binding sites (ABS1, ABS2 and ABS3) (Hemmings *et al.*, 1996). ABS1 is the only actin binding site found in the talin head in sub-domains F2 and F3 (Lee *et al.*, 2004); ABS1 is important for capping actin filaments to prevent actin polymerisation (Ciobanasu *et al.*, 2018).

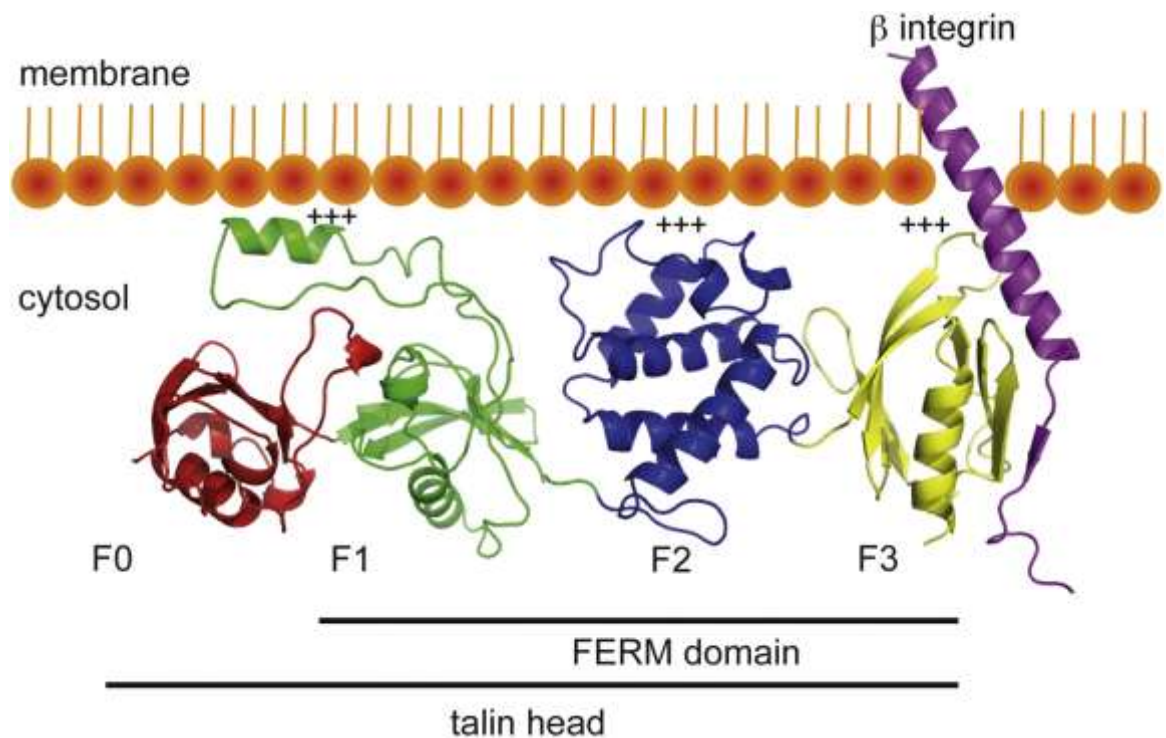


**FIGURE 2.9: TALIN1 FERM DOMAIN INTERACTING WITH THE MEMBRANE**

Schematic model of the complex between the talin FERM and  $\beta_3$ -integrin tail docked against the membrane surface. The talin FERM domain is in an elongated conformation and the + indicate areas of electrostatic interactions between talin and the membrane. Figure from (Elliott, et al., 2010).

### 2.5.3 The talin rod

The talin head is connected to the talin rod via an 82 amino acid unstructured linker (Bate *et al.*, 2012). The talin rod is comprised of 62 alpha helices which are folded into 13 alpha helical bundles of either four or five helices (see **FIGURE 2.7**) (Goult, Zacharchenko, *et al.*, 2013). Four-helix bundles are commonly found in nature; in contrast five-helix bundles are quite unusual. The extra helix that packs onto the side of a four-helix bundle (creating a five-helix bundle) has a great impact on the talin structure and functional ability in the cell. Five-helical bundles determine that the N and C-terminus of the bundle are at opposite ends which allows the bundles to pack side by side in a linear rod-like arrangement as shown in **FIGURE 2.7**; this rod like arrangement allows talin to transmit force. Furthermore, five-helix bundles provide more mechanical stability than four-helix bundles due to extensive contacts throughout the length of the helices and more hydrogen bonding (B. T. Goult *et al.*, 2010).

The talin rod contains a C-terminal dimerisation domain (DD) which enables talin to form an antiparallel dimer with another talin molecule (Gingras *et al.*, 2008). Talin dimers in literature have

been found to be homodimers. Dimeric talin is able to form an autoinhibited confirmation in the cytosol whereby, the two talins wrap around each other to form a 'double-doughnut' shape with the talin FERM domain buried inside (Goult, Xu, *et al.*, 2013). Activation of talin from this inactive state does not appear to happen via one interactor instead a variety of activators have been discovered including: RIAM and G $\alpha$ -switch (Lee *et al.*, 2009; Schiemer *et al.*, 2016).

### 2.5.3.1 The R7R8 fold

In the centre of the talin rod there is an unusual 9-helix bundle comprised of domains R7 and R8. These domains are in an unusual confirmation that is not seen anywhere else in talin; R8 is a four-helix bundle that is inserted into the R7 five-helix bundle as shown in

**FIGURE 2.10** (Gingras *et al.*, 2010). This confirmation of one bundle inserted into another was probably created by chance however, due to importance in function it has remained in this confirmation throughout evolution.

The R7R8 fold is conserved in both talin isoforms; the R8 domain is inserted between the  $\alpha$ 3 and  $\alpha$ 4 helices on R7 (see **FIGURE 2.10**) and the two domains are joined via flexible linkers between helices 30-31 and 34-35 (see **FIGURE 2.10**). The flexible linkers are joined together through hydrogen bonding and allow the R7R8 domain to be in different confirmations of 'open' and 'closed' dependent on what ligand is bound.

As described a four-helix bundle is less mechanically stable than a five-helix bundle and so it would be predicted that the R8 domain should unfold at low force however, due to the insertion into R7 the bundle is protected from unfolding (Yao *et al.*, 2016). This 'protection' of R8 is integral for many talin functions; the folded R8 helix binds many ligands including; actin, RIAM, DLC1 and as discussed in this thesis, CDK1 (see **Chapter 6**).

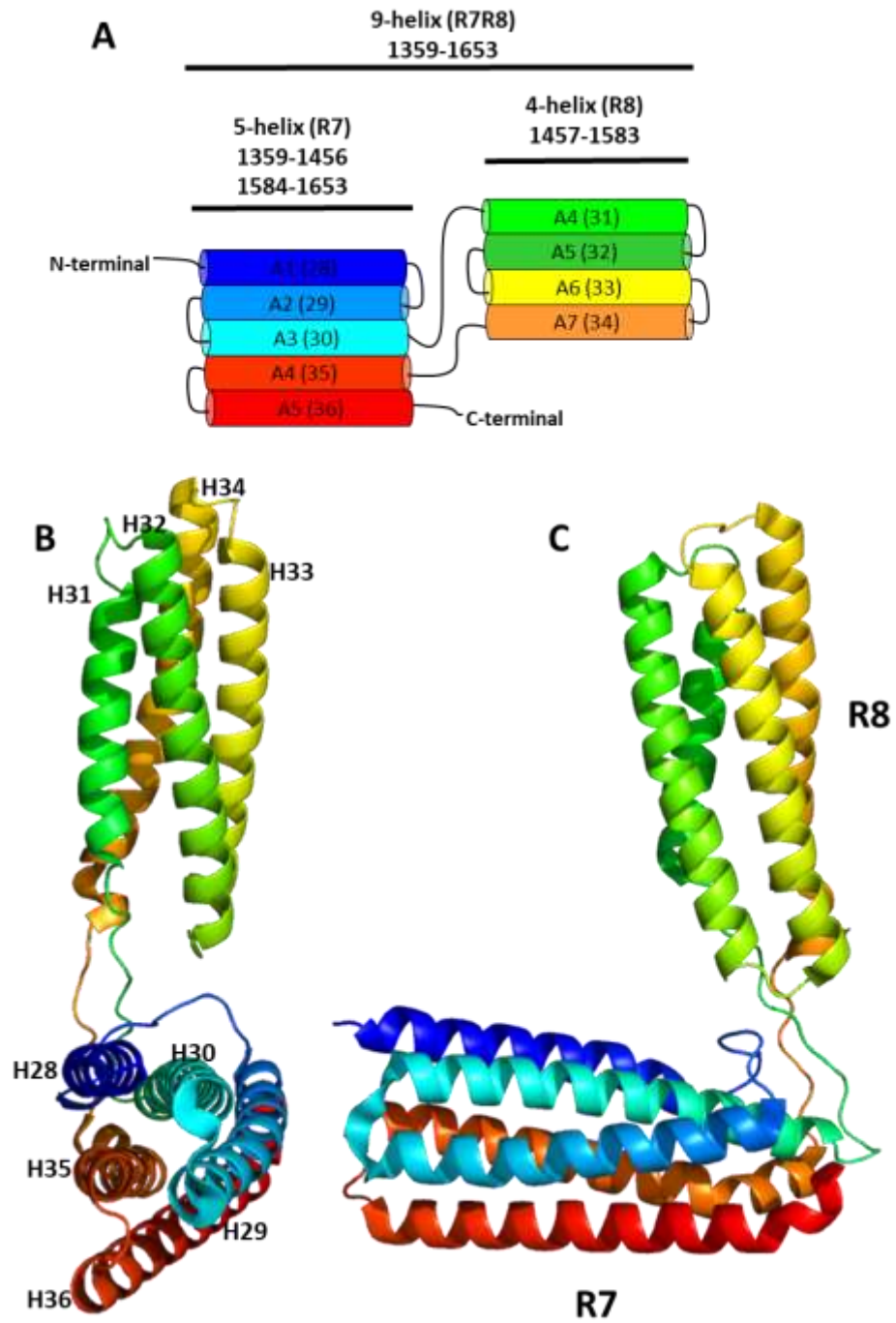


**FIGURE 2.10: TALIN R7R8 DOMAIN STRUCTURE**

(A) Schematic of the helices in talin R7 and R8 indicating in brackets the helix number in full length talin and the alpha-helix position of each helix within the bundle. (B) Structure of talin R7R8 domains (PDB ID: 5FZT).

## 2.6 Talin rod interactions within adhesions

### 2.6.1 Actin

As previously mentioned both talin isoforms have three actin binding sites; ABS1, ABS2 and ABS3. The talin rod contains ABS2 and ABS3 as shown in **FIGURE 2.11A** and both are important for adhesion assembly and creating the force for mechanosensing capabilities of talin.

ABS2 is positioned across talin domains R4 and R8 (Hemmings *et al.*, 1996; Atherton *et al.*, 2015; Kumar *et al.*, 2016) and the main actin contacts are with talin domains R4 and R8 domains (Atherton *et al.*, 2015). R4 and R8 domains have abnormally high pI values (compared with the other talin rod domains), causing the talin surface to be positively charged at a physiological pH as shown in **FIGURE 2.11B** and **C**. This positively charged surface can form electrostatic interactions with negatively charged actin; ABS3 and ABS1 also demonstrate similar properties.

ABS3 is located at the talin C-terminus across domains R13-DD (McCann and Craig, 1997; Gingras *et al.*, 2006). ABS3 is essential for adhesion assembly, and the current working model indicates that ABS3 is the initial site that binds to actin which in turn creates enough force on the talin rod to unfold the mechanosensitive R3 domain, and allowing vinculin to bind. This interaction between talin ABS3 and actin promotes maturation of focal adhesion assemblies (Yao *et al.*, 2014). Following the un-folding of talin R3 (through force generated by actin binding to ABS3), the ABS2 site on talin is activated and can bind actin. This interaction has been found to be essential for FA maturation and cell polarisation (Atherton *et al.*, 2015; Klapholz and Brown, 2017).

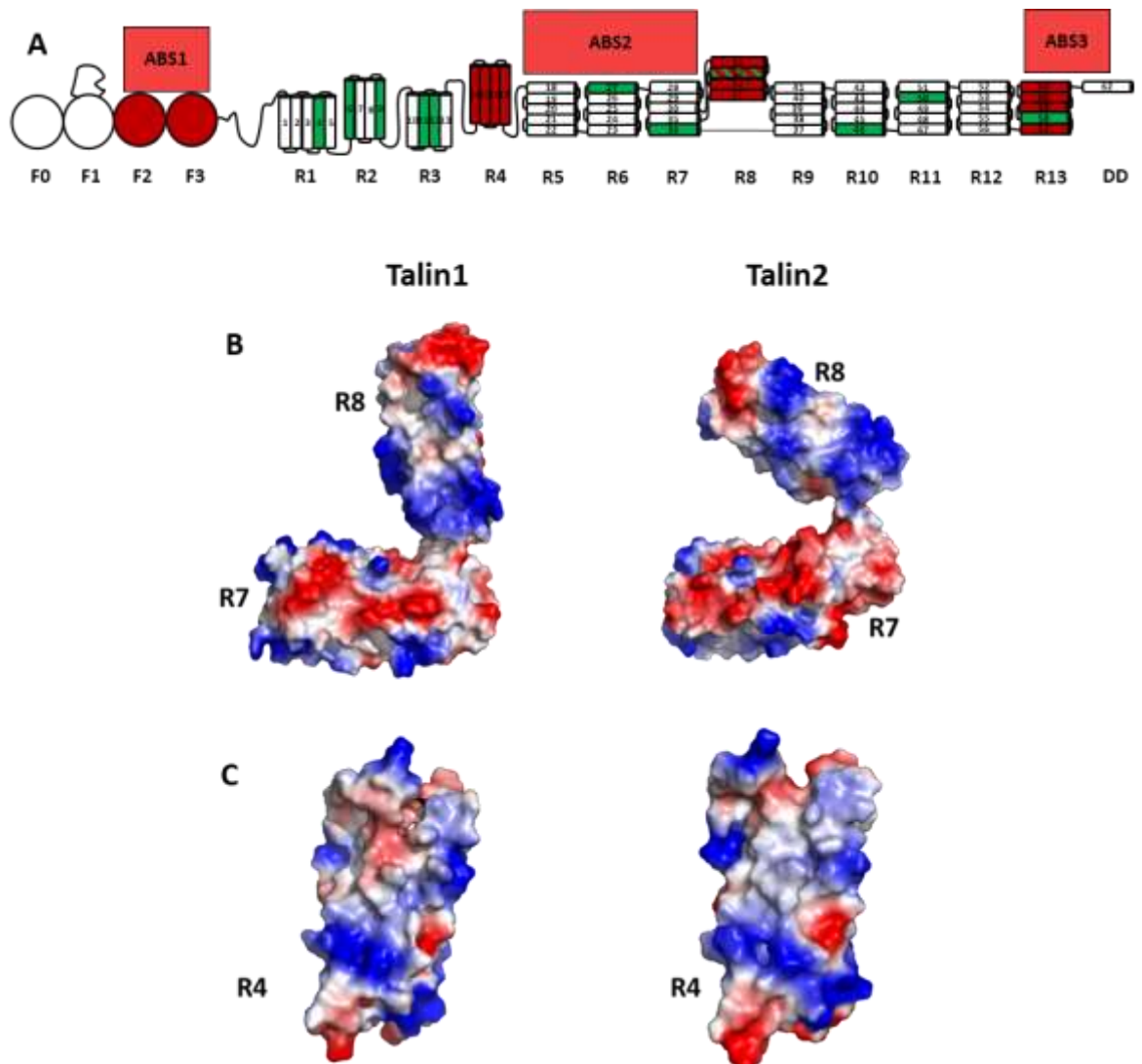


**FIGURE 2.11: ACTIN BINDING SITES ACROSS TALIN**

(A) Schematic of talin, red domains indicate areas of talin involved in actin binding and green helices represent vinculin binding sites. (B) Talin1 and talin2 R7R8 domain structures (tal1n1 R7R8 PDB ID:2X0C and talin2 R7R8 modelled using Phyre2). (C) Talin1 and talin2 R4 domain structures modelled using Phyre2. Structures in both B and C were modelled in PyMOL with electrostatic surfaces indicating the surface charge on the protein. Blue indicates positively charged and red indicated negatively charged.

## 2.6.2 Vinculin

Vinculin is a cytoplasmic actin binding protein that was first discovered in 1979 (Geiger, 1979; Peng *et al.*, 2011). Vinculin is enriched at focal adhesions and is found to be a key talin interactor binding to 11 of the 62 talin helices in the rod domain (Gingras *et al.*, 2005). Vinculin binding sites (VBS) on talin are not found on the helical bundle surfaces (like other talin interactors) but instead are buried inside the helical core and can only be accessed when talin is under mechanical force as



shown in **FIGURE 2.12F** (Yao *et al.*, 2014, 2016). Vinculin has also been shown to activate talin (Carisey *et al.*, 2013) and the exposed VBS on talin can activate vinculin (Bois *et al.*, 2006).

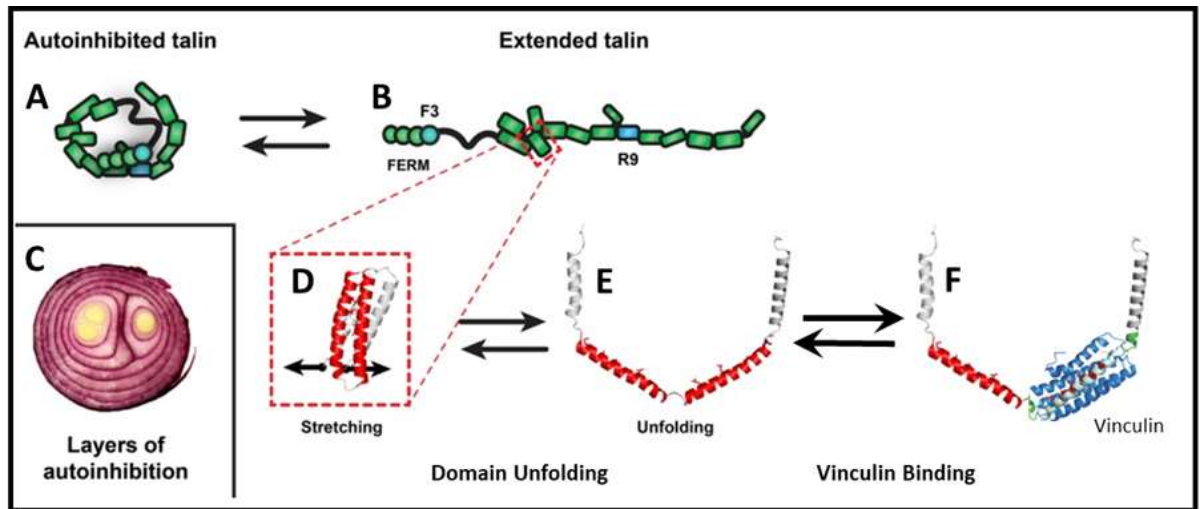


**FIGURE 2.12: LAYERS OF AUTOINHIBITION IN TALIN**

Schematic diagram representing the layers of talin autoinhibition. (A) Represents talin in closed cytoplasmic conformation with the FERM domain buried inside. (B) Open talin conformation commonly found at adhesion sites under no force. (C) A representation of the layers found in talin. (D) Talin rod domain R3 (white) with buried vinculin binding sites shown in red. (E) R3 domain stretched as a result of being under force exposing the buried vinculin binding site, (F) shows the now exposed VBS with vinculin bound. Figure adapted from (Goult, Zacharchenko, *et al.*, 2013; Gough and Goult, 2018)

### 2.6.3 Integrin

As discussed previously talin has an integrin binding site on the F3 sub-domain in the talin head which is known as integrin binding site 1 (IBS1). IBS1 is crucial for activating integrin through ‘inside-out’ integrin activation and increasing ECM binding (Shattil, Kim and Ginsberg, 2010).

Talin also contains a second integrin binding site known as IBS2 (shown **FIGURE 2.14**), which is located in the rod between helical bundles R11 and R12. The structural mechanism of how talin IBS2 binds integrin is currently unknown and it appears that integrin binds across the two talin rod domains (R11 and R12) without the helical bundles being folded or unfolding instead it is thought to be in some sort of intermediate conformation (Rodius *et al.*, 2008; Gingras *et al.*, 2009; Ellis *et al.*, 2011). The physiological role of talin binding IBS2 in mammals is unknown however, it is thought that in it may be linked to nascent adhesion formation as mutations in the region lead to reduction in nascent adhesion clusters (Changede *et al.*, 2015). Interestingly in flies it has been shown that the role of IBS2 in integrin activation is more clear than IBS1 (Shattil *et al.*, 2010; Ellis *et al.*, 2011).

#### 2.6.4 Talin-moesin

The talin rod also binds directly (via its C-terminus domain) to the FERM domain of moesin (Beaty *et al.*, 2014). Moesin is a member of the ERM family and contains a FERM domain. Moesin is localised to filopodia and helps to attach actin filaments to the plasma membrane making it an important protein for cell signalling and movement (Pearson *et al.*, 2000). This interaction between talin and moesin is required for recruiting the sodium hydrogen exchanger (NHE-1) to adhesion sites at invadopodia (Beaty *et al.*, 2014), which can lead to localised alteration of intracellular pH at the adhesion sites. Even a small change in pH can have a dramatic effect on surrounding residues for example, a histidine residue has an imidazole group in its side chain, at pH 5 the imidazole group is positively charged and hydrophilic whereas at pH 7.4 the group is neutral and hydrophobic (Röttschke *et al.*, 2002). Protonation can be considered a post-translational modification (Schönichen *et al.*, 2013) and many important protein:protein interactions have been shown to be regulated by pH in this manner. One of which is the interaction between talin ABS3 and actin (Srivastava *et al.*, 2008); talin1 *knock-down* decreases the cytosolic pH at invadopodia and blocks cofilin-dependent actin polymerisation which leads to instability of invadopodia and matrix degradation (Beaty *et al.*, 2014).

#### 2.6.5 Talin-alpha synemin could provide a link to intermediate filaments

Talin has been found to link to the actin cytoskeleton and in **chapter 3** it is described how talin also forms a link to the microtubule cytoskeleton. Furthermore, an interaction between the talin rod domain and alpha-synemin (an intermediate filament (IF) protein that is expressed in skeletal muscle) (Sun *et al.*, 2008) reveals that talin may also provide linkage to IF. This suggests that talin could potentially co-ordinate interactions between all cytoskeletal (actin, microtubule and IF) networks.

#### 2.6.6 Talin binds LD-motifs

An emerging mechanism for ligands to bind to the talin rod is via Leucine-aspartic acid (LD) binding motifs, which are short alpha helical interaction motifs. These LD-motifs were first identified in paxillin (Brown, Curtis and Turner, 1998) and since have been identified as crucial players in connecting cell adhesion with cell mobility and survival (Alam *et al.*, 2014). LD sequences are named because of their core amino acid sequence LDxLLxxL (where x is any amino acid) which is made up of a hydrophobic cluster with an embedded positive charged amino acid. LD-motifs are

recognised by LD-motif binding domains (LDBDs) (Zacharchenko *et al.*, 2016) and in some cases the same LD-motif can be recognised by different LDBDs (Alam *et al.*, 2014).

Talin R8 has been identified as a LDBD and can bind to multiple LD ligands including; RIAM and DLC1 (Goult, Zacharchenko, *et al.*, 2013; Zacharchenko *et al.*, 2016). RIAM is a Rap1 effector protein and has been found to have a central role in integrin activation through its ability to bind to both talin and Rap1 (Lee *et al.*, 2009; Goult, Zacharchenko, *et al.*, 2013; Chang *et al.*, 2014). DLC1 is a tumour suppressor gene which is frequently inactivated during cancer and it encodes a Rho-GAP focal adhesion protein needed for GTPase activation; negative regulation of RhoGTPases are required but not entirely sufficient for tumour suppression (Li *et al.*, 2011). These LD-motifs bind to the talin R8 domain by helix addition, the ligand forms a helix and packs against the side of the talin rod domain as shown in **FIGURE 2.13**.

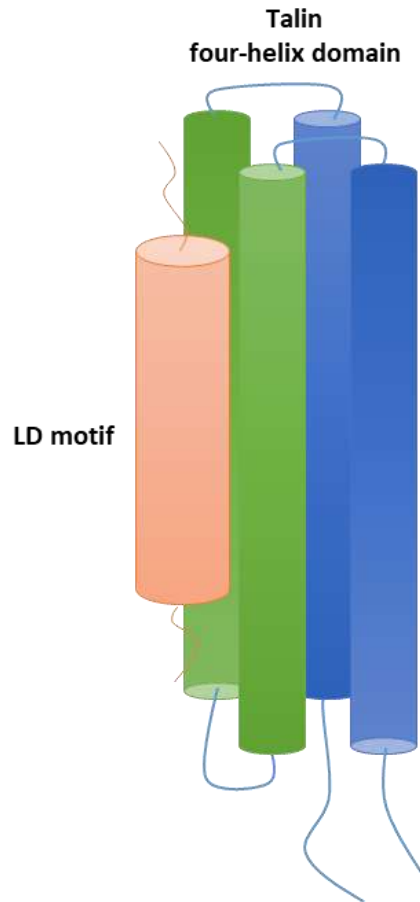


**FIGURE 2.13: LD LIGAND BINDING TO TALIN ROD DOMAIN**

A schematic of an LD-motif packing against a talin helical bundle via helix addition.

Other domains within the talin rod can also bind LD-motifs including R3 which binds RIAM. More recently, and discussed in this thesis, we have discovered that the R7 domain could bind to the LD-motif in KANK (see **chapter 4**), this was a breakthrough for the understanding of LD-motifs and identifying that LD-motifs could bind to five-helix bundles in talin. This was a critical realisation, as it opens up the possibility that every talin rod domain has the potential of binding to an LD-motif. Talin has the possibility to bind numerous LD talin-binding motifs making the talin rod act as a signalling hub (Goult, Yan and Schwartz, 2018).

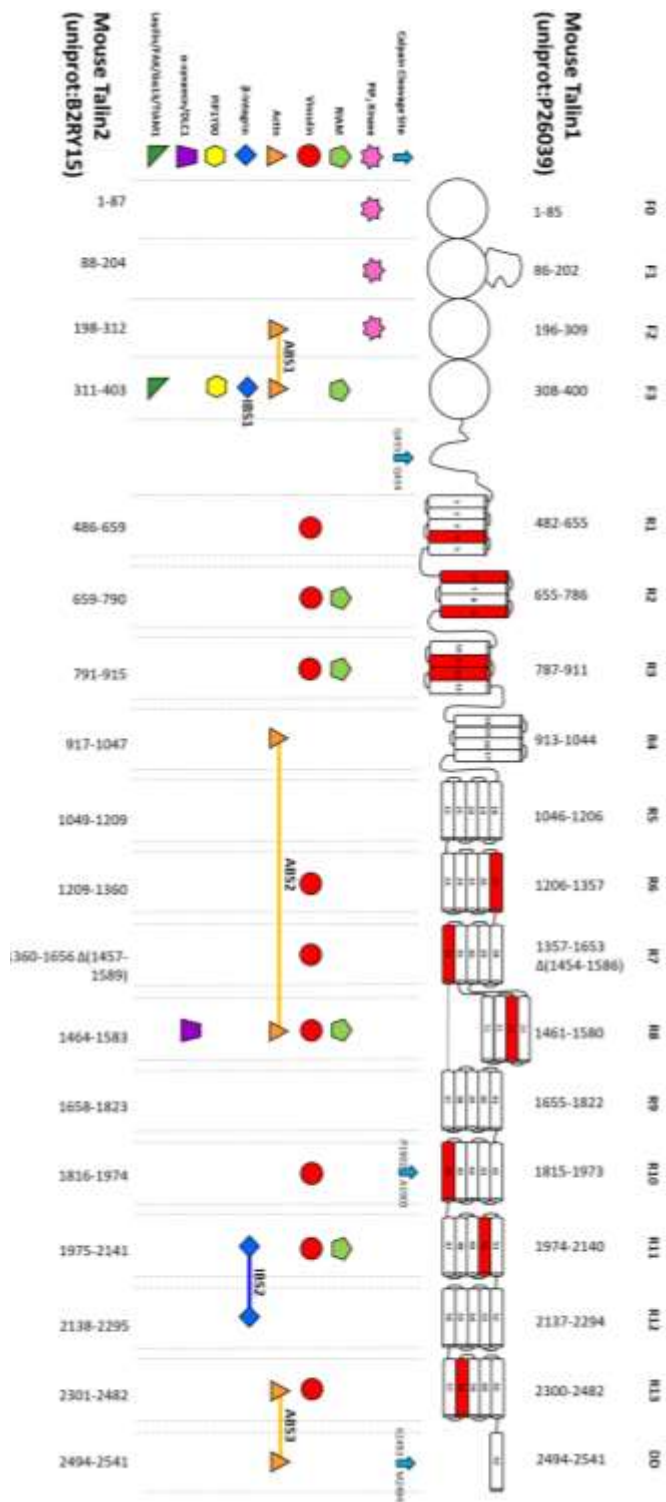


**FIGURE 2.14: DOMAIN STRUCTURE OF TALIN1 SHOWING THE LOCATION OF LIGAND BINDING SITES**

Schematic diagram of talin highlighting the domain arrangement; vinculin binding sites are highlighted in red. Talin domain boundaries for both talin1 (UniProt: P206039) and talin2 (UniPro: B2RY15) are highlighted, if these domain boundaries are used then it is possible to make any fragment of talin and delete any domain whilst maintaining the proteins structural integrity. The ligands that can bind to talin are highlighted under the corresponding talin domain.

## 2.7 Layers of talin autoinhibition and mechano-sensing properties

When describing vinculin binding to talin (**Section: 2.6.2**) it was revealed that talin had multiple layers of folding, and the vinculin binding site was only exposed on talin when talin was under force. We dubbed these multiple layers 'talins layers of autoinhibition' and they appear to be a vital feature of talin as a mechanosensor. Talin has the ability to mask binding sites at certain times allowing talin to respond to different signals within the cell.

**FIGURE 2.12A** shows a schematic representation of autoinhibited talin, here it maintains a compact globular shape and is found in the cytosol (Goksoy *et al.*, 2008; Goult *et al.*, 2009; Banno *et al.*, 2012; Song *et al.*, 2012). The autoinhibited state is achieved through interaction between the FERM F3 sub-domain and the talin rod domain R9. The process by which the interaction between these two domains is relieved and talin switches into an active confirmation is not yet fully understood. However, it would appear that a number of proteins are able to relieve talin autoinhibition including; G $\alpha$ 13 (Schiemer *et al.*, 2016), RIAM and the phospholipid, PIP2 (Goksoy *et al.*, 2008). Once in an open confirmation talin takes on more of a linear confirmation as shown in **FIGURE 2.12B**. This is crucial for the talin F3 sub-domain being able to bind to the integrin  $\beta$ -tail leading to integrin activation (Anthis *et al.*, 2009). Furthermore, the talin rod comprises 13 alpha helical bundles which when in this active confirmation all remain intact and provide binding surfaces for a number of ligands, including the LD-motif containing proteins: RIAM, DLC1 and paxillin (shown in **FIGURE 2.15**).

In the activated confirmation talin still has binding sites such as VBS that are buried and inaccessible, which ensures talin can only bind to these ligands when mechanical force is applied. Force exerted on talin causes the helical bundles to begin to unfold as shown in **FIGURE 2.15B**, this process also simultaneously destroys binding sites on the surface of helical bundles. For example, if RIAM activates talin and helps translocate it to the plasma membrane, it would then no longer be required to bind to talin and so through unfolding the talin domain is repurposed for alternative functions.

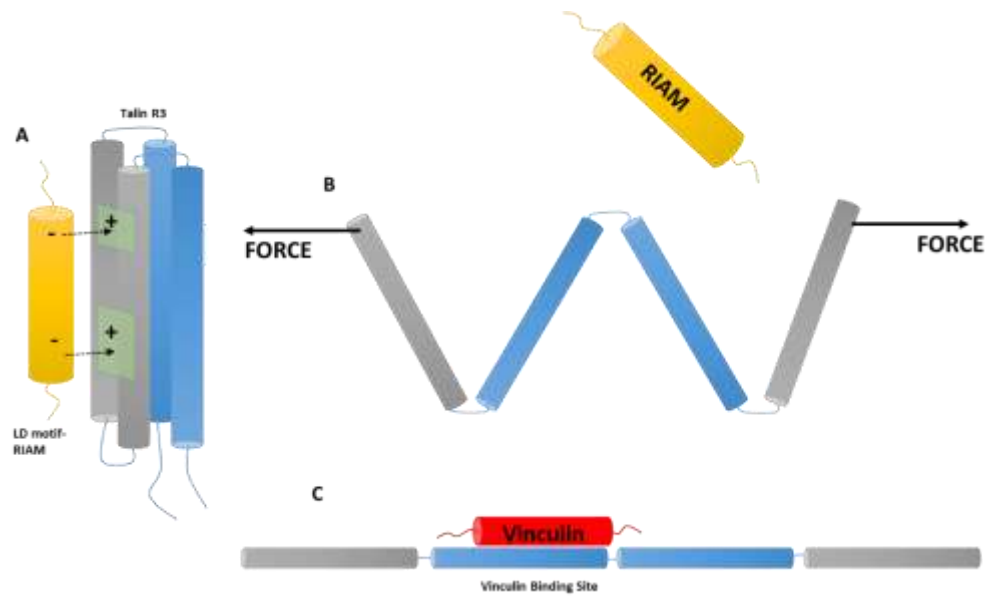


**FIGURE 2.15: DIFFERENT BINDING SITES ON TALIN REVEALED UNDER FORCE**

(A) Schematic of talin R3 folded helical domain illustrating where RIAM LD containing ligand can bind. (B) Schematic demonstrating what happens to the R3 domain when force is applied, the domain begins to unfold revealing the vinculin binding site (blue) this process destroys the RIAM binding site on R3 so it can no longer bind. (C) The talin R3 domain fully unfolded with vinculin binding site exposed allowing vinculin to bind (red).

It has been shown that all thirteen of the talin rod domains can be unravelled when mechanical force is applied (Yao *et al.*, 2016) and the structural stability of each of the helical bundles is different, resulting in some domains unfolding at lower force than others. This difference is due to talin having both four-helix and five-helix bundles; four-helix bundles have a lower stability and can unravel at lower force than five-helix bundles (Yao *et al.*, 2014; Yan *et al.*, 2015). Talin domains R2, R3, R4 and R8 are four-helix bundles and of these R3 is shown to be the 'weakest' domain in the talin rod un-folding at 5 pN (Yao *et al.*, 2014, 2016).

Force is exerted on talin when it binds to actin and the force of a single actomyosin contraction (5 pN) is enough to un-fold R3 and reveal the VBS (Yao *et al.*, 2014). When vinculin binds to talin R3 it prevents R3 from re-folding into a helical bundle; as more force is exerted on talin, further domains unfold and more vinculin binding sites become exposed. The crosslinking of talin to actin via vinculin strengthens the adhesion, allowing it to withstand greater force. Excessive forces on talin (~25 pN) can lead to vinculin being displaced (Yao *et al.*, 2014). When force is released talin helical bundles can re-fold and this ability for talin to un-fold and re-fold is critical for its role as a mechanosensor. It also allows talin to be a force buffer across the talin-integrin interactions setting a physiological force range of only a few pN across the transmission pathway (Yao *et al.*, 2016).

## 2.8 Talin in disease

Talin1 *knockout* in mice was found to be embryonically lethal (Monkley *et al.*, 2000), this implies that any severe mutations or deletions of talin would also be lethal in humans. This is evidenced by the fact that no disease-causing mutations have been identified in talin1 to date. However, talin has a prominent role to play in cell-matrix adhesions and cell migration which has led to extensive research into possible roles talin may have in cancer progression. Talin1 is located on chromosome 9 which is observed to contain numerous mutations and deletions that have led to cancerous phenotypes (Gilmore *et al.*, 1995). Several studies have revealed that talin1 is overexpressed in cancer cells and particularly in metastatic cells (Desiniotis and Kyprianou, 2011). An example of this is where talin1 has been found to be significantly upregulated in prostate cancer compared to normal prostate tissue which led to greater invasion and migration of the cancerous cells (Desiniotis and Kyprianou, 2011). This overexpression of talin1 led to increased activation of  $\beta_1$  integrin at the membrane, which was found to promote the metastatic potential in the cells. In prostate cancer it was found that phosphorylation of talin (at Ser425) was required to activate  $\beta_1$  integrin (Huang *et al.*, 2009). Using a non-phosphorylatable mutant of the Ser425 site the activation of  $\beta_1$  integrin could be blocked. Further understanding of talin at a molecular level within adhesions could enable us to target drugs for specific cancer types.

Talin1 has also been found to be at reduced levels in platelet cells, in patients suffering from myelodysplastic syndrome (MDS) (Fröbel *et al.*, 2013). MDS is a rare type of blood cancer developed through having a shortage of healthy blood cells. Talin is an integral protein in activating the  $\alpha II\beta_3$  integrin found in platelets, which enables aggregation and spreading of platelets. In patients with MDS the critical integrin  $\alpha II\beta_3$  is impaired and this is due to reduced talin expression (Fröbel *et al.*, 2013).

Diseases related to the talin2 isoform are not so well understood nonetheless, studies of talin isoforms in the heart revealed that both isoforms are tightly regulated and highly expressed in cardiomyocytes (Manso *et al.*, 2017). However, as heart cells mature talin2 becomes the predominant talin isoform and is found to localise to the costameres (see

**FIGURE 2.16**(Manso *et al.*, 2013, 2017). Costameres are part of striated muscle and are involved in the assembly of sarcomeres (Jaka *et al.*, 2015). Cardiac specific talin1 *knockout* mice do not display abnormal cardiac function (Jaka *et al.*, 2015) however, talin1 is upregulated in a failing human heart (Manso *et al.*, 2017). The mechanism that leads to talin isoform switching in the heart is still not understood but it would appear the two isoforms play distinct roles in cardiac muscle.



A mutation in talin2, S339L, was found through exon sequencing to cause a fifth-finger Camptodactyly (a medical condition that causes a permanent bend in the fifth finger) (Deng *et al.*, 2016). It seems likely to suggest that further sequencing will reveal additional talin2 mutations that are associated with disease which will shed further light on the functions of talin2.

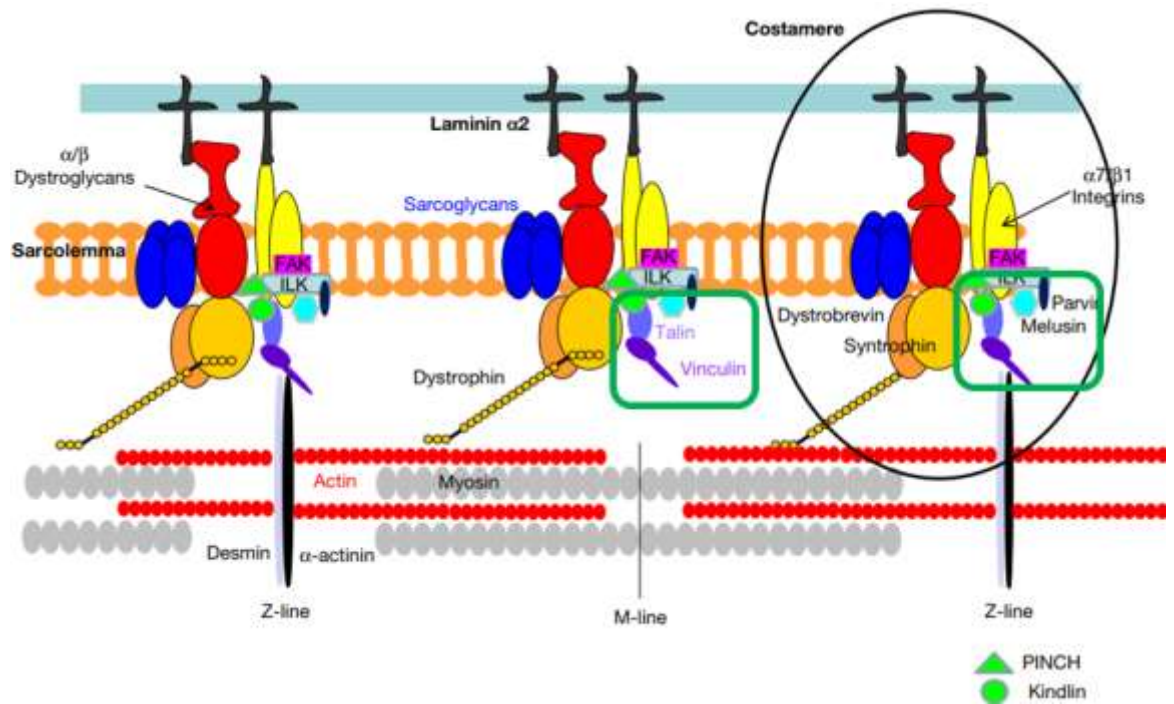


FIGURE 2.16: TALIN IN A COSTAMERE

Diagram of a costamere which assembles to form part of the striated muscle in a heart. Talin is highlighted by a green box. Figure adapted from (Jaka *et al.*, 2015).

## 2.9 Talin post-translational modifications

Proteomic studies on talin have identified many post-translational modifications and phosphorylation sites (summarised in (Gough and Goult, 2018)). Phosphorylation sites of talin 1 were mapped in platelet cells (Ratnikov *et al.*, 2005) and proteomic studies of the 'adhesome' (the network of structural and signalling proteins that assemble on integrin cytoplasmic tails) revealed further phosphorylation sites of talin (Robertson *et al.*, 2015). These sites are shown in **TABLE 1**.

Phosphorylation of adhesions protein are important for cell signalling and phosphorylation of FERM domain proteins has been found to regulate transmembrane proteins (Tsukita and Yonemura, 1999). The talin FERM domain is no exception, the three most abundant phosphorylation sites in talin1 are found in the talin FERM domain; Thr144, Thr150 and Ser446.

Thr144 and Thr150 are found in the F1-Loop; phosphorylation of these residues has been found to negatively regulate integrin activation (Ratnikov *et al.*, 2005; B. T. Goult *et al.*, 2010).

The rod domain also has multiple phosphorylation sites a number of which are shown to be Cyclin Dependent Kinase (CDK) targets. The CDK family plays a vital role in regulating the cell cycle but in literature they are not generally regarded as being involved with the regulation of cell adhesions (Robertson *et al.*, 2015). However, proteins within the adhesome are now being found to be phosphorylated by the CDK family which has led to the belief that CDKs could be regulating adhesions. Talin is also phosphorylated by CDKs including; Ser425 phosphorylation by CDK5 (Huang *et al.*, 2009) and in this thesis I describe novel CDK1 phosphorylation sites on the talin rod R7 and R8 domains (see **chapter 6**). These findings give the beginnings into understanding how adhesions are regulated and could suggest a link between the cell cycle and cell adhesions.

A further talin PTM is calpain cleavage which is non-reversible. Talin has three calpain cleavage sites as shown on **FIGURE 2.14**; one of which is located in the unstructured linker region between residues Gln433 and Gln434. Cleavage at this site results in the separation of the talin head from the rod domain which is a fundamental step in adhesion disassembly (Franco *et al.*, 2004). Expression of non-cleavable talin in cells blocks growth, adhesion maturation and mechanosensing of the protein. If the cells are rescued with talin rod fragments then these functions are rescued (Saxena *et al.*, 2017). Interestingly, cleavage of talin at Gln433-Gln434 is predominantly found in early adhesions, where adhesion turnover is very high. With adhesion turnover being regulated through the calpain cleavage of talin it would suggest that an important function of talin is in control of cell cycle progression via cleavage in early adhesions (Saxena *et al.*, 2017).

Furthermore, when calpain cleaves the linker region a recognition site for E3 ubiquitin ligase SMURF1 is revealed in the talin head (Huang *et al.*, 2009). SMURF1 binds to this site on the FERM domain and this interaction leads to ubiquitination and degradation of the talin FERM domain (Huang *et al.*, 2009). This degradation can be stopped by phosphorylation of the residue Ser425 by CDK5 which inhibits SMURF1 binding (Huang *et al.*, 2009). This complexity arising from talin PTMs hints at a complex signalling network where the cell fine-tunes talin function to regulate adhesion turnover, stability and cell cycle regulation.

Evidence of mechanical regulation of PTMs across talin is evidenced via the third calpain cleavage site located on the talin rod domain between residues Pro1902 and Ala1905 (Zhang, Saha and Kashina, 2012). This site is located within the R10 helical bundle and it is not exposed until talin is

under-force and the helical bundle unfolds. This calpain cleavage site is regulated by arginylation (Zhang, Saha and Kashina, 2012).

Most research on talin PTMs have been carried out with talin1; to determine if these sites are found in talin2, the talin1 and talin2 sequences were aligned. Then all reported talin1 PTM sites were collated and searched for in the talin2 sequence, this information is shown in **TABLE 1**. On the whole it was found that most talin1 PTM sites were found in both talin isoforms, suggesting that the isoforms are regulated in similar ways. However, the sites which differed were of interest as it could give insight onto the differences between the two talin isoforms. One 'difference' of interest is the acetylation site on talin1 R8 domain (Lys1544). This site is not found on talin2 but interestingly, it would appear that in the same region on talin2 there is a phosphorylation sequence (see **chapter 6**). This difference could be a way that the cell uses the talin isoforms to fine tune signalling. Another difference between isoforms was the glycosylation sites found on talin1 R8 and R10 domains which are not found in talin2.

Talin1 Phosphorylation site	Domain of talin1	Site Conserved in talin2	Talin1 Phosphorylation site	Domain of talin1	Site Conserved in talin2
S5	F0	YES	S729	R2	YES
Y26	F0	YES	S815	R3	YES
Y70	F0	YES	S940	R4	NO
T78	F0	NO	S979/981	R4	NO/YES
T96	F1	NO	S1021	R4	YES
T114	F1	YES	Y1116	R5	YES
Y127	F1	YES	T1142	R5	YES
S128	F1	YES	S1201	R5	NO
T144	F1	YES	S1225	R6	NO
T150	F1	YES	T1263	R6	NO
T167	F1	YES	S1323	R6	YES
T190	F1	YES	S1508	R8	NO
S311	F3	YES	S1641	R7	YES
S405	LINKER	YES	S1684	R9	YES
S425	LINKER	YES	S1849	R10	NO
S429/T430	LINKER	YES	T1855	R10	YES
Y436	LINKER	NO	S1878	R10	NO
S446	LINKER	YES	S2040	R11	NO
S455/S458	LINKER	YES	S2127	R11	YES
S467	LINKER	YES	S2338	R12	NO
S620	R1	YES	Y2530	DD	YES
S677	R2	NO	S2535	DD	NO

Talin1 PTM	Domain of talin1	Conserved in talin2	Talin2 Phosphorylation site	Domain of talin2	Site Conserved in talin1
K1544 (acetylation)	R8	YES	Y1665	R9	NO
K2031 (acetylation)	R11	YES	T1843	R10	NO
K2115 (acetylation)	R11	YES			
A1903 (arginylation)	R10	YES			
T1487 (glycosylation)	R8	NO			
T1890 (glycosylation)	R10	YES			
K2454 (methylation)	R13	YES			

**TABLE 1: POST-TRANSLATIONAL MODIFICATIONS IN TALIN ISOFORMS**

A summary table of the known post-translational modifications found in both talin1 and talin2. For each PTM the talin residue is listed along with the domain it is located and whether it is conserved in the other talin isoform. Phosphorylation sites are from (Ratnikov *et al.*, 2005; Robertson *et al.*, 2015) acetylation sites (Choudhary *et al.*, 2009), arginylation (Zhang, Saha and Kashina, 2012), glycosylation (Hagmann, Grob and Burger, 1992) and methylation (Gunawan *et al.*, 2015).

## 2.9.1 Objectives of work

Talin is a large adapter protein that provides a critical link between integrins and the actin cytoskeleton in cell-matrix adhesions. Every talin domain has been conserved over evolution giving strong evidence that each domain has a biological purpose and function. For some of these domains there are defined functions and known binding ligands however, there are still some domains in the talin rod such as talin R7 and R5 with no known role. Are these domains of relevance to talin and do they have a function within adhesions?

In my thesis I will be focussing on identifying novel binding partners to the talin rod domains and exploring the mechanism of LD-motifs binding to talin. Through identifying new talin interactors we believe this will enable a deeper understanding of talin-integrin adhesions and shine a light on how the different assemblies in the cell link together.

1. The first aim of the thesis is to characterise the interaction between talin and the adapter protein KANK by using a variety of different biochemical and biophysical techniques including: florescence polarisation, NMR and X-Ray crystallography. After identifying the individual talin domain required for the talin:KANK interaction I used nuclear magnetic resonance (NMR) to define the talin surface that KANK binds to.

After identifying the talin:KANK binding site I aim to obtain structural information of the talin:KANK interaction in order to design a series of talin point mutations that can perturb the interaction and allow us to study the role of the interaction in a cellular environment. This will enable me to further explore the talin:KANK interaction and look at how it may affect binding of other focal adhesion proteins.

2. The identification of the talin:KANK interaction taught us more about how LD-motifs bind to talin, using this information I sought to design an LD talin-binding motif that can be used to search for other talin binding partners. I designed and implemented a novel pipeline that used this motif and allowed us to identify talin binding proteins and rapidly identify the region of talin that binds the LD-motif.

3. From the LD talin-binding motif search one of the proteins identified was Cyclin Dependent Kinase 1 (CDK1). Using biochemical and biophysical techniques I was able to identify the talin binding surface and design mutants both in CDK1 and talin to perturb the interaction. Using these mutants we sought to understand the dynamics and physiological role of the interaction within a cell.
  
4. My final aim of the project was to biochemically characterise how talin binding CDK1 would affect CDK1 kinase activity. Using an *in vitro* kinase assay we determined talin R7R8 is phosphorylated by CDK1 and through phosphomimetic-mutagenesis of the phosphorylated talin residue we sought to identify the phenotype of talin phosphorylation and if it links to cell adhesions.

# Chapter 3. Materials and methods

---

## 3.1 Materials

### 3.1.1 Chemicals

All chemicals were purchased from: Fisherbrand; Sigma-Aldrich; Melford and BIO-RAD unless specified in **TABLE 2** below. All buffers were dissolved in  $d_4H_2O$  and are listed in **TABLE 3** below.

Reagent	Company
Instant Blue	Expedeon
Ammonium Sulphate $^{15}N$	Cambridge Isotope Lab
Glucose $^{13}C$	Cambridge Isotope Lab

**TABLE 2: CHEMICAL REAGENTS**

### 3.1.2 Buffers

Buffer	Components
NiNTA Buffer A	500 mM NaCl, 20 mM Imidazole and 20 mM Tris pH 8
NiNTA Buffer B	500 mM NaCl, 1 M Imidazole and 20 mM Tris pH 8
Q Buffer A	50 mM NaCl and 20 mM Tris pH 8
Q Buffer B	1 M NaCl and 20 mM Tris pH 8
S Buffer A	20 mM Phosphate Buffer pH 6.5 (1.9 g $NaH_2PO_4$ , 0.9 g $Na_2HPO_4$ ), 50 mM NaCl, 2mM DTT
S Buffer B	20 mM Phosphate Buffer pH 6.5 (1.9 g $NaH_2PO_4$ , 0.9 g $Na_2HPO_4$ ), 1 M NaCl, 2mM DTT
S Buffer A (Crystallography)	20 mM MES pH 6.5, 50 mM NaCl, 2mM DTT



S Buffer B (Crystallography)	20 mM MES pH 6.5, 1 M NaCl, 2mM DTT
NMR Buffer SolutionA	12.5 g Na <sub>2</sub> HPO <sub>4</sub> , 7.5 g KH <sub>2</sub> PO <sub>4</sub> Make to 1L
NMR Buffer SolutionB	4.0 g C <sub>6</sub> H <sub>12</sub> O <sub>6</sub> , 10.0 mL H <sub>2</sub> O, 10.0 mL BME Vitamins, 2.0 ml MgSO <sub>4</sub> (1M), 0.1 ml CaCl <sub>2</sub> (1M), 1.0 ml Antibiotic (1000x), 1.0 g <sup>15</sup> NH <sub>4</sub> Cl
NMR phosphate Buffer	50 mM NaCl, 15 mM NaH <sub>2</sub> PO <sub>4</sub> , 6 mM Na <sub>2</sub> HPO <sub>4</sub> and 2 mM DTT pH 6.5
PBS	137 mM NaCl, 2.7 mM KCl, 8 mM Na <sub>2</sub> HPO <sub>4</sub> , and 2 mM KH <sub>2</sub> PO <sub>4</sub> pH 7.4
SDS Running buffer	50 mM MOPS, 50 mM Tris Base, 0.1% SDS, 1 mM EDTA, pH 7.7
5x Sample Buffer	0.625 M Tris base, 40 % Glycerol, 10 % SDS, 10% 2 mercaptoethanol, 0.005% Bromophenol Blue
TBS	50 mM Tris-HCl, pH 7.6 ; 150 mM NaCl
TBS Tween	0.1% Tween-20, 50 mM Tris-Cl, pH 7.6 ; 150 mM NaCl
BSA in TBS	10 mM Tris-HCl, pH 7.4, and 150 mM NaCl containing 0.05% (WT/vol) Tween-20 (TBST)
Transfer Buffer	25 mM Tris, 0.01% SDS, 20% MeOH and 190 mM Glycine

**TABLE 3: BUFFER COMPOSITIONS**

### 3.1.3 Hardware and apparatus

<b>Laboratory Equipment</b>	<b>Company</b>
Advance III 600 MHz QCI cryoprobe Spectrophotometer	Bruker
5 mm Shigemi tubes	Sigma Aldrich
ÄKTA Pure	GE Healthcare
HiTrap Q HP 5 ml column	GE Healthcare
HiTrap S HP 5 ml column	GE Healthcare
HiPrep 26/10 G25 resin Desalting Column	GE Healthcare
ClarioStar Plate Reader	BMG LABTECH
black 96 well plates (Plate Reader)	Nunc
Prometheus NT.Plex	Nano Temper
7315-Spectrophotometer	Jenway
Weighing Scales	VWR
16R Megafuge Centrifuge	Thermo scientific
Microstar centrifuge	VWR
NanoPhotometer	IMPLEN
Heat block- Dry Block thermostat	Grant-Bio
pH-Meter	Mettler Toledo
Pipettes	Gilson
Gel Rocker	Grant-Bio
SDS-PAGE Gel tank	Novex
DNA tank	Gene Flow
Autoclave	Classic Prestige Medical
Incu-shake Incubator	SciQuip

**TABLE 4: LABORATORY EQUIPMENT**

### 3.1.4 Plasmids

Protein	Plasmid Vector	Description	Source
mTalin1_R1R3	pET151TOPO	Ampicillin Resistant plasmid expressing mouse talin1 rod domains R1,2,and 3.	Dr Ben Goult
mTalin1_R4R8	pET151TOPO	Ampicillin Resistant plasmid expressing mouse talin1 rod domains R4,5,6,7 and R8	Dr Ben Goult
mTalin1_R9R12	pET151TOPO	Ampicillin Resistant plasmid expressing mouse talin1 rod domains R9,10,11 and 12.	Dr Ben Goult
mTalin1_R13DD	pET151TOPO	Ampicillin Resistant plasmid expressing mouse talin1 rod domains R13 and DD	Dr Ben Goult
mTalin1_R7	pET151TOPO	Ampicillin Resistant plasmid expressing mouse talin1 rod sub domain R7	Dr Ben Goult
mTalin1_R8	pET151TOPO	Ampicillin Resistant plasmid expressing mouse talin1 rod sub domain R8	Dr Ben Goult
mTalin1_R7R8	pET151TOPO	Ampicillin Resistant plasmid expressing mouse talin1 rod domains R7 and R8	Dr Ben Goult

mTalin2_R7	pET151TOPO	Ampicillin Resistant plasmid expressing mouse talin2 rod sub domain R7	Gene Art
mTalin2_R8	pET151TOPO	Ampicillin Resistant plasmid expressing mouse talin2 rod sub domain R8	Gene Art
mTalin2_R7R8	pET151TOPO	Ampicillin Resistant plasmid expressing mouse talin2 rod domains R7 and R8	Gene Art
mTalin2_R4R8	pET151TOPO	Ampicillin Resistant plasmid expressing mouse talin2 rod domains R4,5,6,7 and R8	Gene Art
mTalin1_R7R8_S1641E	pET151TOPO	Ampicillin Resistant plasmid expressing mouse talin1 rod domains R7 and R8 with mutation S1641E.	Gene Art
mTalin1_R7R8_KKR	pET151TOPO	Ampicillin Resistant plasmid expressing mouse talin1 rod domains R7 and R8 with mutation KKR.	Gene Art
mTalin1_R7R8_G1404L	pET151TOPO	Ampicillin Resistant plasmid expressing mouse talin1 rod domains R7 and R8 with mutation G1404L.	Gene Art
mTalin1_R7R8_W1630A	pET151TOPO	Ampicillin Resistant plasmid expressing mouse talin1 rod domains R7 and	Gene Art

		R8 with mutation W1630A.	
mTalin1_R7_G1404L	pET151TOPO	Ampicillin Resistant plasmid expressing mouse talin1 rod sub domain R7 with mutation G1404L.	Gene Art
mTalin1_R7_W1630A	pET151TOPO	Ampicillin Resistant plasmid expressing mouse talin1 rod sub domain R7 with mutation W1630A.	Gene Art
mTalin1_R7R8_A1495L	pET151TOPO	Ampicillin Resistant plasmid expressing mouse talin1 rod domains R7 and R8 with mutation A1495L.	Gene Art
mTalin1_R7R8_A1495L+A1499L	pET151TOPO	Ampicillin Resistant plasmid expressing mouse talin1 rod domains R7 and R8 with mutation A1495L+A1499L.	Gene Art
mTalin1_R7_S1513+A1499L	pET151TOPO	Ampicillin Resistant plasmid expressing mouse talin1 rod domains R7 and R8 with mutation S1513+A1499L.	Gene Art
mTalin1_R7_V1540D+K1544D	pET151TOPO	Ampicillin Resistant plasmid expressing mouse talin1 rod domains R7 and R8 with mutation V1540D+K1544D.	Gene Art

**TABLE 5: PLASMIDS**

## **3.2 General microbiology techniques**

### **3.2.1 Bacteria strains used**

Throughout my work DH5 $\alpha$  competent cells were used for plasmid DNA transformation to make large quantities of DNA needed for mammalian cell transfection, DH5 $\alpha$  is a commonly used *Escherichia coli* (or *E. coli*) strain for cloning procedures (Hanahan, Jessee and Bloom, 1991). BL21 DE3 competent cells were used for protein purification.

### **3.2.2 Making competent cells**

Competent *E. coli* cells were made from a bacterial overnight starter culture made from a single colony of DH5 $\alpha$  or BL21 DE3 and inoculated into 10 mL fresh Lysogeny Broth (LB) and grown overnight at 37 °C. The overnight culture was then diluted (1:50) into LB and grown to an OD600 of 0.5-0.7.

The cells were then cooled on ice for 15 minutes and pelleted at 4 °C 850 *xg*. For each 50 mL of culture, the pellets were gently re-suspended in 25 mL of ice-cold 0.1 M CaCl<sub>2</sub> and incubated on ice for 30 min. Cells were collected again by centrifugation and re-suspended in 0.25 mL of 0.1 M CaCl<sub>2</sub>, containing 25% (v/v) glycerol. Aliquots were frozen rapidly and stored at -80 °C.

### **3.2.3 Making agar plates**

Agar plates are used as a selective growth media to grow *E.coli* colonies with the desired plasmid, based on antibiotic resistance. 10 cm Agar plates are made by autoclaving 500 mL LB-Agar and adding the desired antibiotic (Kanamycin 50  $\mu\text{g}/\mu\text{L}$  or Ampicillin 100  $\mu\text{g}/\mu\text{L}$ ) when the LB-agar has reached an approximate temperature of 40 °C. The plates are then poured under sterile conditions and left to stand until set.

### **3.2.4 Transformation**

50  $\mu\text{L}$  of DH10- $\beta$ / BL21 competent cells were thawed on ice and 2  $\mu\text{L}$  of the required plasmid DNA was added and gently mixed by inversion. The cells and plasmid were incubated on ice for 20 minutes and then heat shocked at 42 °C for 60 seconds, before being placed immediately back on ice for a further 2 minutes. 500  $\mu\text{L}$  of autoclaved LB was added to the cells and they were left to grow for 90 minutes, shaking at 200rpm at 37 °C. 100  $\mu\text{L}$  of this was then added to an agar plate

containing the appropriate antibiotic and spread using a glass spreader. Plates were left at 37 °C in an incubator overnight.

### **3.2.5 Plasmid DNA isolation from bacterial cells**

#### **3.2.5.1 Small scale isolation- mini prep**

The small-scale isolation of plasmid DNA was performed by picking a single colony from agar plate using a sterile pipette tip and adding to 10 mL of autoclaved LB media. The appropriate antibiotic is added to the culture and then it is left shaking at 200 rpm for 12-16 hours at 37 °C.

The overnight culture is pelleted at 4000 rpm for 3 minutes. The QIAprep Spin Miniprep kit (Qiagen) is used and manufacturer's instructions were followed, and the plasmid DNA was eluted into 50 µL of Elution Buffer (10mM Tris/HCl, pH 8.5) or water.

#### **3.2.5.2 Large scale isolation- midiprep**

For larger scale isolation of plasmid DNA a midiprep was performed. Initially a single colony was picked from an agar plate and added to 100 mL of autoclaved LB and left shaking at 200 rpm for 12-16 hours at 37 °C. The Midi prep kit (Qiagen) was used and manufacturer's instructions were followed; the plasmid DNA was eluted into 150 µL of buffer Elution Buffer (10mM Tris/HCl, pH 8.5) or water.

## **3.3 Protein purification methods**

### **3.3.1 Making a glycerol stock**

After transformation of BL21 competent cells with the required DNA plasmid, following the steps described in (section 3.3.4). 750 µL of the overnight culture were added to 300 µL of filter sterilised 50% Glycerol and stored at -80 °C.

### **3.3.2 Inoculating a liquid bacterial culture**

An overnight culture is made by taking a scraping of glycerol stock on a sterile pipette tip and dropped into autoclaved LB media. The appropriate antibiotic is added to the culture (Ampicillin 50 µg/mL or Kanamycin 100 µg/mL) and then it is left shaking at 200 rpm for 12-16 hours at 37 °C.

### 3.3.3 Protein expression

The overnight culture is then added to an autoclaved bevelled glass flask containing 750 ml of LB (dilution 1:200). Ampicillin is added to a concentration of 100 µg/ml. The flask is placed in a rotating incubator 200 rpm at 37 °C, the culture is grown until cell density reaches 0.7 (this is measured using spectrophotometer at OD 600). The cells are then induced with 200 µM IPTG and left overnight at 18 °C.

The cells were harvested by centrifugation at 4000 rpm for 20 minutes. The supernatant was discarded, and the pellet re-suspended in 30 mL of NiNTA buffer A. This pellet was then stored at -20 °C or used straight away.

### 3.3.4 Cell lysis by sonication

Cell pellets were defrosted on ice and sonicated using an MSE Soniprep 150 sonicator to lyse the cells and release the protein into solution. Cell pellets were placed on ice, in a 50 mL falcon tube. Sonicating cycles of 30 seconds ON and 30 seconds OFF were repeated for 4 minutes. The sample was placed into a 30 mL centrifuge tube (Oakridge) and centrifuged for 20 minutes at 20,000 rpm. The supernatant, containing the soluble protein, was retained and kept on ice.

### 3.3.5 Protein purification by immobilized metal affinity chromatography

All the talin constructs were in pET-151 vectors (see Table 3), which contained a His<sub>6</sub>-tag sequence for protein purification by affinity chromatography. The His<sub>6</sub>-tag has a high affinity for Ni<sup>2+</sup> ions, which meant the protein could be purified using either a Ni-NTA column on the ÄKTA purifier system or using Ni-NTA resin beads (Thermo Fisher) in the batch method.

#### 3.3.5.1 Batch purification

For the batch purification method 0.5 mL of beads was used for every 0.5 L of *E. coli* used in protein expression. The beads were equilibrated with 20 mL Ni-NTA buffer A, by inverting the solution 3-4 times and pelleting at 3000 rpm for 4 minutes. The supernatant was discarded and this step was repeated three times. The cell lysate from **section 3.3.4** was incubated with the beads on a roller at room temperature for 45 minutes. They were then spun down at 3000 rpm for 4 minutes and supernatant was discarded (50 µL was kept for SDS-PAGE analysis). The beads were then washed with 20 mL Ni-NTA buffer A, by inverting the tube 2-3 times before centrifuging at 3000 rpm for 4 minutes and removing the supernatant, this process was repeated 6 times. The beads were then



poured into an empty eluting column and the protein was eluted from the beads by adding 5 mL of Ni-NTA buffer B. Buffer was added 1 mL at a time and 1 mL fractions were collected and analysed using SDS-PAGE.

#### **3.3.5.2 Ni-NTA column purification**

A 5mL Ni-NTA HiTrap HP column (GE Healthcare) was used on an ÄKTA system for affinity purification of His<sub>6</sub>-tag proteins. Following column equilibration, using 6x column volumes of Ni-NTA Buffer A, at a flow rate of 5mL/min, the supernatant was loaded at a flow rate of 3 mL/min, using a peristaltic pump. Following this, 6 column volumes of Ni-NTA buffer A were loaded (also using the pump) to remove any non-specific binding proteins. An additional wash cycle was run on the ÄKTA main system; with 6 column volumes of Ni-NTA buffer A. The protein was eluted with a 30 mL linear gradient of 0-500 mM imidazole, at a flow rate of 3 mL/min and fractions were collected in a 96 well plate. The fractions with a peak at A<sub>280</sub> were collected and analysed on SDS-PAGE.

#### **3.3.6 Buffer exchange**

After affinity purification using Ni-NTA resin or columns, the protein is in a high concentration imidazole buffer. For TEV cleavage to be successful, all imidazole must be removed from the buffer (Kinsland, 2010). To buffer exchange, a G25 resin-desalting column (GE Healthcare) was used on the ÄKTA. The protein sample from the Ni-NTA purification step was loaded onto the column using a peristaltic pump at a flow rate of 3 mL/min. After this step, Q buffer A was used at a flow rate of 5 mL/min to wash the column. A<sub>280</sub> was monitored to determine when the protein fractions were eluting from the column, and these were collected in a falcon tube. The protein is then in Q buffer A and ready for TEV cleavage.

#### **3.3.7 TEV cleavage**

Purified TEV was added to the protein sample, to a final concentration of 2 mg/mL and incubated on a roller at room temperature overnight. A sample was taken before addition of TEV to run on an SDS PAGE gel.

#### **3.3.8 Ion exchange chromatography**

Ion exchange chromatography separates proteins based on differences in charge; there are two choices of columns for ion exchange - anion exchange column (Q column) or a cation exchange

column (S column). The column was selected, based on the Isoelectric Point (pI) of the protein of interest. The pI is the pH at which the net charge of the protein is zero, all proteins are made up from different combinations of amino acids which gives different proteins different net surface charges. The pI was determined using ExPASy's ProtParam (Gasteiger *et al.*, no date). For proteins with a pI above 7 an S column was used and for proteins with a pI below 7 a Q column was used.

The protein sample with added TEV was spun down at 4000 rpm and the supernatant was decanted into a falcon tube. This was loaded onto either a 5 mL HiTrap HP Q column (GE healthcare) or 5 mL HiTrap HP S column (GE healthcare) using a peristaltic pump at a flow rate of 3 mL/min. Six column volumes of Q/S buffer A were loaded through the pump to remove any non-specific bound proteins. An additional wash cycle was run from the ÄKTA main system, with 6 column volumes of Q/S Buffer A, followed by a 30 mL linear gradient of 0-1 M NaCl for protein elution. All fractions displaying peaks at  $A_{280}$  were collected in a 96 well plate analysed on SDS-PAGE.

### **3.3.9 Protein concentration estimation**

Purified protein samples concentration was quantified using a NanoPhotometer N60/N50 (Implen). The proteins molecular weight and extinction coefficient were calculated using ProtParam. The protein concentration was calculated in mg/mL according to Beer-Lamberts Law.

### **3.3.10 SDS-PAGE gels**

Samples for SDS-PAGE analysis were boiled with 5x sample Buffer at 95 °C for 5 minutes.

Typically, gels were made in gel cassettes (Novex) with a 12 % separating component and a 4 % stacking component. Buffers can be seen in

**TABLE 6.** SDS PAGE gels were run in SDS running buffer at 200V.

Separating Gel - 12%		Stacking Gel - 4%	
40 % Acrylamide	7.5 mL	40 % Acrylamide	1.25 mL
Separating Gel Buffer (1 M Tris-HCL pH 8.8)	9.4 mL	Stacking Gel Buffer (0.375 M Tris-HCL pH 6.8)	4.2 mL
10% SDS	250 µL	10% SDS	125 µL
50% Sucrose	4 mL	Water	6 mL
Water	3.3 mL	TEMED	5 µL
TEMED	6.25 µL	Ammonium Persulphate	1 mL
Ammonium Persulphate	625 µL		

TABLE 6: GEL CONTENTS

## 3.4 Biochemical methods

### 3.4.1 Differential scanning fluorimetry

Nano differential scanning Fluorimetry (nanoDSF) is a technique used to determine protein stability by looking for changes in intrinsic fluorescence from aromatic amino acid residues. The nanoDSF measurements were done with Prometheus NT.48 (NanoTemper Technologies GmbH, Munich, Germany). The Prometheus machine measures protein folding and thermal stability of proteins using a low sample volume capillary system and a dye free approach (Senisterra, Chau and Vedadi, 2012; Muca *et al.*, 2017).

Purified proteins were tested in a range of buffers and at varied concentrations. A Monolith NT.115 standard capillary tube (NanoTemper) was used to pick up 2-3 µL of sample and was placed in the loading tray. A starting temperature was set at 15°C and measurements were taken at 2 °C/minute with fluorescent readings at 350 and 330 nm wavelengths. The ratio of fluorescence 350nm/330nm was used to plot a curve, over the scanning temperatures of the instrument. For

analysis and calculation of the protein's melting point, the first derivative maxima or minima were taken and an 8th order polynomial fit was calculated for the transition region. Next, the first derivative of the fit was formed and the peak position (at  $T_m$ ) was determined. (Martin, Schwarz and Breitsprecher, 2014).

### 3.4.2 Fluorescence polarisation

Fluorescence polarization is a method in which the binding interaction between two molecules can be measured and the binding constant determined. It works on the principle that there is a size difference between the two molecules being measured. The smaller molecule is coupled to a fluorophore that can be excited by polarised light (light waves that only travel in a single direction) and will also then emit polarised light. However, if this small molecule is tumbling quickly in solution it will 'scramble' the polarised light and emit light in all directions. If this small fluorescent molecule binds to a target molecule the tumbling rate will decrease and the amount of polarised light will increase, shown in **FIGURE 3.1**. This change in polarised light is measured and can be plotted to determine a binding constant.

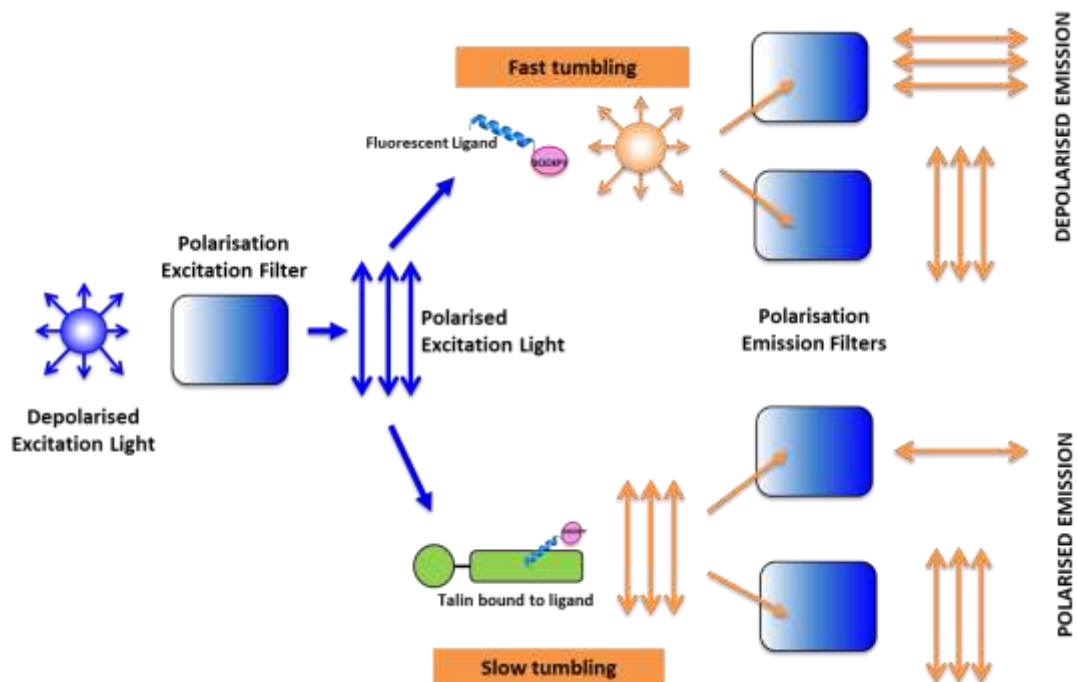


**FIGURE 3.1: FLURESCENCE POLARISATION**

Fluorescence polarisation is a method in which the binding interaction between two molecules can be measured and the binding constant determined. Diagram shows how a small fluorescent ligand not bound to anything will tumble quickly and scramble the polarisation of light by emitting at a different direction from the incident light.

### 3.4.2.1 Coupling peptides

Synthetic peptides (shown in the **TABLE 7** below) were ordered with an additional N-terminal or C-terminal Cys, which allowed coupling to a fluorescent tag; BODIPY-TMR (ThermoFisher Scientific) or fluorescein (ThermoFisher Scientific). The Cys residue forms a di-sulphide bond with the fluorescent tag allowing a signal for the peptide to be measured on the plate reader. The peptides were coupled to the dye using: 100 µM peptide, 25 µL dye (fluorescein or BODIPY-TMR), 0.005 M TCEP (1 M stock), 0.05% (v/v) Triton X-100. The coupling was performed at room temperature, in the dark, with stirring for 2 hours.

To remove the excess of uncoupled dye from the reaction, a PD-10 column (GE Healthcare) was used. 1.5 mL of peptide mix was loaded onto the column and allowed to flow through, before adding 2.5 mL of PBS and collecting the flow through. The coloured fractions were kept and stored in the dark at -80 °C.

### 3.4.2.2 Fluorescence polarisation assay

The assay uses a 1 mM stock solution of fluorescently labelled peptide and dilutes it to 1 µM in PBS. 100 µL of 1µM peptide is pipetted into the first 11 wells of a black 96 well plate (Nunc). 100 µL of the protein of interest (PBS buffer) is added to well 11, along with 1 µL of 1 mM stock solution of the labelled peptide. The well solution is mixed up and down twice with a pipette and 100 µL of solution removed from well 11 and pipetted into well 10. The serial dilution was continued all the way down the plate until well 2; where the extra 100 µL was discarded. The plate is then placed into the plate reader (BMG LABTECH, CLARIOstar) at room temperature and the settings were adjusted according to the fluorescence tag used.

### 3.4.2.3 Calculating $K_D$ from binding curves

In order to determine the binding constant  $K_D$  the fluorescence polarisation data is entered into GraphPad Prism v7.00 software and data is fitted to the non-linear binding equation 'one site total binding' shown in **EQUATION 1**.

$$Y = \frac{Bmax * X}{KD + X} + NS * X + Background$$

#### **EQUATION 1: ONE SITE BINDING EQUATION FOR FLUORESCENCE POLARISATION**

Equation used to determine binding constant  $K_D$ . Here Y represents the protein concentration and X represents the ligand concentration. NS is the slope of nonspecific binding in Y units divided by X units and

Background is the amount of nonspecific binding with no added ligand. The binding constant is defined as the amount of ligand needed to achieve half-maximum binding at equilibrium; the  $K_D$  unit is the same as X.

Peptide	Sequence	Supplier
KANK1 (30-68)	PYFVETPYGFQLDLDFVKYVDDIQKGNTIKKLNQKRRKC	Biomatik
KANK1 (30-60)	PYFVETPYGFQLDLDFVKYVDDIQKGNTIKKC	Biomatik
KANK1_4A (30-68)	PYFVETPYGFQAAAAFVKYVDDIQKGNTIKKLNQKRRKC	Biomatik
KANK2 (31-61)	PYSVETPYGYRLDLDFLKYVDDIEKGHTLRRC	Biomatik
KANK3 (32-62)	PYSVETPYGFHLDLDFLKYVEEIERGPASRRC	Biomatik
KANK4 (24-54)	PYSVETPYGFHLDLDFLKYVDDIEKGHTIKRC	Biomatik
KANK_L43A (30-60)	PYFVETPYGFQLDADFVKYVDDIQKGNTIKKC	Biomatik
CDK1 (283-297)	CNHPYFNDLDNQIKKM	GL Biochem
CDK1 (206-223)	GDSEIDQLFRIFRALGTPC	GL Biochem
CDK1 (206-232)	GDSEIDQLFRIFRALGTP	GL Biochem
CDK1_2A (206-223)	GDSEAAQLFRIFRALGTPC	GL Biochem
CDK1_4A (206-223)	GDSEAAAAFRIFRALGTP	GL Biochem
CDK1_EA FitC (206-223)	<i>FITC</i> -GDSAIDQLFRIFRALGTP	GL Biochem
CDK1_EP FitC (206-223)	<i>FITC</i> -GDSPIDQLFRIFRALGTP	GL Biochem
CDK1 FitC (206-223)	<i>FITC</i> -GDSEIDQLFRIFRALGTP	GL Biochem
HSF2 (519-535)	CLCELAPAPLDSMPLLD	GL Biochem
HSF2 (280-305)	QYPDIVIVEDDNEDEYAPVIQSGEQNC	GL Biochem
SEPTIN2 (159-174)	CGLKPLDVAFMKAIHMK	GL Biochem
DLC1 (465-489)	IFPELDDILYHVKGMRIVNQWSEKC	GL Biochem
RIAM (4-30)	SEDIDQMFSTLLGEMDLLTQSLGVDTC	GL Biochem

**TABLE 7: PEPTIDE SEQUENCES**

### 3.4.3 Nuclear magnetic resonance- NMR

#### 3.4.3.1 Inoculating a liquid bacterial culture in <sup>15</sup>N media

Talin constructs were transformed into BL21 cell as described in **section 3.2.4** and grown in a 10 mL overnight of minimal media solution (10 mL SolutionA and 270  $\mu$ L SolutionB), for 18 hours at 200 rpm, 37 °C. SolutionB could be adjusted according to the sample-label needed for the experiment; for all samples used here <sup>15</sup>N Ammonium Sulphate was added to SolutionB. The overnight solution (1:100) was added to 500 mL flasks of autoclaved NMR SolutionA and 30 mL SolutionB filter-sterilised through a 0.2  $\mu$ M Millex filter (MerckMillipore). Flasks were incubated with shaking at 37 °C, until an OD 600 density of 0.5 was reached, 0.4 mM of IPTG was added to the flask and the temperature changed to 18°C and the flasks were left shaking overnight. The rest of the purification process is the same as described in **section 3.3**.

#### 3.4.3.2 Buffer exchange

Purified protein must be buffer exchanged into NMR buffer, so that the pH and salt concentration is the same for all samples and the data can be effectively compared. Buffer exchange was carried out using a PD-10 column (GE Healthcare) following manufacturer's instructions.

#### 3.4.3.3 1D NMR experiments

All NMR experiments were performed on a Bruker Avance III 600 MHz NMR spectrometer equipped with QCI-P CryoProbe. Purified <sup>15</sup>N labelled protein with 5% D<sub>2</sub>O added was used for all experiments in a Shigemi tube (Sigma-Aldrich) final sample volume 450  $\mu$ L and carried out at a temperature of 298 °K.

1D spectra allowed us to assess if the water suppression was sufficient for the 2D experiment and to determine if the protein sample looked an adequate concentration for the experiments. It also allowed us to determine that the added ligand was present in titrations. However, 1D spectra signals are highly overlapped making direct interpretation of data challenging. Instead analyse an additional dimension (<sup>15</sup>N) is introduced and this is measured in a 2D experiment.

#### 3.4.3.4 2D HSQC experiments

The 2D experiment that was most used was heteronuclear single quantum correlation (HSQC) experiment (Mori *et al.*, 1995). The HSQC (and TROSY) experiment makes use of the fact that every amino acid (apart from proline) has a proton attached to the peptide bond. The experiments

provide a correlation between the proton and the nitrogen atoms that are visualised as a peak in the spectrum; meaning every peak corresponds to an amino acid in the protein sequence. A HSQC does also show the aromatic H<sup>N</sup> protons of Trp and His residues (which are shown as a second peak for that residue as well as the amide peak).

To run a HSQC the sample from **section 3.4.3.3** was kept in the spectrometer at 295K and then a 2D <sup>15</sup>N, <sup>1</sup>H (HSQC) experiment was carried out. Spectra were acquired using a HSQC pulse sequence at 600 MHz; data were acquired with 1024 points in the 1 H dimension over a sweep width of 10 484 Hz and 124 increments in the indirect <sup>15</sup>N dimension over a sweep width of 4600 Hz.

#### 3.4.3.5 2D TROSY experiments

For larger proteins such as the talin1 R7R8 domain (32 kDa) a transverse relaxation optimised spectroscopy (TROSY) experiment was used (Pervushin, Wider and Wüthrich, 1998). TROSY is collected in a similar way to a <sup>1</sup>H<sup>15</sup>N HSQC experiment although; TROSY gives an increased resolution and better sensitivity for larger proteins compared to a HSQC experiment. This increase in resolution is acquired due to the relaxation rates of non-decoupled HN multiplets in a HSQC experiment. **FIGURE 3.2A** shows a peak multiplet (multiplet is what a peak representing a single chemical shift turns into when it is coupled to other nuclei) for both a large protein and a small protein in a coupled HSQC experiment. The small protein (15 kDa) can be seen as four sharp signals whereas the larger protein (30 kDa) is shown as: one sharp peak which is dubbed the TROSY peak, two broadened “semi-TROSY” peaks and a broad peak named the anti-TROSY peak.

The TROSY experiment works by only detecting the sharp TROSY peak and avoids mixing of all four signals (as done in a HSQC experiment). This allows for a sharper peak and better peak dispersion in experiments. **FIGURE 3.2A** demonstrates how there is no benefit to using a TROSY experiment on smaller proteins due to no increase in signal furthermore, hence where possible a HSQC experiment was used. HSQC and TROSY spectrum can be compared and spectra can be overlaid, it is just important to remember there is a slight shift offset with TROSY experiments equivalent to  $\frac{1}{2} J_{HN}$  in both <sup>15</sup>N and <sup>1</sup>H dimension as can be seen in **FIGURE 3.2B** which needs to be corrected for before comparison. <sup>15</sup>N, <sup>1</sup>H (TROSY) spectra were acquired with a sensitivity enhanced sequence using an echo anti echo for phase discrimination and Watergate for water suppression.

#### 3.4.3.6 Spectra analysis

Spectra were displayed and analysed in CcpNmr analysis version 2.5.2 (Vranken *et al.*, 2005; Skinner *et al.*, 2015). Protein assignments could be read directly into CCPN from the Biological



Magnetic Resonance Bank (BMRB) allowing the identity of each peak to be determined and assigned a residue from the talin sequence. In titration experiments each spectrum was assigned and this allowed for peak comparison between the talin spectrum and the titrations with ligand added. Shift distances were measured between talin peak and titration peak using the weighted combination of  $^1\text{H}$  and  $^{15}\text{N}$  amide secondary shifts  $(\Delta(\text{H},\text{N})) \cdot \Delta(\text{H},\text{N})$ . Secondary shifts are determined whereby,  $W_{\text{H}}$  and  $W_{\text{N}}$  are weighting factors for the  $^1\text{H}$  and  $^{15}\text{N}$  amide shifts ( $W_{\text{H}} = 0.15$  and  $W_{\text{N}} = 1$ ) (Ayed *et al.*, 2001; Goult *et al.*, 2009).

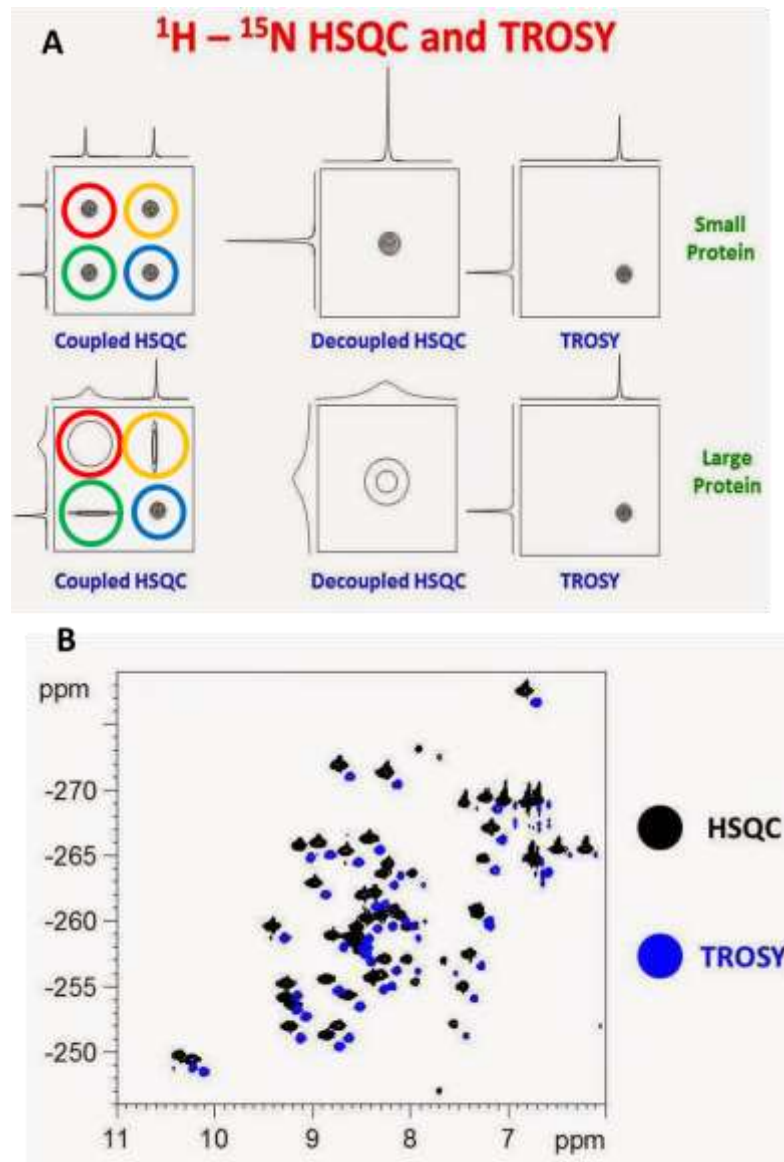


**FIGURE 3.2: DIFFERENCES IN TROSY AND HSQC EXPERIMENTS**

(A) Peak multiplet for both a large protein and a small protein in a coupled HSQC experiment. Blue circle indicates TROSY peak, yellow and green identify semi-TROSY peaks and red identifies the broad peak named the anti-TROSY peak. (B) A  $^1\text{H}^{15}\text{N}$  HSQC (black) and  $^1\text{H}^{15}\text{N}$  TROSY experiment (blue) indicating spectrum shift differences of  $\frac{1}{2} J_{\text{HN}}$  in both  $^{15}\text{N}$  and  $^1\text{H}$  direction. Figure adapted from: (Facey, 2015)

### 3.4.4 X-Ray crystallography

#### 3.4.4.1 Crystallisation by hanging drop method

Crystals were obtained by using the hanging drop vapour diffusion technique at 21 °C. Crystallisation screens: Hampton crystal screen 2 (Hampton), JCSG (Molecular Dimensions), Wizard (Molecular Dimensions) and Pact (Molecular Dimensions) were used and 100 µL of each condition was transferred into a 96 well plate (Hampton Research). A Mosquito (TTP Labtech) robot was used to produce a 1:1 protein: well solution drop, which was then placed over the 96 well plates. Varying concentrations of protein were tried along with differing buffering conditions, furthermore peptide: protein ratio was also varied in order to facilitate crystal growth.

If crystals were obtained from a screening condition further optimisation was carried out. Optimisation was used to increase the size of crystals and improve their quality in order to maximise diffraction quality. Optimisation was carried out in a 24 well plate (Hampton Research) and 500 µL of well solution was used. In the 24 well plates differing the precipitant concentration and the pH across the 24 well plates further optimised the original screening condition.

On successful growth of crystals they were harvested using a loop with a cryo-protectant (cryo-protectants contained the well solution with additional 20% glycerol) and frozen in liquid nitrogen. Diffraction dataset was collected at 100 K on beamline I03 at Diamond Light Source (Didcot, UK) using a Pilatus3 6M detector (Dectris, Baden, Switzerland). To solve the talin:CDK1 and talin:KANK structures the talin1 R7R8 in complex with DLC1 (PDB ID: 5FZT) was used as a template for molecular replacement. Molecular replacement was carried out using PHASER (McCoy *et al.*, 2007) and then manual model adjustment and refinement were performed with COOT (Emsley *et al.*, no date) and REFMAC (Murshudov, Vagin and Dodson, 1997) respectively.

#### 3.4.5 Actin co-sedimentation assay

Proteins to be used in the actin co-sedimentation assay were expressed and purified as described in **section 3.3**. Purified F-Actin was used for experiments and for this G-Actin was purified from Rabbit skeletal muscle and polymerised to F-actin in 10 mM Tris, 50 mM NaCl, 100 µM ATP, 1 mM DTT, 1 mM MgCl<sub>2</sub>, pH 7.0. The co-sedimentation assays were performed using 20-µM talin R4-R8 (residues 913-1653), 60 µM KANK 30-60 peptide and 20 µM F-actin. Samples were incubated at room temperature for 60 minutes and then centrifuged in an ultracentrifuge (Beckman Optima) for 20 minutes at 100,000 rpm at 4 °C. The supernatant was removed and mixed at a 1:1 ratio with

2-mercaptoethanol loading buffer and boiled at 95 °C for 10 minutes. The Pellet was mixed with co-sed buffer (10 mM Tris, 50 mM NaCl, 1 mM DTT, 1 mM MgCl<sub>2</sub>, pH 7.0) and 2-mercaptoethanol loading buffer in a 1:1:1 ratio and boiled at 95 °C for 10 minutes. The supernatant and pellet samples were analysed on 8-12% gradient SDS-PAGE gels and stained using InstantBlue (Expedon).

Image-J software (Rueden *et al.*, 2017) was used to analyse SDS-PAGE gels and quantify the band density of the talin R4-R8 band to determine the percentage of talin in the pellet and the supernatant.

### **3.4.6 *In vitro* kinase assay**

An *in vitro* Kinase assay was used to quantify the amount of phosphorylation of different purified recombinant protein constructs by CDK1 and cyclins: A1 and B1. Purified recombinant GST-tagged CyclinA2-CDK1 and His<sub>6</sub>-tagged CyclinB1-CDK1 were purchased from Invitrogen and stored in 20 mM Tris, pH 7.5, 150 mM NaCl, 0.5 mM EDTA, 0.01% (v/v) Triton X-100, 2 mM DTT, 20% (v/v) glycerol.

30 ng of each protein was mixed with 0.1 µg of substrate (talín/FMNL2) and incubated in 50 mM HEPES (pH 7.4), 150 mM NaCl, 5 mM EDTA, 5 mM DTT, 25 mM MgCl<sub>2</sub>, 0.02% Triton X-100 and 1 mM ATP at 30 °C (shaking 100 rpm) for 20min. The reaction was stopped by adding 10 µL of 5x SDS sample buffer and boiled at 95 °C for 10 minutes. A gradient SDS-PAGE 4-12% Bis-Tris gel (Thermo Fisher Scientific) was loaded with the entire sample and ran at 200 V for 45 minutes in 1x SDS running buffer (NuPAGE). When finished the gel was placed in transfer buffer (see table of buffers).

#### **3.4.6.1 *In vitro* kinase analysis**

Western blotting is a technique used to isolate and identify proteins resolved by SDS-PAGE. Protein bands from the SDS-PAGE gel are transferred to a Polyvinylidene difluoride (PVDF) membrane (Immobilon P, Millipore Inc.) before being probed with a primary antibody (selected for the protein of interest) and detected with a secondary antibody, raised against the primary and labelled with a fluorescent tag.

The protein from the *in vitro* kinase assay SDS-PAGE gels were transferred to a PVDF membrane using a wet transfer. After transfer the membrane was washed with 1x PBS buffer (see buffer table) before being incubated with blocking buffer (5% (m/v) BSA TBS Tween) for 30 minutes at room temperature rocking. After blocking, the membrane was washed with TBS tween and incubated

with 1 µg/µL primary antibody. The primary antibody was prepared in 1.5 mL 5% (m/v) BSA in TBS tween and added to the membrane in a sealed plastic wallet and left rocking overnight at 4 °C.

The membrane was then washed thrice with 30 mL TBS tween (10 minutes each wash) before incubating with the secondary antibody. The secondary antibody was prepared in 10 mL of blocking buffer (5% (m/v) BSA TBS Tween) and added to the membrane for 45 minutes in the dark to avoid any photo bleaching. After incubation, the membrane was washed twice with TBS Tween and scanned using the Odyssey infrared imaging system (LI-COR Biosciences), and band intensities were analysed by using Odyssey software (LI-COR Biosciences). All antibodies used in these experiments are listed in **TABLE 8** below:

Primary Antibody	Supplier	Secondary Antibody	Supplier
Anti- MPM2 (1:1000)	Millipore	Mouse 800 (1:10,000)	Cell Signalling Technology
Anti- CDK1 (1:1000)	Cell Signalling Technology	Mouse 800 (1:10,000)	Cell Signalling Technology
Anti-HIS (1:500)	Cell Signalling Technology	Rabbit 600 (1:10,000)	Thermo Fisher Scientific
Anti-GST (1:500)	Cell Signalling Technology	Mouse 800 (1:10,000)	Cell Signalling Technology

**TABLE 8: PRIMARY AND SECONDARY ANTIBODIES**

### **3.4.7 Identification of talin phosphorylation sites by mass spectrometry**

Phosphorylation sites of talin1 R7R8 and talin2 R7R8 were determined using Mass spectrometry. The *in vitro* kinase assay (see **section: 3.4.6**) was carried out with the substrates talin1 R7R8, talin2 R7R8 and CDK1-cyclinA2. Reaction was left for 45 minutes at 30 °C and stopped by adding 10 µL 5x SDS sample buffer and boiling for 10 minutes at 95 °C.

All samples were loaded onto an SDS PAGE 4-12% Bis-Tris gel (Thermo Fisher Scientific) and separated by running at 200 V for 60 minutes. Gels were stained with Instant-Blue (Expedeon) for 15 minutes, and washed in water overnight at 4°C. The talin R7R8 bands were cut from the gel and processed by in-gel tryptic digest. Peptides were analysed by LC-MS/MS by using an UltiMate 3000 Rapid Separation LC (Dionex Corporation) coupled to an Orbitrap Elite MS (Thermo Fisher

Scientific). Peptides were separated on a bridged ethyl hybrid C18 analytical column (250 mm × 75 µm internal diameter, 1.7-µm particle size; Waters) over a 45-min gradient from 8 to 33% v/v acetonitrile in 0.1% v/v formic acid. LC-MS/MS analyses were operated in data-dependent mode to automatically select peptides for fragmentation by collision-induced dissociation. For phosphoproteomic analyses, multistage activation was enabled to fragment product ions resulting from neutral loss of phosphoric acid. Quantification was performed using Progenesis LC-MS/MS software.

### **3.4.8 Cell culture techniques**

#### **3.4.8.1 Media and cell culture**

The growth medium used for HEK-293T cells was DMEM (Dulbecco's Modified Eagles Medium) with L-Glutamine, glucose, Pyridoxine-HCl, NaHCO<sub>3</sub> (PAA-GE Healthcare) supplemented with 10% of FBS (Biosera) and 50 µg/mL gentamicin (Life Technologies-Invitrogen). All cells were maintained at 37°C and 5% CO<sub>2</sub>.

#### **3.4.8.2 Trypsinization and cell splitting**

For my studies I required the cells to grow as an adherent monolayer and required passaging when they were 70-80% confluent. To re-suspend cells or split cell flasks, the cells needed to be removed from their adherent surface. This was achieved using Trypsin-EDTA (Sigma-Aldrich). To trypsinise, all media was removed from the cells and the surface was gently washed with 1X PBS. Trypsin-EDTA (sigma) was added to the cells and incubated at 37 °C for 5 minutes. Cells were removed and added to 20 mL pre-warmed media. The cells were counted, and the cell suspension was then centrifuged at 2000 rpm for 5 minutes. The supernatant was carefully aspirated and the cell in the pellet re-suspended in fresh media.

#### **3.4.8.3 Cell transfections**

Lenti-X HEK293T cells (Takara Bio Inc.) were used for all experimental assays. The cells were transfected with the DNA constructs seen in table 2. To transfect the plasmid DNA into the HEK 293T cells, 5 µg of DNA pre-incubated in 500 µL of Opti-MEM (Sigma-Aldrich) was mixed to 500 µL of optimum pre-incubated with 25 µL lipofectamine 2000 (Sigma-Aldrich). After 20 minutes of incubation, the mixture was drop-pipetted over the seeded cells in a 10 cm plate or 2x3 well plate. The cells were then incubated for 24 hours at 37 °C before being visualised under a microscope.

# **Chapter 4. Identifying and characterising the interaction between talin and KANK**

---

## 4.1 Introduction

The mechanism that targets microtubule (MT) plus-ends to grow towards focal adhesions (FA) at the cell cortex has been a long-standing question. Here I look to find the missing link between these two macromolecular assemblies and characterise the interaction that can regulate adhesion turnover and stabilise MTs in their vicinity.

### 4.1.1 Microtubules

Microtubules form an integral part of the cell cytoskeleton and help to influence cell shape and cell polarity. MTs are comprised of long protofilaments that assemble together to form hollow tubes (of approximately 25 nm in diameter) (shown in **FIGURE 4.1A**). Protofilaments are made from two globular proteins:  $\alpha$ -tubulin and  $\beta$ -tubulin, which form dimers and polymerise by arranging themselves in a head-to-tail fashion. This assembly results in one end of the MT being exposed with  $\beta$ -tubulin and one end exposed with  $\alpha$ -tubulin. Due to this, MTs have polarity, an attribute that is critical for their function (Cooper, 2000). The  $\alpha$ -tubulin subunits provide a slow growing 'minus-end' and the  $\beta$ -tubulin provides a fast growing 'plus-end'. Although growth can occur at either end of the MT, it is significantly more rapid at the plus-end (Cooper, 2000).  $\beta$ -Tubulin binds GTP, which stimulates polymerisation of the MT protofilament plus-end resulting in growth. MTs are highly dynamic and are susceptible to catastrophe, whereby the filament breaks down. MTs growth/ catastrophe rate is influenced by the rate of which GTP hydrolysis occurs; GTP at the plus-end forms a GTP cap allowing for growth and protects the MT from catastrophe. However, GTP can be hydrolysed to GDP, which prevents the tubulin subunits from binding tightly to the polymer and allows them to break away causing catastrophe shown in **FIGURE 4.1B** and loss of the GTP cap.

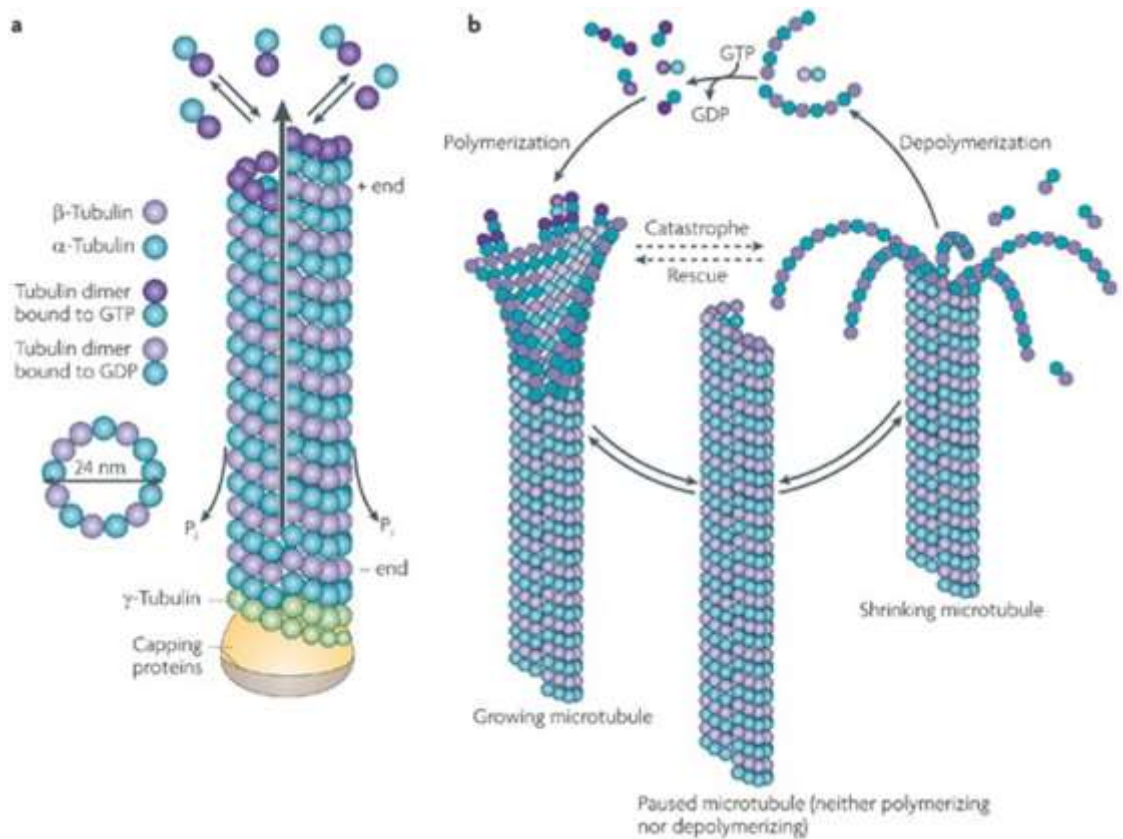


**FIGURE 4.1: THE STRUCTURE OF MICROTUBULES AND THE CYCLE OF GROWING AND SHRINKING**

(A) Schematic diagram showing the composition of a microtubule;  $\alpha$ -tubulin (purple) and  $\beta$ -tubulin (blue). (B) The cycle of growing MT and shrinking MT through GTP hydrolysis. Figure from (Rochlin, Dailey and Bridgman, 1999).

#### **4.1.2 Microtubules are found to localise to focal adhesions and assist in adhesion turnover**

MTs play a role in cells both during mitosis and interphase. During mitosis, MTs completely reorganise to form the mitotic spindle, which allows the cell to divide into two daughter cells (Cooper *et al.*, 2000). Alternatively, during interphase MTs direct their growth towards the cell periphery via their dynamic plus-end (Howard and Hyman, 2003). A process that from very early on has been recognised as a requirement for directional migration of cells (Vasiliev *et al.*, 1970). These dramatic changes in MT organisation highlight the dynamic instability of these structures and the importance this has on cell growth and division.

In the late 1980s it was found that, in migrating cells, MTs localise near FAs (Rinnerthaler, Geiger and Small, 1988). This interaction did not appear to happen by chance, but, instead was a targeted phenomenon whereby MTs would change their growing direction in order to make connection with FAs (Rinnerthaler, Geiger and Small, 1988). This cross-talk between FAs and MTs is important,

61



as it directs MT growth and enables MTs to exert their influence on cell shape and polarity in a migrating cell (van der Vaart *et al.*, 2013). Furthermore, the targeting of MTs to FAs encourage FA turnover which is critical for a cell to move forward during migration (Stehbens and Wittmann, 2012). Since the first identification of a link between MTs and FA turnover, researchers have been trying to identify the mechanism that targets MTs to FAs to understand what controls directional cell growth and migration in a spatially and temporally controlled migrating cell.

The molecular mechanisms involved in adhesion disassembly are thought to be complex due to the number of proteins involved. Because of the multifaceted interaction of proteins, it seems highly unlikely that adhesion disassembly occurs in reverse motion to that of adhesion assembly (Ezratty *et al.*, 2005). Which then questions- what does control adhesion disassembly and what are the key FA players in regulating disassembly? When looking at cell-matrix interactions, two key players activate  $\beta$  integrin- talin and kindlin. These proteins could both make a good converging point for adhesion disassembly and as such MTs could be targeting FAs via one of these proteins.

Microtubules not only regulate FA turnover but also control FA dynamics through the regulation of endocytosis. Endocytosis is the process in which the cell can traffic cargo into the cytoplasm via vesicular transport. One way in which adhesions utilise this process is in integrin recycling. Integrin recycling transports integrins from the back of the cell (cell rear end) and recycles them to the front of the cell (leading edge) (Caswell *et al.*, 2008; Bridgewater, Norman and Caswell, 2012). This process occurs through clathrin-mediated endocytosis and uses rab-labelled endocytic compartments (Ezratty *et al.*, 2009). Clathrin-mediated endocytosis selects its cargo through the use of adapter protein-2 (AP2), this protein coats the cargo and allows a clathrin cage to assemble around it. Dynamin is a GTPase protein that coats around the neck of the clathrin coated pit and when hydrolysed causes a change in confirmation constricting the cell and allowing the break off of the clathrin coated vesicle (De Camilli, Takei and McPherson, 1995).

MTs are often used in endocytosis acting as railroads to facilitate transport of endocytic adapter proteins (Stehbens and Wittmann, 2012). MTs could also play a role in integrin recycling and subsequent disassembly of adhesions; at the point of integrin recycling it is thought MTs would already be attached to adhesion (Stehbens and Wittmann, 2012). These MTs could act as railway tracks transporting in endocytic adapters such as AP2, Dab2, clathrin and dynamin. However, it has been found that when cells are treated with nocodazole (a MT interfering drug) the levels of AP2, dab2 and clathrin are not altered at adhesion sites (Ezratty *et al.*, 2009).

### 4.1.3 Microtubules are stabilised at the cell edge through the cortical microtubule stabilising complex

MTs direct their growth towards the cell periphery, where, once the plus-end of the MT has reached the cell cortex, the MT can do one of the following:

- Catastrophize and shrink
- Promote formation of a cell protrusion
- Continue to grow parallel to the plasma membrane
- Get captured and stabilised at the cell cortex by MT-stabilising proteins

MT capture and stabilisation at the cell cortex can be regulated by MT-stabilising proteins, known as 'plus tip proteins' (+TIP) (Akhmanova and Steinmetz, 2008). An important +TIP is the cytoplasmic linker associated protein (CLASP), which acts as rescue factor and attaches MTs to the cell cortex through the formation of a complex with other proteins: LL5 $\beta$  and the ETS domain-containing protein (ELKS) (van der Vaart *et al.*, 2013). These proteins are found in concentrated plasma membrane bound patches which are tightly associated with FAs around the cell cortex (Lansbergen *et al.*, 2006; Hotta *et al.*, 2010).

In low motility cells, most MTs are found to terminate at the cell edge despite the high concentration of the +TIP protein CLASP (rescue factor) in close vicinity (van der Vaart *et al.*, 2013). This is an interesting observation, as in the absence of protrusions the MTs could be predicted to form a bundle parallel to the cell edge due to continued growth; however, this was not the case. MT termination at the cell edge could also not be due to the cell membrane acting as a barrier to stop growth because MTs have been proven to be flexible (Brangwynne *et al.*, 2007). Instead, it was found that the protein kinesin family member 21A (KIF21A) counterbalanced CLASP'S activity and inhibited MT growth at the cell cortex (van der Vaart *et al.*, 2013). KIF21A had also been previously found to interact with the KANK family of proteins via KANK's ankyrin repeat domain (Kakinuma and Kiyama, 2009). KANK, in turn, is also known to bind to liprin- $\beta$ 1 and liprin- $\alpha$ 1 at the cell cortex (van der Vaart *et al.*, 2013). KIF21A, Liprin- $\beta$ 1, liprin- $\alpha$ 1 and KANK have been found to associate to the plasma membrane-bound patch proteins (LL5 $\beta$ , ELKS and CLASPs) and together this group of proteins form the cortical microtubule stabilising complex (CMSC) (**FIGURE 4.2**).

The CMSC stabilises MT growth at the cell periphery and accumulates around FAs but with no overlap with FA proteins (van der Vaart *et al.*, 2013). Further evidence shows that KANK protein

was found very close to the FA assemblies, raising the question of whether it could be interacting with any FA proteins.

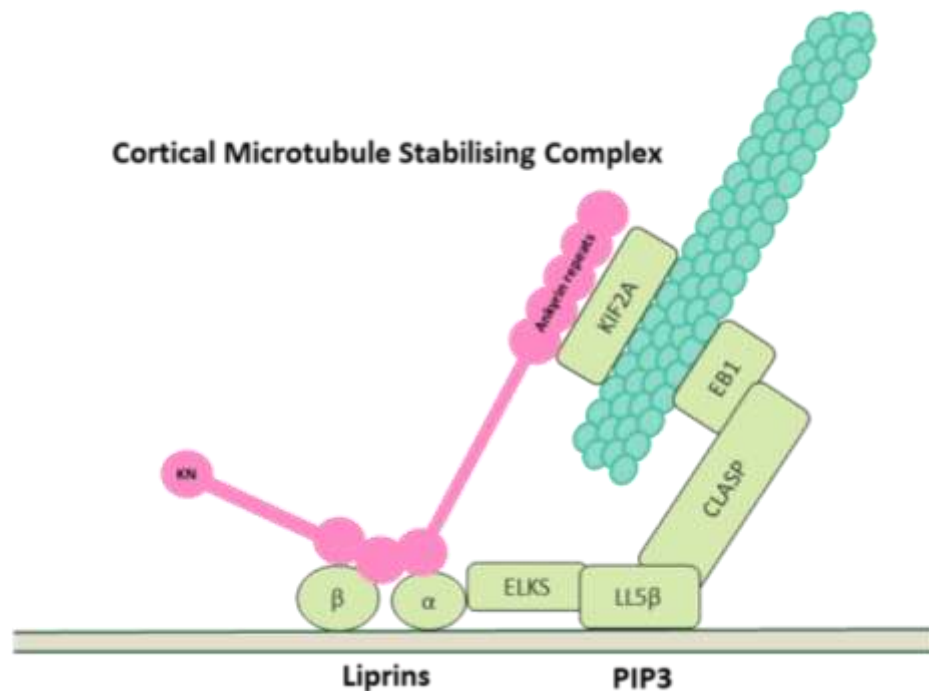


**FIGURE 4.2: THE CORTICAL MICROTUBUE STABILISING COMPLEX**

A schematic diagram of the proteins involved in the CMSC (cortical microtubule stabilising complex). KANK binds to liprin  $\beta$ 1 via its C1 coiled coil domain, completion of the CMSC occurs with further clustering of liprins and the KANK ankyrin repeat domain binding to KIF21A, which captures the microtubules and allows ELKS, CLASP, LL5 $\beta$  all to cluster around the focal adhesion.

#### 4.1.4 KANK protein family

The KANK family of proteins are comprised of four members KANK1-KANK4. KANK stands for 'KN motif and ankyrin repeat domains' and the KANK1 gene was originally identified as a candidate tumour suppressor gene in analysis of renal cell carcinoma (Zhu *et al.*, 2008). Subsequent homology search across the human genome identified three other proteins in the family KANK2, KANK3 and KANK4 (Zhu *et al.*, 2008). All four KANK isoforms have a similar domain structure as shown in **FIGURE 4.3**. Each isoform has a conserved N-terminal KN domain which spans around 38 amino acid residues, which until recently had no known function (Zhu *et al.*, 2008). Our work here demonstrates that the KN domain plays a critical role in binding the adhesion protein talin and through collaboration with the Akhmanova group, we describe that this interaction is the mechanism that links FAs to cortical microtubule stabilising complexes (CMSC).

The KANK C-terminus comprises a series of five ankyrin repeats, preceded by an additional ankyrin-0 domain shown in **FIGURE 4.3**; the ankyrin repeats are well conserved across the KANK family and across species and are important for binding to KIF21A (van der Vaart *et al.*, 2013), a key component of CMSC complexes.

The middle region of KANK is the region that differs most between the KANK isoforms and is largely unstructured apart from coiled-coils regions. KANK1 has 3 predicted coiled-coils, KANK 2 and KANK3 have two coiled-coils and KANK4 has just one single coiled-coil. KANK1 and KANK2 coiled-coil 1 region (CC1) is required to bind to liprin  $\alpha$ 1 and  $\beta$ 1 (van der Vaart *et al.*, 2013).

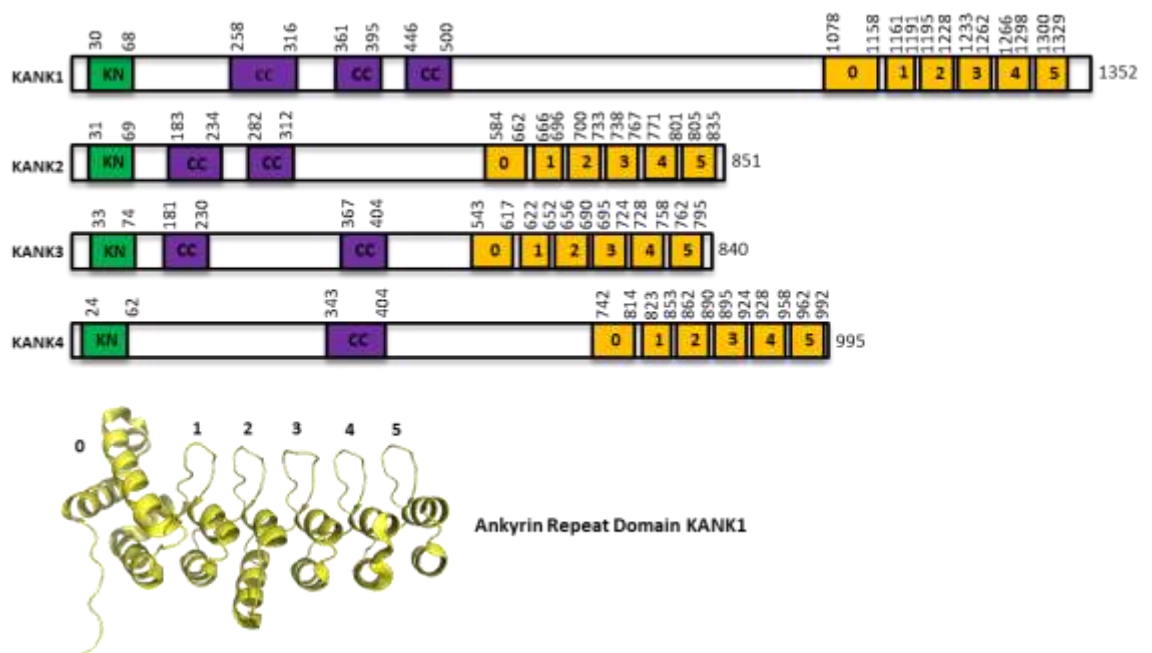


**FIGURE 4.3 SECONDARY STRUCTURE OF KANK FAMILY PROTEINS**

Domain structure of human KANK family proteins the domain regions are predicted using secondary structure prediction (PSIPRED(Jones, 1999)). KANK domains highlighted: KN domain (green), coiled coil regions (purple) and the ankyrin repeats (yellow). (B) The ankyrin repeat domain crystal structure (PDB ID: 5YBJ).

#### 4.1.5 Identifying talin as a KANK binding protein

To address the question of whether KANK can bind to adhesion proteins, Anna Akhmanova's group from the University of Utrecht, carried out a proteomics study for KANK1, using full-length GFP-KANK1, in HEK239T cells. The top hits for this study are shown in **FIGURE 4.4B**. One of the top hits was talin1, the only FA protein present in the proteomics dataset. This suggested that talin is the FA protein involved in the KANK:FA interaction. In parallel to this, we found that a talin1 proteomics set previously obtained by Ben Goult in a collaboration with Martin Humphries' group (unpublished data) identified KANK as one of the most abundant proteins bound to GFP-talin1 in human fibroblasts (shown in **FIGURE 4.4A**).

In order to identify the region of KANK responsible for talin binding, the Akhmanova lab used pull-downs from HEK293T cells, combined with mass spectrometry, to show that only the N-terminal region of KANK1 (1-339) interacts with talin. Taken together, these studies suggest that talin might be the FA mechanosensitive protein linking the FA and the CMSC (via KANK).

**A**

Identified Proteins	Accession Number	Molecular Weight (kDa)	Spectral Counts
Talin-2	TLN2_HUMAN	272	502
<b>KN motif and ankyrin repeat domain-containing protein 2</b>	<b>KANK2_HUMAN</b>	<b>91</b>	<b>88</b>
Septin-2	SEPT2_HUMAN	41	12
Cyclin-dependent kinase 1	CDK1_HUMAN	34	11
Talin-1	TLN1_HUMAN	270	7235

**B**

BioGFP-KANK1 Full Length Pull Down			
Protein	Accession Number	Mascot Score	Unique Peptide
KANK1	Q14678	6279	59
KIF21A	Q7Z456	3398	55
Liprin-β1	Q86W92	2544	50
Liprin-α1	Q13136	261	9
<b>Talin1</b>	<b>Q9Y490</b>	<b>212</b>	<b>9</b>
LL5β	Q865QD	150	8
BioGFP-KANK1 1-339 Pull Down			
<b>Talin1</b>	<b>Q9Y490</b>	<b>4014</b>	<b>72</b>
Talin2	Q9Y4G6	1508	42
KANK1	Q14678	245	8
BioGFP-KANK1 516-1352 Pull Down			
KIF21A	Q7Z456	7410	75
KANK1	Q14678	2855	29

**FIGURE 4.4: GFP-TALIN1 AND GFP-KANK1 PROTEOMIC DATA SETS.**

(A) Data from the Goult and Humphries lab showing identified GFP-tagged talin1 binding partners using mass spectrometry. (B) Data from the Akhmanova lab showing identification of the binding partners of Bio-GFP-tagged KANK1 from a series of pull-down assays from HEK293T cells. Proteins were identified using mass spectrometry and data was analysed using Mascot.

#### 4.1.6 Identifying the region of KANK involved in interaction talin

To further define the region of KANK involved in talin binding, the Akhmanova group used deletion mapping of KANK1. This revealed that the KN domain is essential for KANK1 to localise to the FA rim. The KN domain was identified in KANK1 as a conserved region spanning residues 31-72 (Zhu *et al.*, 2008). Previously, and despite its high conservation, the region had no known function other than harbouring a potential nuclear export sequence (NES) and nuclear localisation signals (NLS) which were found to contribute to nucleo-cytoplasmic shuttling of KANK1 (Zhu *et al.*, 2008).

The KANK1 KN domain boundary was slightly refined to 30-68 and used to make a series of GFP-KANK constructs. These GFP-KANK constructs were then transfected into HeLa cells along with mCherry-paxillin (FA marker). **FIGURE 4.5** shows both full-length KANK1 and KANK1\_KN constructs localise to FAs, whereas the KN deletion (KANK1\_ΔKN) is, instead, found to be diffuse around the cell cortex. These data strongly indicate that the KANK KN domain is required for FA targeting. Combined with the data obtained through proteomics whereby KANK1 binds to talin, it is possible that KANK1 is targeting to FAs via talin.

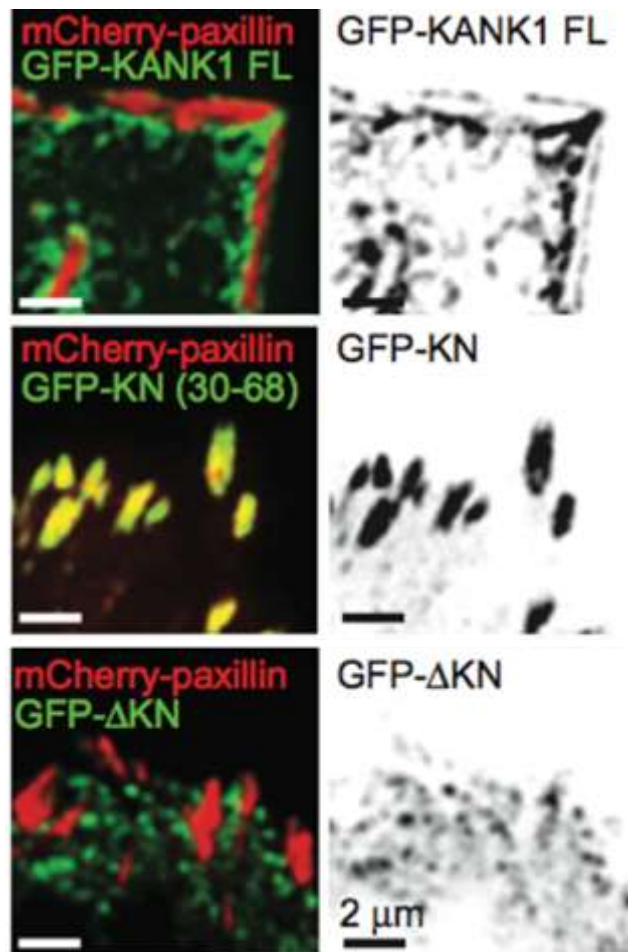


**FIGURE 4.5: KANK1 KN DOMAIN IS RESPONSIBLE FOR LOCALISATION TO FOCAL ADHESIONS**

TIRFM images of live HeLa cells transiently expressing GFP-tagged KANK1 constructs: KANK1, KANK1\_KN and KANK1\_ΔKN along with mCherry-paxillin (focal adhesion marker). In these experiments, endogenous KANK1 and KANK2 were also expressed. Data adapted from (Bouchet *et al.*, 2016).

## 4.2 Results

With strong evidence that the KANK KN domain binds to talin, I sought to explore the interaction by employing a series of biochemical and biophysical techniques, including: Fluorescence Polarisation (FP), Nuclear Magnetic Resonance (NMR) and X-Ray Crystallography. After identifying the individual talin domain required for the talin:KANK interaction, I used NMR to define the talin surface to which KANK binds to. From this I aim to obtain structural information of the talin:KANK interaction in order to design a series of talin point mutations that can perturb the interaction. This is of importance, as it would allow the study of the interaction in a cellular environment and improve our understanding of the combined function of talin and KANK1 in the context of FAs. I also look at how the interaction between talin and KANK1 affects binding of other FA proteins to talin.

### 4.2.1 Designing KANK1 KN domain peptide

The cell biology experiments from the Akhmanova lab, in **section: 4.1.6**, identified that the N-terminal region of KANK contains the region responsible for binding to talin. In light of this, we designed a KANK1 synthetic peptide for binding experiments. To design the KANK1 KN peptide, a secondary structure prediction software (PSIPRED (Jones, 1999)) and a KANK1 sequence alignment across different species was carried out. PSIPRED is a two-stage neural network that can be used to predict protein secondary structure based on position-specific scoring matrices generated by PSI-BLAST(Jones, 1999). PSIPRED gives a predicted secondary structure:  $\alpha$ -helix,  $\beta$ -sheet or disordered. The predicted secondary structure is given a confidence score, which is depicted as a series of blue bar graphs; the higher the bar, the higher the confidence of the predicted structure. The results of the PSIPRED analysis on human KANK1 have been over-laid on the sequence alignment on **FIGURE 4.6** to highlight the region of the sequence with predicted structure. The algorithm shows that the N-terminal of KANK1 is unstructured, except between residues 38-50, where it predicts an  $\alpha$ -helix (with 50-60% confidence).

To highlight the areas of high conservation in the KANK1 sequence across species, a BLAST search using the KANK1 human sequence (Uniprot: Q14678) was performed. A BLAST query highlights proteins from different species sequences that have regions of similarity. This search enabled identification of KANK1 sequences from a range of species including: Horse; Sheep; Chicken; Mouse and Human. The N-terminal region of KANK1 across all species had a patch of high conservation between residues 30-68 (human KANK1). In contrast, the sequence conservation for the regions



either side of 30-68 was much lower. Furthermore, inspection of the highly conserved 30-68 sequences revealed the presence of a putative LD-motif.

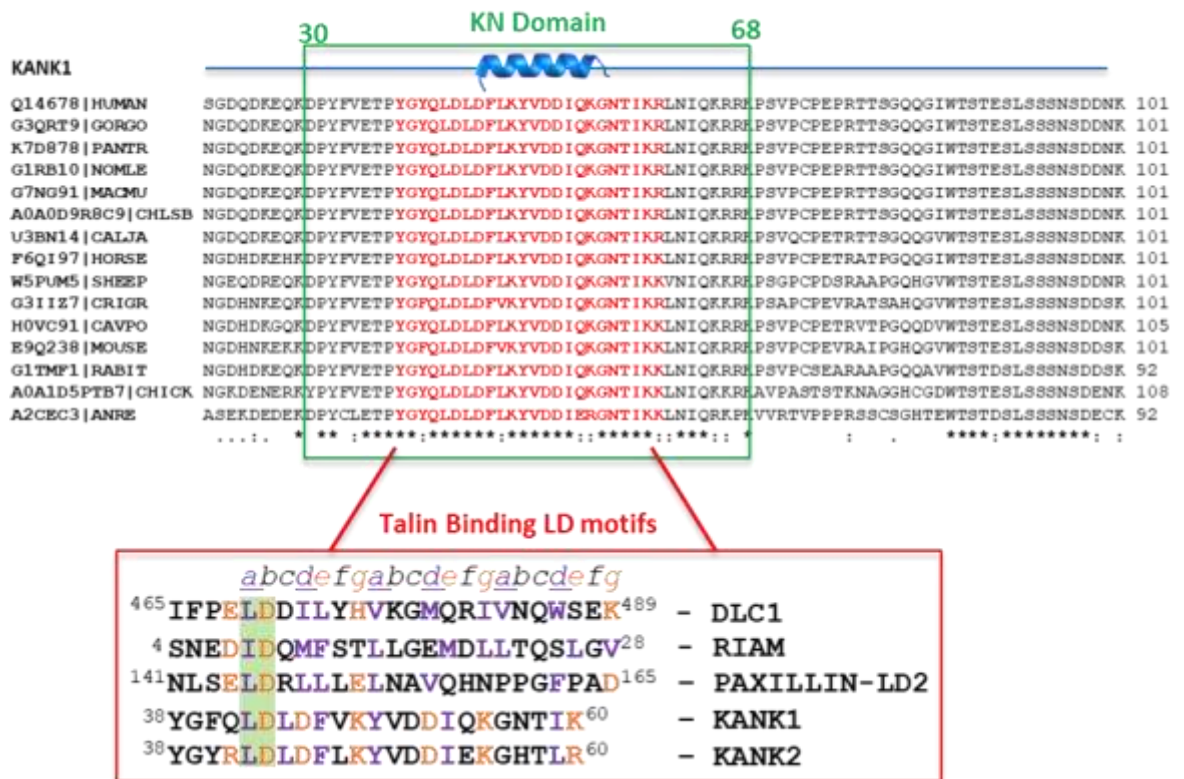


FIGURE 4.6: CONSERVATION ALIGNMENT OF KANK1 TO DESIGN A KANK PEPTIDE

Conservation of KANK1 N-terminal residues using sequences from: human, gorilla, chimpanzee, gibbon, green monkey, marmoset, horse, sheep, Chinese hamster, guinea pig, mouse, rabbit, chicken and zebrafish. Sequences were aligned in UniProt and all had similar secondary structure predictions (PsiPred), which is shown above the sequence in blue. Conserved residues are highlighted by a \*, semi-conserved amino acids (with similar properties) are shown by a :. Sequence alignment of talin binding motifs: paxillin LD2 (UniProt: P49023); RIAM (UniProt: Q7Z5R6); DLC1 (UniProt: Q96QB1); KANK1 (UniProt: Q14678) and KANK2 (UniProt: Q63ZY3). The sequences were aligned via the Leu-Asp residues in the LD, interacting hydrophobic residues are highlighted orange and additional hydrophobic residues are highlighted in purple.

#### 4.2.1.1 KANK proteins contains an LD-Motif

LD-motifs are short helical protein-protein interaction motifs that are crucial in connecting cell adhesion with cell motility and survival (Alam *et al.*, 2014). LD-motifs were first discovered over 20 years ago in the paxillin family of scaffolding proteins (Bellis, Miller and Turner, 1995), with the sequence LDxLLxxL (where x is any residue). The N-terminus of paxillin was found to contain five of these LD-motifs which are highly conserved both across species, and across the paxillin superfamily (Tumbarello, Brown and Turner, 2002).

LD-motifs are recognized by LD binding domains (Zacharchenko *et al.*, 2016) (LDBDs). LD-motifs bind to LD binding domains via helical addition, whereby the LD-motif forms a helical structure which packs against the side of a helical bundle as shown in **FIGURE 4.7**. The core LD-motif sequence LDxLLxxL binds to the LD recognition box via its Asp residue, which forms a salt bridge with a negatively charged residue on the LDBD. In some cases, the same LD recognition box can recognize multiple different LD-motifs and the mechanism that distinguishes how LD-motifs are selective for their target molecule is still not fully understood. Fully understanding this mechanism is important, as dysfunction in LD-motifs often contributes to diseases, such as cancer metastasis and viral infections (Mitra and Schlaepfer, 2006). A more detailed discussion of LD-motif recognition is given in **Chapter 5**.

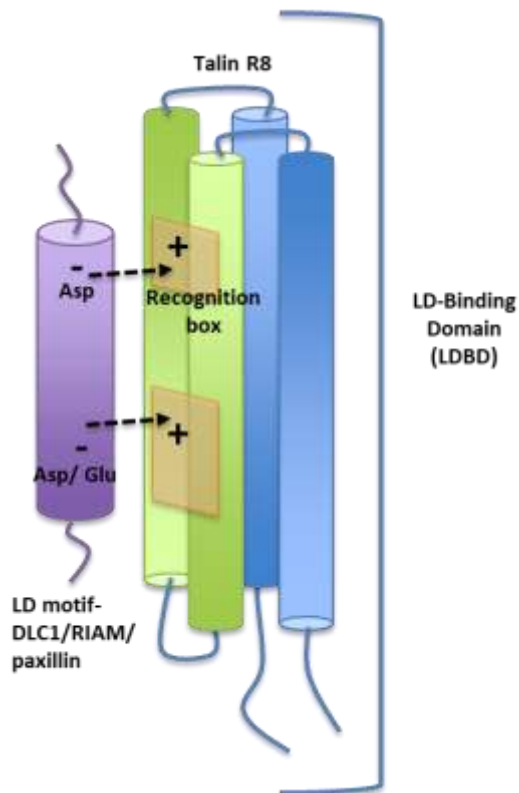


**FIGURE 4.7: TALIN1 R8 DOMAIN IS LD RECOGNITION BOX**

A schematic of the LD recognition box on the talin R8 domain. Purple cylinder represents an LD-motif showing how the Asp residue would bind to a charged amino acid on the LDBD via the recognition box. Further down the LD-motif a second charged residue makes contact with talin in what is known as the specificity region (Zacharchenko *et al.*, 2016).

#### 4.2.1.2 Talin can bind LD-motifs

The first realisation of LD-motif binding to talin was found when looking at the interaction between the protein DLC1 (Deleted in Liver Cancer 1) and talin (Zacharchenko *et al.*, 2016). This interaction was mapped to the R8 domain of talin, and since then R8 has become recognised as an LDBD that

forms a hot spot for LD binding proteins with: DLC1, RIAM, and Paxillin all binding to the domain. The best studied mode of LD-motif recognition is via binding to four helix bundles (Hoellerer *et al.*, 2003). **FIGURE 4.6** shows an alignment of the known talin binding LD-motif proteins identified to date and aligns the KANK1 KN domain with the canonical LDxLLxxL motif. This analysis was interesting as it shows that the KANK1 region does not quite fit the consensus LDxLLxxL motif of other LD binding proteins; the KANK sequences have an additional charged Asp residue in place of the hydrophobic residues found in the other sequences. This extra Asp residue comes because of an LDLD motif found in KANKs sequence, which has not been found in other LD containing proteins. We were not sure if the charged residue would prevent the region from binding to the LD recognition box. However, the rest of the KANK sequence looked to fit the LD-motif pattern and so we concluded the KANK KN domain did include an LD-motif. This led us to hypothesize that KANK would bind to the talin R8 domain where the other LD-motifs have been found to bind to talin. A series of KANK1 peptides were designed encompassing the potential LD-motif predicted to bind to talin. The constructs differed slightly in length with the hope they would narrow down the talin-binding site; peptides are shown in **FIGURE 4.8**.

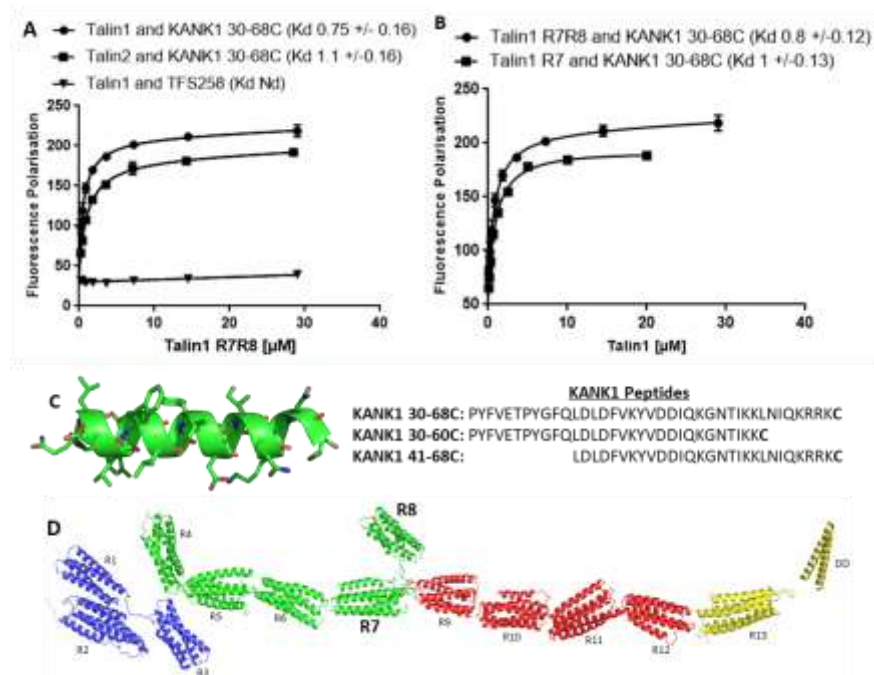


**FIGURE 4.8: BIOCHEMICAL CHARACTERISATION OF KANK BINDING TO TALIN**

(A-B) Binding of BODIPY-TMR labelled KANK1(30–68)C peptide to talin1 R7R8 (1357–1653), talin2 R7R8 (1360-1656) and Talin1 R7 (1357-1653  $\Delta$ 1454-1586) was measured using fluorescence polarization. BODIPY-TMR labelled TFS258 peptide was used as a negative control. Dissociation constants  $\pm$  SE ( $\mu$ M) for the interactions are indicated in the legend. All measurements were performed in triplicate. ND, not determined. (C) helical prediction of KANK peptide based on the DLC1 peptide (PDB ID: 5FZT) KANK1 30-60 residues were threaded onto the DLC1 helix using PyMOL and the designed peptides for FP: KANK1 30-60C, KANK1 30-68C and KANK1 41-68C. (D) Structural model of the talin rod domains highlighting R7 and R8 talin domains.

## 4.2.2 Determining the region of talin involved in the talin:KANK interaction

To investigate if talin R8 was the binding domain for KANK1, we used the designed human KANK1 synthetic peptide (KANK1 30-68C), shown in **FIGURE 4.8C**. A C-terminal cysteine residue was added to the peptide to allow coupling to a fluorescent label. To test the relative binding affinities, an *in vitro* fluorescence polarization (FP) assay was used. In the assay, the KANK1 30-68C peptide was coupled to BODIPY-TMR (see material and method **Chapter 3**) and titrated against an increasing concentration of talin1 (residues 1357-1653) or talin2 (residues 1360-1656). An increase in FP signal generates a binding curve that corresponds to binding of the peptide and protein, the FP binding curve was fitted to a binding equation (see materials and method **Chapter 3**) to obtain dissociation constant,  $K_D$ . **FIGURE 4.8** shows the binding data for talin1 R7R8 domain with the KANK1 30-68C peptide. **FIGURE 4.8A**, shows that talin1 binds KANK1 with a  $K_D$  of 0.75  $\mu\text{M}$  and talin2 with  $K_D$  1.2  $\mu\text{M}$ . Interestingly, this sub-micromolar affinity of KANK1 for talin makes KANK the strongest talin-binder identified so far.

To confirm if talin R8 was the KANK binding domain, the same FP assay was used with individual domains R7 (residues 1359–1653  $\Delta$ 1454–1586) and R8 (residues 1461-1580) (**FIGURE 4.8B**). This gave a surprising result - KANK1 bound to talin1 R7 with a  $K_D$  of 1  $\mu\text{M}$  only barely to the R8 domain ( $K_D$  nd, data not shown), revealing that it is actually the talin R7 domain that contains the major KANK binding site. The fact that KANK1 bound with lower affinity to the R8 domain indicates that there is a weak interaction (possibly between the LD residues and the LD recognition box in R8). This was unanticipated because evidence of LD-motifs binding to 5-helix bundles had not yet been reported. This finding shows KANK is binding to talin in a novel-binding site, and talin R7 could be a new talin LD binding domain (LDBD).

## 4.2.3 Chemical shift mapping of talin1 R7R8 domain with KANK peptide

To explore the talin:KANK1 interaction further, NMR chemical shift mapping was used. Chemical shift mapping is a technique that follows the changes in chemical shifts of a protein when a ligand is added, these shifts can be used to determine the binding site and in some cases the affinity of the ligand. Typically for chemical shift mapping  $^1\text{H}^{15}\text{N}$  HSQC or  $^1\text{H}^{15}\text{N}$  TROSY experiments are used (see materials and methods 3.4.3.4) and the protein is expressed with an  $^{15}\text{N}$  label such as  $^{15}\text{N}$  ammonium sulphate. The HSQC and TROSY experiment makes use of the fact that every amino acid (apart from Pro) has a proton (hydrogen) attached to the peptide bond see **FIGURE 4.9**. The

experiments provide a correlation between the proton and the nitrogen atoms which are visualised as a peak in the spectrum; meaning every peak correlates to an amino acid in the protein sequence.

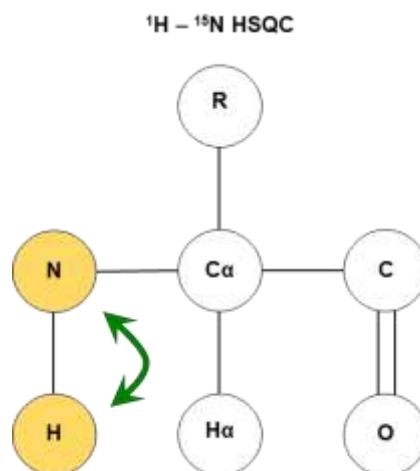


**FIGURE 4.9:  $^1\text{H}^{15}\text{N}$  HSQC CORRELATION BETWEEN THE PROTON AND THE NITROGEN ATOM**

Schematic diagram showing the correlation between nitrogen and proton atoms in a amino acid that a HSQC and TROSY measure.

$^{15}\text{N}$ -labeled talin1 R7R8 (residues 1357-1653) were expressed and purified for NMR see materials and methods 3.4.3.1. A  $^{15}\text{N}$  TROSY spectrum of talin1 R7R8 (80  $\mu\text{M}$ ) (black **FIGURE 4.10**) showed good peak dispersion indicating the talin1 R7R8 domain was folded as reported previously (Gingras *et al.*, 2010). The addition of the KANK1 peptide 30-68C to talin1 R7R8 at a ratio of 3:1 (blue **FIGURE 4.10**) caused large peak changes in the NMR spectra; the peaks were still well dispersed, indicating that the overall structure of the R7R8 talin domain had been maintained. A significant number of peaks that shifted upon addition of KANK1 were found to be in slow exchange, which on the NMR shift timescale is indicative of a tight interaction, complementing the 1  $\mu\text{M}$   $K_D$  measured with the FP assay. Slow exchange is where the protein is found to be in two states: free protein and protein bound to the ligand. Because the exchange between these two forms is happening slowly the NMR is capturing both states that is visualised as two peaks. These two peaks will disappear and become one when the interaction is saturated enough to only see the bound form.

To determine which talin peaks had shifted when KANK peptide was added the talin:KANK spectrum was overlaid with talin1 R7 spectrum (data not shown). This showed that the large majority of the peaks that shifted were h the talin R7 peaks, there were some smaller shifts recorded on R8 talin peaks. The chemical shift changes on the R8 domain were in fast exchange, which on the NMR timescale is indicative of a weak binding interaction, thus supporting the finding that the KANK peptide binds weakly to R8 and that R7 is the main KANK binding site.

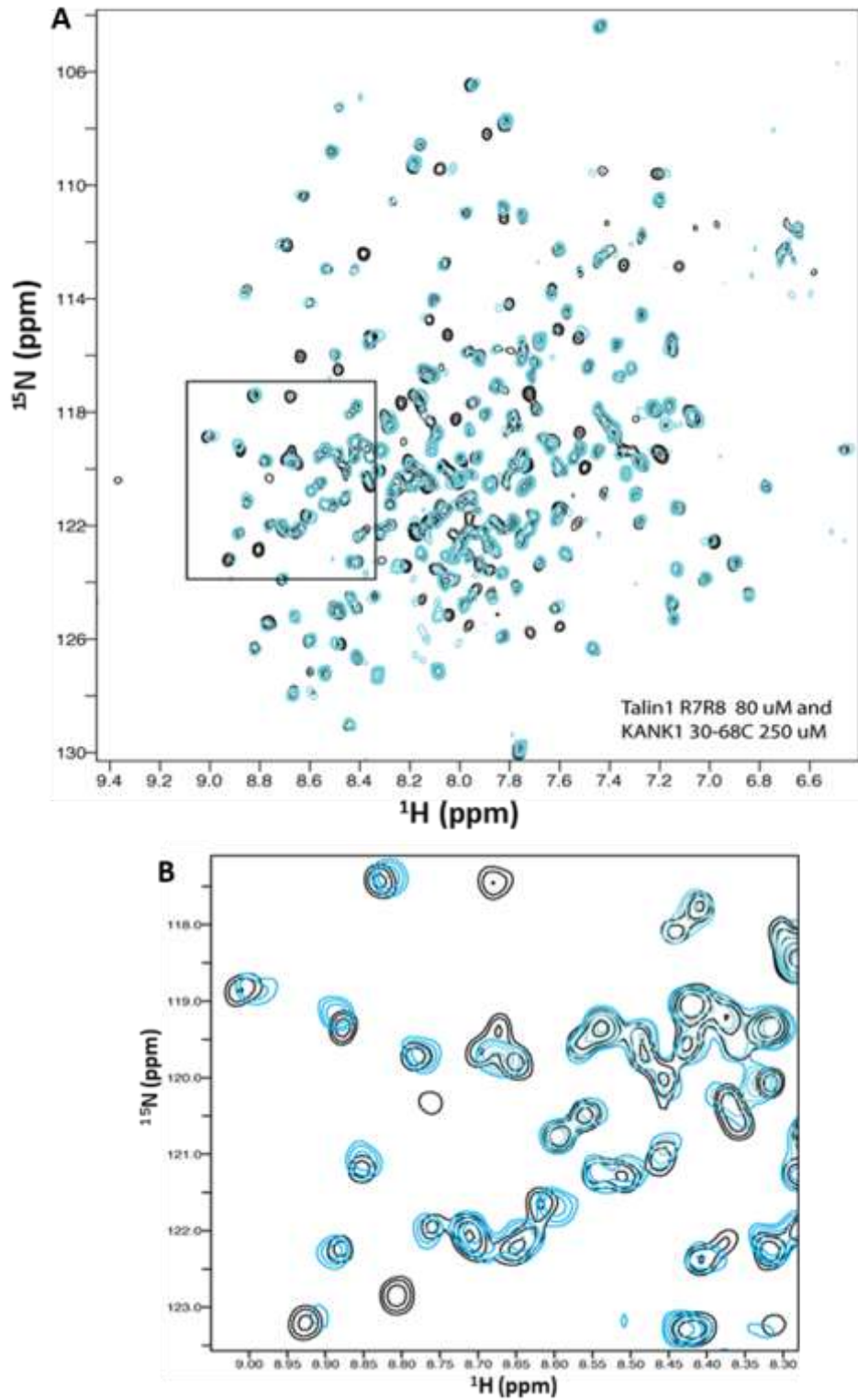


**FIGURE 4.10:  $^{15}\text{N}$  TROSY NMR TITRATION TALIN1 R7R8 AND KANK1 30-68C PEPTIDE**

(A)  $^1\text{H},^{15}\text{N}$  TROSY spectra of 80  $\mu\text{M}$   $^{15}\text{N}$ -labelled talin1 R7R8 (residues 1357–1653) in the absence (black) or presence of KANK1(30–68)C peptide (blue) at a ratio of 1:3. (B) Shows a zoomed in region of spectra (A) (highlighted by the black box) showing slow exchange of peaks when the KANK1 peptide has been added.

#### 4.2.4 Chemical shift mapping of talin1 R7 domain with KANK peptide

To identify where on the R7 domain the KANK was interacting a  $^{15}\text{N}$  HSQC titration was carried out on the single talin1 R7 (1359–1653  $\Delta$ 1454–1586).  $^{15}\text{N}$ -labelled talin1 R7 was titrated against increasing concentrations of the KANK1 30-68C peptide. The overall spectra are shown in **FIGURE 4.11A**, with talin1 R7 on its own (black) and KANK1 titrated at a ratio 1:2 (talin:KANK) (blue). The peak shifts were much clearer to analyse compared to the double R7R8 domain due to less overlap of individual peaks, allowing the tracking of each individual peak. The peaks are in slow exchange on the NMR timescale after the addition of the KANK1 30-68C peptide, confirming the high affinity between talin1 R7-KANK1.

Evidence of an R7 peak in slow exchange is shown in **FIGURE 4.11B**. Talin1 Asp1362 (black) is found as a single peak when not bound to KANK1. When KANK1 is added at a 0.5:1 ratio (talin: KANK1) (green) half the talin R7 molecules are bound to KANK1 and half are in the free form which gives rise to two Asp1362 peaks. In contrast, if the interaction were in fast exchange we would see a single peak at the average position of free and bound. When KANK1 is then added to talin at a ratio of 1:1 (pink) the entire population of talin in the sample is now bound to KANK1 and so the Asp1362 signal appears as a single peak again but in a different position to when not bound to KANK1.

A region of the R7 spectrum is shown in **FIGURE 4.11C** and **D**. **FIGURE 4.11C** shows talin1 R7 (black) with KANK1 30-60C added at a ratio 1:0.5 (green) and **FIGURE 4.11D** KANK1 30-68C added at a ratio 1:1 (purple). **FIGURE 4.11C** has more peaks than **FIGURE 4.11D** as it is showing both the bound and non-bound forms of talin. Mapping which peaks shift upon addition of KANK allows us to understand which talin residues are involved in the interaction and define the interacting surface on talin.

In order to determine which peaks have shifted, amide chemical shift assignments from the Biological Magnetic Resonance Bank (BMRB) of talin1 R7 were downloaded (BMRB: 19139). The assignments were used to assign the corresponding residue number to each peak in the talin1 R7 HSQC spectrum. For each peak the chemical shift changes on addition of KANK1 were measured between talin1 R7 on its own and talin1 R7:KANK1 (at a ratio 1:2). This however was harder than anticipated, as it was not clear for every talin peak where it had shifted upon the addition of KANK1 and a confident prediction could not be made.



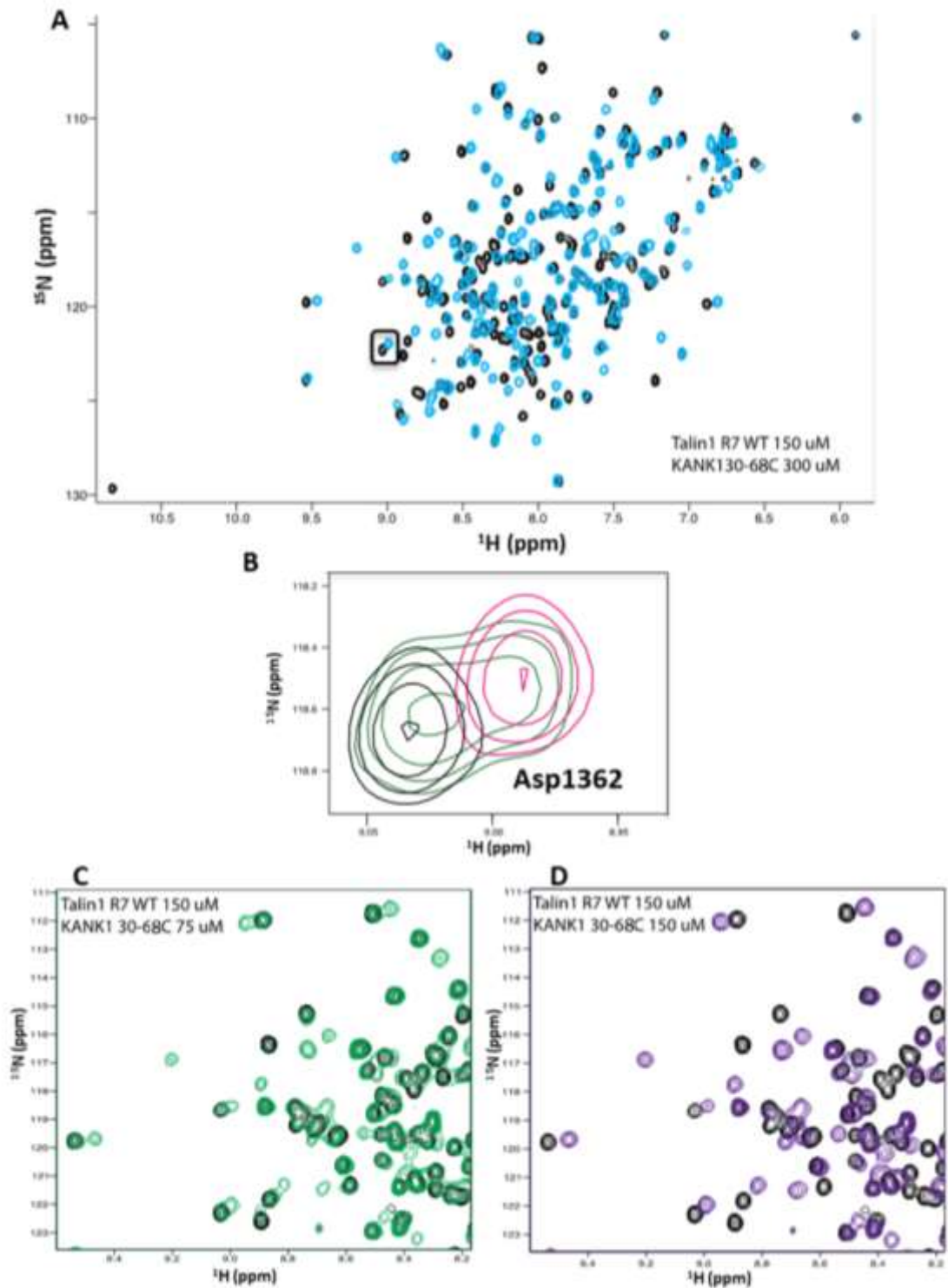


**FIGURE 4.11:  $^{15}\text{N}$  HSQC NMR TITRATION TALIN1 R7 AND KANK1 30-68C PEPTIDE**

(A,C,D)  $^1\text{H}$ , $^{15}\text{N}$  HSQC spectra of 150  $\mu\text{M}$   $^{15}\text{N}$ -labelled talin1 R7 (residues 1357–1653  $\Delta$ 1454-1586) in the absence (black) or presence of KANK1(30–68)C peptide (blue/green/purple). Blue peaks shows a 1:2 ratio of talin:KANK1, green peaks 1:0.5 ratio and purple peaks 1:1 ratio. Black box highlights residue Asp1362. (B) Shows the peak corresponding to Asp1362: black peak is on its own, green is with KANK1 30-68C peptide added at a ratio of 1:0.5 and pink is KANK1 peptide added at a ratio of 1:1. The peak splitting is evidence that the interaction is happening in slow exchange.



To solve this problem, we needed to find a way to put the talin:KANK interaction into fast exchange on the NMR timescale. Fast exchange binding has a distinct peak tracking pattern; peaks shift in a line upon addition of binding ligand. This is because the ligand is binding on and off the protein quickly resulting in an average position being taken, so as more ligand is added the average peak position will be closer to fully bound resulting in a linear line of peaks. This line of peak shifts allows for more confident tracking and recognition of where each peak has shifted.

In preliminary characterization of the talin:KANK interaction a KANK1 peptide- KANK1 42-68 was designed. The KANK1 42-68 peptide did not encompass any residues before the LD-motif unlike the longer KANK1 30-68C peptide. Instead, the first residue was Leu48, which was likely to have reduced helical propensity of the region reducing its ability to bind to talin R7.

The FP assay showed this peptide had a much weaker binding  $K_D$  (data not shown) to talin R7R8 than the 30-68C peptide. The reduced affinity to talin worked to our advantage, as it changed the talin:KANK interaction to a fast exchange regime on the NMR timescale.

A point in the  $^{15}\text{N}$  HSQC titration with talin1 R7 (black) is shown in **FIGURE 4.12A**. KANK1 42-68 peptide was added to talin1 R7 at a ratio of 6:1 (blue). The addition of KANK peptide caused the talin peaks to shift. Talin1 R7 amide chemical assignments (BMRB: 19139) were used to determine which peaks in the HSQC had shifted and peak distances were measured using **EQUATION 2**:

$$\Delta(H, N) = \sqrt{\Delta_H W_H^2 + \Delta_N W_N^2}$$

#### **EQUATION 2: WEIGHTED COMBINATION OF AMIDE SECONDARY SHIFTS**

Chemical shift changes are determined using the weighted combination of  $^1\text{H}$  and  $^{15}\text{N}$  amide secondary shifts ( $\Delta(H,N)$ ).  $\Delta(H,N)$ . Secondary shifts are determined whereby,  $W_H$  and  $W_N$  are weighting factors for the  $^1\text{H}$  and  $^{15}\text{N}$  amide shifts ( $W_H= 0.15$  and  $W_N= 1$ ) (Ayed *et al.*, 2001).

The shift differences for each peak in talin1 R7 are shown in **FIGURE 4.12B**; residues where the peak shifted over 0.005 ppm are highlighted in red on the graph and also on the talin1 R7R8 structure (PDB ID: 5FZT) shown in **FIGURE 4.12D**. Shifts over 0.005 ppm were chosen to be mapped because it represented a significant peak shift when KANK1 was added which likely correlates to the peak being involved in binding or can also be due to induced conformational change upon binding. Shifts below this range were not deemed significant in the talin:KANK interaction. The shift changes mapped to the surface of talin R7 between helices 2 and 5 of the R7 5 helix bundle (talin rod helices 29 and 36)(**FIGURE 4.12C**). Confirming that talin R7 is a new LD binding domain.

**A** KANK1 30-68C: PYFVETPYGFQ**LDLD**FVKYVDDIQKGNTIKKLNIQKRRKC  
 KANK1 42-68C: **LDLD**FVKYVDDIQKGNTIKKLNIQKRRKC

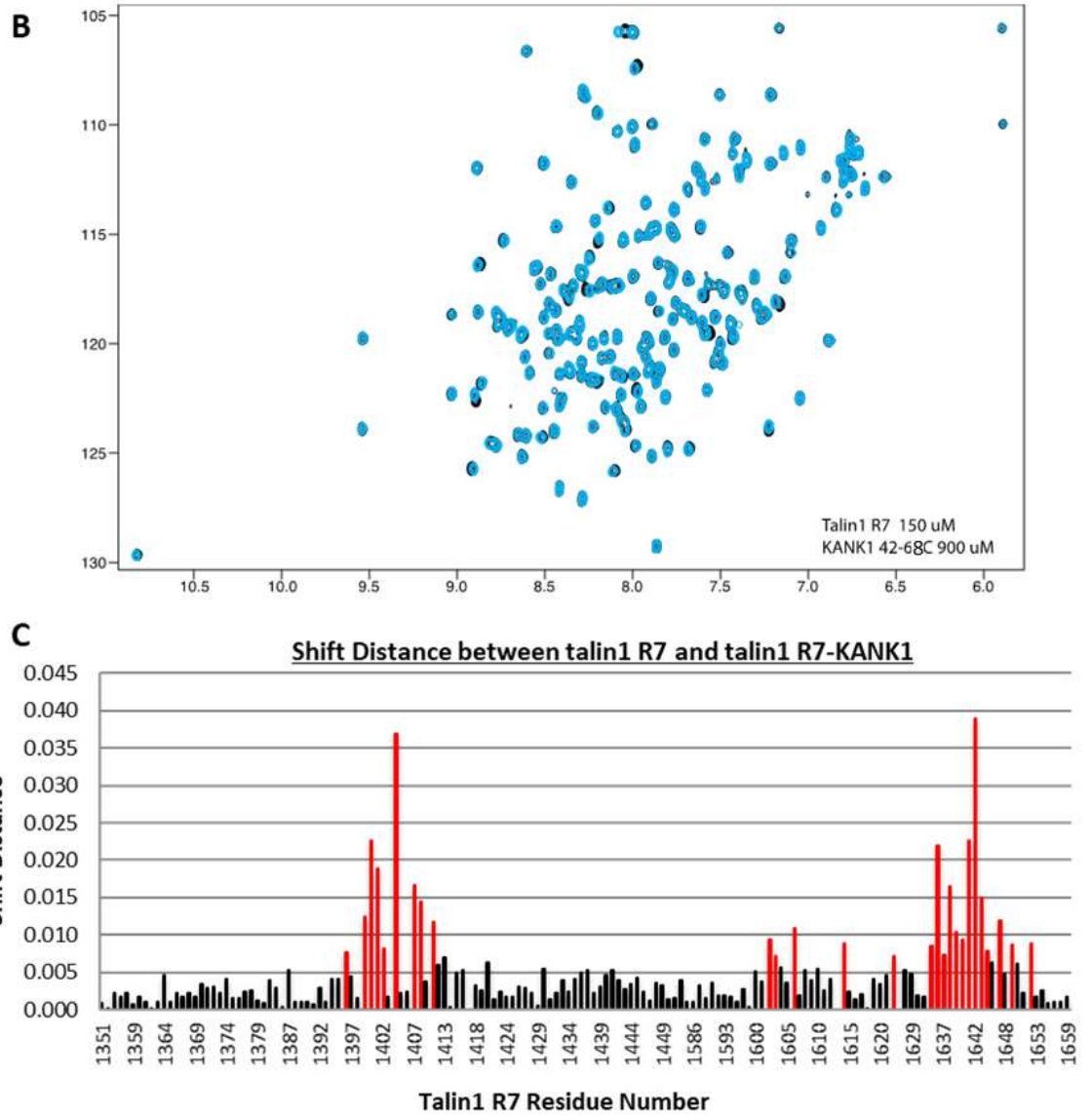


**FIGURE 4.12: CHEMICAL SHIFT MAPPING OF TALIN1 R7R8 AND KANK1 42-68C**

(A) KANK1 30-68C and KANK1 42-68C peptides aligned. (B)  $^1\text{H}$ ,  $^{15}\text{N}$  HSQC spectra of 150  $\mu\text{M}$   $^{15}\text{N}$ -labelled talin1 R7 (residues 1357–1659  $\Delta$ 1454–1586) in the absence (black) or presence of KANK1(42–68)C peptide (blue) at a ratio of 1:6. (C) Mapping the chemical shift distances of the KANK142-68 peptide with talin1 R7 as detected by NMR peaks that shifted more than 0.005 are highlighted in red.

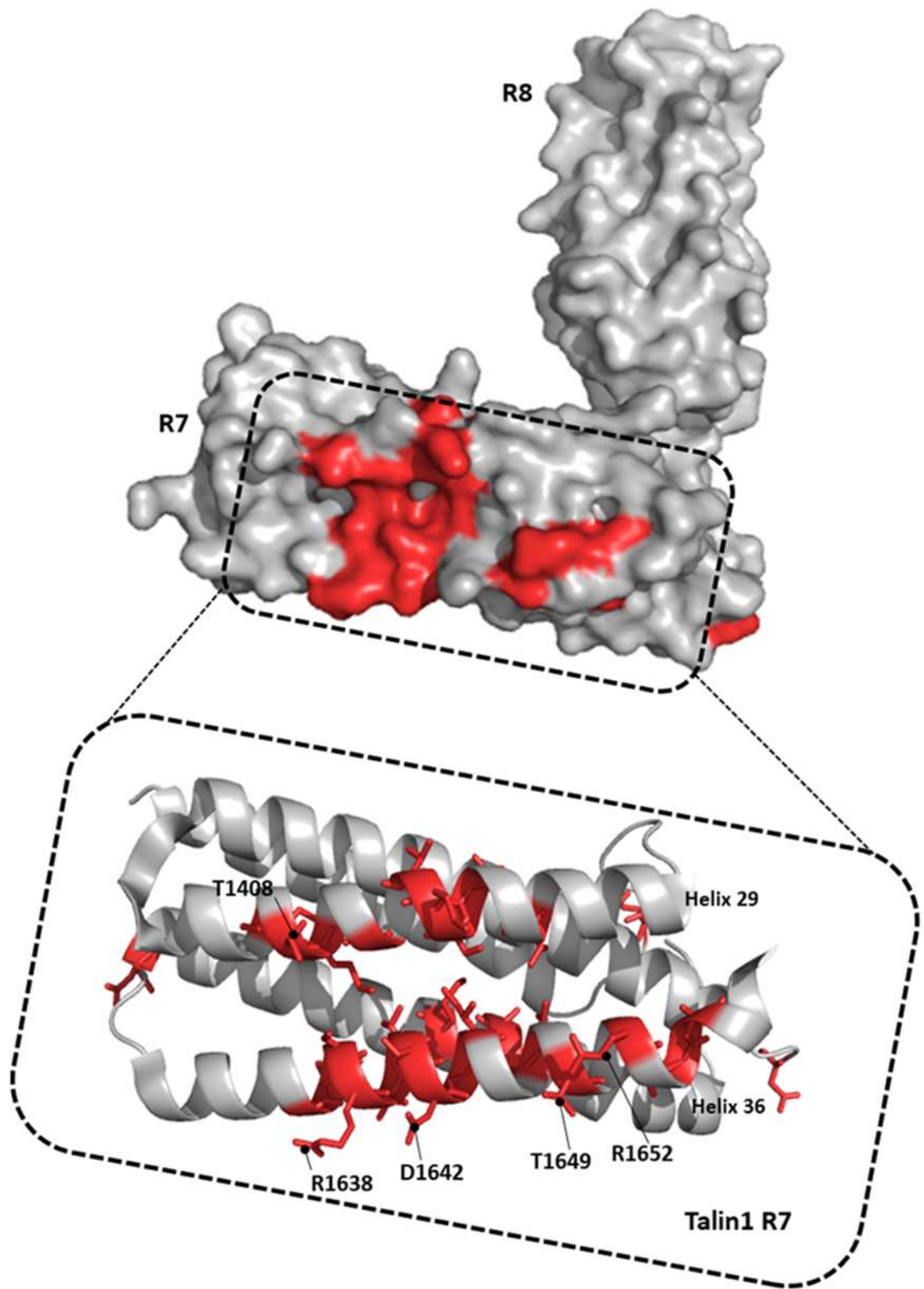


**FIGURE 4.13: CHEMICAL SHIFT MAPPING OF THE KANK1 BINDING SURFACE ON TALIN1 R7**

Mapping of the KANK1 binding site on R7 as detected by NMR using weighted chemical shift distances, residues that shifted  $> 0.005$  are mapped onto the talin1 R7R8 structure (highlighted in red).

## 4.2.5 Structural characterisation of the talin:KANK complex

We wanted to gain an atomic structure of the talin:KANK1 interaction in order to determine which KANK1 residues were interacting with talin R7. Through doing so we hoped to design both a KANK mutant to disrupt talin binding and a talin mutant to disrupt KANK binding.

### 4.2.5.1 Crystal trials of talin1R7R8:KANK1 structure

To get an atomic structure of talin1:KANK1 crystallography trials were set up with talin1 R7R8 (residues 1357-1659) and the KANK1 30-60C peptide. Talin1R7R8 and KANK1 were incubated together at varying ratios (1:1,1:2,1:4) and then plated onto a number of different crystallography screens including: Hampton crystal screen 2 (Hampton), JCSG (Molecular Dimensions), Wizard (Molecular Dimensions) and Pact (Molecular Dimensions). All screens were plated at a 1:1 ratio of protein: well solution and left at both 4 °C and 20 °C. No crystals were found in any condition at either temperature.

### 4.2.5.2 Predicted talin:KANK1 structure

To design KANK and talin mutations in the absence of an atomic structure of talin:KANK1, a structural model was generated by docking the talin1 R7R8 and the KANK1 30-68C peptide together. This was achieved using the known talin1 R7R8:DLC1 structure (PDB ID:5FTZ), where the DLC1 forms a short alpha helix when bound to talin. The DLC1 helix was used as a base and the KANK1 peptide 30-68C was threaded onto the DLC1 helix using PyMOL to create a helical KN domain structural coordinates. The DLC1 helix was docked onto the R7 helices 29 and 36 based on the NMR chemical shift mapping data. Multiple binding models were initially created; switching which end of the talin bundle the KANK LD-motif docked, i.e. with the KN domain flipped 180° along the domain axis. After structural analysis of the residues involved it was decided that the most plausible model had the KANK Asp42 and Asp44 forming salt bridges with talin Arg1652 and Lys1401 (respectively). We know from previous studies in the lab that the formation of a salt bridge with the Asp residue in an LD protein is essential for talin binding (Zacharchenko *et al.*, 2016). The final docking model is shown in **FIGURE 4.14**.

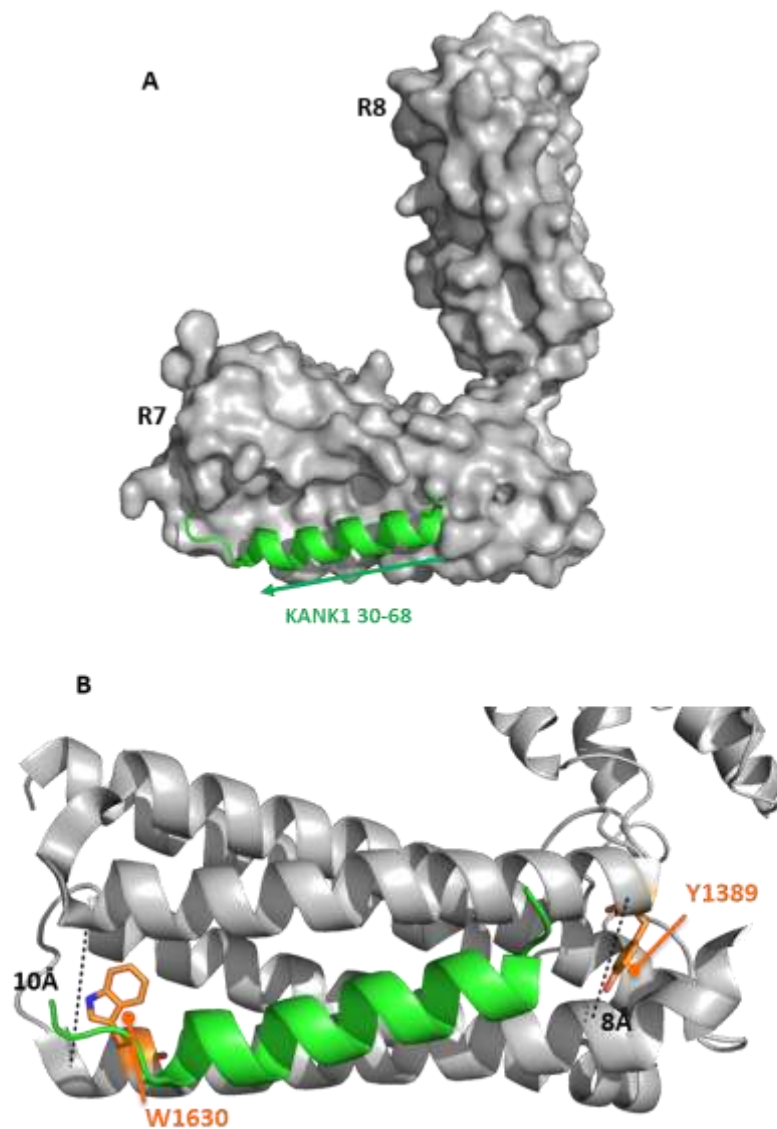


**FIGURE 4.14: STRUCTURAL MODEL OF THE TALIN1 R7R8: KANK1 INTERACTION**

(A) Talin1 R7R8 structure showing the predicted binding site of KANK 30-60 (green) on the talin1 R7 surface. (B) Highlights talin1 R7 residues Trp1630 and Tyr1389 that act as molecular rulers separating helices 29 and 36.

#### 4.2.6 Designing KANK mutations to perturb talin:KANK1 interaction

The talin binding site (TBS) on KANK1 is unusual, it contains an LDLD motif, which has not been seen before in an LD-motif. In order to further investigate and confirm that the LDLD residues were integral for talin binding, we designed a KANK1 mutant that removed the LDLD residues and mutated them to alanine's (KANK\_4A mutant).

We anticipated that the substitution to alanine residues would perturb KANK binding to talin. The talin:KANK model shows KANK residues Asp42 and Asp44 form salt bridges with talin Arg1652 and Lys1401 (respectively). **FIGURE 4.15** shows how aspartate interactions position the KANK peptide in relation to talin and allow the KANK1 hydrophobic residues to be directed between the talin helices to form hydrophobic interactions. Mutating Asp42 and Asp44 to a non-charged residue such as alanine would prevent the ability of KANK to form salt bridges with talin.

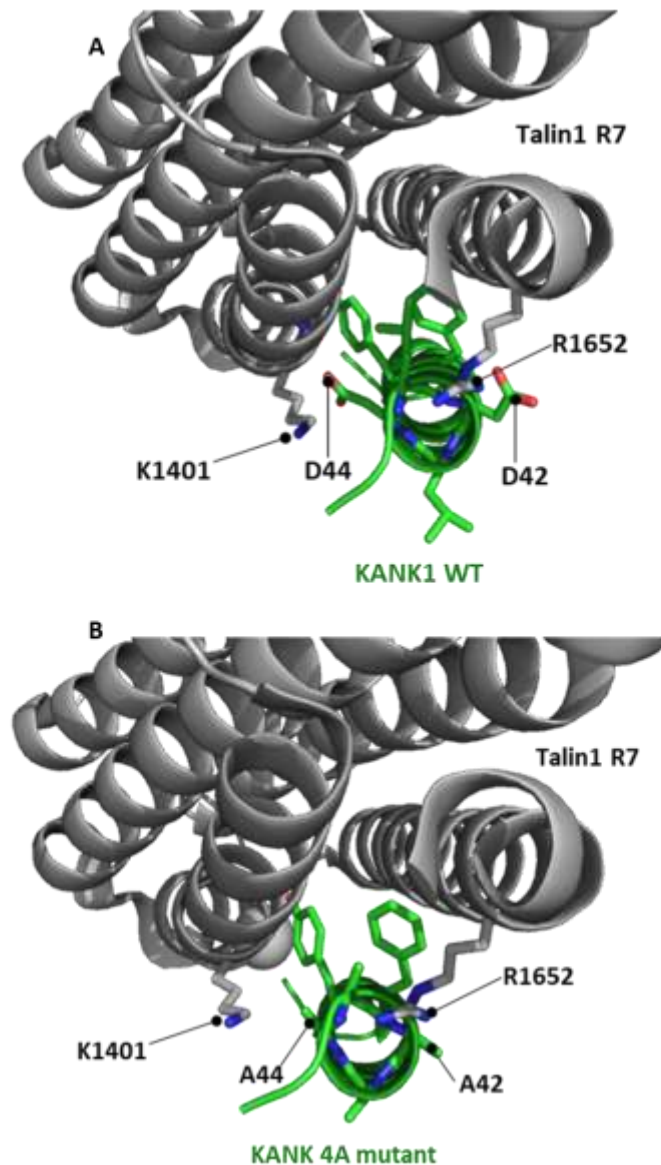


**FIGURE 4.15: STRUCTURAL REVIEW KANK\_4A MUTANT**

(A) Talin1 R7 structure with predicted KANK1 30-60 (green) bound; KANK1 Asp42 and Asp44 residues are highlighted and the talin residues predicted to form salt bridges which are integral for KANK binding. (B) Talin1 R7 with KANK1\_4A peptide, KANK LDLD residues mutated in PyMOL which demonstrates how Ala mutations prevent the formation of salt bridges with talin1 R7 and thus would prevent talin:KANK binding.

#### 4.2.7 Biochemically characterisation of the KANK1\_4A mutant

To determine if KANK\_4A mutation would prevent binding to talin a KANK1\_4A 30-68C peptide was designed **FIGURE 4.16A**, the peptide was designed to be the same length as the KANK1 30-68C peptide and contain a C-terminal cysteine residue that would allow it to be coupled to a fluorescent label.

Using the FP assay, both KANK1 30-68C and KANK1\_4A 30-68C peptides were titrated against increasing concentrations of talin1 R7R8 (residues: 1357–1653) and talin2 R7R8 (residues: 1360-1656) the relative binding affinities measured are shown in **FIGURE 4.16B**. The binding between talin and KANK1 was completely abolished in both talin isoforms when the KANK\_4A peptide was used, highlighting that the KANK LDLD residues are required for binding to talin.

**A** **KANK1 30-68C:** PYFVETPYGFQ**LDLD**FVKYVDDIQKGNTIKKLNIQKRRKC  
**KANK1\_4A\_30-68C:** PYFVETPYGFQ**AAAA**FVKYVDDIQKGNTIKKLNIQKRRKC

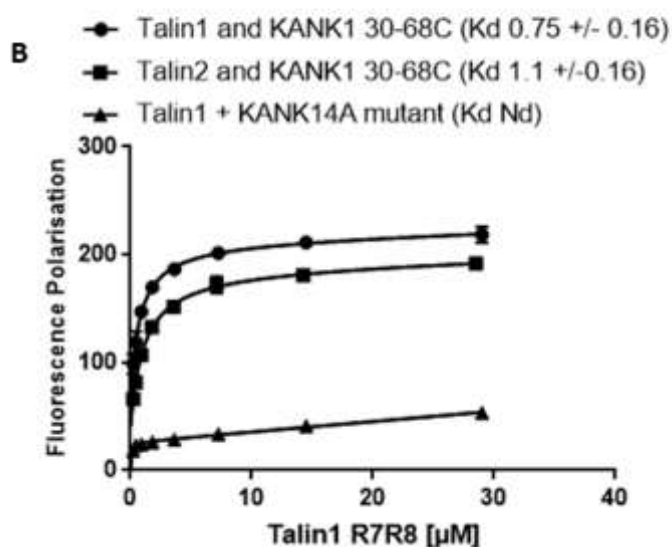


**FIGURE 4.16: KANK\_4A MUTANT PERTURBS BINDING TO TALIN**

(A) Alignment of KANK1 peptides used in FP assays green highlights LD-motif and red highlights mutation added to sequence. (B) Binding of BODIPY-TMR labelled KANK1 (30–68)C and KANK1\_4A (30-68)C peptides to talin1 R7R8 (1357–1653) and talin2 R7R8 (1360-1656). Dissociation constants  $\pm$  SE ( $\mu$ M) for the interactions are indicated in the legend. All measurements were performed in triplicate. ND, not determined.

#### 4.2.7.1 NMR analysis of the KANK1\_4A mutant

NMR was used to further investigate the effect of the KANK1\_4A mutation on talin:KANK binding and to look for the presence of weaker binding events that may not be detectable by FP. A  $^{15}\text{N}$  TROSY titration of  $^{15}\text{N}$  labelled talin1 R7R8 (residues 1357-1653) (black) shown in **FIGURE 4.17** with addition of KANK1\_4A 30-68C peptide (orange) and addition of KANK1 30-68C (blue). No shifts were observed with the addition of KANK1\_4A peptide confirming the absence of binding events. Interestingly, there was also no peak movement on the talin R8 residues when the KANK\_4A mutant was added unlike with the KANK 30-68C peptide, supporting the idea that the weak KANK1 binding to talin R8 is via its LD domain.

To further confirm the KANK\_4A mutant was effective, a  $^{15}\text{N}$  HSQC was carried out with the single R7 talin domain. **FIGURE 4.17** shows talin1 R7 (black) with KANK1 30-68 (blue) and KANK1\_4A 30-68 (orange) added. No shifts were observed when the KANK1\_4A mutant was added confirming that the KANK\_4A is an effective mutant to disrupt talin:KANK1 binding.



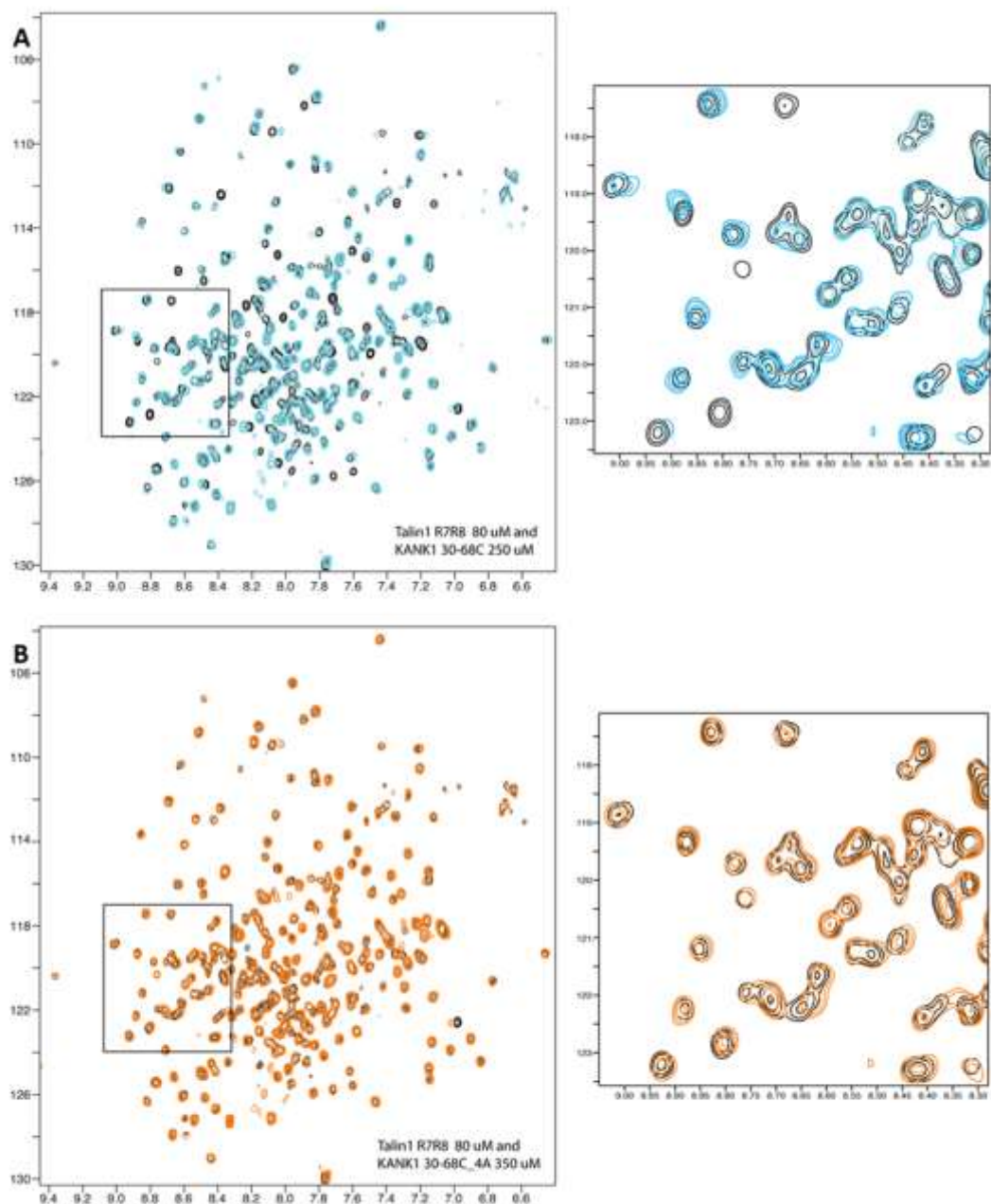


**FIGURE 4.17: KANK\_4A MUTANT PERTURBS BINDING TO TALIN1 R7R8**

(A)  $^1\text{H}$ ,  $^{15}\text{N}$  TROSY spectra of 80  $\mu\text{M}$   $^{15}\text{N}$ -labelled talin1 R7R8 (residues 1357–1653) in the absence (black) or presence of KANK1(30–68)C peptide (blue) at a ratio of 1:3. (B) Shows  $^1\text{H}$ ,  $^{15}\text{N}$  TROSY spectra of 80  $\mu\text{M}$   $^{15}\text{N}$ -labelled talin1 R7R8 (residues 1357–1653) in the absence (black) or presence of KANK1\_4A mutant peptide (orange) at a ratio of 1:4.

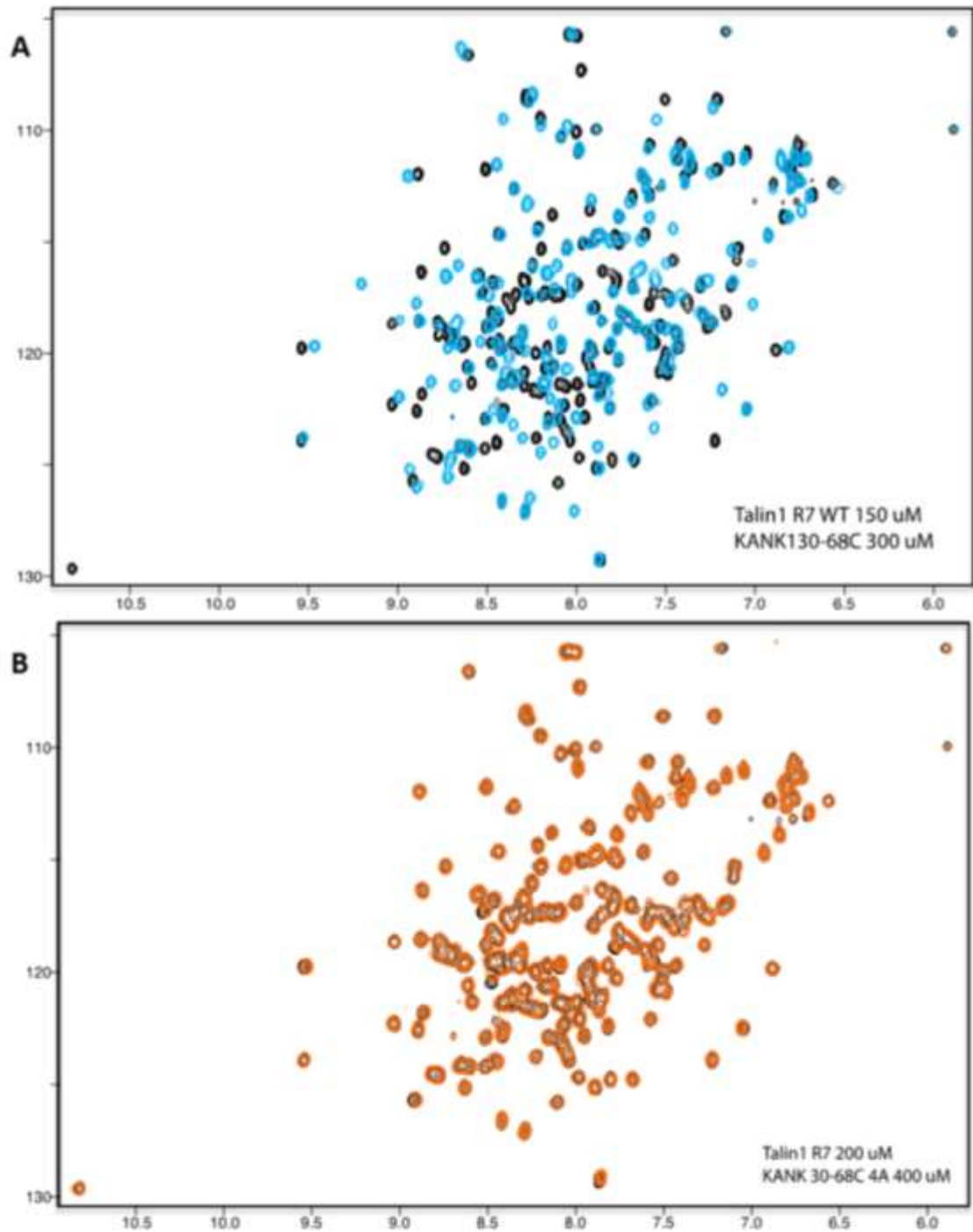


**FIGURE 4.18: KANK\_4A MUTANT PERTURBS BINDING TO TALIN1 R7**

(A)  $^1\text{H},^{15}\text{N}$  HSQC spectra of 150  $\mu\text{M}$   $^{15}\text{N}$ -labelled talin1 R7 (residues 1357–1659  $\Delta$ 1454-1586) in the absence (black) or presence of KANK1(30–68)C peptide (blue) at a ratio of 1:2. (B)  $^1\text{H},^{15}\text{N}$  HSQC spectra of 150  $\mu\text{M}$   $^{15}\text{N}$ -labelled talin1 R7 (residues 1357–1659  $\Delta$ 1454-1586) in the absence (black) or presence of KANK\_4A mutant (orange) at a ratio of 1:2.

#### 4.2.8 Designing talin1 R7 mutants to perturb the talin: KANK1 interaction

A major aim of the biochemical characterisation of the talin:KANK interaction was to design and validate mutations that perturb the interaction, so to be able introduce them into cells and ultimately animals, to explore the physiological role of the interaction. Having already designed a successful KANK\_4A mutant we wanted to design a point mutation on talin R7. The mutation needed to perturb the interaction between talin and KANK, but also maintain talins structural integrity so as not to perturb its mechanical properties or other interactions with adhesion proteins.

The distance between the talin R7 helices 29 and 36 (**FIGURE 4.19**) is larger than between other adjacent helices, both within R7 but also in other talin bundles. Helices 29 and 36 are separated by a distance of 8-10Å, compared to the other helices in R7 that are only 5-6Å apart. Analysis of the structure revealed that two residues, Trp1630 on helix 36 and Tyr1389 on helix 29, are the reason for this helix separation. These residues act as “molecular rulers” and fix the distance between the two talin helices. This is due to the large size of Trp and Tyr side chains forcing the talin helices apart.

The space between the two helices is enhanced further due to smaller residues Ser1400, Gly1404 and Ser1411 on helix 29 and Ser1637 and Ser1641 on helix 36 (**FIGURE 4.19**). These residues are located on the inner helical surfaces and their small side chains create two conserved pockets midway along the KANK1 binding site. We predict that these pockets create space for the KANK1 peptide to fit and allow KANK1 bulky hydrophobic residues to point in between the talin helices.

A key KANK1 residue that looks to be burying in between the talin helices is Tyr48. Our structural talin:KANK1 model shows the Tyr48 residue binding in the talin binding pocket described above. It looks as though when bound, the KANK1 Tyr48 residue is in close proximity to talin Gly1404. We therefore rationalized that if Tyr48 could be prevented from engaging R7 it might disrupt the talin:KANK1 interaction. To achieve this the talin Gly1404 residue was mutated to a leucine residue. Leucine residues have big side chains, we predicted that it would fill the gap between the two-talin helices and prevent Try48 from slotting into the helical groove **FIGURE 4.20**.

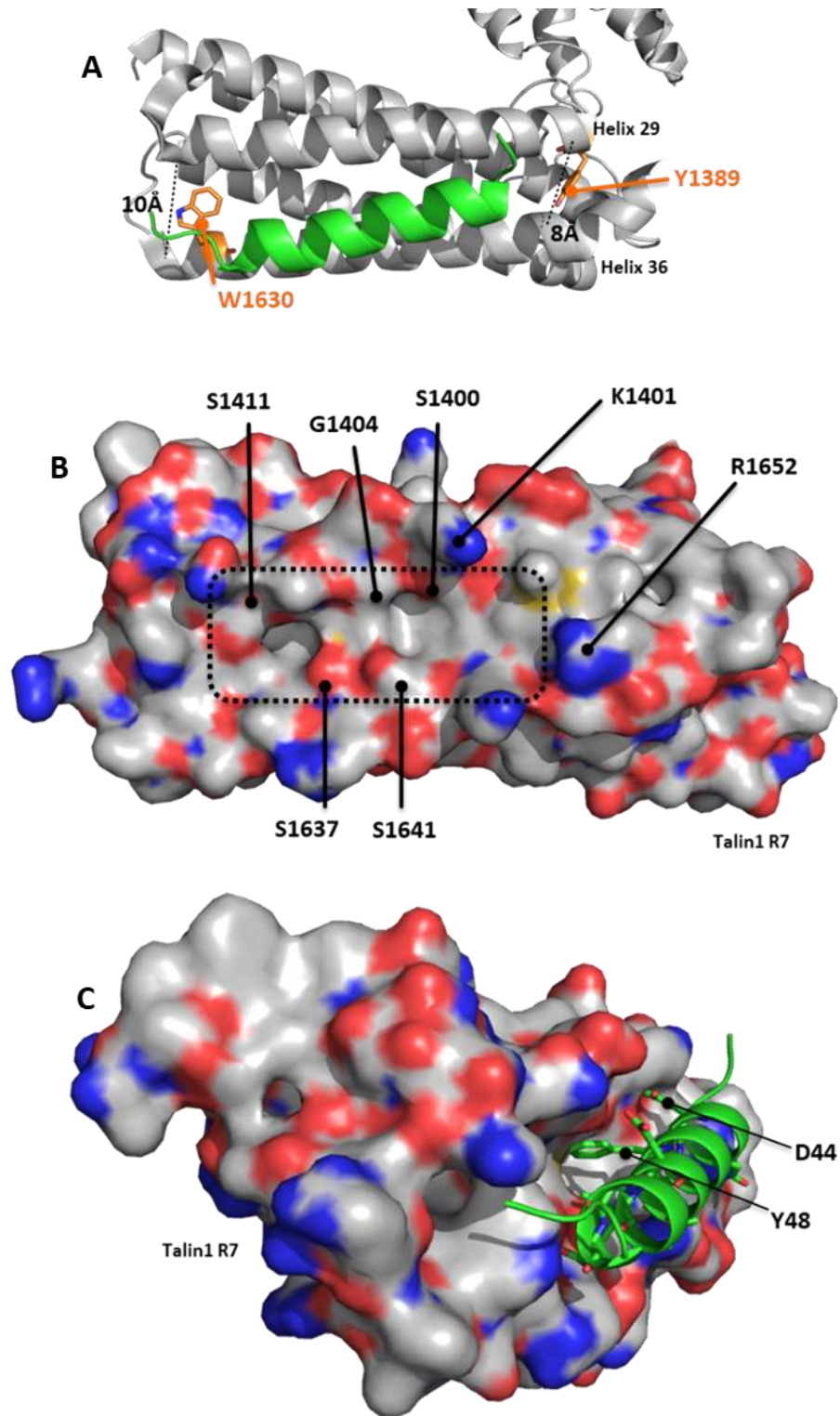


**FIGURE 4.19: STRUCTURAL ANALYSIS OF TALIN1 R7 TO DESIGN TALIN MUTANTS TO PERTURB KANK INTERACTION**

(A) KANK 30-60 peptide (green) binding to talin R7 highlighting the Tyr and Trp residues acting as molecular rulers and keeping helices 29 and 36 at a fixed distance apart. (B) Talin R7 helices 29 and 36 surface showing acidic residues (red) and basic residues (blue); black dotted box indicates the conserved pockets on the talin surface important for KANK binding. (C) Talin1 R7 surface with KANK 30-60 (green) peptide docked onto the side.

Additionally, on the opposite helix to Gly1404 (helix 36) is the residue Ser1641 (helix 29). Ser1641 was of particular interest as it was identified in the 2005 paper by Ratnikov *et al.* as a phosphorylation site on the talin R7 domain; this residue was predicted to be phosphorylated by CKII (casein kinase 2), PKC (protein Kinase C) and RSK (ribosomal S6 Kinase)(Ratnikov *et al.*, 2005). With the location of this phosphorylation site being close to the KANK binding site we hypothesized that phosphorylation of Ser1641 may serve as a kinase dependent regulation of talin:KANK binding. To further investigate this, a phosphomimetic mutant, S1641E was designed.

Lastly, a triple talin mutation was designed; Lys1401Glu, Lys1645Glu and Arg1652Glu (KKR). The KKR mutant replaced three positively charged residues is shown in **FIGURE 4.20**, the talin Lys1401 and Arg1652 residues are predicted to form salt bridges with KANK Asp42 and Asp44. Through mutating the positively charged talin residues to negatively charged Glutamates it was predicted to repel the KANK Asp and prevent the talin:KANK interaction.

These observations lead us to designing a series of talin1 R7 mutants:

- i. **G1404L** - Filling the gaps between helices 29 and 36 preventing KANK Tyr48 from binding into talin groove.
- ii. **W1630A** - Removing the 'molecular ruler' that is holding the two talin helices 29 and 36 apart.
- iii. **S1640E** - A phosphomimetic of the phosphorylation site.
- iv. **KKR (K1401E, K1645E and R1652E)** - Trying to disrupt electrostatic interactions between the KANK LD Asp42 and Asp44 residues binding to talin.

The mutants were introduced into talin1 R7R8 (residues 1357-1653) for protein solubility purposes as creating them in the R7 domain alone might be disruptive to the helical bundle and prevent appropriate folding of the protein. The constructs were cloned into apET-151 expression vector with a TEV cleavage site, to allow for removal of the HIS<sub>6</sub>-tag.



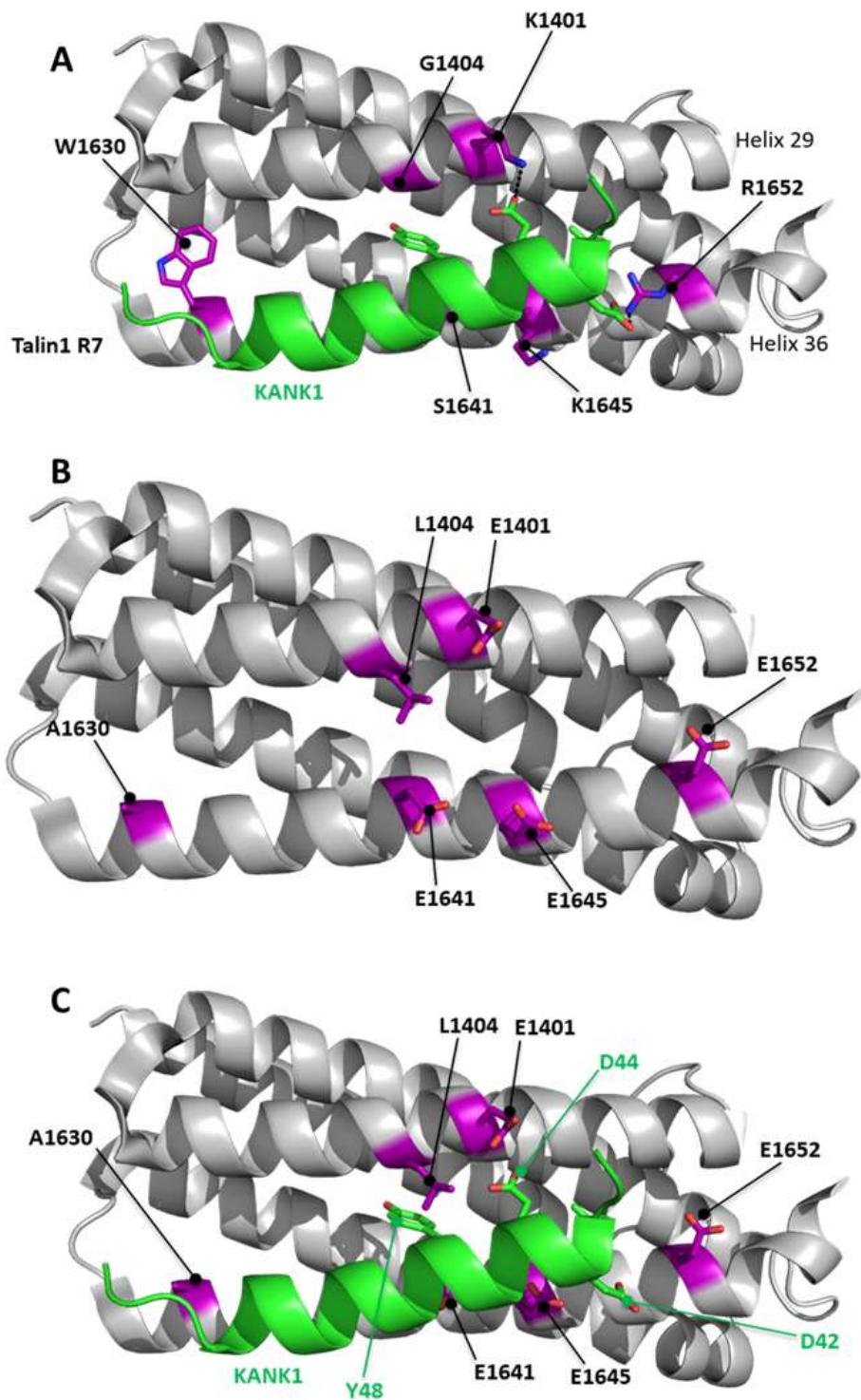


**FIGURE 4.20: STRUCTURAL ANALYSIS OF DESIGNED TALIN MUTANTS TO PERTURB KANK INTERACTION**

(A) Talin1 R7 bound to KANK1 indicating the talin residues selected for mutation to perturb the talin:KANK interaction. The salt bridges between Asp residues on KANK and talin Lys1401 and Arg1652 are indicated on the structure. (B) Talin1 R7 indicating the mutated talin residues for mutants; G1404L, S1641E, W1630A and KKR. (C) Talin1 R7 bound to KANK1 highlighting how talin mutants will affect talin:KANK interactions.

#### 4.2.9 Validating the structural integrity of the talin1 R7R8 mutants

The validation and analysis of the talin mutants is essential in ensuring that the domain integrity is not compromised by the modification, and a combination of techniques was used, including: NMR, CD and Nanoscale Differential Scanning Fluorimetry to assess this.

To determine the structural stability of the talin1 R7R8 mutants: G1404L, W1630A, S1640E and KKR, the proteins were recombinantly expressed and purified (gel shown in **FIGURE 4.21**). Thermal stability was measured using Nanoscale Differential Scanning Fluorimetry (Nano Temper Technologies GmbH) see materials and methods **Chapter 3**.

Thermal unfolding of R7R8 mutants was followed through changes in intrinsic fluorescence (ratio at 350/330 nm) as a function of temperature (temperature gradient from 20 to 90 °C) and plotted as shown in **FIGURE 4.21**. The maxima and minima of the first derivatives these curves were used as the midpoints ( $T_m$ ) of the thermal unfolding and the values are summarized in the table in **FIGURE 4.21**. Whilst *WT* talin1 R7R8 has a  $T_m$  of 47.6 °C, the thermal stability of the different mutants were mixed. W1630A had a similar unfolding temperature to the *WT*, indicating that this particular mutation had no major effect on the overall stability of the helical bundle. The G1404L mutation also had negligible effect on the stability of R7R8.

Intriguingly, the S1641E mutant appeared to stabilize the R7R8 domain, increasing the  $T_m$  to 50.3 °C. The KKR mutant, however, was surprisingly unstable in solution and appeared to undergo two unfolding events, the first being at 36.5 °C; this suggests that the KKR mutation may have disrupted the integrity of the domains and the separate unfolding events could represent the different talin domains unfolding: R7, where the mutation lies, could unfold at the lower temperature before the final unfolding of the R8 domain.

Protein aggregation midpoints were also calculated for all versions of the R7R8 domains, by measuring light scattering as a function of temperature – the values used represent the maxima or minima of the first derivatives of the scattering curves. Whilst most mutants had aggregation temperatures close to the *WT* R7R8 domain, the aggregation temperature for KKR mutant was much lower, confirming its instability and indicating that this would not be a useable mutant for either biochemical analysis or for cell work, as it wouldn't be stable and could affect more than the talin:KANK1 binding site.

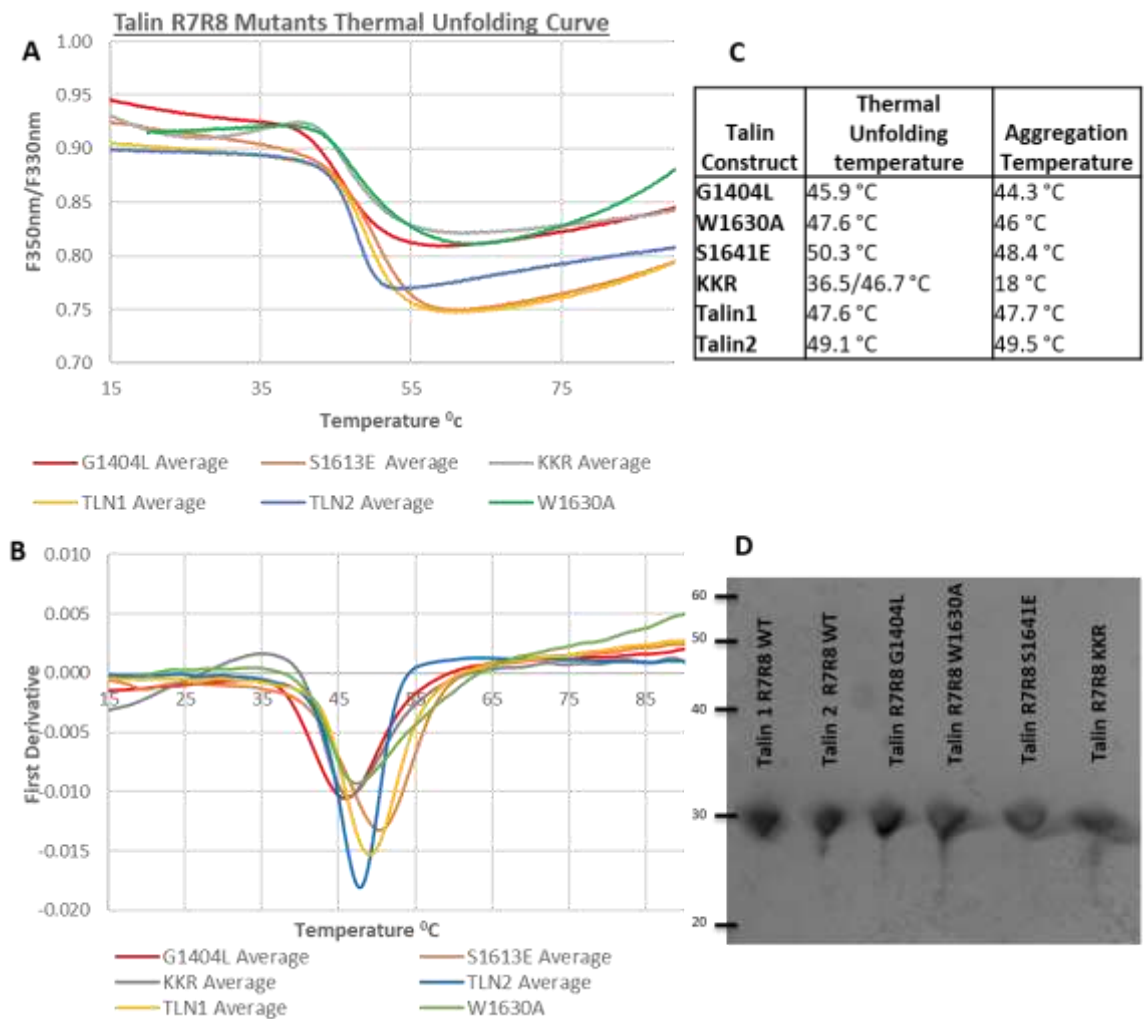


**FIGURE 4.21: THERMAL STABILITY OF TALIN R7R8 MUTANTS**

(A-B) Thermal stability of a series of talin R7R8 (1357-1653) constructs (Talin1, Talin2, S1641E, G1404L, W1630A and KKR) was determined. The unfolding temperature was calculated using the first derivative of thermal unfolding curves obtained using Prometheus NT.plex instrument (NanoTemper Technologies GmbH). (C) A table of all unfolding temperatures and aggregation temperatures, aggregation temperatures calculated from first derivative of scattering data. (D) SDS-page gel of all talin R7R8 constructs used in the thermal stability measurements.

#### 4.2.10 Measuring the binding affinity of KANK1 to the talin mutants

To determine if the talin mutants were effective in disrupting the talin:KANK interaction, the relative binding affinities of the talin mutants and the KANK1 30-68C peptide were measured using *in vitro* FP assays (**FIGURE 4.22**). The KANK1 30-68C peptide was coupled to the fluorescent label BODIPY-TMR and titrated with an increasing concentration of the talin1 R7R8 mutants.

The relative binding constant showed that the S1641E mutation had a small effect on the binding of KANK1 to talin with a measured  $K_D$  of 2.1  $\mu$ M compared to the talin1 R7R8 WT  $K_D$  0.5  $\mu$ M, suggesting that the proposed phosphorylation of the Ser1641 residue may be playing only a minor



role in regulating the binding of KANK1 to talin. However, this still represents a four-fold change in affinity, which may be of importance and it is also possible that the Glu1641 was not a sufficient phosphomimetic. In the cell, phosphorylation may have a larger effect on the R7 surface properties an effect that is not being mimicked completely by a single Glu substitution.

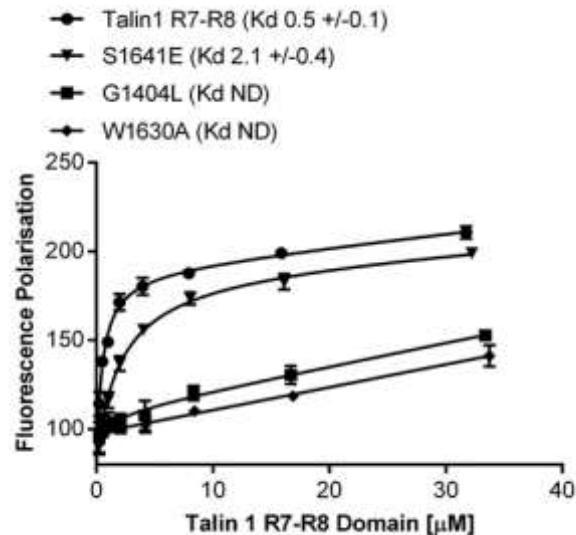


**FIGURE 4.22: TALIN R7R8 MUTANTS BINDING TO TALIN**

Binding of BODIPY-TMR labelled KANK1(30–68)C peptide to talin1 R7R8 (residues 1357–1653), talin1 R7R8 G1404L(residues 1357–1653), talin1 R7R8 S1641E (residues 1357–1653), and talin1 R7R8 W1630A (residues 1357–1653). Relative binding affinities were measured using fluorescence polarization and dissociation constants  $\pm$  SE ( $\mu\text{M}$ ) for the interactions are indicated in the legend. All measurements were performed in triplicate. ND, not determined.

The W1630A and G1404L mutations both had striking effects on the talin:KANK interaction, abolishing any binding and therefore a  $K_D$  could not be determined. This gives further confidence in the talin:KANK structural model we predicted, as it confirms the importance of the Gly1404 for the KANK1 Tyr48 to dock. G1404L and W1630A were taken forward for further biochemical analysis.

NMR was used to further validate the G1404L and W1630A mutants. Initially a  $^{15}\text{N}$  TROSY spectrum of talin1 R7R8 WT, G1404L and W1630A mutants were run and are shown in **FIGURE 4.23**. Each of the mutant spectra look well dispersed and similar to the R7R8 WT, indicating the R7 helical bundle has folded and is stable, supporting the thermal stability data.

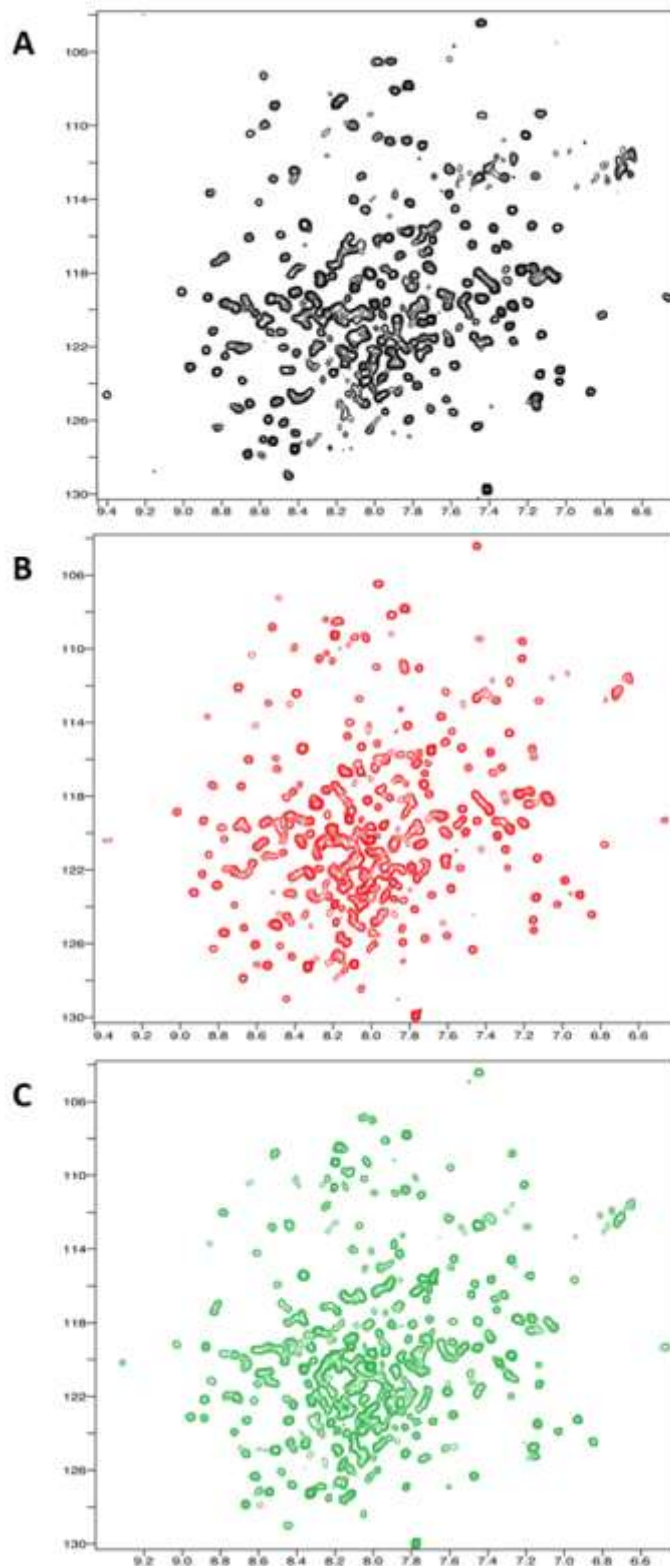


**FIGURE 4.23:  $^{15}\text{N}$  TROSY SPECTRA OF THE R7R8 TALIN MUTANTS**

(A)  $^1\text{H},^{15}\text{N}$  TROSY spectra of  $80\ \mu\text{M}$   $^{15}\text{N}$ -labelled talin1R7R8 (residues 1357–1653)(black).  $^1\text{H},^{15}\text{N}$  TROSY spectra of  $80\ \mu\text{M}$   $^{15}\text{N}$ -labelled talin1R7R8 G1404L (red) (residues 1357–1653).  $^1\text{H},^{15}\text{N}$  TROSY spectra of  $80\ \mu\text{M}$   $^{15}\text{N}$ -labelled talin1R7R8 W1630A (green) (residues 1357–1653)(black).

To look at the binding of KANK1 30-68C with talin1 R7R8 G1404L mutant a <sup>15</sup>N TROSY NMR titration (shown in **FIGURE 4.24**) of talin1 R7R8 (residues 1357-1653) (black) and talin1 R7R8 G1404L (black) were titrated against increasing concentrations of the KANK1 30-68C peptide (*WT* blue, G1404L red). The addition of the KANK1 30-68C peptide caused shifts in the *WT* R7R8 spectra consistent with binding occurring, however, there were also some small shifts in the G1404L mutant spectra. Further analysis showed these shifts could be mapped to the talin R8 domain, showing that the KANK1 peptide could still bind weakly to the talin1 R8 domain.

To further characterize the effects of the point mutations on R7 binding to KANK, the G1404L and W1630A mutations were introduced into the single talin1 domain R7 (1359–1653 Δ1454–1586), recombinantly expressed and purified. <sup>15</sup>N HSQC of talin1 *WT* R7, G1404L and W1630A were run to determine if the mutants affected the overall structure of the talin1 R7 domain. The spectra (G1404L red, W1630A green) shown in **FIGURE 4.25** confirm the mutations did not affect the folding of the five-helix bundle; the peaks were well dispersed and looked similar to the *WT* spectra (shown in black), although a number of residues shifted in the mutants in comparison to the *WT*, presumably close to the mutation site. The 2D NMR spectra nicely highlights the tryptophan mutation in W1630A - talin1 R7 only has one tryptophan residue and the indole peak from the tryptophan is not present in the W1630A spectra, as highlighted by a red circle in **FIGURE 4.25**.

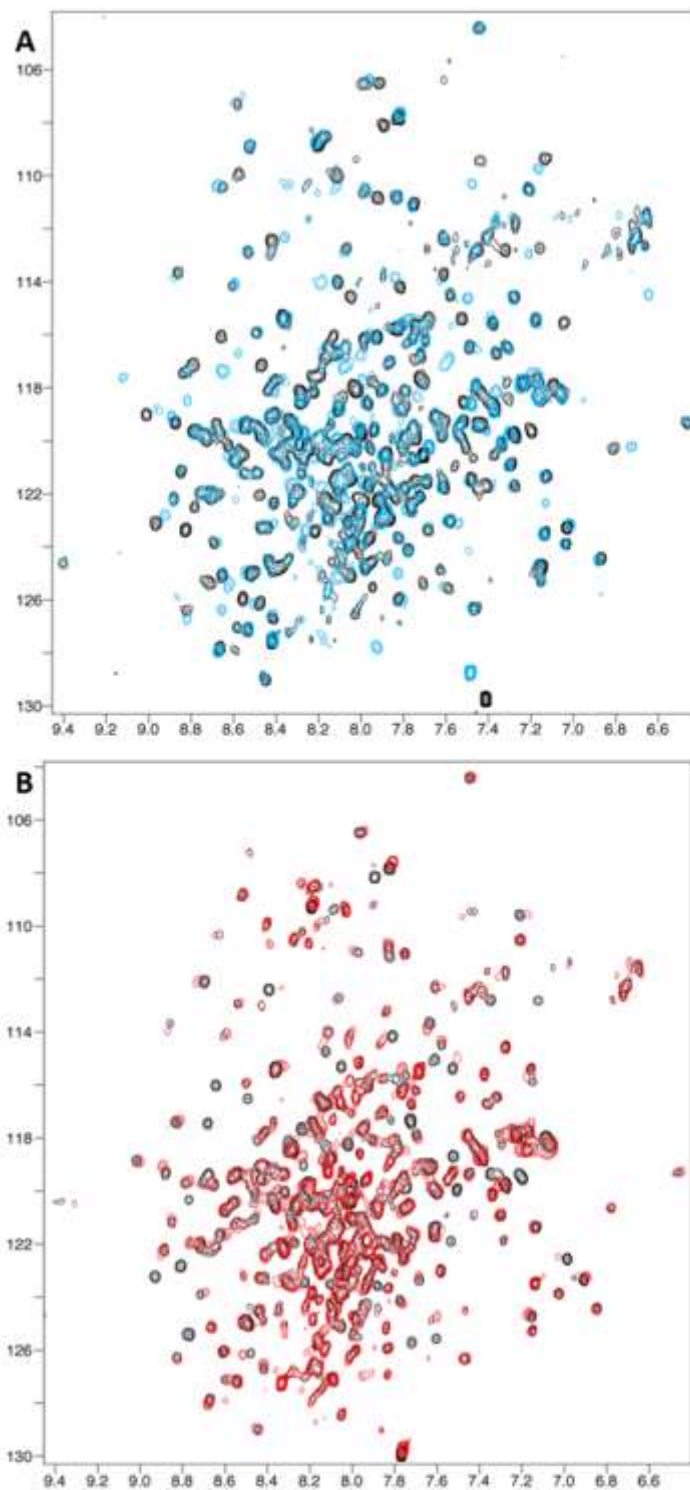


**FIGURE 4.24: TALIN G1404L MUTANT PERTURBS BINDING TO TALIN R7**

(A)  $^1\text{H},^{15}\text{N}$  TROSY spectra on the left  $80\ \mu\text{M}$   $^{15}\text{N}$ -labelled talin1 R7R8 (residues 1357–1653) in the absence (black) or presence of KANK1(30–68)C peptide (blue) at a ratio of 1:3. Right spectra shows  $^1\text{H},^{15}\text{N}$  TROSY spectra of  $80\ \mu\text{M}$   $^{15}\text{N}$ -labelled talin1 R7R8 G1404L mutant (residues 1357–1659) in the absence (black) or presence of KANK1(30–68)C peptide (red) at a ratio of 1:3.

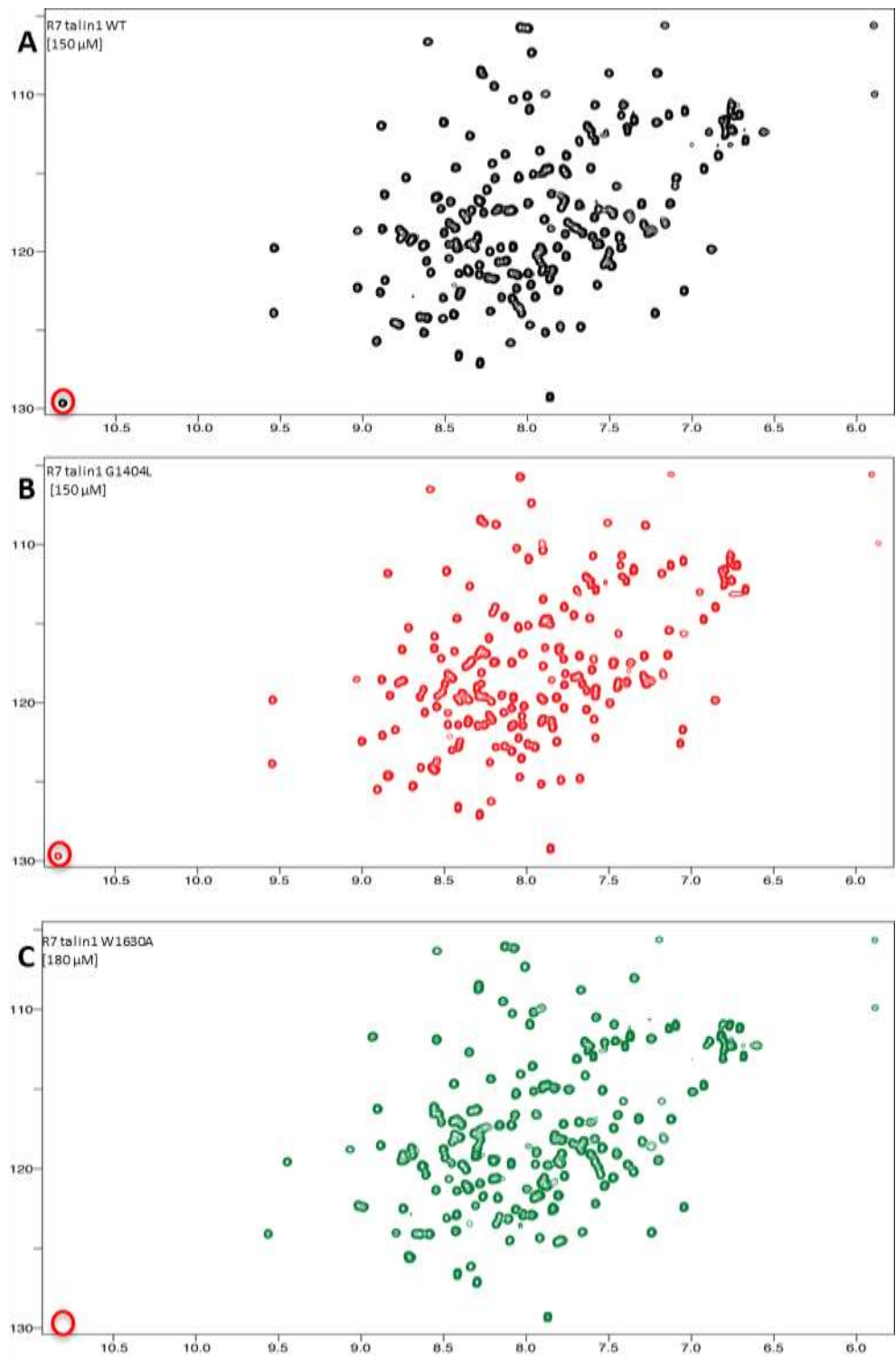


**FIGURE 4.25:  $^{15}\text{N}$  HSQC SPECTRA OF THE TALIN R7 MUTANTS**

(A)  $^1\text{H},^{15}\text{N}$  HSQC spectra  $80\ \mu\text{M}$   $^{15}\text{N}$ -labelled talin1 R7 (residues 1357–1653  $\Delta$ 1454-1586). (B)  $^1\text{H},^{15}\text{N}$  HSQC spectra  $80\ \mu\text{M}$   $^{15}\text{N}$ -labelled talin1 R7 G1404L (red) (residues 1357–1653  $\Delta$ 1454-1586). (C)  $^1\text{H},^{15}\text{N}$  HSQC spectra  $80\ \mu\text{M}$   $^{15}\text{N}$ -labelled talin1 R7 W1630A (green) (residues 1357–1653  $\Delta$ 1454-1586). Red circle indicates Trp1630 residue indol peak.

Having determined that the mutations do not affect the talin R7 structurally  $^{15}\text{N}$  titrations with talin1 R7 *WT*, G1404L and W1630A mutants and increasing amounts of KANK1 30-68C peptide were carried out and shown in **FIGURE 4.26**. The talin1 R7 *WT* peaks shifted when the KANK1 peptide was added, as previously shown, demonstrating the tight interaction between KANK1 and talin1 R7 *WT*. In contrast, the two talin mutants showed only very slight changes in their spectra when the KANK1 peptide was added (G1404L green, W1630A red), indicating lack of interaction. The presence of slight changes in the spectra for the R7 mutants with KANK1 are likely to represent weak residual interactions as NMR can detect very weak interactions down to the mM  $K_D$  range.

The NMR titrations do confirm that the talin G1404L and W1630A mutants successfully perturb the binding of KANK1 30-68C to the talin R7 domain.

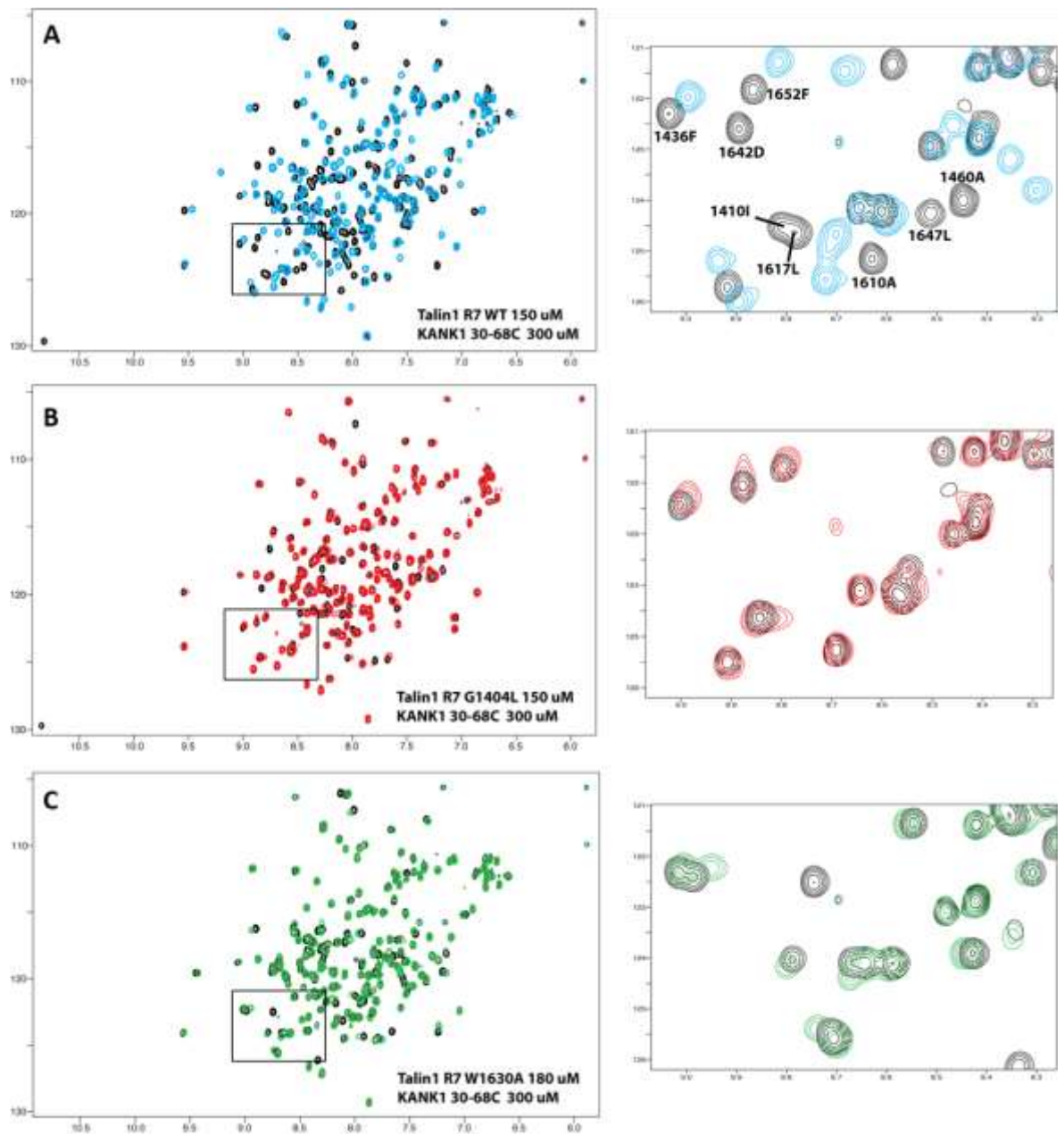


**FIGURE 4.26: TALIN R7 MUTANTS PERTURB BINDING TO KANK1**

**(A)**  $^1\text{H}$ ,  $^{15}\text{N}$  HSQC spectra: 150  $\mu\text{M}$   $^{15}\text{N}$ -labelled talin1 R7 (residues 1357–1653  $\Delta$ 1454-1586) in the absence (black) or presence of KANK1(30–68)C peptide (blue) at a ratio of 1:2. **(B)**  $^1\text{H}$ ,  $^{15}\text{N}$  HSQC spectra: 150  $\mu\text{M}$   $^{15}\text{N}$ -labelled talin1 R7 G1404L mutant (residues 1357–1653  $\Delta$ 1454-1586) in the absence (black) or presence of KANK1(30–68)C peptide (red) at a ratio of 1:2. **(C)**  $^1\text{H}$ ,  $^{15}\text{N}$  HSQC spectra: 180  $\mu\text{M}$   $^{15}\text{N}$ -labelled talin1 R7 W1630A mutant (residues 1357–1653  $\Delta$ 1454-1586) in the absence (black) or presence of KANK1(30–68)C peptide (Green) at a ratio of 1:2.

#### 4.2.11 Investigating talin binding to different KANK isoforms

All our initial experiments aimed to characterise the interaction between talin and KANK1. However, the proteomics data set (from fibroblast cells) for talin1, suggested that talin could also bind to KANK2. Therefore, we sought to test whether the other KANK isoforms were also capable of binding to talin. As described earlier **FIGURE 4.3**, all four isoforms of KANK have a KN domain. To predict whether they could bind to talin, human KANK isoforms were aligned to determine if the LD region was conserved; this is shown in **FIGURE 4.27**. When all four human isoforms were aligned, not all of the 30-68 residues that make up the KN domain were fully conserved. Only residues 30-60 were conserved across all four isoforms, shown in red on **FIGURE 4.27**, with KANK3 being the most divergent. KANK3 had 58% sequence homology to the KANK1 KN domain whereas KANK2 and KANK4 had 73% and 77% sequence homology (BLAST results), respectively, raising the question of whether KANK3 will bind more weakly than the other isoforms to talin.

Due to low conservation of residues 60-68 across all KANK isoforms I wanted to determine if residues 60-68 (shown in blue on **FIGURE 4.27**) were important for talin binding. To achieve this a shorter KANK1 KN peptide, with only residues 30-60, was designed shown in **FIGURE 4.28**. The relative binding affinities of KANK1 30-60c and KANK1 30-68C to talin R7R8 were measured, using the *in vitro* FP assay. The KANK1 30-60C peptide coupled to the fluorescent label BODIPY-TMR, was titrated with an increasing concentration of the talin1 R7R8. The results are shown in **FIGURE 4.28**; there was not a noticeable difference in relative affinities between KANK1 30-60 and KANK1 30-68C, revealing that the 60-68 residues do not play a major role in the talin interaction.

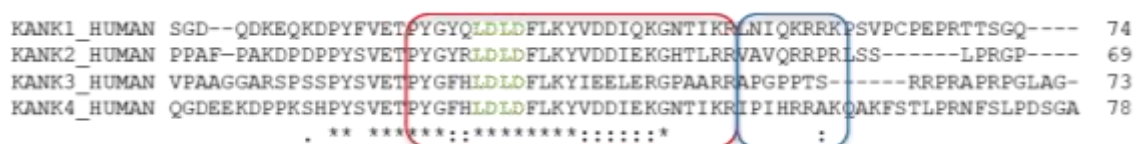
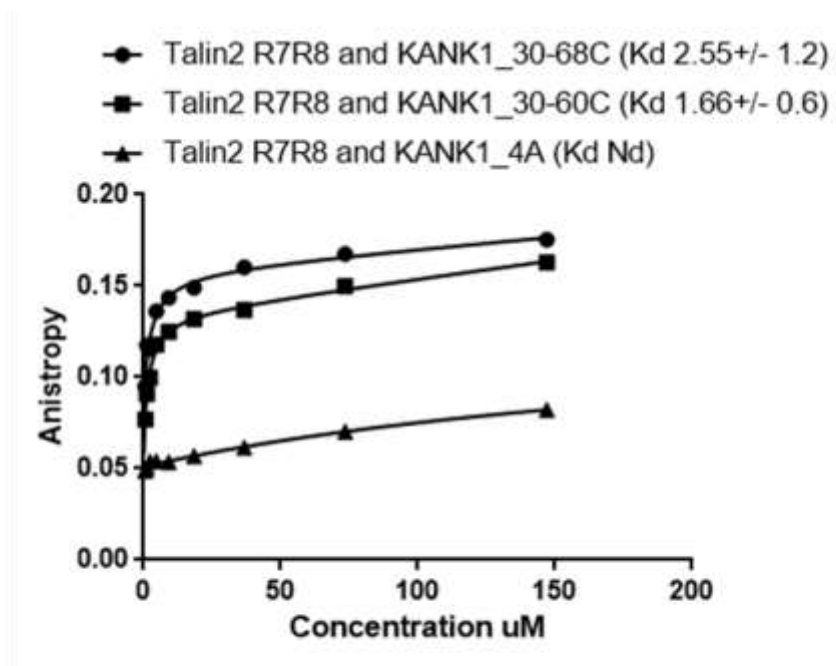


**FIGURE 4.27: KANK KN DOMAIN ALIGNMENT**

Alignment of Human KANK proteins (KANK1 Q14678, KANK2 Q63ZY3, KANK3 Q6NY19, KANK4 Q5T7N3) LD residues highlighted in green. Conserved residues are highlighted by a \*, similar property amino acids are shown by a :. Red box indicates the region highly conserved 30-60 residues across all four KANK isoforms and the blue box indicates region the 60-68 residues not well conserved across the four isoforms.





**KANK1 30-68C:** PYFVETPYGFQ**LDLD**LVKYVDDIQKGNTIKKLNIQRRKC  
**KANK1 30-60C:** PYFVETPYGFQ**LDLD**LVKYVDDIQKGNTIKKC

**FIGURE 4.28: CHARACTERISING THE KANK1 KN DOMAIN BOUNDARY**

Binding of BODIPY-TMR labelled KANK1(30–68)C and KANK1 (30-60)C peptides to talin2 R7R8 (1360-1656). Dissociation constants  $\pm$  SE ( $\mu$ M) for the interactions are indicated in the legend. All measurements were performed in triplicate. ND, not determined.

As residues 30-60 are highly conserved across the isoforms of KANK, narrowing down the TBS on KANK1 to residues 30-60 strongly suggested that the other isoforms of KANK may also bind talin. To determine if the other KANK isoforms could bind to talin R7R8 via the KN domain, synthetic peptides of the other KANK isoform KN domains were designed, encompassing the '30-60' residues of KANK1 as shown in **FIGURE 4.29**.

Relative binding affinities of the different KANK isoforms (KANK1 30-60, KANK2 31-62, KANK3 32-62 and KANK4 24-54) and talin1 and 2 R7R8 were determined using FP assays, and the results are shown in **FIGURE 4.29**. It is apparent that all the four KANK KN domains can bind to talin1. KANK1 and KANK2 have similar binding affinities to both talin isoforms, whereas KANK4 shows a stronger affinity to talin2 than talin1. KANK4 24-54 bound to talin1 with a  $K_D$  2.55  $\mu$ m and talin2 with a  $K_D$  of 0.6  $\mu$ m. The measured  $K_D$  of KANK3 and talin1 R7R8 was 1  $\mu$ m the same affinity as KANK1 and talin1. It was unexpected that the KANK3 binding affinity was same as KANK1 due to the biggest sequential difference was between KANK1 and KANK3. The similarity in binding highlights the importance of the LD-motif in the talin:KANK interaction.

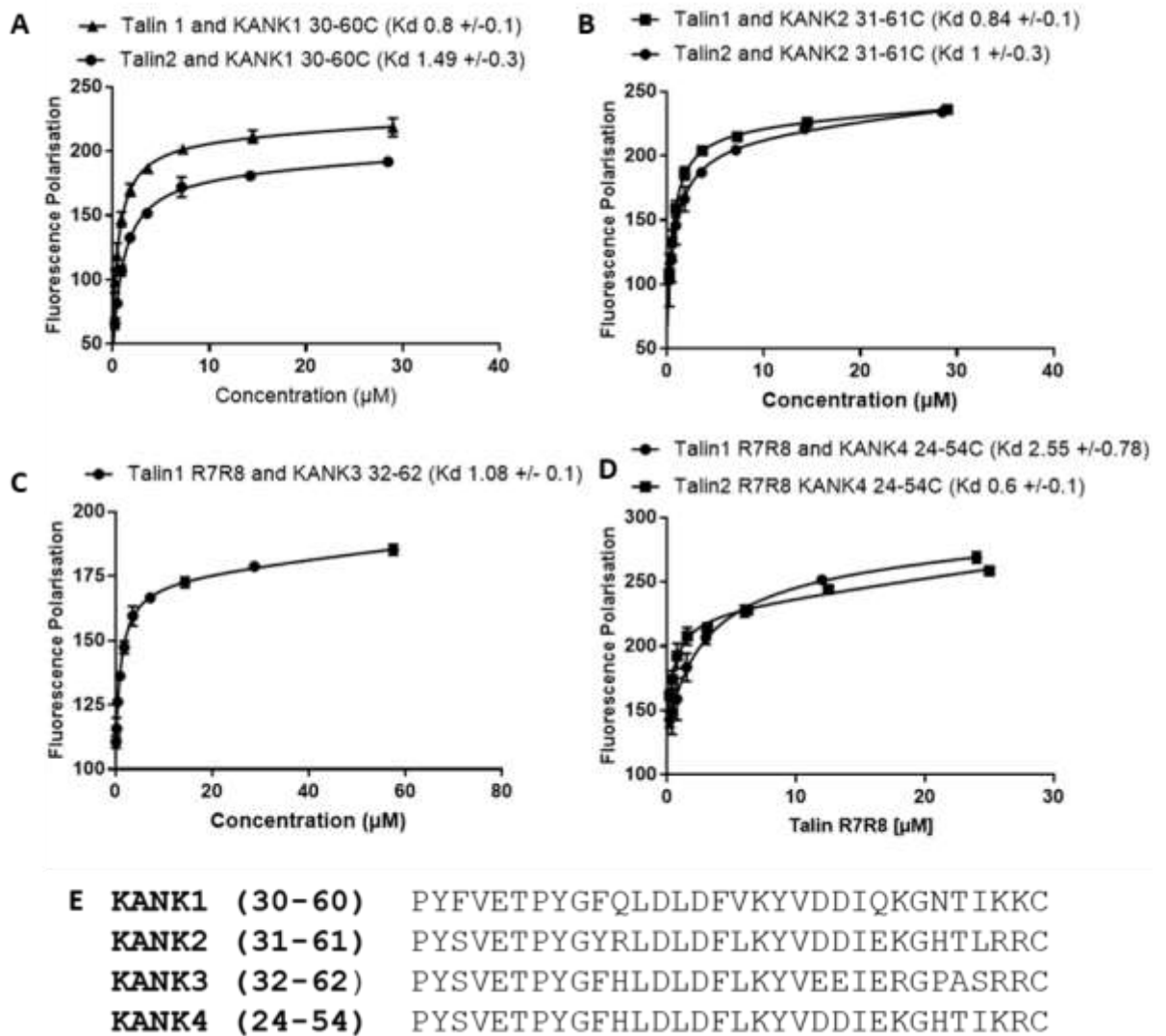


**FIGURE 4.29: CHARACTERISING KANK ISOFORMS 1-4 BINDING TO TALIN1 R7R8 AND TALIN2 R7R8**

(A-D) Binding of BODIPY-TMR labelled KANK1(30-60)C, KANK2(31-61)C, KANK(32-62)C and KANK4(24-54)C peptides to talin1 R7R8 (1357-1653) and talin2 (1360-1656) measured using fluorescence polarisation. Dissociation constants  $\pm$  SE ( $\mu$ M) for the interactions are indicated in the legend. All measurements were performed in triplicate. ND, not determined. (E) Alignment of KANK1-4 peptides used in assay.

#### 4.2.12 Does the binding of KANK to talin R7 increase thermal stability?

Our structural model of talin:KANK shows KANK1 binding to the talin R7 domain through a helix-addition interaction, where the KN domain peptide packs on the side of R7 between helices 29 and 36. This would imply that, when KANK1 is bound to R7 (a five-helix bundle) it would become like a six-helix bundle. In literature there is little evidence of six-helix bundles in nature other than those found in virus proteins such as HIV (Hu *et al.*, 2012).

We know that talin is a mechanosensitive protein and if enough force is applied then the talin R7R8 domain can be unfolded and the helical bundle formation is lost (Yan *et al.*, 2015; Yao *et al.*, 2016). If the talin R7 bundle is unfolded by force, then the KANK1 binding site would be lost and KANK1 would no longer be able to bind to talin. Does KANK1 binding to talin increase the stability of bundles and prevent their unravelling, by reducing susceptibility to force?

To begin to address this question we initially looked at the thermal stability of talin R7R8 domain with both KANK1 and KANK2 30-60C peptides. Although thermal stability does not directly link to mechanostability it would give an indication of whether KANK binding was altering the talin R7R8 domains. Thermal unfolding was measured using the Prometheus software and the results are shown in **FIGURE 4.30**. For both KANK1 and KANK2 peptides, binding to talin increases the thermal stability of talin1 and talin2 R7R8 domains;  $T_m$  values in talin1 and KANK2 were increased by 10 °C, compared to talin1 R7R8 on its own.

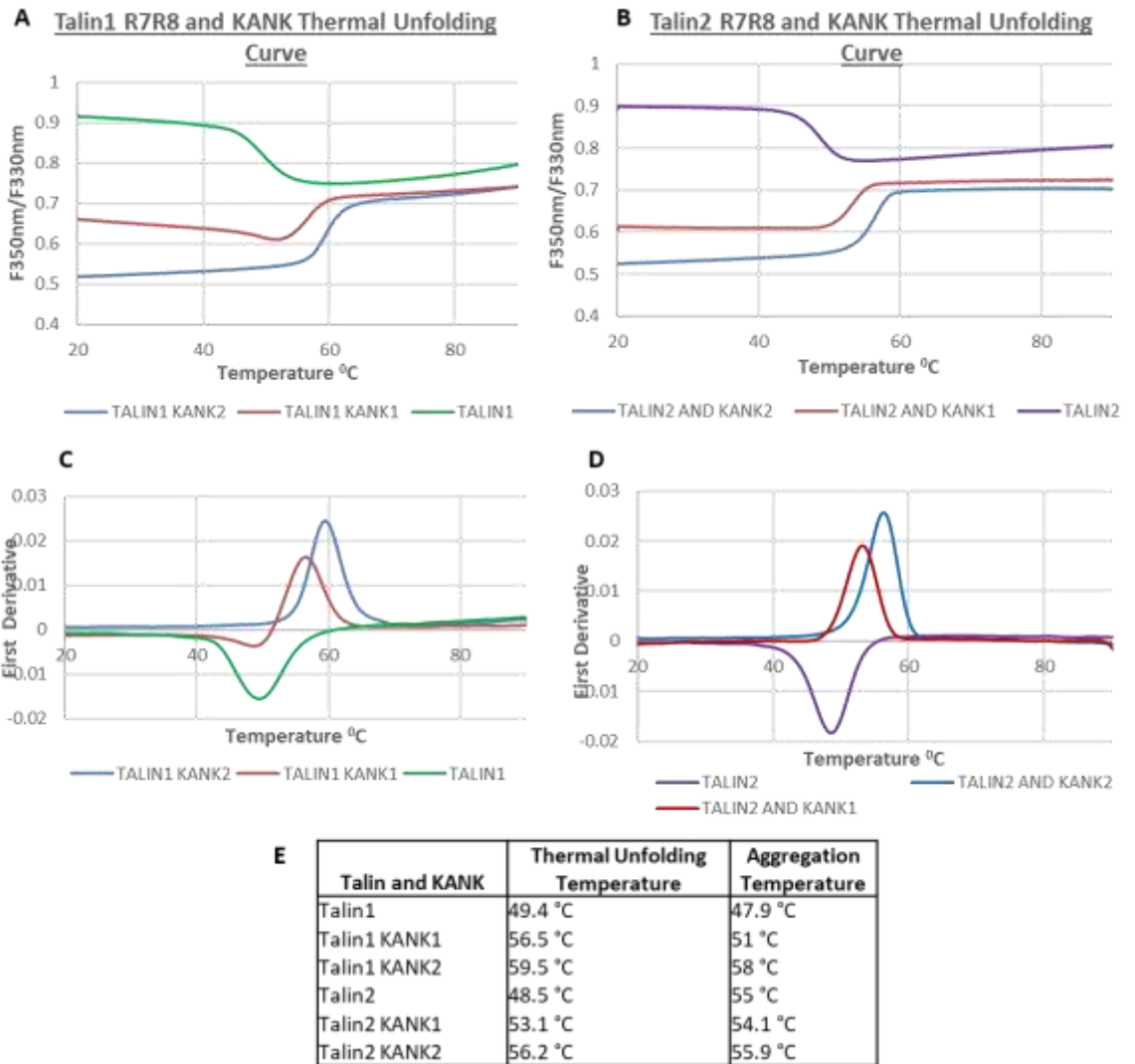


**FIGURE 4.30: KANK EFFECTS STABILITY OF TALIN HELIX**

(A-B) 141  $\mu$ M Talin1 R7R8 and Talin2 R7R8 thermal stability measured in the presence and absence of KANK1 and KANK2 (150  $\mu$ M) peptides. (C-D) The unfolding temperature was calculated using the first derivative of thermal unfolding curves obtained using Prometheus NT.plex instrument (NanoTemper Technologies GmbH). (E) A table of all unfolding temperatures and aggregation temperatures. Aggregation temperatures calculated from first derivative of scattering data.

### 4.2.13 Can KANK influence the interaction between talin and actin?

As mentioned in the introduction (**Chapter 2**) talin has three actin binding sites; ABS1, ABS2 and ABS3, which all play different roles in adhesions (Atherton *et al.*, 2015). ABS2 is positioned across talin domains R4 and R8 (shown **FIGURE 4.31C**) at the centre of the talin rod and provides the tension-bearing actin connection which has been found to be crucial for focal adhesion maturation and generating maximum traction force (Atherton *et al.*, 2015; Kumar *et al.*, 2016).

Talin ABS2 is present in both talin isoforms and the main binding surfaces for actin have been narrowed down in previous actin pull-down experiments, showing R4 and R8 domains to be the key helical bundles involved in the interaction (Atherton *et al.*, 2015). Both R4 and R8 domains have atypically high isoelectric point (pI) values, compared with the other talin rod domains, causing the surface of these domains to be positively charged at physiological pH. A positive binding surface enables the domains to form an interaction with the negatively charged actin; these high pI values are also shown on the actin binding helices in ABS1 and ABS3 (Atherton *et al.*, 2015).

The R7 domain is only weakly involved in actin binding but is crucial in correctly positioning the R8 domain in the ABS2 site. Since we show that KANK binds weakly to the R8 helical bundle, we questioned whether KANK binding to talin R7R8 could have an overall effect on the affinity of actin to talin ABS2.

To observe the effects that KANK had on the interaction between actin and talin1 ABS2, a series of actin pull-down experiments were carried out using talin1 R4R8 (residues 913-1580), filamentous actin and KANK1 30-68C peptide. Initially the percentage of actin pulled down with talin1 ABS2 was measured (see materials and methods **Chapter 3**) and visualised using SDS PAGE. Image J was used to measure grey-scale value of the talin bands in the pellet and supernatant (Rueden *et al.*, 2017). The intensities were converted into a percentage of overall talin in the supernatant and pellet and are shown above the band on the gel in **FIGURE 4.31**.

The difference in talin R4R8 co-sedimentation with actin, compared to KANK:talin R4R8 co-sedimentation with actin was measured and is shown in **FIGURE 4.31**. The KANK1 30-68C peptide is 3 kDa in molecular weight so could not be visualized on an SDS-PAGE gel. The experiment was carried out in triplicates and a re-producible difference in the amount of talin in the actin pellet when KANK1 was present compared to when it was absent is noticeable. More talin was pulled-down when KANK1 was present 41% compared to 29%.

The increased amount of talin in the pellet, when KANK1 is present, could be due to KANK1 binding the talin1 R7 domain and opening up the R7R8 structure allowing the R8 domain to be in a more open confirmation to bind actin. The negative effect on talin:actin binding predicted if KANK bound to talin R8 was not seen, this could be due to not enough KANK1 being added, saturation of the R7 domain had not been reached meaning that there was no KANK1 bound to talin1 R8.

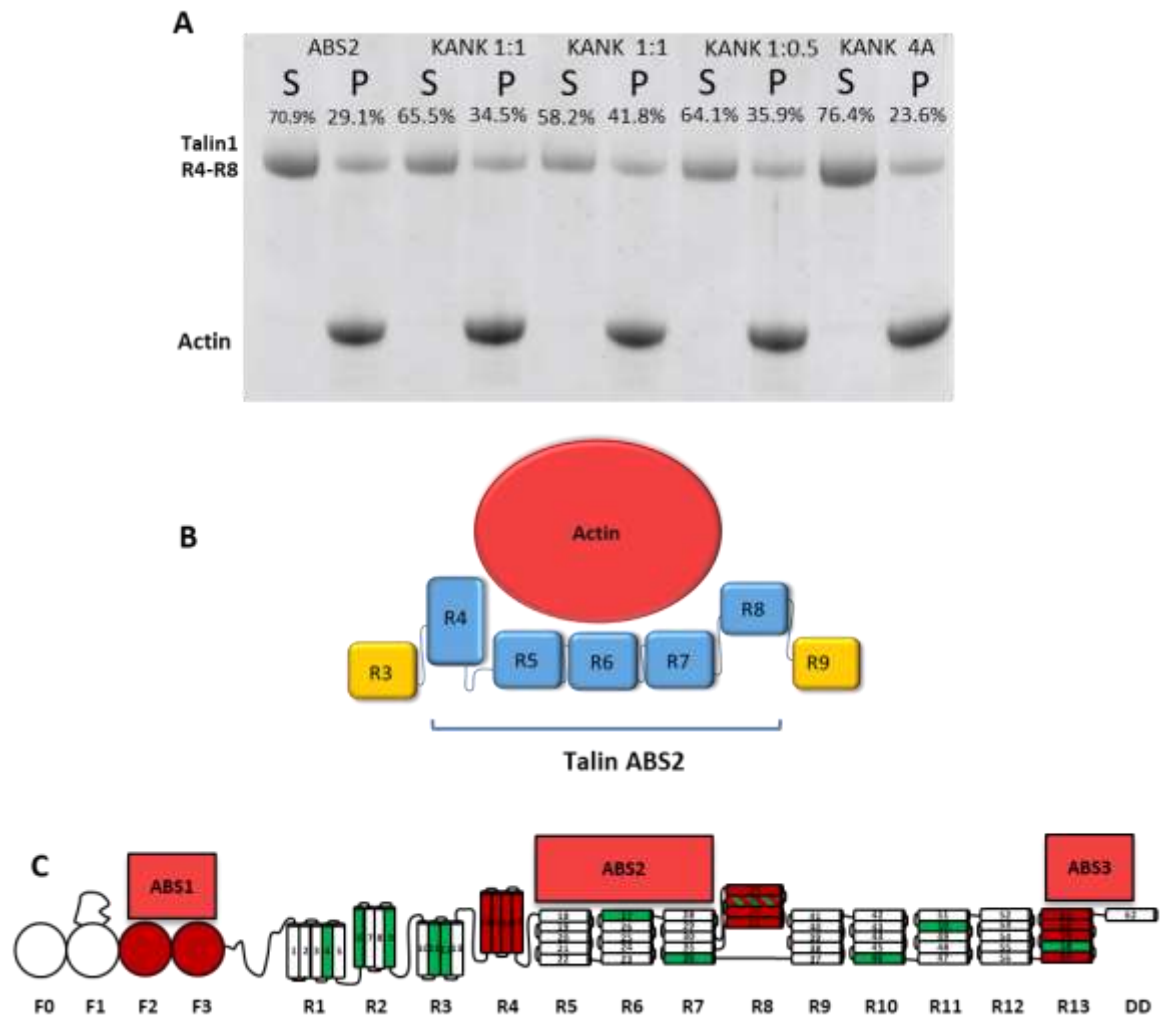


**FIGURE 4.31: TALIN1:KANK1 INTERACTION INCREASES ACTINS AFFINITY TO TALIN ACTIN BINDING SITE 2**

**(A)** Recombinant talin domain ABS2 (residues 913-1580) was incubated with F-actin and KANK1 peptide, actin was then pelleted and the supernatant (S) and pellet (P) were analysed via SDS-PAGE, the percentage of talin found in either the S or P is shown above the band. Actin co-sedimentation assay shows that actin binding to ABS2 is increased when KANK 30-68C peptide is present. **(B)** A schematic of talin actin binding site 2, blue highlights bundles involved in the interaction and yellow shows neighbouring domains. **(C)** A full length talin schematic highlighting the three talin actin binding sites ABS1-ABS3 across the protein, green helices represent vinculin binding sites.

## 4.3 Testing the physiological role of KANK mutants in a cellular context

Having designed and biochemically characterised both a successful KANK mutant (KANK\_4A) and a talin mutant (G1404I and W1630A) to perturb the talin:KANK interaction it was paramount to next understand the significance the talin:KANK interaction in conjunction with the rest of the cell. In order to achieve this our collaborator Anna Akhmanova from the University of the Utrecht carried out cellular experiments using our designed talin and KANK1 mutants. The following sections describe the cell biology results generated with the reagents generated in this chapter.

### 4.3.1 Characterisation of KANK1\_4A mutant in mammalian cells

In collaboration with Anna Akhmanovas' group, the KANK\_4A mutant was transfected into mammalian HEK293T cells to explore the importance of the talin:KANK interaction within the cell. The Utrecht group also generated: a full-length KANK1  $\Delta$ coiled-coil ( $\Delta$ CC), a  $\Delta$ coiled-coil\_4A ( $\Delta$ CC\_4A) and a KN domain 4A (KN\_4A). The  $\Delta$ CC mutant corresponds to the coiled-coil region of KANK1, designed to test if KANK1 requires binding to liprin  $\beta$ 1 in order for the KN domain to bind to talin. The hybrid mutant  $\Delta$ CC\_4A was designed with both the coiled-coils missing and the 4A mutation in the KN domain incorporated.

To determine if the KANK1 mutants perturbed the talin1:KANK1 interaction bioGFP-tagged: KANK1 *WT*, KANK\_4A,  $\Delta$ CC,  $\Delta$ CC\_4A and KN\_4A constructs were co-transfected with GFP-talin1 into HEK293T cells. Streptavidin pulldown assays were performed, as shown in **FIGURE 4.32**, and these showed that both the KANK1\_4A and the KN\_4A mutants reduced the interaction between KANK and talin1. This corroborated my biochemical finding that the KANK\_4A mutant disrupted the interaction between talin and KANK. Whilst the  $\Delta$ CC mutant did not appear to affect the talin:KANK interaction, the  $\Delta$ CC\_4A mutant had a stronger inhibitory effect than the full length 4A mutant on its own. The deletion of the coiled-coil region in the  $\Delta$ CC\_4A mutant prevented KANK1 from localising to the cell cortex and binding to liprin  $\beta$ 1, which can account for the difference observed between this form of the protein and the KANK\_4A mutant.

To investigate effects of the different mutations on KANK1's localisation in the cell, HeLa cells were depleted of endogenous KANK1 and KANK2 using siRNA. KANK1 and KANK2 were targeted, as they were the two isoforms the Utrecht group found to be present in HeLa cells in previous proteomic studies (van der Vaart *et al.*, 2013). Rescue experiments were performed with GFP-KANK1 *WT* and

mutants. **FIGURE 4.32B** shows images taken using total internal reflection fluorescence microscopy (TIRFM) live imaging. The FL-KANK1 *WT* strongly accumulates in cortical patches that cluster around the edge of FAs, as expected. However, this clustering is absent when cells are transfected with the FL-KANK1\_4A and instead KANK1 is dispersed throughout the cell cortex. Whilst the  $\Delta$ CC mutant of KANK1 localised almost entirely around FAs in the shape of tight rings, the  $\Delta$ CC\_4A mutant was completely dispersed around the cell with no localisation to FAs or the cell cortex. For the KN domains, the *WT* version localised to focal adhesions but did not accumulate around the edge of FA assemblies; instead, it entered into focal adhesion assemblies, possibly due to the small size of the domain. The KN\_4A mutant, however, was completely diffused across the cell.

The KANK1 mutants provided further evidence that the KANK1 KN domains interaction with talin provides an essential link for KANK1 to be recruited to focal adhesion assemblies. The different KANK1 mutations also highlighted the importance of the different KANK domains. They showed that the coiled-coil region is essential for KANK to accumulate in the cell cortex, where it interacts with liprin  $\beta$ 1, and that the KN domain is critical to create a link with talin and cluster KANK around the focal adhesions.



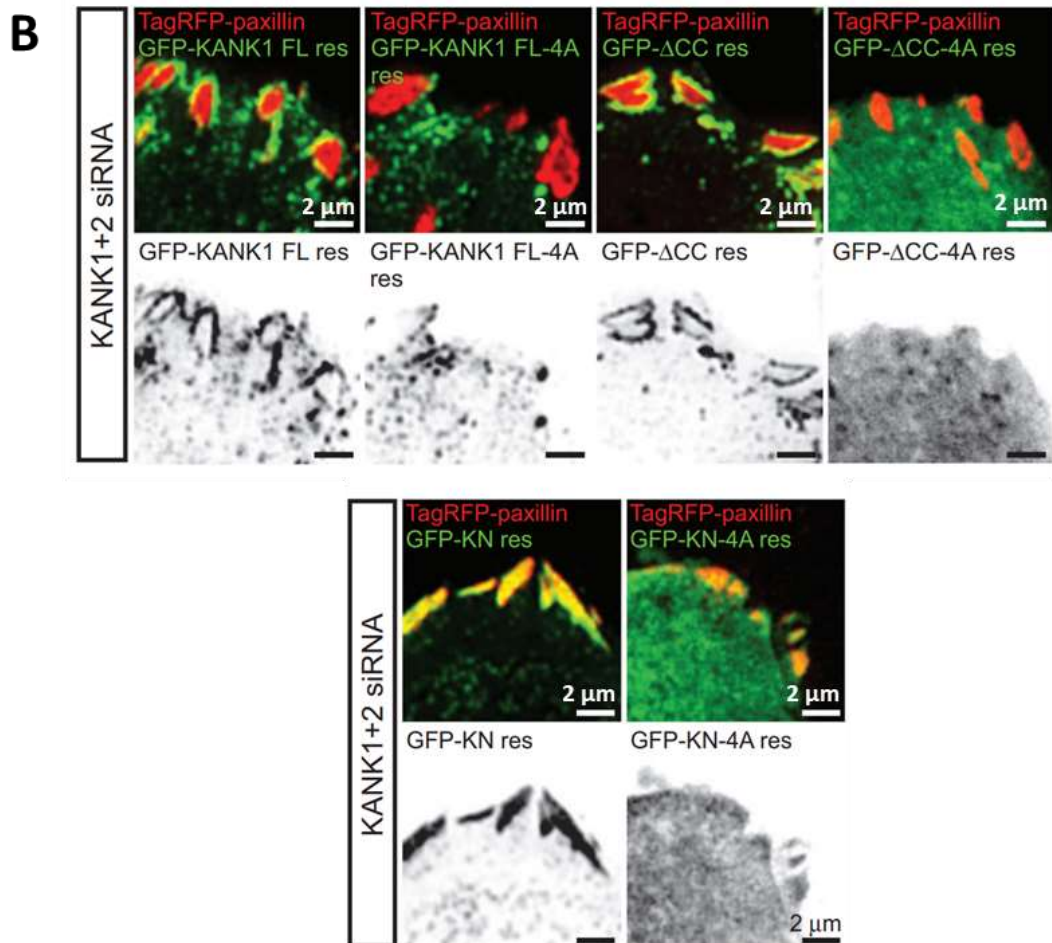
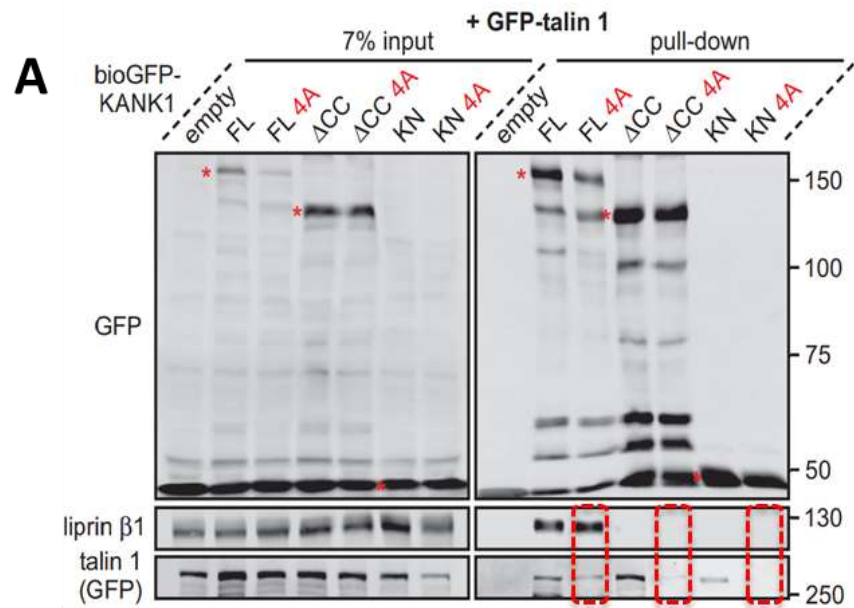


**FIGURE 4.32: CHARACTERISATION OF KANK LOCALISATION IN MAMMALIAN CELLS**

(A) Streptavidin pull-down assays with the BioGFP-tagged KANK1 or the indicated KANK1 mutants, co-expressed with GFP-talin1 in HEK293T cells, analysed by Western blotting with the indicated antibodies. (B) TIRFM images of live HeLa cells depleted of KANK1 and KANK2 and co-expressing the indicated siRNA-resistant GFP-KANK1 fusions and TagRFP-paxillin. Data from (Bouchet *et al.*, 2016).

### 4.3.2 Characterisation of talin1 G1404L mutant in mammalian cells

Our biochemistry data identified two talin1-R7 point mutants that could abrogate the talin1:KANK1 interaction: W1630A and G1404L. To further our understanding of talins' role in recruiting KANK1 to focal adhesion assemblies one of the talin mutants was chosen for transfection in mammalian cells.

Biochemically both the W1630A and G1404L mutations perturbed talin binding to KANK. However, for the cellular studies G1404L was chosen over W1630A. G1404L changes the talin binding surface and not the domain structure whereas, removal of Trp1630 would remove the 'molecular ruler' that is holding apart the two talin helices making up the KANK binding site; this structural change could have an off target effect of disrupting the mechanostability of the talin R7 domain, which is known to be important for protecting talin R8 from force induced extension (Yao *et al.*, 2016).

#### 4.3.2.1 Does the G1404L mutant effect focal adhesion formation?

To determine if the G1404L talin mutant had any off-target effects on focal adhesion formation or maturation, the Akhmanova lab used HeLa cells and depleted them of both endogenous talin1 and talin2 before rescuing with mouse GFP-talin1 or the GFP-talin1\_G1404L mutant. The depletion of talin1 and talin2 resulted in near total loss of FAs and caused detachment from coverslips, which supports the well-established role of talin1 in focal adhesion formation (del Rio *et al.*, 2009; Calderwood, Campbell and Critchley, 2013; Yao *et al.*, 2014; Yan *et al.*, 2015). Therefore, only cells expressing the GFP-talin1 could be imaged, since they exhibit normal attachment and spreading. **FIGURE 4.33A** shows HeLa cells expressing GFP-talin1 and GFP-talin1-G1404L. **FIGURE 4.33B-D** also show that talin-G1404L can fully support normal cell attachment and spreading. Further the number or size of focal adhesions is not significantly different between talin1 *WT* and G1404L. This leads to the conclusion that the talin1 G1404L point mutation did not interfere with talins' functional role in FA formation.

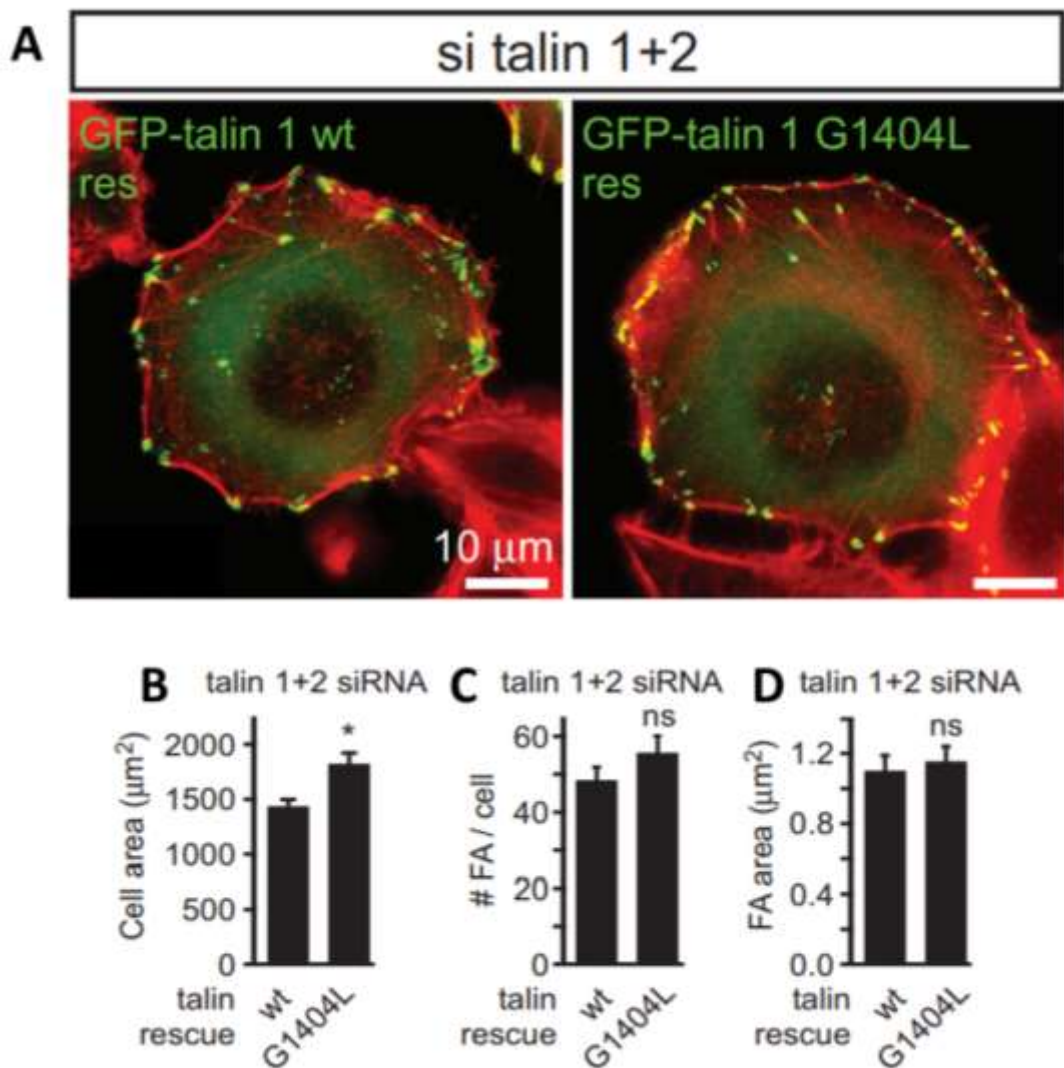


**FIGURE 4.33: G1404L TALIN1 MUTANT DOES NOT AFFECT TALINS ABILITY TO FORM FOCAL ADHESIONS**

(A) Fluorescent F-actin staining (red) in HeLa cells co-depleted of talin1 and talin2 transfected with the indicated GFP-talin1 fusions. (B) Cell area (C) Focal Adhesion number per cell (D) Focal Adhesion area in cells treated the same way as (A). (n=12 cells, 577–664 FAs analysed). In all plots: error bar, SEM; ns, non-significant, \*p<0.05. Data taken from (Bouchet *et al.*, 2016).

#### 4.3.2.2 Does the G1404L mutant perturb talin:KANK interaction in cells?

To investigate the impact of the talin mutant G1404L on the talin:KANK1 interaction, the Akhmanova group used bioGFP-tagged talin1, talin1-G1404L, talin1 R7 and talin1 R7 G1404L constructs for co-transfection with HA-KANK1 in HEK293T cells. Streptavidin pull-down assays were performed and Western Blots against GFP and HA are shown in **FIGURE 4.34A**. The assays show that both the talin1-G1404L and talin1 R7 G1404L mutants abrogated the interaction with KANK. This finding fully supports our biochemical evidence where we observed that recombinant talin1 R7 G1404L stops binding with KANK.

Following pull-down assays, the Akhmanova group used HeLa cells with *knock-downs* of both talin1 and talin2 for rescuing with GFP-talin1 *WT* and GFP-talin-G1404L. Following transfection, cells were immunolabelled for endogenous KANK1 and imaged (shown in **FIGURE 4.34B and D**). KANK1 localises around the rim of adhesions when *WT* talin is present but in cells expressing talin-G1404L, KANK1 is no longer localised to FAs and appears to be diffuse across the cell.

Overall, our biochemical data and the Utrecht group's cell data leads to the conclusion that it is possible to perturb the talin:KANK1 interaction with a single point mutation in the approximately 2500 amino acid long talin1 protein. As previously discussed, the point mutation does not disrupt talin's role in focal adhesion formation; however, it abolishes KANK1s' ability to cluster around the edge of FAs.

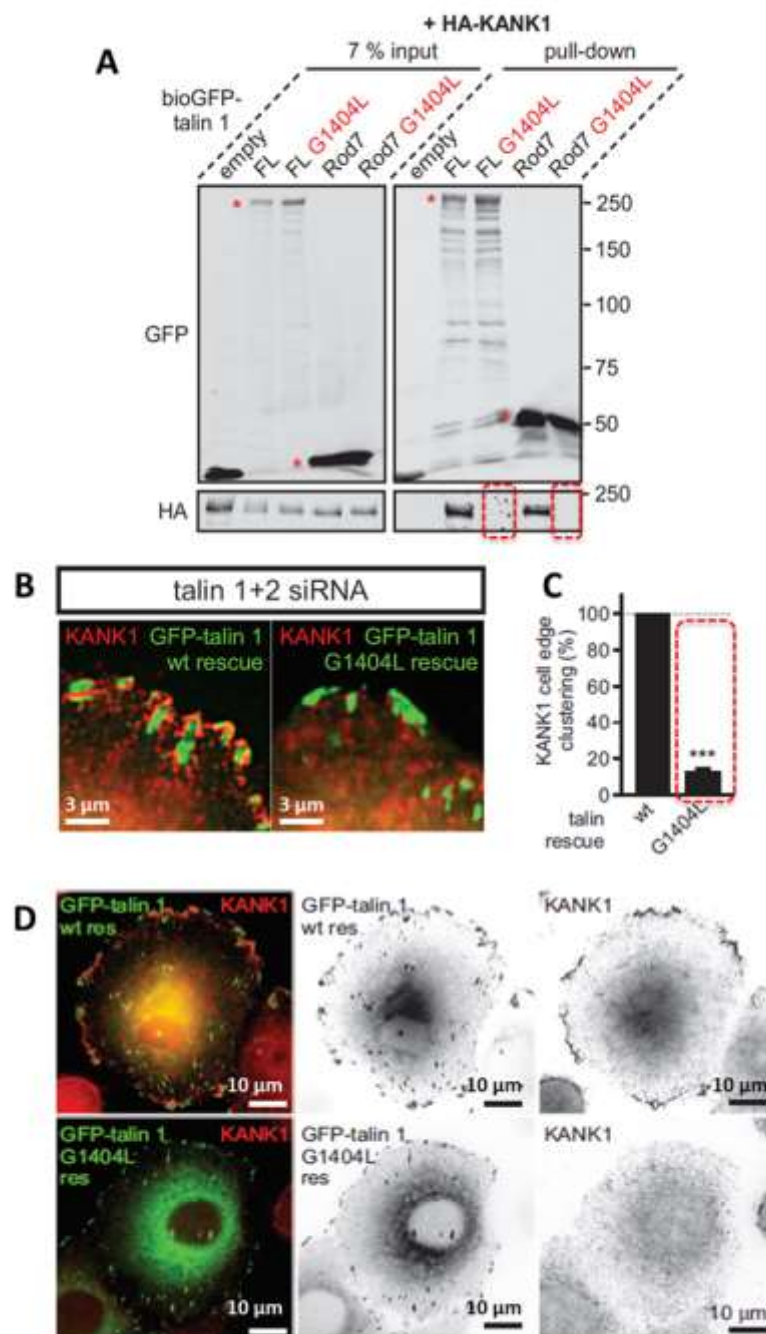


**FIGURE 4.34: CHARACTERISATION OF THE TALIN1 G1404L MUTANT IN CELLS**

(A) Streptavidin pull-down assays with the BioGFP-tagged *WT* talin1 or the indicated talin1 mutants, co-expressed with HA-KANK1 in HEK293T cells, analysed by Western blotting with the indicated antibodies. (B) Widefield fluorescence images of HeLa cells depleted of endogenous talin1 and talin2, rescued by the expression of the wild type GFP-tagged mouse talin1 or the G1404L mutant and labelled for endogenous KANK1 by immunofluorescence staining. (C) Quantification of peripheral clustering of KANK1 in cells treated and analysed as in (E) ( $n=12$ , 6 cells per condition). Error bar, SEM; \*\*\*  $p<0.001$ . (D) HeLa cells co-depleted of talin1 and talin2 transfected with the indicated talin1 fusions and stained for the endogenous KANK1. Data taken from (Bouchet *et al.*, 2016).

### 4.3.3 How does mislocalisation of KANK1 due to perturbed talin1:KANK1 binding affect other CMSC components?

Disruption of the talin:KANK interaction prevents KANK from being recruited to the rim of FA assemblies and, instead, KANK is distributed across the cell. Following this finding, we wanted to explore what happens to CMSC components when KANK is no longer localised to the cell cortex or adhesions.

For this, the Akhmanova group *knocked-down* KANK1 and KANK2 in HeLa cells, which resulted in the complete abolishment of clusters of CMSC components such as LL5 $\beta$  and KIF21A around the cell cortex. Rescue experiments with GFP-KANK1 showed that cortical clustering of these proteins could be restored upon expression of KANK1 *WT* (**shown in FIGURE 4.35**). However, clustering of LL5 $\beta$  and KIF21A could not be fully restored with the addition of either GFP-KANK1-4A, GFP- $\Delta$ CC or GFP- $\Delta$ CC\_4A mutants. Importantly, although the KANK\_4A mutant did not localise to adhesions, it could still be found to co-localise with LL5 $\beta$  across the cell due to KANK-liprin $\beta$ 1 binding. The KANK  $\Delta$ CC mutant localised around FA assemblies in ring like structures, but could not bind LL5 $\beta$  due to mutually exclusive localisation with liprin  $\beta$ 1 and LL5 $\beta$ .

The CMSC component, KIF21A, binds to KANK1 via the ankyrin repeat domain. In contrast to LL5 $\beta$ , KIF21A could still localise with the KANK  $\Delta$ CC mutant at the FA assembly rim. However, overall KIF21A localisation at the cell periphery was significantly reduced in both KANK  $\Delta$ CC, KANK  $\Delta$ CC\_4A and KANK\_4A compared with KANK1 *WT* (**FIGURE 4.35**). Furthermore, all the KANK mutants prevented efficient accumulation of CLASP2 (MT binding protein) at the cell cortex, which confirms that cortical recruitment of CLASPS depend on LL5 $\beta$  (Lansbergen *et al.*, 2006).



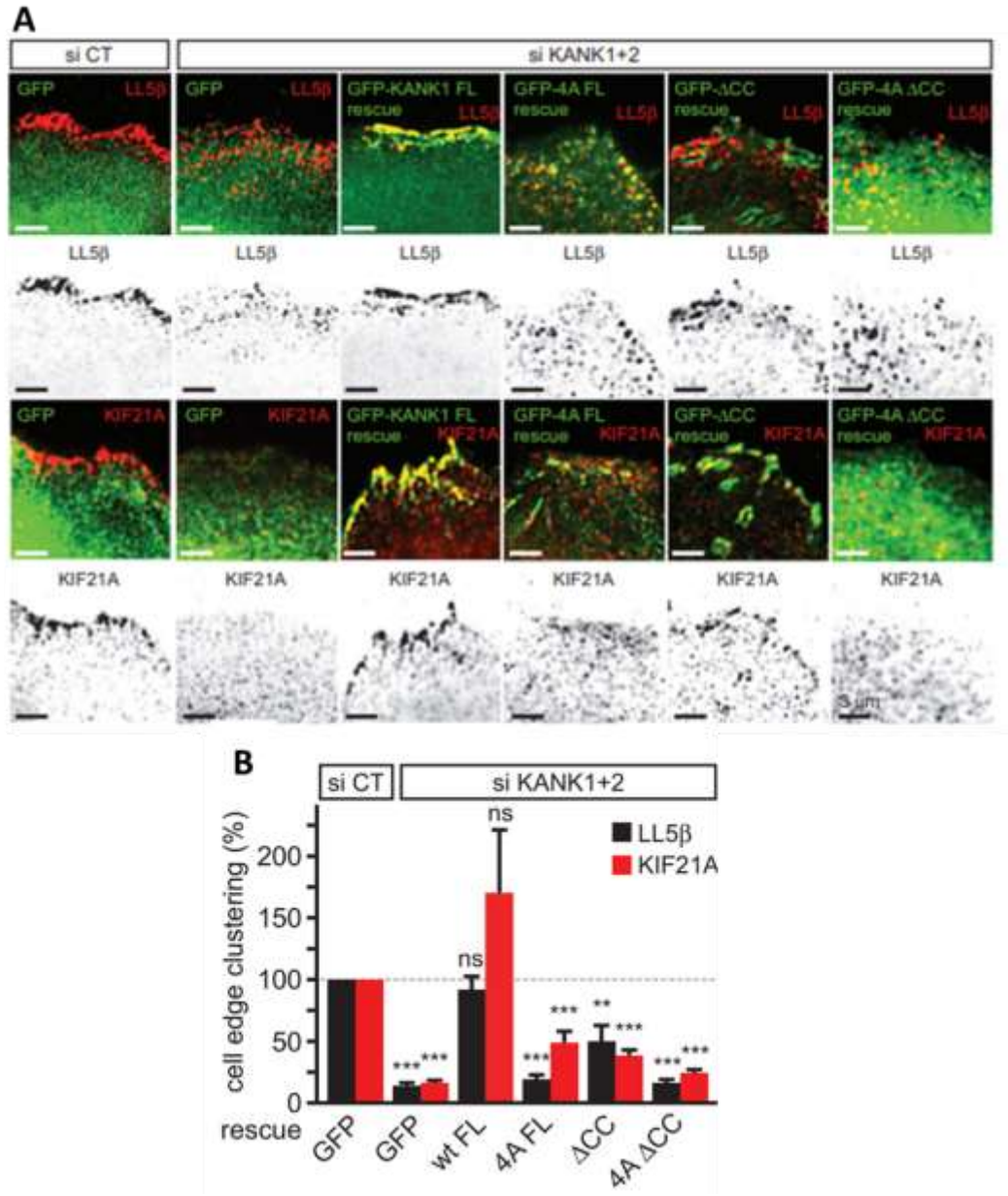


**FIGURE 4.35: KANK1 MUTANTS AFFECT ON CMSC COMPONENTS CLUSTERING AROUND FOCAL ADHESIONS**

(A) Wide field fluorescence images of HeLa cells co-depleted of KANK1 and KANK2 then transfected with indicated GFP-KANK mutants ( $\Delta$ CC\_4A,  $\Delta$ CC and KANK\_4A) (green) and stained for endogenous LL5 $\beta$  or KIF21A (red), magnification bars represent 3  $\mu$ M. (B) Quantification for cell edge clustering of both CMSC proteins LL5 $\beta$  (black) and KIF21A (red) in cells with indicated KANK1 mutant. Error bars, SEM; \*\*\* $p$ <0.001, Mann-Whitney U test. Data taken and adapted from (Bouchet *et al.*, 2016).

To determine if disrupting the talin:KANK interaction from the ‘talin side’ would have a similar effect on CMSC localisation as the KANK mutants, HeLa cells depleted of talin1 and talin2 were rescued with either GFP-talin1 or GFP talin1 G1404L. **FIGURE 4.36** shows that the cells rescued with talin1 *WT* had both MSC components, LL5 $\beta$  and KIF21A, clustered around the adhesion. However, cells rescued with GFP-G1404L talin1 (deficient in KANK binding) were no longer able to recruit LL5 $\beta$  and KIF21A to FA clusters.

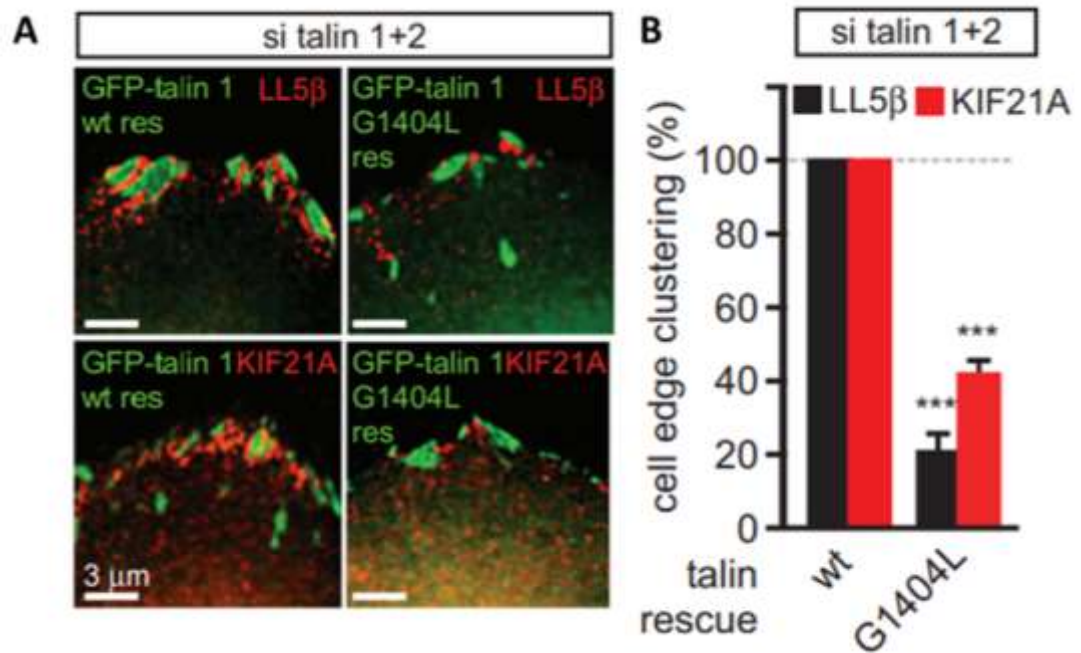


**FIGURE 4.36: TALIN G1404L MUTANT STOPS CLUSTERING OF CMSC COMPONENTS TO FOCAL ADHESIONS**

(A) Wide field fluorescence images of HeLa cells co-depleted of talin1 and talin2 then transfected with indicated GFP-talin1 construct (green) and stained for endogenous LL5 $\beta$  or KIF21A (red), magnification bars represent 3  $\mu$ m. (B) Quantification for cell edge clustering of both CMSC proteins LL5 $\beta$  (black) and KIF21A (red) in both cells with GFP-talin1 and GFP-talin1 G1404L Error bars, SEM; \*\*\* $p$ <0.001, Mann-Whitney U test. Data taken and adapted from (Bouchet *et al.*, 2016).



#### 4.3.4 Disruption of talin1:KANK1 leads to microtubules plus-end disorganisation at the cell periphery

To understand the importance of the focal adhesion and cortical microtubule stabilising complex crosstalk, we investigated the effect of disruption of the talin:KANK interaction on microtubule organisation at the cell periphery, using our talin1 G1404L and KANK\_4A mutants.

For the MT study the Akhmanova group used HeLa cells due to their stereotypically round shape (van der Vaart *et al.*, 2013). In HeLa cells, MTs are found to grow rapidly in central parts of the cell whereas at the cell margin (where CMSCs group in the vicinity of FAs), MT plus-ends are tethered to the cortex and exhibit much slower growth rate due to MT regulators; CLASP and KIF21A (Mimori-Kiyosue *et al.*, 2005; Drabek *et al.*, 2006; van der Vaart *et al.*, 2013). These regulators are important as they prevent MT overgrowth at the cell edge, which causes disorder.

The Utrecht group *knocked-down* both endogenous KANK1 and KANK2 from HeLa cells before co-transfecting GFP KANK1 *WT* or GFP KANK1\_4A with EB3-mRFP (a microtubule plus-end marker). Additionally, *knock-downs* of talin1 and talin2 were also performed in HeLa cells, before co-transfection with GFP-talin1 *WT* or GFP-talin1 G1404L and EB3-mRFP. TIRFM live imaging was used to image cells, as shown in **FIGURE 4.37B and C**. The plus-ends of MTs, in cells expressing talin1 and KANK1, grew at a 60-80° angle and approximately 2.5 times slower than the central region of MTs. However, when either the KANK\_4A mutant or the talin1 G1404L mutant were expressed, the MT central regions were not affected but the growth rate of plus-ends increased and the characteristic growth at 60-80° angles was no longer observed. Instead, MTs grew at oblique angles to the cell margin.

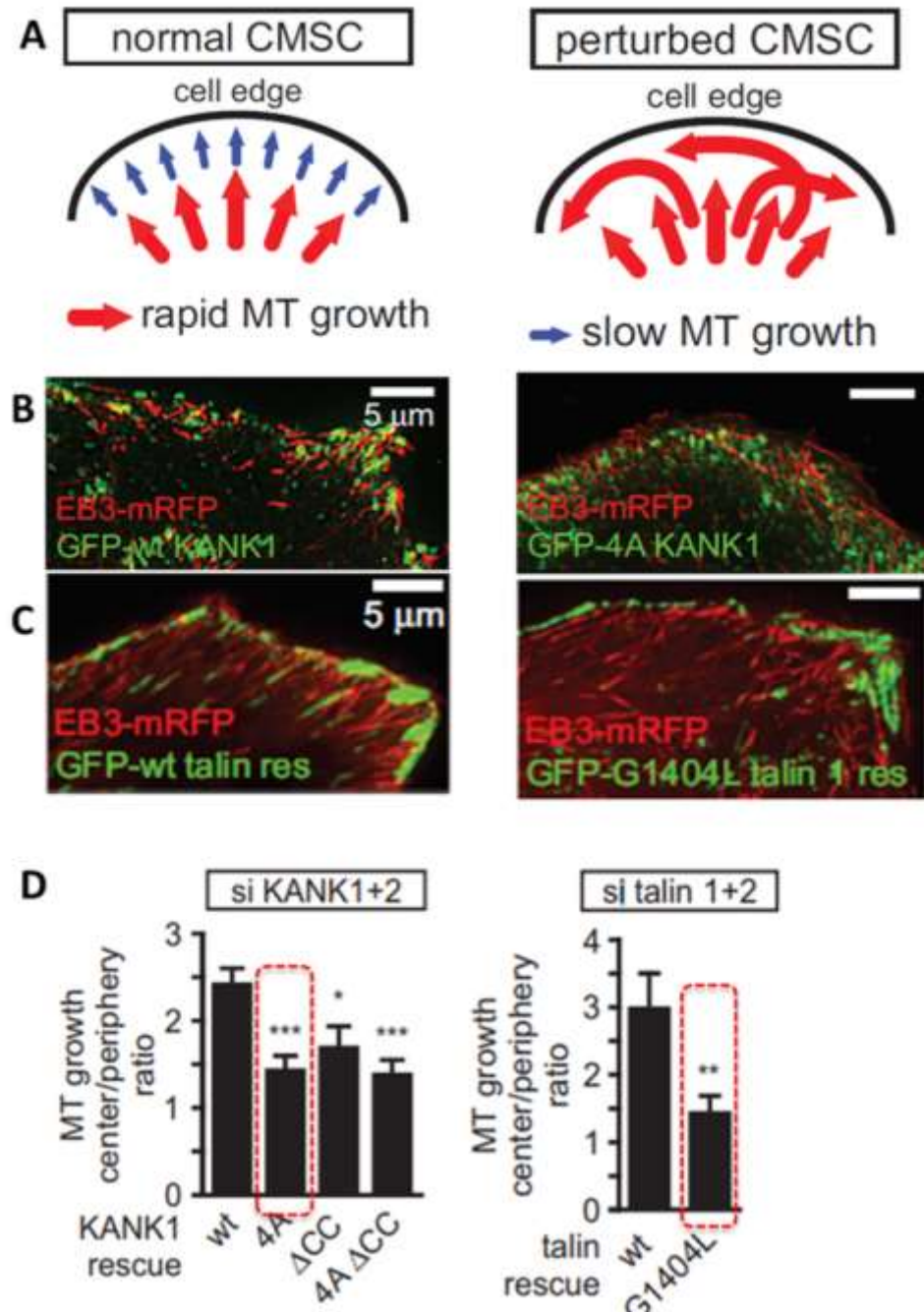


**FIGURE 4.37: DISRUPTION OF THE TALIN:KANK INTERACTION DISORDERS MICROTUBULE PLUS END ORGANIZATION AT THE CELL PERIPHERY**

(A) Schematic representation of the pattern of microtubule growth in control HeLa cells and in cells with perturbed CMSCs, based on (van der Vaart *et al.*, 2013). (B) TIRFM images of live HeLa cells depleted of both KANK1 and KANK2 then co-expressed with siRNA-resistant GFP-KANK1 and EB3-mRFP, magnification bars represent 5 μM. (C) TIRFM images of live HeLa cells depleted of talin1 and talin 2 and then co-expressed with GFP-talin1 and EB3-mRFP. Magnification bars represent 5 μM (D) Ratio of microtubule growth rate in the cell centre and at the cell edge for the cells treated with varying talin and KANK mutants described in B and C. Data taken from (Bouchet *et al.*, 2016).

This phenotype observed with the GFP-talin1 G1404L mutant fully supports our biochemistry data. This single point mutation, G1404L in talin1, presents a powerful tool for exploring the connections between adhesion and the microtubules as it does not interfere with adhesion formation but is sufficient to perturb CMSC clustering and through doing so induces complete disorder of the microtubule plus ends at the cell cortex.

## 4.4 Conclusion

### 4.4.1 Does talin nucleate CMSC assembly?

In the cell, CMSC proteins have not been found to coalesce around the FAs, so what is driving them to accumulate around the focal adhesion rim? CMSC complexes form through an intricate network of interactions, and at the heart of this network is a trio of core proteins: KANK; LL5 $\beta$  and liprins (Lansbergen *et al.*, 2006; van der Vaart *et al.*, 2013; Astro and De Curtis, 2015). These core components can be independently recruited to the plasma membrane. The KANK mutant  $\Delta$ CC (**FIGURE 4.38**) was unable to support proper clustering of CMSC components at the cell cortex despite being able to co-localise around FA assemblies. These data suggest that the liprin $\beta$ 1-KANK1 interaction is required for CMSC recruitment along with the talin:KANK1 interaction.

It would seem that the talin:KANK interaction initiates the platform for assembly of CMSC components. Talin acts as the seed for KANK1 to bind via the KN domain and in turn KANK serves as a platform to bind liprin  $\beta$ 1 at the cell cortex (via KANK coiled-coil domain). This then allows CMSC proteins to assemble forming CMSC 'patches'. These patches can remain stable for around 10 minutes at a time, whilst individual CMSC proteins are dynamic and have much shorter turnover rates (van der Vaart *et al.*, 2013). Additional proteins then bind to these 'patches', including KIF21A and CLASPS, MT-binding proteins that ultimately capture MTs at the CMSC (**FIGURE 4.38A**).

We speculate that increasing the KANK concentration at the FA rim helps nucleate CMSC assembly (**FIGURE 4.38B**). Through this nucleation, large macromolecular assemblies form around the adhesions, attracting different membrane bound proteins to bind such LL5 $\beta$  (Bouchet *et al.*, 2016) and, in turn, concentrating the number of CMSC proteins in the region. This model correlates with data indicating that CMSC accumulation is reduced but not abolished when PI3 kinase is inhibited (Lansbergen *et al.*, 2006). Most importantly this model provides the answer to a key unanswered question of the last 25 years what links the focal adhesion assemblies to microtubule plus ends?

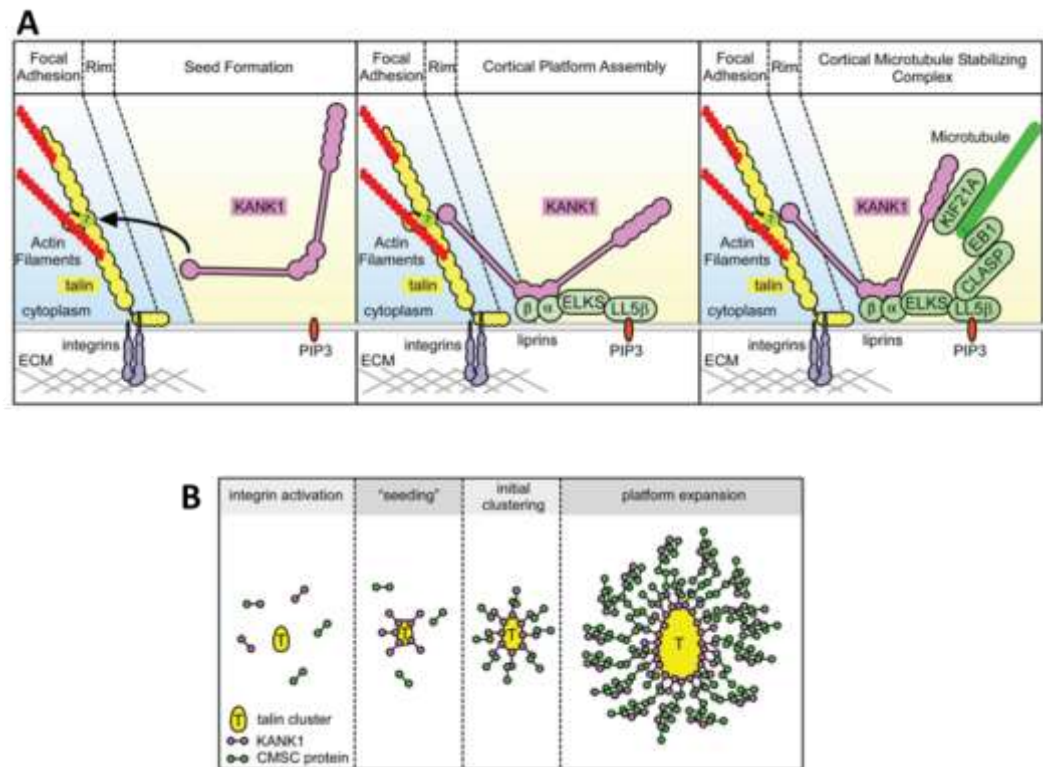


**FIGURE 4.38: TALIN NUCLEATES CMSC ASSEMBLY BY INITIATING A SEEDING COMPLEX WITH KANK1**

(A) Model of how talin1 directs the assembly of the cortical microtubule-stabilizing complex in three stages. 1) KANK1 binds to talin R7, 2) KANK1 coiled-coil domain binds to liprin  $\beta$ 1, 3) this allows LL5 $\beta$  to bind and the final CMSC proteins to assemble including ELKS, CLASP and KIF21A. (B) KANK1 binds to the rim of adhesion complexes and acts as a 'seed' for the CMSC proteins to bind, which generates a macromolecular assembly around the FA rim. Figure taken from (Bouchet *et al.*, 2016).

#### 4.4.2 Why is KANK kept at the rim of focal adhesions?

The cell images from the Akhmanova group showed that KANK1 was able to bind to talin and localise to focal adhesion assemblies. Interestingly though, KANK1 formed a belt around the edge of the adhesion and was not found distributed through the adhesion; this was also observed in another KANK study (Sun *et al.*, 2016). **FIGURE 4.39** shows the different KANK mutants and their abundance (shown as a measure of fluorescence) across a cross section of an adhesion. **FIGURE 4.39** show that the only KANK1 construct able to enter the adhesion was the small KN domain. What is keeping KANK at the rim of adhesions and is it biologically important that KANK doesn't enter the adhesion?

A logical answer is that steric hindrance prevents KANK from doing so, whilst the smaller KN domain can easily penetrate the dense actin core of the adhesion. This steric hindrance would be further compounded due to binding of CMSC proteins to KANK and the formation of large macromolecular assemblies.

This however, may be a slightly too simplistic model. Unpublished data from the Akhmanova lab shows that when ROCK1 inhibitors are introduced in the cell there is more of an overlap between KANK1 and FA markers. ROCK1 is a key regulator in actin cytoskeleton organisation and is found to be involved in stress fibre and adhesion formation (Maekawa *et al.*, 1999). Because ROCK1 inhibitors would reduce the tension across the cell and at adhesions, a higher overlap with FA markers suggests that the interaction between talin and KANK1 is mechanosensitive.

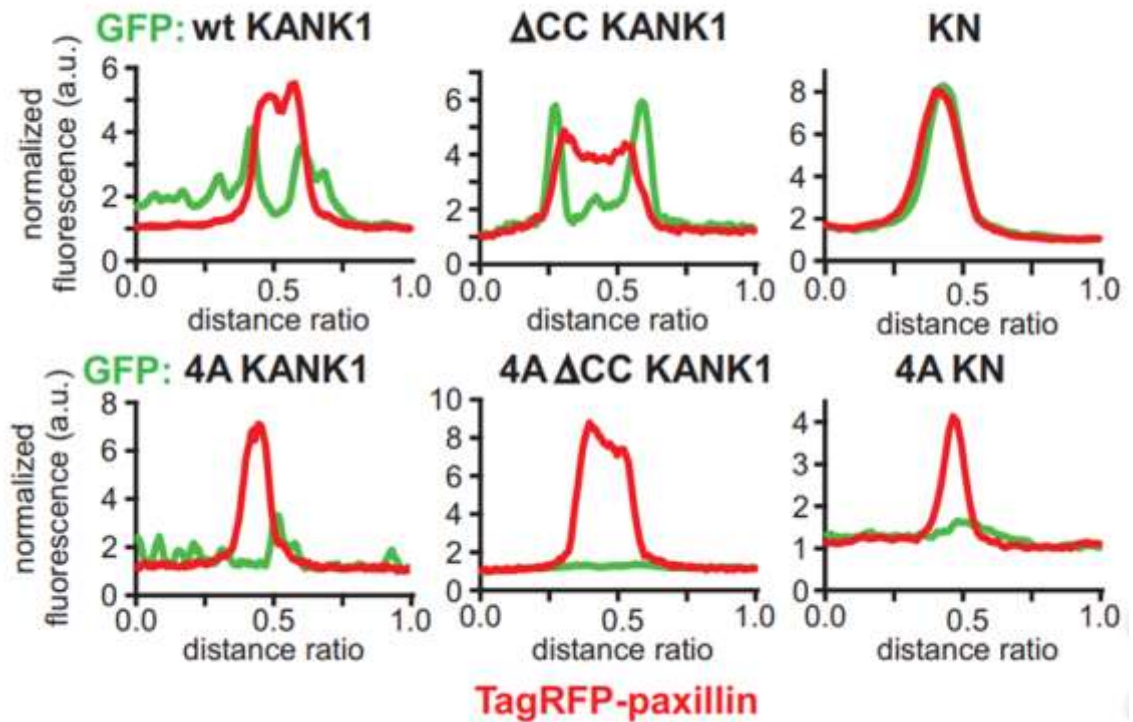


**FIGURE 4.39: TALIN:KANK INTERACTION IS REQUIRED FOR KANK TO BE RECRUITED TO FOCAL ADHESIONS RIM.**

Fluorescence profile of GFP-tagged KANK1 and KANK mutants: KANK\_4A,  $\Delta$ CC, 4A\_  $\Delta$ CC, KN and KN\_4A and TagRFP-paxillin (adhesion marker) based on line scan measurement across the FA area in TIRFM images.

As mentioned in **Chapter Chapter 2**, talin is a mechanically sensitive protein (Yan *et al.*, 2015; Kumar *et al.*, 2016; Yao *et al.*, 2016). The helical bundles in the rod domain can unfold under force. Unfolding of the R7 helical bundle would lead to the loss of the KANK binding site. The KANK1 binding site overlaps with the ABS2 on the talin rod (between R4-R8) (Atherton *et al.*, 2015). Actin binding puts talin under force and with multiple actin binding sites across talin it is possible to hypothesise that different talin molecules are under differing amounts of force across the adhesion. This results in KANK1 only binding at the periphery of the adhesion, where talin is not fully

embedded into the adhesion and not under tension, allowing the R7 domain to maintain helical bundle formation.

Finally, post-translational modifications on or surrounding the KANK1 binding site may prevent KANK1 from binding talin. A recognised phosphorylation site Ser1614 was found in the KANK1 binding site (Gough and Goult, 2018) and our FP data showed that a phosphomimetic S1641E caused a four-fold decrease in binding affinity for KANK1. Even though this did not abolish binding, it does weaken the interaction and it is certainly rational to suggest a PTM in this region could disrupt binding. It will be important in the future to test a phosphomimetic and non-phosphorylatable mutant of this site in cells and look to see if a similar phenotype to the G1404L mutant is observed.

### **4.4.3 KANK proteins in disease**

Mutations and deletions within the KANK proteins have been implicated with a number of rare genetic human diseases. A large deletion of KANK1 has been found to lead to cerebral palsy: a four generation family with congenital cerebral palsy were found to have a 225 Kb deletion of the ankyrin repeat domain in KANK1 (Lerer *et al.*, 2005).

Inactivation of genes by mutations and loss of heterozygosity (gene locus containing two different alleles) often lead to carcinomas (Kakinuma *et al.*, 2009). Loss of heterozygosity in the KANK gene locus has been found to be linked to renal cell carcinomas (RCC); this has also been reported in other cancers including lung cancer, breast cancer, pancreatic carcinoma and bladder cancer (Kakinuma *et al.*, 2009). These studies give a clear indication that loss of KANK1 function within the cell can lead to disease. Reduced expression of KANK has also been reported in myeloproliferative disorders a group of slow-growing blood cancers, whereby abnormal red blood cells are produced and accumulate in the blood (Kakinuma *et al.*, 2009). Other diseases where KANK is mis-regulated obsessive compulsive disorder (Willour *et al.*, 2004) and autism (Vinci *et al.*, 2007).

### **4.4.4 Expression of KANK family members**

**TABLE 9** highlights information of the different KANK isoform expression levels across different tissues. These data would suggest that KANK1 and KANK2 are the most dominant KANK isoforms and have been found in all tissues tested whereas; KANK3 and KANK4 appear more tissue specific. KANK1 is shown to be the predominant isoforms expressed in the heart, liver and kidney (Zhu *et*

*al.*, 2008). KANK2 was shown to also have high expression in kidney cells but in contrast, KANK3 and KANK4 were shown to have low expression levels (Zhu *et al.*, 2008). Current evidence reveals slight differences in expression between the different KANK isoforms in tissues and could these differences reveal differences in functions between the isoforms? We are still yet to determine the functional differences between KANK1-4 and in the future it would be interesting to introduce *knockouts* of the individual KANK isoforms into mice and study the effects. Furthermore, with the advancement in super-resolution microscopy it could now be possible to study the KANK isoforms localisation in cells and determine functional aspects of the different isoforms.

Tissue expression	KANK1	KANK2	KANK3	KANK4
cervix	**	**		
lung	**	**	**	**
colon	**	**		**
heart	**	**		
kidney	**	**	**	**
liver	**	**	**	**
skeletal muscle	**	*	**	**
breast	**	*	**	

**TABLE 9: EXPRESSION LEVELS OF KANK1,2,3 AND 4 GENES**

Table indicating (\*) expressed and (\*\*) highest level of expression of the different KANK isoforms from different tissues. Data collated from Human protein atlas (Uhlén *et al.*, 2015) and (Zhu *et al.*, 2008).

#### 4.4.5 Why do humans have four KANK isoforms?

As described earlier humans have four KANK isoforms KANK1-4, the originally identified member was KANK1 and through a homology search across the human genome three further KANK isoforms (KANK 2, 3 and 4) were identified (Kakinuma *et al.*, 2009). These four KANK proteins all have a very conserved C-terminal ankyrin repeat domain and a conserved N-terminal KN domain. The only major difference in terms of structure between the four isoforms is the coiled-coil region (CC) in the middle of the protein. KANK1 has three CC regions, KANK2 has two CC, KANK3 has two CC and



KANK4 has one CC region as shown in **FIGURE 4.40**. These differences between the isoforms might be providing a clue into the different functions the KANK isoforms have within the cell. The first coiled coil (CC1) in KANK1 binds to liprin $\beta$ 1 (van der Vaart *et al.*, 2013) this interaction is crucial for LL5 $\beta$  binding and the co-localisation of the other CMSC components. KANK2 is also shown to have a strong association with liprin $\beta$ 1 (Luo *et al.*, 2016). After aligning the KANK CC regions of all KANK isoforms in Clustal Omega, it was clear that KANK1-3 contained a similar sequence (shown in **FIGURE 4.40**). This suggests that KANK3 would also be able to bind to liprin $\beta$ 1 and could be helping to regulate the assembly of the CMSC. I also showed that the KANK3 KN domain could bind to talin1 R7 and, therefore, it is feasible to suggest that KANK3 could be playing a similar role to KANK1. KANK4 does not contain this potential liprin $\beta$ 1 binding sequence and, as a consequence, cannot recruit CMSC components to FA.

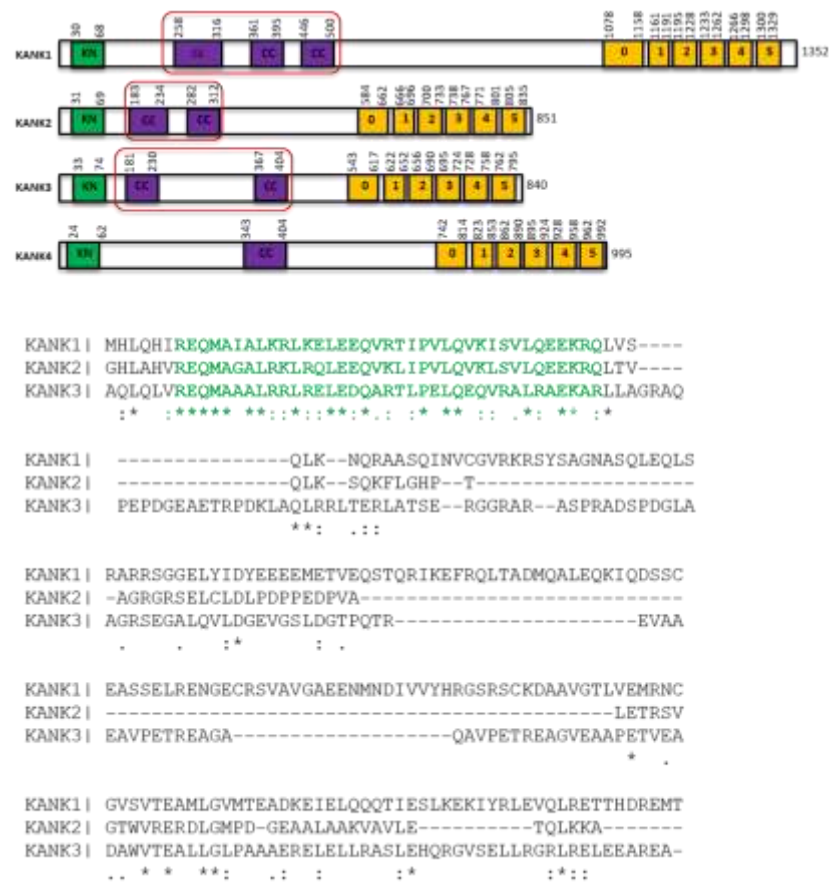


**FIGURE 4.40: HUMAN KANK ISOFORMS COILED COIL ALIGNMENT**

Schematic of the human KANK isoforms 1-4. Highlighted in red boxes are the regions of sequence aligned using Clustal Omega that can be seen in the bottom panel. Residues not be recruiting CMSC components to FA. Highlighted in green shows region of high conservation and indicates predicted Liprin  $\beta$ 1 binding region.



#### 4.4.6 What is the role of the talin:KANK interaction in organisms?

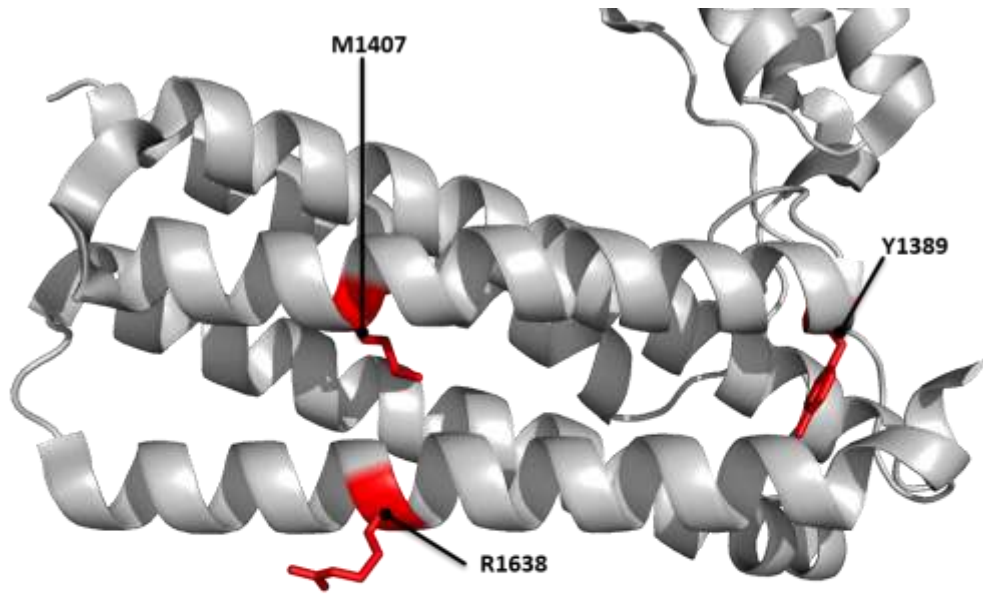
So far, KANK proteins have been poorly studied due to their unknown function and structure. This is beginning to change with the recent emerging role of KANK1 as a microtubule targeting protein (Bouchet *et al.*, 2016) and a possible connection to the regulation of force transmission across adhesions (Sun *et al.*, 2016). Although the KANK family is becoming more studied both *in vitro* and *in vivo* the main study on KANK1 function comes from studies in *C.elegans*. Unlike humans, *C.elegans* have only one isoform of KANK named VAB19, which was found to localise to muscle-epidermal attachment sites (Ding, 2003). For interaction with epidermal attachment structures both the KN motif and the coiled-coil domains are required for localisation. VAB19 mutants are defective in epidermal elongation (growth from embryo to larva) and muscle attachment to the epidermis, which results in developmental arrest and subsequent embryonic lethality (Ding, 2003). Furthermore, the VAB19 is required for normal epidermal actin reorganisation and VAB19 mutants caused abnormal actin cytoskeletal reorganisation, preventing attachment structures to develop beyond a certain stage (Ding, 2003).

KANK *knock-down* experiments have been reported in zebra fish, where the authors looked at the roles of both KANK2 and KANK3. In this particular study, *Knock-down* of KANK2 showed a nephrotic syndrome phenotype (a kidney disorder that leads to progressive renal function decline) (Gee *et al.*, 2015). *Knock-down* of KANK3 in zebra fish was shown to enhance cell migration and invasion however, whilst overexpression of the protein inhibited these characteristics (Kim *et al.*, 2018). Cell work of the KANK1 family in mammals is also still very limited. Our work with the Akhmanova group found strong phenotypes in HeLA cells when the talin:KANK interaction was removed, MT growth at the cell cortex was no longer co-ordinated and MTs grew at an accelerated rate in random directions. CMSC components were no longer able to recruit to focal adhesions and form macromolecular assemblies around adhesions helping to regulate the turnover of adhesions (Bouchet *et al.*, 2016). These data suggest that if a KANK *knock-out* was introduced into a mammal it would have severe effect and possibly lead to death.

Further experiments need to be carried out to determine the importance of MT localisation to FAs in determining cell polarisation. If the link between FAs and MTs was found to be critical in determining cell polarity, then this would give more weight to the hypothesis that a KANK1 *knock-out* would be fatal in a model organism, as cell polarity is essential in determining direction of migration and co-ordinating the migration and formation of tissues and organs during embryogenesis (Campanale, Sun and Montell, 2017).

A good indication of how important KANK1 is in the cell is to look at known mutations found within the KANK gene. Extensive mutational studies of KANK1 have been carried out and, to date, whilst missense variants and single nucleotide polymorphisms (SNPs) can be found in KANK1, no KANK1 deletions or nonsense mutations have been found. Although, interestingly, no SNPs have been found in the KANK1 KN domain (Kakinuma *et al.*, 2009), indicating that a mutation in this region could also be lethal.

To investigate if there are human mutations found on the talin KANK1 binding site (talin R7) the human 1000 genome project (Gibbs *et al.*, 2015) and the Catalogue Of Somatic Mutations In Cancer (COSMIC) (Bamford *et al.*, 2004) were used. **FIGURE 4.41** shows the SNPs across the KANK1 binding site on talin1. Across R7 helices 29 and 36 that form the KANK binding site, there are three SNPs, one of which is of particular interest: the mutation of residue Tyr1389. This residue was one of the residues identified (along with Trp1630) to hold the helices 29 and 36 at a fixed distance apart and was found to be crucial for talin-binding. In humans, SNPs where the Tyr residue is replaced by a His or Ile can occur. The His residue is less hydrophobic and would not disrupt the hydrophobic core of the domain, likely pushing the helices apart, potentially leading to KANK1 no longer being able to bind talin. SNPs for this residue (Tyr1389) are very rare since this is highly conserved residue across species, and this particular mutation was found in patients with carcinoma. The next most critical KANK1 experiments are to explore the effect of KANK1 *knock-out* in a model organism. This will determine the importance of the interaction and start to unlock some of the questions around the different KANK1 isoforms and their role within the cell.



Cosmic/ 1000 Genome Identifier	Talin1 Residue	Mutation Found	Tissue
rs538218511	Y1389	His/Ile	Liver/Lung
COSM3367704	M1407	Ile	Kidney
COSM2774493	R1638	His	N/A

**FIGURE 4.41: SINGLE NUCLEOTIDE POLYMORPHISMS FOUND IN THE KANK BINDING SITE ON TALIN R7**

Talin1 R7 structure (PDB: 5FZT) residues highlighted in red indicate the found human SNPs from either COSMIC or the Human 1000 genome identifier.

# **Chapter 5. Defining an LD talin-binding motif**

---

## 5.1 Introduction

In **Chapter 4**, the interaction between talin and the adapter protein KANK was biochemically characterised and we identified KANK bound to talin R7 via an LD-motif in the KANK KN domain. This KANK LD-motif was the first LD-motif found to bind to a talin five-helix bundle (aside from potentially RIAM binding to R11) and subsequently identified talin R7 as a new LDBD. Biochemical characterisation of this interaction has increased our understanding of LD-motifs binding to talin and has raised the question: can any of the other 11 five-helix bundles on the talin rod bind LD-motifs?

In this chapter a strategy was developed to search for novel talin interactors from proteomics data sets in the view that identifying novel LD-motif interactions with talin will give new insight into talins role in regulating adhesion assemblies.

### 5.1.1 What are Leucine-Aspartic acid motifs

Leucine-Aspartic acid (LD) motifs are short helical interaction motifs that have been found in a number of adhesion proteins and mediate protein:protein interactions; they have been identified as crucial players in connecting cell adhesion with cell motility and survival (Alam *et al.*, 2014). LD-motifs are identified through the canonical sequence LDxLLxL (where x is any amino acid) and were first discovered in the paxillin family (Brown, Perrotta and Turner, 1996).

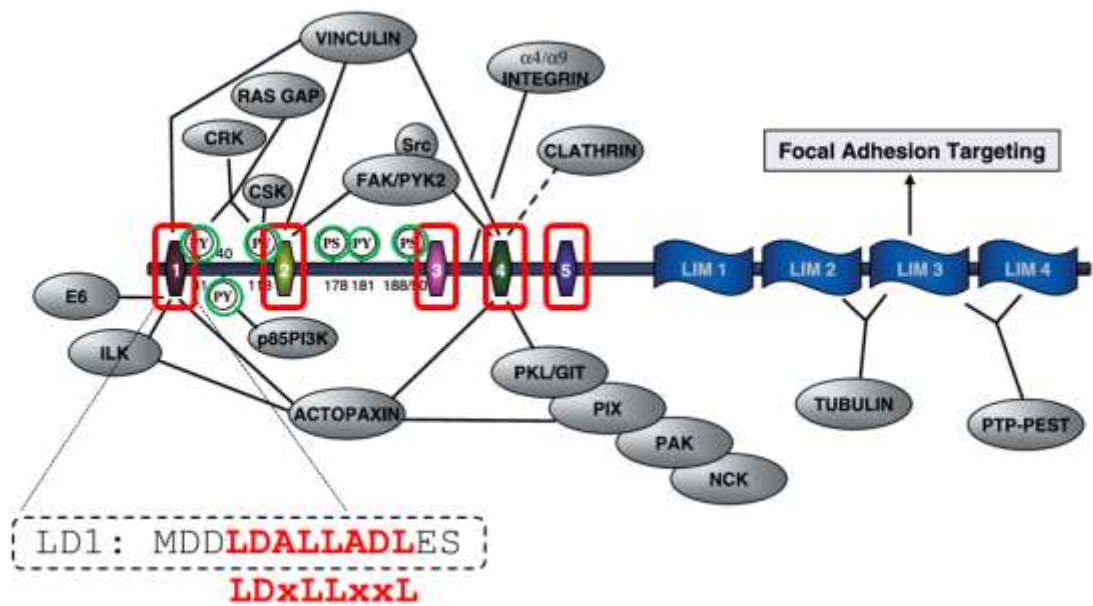


**FIGURE 5.1: PAXILLIN DOMAIN STRUCTURE AND KNOWN BINDING PARTNERS.**

Schematic diagram of paxillin showing the proteins domain structure and highlighting the five LD-motif domains (highlighted by red boxes) and LIM domains. LD1 has been expanded and the protein sequence is shown in black box, the corresponding LDxLLxxL motif has been highlighted in red. Green circles highlight the multiple; tyrosine (PY), serine (PS) and threonine (PT) residues that are phosphorylated along the protein also shown in grey are some of the current recognised paxillin binding partners and where they bind on the paxillin structure. Diagram adapted from: (Brown, 2004).

#### 5.1.1.1 Paxillin LD-Motifs

Paxillin is a large 68 kDa focal adhesion adapter protein, and its biological function is to regulate cell spreading and motility through its involvement in the integrin-mediated signalling pathway (Schaller, 2001). The protein has multiple domains which encompass a number of different protein-binding motifs.

**FIGURE 5.1** shows the five N-terminal LD-motifs (highlighted by red boxes) and four C-terminal double zinc finger LIM (lin-a, isl-1, mec-3) domains. The protein also contains multiple phosphorylated tyrosine (PY), serine (PS) and threonine (PT) residues that can be phosphorylated in response to cell adhesion (highlighted on **FIGURE 5.1** by green circle). Phosphorylated tyrosine residues generate docking sites for SH2 domain containing proteins to bind (Brown, 2004). Furthermore, **FIGURE 5.1** shows the multiple binding partners that can interact with the paxillin domains including LD-motif binding proteins, focal adhesion kinase (FAK) and vinculin (Schaller, 2001).

The five LD-motif domains are named LD 1-5, these domains are well conserved across all members of the paxillin superfamily (paxillin, Hic-5, paxB and Leupaxin) and across species (Brown, 2004). The paxillin LD-motifs contain a short leucine rich sequence; LDxLLxxL (where x is any residue) which has been defined as the canonical LD-motif (Alam *et al.*, 2014). This sequence is found in all five of the paxillin LD domains, apart from LD3, (which has a conserved Val-Glu instead of the Leu-Asp). The motif has been shown to be important in mediating interactions between several proteins central to the regulation and co-ordination of the actin cytoskeleton including proteins FAK and vinculin (Schaller, 2001).

Interestingly, each of the paxillin LD-motifs can bind multiple proteins for example, paxillin LD2 and LD4 can bind FAK and paxillin; LD1, LD2, LD4 could bind to vinculin (Turner *et al.*, 1999). This started to raise questions around how the LD-motifs could dictate specificity. To further investigate how LD binding partners are interacting with LD domains the FAK:paxillin interaction was more closely studied (Hoellerer *et al.*, 2003). Hoellerer *et al.*; corroborated that FAK could only bind to paxillin via LD2 and LD4 domains and this selectivity could be due to modulated affinity of side chain pairing between the paxillin LD domain and FAK. It was also thought that the length and helical propensity of the paxillin LD-motif determined binding affinity to an LD-binding ligand. Overall it was concluded that the LD-motif is a fairly promiscuous recognition sequence.

### **5.1.2 Leucine-Aspartate binding domains (LDBDs)**

Molecular recognition of LD-motifs comes through Leucine-Aspartic acid binding domains (LDBDs). The common binding mechanism of LD-motifs to the corresponding LDBD is through helical addition as shown in **FIGURE 5.2**. Several different proteins have been shown to contain an LDBD including the already been discussed proteins, FAK and vinculin. Other proteins include parvins, which are an actin binding protein directly responsible for the initial nucleation of actin at FAs (Nikolopoulos and Turner, 2000), and PV E6 protein from the papilloma virus. PV E6 has specifically evolved to recognise the LD-motifs on paxillin (LD1, LD2 and LD4) it is thought the interaction disrupts the actin cytoskeleton which in turn disrupts migrating cells (Wade, Brimer and Vande Pol, 2008). This demonstrates how pathogens have learnt to exploit the 'promiscuous' LD pathway for their own purposes and also highlights the functional importance of the LD interactions.

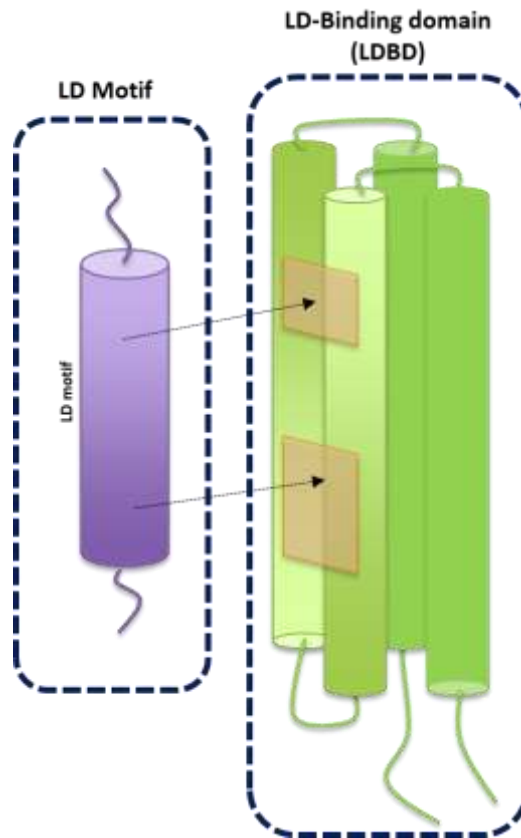


**FIGURE 5.2: LD-MOTIF BINDING TO AN LDBD**

Schematic of an LD-motif (purple) forming an interaction with corresponding LDBD (green). LD-motif binds via a helix addition to the side of the helical bundle on the LDBD.

### 5.1.3 Talin can bind LD-motifs

More recently, talin has been found to be bind LD-motifs with the R8 domain being an important LDBD. The R8 domain binds the deleted in liver cancer (DLC1) protein between helices 32 and 33 (Zacharchenko *et al.*, 2016), this same region also binds to paxillin LD1 (Zacharchenko *et al.*, 2016) and to Rap1 –interacting adaptor molecule (RIAM) (Goult, Zacharchenko, *et al.*, 2013). Furthermore, our recent findings have found the R7 domain to be an LDBD and can bind the KANK LD-motif between helices 29 and 36. This was a breakthrough in terms of identifying talin as a protein with multiple LDBDs. Previous literature has shown only four-helix bundles to bind LD-motifs and in the talin rod only four domains contain four-helix bundles: R2, R3, R4 and R8. KANK binding to R7 raised the intriguing possibility that every talin rod domain could be an LDBD and thus could suggests a role for talin as a signalling platform.



### 5.1.3.1 DLC1 an LD-motif

DLC1 is a tumour suppressor gene which is frequently inactivated during cancer and it encodes a Rho-GAP focal adhesion protein needed for GTPase activation; negative regulation of RhoGTPases are required but not entirely sufficient for tumour suppression (Li *et al.*, 2011). The structure of talin1 R7R8 and the DLC1 LD-motif (residues 467-489) show DLC1 binds to talin1 R8 domain between helices 32 and 33 (Zacharchenko *et al.*, 2016) (shown in **FIGURE 5.3B**).

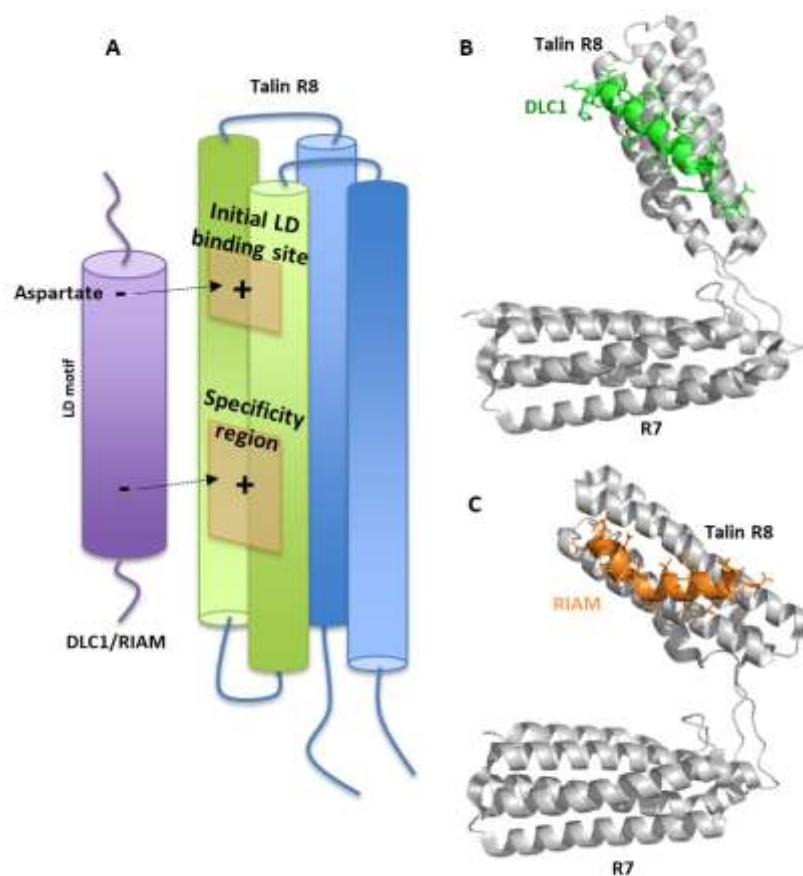


**FIGURE 5.3: TALIN R8 DOMAIN IS AN LD BINDING DOMAIN**

(A) Schematic of an LD-motif i.e RIAM or DLC1 binding to the LDBD (talin R8) (B) structure showing binding of LD-motif DLC1 (green) to talin1 R8 (grey) via the LD recognition box (PDB ID: 5FZT). (C) Structure showing the binding of LD-motif RIAM (orange) to talin1 R8 (grey) (PDB ID: 4W8P).

### 5.1.3.2 RIAM- a previously unrecognised LD-motif

RIAM is a Rap1 effector protein and is a member of the MRL (Mig10/RIAM/lamellipodin family) adaptor proteins (Lee *et al.*, 2009). RIAM has been found to have a central role in integrin activation through its ability to bind to both talin and Rap1 (Lee *et al.*, 2009; Goult, Zacharchenko, 134

*et al.*, 2013; Chang *et al.*, 2014). Integrin activation by talin is instigated by a Rap1-induced signalling pathway, these integrin activation pathways initiated from inside the cell are known as inside-out signalling (Bivona *et al.*, 2004; Banno and Ginsberg, 2008) (see **section 2.5.2**).

Rap1 is a small plasma membrane bound GTPase that recruits RIAM which then in turn recruits talin via its TBS between residues 1-30 (Lee *et al.*, 2009). Talin then activates integrin via the F3 sub-domain in the FERM head (Critchley & Gingras, 2008; J. H. Wang, 2012), mutations introduced in the RIAM 1-30 region prevented talin binding and in turn prevented the activation of integrin (Lee *et al.*, 2009).

RIAM was found to bind to talin by Goult *et al* along multiple sites across talin one of which was talin rod domain R8 (Goult, Zacharchenko, *et al.*, 2013). RIAM has not been classed as an LD-motif but it does contain a very similar sequence to the other LD-motifs that bind to talin R8, although instead of the Leu-Asp at the beginning of the motif it contains an Ile-Asp. Like the other talin R8 binding proteins, RIAM also binds between the hydrophobic groove of talin helices 32 and 33 via helix addition (Goult, Zacharchenko, *et al.*, 2013) (shown in **FIGURE 5.3C**).

For my study into talin binding LD-motifs I agree with the findings of Zacharchenko *et al* and have classed RIAM to be an LD-motif (Zacharchenko *et al.*, 2016). This classification is for two reasons. Firstly, the RIAM sequence binds to talin R8, a known LDBD, and the RIAM LD motif closely fits the canonical paxillin LDxLLxxL pattern. Secondly, RIAM binds to talin R8 through helical addition and via similar residues as other talin binding LD-motifs.

### **5.1.3.3 LD-motif Binding mechanism**

The best characterised mode of LD-motif recognition is by binding to four-helix bundles via helix addition (as shown in **FIGURE 5.3A**). LD-motifs can have helical propensity before binding to an LDBD or can form a helical structure upon interaction with the LDBD (Alam *et al.*, 2014). The charged Asp residue is thought to make the initial connection with the LDBD and form an electrostatic interaction with a conserved basic residue (Lys/Arg/His) (Zacharchenko *et al.*, 2016). Talin R8 has been found to bind multiple LD-motifs: DLC1, RIAM, Paxillin. These LD-motifs all bind to talin R8 using the same mechanism whereby the initial aspartate residue (in the LD-motif) binds to a basic residue on talin in what had been named the initial LD binding site (Zacharchenko *et al.*, 2016) (shown in **FIGURE 5.3A**). On talin R8 this charged residue is Lys1544 and it forms a salt bridge with the aspartate on the LD-motif. This initial interaction then positions the LD-motif along the furrow of the talin R8 helices 32 and 33 allowing the hydrophobic Leucine residue to form hydrophobic interactions with talin. Zacharchenko *et al* proposed in their talin:DLC1 structure that

135

there is then a second binding site along the talin R8 LDBD called the specificity region shown in **FIGURE 5.3A**. The residues in the specificity region differ between the LD-motifs and this allows for difference in specificity of binding to LDBD surfaces. The specificity region is thought to be a way that helps to regulate which LD-motif can bind when (Zacharchenko *et al.*, 2016).

#### **5.1.4 Searching for additional non-paxillin LD-motifs**

To identify LD-motifs in proteins other than paxillin, the canonical LDxLLxxL motif was used as a query to search protein data bases. This method only identified three LD-motif containing proteins, Gelsolin, Deleted Liver Cancer 1 (DLC1) and RoXaN (Alam *et al.*, 2014). Gelsolin is a cytoplasmic protein that is important for actin cytoskeletal organisation in multiple cell types including osteoclasts (Wang *et al.*, 2003) and RoXaN (rotavirus X protein associated with NSP3) is a rotavirus interacting protein (Vitour *et al.*, 2004).

The limitation with searching for LD-motifs by sequence alone is that the sequence is so similar to other motifs such as transcriptional regulation sequences (LxxLL) and Nuclear export sequences (Alam *et al.*, 2014). In order to have a better chance at identifying genuine LD-motifs a structural characterisation could also help to reduce the number of false positives identified.

## **5.2 Results**

The structure of talin domain is highly conserved across evolution. This provides compelling evidence that every domain within talin has an important functional role. Furthermore, the talin:KANK interaction gives us some insight into how the five helix domains in the talin rod can bind LD motifs. Altogether, this gives us reason to suggest that every talin rod domain has the potential to be an LDBD and bind multiple LD motifs.

Previously, the Goult group produced a talin1 proteomics data set (unpublished data); the data set contains over 800 potential talin binding partners and, from this, only KANK had been confirmed and characterised as a talin binding protein. Interrogating this vast data is an important step into uncovering further talin binding proteins; however, due to large size of talin, it is difficult to narrow down the binding sites on both talin and the putative talin binding protein.

To overcome this, we used the current knowledge of LD motifs and, in particular, the LD motifs that have been found to bind to talin, to design an LD talin-binding search motif (LD-TBM) that could be used to search through the proteomics dataset and identify new talin binding partners

with LD motifs. This method has the advantage of having the binding site on talin already identified, allowing for an easier characterisation of the interaction.

### 5.2.1 Designing a search query to identify novel LD talin-binding motif (LD-TBM) containing proteins

As discussed previously, LD motifs were initially found in paxillin, where they follow the consensus sequence LDxLLxxL. Previous attempts to search for proteins containing LD motifs using this sequence (LDxLLxxL) uncovered only three hits: DLC1, RoXan and Gesolin (Alam *et al.*, 2014). On the other hand, further attempts to search for LD motifs using a ‘more relaxed’ search sequence has led to the identification of many false-positives. Searching for LD motifs is a challenging task due to the lack of common features in the known LD motifs that would allow them to be distinguished from other helical motifs.

To combat these problems and define a LD talin-binding motif (LD-TBM) that could accurately determine potential talin binding proteins, a common set of features needed to be identified. To search for common sequence features, all the known talin binding LD-motifs were aligned (as shown in **FIGURE 5.4**). From this alignment any differences between the talin-binding LD-motifs and the paxillin LD-motifs were identified. Position numbers were given to the residues; 0 was given to the first Leu residue in the (LDxLLxxL) sequence and 1 to the Asp residue, ect. The residues were also coloured based on their properties; acidic (red), basic (blue) and hydrophobic (green).

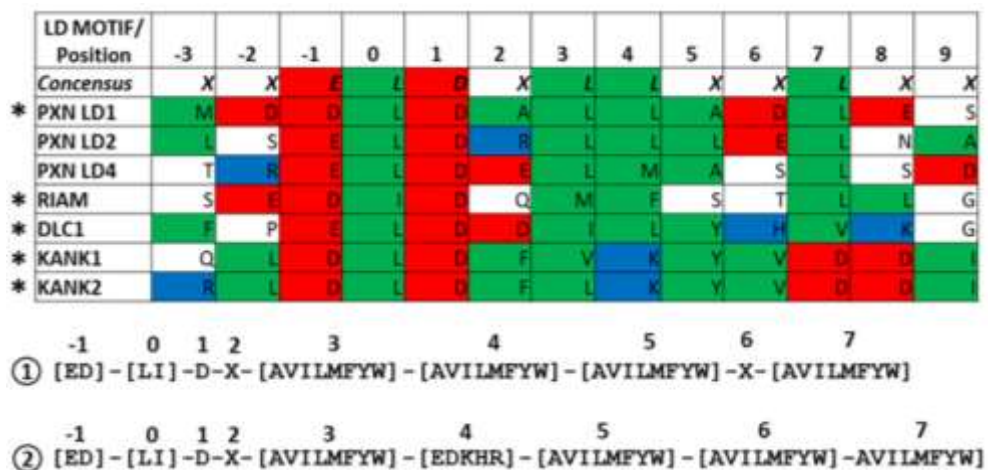


**FIGURE 5.4: SEQUENCE ALIGNMENT OF KNOWN OF LD TALIN-BINDING MOTIFS**

(A) Sequence alignment of: paxillin LD1, LD2 and LD4 (UniProt ID: P49023); RIAM (UniProt ID: Q7Z5R6); DLC1 (UniProt ID: Q96QB1); KANK1 (UniProt ID: Q14678) and KANK2 (UniProt ID: Q63ZY3). Red highlights acidic residues, blue basic residues and green hydrophobic residues. Known talin binding sequences are highlighted with an \*. (B) The designed LD talin-binding sequences which were entered into the PROSITE scanning tool.

The first difference noted between the LD-TBM and paxillin LD motifs is that, in position 0, the residue can be an Ile (as found in RIAM) or a Leu (paxillin LD motifs only contain a Leu at position 0). Additionally, from the alignment it appeared that the residue in position -1 was important to the sequence. In both paxillin LD motifs and LD-TBM, a charged residue (either Asp or Glu) was present, possibly allowing an interaction with the LDBD surface. From the alignment, it was also clear that whilst Leu residues always occupied positions 3, 4 and 7 in the paxillin sequences, the same was not true for talin-binding LD proteins. Instead, in the latter case, position 3 could be any hydrophobic residue and position 4 could be occupied either by a charged or hydrophobic residue. This information was taken into consideration when designing the LD-TBM. Finally, position 6 in the paxillin LD consensus sequence is defined as x (any amino acid); however, from the alignment we observed that the talin-binding LD proteins all contained a hydrophobic amino acid.

From these findings two new LD talin-binding sequences were designed:

**Sequence 1:** Asp/Glu-Leu/Ile-Asp-x-( $\phi$ )-( $\phi$ )-( $\phi$ )-x-( $\phi$ )

**Sequence 2:** Asp/Glu-Leu/Ile-Asp-x-( $\phi$ )- (+/-)-( $\phi$ )- ( $\phi$ )-( $\phi$ )

(where  $\phi$  is a hydrophobic residue, x is any residue and +/- indicate a charged residue)

Sequence 1 and sequence 2 are similar but differ in positions 6 and 7. In some of the talin-binding LD sequences a charged residue was found at position 6 whereas in others it was a hydrophobic residue. Designing two sequences with more-specific residues rather than one sequence with a more generalised approach was thought to lead to less false positives.

## 5.2.2 Searching for LD talin-binding motifs

When searching for LD-TBMs two different approaches were used: a manual approach and a bioinformatics approach. The manual method allowed the manual search of proteins containing either sequence 1 or sequence 2 from the top 20 proteins identified in the talin1 proteomics data set. The bioinformatics approach utilised the programme PROSITE (Sigrist *et al.*, 2002), with sequences 1 and 2 used as search queries to analyse the entire talin1 proteomics dataset for potential LD-TBMs.

### 5.2.2.1 Manually searching for LD talin-binding motifs

The manual search was used initially as a proof of concept to determine if the LD-TBM would be recognised in any protein sequences. The sequences for the twenty highest scoring proteins from the talin1 proteomics dataset, were manually screened to identify any motifs similar to the

designed sequences 1 and 2 (**section: 5.2.1**). From this search, two proteins were identified to contain the LD-TBM: cyclin dependent kinase 1 (CDK1) and septin2 (SEPT2).

The CDK1 sequence appeared to have two possible LD-TBM: one in the middle region of the protein (residues 206-223) that fitted the designed LD-TBM sequence 1 exactly and one at the very C-terminus of the protein that closely fitted the LD-TBM sequence. The sequence for SEPT2 had one LD-TBM that closely fitted the LD-TBM sequence but not exactly.

#### **5.2.2.2 Searching for LD talin-binding motifs using PROSITE**

The bioinformatics approach used the programme PROSITE which is a protein data base tool that allows an imputed query sequence to be searched against a chosen protein database. The query sequence used both the designed sequences. These were written using the PROSITE parameters, square brackets surrounding groups of amino acids such as hydrophobic amino acids [AVILMFYW] and X representing any amino acid (shown in **FIGURE 5.5B**).

All UniProt identities from the 800 proteins identified in the talin proteomics were submitted to PROSITE and this formed the protein database. The dataset was then searched using the imputed sequences and any matching hits were listed as shown in **FIGURE 5.5C**. The PROSITE software identified multiple proteins that contained the LD-TBM the first of which was the protein CDK1. The PROSITE software only identified one LD-TBM in the CDK1 sequence and this matched the 206-223 sequence also identified using the manual approach. The other sequences included RIAM and DLC1 which are both confirmed LD-TBM giving greater confidence in the search method.

**A** STEP 1 - Submit PROTEIN sequences [help]

- Submit PROTEIN sequences (max. 1'000) [Examples](#)
- Submit a PROTEIN database (max. 16MB) for repeated scans (The data will be stored on...

```

TLN2_HUMAN
KANK2_HUMAN
1433G_HUMAN
RUXE_HUMAN
EHD_HUMAN
PROF2_HUMAN
ERLN1_HUMAN
DNJA2_HUMAN
MK67I_HUMAN
PSA3_HUMAN

```

Supported input:

- UniProtKB accessions e.g. P98073 or identifiers e.g. ENTK\_HUMAN
- PDB identifiers e.g. 4DGJ
- Sequences in FASTA format

**B** STEP 2 - Enter a MOTIF or a combination of MOTIFS [Examples](#) [help]

[ED]-[LI]-D-X-[AVILMFYW]-[AVILMFYW]-[AVILMFYW]-X-[AVILMFYW]

**prosite** ScanProsite Results Viewer

Output format: Graphical view - this view shows ScanProsite results together with ProRule-based predicted intra-domain features [\[help\]](#)

Hits for USERPAT1{[ED]-[LI]-D-X-[AVILMFYW]-[AVILMFYW]-[RKHED]-[AVILMFYW]-[AVILMFYW]} motif on

found: 5 hits in 5 sequences

**C** P06493 CDK1 HUMAN (297 aa)  
 RecName: Full=Cyclin-dependent kinase 1; Short=CDK1; EC=2.7.11.22; EC=2.7.11.23; AltName: Full=Cell division control pro

```

MEDYTKIEKIGEGTYGVVYKGRHKTTGQVWANKKIRLESEEEGVPSTAIRREISLLKELRHPNIVSL
QDVLMDGSRALYLIFEF LSPDLKKYLDISIPPGQVMDSSLVKSYLELQGIIVFCHSRVLRDLKPKQ
NLLDDKGTIKLADFGLARAFGIPIRVYTHEVVTLWYRSPVLLGSARYSTPVDIHSIGTIFAEALA
TKKPLFHGDSEIDQLFRIFRALGTPMNEWPEVESLQDYKNTFPKXKPGSLASHVKNILDENGLDL
SKMLIYDPAKRISGKIALNHPYFIDLDNIKKKI

```

**B** [ED]-[LI]-D-X-[AVILMFYW]-[AVILMFYW]-[RKHED]-[AVILMFYW]-[AVILMFYW]

**FIGURE 5.5: PROSITE SOFTWARE USED TO IDENTIFY LD TALIN-BINDING MOTIFS**

(A) An overview of the protein sequences imputed into the PROSITE software from talin1 proteomics database. (B) The LD talin-binding motif (sequence 2) imputed to the ScanProsite software. (C) The first hit identified, cyclin dependent kinase 1 (highlighted green box), to contain a potential LD talin-binding motif.

### 5.2.3 Validating the potential LD talin-binding motifs

The manual and bioinformatics-based approaches identified nine proteins that contained potential LD-TBMs. From the proteins identified, CDK1 (which was identified as a LD-TBM in both the manual and bioinformatics searches), and SEPT2 (identified in manual search), were chosen for further analysis, as both had high scoring in the talin proteomics.

Past searches for LD-motifs found that sequence searching alone identified many false positives. In order to further validate the LD-TBMs identified through a sequence search, a structural

evaluation was also carried out. This involved analysing both the structural position, secondary structure and sequence conservation of the LD-TBM.

### 5.2.3.1 Structural evaluation of septin2

Septins are a family of GTP-binding and membrane interacting proteins that were first discovered in yeast, where they were found to have a role in cytokinesis and cell morphology (Hartwell *et al.*, 1974). Septins are found in all eukaryotes and, in mammals, thirteen isoforms have been identified: septin 1-12 and septin 14 (Neubauer and Zieger, 2017). Septins are highly conserved through evolution with a common domain structure consisting of: an N-terminus region, central core domain with a GTP-binding domain and a coiled coil region (as shown in **FIGURE 5.6A**). In most isoforms a short polybasic region (PBR) can bind directly to phosphatidylinositol bisphosphate (PIP2) in the cell membrane (Neubauer and Zieger, 2017). Septin isoforms can be split into four sub groups as shown in **FIGURE 5.6B**, and septin isoforms within these subgroups can assemble into multimeric complexes of two or more subunits (Neubauer and Zieger, 2017; Xu *et al.*, 2018).

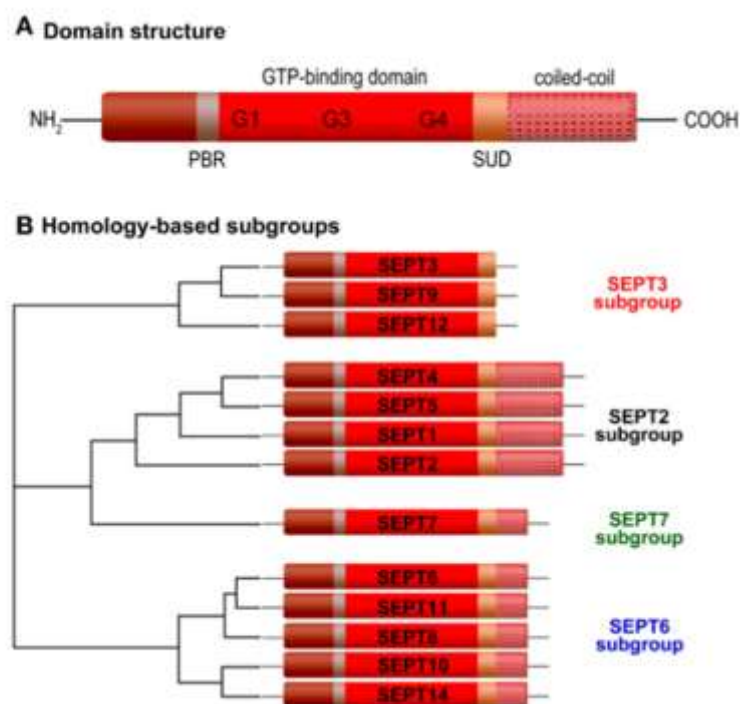


**FIGURE 5.6: SEPTIN ISOFORMS DOMAIN STRUCTURE AND SUBGROUPS**

(A) Schematic representation of septin domain structure. (B) Human Septin isoforms SEPT1-12 and SEPT14 subgroupings -based on homology sequence and coiled-coil domains. Figure from: (Neubauer and Zieger, 2017).

These complexes can form hexamer and octamer-like structures, which are believed to be stable within the cell (Neubauer and Zieger, 2017). Human septins predominantly form hetero-hexamers



and hetero-octamers composed of SEPT2, SEPT6, SEPT9 and SEPT7. The composition of septin complexes is cell type specific and is essential in determining the proteins function within the cell (Neubauer and Zieger, 2017).

It has been shown that mis-regulation of septin expression is associated with human tumorigenesis (Xu *et al.*, 2018). High expression levels of SEPT2 and SEPT7 have been detected in breast cancers and in particular down regulation of SEPT2 has been shown to suppress hepatoma cell growth (Xu *et al.*, 2018). In the talin1 proteomics SEPT2 was the most abundantly found septin; but, SEPT7 and SEPT9 were also present.

To further determine if the LD-TBM found within the SEPT2 sequence was likely to bind to talin; structural position, secondary structure and sequence conservation were all considered. **FIGURE 5.7** shows a SEPT2 sequence alignment of different vertebrate species from residues 150-195(inclusive of the LD-TBM). This alignment shows good conservation across species not only in this region but also in the region immediately before the Leu-Asp (position -1 - -4).

The crystal structure of SEPT2 has been solved (PDB ID: 2QA5) and is shown in **FIGURE 5.7B** and **C**. The LD-TBM region is highlighted in green and has a helical structure giving greater confidence that it could bind to talin via helical addition in a similar way to the known LD-motifs DLC1 and RIAM. Importantly, the motif appears to be exposed, enabling a possible interaction with talin. This binding site, however, could potentially be restricted if a hexamer or octamer structure is formed. After evaluating the structure and sequence of SEPT2, I would predict that it could form an interaction with talin via potential LD-TBM between residues 164-170.

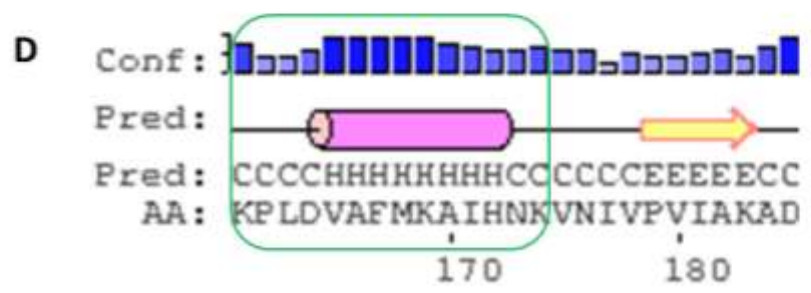
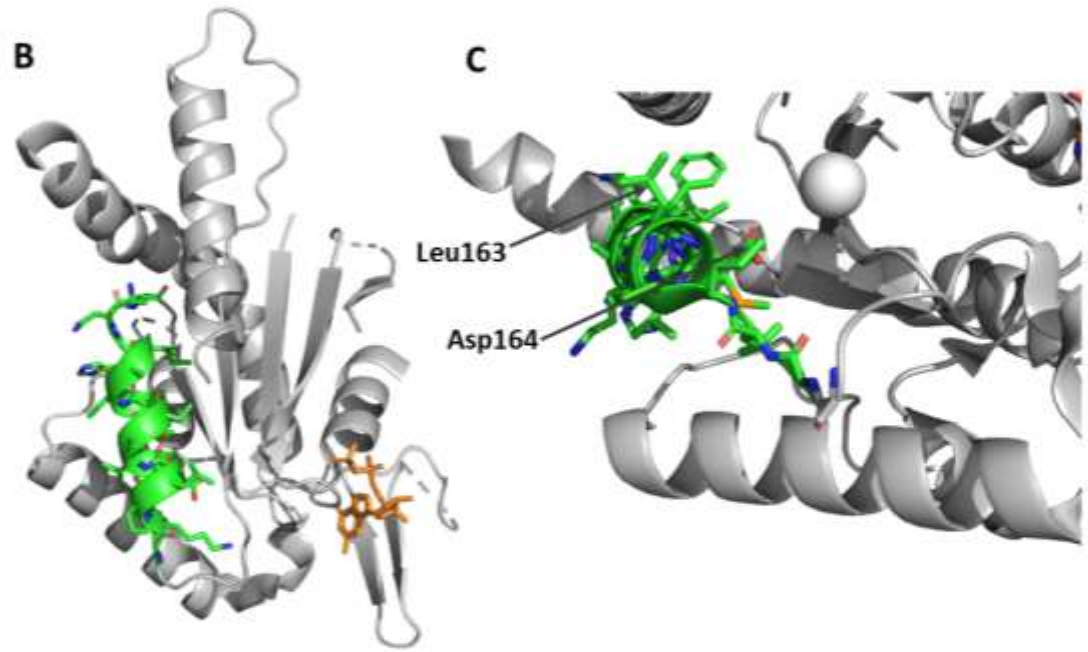
To determine if SEPT2 can bind to talin, we designed a synthetic peptide. The peptide encompassed the core LD-TBD between residues 164-170 and also included a few residues on both sides; to allow the peptide to adopt the correct helical fold. The inclusion of residues before position 0 is an important step learnt from designing the KANK1 peptides (**section: 4.2.1**), where the shorter KANK1 peptide (KANK1 42-68) started on the Leu residue (position 0) which significantly impaired binding to the talin LDBD.

The final SEPT2 peptide designed encompassed the residues 159-174 and an additional N-terminus Cys was attached to allow coupling to a fluorescent tag for binding experiments.

**A**

SEPT2_HUMAN	DNRVHCCFYFISPF <del>GHGLKPLDVAFMKAIHNK</del> VNIVPVIAKADTLTLKERERL	195
SEPT2_MOUSE	DNRVHCCFYFISPF <del>GHGLKPLDVAFMKAIHNK</del> VNIVPVIAKADTLTLKERERL	195
SEPT2_RAT	DNRVHCCFYFISPF <del>GHGLKPLDVAFMKAIHNK</del> VNIVPVIAKADTLTLKERERL	195
SEPT2_FLY	DSRIHICLYFICPTG <del>HGLKSLDLVCMKLD</del> SKVNIIPVIAKADTISKVELQRF	194
SEPT2_COW	DNRVHCCFYFISPF <del>GHGLKPLDVAFMKAIHNK</del> VNIVPVIAKADTLTLKERERL	195
SEPT2_CHICK	DNRVHCCFYFISPF <del>GHGLKPLDVEFMKALHGK</del> VNIVPVIAKADTLTLKERERL	194
SEPT2_C_ELEGANS	DKCVHLCLYFIEPSG <del>HGLKPIDIELMKHLHGR</del> VNIVPVISKADCLTRDELLRF	205
SEPT2_MONKEY	DNRVHCCFYFISPF <del>GHGLKPLDVAFMKAIHNK</del> VNIVPVIAKADTLTLKERERL	195

\*. :\* \*:\* \* :\*\*\* \* :\*\*\*\*\* :\*: \*\* :...:\*\*\*:\*\*\*:\*\*\* :: \* \*\*



**E** SEPTIN2 159\_174 CGLKPLDVAFMKAIHNK

**FIGURE 5.7: STRUCTURAL EVALUATION OF SEPTIN2 159-174 PEPTIDE**

(A) Sequence alignment of septin2 proteins from different vertebrates, the septin2 159-174 peptide highlighted in green. (B-C) show the structure of septin2 (PDB ID:2QA5) with the peptide residues coloured in green, (C) highlights the residues that are on the potential talin binding surface (Asp164 and Leu163). (D) Shows the PSIPRED predicted secondary structure for the peptide residues (highlighted by a green box) in human septin2. (E) shows the residues in the final ordered peptide with a N-terminal cysteine residue synthetically added.

### 5.2.3.2 Structural evaluation of Cyclin Dependent Kinase 1

CDK1 is part of a large family of Ser/Thr kinases, whose kinase activity is dependent of the addition of a regulatory subunit called cyclin (Malumbres *et al.*, 2009). CDKs regulate many cellular functions, including the cell cycle, transcription, mRNA processing, stem cell self-renewal and spermatogenesis (Lim and Kaldis, 2013). CDK1 is largely involved in regulating progression through the cell cycle and, in yeast, is the only cyclin-dependent kinase required to drive the cell cycle (Santamaría *et al.*, 2007).

CDK1 was identified as containing an LD-TBM in both the manual and bioinformatics searches, where the protein sequence appeared to have not one but two potential LD-TBMs. Both the manual and PROSITE search identified an LD-TBM within residues 210-220 and the manual search identified a second potential LD-TBM between residues 283-290. To determine if the site(s) were structurally viable to bind to talin and examine if these regions were conserved across species, we analysed CDK1's structure and performed protein sequence alignments.

### 5.2.3.3 CDK1 206-223 sequence evaluation

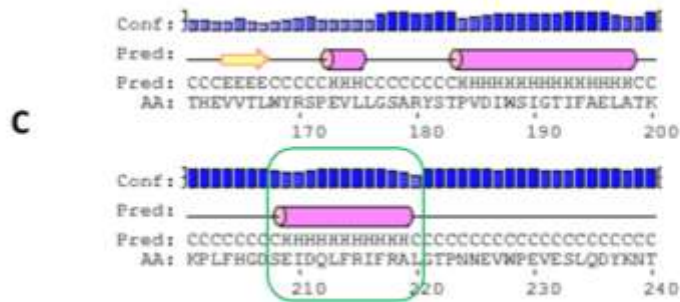
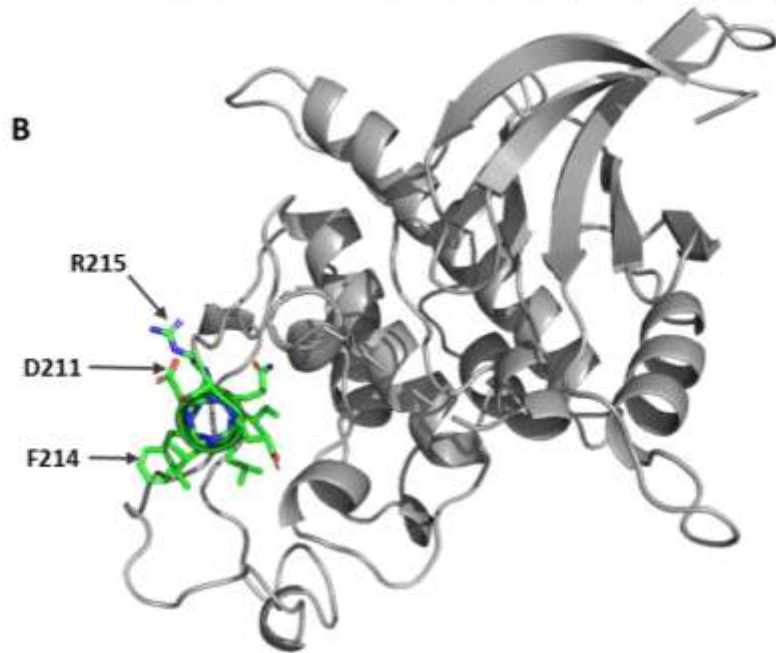
CDK1 residues 210-220 were identified in both the manual and PROSITE search, **FIGURE 5.8A** shows a sequence alignment of CDK1 from a number of vertebrates and single cellular organisms. The predicted LD-TBM (between residues 210-220) is highlighted in green and shows that the region is highly conserved across all species, further suggesting that the region is functionally important.

The crystal structure of CDK1 is shown in **FIGURE 5.8B** and again the LD-TBM (210-220) is highlighted in green. The LD-TBM is located in an accessible region of the structure and the region does not clash with the cyclin binding site on CDK1. The region has a clear helical structure that as previously discussed is important for the binding of an LD-motif to an LDBD. **FIGURE 5.8B** also highlights both the Leu210 and Asp211 residues on the structure (positions 0 and 1, respectively). The Asp residue points out into space, which could allow formation of a salt bridge with talin.

After evaluating both the conservation and the positioning of the LD-TBM on the CDK1 structure, we predicted that the CDK1 210-220 region would to bind talin. In a similar fashion to SEPT2, a synthetic CDK1 peptide encompassing the LD-TBM was designed. The peptide was designed to include residues 206-223 with a Cys at the N-terminus to allow coupling of a fluorescent tag. The peptide sequence is shown in **FIGURE 5.8C**.

**A**

CDK1_HUMAN	VLLGSARYSTPVDIWSIGTIFAELATKKPLFHGDSEIDQLFRIFRA	219
CDK1_MOUSE	VLLGSARYSTPVDIWSIGTIFAELATKKPLFHGDSEIDQLFRIFRA	219
CDK1_FLY	VLLGSPRYSCPVDIWSIGCIFAEMATRKPLFQGDSEIDQLFRMFRI	219
CDK1_SLIME MOULD	VLLGSKSYSVPVDMWSVGCIFGEMLNKKPLFSGDCEIDQIFRIFRV	220
CDK1_POMBE.YEAST	VLLGSRHYSTGVDIWSVGCIFAEMIRRSPLFPGDSEIDEIFKIFQV	224
CDK1_C.ELEGANS	ILMGAQRYSMGVDMWSIGCIFAEMATKKPLFQGDSEIDELFRIFRV	236
CDK1_COW	VLLGSARYSTPVDIWSIGTIFAELATKKPLFHGDSEIDQLFRIFRA	219
CDK1_GOLD FISH	VLLGASRYSTPVDVWSIGTIFAELATKKPLFHGDSEIDQLFRIFRT	219
CDK1_CHICK	VLLGSALYSTPVDIWSIGTIFAELATKKPLFHGDSEIDQLFRIFRA	219
	::*: . ** ** **:* **.*: .:.* **.***::**::**:	



**D** CDK1 206\_223 GDSEIDQLFRIFRALGTPC

**FIGURE 5.8: STRUCTURAL EVALUATION OF CDK1 206-223 PEPTIDE**

(A) Sequence alignment of CDK1 proteins from different vertebrates with the CDK1 206-223 peptide highlighted in green. (B) Models the structure of CDK1 (PDB ID:4YC6) with the peptide residues coloured in green and the potential talin binding residues are also highlighted (Asp211 and Ile210). (C) Shows the human CDK1 PSIPRED predicted secondary structure for the peptide residues (highlighted by a green box); the peptide looks to be in a helical region. (D) shows the residues in the final ordered peptide with a C-terminal cysteine residue synthetically added.

#### 5.2.3.4 CDK1 283-297 sequence evaluation

The additional LD-TBM identified within residues 287-297 of CDK1 was only identified in the manual search as this method is less stringent and does not fit strictly to sequence1 or sequence2 (section 5.2.1). To determine if this region could bind talin, the same structural evaluation process was carried out as with the CDK1 210-220 region.

**FIGURE 5.9A** shows the sequence alignment of CDK1 across different species highlighting the 290-297 region in green. This revealed that the LD-TBM is not conserved across species and that the Leu-Asp residues (position 0 and 1, respectively) are not found in all species. Residues 287-297 are highlighted on the CDK1 structure in **FIGURE 5.9B** and unlike with the SEPT2 and CDK1 210-220 region there is no helical propensity but instead the region is disordered. This was also confirmed when the sequence was run through the secondary prediction software PSIPRED (D. T. Jones, 1999). The results of the secondary structure prediction correlate with the CDK1's crystal structure and indicate a low level of confidence in helical formation (shown in **FIGURE 5.9D**).

The sequence is however, located in an accessible region of CDK1 meaning that talin could potentially bind without hindrance. Furthermore, Asp288 in position 1 points out into space allowing the possible formation of a salt bridge with talin.

After evaluating the structure and sequence of CDK1's 287-297 region, it appeared unlikely the possibility of an interaction with talin. In spite of this, the region was ordered as a synthetic peptide to confirm this and thus determine how accurate and relevant the structural analysis of the LD-TBM was. A synthetic peptide of residues 283-297 was designed and an N-terminal Cys was added (shown in **FIGURE 5.9E**).

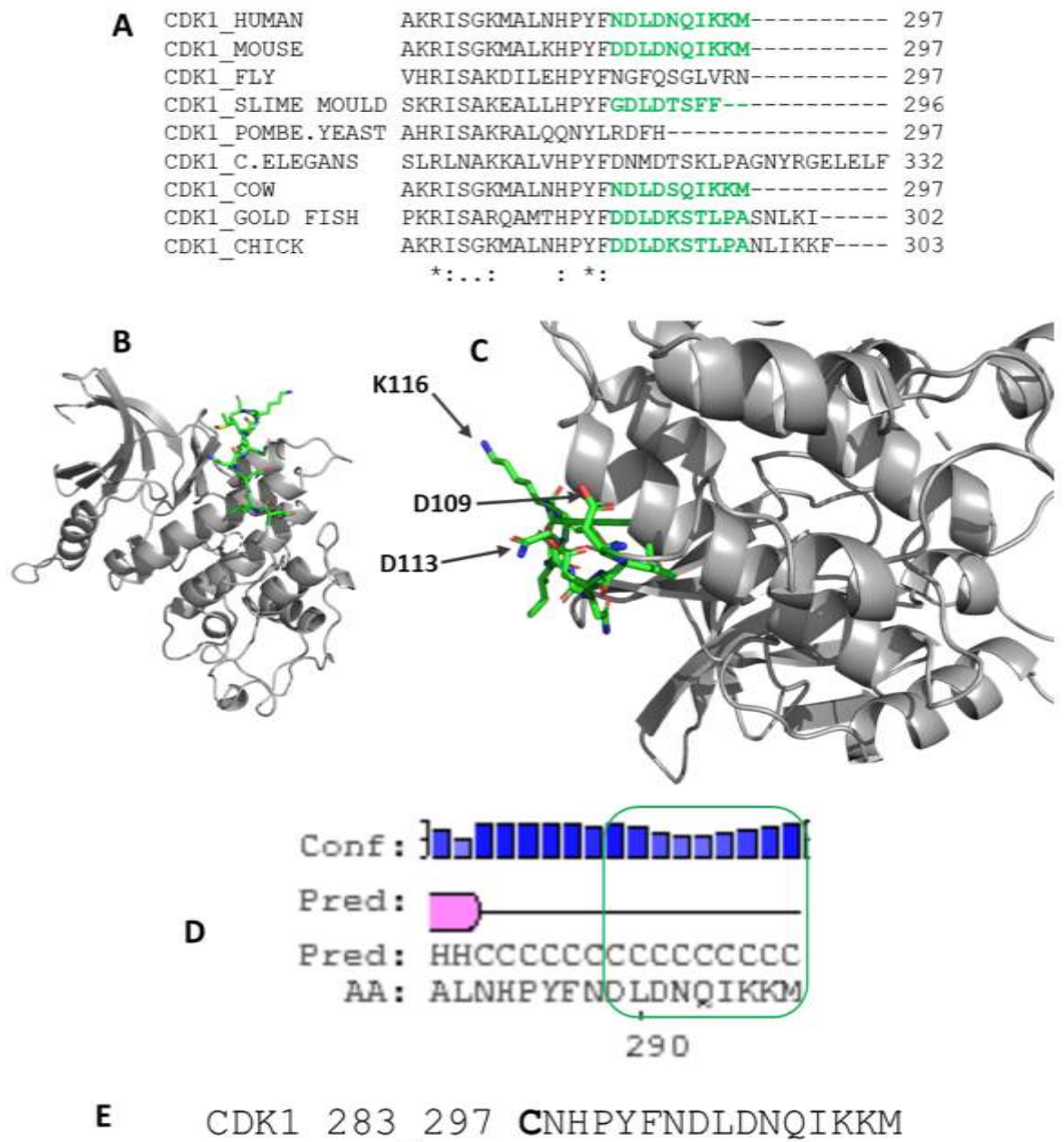


**FIGURE 5.9: STRUCTURAL EVALUATION OF CDK1 283-297 PEPTIDE**

(A) Sequence alignment of CDK1 proteins from different vertebrates with the CDK1 283\_297 peptide highlighted in green. (B-C) show the structure of CDK1 (PDB ID:4YC6) with the CDK1 283\_297 peptide residues coloured in green, (C) highlights the residues of the potential talin binding motif Leu and Asp residues. (D) PSIPRED secondary structure prediction for the peptide residues (highlighted by a green box) in human CDK1; the peptide looks to be in an unstructured region. (E) shows the residues in the final ordered peptide with a N-terminal cysteine residue synthetically added.

## 5.2.4 Determining if the LD talin-binding motifs bind talin

Through the design of a novel LD-TBM and the use of structural evaluation methods, we were able to identify two potential proteins that could bind to talin. From these hits, three synthetic peptides were designed encompassing three potential LD-TBM in proteins SEPT2 and CDK1.

- |      |                |                     |
|------|----------------|---------------------|
| I.   | SEPT2: 159-174 | CGLKPLDVAFMKAIHNK   |
| II.  | CDK1: 206-223  | GDSEIDQLFRIFRALGTPC |
| III. | CDK1: 283-297  | CNHPYFNDLDNQIKKM    |

The synthetic peptides are predicted to bind to talin via helical addition to a folded helical bundle in the talin rod. The talin rod is comprised of 13 helical bundles (as shown in **FIGURE 5.10**) and so to determine which bundle(s) the peptide can bind, a talin-screening assay was developed.

Talin is a large 250 kDa protein and although the full-length protein can be purified from *E. coli*, only very low yields can be produced, making many of the available biochemical assays unfeasible. Furthermore, using the whole talin protein would allow us to gauge if the peptide binds but it would not enable the refinement of the binding site. To overcome these issues, the talin rod was broken down into four large fragments: R1-R3 (residues 482-911), R4-R8 (residues 913-1653), R9-R12 (residues 1461-2294) and R13-DD (residues 2300-2541). These regions are shown in **FIGURE 5.10** and all can be expressed with high yields from *E. coli*, allowing the use of biochemical assays such as FP allowing us to screen for multiple ligands in quick succession against different regions of the rod domain.



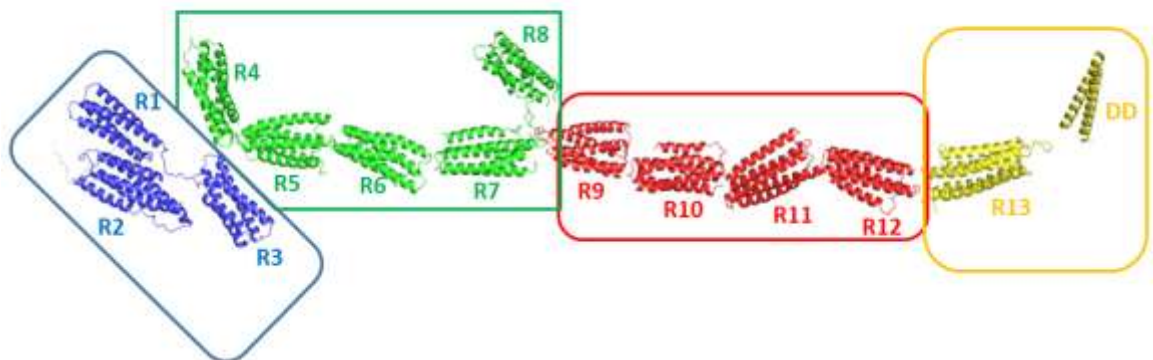


**FIGURE 5.10: THE TALIN ROD DIVIDED INTO FOUR BIG FRAGMENTS**

Schematic diagram of talin rod domains. Talin rod has been separated into the four talin fragments the blue box indicates R1-R3 fragment (residues 482-911), green box indicates R4-R8 fragment (residues 913-1653), red box indicates R9-R12 fragment (residues 1461-2294) and yellow box indicates R13-DD fragment (residues 2300-2541).

#### 5.2.4.1 Fluorescence polarisation with talin1 'big fragments'

The synthetic peptides (CDK1 206-223, CDK1 283-297, SEPT 159-174) were each coupled to the fluorescent tag, BODIPY-TMR, to be used in the FP assay (see methods **section: 3.4.2**). The four talin fragments (R1-R3, R4-R8, R9-R12 and R13-DD) were all concentrated to 200  $\mu$ M and increasing amounts of each fragment were titrated against each of the synthetic peptides. The binding of the KANK1 30-60C peptide (from **Chapter 4**) was also tested against each of the four talin fragments as a positive control for the R4-R8 fragment of talin.

The binding affinity of each peptide for the talin fragments are shown in **FIGURE 5.11**. As expected KANK1 30-60C bound to the talin1 R4-R8 domain region but displayed no binding to any of the other large fragments. Of the remaining peptides, only the CDK1 206-223 peptide was bound to talin. In this case, the peptide appeared to bind in multiple places within the talin rod, as there was binding affinity for talin1 R9-R12 and talin1 R4-R8. Neither the SEPT2 159-174 or the CDK1 283-297 peptides showed binding affinity to any of the talin fragments.



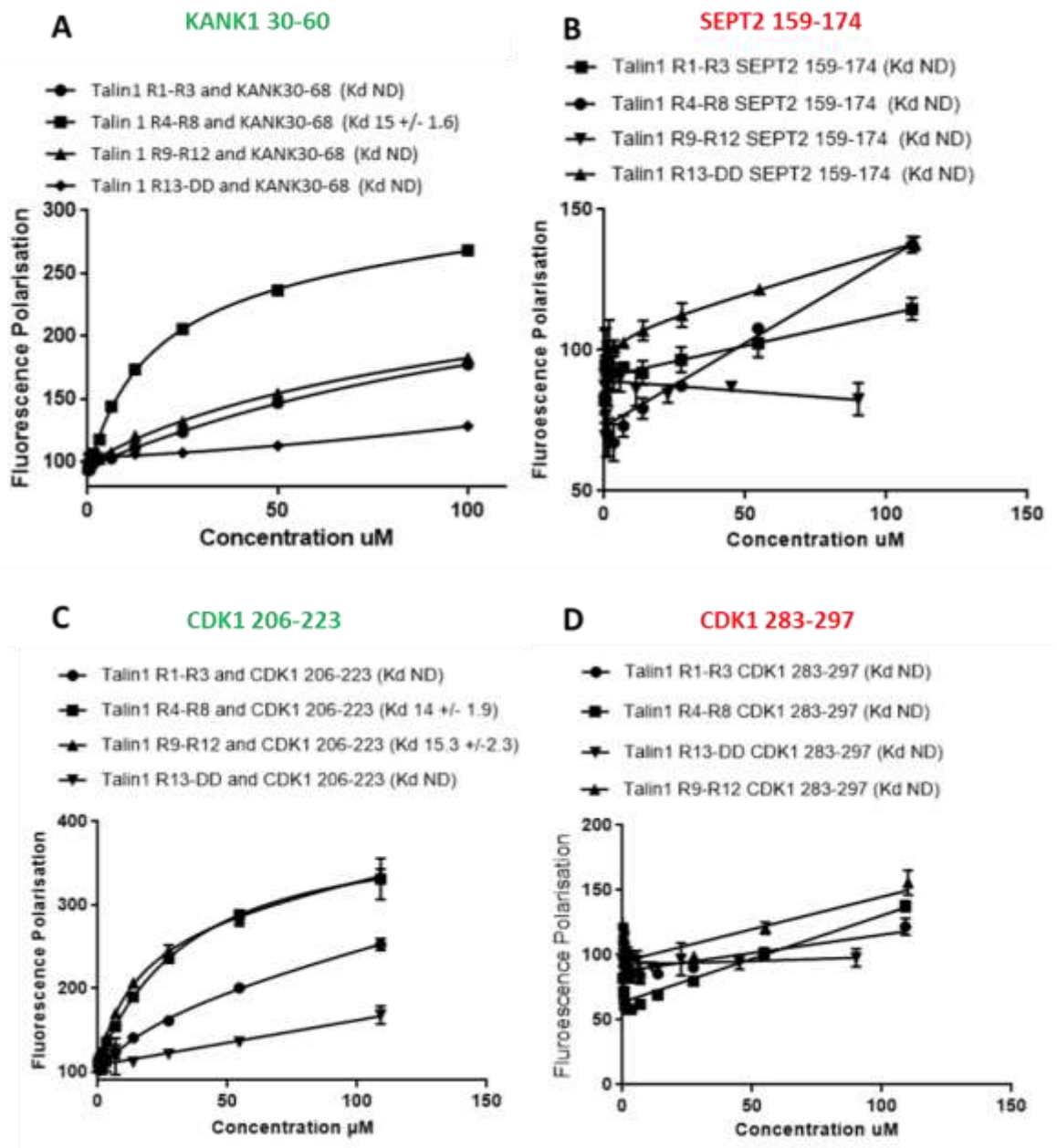


**FIGURE 5.11: BIOCHEMICAL CHARACTERISATION OF LD TALIN-BINDING MOTIFS TO TALIN ROD FRAGMENTS**

(A-D) Binding of BODIPY-TMR labelled; CDK1 206-223C, CDK1 283-297, SEPT2 159-174, KANK1 30-60 peptides to talin domains; R1-R3 (residues 482-911), R4-R8 (residues 913-1653), R9-R12 (residues 1655-2294) and R13-DD (residues 2300-254). Binding affinities were measured using a Fluorescence Polarization assay. Dissociation constants  $\pm$  SE ( $\mu$ M) for the interactions are indicated in the legend. All measurements were performed in triplicate. ND, not determined.

#### 5.2.4.2 Refining the talin binding site of CDK1 206-223

The binding curves shown in **FIGURE 5.11** indicate that CDK1 206-223 could bind to both talin fragments, R4-R8 and R9-12, with an equal affinity of  $\sim 15 \mu\text{M}$ . However, through optimisation of the assay with the large talin fragments, we noticed that talin1 R9-R12 can bind to BODIPY-TMR (data not shown) leading to potential artifacts on the FP data. To overcome this problem, the talin1 R9-R12 fragment was split into two smaller domains: R9-R10 (residues 1655-1973) and R11-R12 (residues (1974-2294)). These seemed to be a good compromise, as both double-domains were easily expressed and do not bind to BODIPY-TMR.

The same FP assay was then carried out with the two smaller fragments, R9-R10 and R11-R12. The binding affinity of CDK1 206-223 peptide to the five talin fragments is shown in **FIGURE 5.12C**. This time no interaction was observed between the peptide and talin domains R9-R10 or R11-R12. This leads to the conclusion that CDK1 206-223 can only bind to talin1 R4-R8 and does so with an affinity of  $14 \mu\text{M}$ .

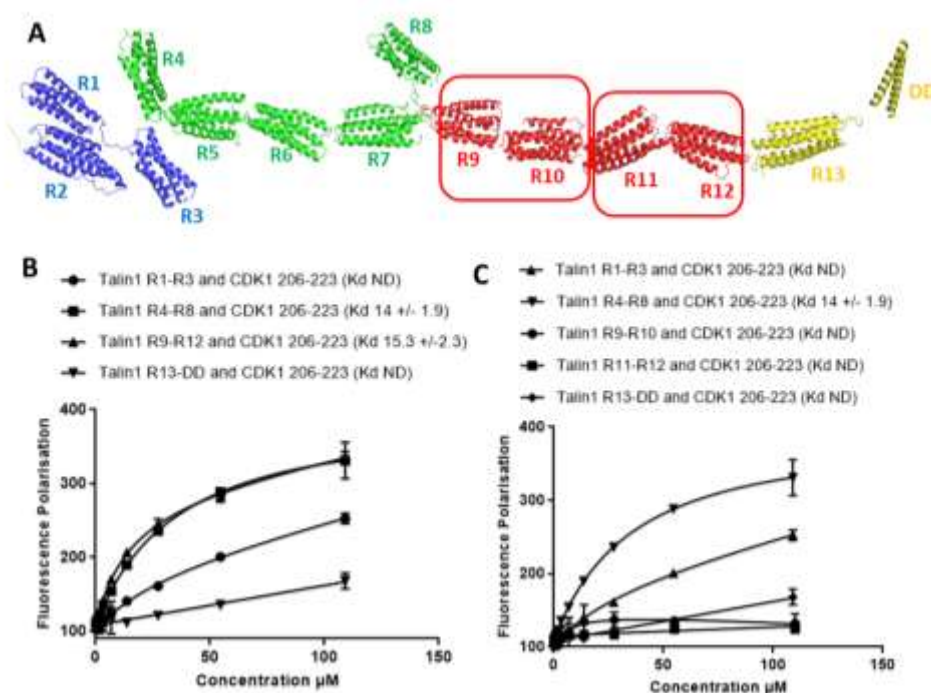


**FIGURE 5.12: BIOCHEMICAL CHARACTERISATION OF CDK1 206-223 PEPTIDE**

(A) Talin rod domains predicted structure highlighting the rod fragments used in the corresponding FP assay, red box highlights the splitting of the R9-R12 fragment into smaller R9-R10 and R11-R12 fragments. (B-C) Binding of BODIPY-labelled CDK1 206-223C peptide to talin domains; R1-R3 (residues 482-911), R4-R8 (residues 913-1653), R9-R10 (residues 1655-1973), R11-R12 (residues 1974-2294) and R13-DD (residues 2300-254). Binding affinities were measured using a Fluorescence Polarization assay. Dissociation constants  $\pm$  SE ( $\mu\text{M}$ ) for the interactions are indicated in the legend. All measurements were performed in triplicate. ND, not determined.

## 5.3 Discussion

### 5.3.1 Identifying future talin binding partners

Of the chosen LD-TBMs identified in the manual and bioinformatics approaches only the CDK1 206-223 peptide was found to have a binding affinity to talin. The SEPT2 159-174 and CDK1 283-297 peptides were not identified to bind to talin. Can the lessons from this initial screening help refine the LD-TBM sequence and enable us to search for further talin binding proteins?

Initially, it was believed that all the chosen peptides fitted the LD-TBM closely enough to bind to talin. However, a structural evaluation was carried out on each peptide whereby the secondary structure of the peptide, sequence conservation and structural positioning were analysed. The structural evaluation determined that, the CDK1 206-223 and the SEPT2 159-174 peptide would be likely to bind talin and the CDK1 283-297 peptide would be unlikely to bind talin. This was due to the CDK1 283-297 peptide not having a helical structure and also not being conserved across species, implying the region was not of functional importance. From the structural analysis it was not a surprise to determine the CDK1 283-297 peptide had no binding affinity to talin. It was however, a surprise that the SEPT2 159-174 peptide had no binding affinity to talin.

LD MOTIF/ Position	-3	-2	-1	0	1	2	3	4	5	6	7	8	9
<i>Consensus</i>	X	X	F	L	D	X	L	L	X	X	L	X	X
*PXN LD1	M	D	D	L	D	A	L	L	A	D	L	E	S
*RIAM	S	E	D	L	D	Q	M	F	S	T	L	L	G
*DLC1	F	P	E	L	D	D	L	L	Y	H	V	K	G
*KANK1	Q	L	D	L	D	F	V	K	Y	V	D	D	I
*KANK2	R	L	D	L	D	F	L	K	Y	V	D	D	I
*CDK1_206	D	S	E	L	D	Q	L	F	R	I	F	R	A
CDK1_283	F	N	D	L	D	M	Q	L	K	K	M		
Septin2	L	P	P	L	D	V	A	F	M	K	A	I	H

**FIGURE 5.13: SEQUENCE ALIGNMENT AND EVALUATION OF LD TALIN-BINDING MOTIFS**

Sequence alignment of: paxillin LD1 (UniProt ID: P49023); RIAM (UniProt ID: Q7Z5R6); DLC1 (UniProt ID: Q96QB1); KANK1 (UniProt ID: Q14678); KANK2 (UniProt ID: Q63ZY3); CDK1 (UniProt ID: P06493) and SEPT2 (UniProt ID: Q15019). Red highlights acidic residues, blue basic residues and green hydrophobic residues. Known talin binding sequences are highlighted with an \*.

To determine why the SEPT2 peptide did not bind to talin, the tested LD-TBM peptides were aligned alongside known LD-TBMs (shown in **FIGURE 5.13**). The alignment indicates the only difference between the SEPT2 159-174 peptide and the other successful talin binding peptides is the residue found in the -1 position. Earlier analysis determined the -1 position to be important

for binding talin and a charged Asp needed to be present, the SEPT2 peptide had a Pro in this position not fitting the criteria. Enforcing the -1 position in the LD-TBM to be of high importance. The alignment also highlighted a slight variation in the CDK1 283-297 peptide compared to other known LD-TBMs; the Gln residue at position +3 (highlighted by yellow box) is not a hydrophobic residue like the other LD-TBM in this position. Glutamine is a polar residue and could disrupt binding, potentially indicating that the +3 position is also of importance in the LD-TBM sequence.

This preliminary screening of talin proteomics hits, with a designed LD-TBM sequence has proved successful and the LD-TBM has identified a novel talin binding protein, CDK1. Using the results of successful and non-successful talin binding sequences the eight residue LD-TBM has been refined and important residues (-1,0,1, +3) have been identified. Furthermore, it has been established that 'sequence searching' for LD-TBMs is not enough on its own to identify talin binding partners, further structural analysis helps to reduce the number of false positives identified.

Further analysis of new LD-motifs binding to talin will give a better understanding of the binding mechanism to talin and in the future it is hoped that the designed LD-TBM can be used to search larger databases of proteins helping to identify future talin binding proteins. Furthermore, proteomics with talin1 in different cell types would give more information on talin binding partners in different cell types and different conditions. Equally, it would be interesting to determine if there is any difference in LD-motifs binding the two talin isoforms in order to further understand the functional differences between the two isoforms.

### **5.3.2 LD-motifs can bind to multiple LDBDs**

LD-motifs can be recognised by multiple LDBDs with different three-dimensional structures. For example, paxillin can bind to both vinculin and talin which both have different binding surface residues (Tumbarello, Brown and Turner, 2002). This research identifies that LD-motifs do not have to adhere to the strict LDxLLxxL consensus sequence to bind LDBDs and this sequence adaptability would suggest that the LD-helix is malleable and the hydrophobic side chains on the LD-motif are able to adjust to binding to different surfaces.

This promiscuity between LD-motifs and LDBD raises questions around how LD-motifs are being correctly directed to their target molecule and prevented from forming non-specific interactions. Specificity is important, as an LD-motif binding to the wrong LDBD can trigger the incorrect cellular response (Alam *et al.*, 2014). Understanding this specificity would lead to further understanding of the biological processes LD-motifs are involved in and understand how dysfunction in these

relationships can lead to disease. Our research has identified that the specificity of LD-motifs is incredibly sensitive to sequence, and a single point mutant at the -1 or +3 position can change whether it binds talin or not. Therefore, the specificity between LD and LDBD interactions, whilst not fully understood is likely driven by similar alterations to the sequence of the surrounding residues of the LD-motif.

### 5.3.3 Talin LDBD specificity

Talin1 R8 is a LDBD that has been shown to bind multiple different LD-motifs including: DLC1, RIAM and Paxillin (Goult, Zacharchenko, *et al.*, 2013; Zacharchenko *et al.*, 2016). The talin R8 domain can also bind to multiple non-LD proteins such as actin,  $\alpha$ -synemin and vinculin making it a major signalling hub in the talin tail.

As previously discussed in the introduction (**Chapter 2**) the positioning of talin R8 is unlike any of the other talin rod domains. In the talin rod, each helical bundle provides a link to the next rod domain via a short unstructured linker, talin R8 however, is inserted into the five helical bundle R7 domain, between helices 30 and 36 as shown in **FIGURE 5.14** (Yao *et al.*, 2016). This domain insertion protects the four-helix R8 domain from being 'unravelling' by mechanical force (Yan *et al.*, 2015; Yao *et al.*, 2016). The talin four-helix bundles are less mechanically stable than five-helix bundles; talin1 R8 on its own can be unfolded at 5 pN (Yao *et al.*, 2016). Whereas a five-helix bundle such as R7 is not unfolded until a higher force of 15 pN (Yao *et al.*, 2016). When R8 is inserted into the R7 domain the four-helix R8 domain does not unfold until after the R7 domain unfolds at 15 pN, allowing the R8 domain to remain stable and keep its helical bundle structure. The helical bundle forms the binding site for LD-motifs and other ligands which when bound can help regulate focal adhesion maturation.

With talin R8 acting as a signalling hub and binding many crucial ligands, how are the interactions to the domain regulated?

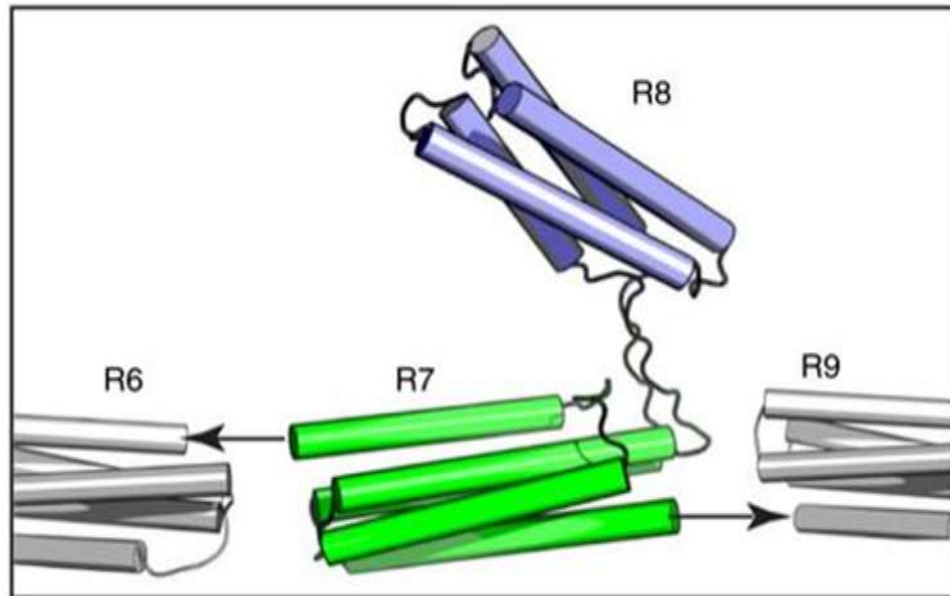


**FIGURE 5.14: TALIN R8 DOMAIN STRUCTURE IN RELATION TO THE TALIN TAIL**

A schematic representation of the talin R7-R8 domain structure. Talin R8 (blue) shown to be inserted into the talin R7 domain (green) via unstructured linkers. The arrows showing the direction of the adjacent domains R6 and R9 and the applied force. Figure from: (Yao *et al.*, 2016).

### 5.3.3.1 Talin auto-inhibition

One way in which the talin could regulate when an LD-motif can bind to the R8 domain is through talin autoinhibition. Talin can form homodimer complexes which are able to adopt a compact auto inhibited conformation in the cytosol (Goult, Xu, *et al.*, 2013). The two talin molecules wrap around each other in a doughnut like conformation with both talin head domains buried in the centre. In this conformation the talin R8 domain is hidden (as shown in **FIGURE 5.15**) meaning that the helices are not exposed to bind to LD-motifs. This conformation could be a way to prevent LD-motifs binding to talin when it is not at the cell periphery or near an adhesion.

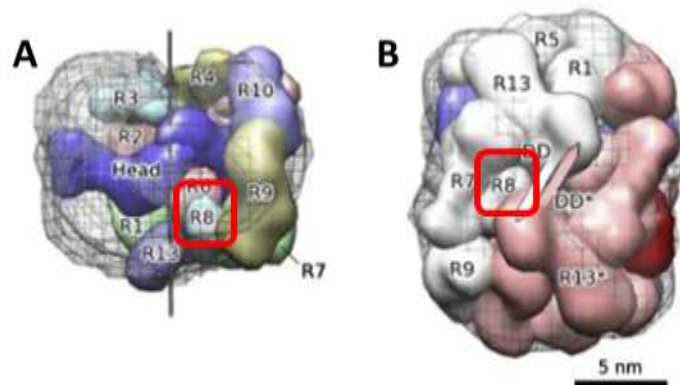


**FIGURE 5.15: TALIN AUTOINHIBITION**

(A) Front view of the talin1 dimer in compacted doughnut like conformation. (B) Top view of the talin dimers the two monomers are coloured either white (rod), blue (head) and pink (rod), red (head) respectively. In both A and B the talin R8 domain is highlighted by a red box. Figure adapted from: (Goult, Xu, *et al.*, 2013).

Furthermore, it was described how talin has many layers of autoinhibition (**section 2.7**) and that individual talin domains can become unfolded when subjected to force. When the helical bundles are unfolded the binding sites for LD-motifs are destroyed thus, preventing LD-motifs from binding to talin. This prevention of LD-motifs binding under high force could be a mechanism in which the cell prevents LD ligands binding and allow other ligands such as vinculin to bind.

### 5.3.3.2 Binding affinity of LD-motifs to talin

LD-motifs bind to talin with micro molar affinity; RIAM and DLC1 ligands bind to talin R8 with an affinity around 4  $\mu\text{M}$  and paxillin binding is found to be much weaker (Zacharchenko *et al.*, 2016). The KANK LD-TBM was the tightest binding talin LD-motif found to date with a binding affinity of 1  $\mu\text{M}$ . The weakness of the binding between talin and the LD-motif could be functionally important as it could prevent non-specificity between LD-motifs and LDBDs. In order to have an interaction between the LD-motif and talin there would need to be a high concentration of the LD-motif in the vicinity of talin or equally a high concentration of talin around the LD-motif. This could prevent interactions between talin and LD-motifs from occurring when not at adhesions.

Spatial and sequential binding of LD-motifs and talin could result indirectly from co-expression and co-localisation of LD-motifs and/or talin proteins. It could also rely indirectly on clustering from their recruiting factors such as integrin clusters at focal adhesions or CMSC clusters.

### 5.3.3.3 Post-translational modifications

Post-translational modifications could also be a way to regulate binding of LD-motifs to talin. When looking at the paxillin LD-motifs binding to LDBDs, phosphorylation of the LD-motif has resulted in weakening of binding to the LDBDs. Phosphorylation of paxillin LD4 weakened the helical propensity of the LD-motif and consequently reduced binding to the FAK FAT domain by a factor of ~2.5 (Schmalzigaug *et al.*, 2007).

No PTMs have been yet found on the sequences of LD-TBMs: DLC1, RIAM and KANK however, the CDK1 206-223 LD-TBM does appear to contain a phosphorylation site at residue Ser206 (information from PhosphoSitePlus (Hornbeck *et al.*, 2015)). This residue is located in position -2 of the LD-TBM, there is also another phosphorylation site found in the CDK1 206-223 LD-TBM at Thr222. Phosphorylation at either of these sites, but in particular Ser206, could prevent or weaken the interaction between talin and CDK1 through a change in binding surface or the LD-motif losing helical propensity.

Furthermore, PTMs on the surface of talin could have an impact on the binding of LD-motifs. **FIGURE 5.16** shows some of the known PTMs on talin R7R8. In our review, we catalogued the published the known talin PTMs and found that Ser1508 (talin R8) and Ser1641 (talin R7) can be phosphorylated and Thr1487 (talin R8) has been reported to be acetylated (Gough and Goult, 2018). These PTMs on talin could have an effect on the binding of LD-motifs. In the characterisation of the talin:KANK interaction (**chapter 3**) a phosphomimetic mutant S1641E was used to disrupt the binding of talin:KANK interaction. This mutant did not completely perturb binding but did result in a four-fold weakening in binding affinity between talin R7R8 and KANK; a similar finding to that in paxillin LD4 and FAT.



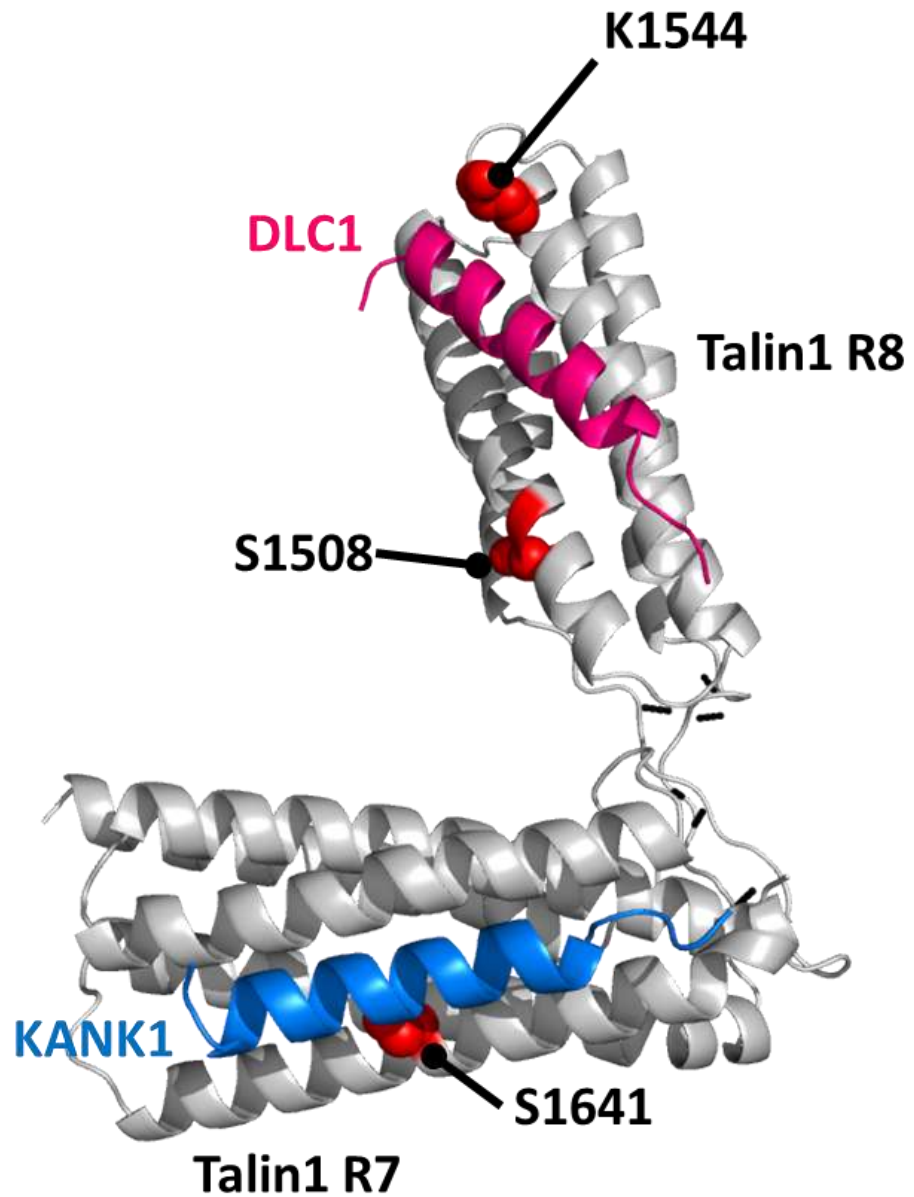


**FIGURE 5.16: TALIN R7R8 POST-TRANSLATIONAL MODIFICATIONS**

Talin1 R7R8 KANK1 30-60 and DLC1 predicted structure, with highlighted PTMs in red (data from PhosphoSitePlus). DLC1 461-489 (pink) and KANK 30-68 (blue).

# **Chapter 6. Identifying and characterising the interaction between talin and CDK1**

---

## 6.1 Introduction

In the previous chapter, I described how a designed LD talin-binding motif was used to screen through talin proteomic datasets in order to identify novel talin binding partners. Sequence conservation and structural characteristics of these potential talin-binding proteins were further assessed and, from this the protein known as cyclin dependent kinase1 (CDK1) stood out as an interesting talin binding protein. In this chapter, I describe the biochemical characterisation of the interaction between talin and CDK1 and look at how talin affects the phosphorylation activity of CDK1, to determine whether there is a link between the cell cycle and adhesion regulation.

### 6.1.1 The cell cycle

The cell cycle is a tightly regulated process that orchestrates gene duplication and accurate segregation of DNA and other factors into two daughter-cells. The cell cycle is split into four distinct phases  $G_1$ ,  $G_2$ , S phase and M phase (mitosis) (see **FIGURE 6.1**). In the  $G_1$  phase metabolic changes prepare the cell for DNA replication, S phase involves the duplication of genetic material to create sister chromatids.  $G_2$  prepares the cell for division and assembles all cytoplasmic components needed for entry into the M phase, where nuclear division also known as mitosis, occurs, which creates two daughter-cells (Lim and Kaldis, 2013). Before entry into each phase of the cycle, the cell has a series of checkpoints it must pass in order to prevent incorrect chromosome replication. When these checkpoints fail and the cell cycle progresses incorrectly, this can lead to disease and is often recognised as a hallmark of cancer (Sherr and Bartek, 2017). One group of molecules used to ensure regulated progression through each of the phases is the family of cyclin dependent kinases (CDKs) and their partnering cyclins.

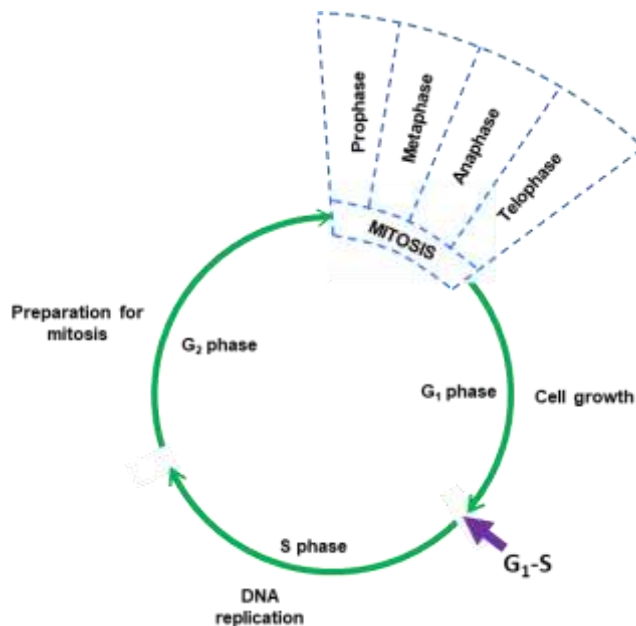


**FIGURE 6.1: THE CELL CYCLE**

A schematic diagram of the cell cycle highlighting each of the four phases involved G<sub>1</sub> phase, S phase, G<sub>2</sub> phase and M phase (mitosis).

### 6.1.2 Cyclin Dependent Kinases

CDKs are a large family of serine/threonine kinases that partner with regulatory subunits known as cyclins, which control the kinase activity and substrate specificity of CDKs (Lim and Kaldis, 2013). The first CDK discovered was in budding yeast, CDC28 (known as CDK1 in mammalian cells, see **FIGURE 6.2**, and was revealed to play a crucial role in controlling cell cycle progression through interactions with different cyclins (Beach, Durkacz and Nurse, 1982). Yeast became a working model to study both CDK proteins and the cell cycle, and it was shown that CDC28 (CDK1) was the only CDK needed to drive cell division in yeast models (Santamaría *et al.*, 2007).

In contrast to yeast, the mammalian cell cycle has several different CDK proteins which aid regulation of entry into each cycle phase although, similarly to yeast, CDK1 is the only CDK required to drive the cell cycle (Santamaría D1, Malumbres M *et al.*, 2007). Humans have twenty identified CDK proteins, named CDK1-CDK20, categorised into two classes: cell cycle related CDKs (these can bind to multiple cyclins), and transcriptional CDKs (these can bind to single cyclins) (Malumbres, 2014) (shown in **FIGURE 6.2**). The main required CDKs for cell cycle are CDK1, CDK2, CDK4 and CDK6 (Malumbres, 2014); these CDKs mediate the cell cycle through association with different cyclins.

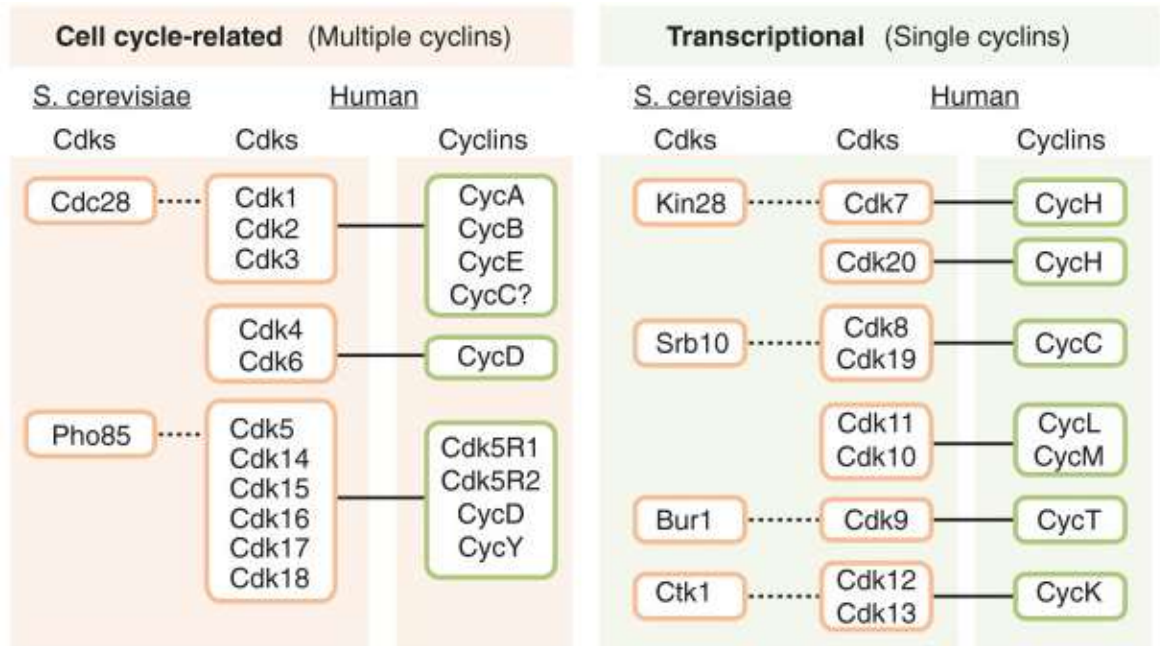


**FIGURE 6.2: CDKS AND CORRESPONDING CYCLINS**

A list of human CDKs and their partnering cyclin, the CDKs are split into two categories cell cycle-related and transcriptional CDKs. Figure is taken from: (Malumbres, 2014).

### 6.1.3 Cyclin-dependent kinase activation

Cyclins are small proteins that bind to CDKs to activate their kinase ability; they are named cyclins because they undergo a cycle of synthesis and degradation over the course of the cell cycle (Yang, 2018). CDK1 can be partnered with either cyclinA, B or E (shown in **FIGURE 6.2**) and the cyclin to which CDK1 is bound, determines the phase of the cell cycle. As such, CDKs could be considered as the 'engine' that drives the cell cycle and cyclins as the 'gears' that have to be changed to aid the transition between the cell cycle phases.

In the first phase, cyclinE is bound to CDK2 which promotes entry to S phase (Pines and Hunter, 1990). Subsequently, cyclin A levels begin to rise driving the binding of CDK1-cyclinA and, by late S phase, there is a detectable level of CDK1-cyclinA in the cell (Malumbres, 2014). This aids entry into G<sub>2</sub> phase, where levels of cyclinA slowly decrease and cyclinB levels rise (see **FIGURE 6.3**). The binding of cyclinB to CDK1 promotes the cells entry into M phase and is known as the 'mitosis promoting factor' (Lohka, Hayes and Maller, 1988).

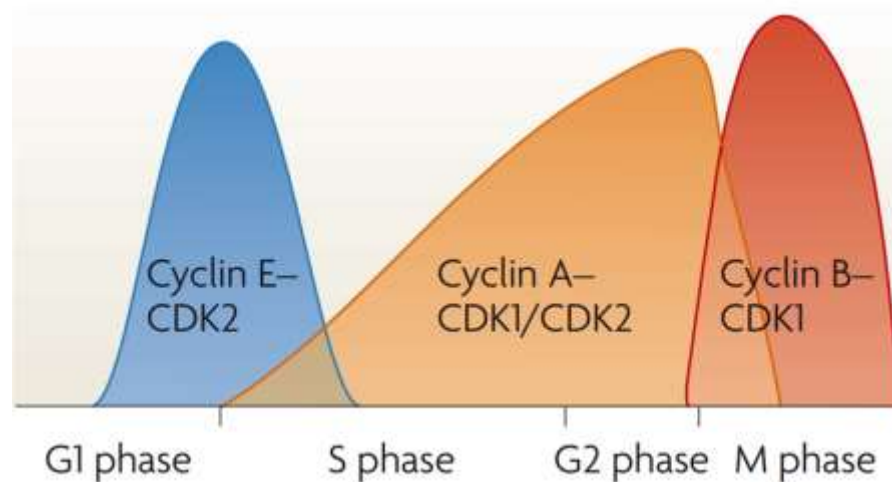


**FIGURE 6.3: LEVELS OF CYCLIN AND CDK COMPLEXES IN THE DIFFERENT PHASES OF THE CELL CYCLE**

A model to show the levels of cyclin-CDK complexes at the different phases of the cell cycle. cyclin E-CDK2 triggers S phase, cyclin A-CDK2 and cyclin A-CDK1 regulate the completion of S phase, and CDK1-cyclin B is responsible for mitosis. Figure from: (Hochegger, Takeda and Hunt, 2008).

To prevent early entry into mitosis, the activity of CDK1-cyclinB is regulated by several feedback loops. When in early G<sub>2</sub> phase, inactive CDK1-cyclin B is maintained in the cytosol through phosphorylation of CDK1 at residue Tyr15, by Wee1 kinase and related kinases (Gould and Nurse, 1989).

The activity of cyclinB then progressively increases once the cell enters prophase and active cyclinB-CDK1 can translocate to the nucleus, triggering several mitotic events such as cell rounding, nuclear envelope breakdown and spindle formation (Gavet and Pines, 2010). Cell rounding is an important stage for entry into mitosis. Throughout the cell cycle, anchorage to a matrix is important requiring both integrin-ECM interactions and the formation of actin-associated complexes. As the cell enters M phase cell rounding occurs (see **FIGURE 6.4**) and adhesion complexes are rapidly disassembled allowing for the cell to retract from the surface and round up to divide (Jones *et al.*, 2018). Cell rounding is required for accurate spindle formation and chromosome capture (Carreno *et al.*, 2008). Integrin mediated adhesion is required for orientation of cell division and efficient cytokinesis to occur (Jones *et al.*, 2018).

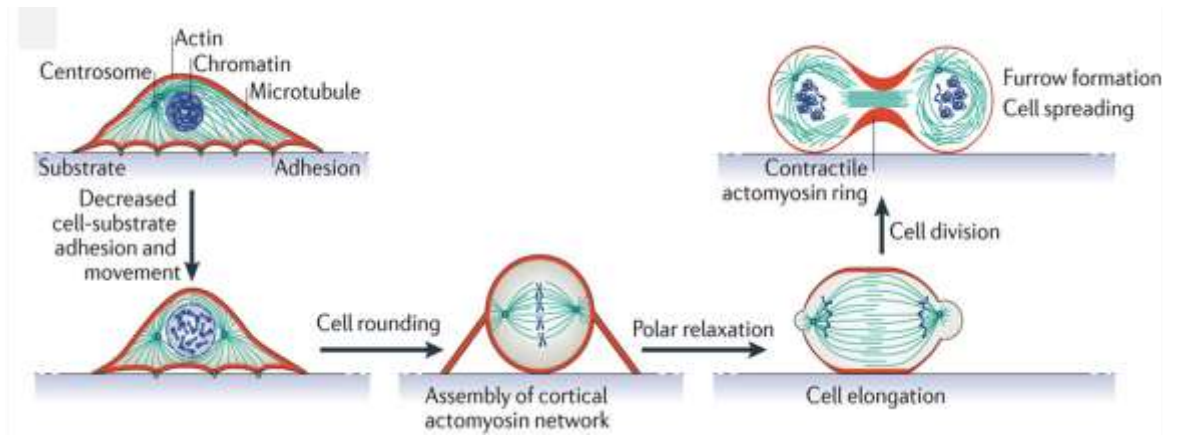


**FIGURE 6.4: CELL ADHESIONS RETRACT BEFORE ENTRY INTO MITOSIS**

A schematic diagram showing cell-matrix adhesions on entry into mitosis. During the onset of mitosis levels of CDK1-cyclinB rise and cell adhesions are lost. Figure adapted from: (Ramkumar and Baum, 2016)

### 6.1.4 CDK1 Phosphorylation

CDK1 has a 'two lobed' structure consisting of an N-terminal lobe and a C-terminal lobe, the kinase also has an important active site found in a cleft between these two lobes (as shown in **FIGURE 6.5**). CDKs have to bind to cyclins in order to become 'activated', when not bound to a cyclin they are completely inactive for two reasons. Firstly, the active site is blocked by the activation loop (a flexible loop region shown in **FIGURE 6.5**) and secondly, several important amino acids in the active site are not correctly positioned for the kinase reaction. Binding of a cyclin induces conformational change in the activation loop exposing the active site. However, for full kinase activity to occur phosphorylation of a conserved threonine residue on the activation loop has to follow.

The CDK family is different to other kinases as it is unable to auto-phosphorylate this site on their activation loop and instead rely on being phosphorylated by other kinases. A key kinase that phosphorylates the CDK1 activation loop at residue Thr160, is CDK Activating Kinase protein (CAK) (Enserink and Kolodner, 2010). CAK is comprised of three subunits' CDK7, cyclin H and MAT1 making it a member of the CDK family (Lolli and Johnson, 2005). CAK phosphorylates the conserved Thr160 residue on the activation loop of CDK1 (shown in **FIGURE 6.5**) resulting in a conformational change of the protein and the exposure of the substrate binding region (Enserink and Kolodner, 2010). Furthermore, phosphorylation of this site increases the number of contacts between the cyclin and CDK1 leading to a stronger binding interaction. Both activation loop phosphorylation and cyclin binding are required for full kinase activity.

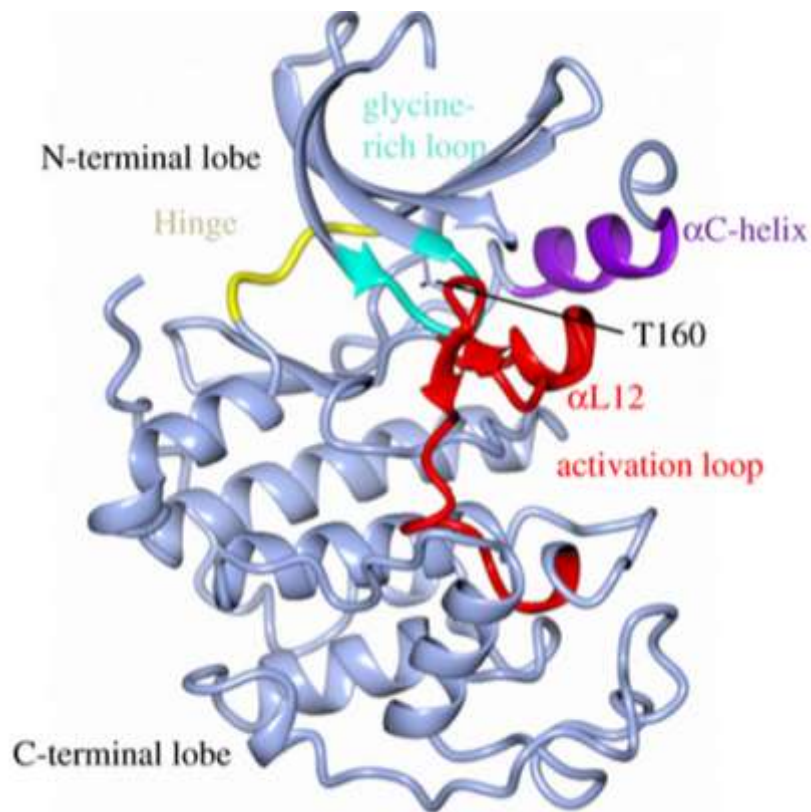


**FIGURE 6.5: STRUCTURE OF CDK2**

The structure of monomeric CDK2 (PDB ID: 1HCK) (silver). CDK2 is composed of a smaller N-terminal lobe formed from a twisted anti-parallel  $\beta$ -sheet and a larger C-terminal lobe. The activation loop (red) runs from residues 145-172 and the Thr160 residue is marked. Figure adapted from: (Wood and Endicott, 2018).

When activated, CDK1 can phosphorylate, Ser, Thr and Tyr residues through the addition of a phosphate group ( $\text{PO}_3^-$ ), as shown in **FIGURE 6.6**. CDK1 phosphorylates proteins that contain the optimal phosphorylation consensus sequence, Ser/Thr-Pro-x-x-Lys/Arg (S/T-P-x-x-K/R) (Rhind and Russell, 2012) although it can also phosphorylate numerous proteins with the minimal consensus sequence: Ser/Thr-Pro (S/T-P) (Suzuki *et al.*, 2015). And more recently it has been shown that CDK1 can also phosphorylate non-S/T-P sites (Enserink and Kolodner, 2010).

Phosphorylation is a reversible post-translational modification (PTM) and plays a critical role in the regulation of many cellular processes including cell growth, cell cycle and apoptosis. It is estimated that one third of proteins in the human proteome are substrates for phosphorylation (Ardito *et al.*, 2017). The addition of a phosphate group changes the amino acid environment through the addition of a negative charge, which can have a large effect on protein function and phenotype within the cell. The addition of a phosphate can cause conformational changes in the protein's structure, which may then regulate catalytic activity or allow the phosphorylated region to recruit neighbouring proteins that can recognise and bind phospho-motifs, such as Src homology domains (SH2) and phosphotyrosine binding domains (PTB) (ThermoFisher, 2018).



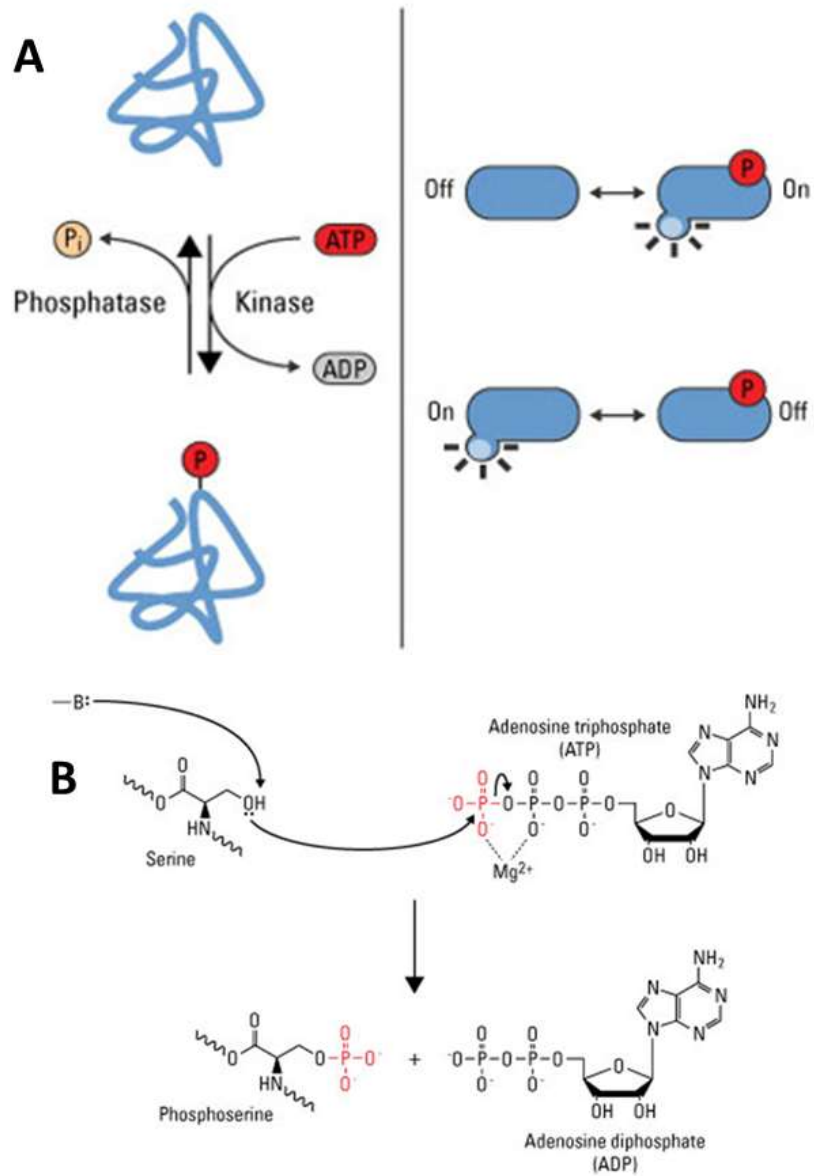


**FIGURE 6.6: MECHANISM OF PHOSPHORYLATION**

(A) Diagram illustrating that the phosphorylation PTM is a reversible reaction, phosphorylation is mediated through a kinase adding a phosphate group from ATP and phosphatases remove phosphate group. (B) Diagram illustrating the phosphorylation of the amino acid serine. The protein transfer from (-OH) group on the Ser stimulates the nucleophilic attack of the  $\gamma$ -phosphate group on ATP resulting in the transfer of a phosphate group (from ATP) to serine to form phosphoserine and ADP. (-B:) indicates the phosphatase enzyme that initiates the proton transfer. Diagram adapted from: (ThermoFisher, 2018).

### 6.1.5 Cell adhesions regulated by CDK1

The CDK family plays a vital role in regulating the cell cycle, but until recently they were not regarded as being involved with the regulation of cellular adhesions (Robertson *et al.*, 2015). Through the publication of the phospho-adesome, a report of the proteomic and phosphoproteomic sites on adhesion complexes, it was revealed that many proteins involved in integrin-matrix adhesions are phosphorylated by CDK1, proposing the idea that the CDK family could play a role in adhesion regulation (Robertson *et al.*, 2015).

Since then, work from *M.C. Jones et al.* have shown that cell adhesions are regulated by CDK1 during the cell cycle. They found that cells transitioning from G<sub>1</sub> to S phase had a CDK1 dependent increase in focal adhesion formation, which was partially mediated by phosphorylation of adhesion proteins such as the formin-like protein 2 (FMNL2) (Jones *et al.*, 2018) (see **FIGURE 6.7**).

Study of CDK1 in adhesions revealed that CDK1 inhibition triggers disassembly of focal adhesions and leads to a decrease in the area of cells covered by adhesions with only smaller nascent adhesion left (Robertson *et al.*, 2015). This provides the first clear evidence that CDK1 may be regulating adhesion sites in non-dividing cells.

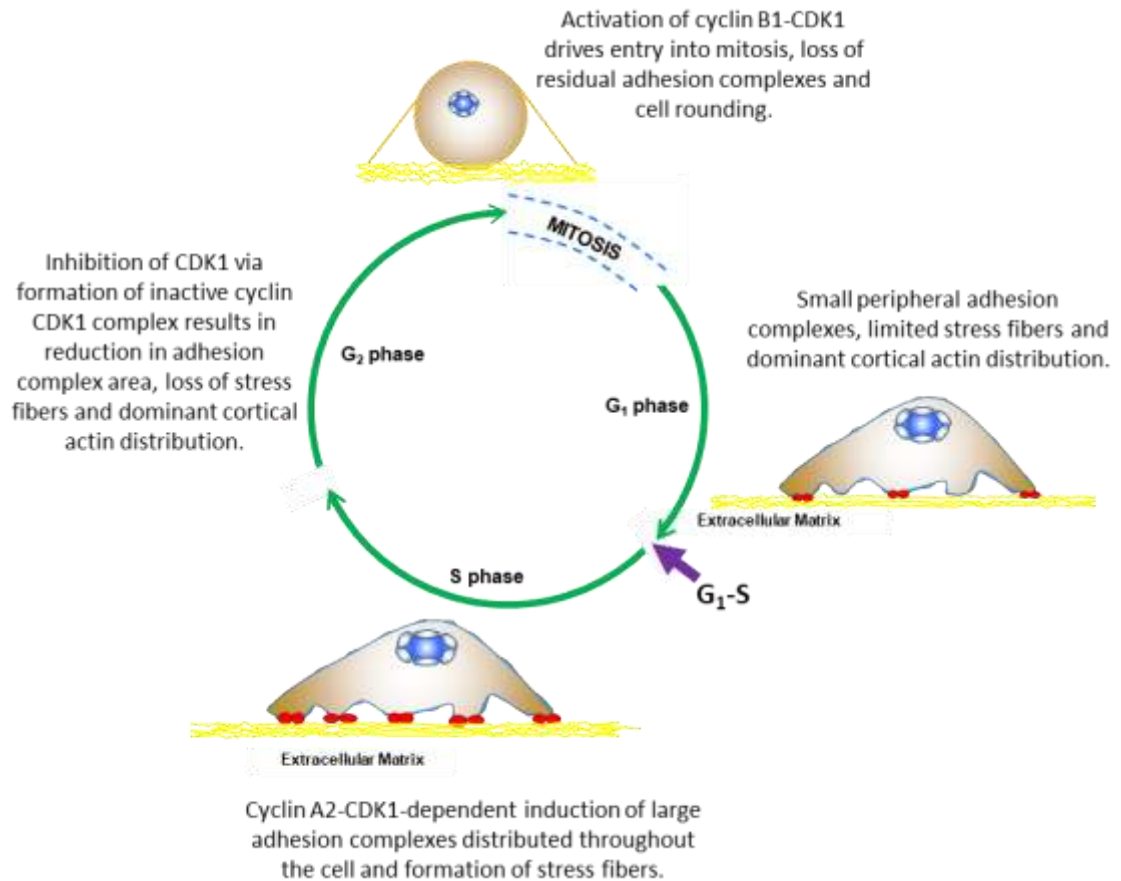


**FIGURE 6.7: ADHESION AREA IS DEPENDENT ON THE CELL CYCLE PHASE**

Schematic diagram of the cell cycle indicating the size of cell-matrix adhesions (red) at different phases of the cell cycle. Figure based from: (Jones *et al.*, 2018)

This role of CDK1 is distinct from its more well-described role with cyclinB-CDK1 (driving the G<sub>2</sub> phase into mitosis), because a *knock-down* of cyclin B did not cause changes in adhesion formation throughout the cell cycle. This finding makes sense as cyclinB-CDK1 is only seen in G<sub>2</sub> phase of the cell cycle (cell adhesion growth found in S phase) and so, instead of cyclinB it appears that cyclinA is required for the CDK1-dependent adhesion regulation.

Furthermore, cell adhesion area increases between G<sub>1</sub> to S phase and decreases as cells enter G<sub>2</sub> phase, following the pattern of cyclin A concentration in the cell (see **FIGURE 6.3**) (Jones *et al.*, 2018). Jones *et al.* concluded, that additional CDK1-cyclinA substrates might be involved in the regulation of adhesion formation. Could the CDK1:talins interaction play a role in the cell adhesion regulation and could talin binding to CDK1 be a recruiting factor of CDK1 to adhesions?

In the previous chapter, it was described how a designed LD talin-binding motif, was used to screen through talin proteomic datasets in order to identify talin-binding partners. Sequence conservation and structural characteristics of these potential talin-binding proteins were further

assessed and from these data, one protein stood out as an interesting talin binding protein. This protein was cyclin dependent kinase1 (CDK1). This chapter describes the characterisation of this protein-protein interaction through biochemical and biophysical methods, and addresses the effects of talin on the phosphorylation activity of CDK1, to attempt to determine the existence of a link between cell cycle and adhesion regulation.

## 6.2 Results

The designed LD talin-binding motif (described in **chapter 5**) identified two regions of CDK1 that could potentially interact with talin: CDK1 206-223 and CDK1 283-297. These regions of CDK1 were designed as synthetic peptides and ordered with C-terminal Cys residues, as previously described in **Chapter 5**. The affinity of both CDK1 peptides to talin was measured using FP assays, which showed that the CDK1 283-297 region did not interact with talin, whilst the 206-223 peptide bound to the talin1 fragment R4-R8.

### 6.2.1 Determination of the CDK1 binding site(s) on talin

**Chapter 5, FIGURE 5.11** shows binding data between the CDK1 206-223 peptide and the large talin rod fragments (R1-R3, R4-R8, R9-R10, R11-R12 and R13-DD). CDK1 binds to the talin1 fragment R4-R8 with a  $K_D$  of 16  $\mu\text{M}$ . To further refine the CDK1 binding site on talin, the large R4-R8 fragment was broken down into smaller domains, no binding was observed for domains R4 (residues 913-1044), R5 (residues 1046-1206), and R6 (residues 1206-1357), leading to the conclusion that the CDK1 binding site is in the R7-R8 region of talin. However, the double domain R7R8 (residues 1357-1653) was found to bind the CDK1 peptide with an affinity of 15  $\mu\text{M}$  (shown in **FIGURE 6.8A**). It was also determined that both talin isoforms (talin1 and talin2) could bind to the CDK1 peptide with similar affinity; talin2 R7R8 bound the CDK1 peptide with an affinity of 11  $\mu\text{M}$ .

Subsequently the individual talin domains: R7 (residues 1357-1365  $\Delta$ 1454-1586) and R8 (residues 1461-1580) binding affinity was measured to the CDK1 peptide. **FIGURE 6.8B** shows the CDK1 peptide bound very weakly to talin1 R7 with a binding  $K_D$  of 56  $\mu\text{M}$ . Talin1 R8 on the other hand, had an affinity of 18  $\mu\text{M}$  to the CDK1 peptide concluding that the CDK1 binds to the talin1 R8 domain.

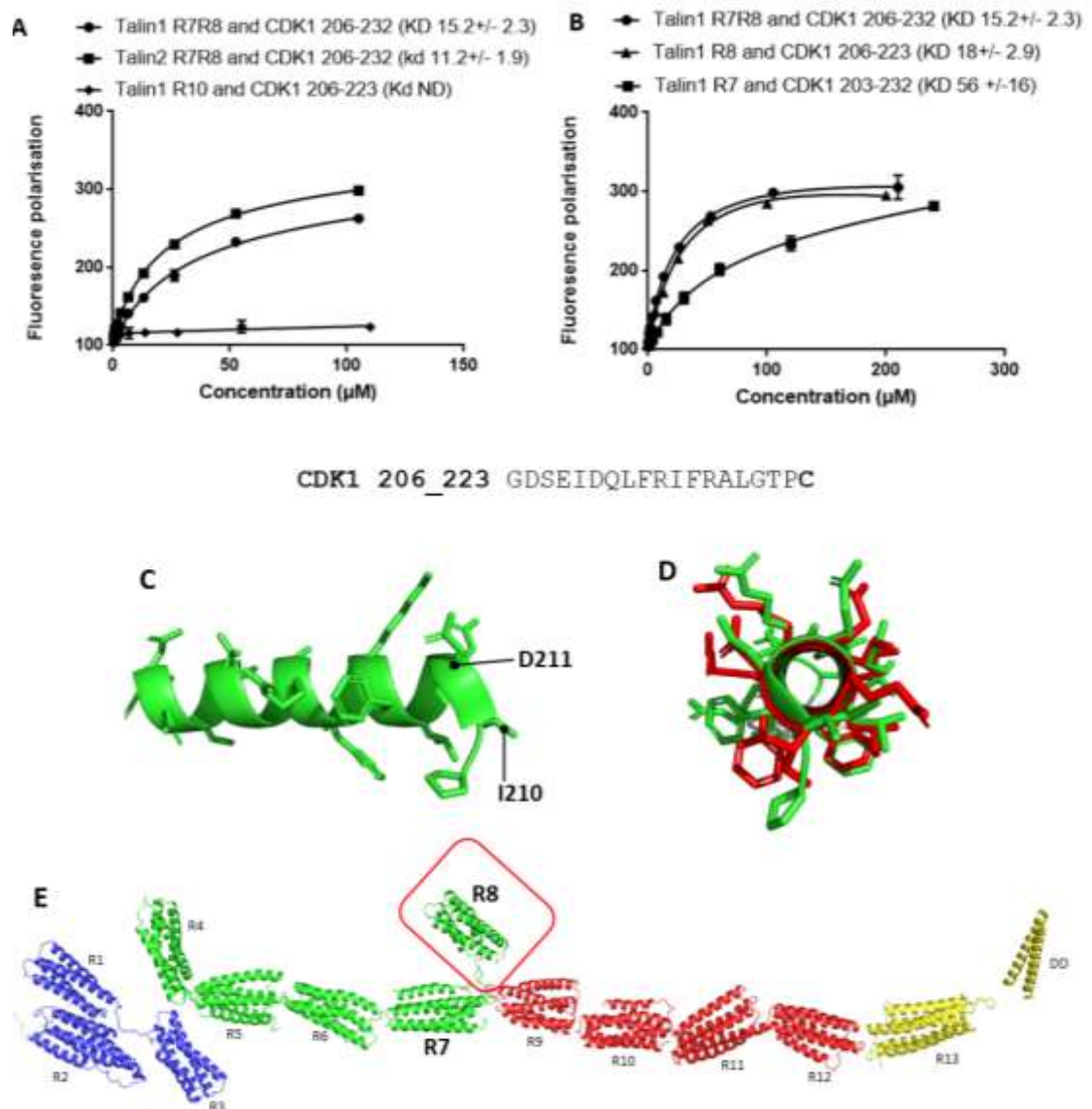


**FIGURE 6.8: BIOCHEMICAL CHARACTERISATION OF CDK1 BINDING TO TALIN**

(A-B) Binding of BODIPY-labelled CDK1 206-223C peptide individual talin domains; talin1 R7-R8 (1357–1659), talin2 R7R8 (1360-1656), talin1 R7 (1357-1653 $\Delta$ (1454-1586) and talin1 R8(1461-1580). Binding affinities were measured using a Fluorescence Polarization assay. Talin domain R10 (1815-1973) was used as a negative control. Dissociation constants  $\pm$  SE ( $\mu$ M) for the interactions are indicated in the legend. All measurements were performed in triplicate. ND, not determined. (C) Helical prediction of CDK1 peptide based on the structure CDK1 (PDB ID:4YC6). (D) structural prediction of CDK1 peptide from CDK1 structure (PDB ID:4YC6) (green) overlaid with DLC1 peptide structure (PDB ID:5FZT) with CDK1 residues threaded onto the helix (red) (E) Talin rod domains predicted structure shown highlighting R8 talin sub domain.

## 6.2.2 Chemical shift mapping of the CDK1 binding site on talin1 R7R8

To further explore the talin:CDK1 interaction and determine the CDK1 binding surface on talin R7R8, NMR chemical shift mapping was used.  $^{15}\text{N}$ -labelled talin1 R7R8 (residues 1357-1653) were expressed and a  $^{15}\text{N}$  TROSY spectrum of talin1 R7R8 (140  $\mu\text{M}$ ) (black **FIGURE 6.9**) was carried out. The talin1 R7R8 spectrum had good peak dispersion indicating that the protein was folded; CDK1 206-223 peptide was then added to talin1 R7R8 at a ratio of 6:1 (green in **FIGURE 6.9**) and a very similar peak dispersion remained indicating that the interaction between talin:CDK1 did not alter the folding of talin1 R7R8. However, a subset of the talin1 R7R8 peaks shifted upon addition of CDK1 whilst some remained in the same position, indicating that the CDK1 peptide bound to a specific region on talin. To determine which peaks had shifted, the CDK1:talin spectrum was overlaid with a talin1 R8 spectrum (data not shown), which highlighted it was talin1 R8 peaks that had shifted with no significant shift changes observed on the R7 peaks; corroborating the FP data (**FIGURE 6.8**) that talin1 R8 is the main CDK1 binding site on talin.

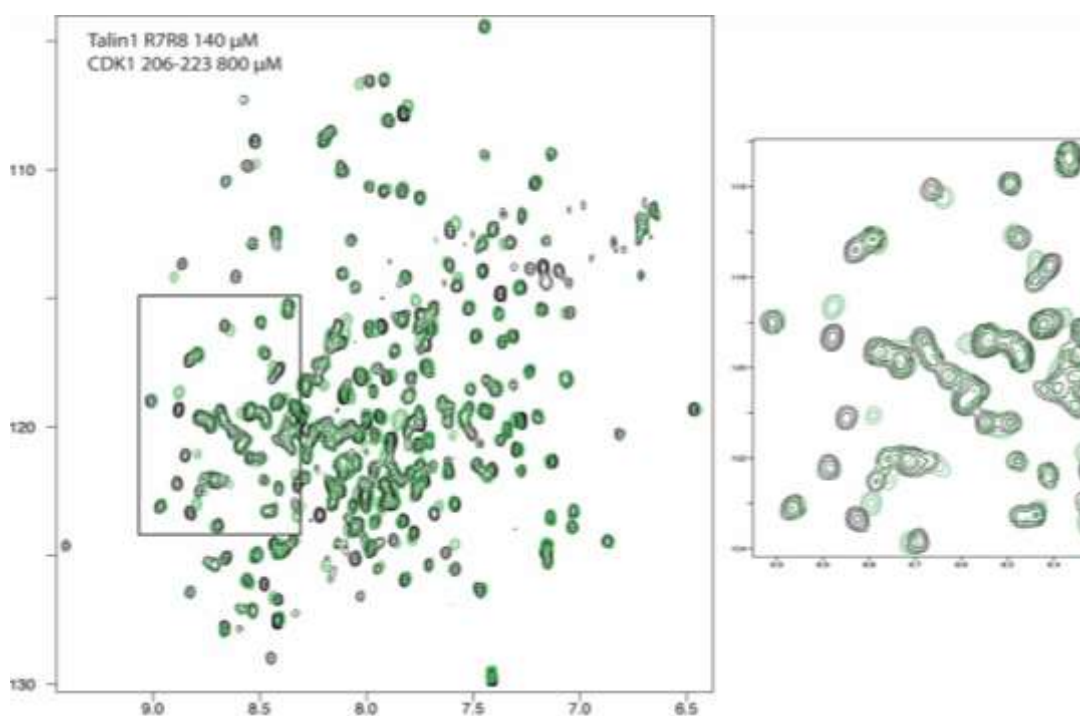


**FIGURE 6.9:**  $^{15}\text{N}$  TROSY NMR TITRATION TALIN1 R7R8 AND CDK1 206-223C PEPTIDE

$^1\text{H}$ ,  $^{15}\text{N}$  TROSY spectra of 140  $\mu\text{M}$   $^{15}\text{N}$ -labelled talin1 R7R8 (residues 1357–1659) in the absence (black) or presence of CDK1 206-223C peptide (green) at a ratio of 1:6.

### 6.2.3 Chemical shift mapping of the CDK1 binding site on talin R8

The peaks in the R7R8 TROSY spectrum (**FIGURE 6.9**) are quite overlapped making the mapping of individual peaks challenging. To overcome this a titration of the individual talin1 R8 (residues 1461-1580) domain was carried out.  $^{15}\text{N}$ -labelled talin1 R8 was titrated against increasing concentrations of the CDK1 206-223 peptide, the most saturated point in the titration is shown in **FIGURE 6.10A**; talin R8 on its own (black) and CDK1 titrated in at a ratio 12:1 (blue). There was less overlap of the individual peaks with the talin1 R8 domain, allowing a clearer tracking of each peak, shown in **FIGURE 6.10B** (talin1 R8 on its own (black), and in the presence of CDK1 at a ratio 3:1 (pink), 6:1 (green) and 12:1 (blue)). The talin peaks move differently compared to when the KANK1 30-60C peptide was added to talin1 R7, instead of splitting (slow exchange) they move progressively in a linear line (with increasing concentrations of CDK1 peptide). This movement is showing the peaks are in fast exchange on the NMR timescale, which allows for easy and accurate peak tracking. **FIGURE 6.10C** highlights one peak, corresponding to talin residue Asn1534 to show the linear shift changes as a higher concentration of CDK1 peptide is added.

To map exactly which talin1 R8 residues shift upon addition of the CDK1 peptide, the talin1 R8 chemical shift assignments were downloaded from the BioMagResBank (BMRB ID:19339) and analysed using CcpNMR Analysis software allowing each peak in the talin R8 spectrum to be assigned to the corresponding talin1 R8 residue. For analysis, the talin1 R8 spectrum was overlapped with the talin1R8:CDK1 1:6 spectra to allow measurement of the distance shifted for each peak.

These shift distances were determined using the weighted combination of  $^1\text{H}$  and  $^{15}\text{N}$  amide secondary shifts ( $\Delta(\text{H,N})$ ).  $\Delta(\text{H,N})$  are determined using **EQUATION 2**: as described in **chapter 4**. The shift distances for each peak were plotted and can be seen in **FIGURE 6.11A**; residues where the peak shifted over 0.02 ppm (which represented a significant shift) are highlighted in red on the graph and on the talin1 R7R8 structure (**FIGURE 6.11B**). The talin residues that shifted upon addition of the CDK1 peptide mapped onto talin helices 32 and 33 (**FIGURE 6.11B**). This was interesting as these talin helices also form the binding surface for several other talin ligands including RIAM and DLC1 (Yang *et al.*, 2014; Zacharchenko *et al.*, 2016) as discussed in **chapter 5**.

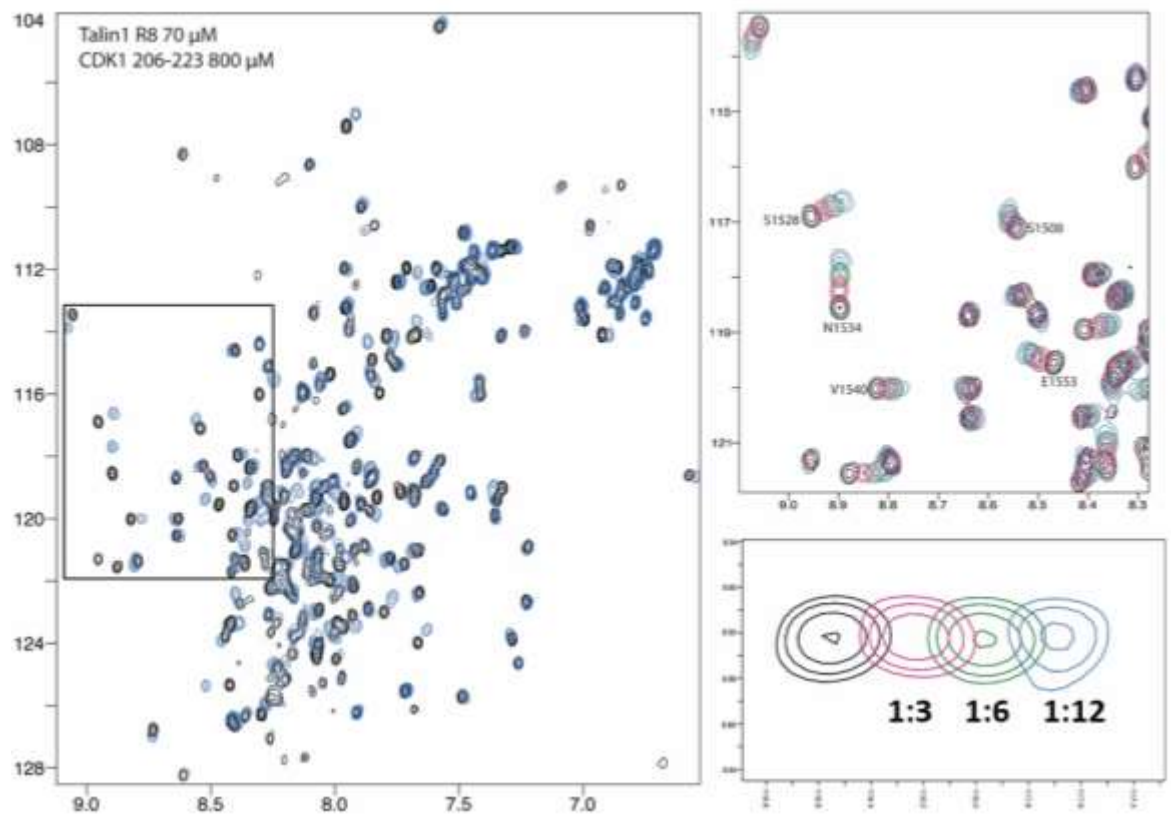


**FIGURE 6.10:  $^{15}\text{N}$  HSQC NMR TITRATION OF TALIN1 R8 AND CDK1 206-223C PEPTIDE**

(A-C)  $^1\text{H}$ ,  $^{15}\text{N}$  HSQC spectra of  $70\ \mu\text{M}$   $^{15}\text{N}$ -labelled talin1 R8 (residues 1461-1580) in the absence (black) or presence of CDK1 206-223C peptide (pink/green/blue). Spectra are talin:CDK1 at a ratios of 1:12 (blue), 1:6 (green) and 1:3 (pink). (B) Zoomed in view of the box shown in (A). (C) Zoomed in region highlighting the peak corresponding to residue Asn1534, showing progressive chemical shift changes, demonstrating the talin:CDK1 interaction is in fast exchange on the NMR timescale.



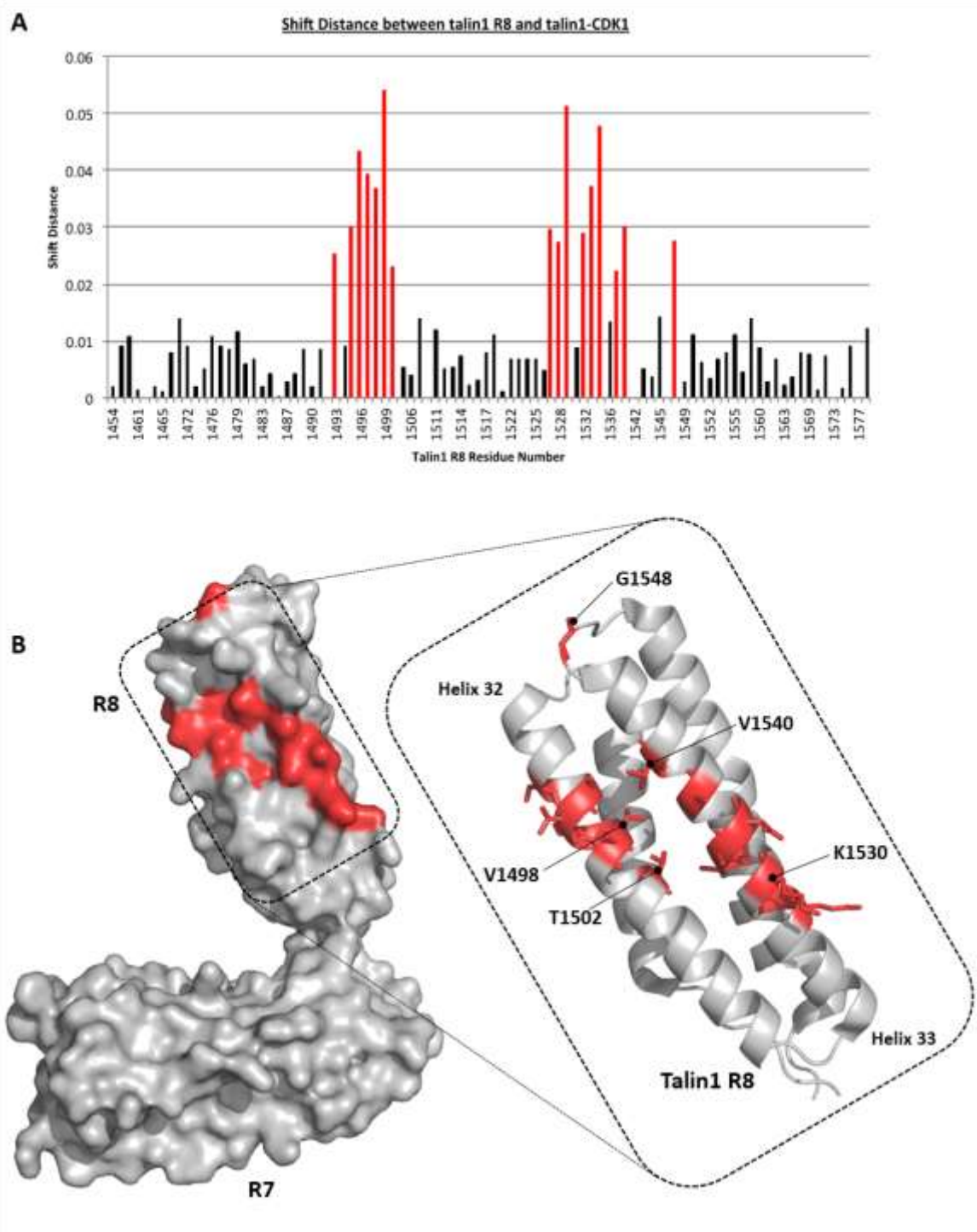


**FIGURE 6.11: CHEMICAL SHIFT MAPPING OF TALIN1 R8 AND CDK1 206-223C**

(A) Chemical shift mapping of the CDK1 binding site on talin1 R8 as detected by NMR using weighted chemical shift distances. (B) Residues that moved more than 0.02 ppm (highlighted in red) mapped onto the talin1 R7R8 structure (PDB ID:5FZT).

## 6.2.4 Biochemical comparison of DLC1 and CDK1 binding talin1 R8

CDK1 binds to talin R8 via helices 32 and 33, which is the same binding surface as DLC1. Our understanding of how LD ligands and their LDBD are regulated is limited so here I wanted to compare how the two ligands, DLC1 and CDK1 interact with talin1 R8.

Both CDK1 and DLC1 bind to talin via a similar LD talin-binding motif; the DLC1 LD-motif is between residues 465-489 (IFPELDDILYHVKGMQRIVNQWSEK). The motif is slightly different to CDK1 shown in **FIGURE 6.12B** as CDK1 contains an 'ID' rather than the canonical 'LD' found in DLC1. To determine if this makes a difference in binding to talin; the FP assay was used to measure affinity between talin1 R7R8 and the DLC1 and CDK1 peptides. The data shown in **FIGURE 6.12A** shows DLC1 binds talin1 R7R8 with a higher affinity than CDK1; DLC1 binds talin R7R8 with a  $K_D$  of 3.5  $\mu$ M whereas CDK1 has a  $K_D$  of 14  $\mu$ M.

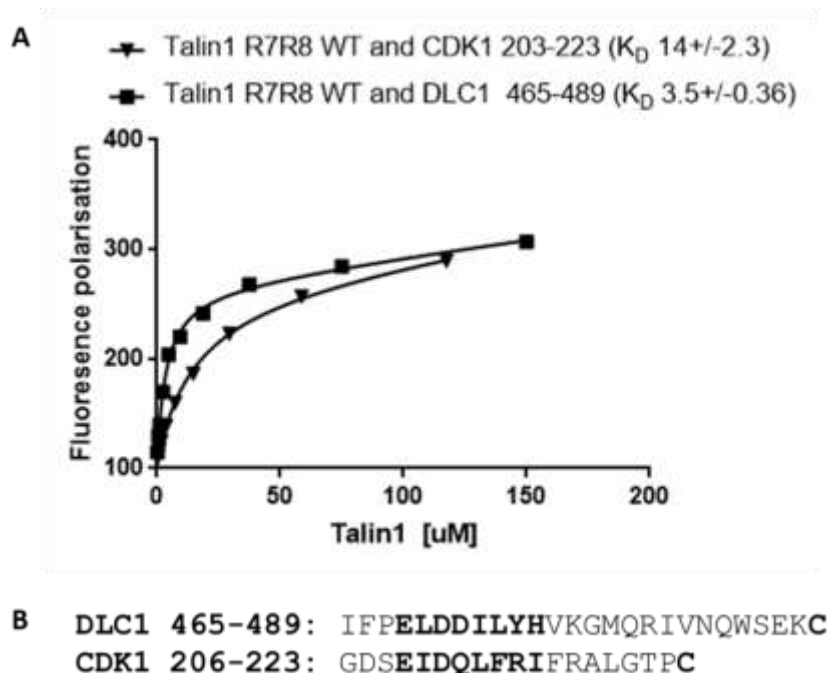


**FIGURE 6.12: BINDING OF DLC1 AND CDK1 TO TALIN1 R7R8**

(A) Binding of BODIPY-TMR labelled CDK1 206-223C peptide and DLC1 465-489C peptide to talin1 R7-R8 (1357-1653). Binding affinities were measured using a Fluorescence Polarization assay dissociation constants  $\pm$  SE ( $\mu$ M) for the interactions are indicated in the legend. All measurements were performed in triplicate. (B) The CDK1 (206-223) and DLC1 (465-489) peptide sequences shown with the LD talin-binding motif highlighted in bold.

A  $^{15}\text{N}$  HSQC of talin1 R8 (black) is shown in **FIGURE 6.13**; both CDK1 (green) and DLC1 (blue) peptides were added to talin R8. The spectra were compared to highlight the differences the two peptides had on the talin R8 environment. The DLC1 spectrum shows more peaks have shifted, compared to the CDK1 spectrum, (red box on **FIGURE 6.13** and **FIGURE 6.13B**). This suggests that more residues may be involved in the binding of talin:DLC1 compared to talin:CDK1.

**FIGURE 6.13C** shows a region of the spectrum where most talin shifts take place when CDK1 is added. In this region the same talin peaks shift in the presence of both DLC1 and CDK1 indicating that the same core residues are mediating the binding of CDK1 and DLC1. Additionally, some talin peaks in this region shift in opposite directions with the two ligands (**FIGURE 6.13C** highlighted by black dotted box). This change highlights the differences in the ligands CDK1 and DLC1 sequences, these different residues cause different environmental changes to talin when binding. This indicates that, even though there is residue variation in the talin binding sequence on CDK1 and DLC1, they still binding to the same talin residues. Together this provides evidence that the same talin binding mechanism is being used between the different LD-motif peptides.

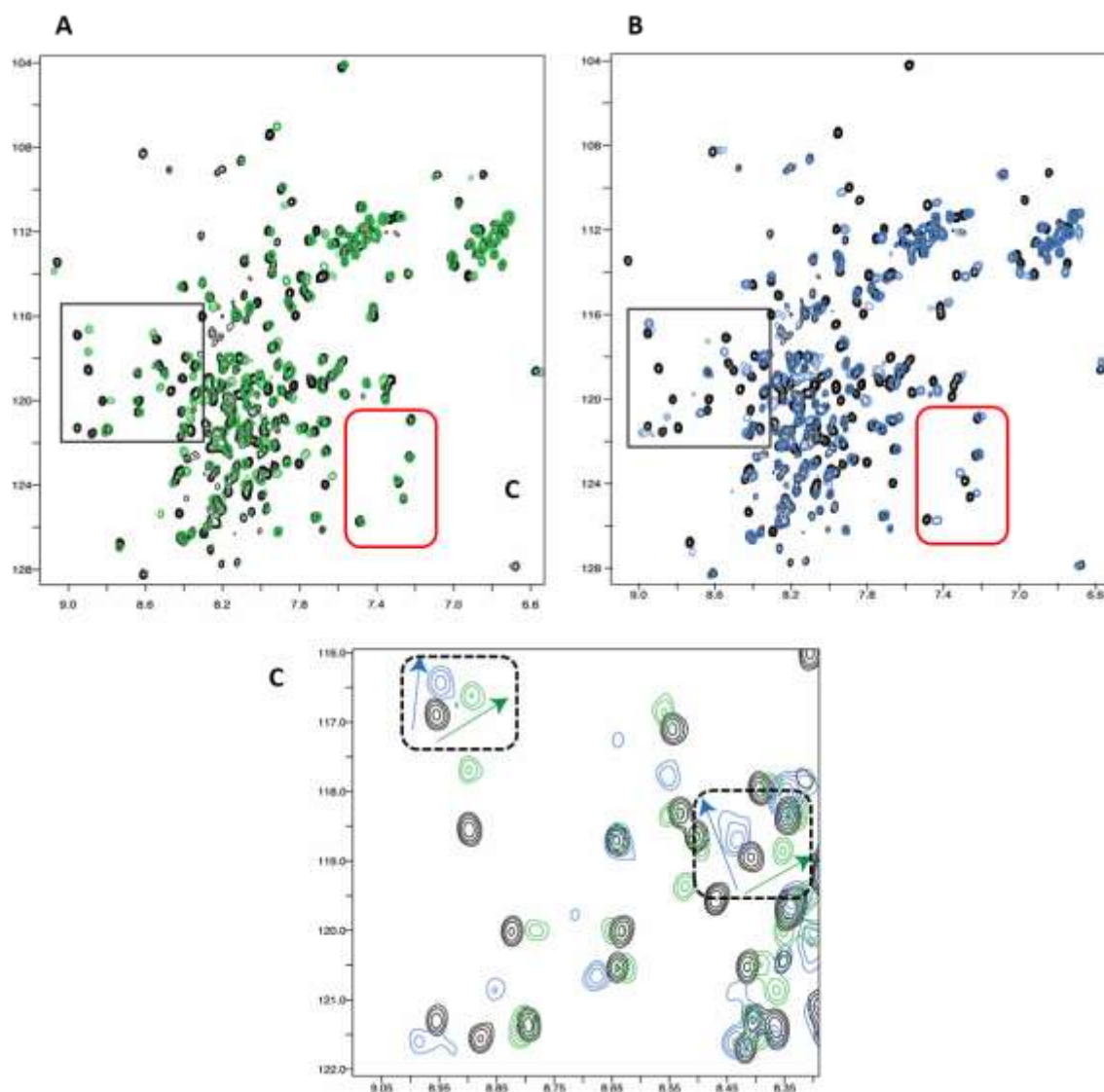


**FIGURE 6.13:  $^{15}\text{N}$  TROSY SPECTRA SHOWING DLC1 AND CDK1 BINDING TO TALIN1 R7R8**

(A-B)  $^1\text{H}, ^{15}\text{N}$  TROSY spectra of  $140\ \mu\text{M}$   $^{15}\text{N}$ -labelled talin1 R7R8 (residues 1357–1659) in the absence (black) and presence of  $400\ \mu\text{M}$  CDK1 206-223C peptide (green) or  $400\ \mu\text{M}$  DLC1 465-489C peptide (blue). Black box highlights region of talin residues shifted upon addition of CDK1. Red box highlights area of the spectra where the peaks have shifted upon addition of DLC1 to talin R7R8 but not CDK1. (C) Zoomed in region of the HSQC spectra, highlighting the different directions of the peaks when CDK1 or DLC1 peptides are added to talin1 R7R8.

## 6.2.5 Designing a CDK1 mutant to disrupt the talin:CDK1 interaction

CDK1 binds to talin through an LD talin-binding motif. This LD-motif is similar to the KANK LD talin-binding motif discussed in **chapter 4**. Designing a CDK1 mutant to perturb talin:CDK1 binding was greatly assisted from the design of the KANK\_4A mutant (see **section 4.2.6**), that successfully perturbed the binding between talin:KANK.

The KANK\_4A mutant was designed to perturb binding via mutating the Leu and Asp residues in the LD-motif for Ala. This prevented KANK from forming the salt bridge between the charged Asp residue and talin and consequently perturbing binding.

**FIGURE 6.14A** shows a model of CDK1 binding to talin R8 which demonstrates how the Asp211 residue (in the LD-motif) likely forms a salt bridge with talin residue Lys1544. This interaction orients the CDK1 peptide and allows the hydrophobic Ile210 residue to form a hydrophobic interaction with talin. Using the same strategy we developed for KANK, we mutated the CDK1 Ile210 and Asp211 residues to Ala. A peptide CDK1\_2A 206-223 (GDSEAAQLFRIFRALGTPC) containing the mutation was ordered (shown **FIGURE 6.14C**) allowing the FP assay to be used to determine the binding of the CDK1\_2A mutant with talin1 and talin2 R7R8. **FIGURE 6.14D** shows the CDK1\_2A mutant is effective as it did not generate a determinable  $K_D$  confirming it is an effective mutant in abrogating the talin:CDK1 interaction.

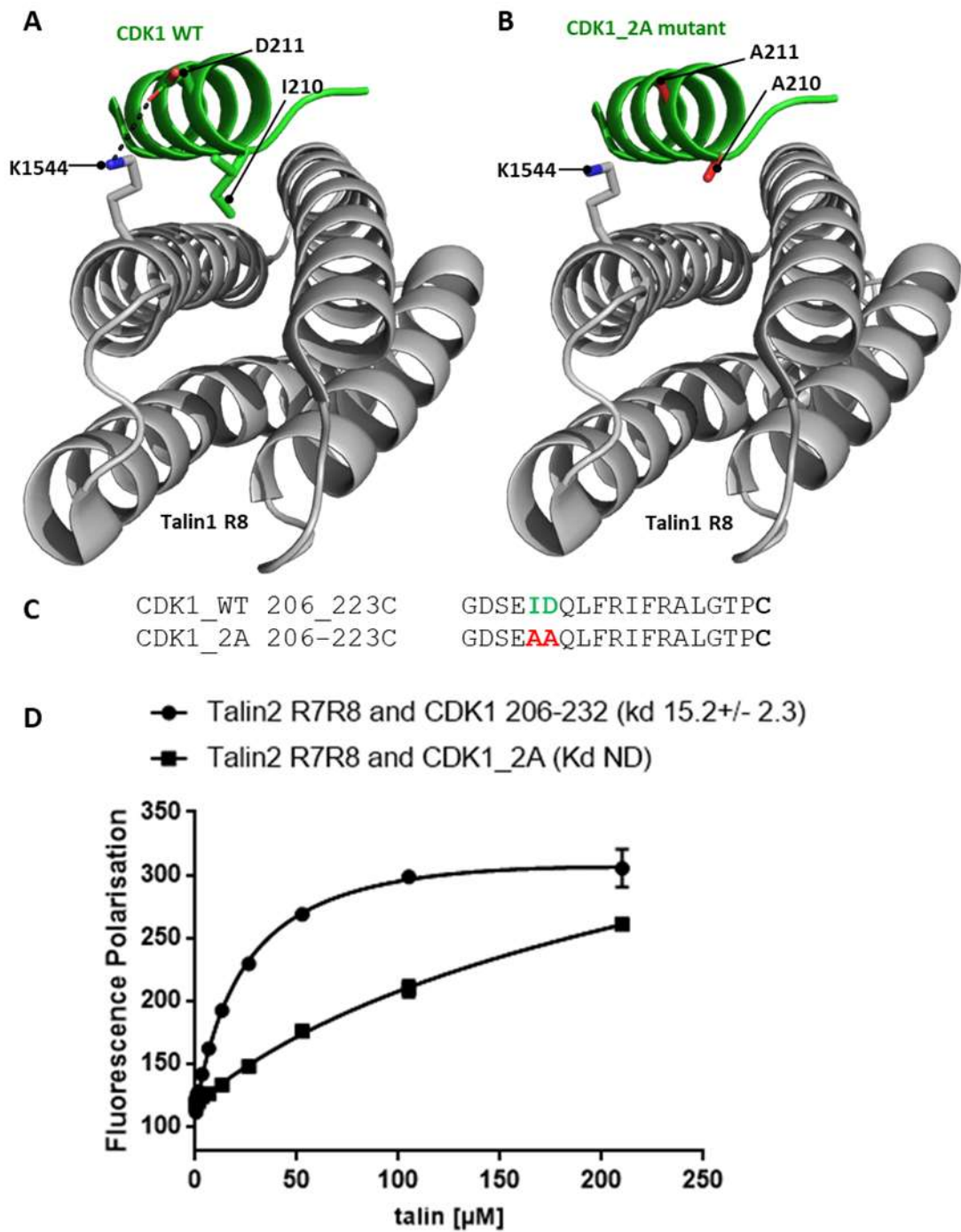


**FIGURE 6.14: DESIGN OF ACdk1\_2A MUTANT TO PERTURB TALIN:CDK1 INTERACTION**

(A-B) Structural model of CDK1 206-223C (green) binding to talin1 R8 domain (grey) - the talin:DLC1 structure used with CDK1 residues threaded onto DLC1 helix (PDB ID: 5FZT). (A) Ile210 and Asp211 residues are highlighted (B) the mutations Ala210 and Ala211 are highlighted. (C) CDK1 and CDK1\_2A peptide sequences: green highlights the Ile and Asp residues in the LD-motif and red highlights the Ala residues in the CDK1\_2A mutation. (D) Binding of BODIPY-TMR labelled CDK1 206-223C and CDK1\_2A 206-223C peptides to talin2

R7R8 (1360–1656). Dissociation constants  $\pm$  SE ( $\mu$ M) are indicated in the legend. All measurements were performed in triplicate. ND, not determined.

To confirm the effectiveness of the CDK1\_2A mutant for disrupting the interaction between CDK1 and talin, NMR titrations were carried out with talin1 R7R8 (residues 1357–1659) and the CDK1\_2A 206-223 peptide. The  $^{15}$ N TROSY talin1 R7R8 spectra are shown in **FIGURE 6.15**. For both **FIGURE 6.15A** and **B**, the spectra in black correspond to talin1 R7R8; in green (**FIGURE 6.15A**) spectrum corresponds to the addition of the CDK1 206-223 peptide (ratio 6:1) and, in red, **FIGURE 6.15B** the spectrum of mutant CDK1\_2A 206-223 added at a ratio of 6:1. No shifts can be observed when the CDK1\_2A peptide is added, in contrast to the addition of CDK1 WT peptide.

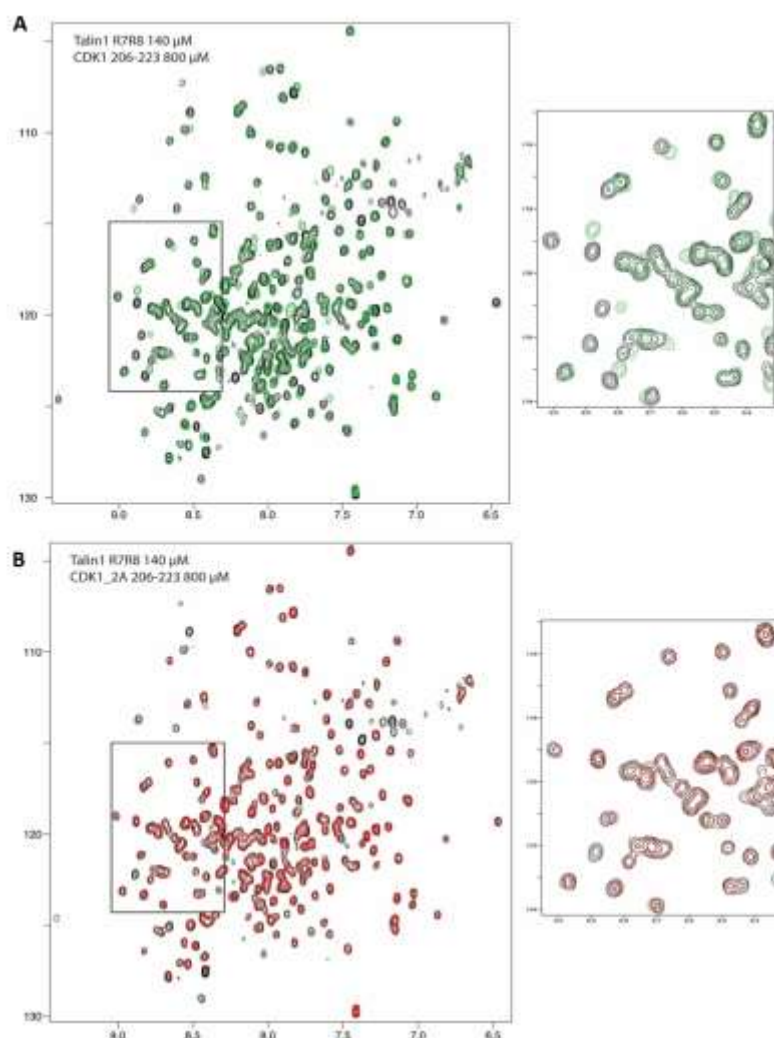


**FIGURE 6.15: NMR TROSY OF THE CDK1\_2A MUTANT ON BINDING TO TALIN R7R8**

(A)  $^1$ H,  $^{15}$ N TROSY spectra of 140  $\mu$ M  $^{15}$ N-labelled talin1 R7R8 (residues 1357–1653) in the absence (black) or presence of CDK1 206-223C peptide (green) at a ratio of 1:6. (B)  $^1$ H,  $^{15}$ N TROSY spectra of 140  $\mu$ M  $^{15}$ N-labelled talin1 R7R8 in the absence (black) or presence of CDK1\_2A mutant peptide (red) at a ratio of 1:6



Furthermore, a  $^{15}\text{N}$  HSQC titration with the individual talin R8 domain was carried out. **FIGURE 6.16** shows the most saturated point of the titration with 420  $\mu\text{M}$  CDK1 added to 70  $\mu\text{M}$  talin R8. The HSQC showed no shifts occurred in presence of the mutant enabling us to conclude that the CDK1\_2A mutant is effective in abrogating the talin:CDK1 interaction and would be a good mutant to use in cellular studies of the CDK1:talin interaction.

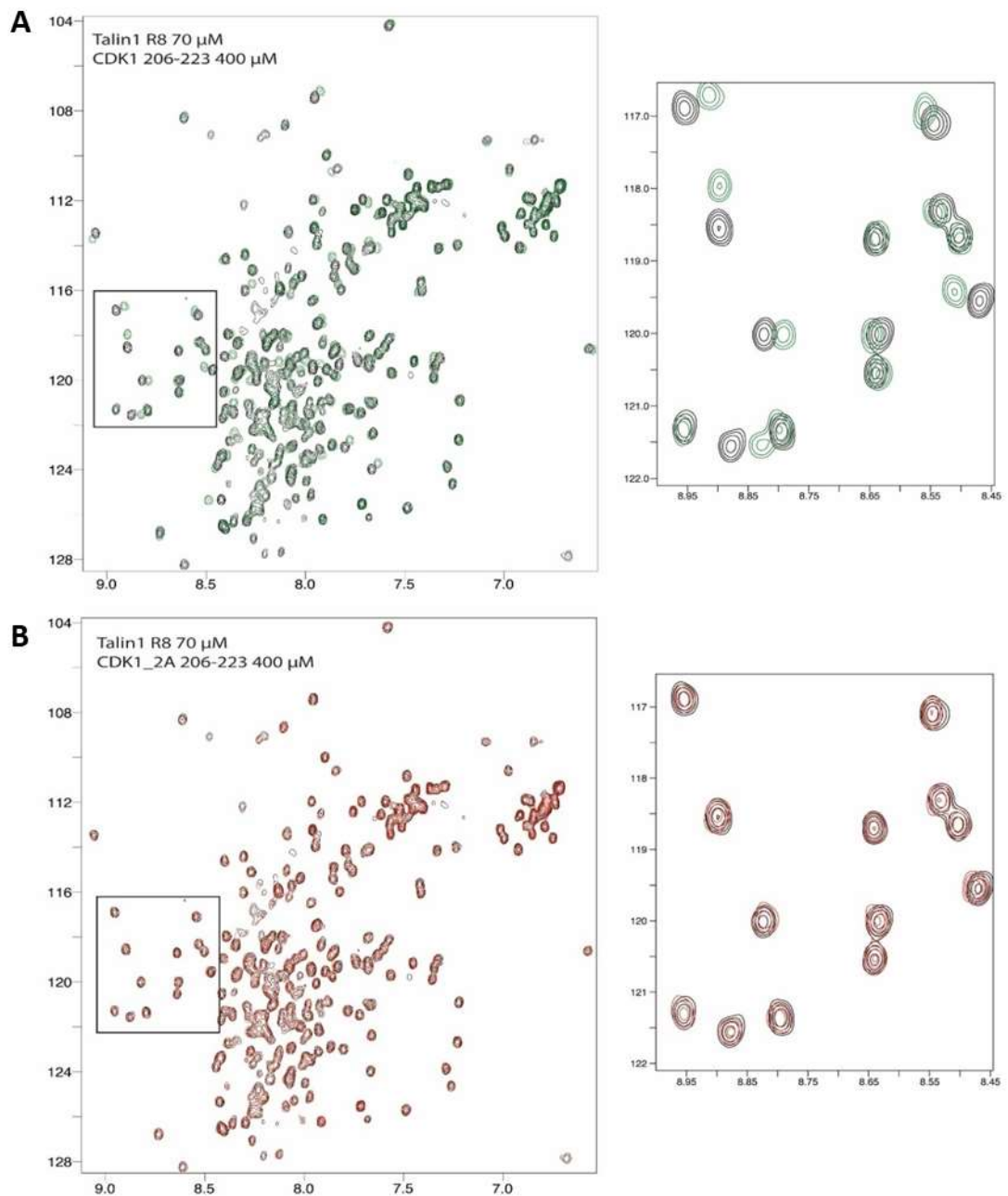


**FIGURE 6.16: NMR HSQC OF THE CDK1\_2A MUTANT AFFECT ON BINDING TO TALIN R8**

(A)  $^1\text{H},^{15}\text{N}$  HSQC spectra of 70  $\mu\text{M}$   $^{15}\text{N}$ -labelled talin1 R8 (residues 1461-1580) in the absence (black) or presence of CDK1 206-223C peptide (green) at a ratio of 1:6. (B)  $^1\text{H},^{15}\text{N}$  HSQC spectra of 70  $\mu\text{M}$   $^{15}\text{N}$ -labelled talin1 R8 in the absence (black) or presence of CDK1\_2A mutant peptide (red) at a ratio of 1:6.



## 6.2.6 Structural characterization of the talin:CDK1 complex

Following the design of a CDK1 mutant to perturb talin:CDK1 binding we wanted to design a talin mutant to perturb the interaction also. In order to achieve this, it was important to understand the talin residues involved in the interaction with CDK1 and so we wanted to obtain an atomic structure of talin1 R7R8 and CDK1 206-223.

### 6.2.6.1 Crystallography

Crystallography screens of the CDK1:talin complex were set up including Hampton crystal screen 2 (Hampton), JCSG (Molecular Dimensions), Wizard (Molecular Dimensions) and Pact (Molecular Dimensions). Initially talin1 R7R8 (residues 1357–1653) was purified and mixed with CDK1 peptide at a ratio of 1:4. All screens were plated at a 1:1 ratio of protein: well solution and left at both 4 °C and 20 °C. A number of crystals grew in the screening trays, some are shown in **FIGURE 6.17**, these crystals were placed into a CryoLoop and frozen in liquid nitrogen. Diffraction datasets was collected at 100 K on beamline I03 at Diamond Light Source (Didcot, UK). However, when solved it was found that the crystals were Apo structures and no CDK1 peptide was present. Different ratios of talin:CDK1 were tried and also talin2 R7R8 but no structure could be obtained.

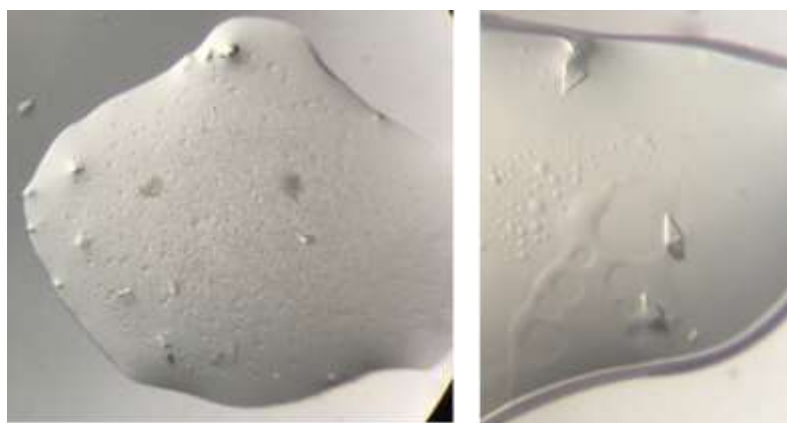


**FIGURE 6.17: CRYSTALLIZATION TRIALS OF TALIN1 R7R8 AND CDK1 206-223C PEPTIDE**

Crystals of talin1 R7R8 grown from a protein complex talin1 R7R8:CDK1 (ratio of 1:8) and laid at a 1:1 protein well solution ratio, crystals were found in JCSG+ optimization screen conditions at 20 °C.

### 6.2.6.2 Predicted docking

In the absence of a talin:CDK1 structure a docking prediction between the talin R7R8 domains and the CDK1 206-223 peptide was created. This was achieved using the known talin1 R7R8:DLC1 structure (PDB ID: 5FTZ), where the DLC1 peptide forms a short alpha helix that packs against the talin helices 32 and 33. The DLC1 helix was used as a base and the CDK1 peptide 206-223 was threaded onto the DLC1 helix using PyMOL. **FIGURE 6.18** shows the structural model of a CDK1 peptide threaded onto talin1 R8. In the model, Asp211 of CDK1 is positioned to form a salt bridge with talin Lys1544 residue; a key interaction found in all LD peptides bound to the talin R8 domain.

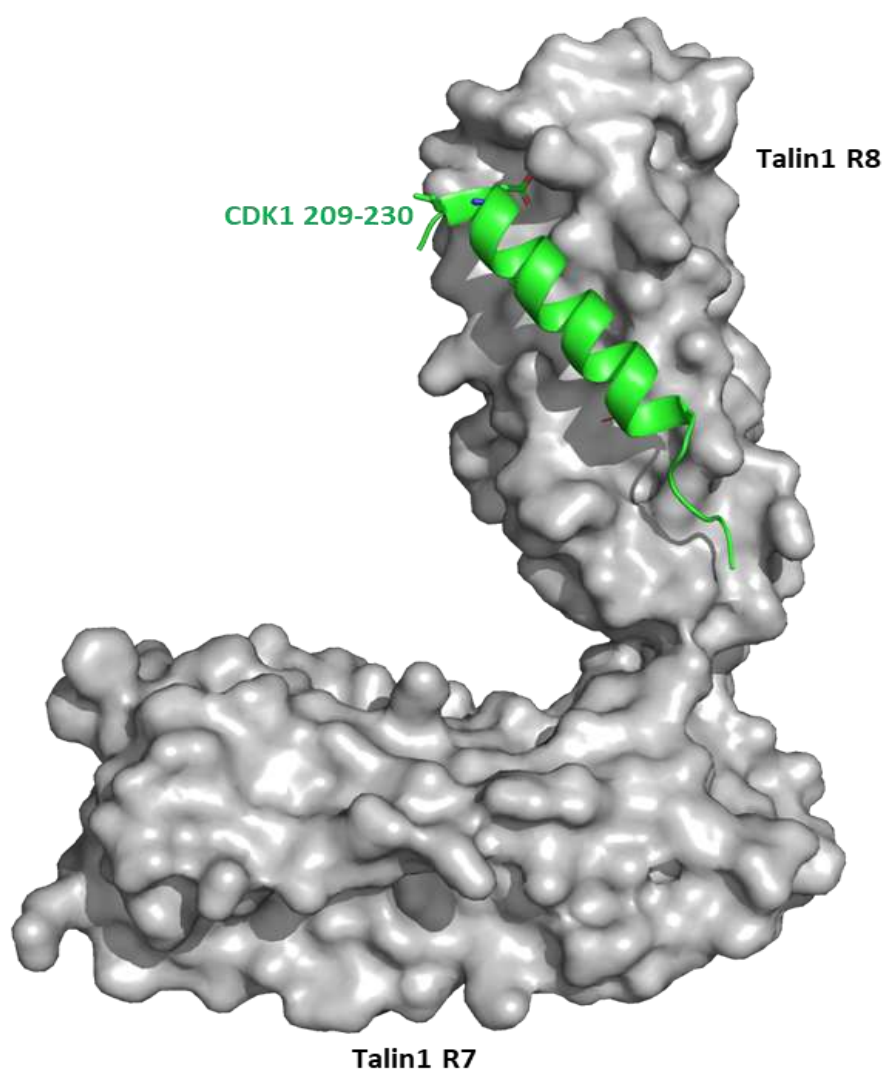


**FIGURE 6.18: STRUCTURAL MODEL OF TALIN1 R7R8:CDK1 206-223**

The binding of talin1 R7R8 and CDK1 peptide 206-223. CDK1 peptide 206-223 was modelled onto the known DLC1 structure using PyMOL and is highlighted in green.

### 6.2.7 Designing a talin mutant to perturb CDK1:talin binding

A major aim of the biochemical characterisation of the interaction between talin and CDK1 was to design and validate mutations that were capable of modulating it, with the ultimate purpose of introducing these mutants into cells to explore the physiological role of the interaction (with and without the mutations).

The CDK1\_2A mutant disrupts talin:CDK1 binding and is useful in helping understand what the CDK1:talin interaction is doing in a cell. However, because CDK1 is a promiscuous Ser/Thr kinase and is known to phosphorylate hundreds of other proteins in different compartments of the cell (M. C. Jones, Askari, Humphries, & Humphries, 2018), having a CDK1 mutant may not give a clear picture of its talin-dependent functions. The mutation in CDK1 may affect phosphorylation of other proteins in the cell, and this would have off target effects other than just disrupting the talin:CDK1 interaction. To resolve this, we proposed that a mutation on the talin R8 domain inhibiting the talin:CDK1 interaction would give a clearer insight in to the role CDK1:talin is playing in the cell.

We wanted to design and test a talin mutant that would perturb the talin:CDK1 interaction and not prevent binding of other known talin R8 binding proteins such as DLC1 or RIAM (Goult, Zacharchenko, *et al.*, 2013; Zacharchenko *et al.*, 2016). To determine if R8 ligand-specific mutations were feasible, the structures of DLC1:talin (PDB ID: 5FZT) and RIAM:talin (PDB ID: 4W8P) and CDK1:talin (predicted) were examined (**FIGURE 6.19**).

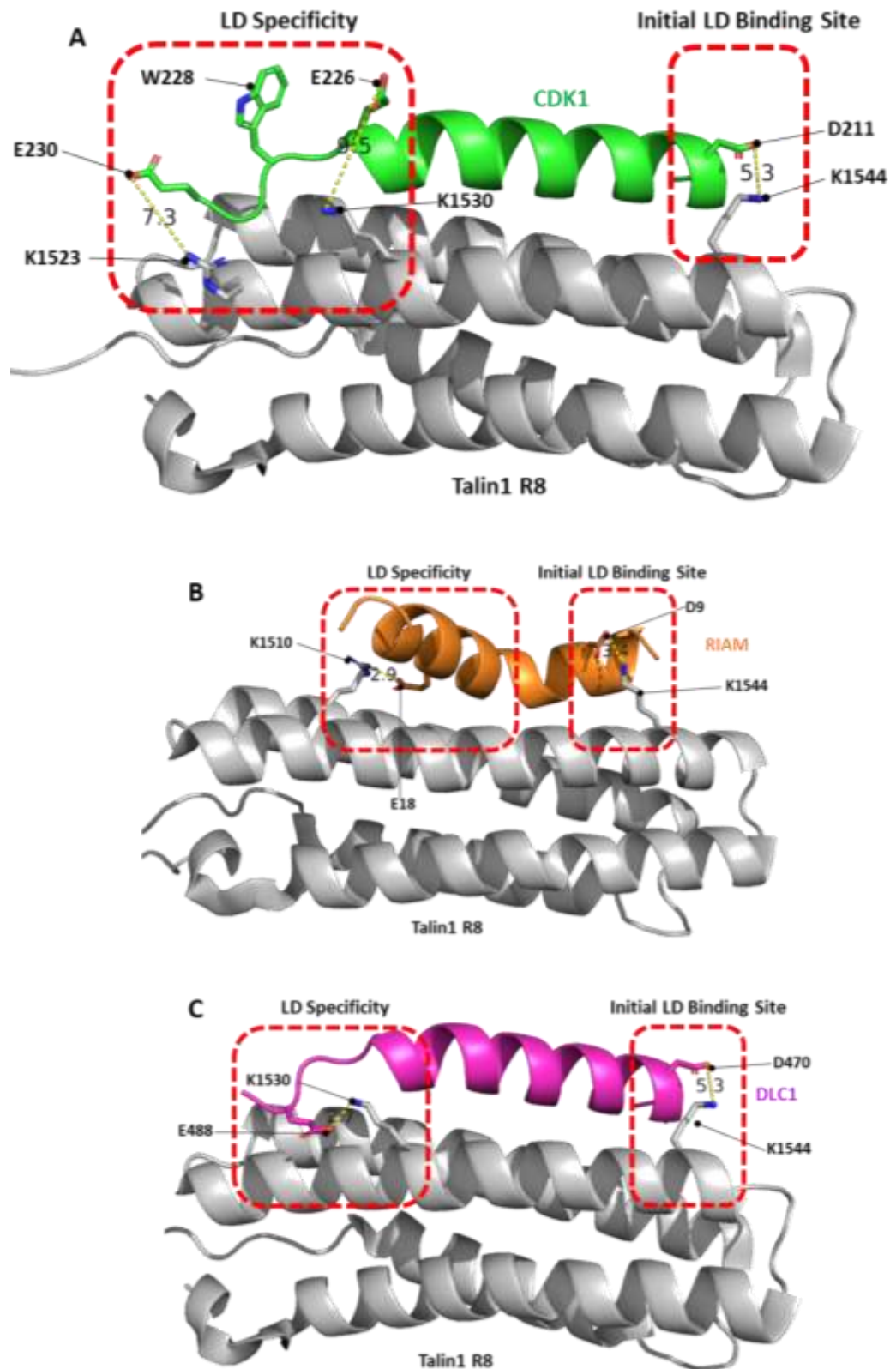


**FIGURE 6.19: LD SPECIFICITY BETWEEN TALIN R8 LIGANDS: DLC1, RIAM AND CDK1**

(A) Structural model of talin: CDK1:tal in highlighting the binding of LD talin-binding motif on the CDK1 peptide (green) initial talin LD binding site shown by a red box and the LD specificity region is also highlighted by a red box. (B) Structure of talin: RIAM (PDB ID: 4W8P) RIAM LD talin-binding motif highlighted in orange. (C) The structure of talin: DLC1 (PDB ID: 5FZT) DLC1 (pink).

The salt bridge interaction that forms between the Asp on the LD-motif and talin1 R8 Lys1544 residue might be the initial contact that defines the interaction. Structural analysis confirms that the LD talin-binding motifs of: CDK1, RIAM and DLC1 dock to the talin R8 domain all form this interaction via the 'initial LD binding site' (see **FIGURE 6.19**).

This interaction orients the LD talin-binding peptide and allows binding of other residues further downstream of the LD to bind to talin in what is known as the 'specificity region' (Zacharchenko *et al.*, 2016). Talin1 Lys1544 was targeted when trying to perturb the DLC1:talin interaction (Zacharchenko *et al.*, 2016), where the basic Lys residue was mutated to an acidic Glu. This mutation however, only had a partial effect on perturbing the interaction between talin and DLC1 suggesting that other interactions downstream of this in the 'LD specificity region' are integral for the interaction (Zacharchenko *et al.*, 2016).

The 'LD specificity region' potentially makes it plausible that a ligand specific mutation could be made to prevent only the perturbation of one LD ligand from talin R8. The talin residue Lys1544 could be mutated to abrogate the 'LD initial binding site' and then a residue making a contact unique to that LD talin-binding ligand could be mutated in the 'specificity region'.

**FIGURE 6.19** shows the 'LD specificity region' in both DLC1 and RIAM; DLC1 Glu488 forms a salt bridge with talin Lys1530 whereas RIAM Glu18 forms a salt bridge with talin Lys1510. A double talin mutant that targeted both the 'initial LD binding site' (Lys1544) and the DLC1 'specificity site' (Lys1530) was designed and tested using NMR (Zacharchenko *et al.*, 2016). This data indicated that the double mutation perturbed the binding of talin and DLC1 (Zacharchenko *et al.*, 2016).

Using a similar strategy we sought to design a talin mutant to perturb talin:CDK1 binding and to achieve this the CDK1 'specificity site' needed to be identified. The CDK1: talin docking structure (**FIGURE 6.19A**) was used as a reference and a potential salt bridge between CDK1 Glu232 and talin Lys1523 was identified. A further contact between CDK1 and talin in the 'specificity region' could come from hydrophobic interactions between CDK1 Trp228 and talin. **FIGURE 6.19A** shows the Trp228 residue to be facing away from the talin helices however, if helical propensity of this region was modelled we would predict that the hydrophobic Trp residue would point in-between the two talin helices forming a hydrophobic interaction.

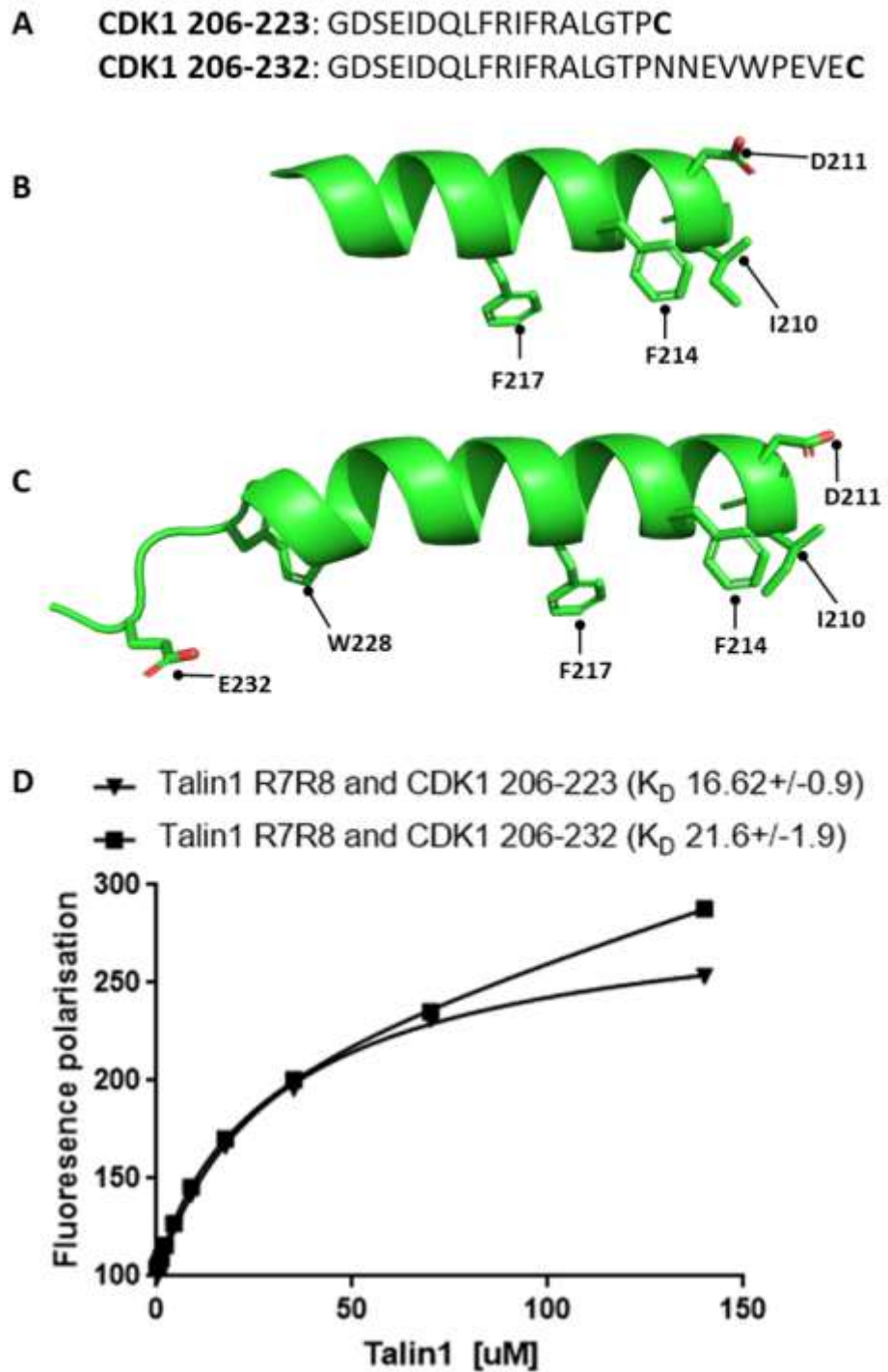


**FIGURE 6.20: IDENTIFYING IF CDK1 TRP228 AND GLU230 RESIDUES ARE IMPORTANT FOR TALIN BINDING**

(A) The CDK1 206-223 and CDK1 206-232 peptide sequences used. (B-C) Helical prediction of CDK1 peptides based on the structure CDK1 (PDB ID:4YC6). (D) Binding of BODIPY-TMR labelled CDK1 206-223C and CDK1 206-232C peptides to individual talin1 R7-R8 (1357–1659). Binding affinities were measured using a Fluorescence Polarization assay. Dissociation constants  $\pm$  SE ( $\mu$ M) for the interactions are indicated in the legend. All measurements were performed in triplicate.

Neither CDK1 residues Trp228 and E230 are found in DLC1 or RIAM nor do DLC1 or RIAM appear to contact talin Lys1523. We hypothesised that if these regions could be targeted in conjunction with the talin Lys1544 residue a CDK1 specific talin mutation could be made.

Before designing the talin mutants we wanted to determine if the CDK1 residues encompassing the predicted LD specificity region would increase the affinity for CDK1 as they were not included in the original CDK1 206-223 peptide. To explore whether Trp228 and Glu230 were involved; we designed a longer CDK1 peptide- CDK1 206-232 (shown in **FIGURE 6.20A**). Fluorescence polarisation was used to measure the binding affinities for the two CDK1 peptides with talin1 R7R8.

**FIGURE 6.20D** shows there was no significant difference between the longer and shorter CDK1 peptides: the short CDK1 206-223 peptide bound with a  $K_D$  of 16  $\mu$ M and the longer peptide bound with a  $K_D$  of 21  $\mu$ M. Therefore, we concluded that Trp228 and Glu230 are not important for the interaction with talin and thus we have determined that the CDK1 residues 206-223 comprise the talin binding site. Determining that only CDK1 residues 206-223 are important for talin binding meant that a new strategy for designing a CDK1 specific mutant had to be implemented as talin residues around Trp228 and Glu230 could no longer be targeted as they were not part of the talin binding site, meaning the 'LD specificity region' was not where originally anticipated. The next strategy we implemented was to disrupt hydrophobic interactions between talin and CDK1 206-223. **FIGURE 6.21** highlights the hydrophobic residues on CDK1 that could interact with talin helices 32 and 33, these include CDK1 residues: Ile210, Phe214 and Phe217.

To target these CDK1 residues, talin1 R7R8 mutants were designed, the CDK1 Phe217 (from the CDK1:talin binding model) looked to be situated near two alanine residues on the talin surface Ala1495 and Ala1499 (shown in **FIGURE 6.21**). Ala1495 and Ala1499 potentially create a pocket for the aromatic ring of Phe217 and Phe214.

This observation of conserved small residues in the interface had some similarity to the docking of KANK to talin R7; KANK had a bulky hydrophobic residue Tyr48, which formed hydrophobic interactions with talin helices 29 and 36. The design of the talin mutant G1404L utilised a bulky leucine residue and prevented KANK1 Tyr48 from interacting with talin. Learning from the success of the G1404L talin mutant we employed a similar strategy of trying to prevent the CDK1 residues; Phe217 and Phe214, from fitting in-between the talin helices. Talin1 Ala1495 and Ala1499 were mutated to leucine residues with the hypothesis that the two Leu residues would fill the gap between talin helices 32 and 33 preventing CDK1 Phe214/ Phe217 from fitting in to the pocket and forming a hydrophobic interaction.

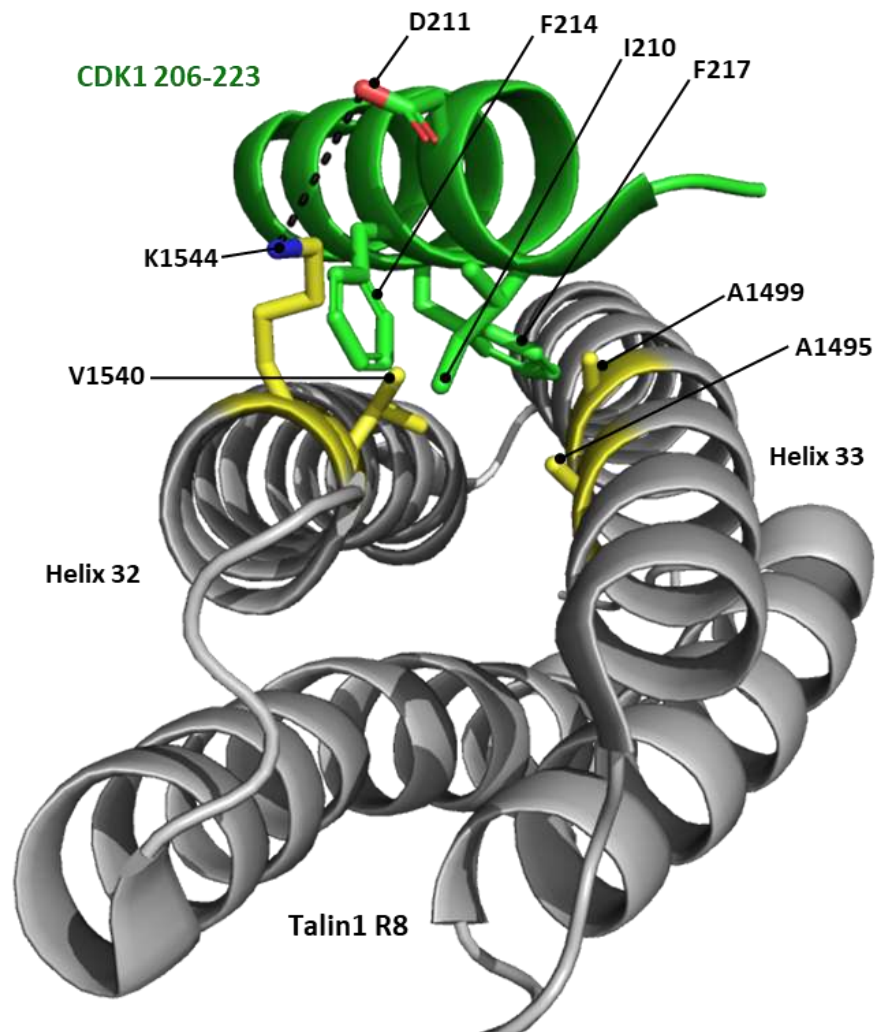


**FIGURE 6.21: DESIGNING A TALIN R8 MUTANT TO PERTURB CDK1 BINDING**

Structural model of Talin1:CDK1 206-223 predicted based on talin:DLC1 structure(PDB ID: 5FZT). Residues on talin R8 that look to be interacting or in close proximity to CDK1 residues are highlighted in yellow. The salt bridge formed between talin Lys1544 and CDK1 Asp211 is highlighted with a black dotted line.



A second mutagenesis approach was to target the CDK1 'initial LD binding site' by designing a talin mutant that could prevent the salt bridge between talin Lys1544 and CDK1 Asp211 as showing in **FIGURE 6.19A**. These included:

- i. A charge reversal mutant K1544D aimed to repel the Asp211 residue on CDK1 and prevent binding.
- ii. A charged mutant V1540D targeting the Ile210 hydrophobic residue on CDK1 to prevent hydrophobic interaction with talin. The addition of a charged aspartate residue in the hydrophobic pocket on talin aimed to repel the CDK1 Ile210 residue.

Our studies with the longer CDK1 206-232 peptide indicated that the region 223-232 was not essential for binding to talin (**FIGURE 6.20**); however, we postulated that by introducing a mutation in talin that would prevent this region of CDK1 being able to bind talin, the entire CDK1 peptide binding to talin R8 could still be disrupted. The talin mutant S1513L was, therefore, designed with a Leu residue filling the gap between the talin helices and thus preventing the CDK1 Trp228 residue (or surrounding residues) from forming hydrophobic interactions with talin.

In summary, we designed a total of four talin1 R7R8 mutants:

- i. A1495L: Targeting the interaction sustained by Phe214 on CDK1
- ii. S1513L+A1495L: Targeting binding of CDK1 through Phe214 and Trp228
- iii. A1499L+A1495L: Targeting binding of CDK1 through Phe214 and Phe217
- iv. V1540D+K1544D: Targeting binding of CDK1 through Asp211 and Ile210

## 6.2.8 Testing of designed talin mutants to perturb CDK1 binding

The designed talin mutants were put into the pET151 talin1 R7R8 vector allowing for recombinant expression and purification. Mutants were not put into the single talin domain R8 due to the domain not being as stable as R7R8. The talin1 R7R8 mutants were all concentrated to an equal concentration of 300  $\mu$ M along with talin1 R7R8 *WT* and used in the FP assay to measure affinity with BODIPY-TMR labelled CDK1 206-232 peptide, results are shown in **FIGURE 6.22**.

The talin Leu mutations (A1495L, A1499L) did not have a big effect on the binding affinity between CDK1 and talin compared to talin1 R7R8 *WT*. These mutations were designed to prevent the hydrophobic Phe residues on CDK1 forming hydrophobic interactions with talin, the fact it had no effect on CDK1 binding suggests either a Leu substitution may not have been enough to disrupt the hydrophobic interaction or instead a charged residue could have been used. It could also have been that the talin residues Ala1495 and Ala1499 were not close enough to the Phe residues on CDK1 or that the Ala residues provided a hydrophobic environment that the Phe could still interact with. On the other hand, it could imply that the CDK1 Phe residues are not involved in the interaction. The double mutant S1513L and A1495L had a slightly bigger effect on CDK1's binding affinity to talin, it doubled the  $K_D$  however, and this would not probably not be enough to perturb binding within a cell. The most effective mutation was the V1540D and K1544D (VDKD) mutation, as it changed the  $K_D$  from 15  $\mu$ M to 91  $\mu$ M, a six-fold difference.

A

Talin1 R7R8 Mutant	Reason for Mutant	$K_D$ $\mu$ M
WT	N/A	16.03 +/- 0.9
A1495L	Targeting CDK1 F214	16.97 +/- 0.8
S1513L + A1495L	Targeting CDK1 F214, W228	33 +/- 4.1
A1499L + A1495L	Targeting CDK1 I210, D211, F214	16.97 +/- 0.9
V1540D + K1544D	Targeting CDK1 I210, D211	95 +/- 22.3

B

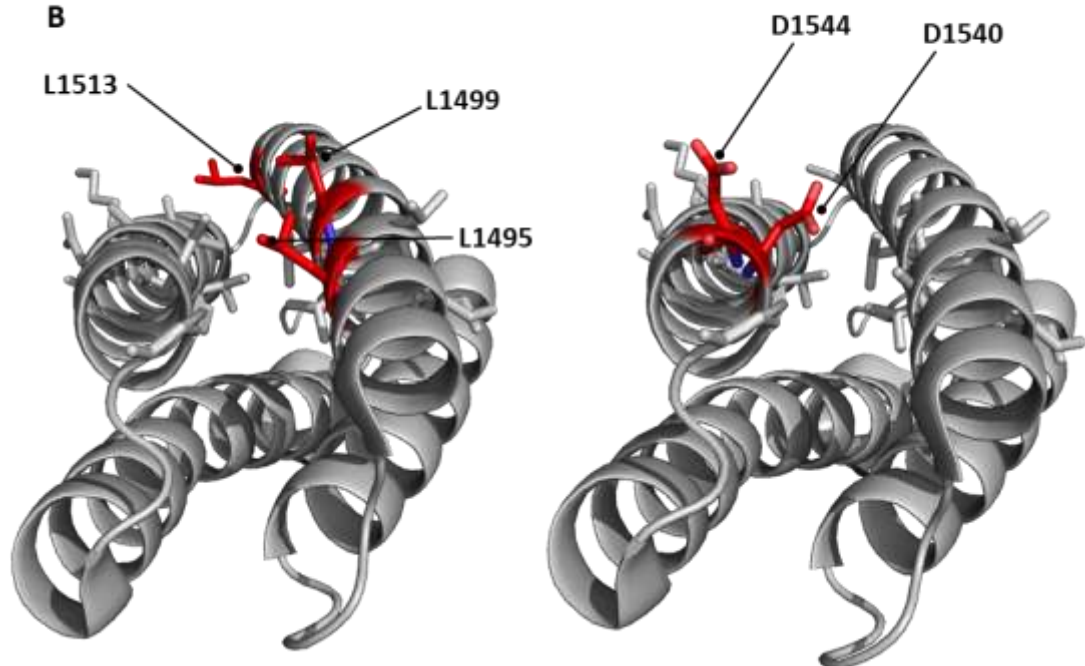


**FIGURE 6.22: DETERMINING IF THE DESIGNED TALIN R7R8 MUTANTS PERTURB CDK1 BINDING**

(A) Table of  $K_D$  values determined from FP assay with CDK1 peptide 206-223 and talin1 R7R8 mutants: V1540D+K1544D, A1499L+A1495L, S1513L+A1495L and A1495L. Dissociation constants  $\pm$  SE ( $\mu$ M) for the interactions are indicated and all measurements were performed in triplicate. (B) talin1 R8 structure (PDB ID: 5FTZ) highlighting talin residues in red that have been mutated.

### 6.2.9 Is the talin mutant 'VDKD' specific to perturbing the talin:CDK1 Interaction?

After determining the talin VDKD mutant to be successful in perturbing the talin:CDK1 interaction it was important to conclude if the mutation only perturbed CDK1 binding or if it affected the binding of other R8 ligands; RIAM and DLC1. To determine this the binding affinities of talin1 R7R8 *WT* and talin1 R7R8 VDKD were tested against DLC1 465-489 and RIAM 4-30 peptides, using *in vitro* FP assays (**FIGURE 6.23**). The VDKD mutation appears to affect both RIAM and DLC1 binding to talin; the  $K_D$  of DLC1 changed from 3.5  $\mu\text{M}$  (talin1 *WT*) to 15  $\mu\text{M}$  with the talin1 VDKD mutation. Likewise, the  $K_D$  for the interaction with RIAM changed from 3.9  $\mu\text{M}$  to 22  $\mu\text{M}$  with *WT* and VDKD mutant, respectively.

The VDKD talin mutation was designed to target the 'LD initial binding site' of CDK1 however, due to this being a common mechanism of binding for all LD talin-binding motifs the mutant also affected RIAM and DLC1 binding to talin. This is a difficult problem to navigate around as the other talin mutants designed to target CDK1 in the 'specificity region' downstream of the LD-motif did not seem to have an effect on talin:CDK1 binding. This is a useful talin mutant for cellular studies as it does perturb the talin:CDK1 interaction. It will just be important to consider that when looking for a talin:CDK1 phenotype within a cell, other ligands (RIAM and DLC1) would also be prevented from binding to talin1 R8.

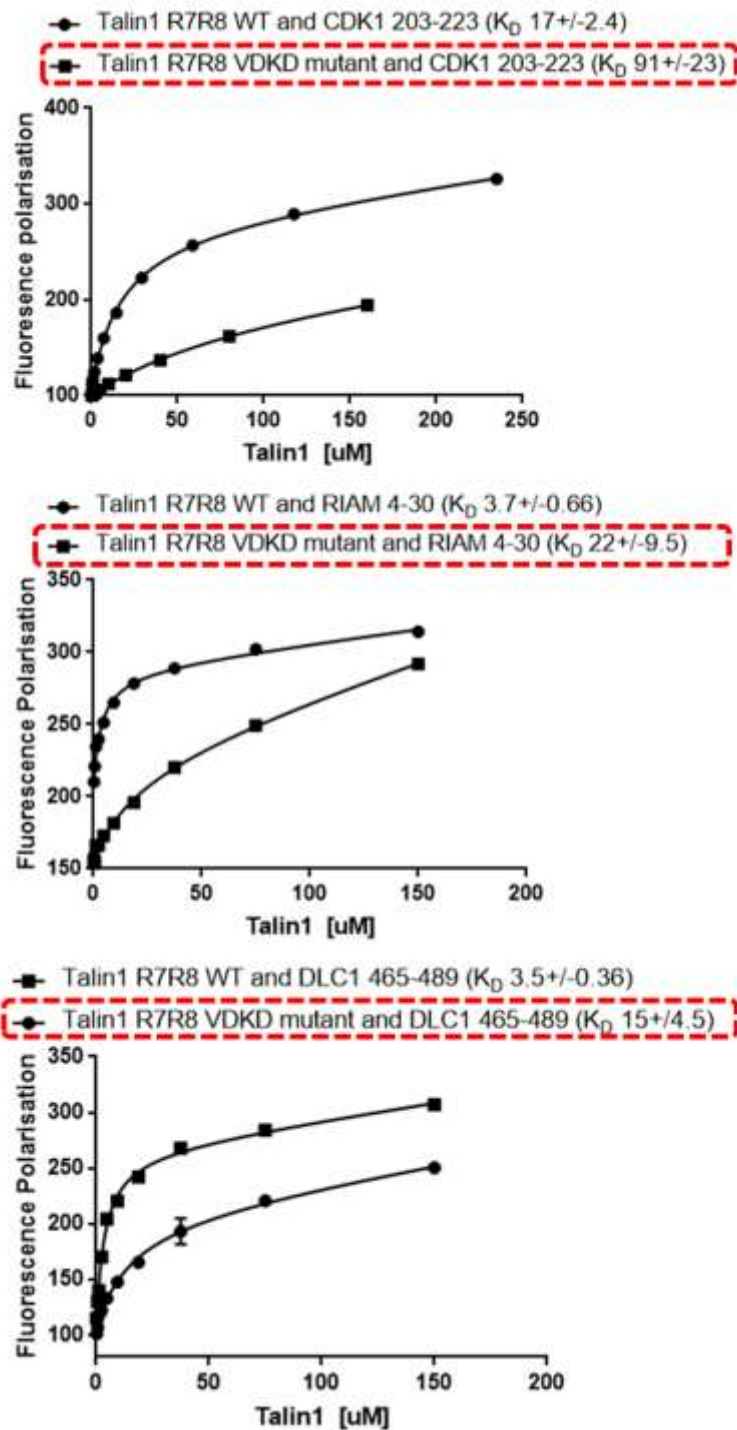


**FIGURE 6.23: DETERMINING THE BINDING AFFINITY FOR DLC1, RIAM AND CDK1 AGAINST THE TALIN1 R7R8 VDKD MUTATION.**

(A-C) Binding of BODIPY-TMR labelled; CDK1 206-223C, DLC1 465-489C and RIAM 4-30C peptides to talin1 R7-R8 (1357–1659). Binding affinities were measured using a Fluorescence Polarization assay. Dissociation constants  $\pm$  SE ( $\mu$ M) for the interactions are indicated in the legend. All measurements were performed in triplicate.

### 6.2.10 Can CDK1:Cyclin:taln form a complex?

In our biochemical studies we have used the CDK1 peptide 206-223 as a representation of the CDK1 protein. We know that this region provides the talin binding epitope. In order to visualize the interaction between talin R7R8 and full-length CDK1, the known CDK1 (PDB ID: 4YC6) and talin1 R7R8 (PDB ID: 5FZT) structures were docked together combining both modelling approaches and the knowledge gained from our biochemical studies. **FIGURE 6.24A** shows CDK1 and R7R8 docked, highlighting that the interaction is sterically feasible and there is space for both proteins to bind. There is a slight clash between talin R8 and the flexible loop near the CDK1 LD talin-binding motif. This region on CDK1 is flexible and would be able to take a different confirmation so would not be anticipated to cause problems.

I was also intrigued to model the tripartite complex of cyclin:CDK1:taln. Cyclin is needed to activate CDK1 and so it would be possible talin-cyclin-CDK1 could form a complex. To determine if the interaction was sterically possible the known structures; CDK1-cyclinB1 (PDB ID:4YC3) and talin1 R7R8 (PDB ID:5FZT), were used to model the interaction (**FIGURE 6.24B**). Again, it looks sterically feasible for talin to bind cyclin-CDK1; there is a small clash between talin R7 and cyclin B1. However, the talin R7R8 domains are connected via a flexible linker which would allow for sufficient movement to prevent a clash with cyclinB1 implying that a tripartite interaction is feasible.

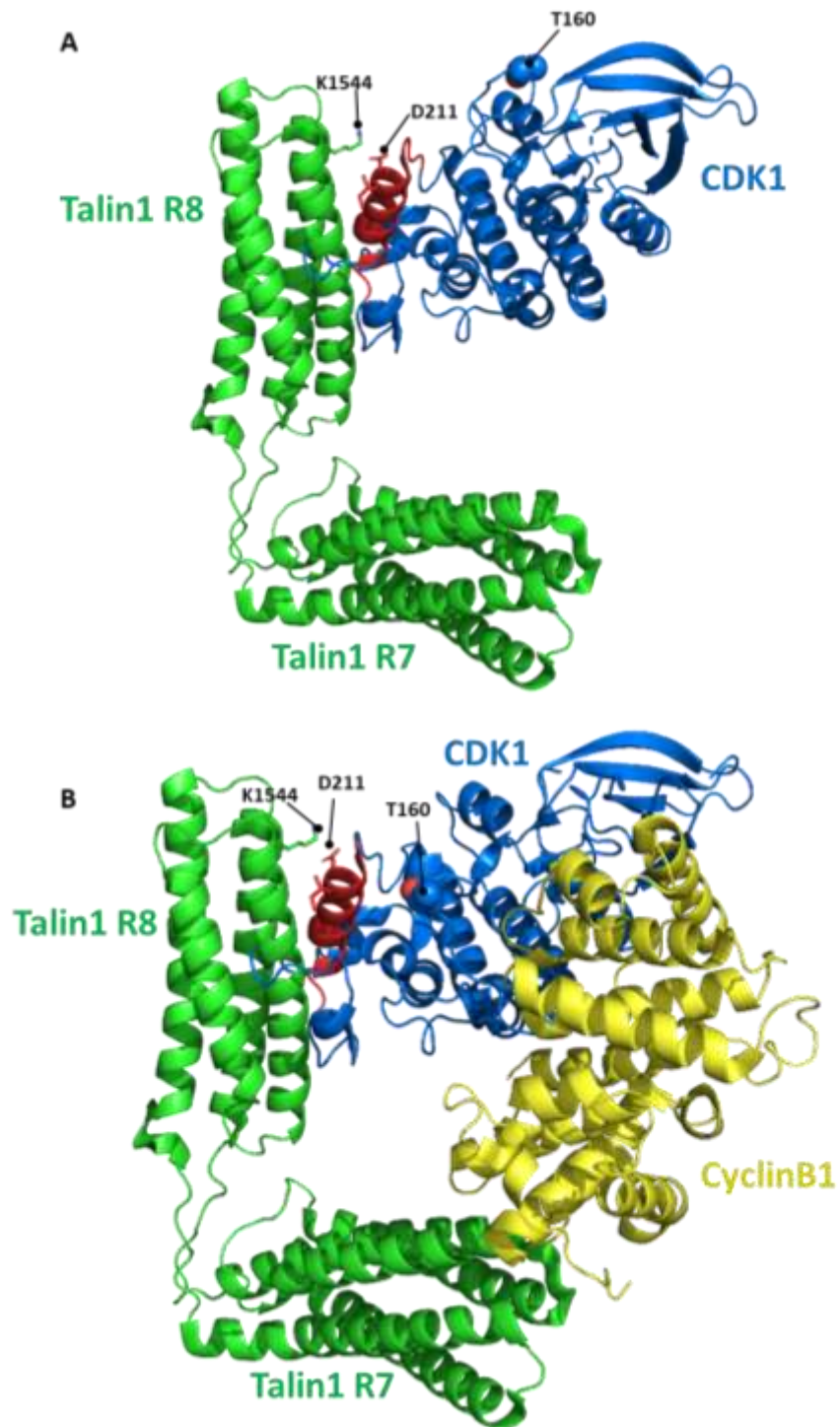


**FIGURE 6.24: STRUCTURAL MODEL OF TALIN1 R7R8:CDK2:CYCLINA2**

(A) Structural model of CDK1:talin1R7R8 using X-Ray crystallography structures of CDK1 (PDB ID:4YC6) and talin R7R8 (PDB ID:5FZT). (B) Structural Model of CyclinB1:CDK1:talin1R7R8 using the CDK1/cyclinB1 structure (PDB:4YC3) and the talin structure (PDB ID:5FZT). CyclinB1 is coloured in yellow, CDK1 (blue) and talin R7R8 (green). Residues from CDK1 206-223 peptide are highlighted in red.

### 6.2.11 How does talin affect CDK1 kinase activity?

We wanted to determine if talin binding to CDK1 would affect the kinase function of CDK1. To explore this further, we collaborated with Martin Humphries from the University of Manchester. The Humphries group had been studying the CDK1-dependent phosphorylation of Formin Like Protein-2 (FMNL2), an adhesion protein required for actin assembly and turnover (Grikscheit *et al.*, 2015). They identified the phosphorylation of FMNL2 using an *in vitro* kinase assay, where GST-tagged FMNL2 was incubated with purified cyclinA2-CDK1/ cyclinB1-CDK1 and ATP. Using pull-down assays and western blots with S/T-P antibody (MPM2); MPM2 is an anti-phospho Ser/Thr-Pro antibody and can be used to detect phosphorylated Ser/Thr residues in the CDK1 phosphorylation sequence Ser/Thr-Pro. The Humphries group found that FMNL2 was phosphorylated by CDK1 in the presence of both cyclinA2 and cyclinB1 (Jones *et al.*, 2018).

This *in vitro* kinase assay with FMNL2 provided an ideal platform to determine if talin was affecting CDK1s kinase activity, by adding talin to the assay we predicted one of three outcomes:

- i. Talin prevents phosphorylation of FMNL2; talin binding to CDK1 inactivates the kinase.
- ii. FMNL2 can be phosphorylated by CDK1 in the absence of cyclin as talin activates the kinase.
- iii. FMNL2 is phosphorylated with cyclin-CDK1 and ATP; talin binding to CDK1 is not affecting the kinase activity.

I carried out the following experiments in the Humphries lab at the University of Manchester. Purified talin1 R7R8 (residues 1357-1653) (in 3-fold excess 3  $\mu$ g) was added to purified FMNL2 1  $\mu$ g/ $\mu$ L, cyclinA2-CDK1 1 ng/ $\mu$ L (Invitrogen), and ATP 1 mM. Following this we performed immunoblotting against MPM2, CDK1 and cyclinA2. The blot shown in **FIGURE 6.15**, shows FMNL2 was phosphorylated at similar levels in both the presence and absence of talin (when ATP was present), confirming talin was not inhibiting the kinase activity of CDK1. Unexpectedly, the assay revealed that the talin1 R7R8 was also being phosphorylated by CDK1 (highlighted by a red box in **FIGURE 6.15**). Talin phosphorylation by CDK1 had not been anticipated due to no known phosphorylation sites on the talin R7R8 domain (despite phosphoproteomic analysis of talin in the phospho-adhesome (Robertson *et al.*, 2015)) and no obvious CDK1 phosphorylation sequence in the talin R7R8 sequence.



A high intensity talin R7R8 band was visualized in the western blot at approximately 32 kDa, in the presence of CDK1-cyclinA2 and ATP when probed with MPM2. In the absence of either cyclinA2 or ATP, no band is observed, indicating that talin could not activate CDK1 and that the activity was still cyclin dependent.

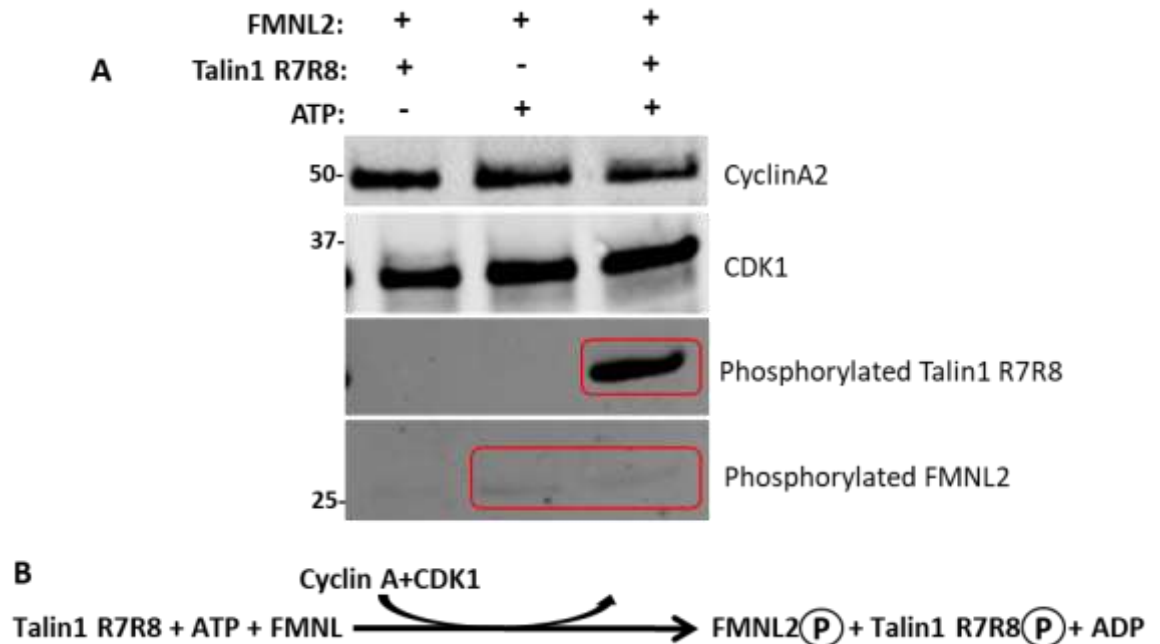


**FIGURE 6.25: CDK1 KINASE ACTIVITY IS NOT AFFECTED BY TALIN BINDING**

(A) Immunoblot analysis of *in vitro* kinase assay with purified talin1 R7R8, FMNL2 and CDK1-cyclinA2 (Invitrogen) with and without ATP. Immunoblot is blotted using anti-CDK1, GST-cyclin and anti-MPM2. Red box indicates talin1 R7R8 phosphorylation by CDK1 and FMNL2 phosphorylation by CDK1. (B) The reaction occurring in the *in vitro* kinase assay.

### 6.2.12 Talin phosphorylation by CDK1 is cyclin specific

To further investigate the phosphorylation of talin R7R8 by CDK1, the *in vitro* kinase assay was repeated in the absence of FMNL2 and at lower concentrations of talin (1  $\mu\text{g}/\mu\text{L}$ ). Both talin1 R7R8 (residues 1357-1653) and talin2 R7R8 (residues 1360-1656) were used in the *in vitro* kinase assay and cyclinA2 and cyclinB1 were used to determine if the interaction was cyclin specific. **FIGURE 6.26** shows a representative western blot of the assays and here the *in vitro* kinase assay was used as a qualitative assessment, rather than a quantitative measurement to determine CDK1 phosphorylation.

The immunoblots shown in **FIGURE 6.26** again confirm talin R7R8 is phosphorylated by CDK1-cyclinA2; a large increase in talin phosphorylation is shown **FIGURE 6.26A** when ATP is added to the assay with both talin1 R7R8. This same increase in talin phosphorylation when ATP is added can be seen in the talin2 R7R8 confirming that both talin isoforms are being phosphorylated by CDK1.

Interestingly the CDK1 phosphorylation on talin 1 and talin2 R7R8 looks to be cyclin specific as less phosphorylation is seen when CDK1-cyclinB1 is added to talin than with the CDK1-cyclinA2. This cyclin isoform specific phosphorylation can also be seen in **FIGURE 6.26B**; talin1 R7R8 and talin2 R7R8 phosphorylation is highlighted by a red box and it is clear that an increase in signal of talin phosphorylation when ATP is added can be identified when cyclinA2 is present but not when cyclinB1 is present.

Further immunoblots were carried out with CDK1-CyclinA2, talin1 R7R8 and talin2 R7R8 that can be seen in **FIGURE 6.27**. The blots provide further evidence that talin R7R8 is phosphorylated by CDK1-cyclinA2.

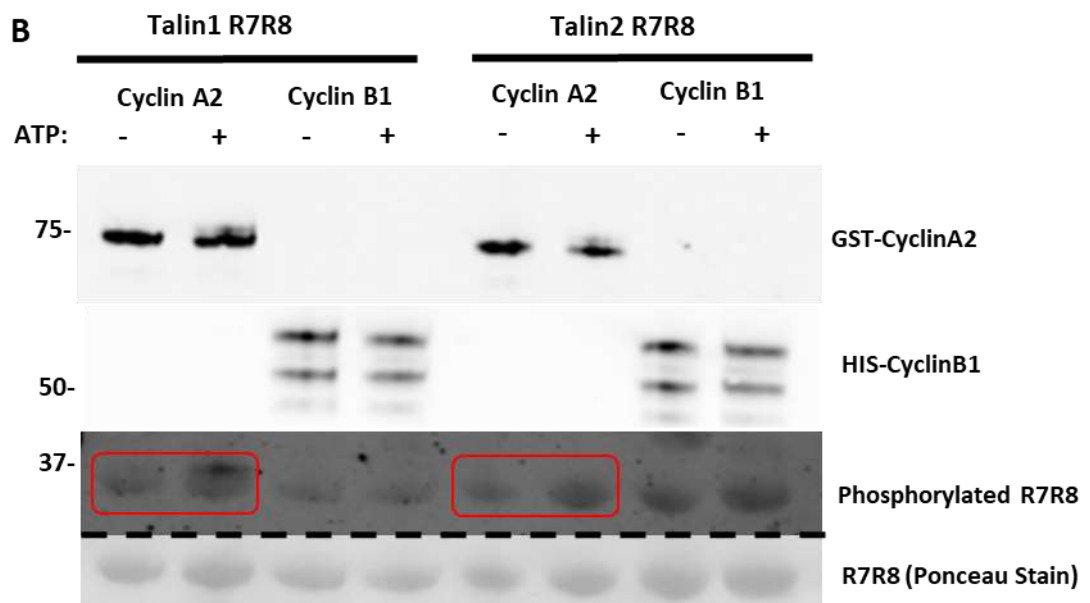
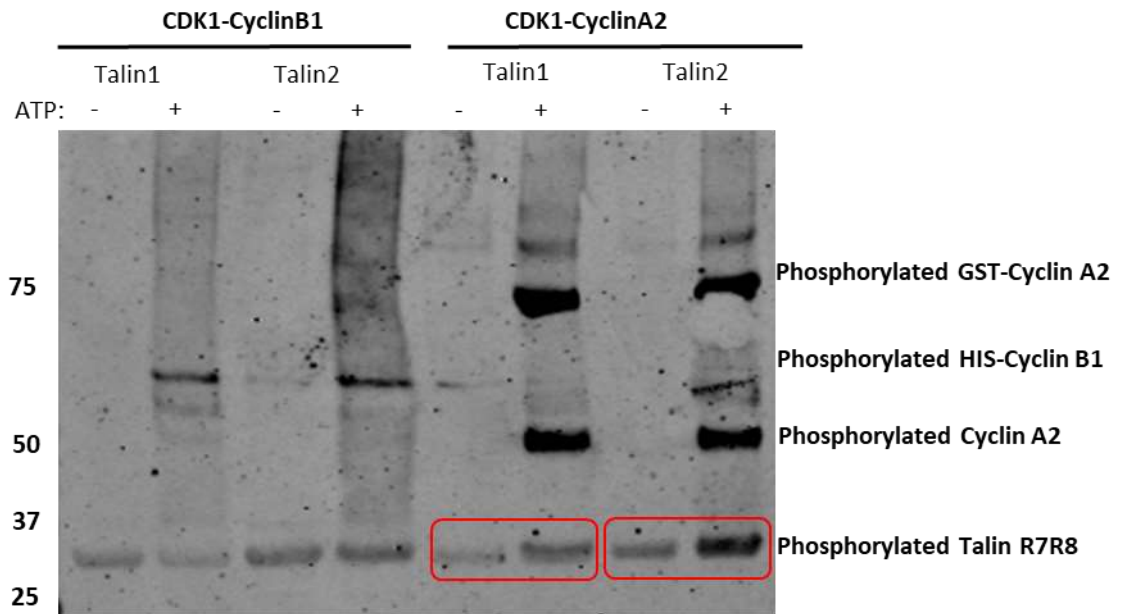


**FIGURE 6.26: TALIN R7R8 IS PHOSPHORYLATED BY CDK1-CYCLINA2**

(A-B) Immunoblot analysis of *in vitro* kinase assay with purified talin1 R7R8/talin2 R7R8, CDK1-cyclinA2 (Invitrogen) or cyclinB2 (Invitrogen) with and without ATP. (A) Immunoblot is blotted using anti-MPM2. Red box indicates talin1 R7R8 phosphorylation by CDK1 cyclinA2. (B) Immunoblot is blotted against anti-MPM2, anti-GST and anti-HIS. Black line separates immunoblot from ponceau stain of talin R7R8 (32 kDa).

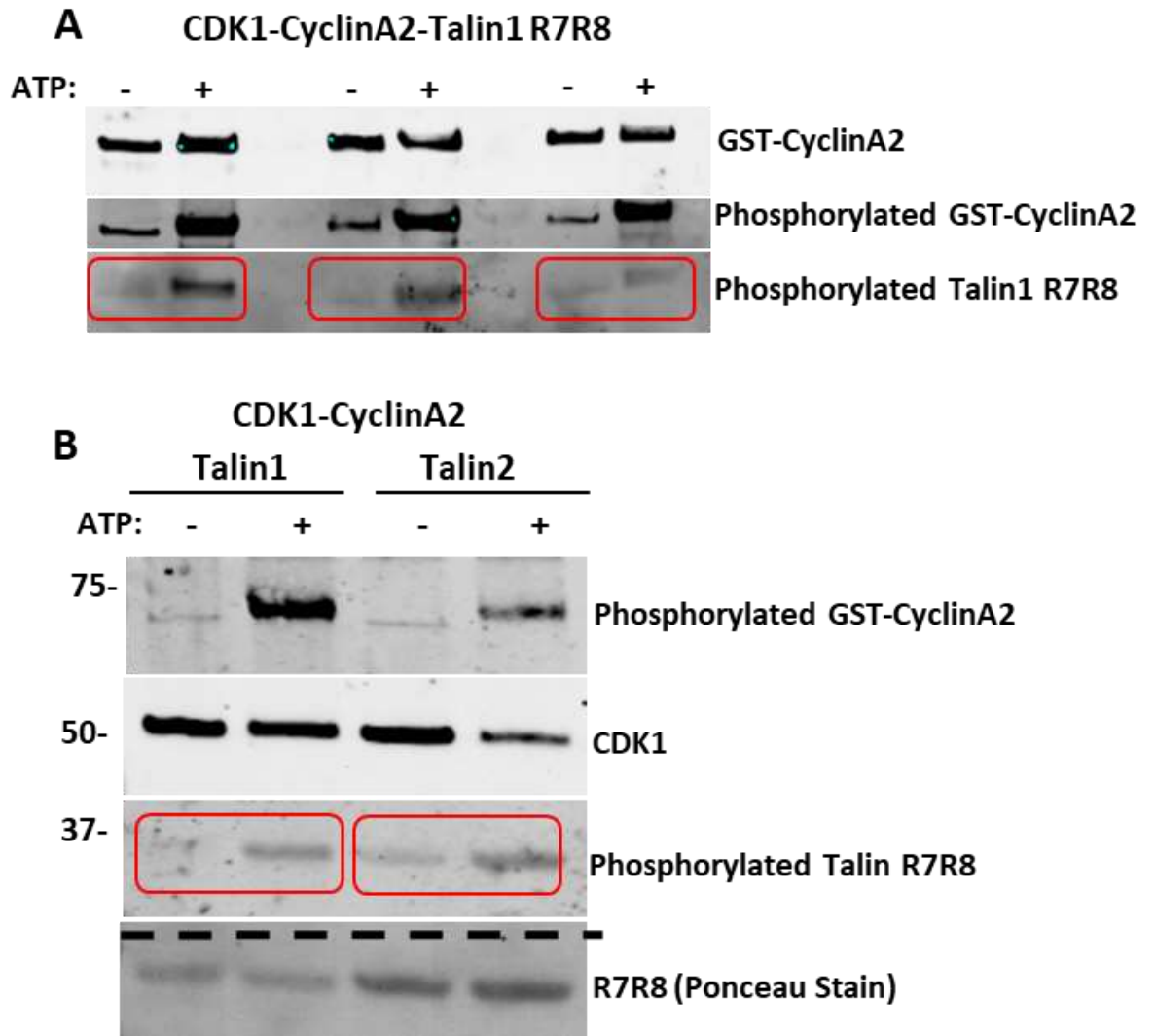


**FIGURE 6.27: IMMUNOBLOTS CONFIRMING TALIN R7R8 IS PHOSPHORYLATED BY CDK1-CYCLIN A2**

(A-B) Immunoblot analysis of *in vitro* kinase assay with purified talin1 R7R8/talin2 R7R8, CDK1-cyclinA2 (Invitrogen) with and without ATP. (A) Immunoblot is blotted using anti-MPM2 and anti-GST, red box indicates talin1 R7R8 phosphorylation by CDK1 cyclinA2. (B) Immunoblot is blotted against anti-MPM2, anti-GST and anti-CDK1. Black line separates immunoblot from ponceau stain of talin R7R8 (32 kDa).

### 6.2.13 Mass spectrometry-based phosphosite mapping of talin phosphorylation

The *in vitro* kinase assays showed that both talin1 R7R8 and talin2 R7R8 could be phosphorylated by CDK1-cyclinA2. From the assay it is not possible to quantify the number of phosphorylation sites or identify the phosphorylation site(s). In order to map the phosphorylation sites on talin1 and 2 R7R8 Mass Spectrometry (MS)-based phosphosite mapping was used.

#### 6.2.13.1 Identifying phosphorylation site(s) on talin1 R7R8

The *in vitro* kinase assay was carried out in triplicate and products were run on an SDS-PAGE gel shown in **FIGURE 6.28A**. Talin1 R7R8 bands were cut from the gel and processed by in-gel tryptic digest as described previously (Horton *et al.*, 2016). The peptides produced from the digest were analysed using liquid chromatography Mass Spectrometry (LC-MS) and the data from LC-MS was analysed using the proteome software Mascot (Perkins *et al.*, 1999).

A screen shot of the Mascot output is shown in **FIGURE 6.28B**. The software lists the proteins identified in MS from the excised SDS-PAGE band (talin1 R7R8). The top panel shows the list of proteins found and the abundance of peptides found in each gel band (1-6); as expected the most abundant protein identified was mouse talin1 (UniProt: P26039). The Mascot software then searches for phosphorylated Ser or Thr residues on the peptides identified through LC-MS. Mascot can identify phosphorylated residues because of the addition of a  $\text{PO}_4^{2-}$  group; which adds 80 Da weight to the peptide. Talin1 R7R8 was found to have a single phosphorylated residue, Ser1589, found in all repeats (where ATP was present). **FIGURE 6.28B** shows the Ser1589 residue (highlighted in green) that is phosphorylated.



### 6.2.13.2 Identifying phosphorylation site(s) on talin2 R7R8

Similarly, to determine the phosphorylation site on talin2 R7R8 the products from *in vitro* kinase assay were separated by SDS-PAGE and the talin2 R7R8 bands at approximately 32 kDa were excised. The talin2 R7R8 bands were processed by in-gel tryptic digest as with talin1 R7R8 and the peptides produced from the digest were analysed using LC-MS and then the proteome software Mascot (Perkins *et al.*, 1999). Mascot identified talin2 R7R8 to be the most abundant protein in the sample and identified a phosphorylated residue between 1488-1491 (Ser, Ser, Pro, Ser). The programme was unable to determine which serine in this sequence was being phosphorylated as the trypsin digestion did not produce overlapping peptides in this region and, therefore, the exact phosphorylated Ser residue could not be determined.

To overcome this problem and determine the exact residue on talin2 undergoing phosphorylation, an Asp-N/trypsin digestion was used. The *in vitro* kinase assay was re-run and separated using SDS-PAGE as seen in **FIGURE 6.29A** and processed by in-gel Asp-N/trypsin digestion.

Asp-N is a highly specific endoproteinase that cleaves at the N-terminal side of Asp and Cys residues (Lahm and Langen, 2000). This approach was used alongside the trypsin digest to obtain additional overlapping peptides and improve sample characterisation. The data from LC-MS was imputed into Mascot; the Asp-N/trypsin digestion appeared to be successful in creating overlapping peptides in the 1489-1491 regions and allowed the software to identify a single phosphorylated residue Ser1489 (shown **FIGURE 6.29B**).

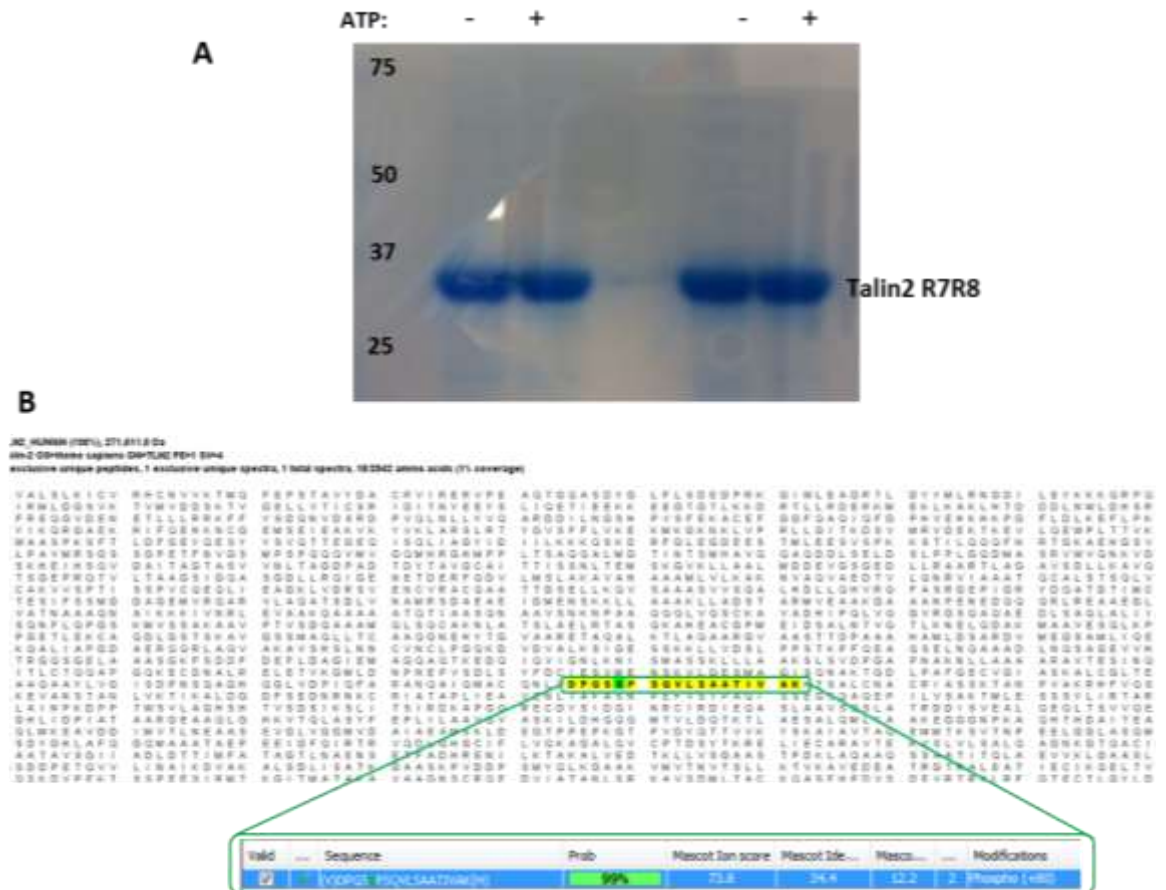


**FIGURE 6.29: PHOSPHOSITE MAPPING OF TALIN2 R7R8 PHOSPHORYLATION SITE**

(A) SDS PAGE gel showing talin2 R7R8 protein bands ~32 kDa that were separated from *in vitro* kinase assay. (B) Scaffold viewer highlighting the sequence in talin2 R8 found to be phosphorylated by CDK1cyclinA2. The residue Ser1489 was shown to have 99% confidence of being phosphorylated.

### 6.2.14 Isoform differences in CDK1 talin phosphorylation

The phosphosite mapping identified that both talin1 and talin2 R7R8 have a single CDK1 phosphorylation site. However interestingly, each talin isoform was phosphorylated at a different site by CDK1 raising the possibility that this is a mechanism to regulate CDK1 binding in the cell. To further explore why there are these differences in the talin isoforms, a sequence alignment of talin1 and talin2 was performed.



#### 6.2.14.1 Talin1 R7R8 Ser1589 phosphorylation site

**FIGURE 6.30** shows a conservation alignment, using Clustal Omega (Larkin *et al.*, 2007), of twenty-one talin1 species (green) and talin2 (red). The species aligned were chosen to cover a wide range of vertebrates across different animal classes. **FIGURE 6.30** shows the talin alignment between residues 1534-1604, encompassing the talin1-phosphorylated residue Ser1589. The blue box highlights the phosphorylated talin1 Ser1589 residue and the surrounding residues. Ser1589 is completely conserved in both talin1 and talin2 species, but the following Pro1590 residue is fully conserved in talin1 and not in talin2. Instead, talin2 has a semi-conserved Ser residue in this position; the removal of the Pro residue in talin2 means that it no longer is a consensus CDK1 phosphorylation site as it does not contain the minimal Ser/Thr-Pro motif, possibly explaining why we did not see this site as a hit in the phosphosite mapping analysis of talin2 R7R8.

The talin1 sequence 'SPEGR' around the Ser1589 is highly conserved across all the species which implies the sequence may have an important function. This sequence makes up the optimal consensus CDK1 phosphorylation sequence Ser/Thr-Pro-X-X-Arg/Lys (Suzuki *et al.*, 2015).



#### 6.2.14.2 Talin2 R7R8 Ser1489 phosphorylation site

To further investigate the talin2 CDK1 phosphorylation site the same talin1 and talin2 sequences as above were aligned using Clustal Omega (Larkin *et al.*, 2007) and **FIGURE 6.31** shows the conservation alignment around the phosphorylated talin2 Ser1489. Ser1489, as well as the surrounding residues Ser-Ser(p)-Pro-Ser-Gln, are completely conserved in talin2 across all species used in the alignment. These conserved residues do not fit the optimal CDK1 consensus sequence (Ser/Thr-Pro-X-X-Arg/Lys) found in the talin1 Ser1589 phosphorylation site. However, the residues do fit the Ser/Thr-Pro site sequence also known to be phosphorylated by CDK1.

Interestingly though, the talin1 sequence in this region is also conserved across species but is conserved differently from talin2. The talin1 sequence Pro-Cys-Thr-Gln is a reported O-glycosylation site with residue Thr1487 being glycosylated (Hagmann, Grob and Burger, 1992).

This concludes the finding of two unique CDK1 phosphorylation sites in talin R7R8. Each CDK1 phosphorylation site is isoform specific and the high conservation across species suggests that they are of functional importance. Determining the role of the different isoform-specific phosphorylation sites could therefore give an insight into the functional differences between talin1 and talin2.

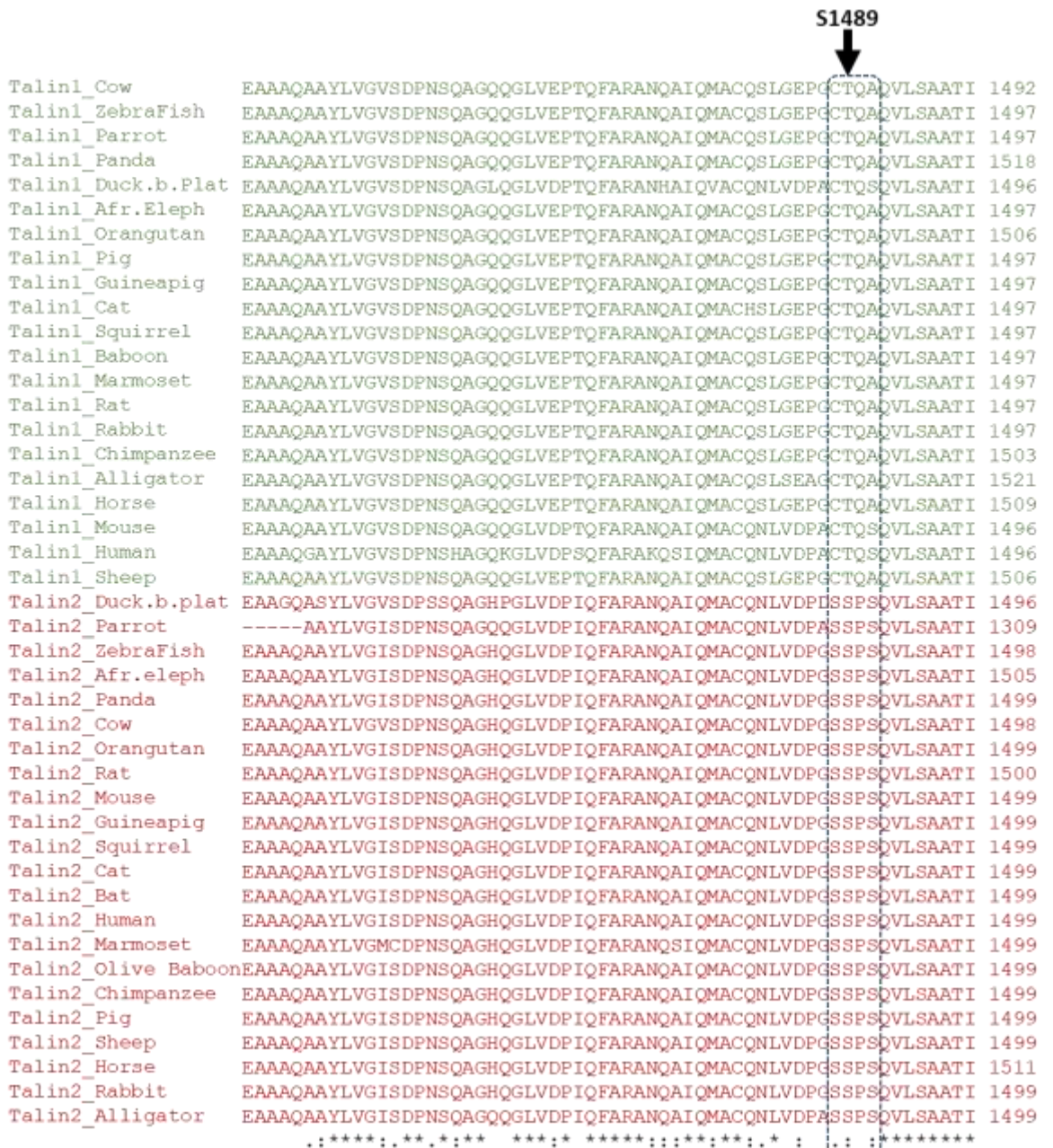


**FIGURE 6.31: ALIGNMENT HIGHLIGHTING THE TALIN2 PHOSPHORYLATION SITE BY CDK1:CYLINA2**

Human talin1 and talin 2 sequences aligned using Clustal Omega (Thompson, Gibson and Higgins, 2002), residues that are conserved in both talin 1 and talin2 are highlighted by a ‘\*’ closely conserved residues with similar properties highlighted with a ‘.’. Talin1 species are in green and talin 2 species are in red; the Ser1489 residue found to be phosphorylated in talin2 by CylinA2:CDK1 are highlighted in a black box.

### 6.2.15 Biochemically characterising the CDK1 phosphorylation site on talin1 R7R8

To determine the functional role of the talin1 CDK1 phosphorylation we looked at its positioning on the talin1 structure; **FIGURE 6.32A** shows the Ser1589 residue is positioned on talin R7 domain. The residue is positioned near the flexible linker region that joins R7 and R8 (**FIGURE 6.32B**). The flexible linker is a beta sheets that is held together by hydrogen bonds.

**FIGURE 6.32B** shows Ser1589 is positioned near two charged residues, Asp1451 and Glu1591. When Ser1589 is phosphorylated a  $\text{PO}_4^{2-}$  group will be added to the residue making the residue have a negative overall charge. This could repel the surrounding negatively charged Asp1451 and Glu1591 residues, which in turn could cause the hydrogen bonds in the beta sheet to break open. The instability generated in the linker could then lead to instability across both R7 and R8 domains potentially weakening the binding of any ligands to R7R8.

To determine if phosphorylation of Ser1589 would cause an effect on the stability of talin R7R8 a phosphomimetic mutant was designed. Ser1589 was substituted for an Asp residue; which is a negatively charged residue that provides a good mimic of phosphorylation. An Asp in position 1589 (S1589D) was introduced into talin1 R7R8 and using the FP assay, the affinity between BODIPY-TMR labelled CDK1 206-223 peptide and the talin S1589D mutant was measured. **FIGURE 6.32** shows the binding between CDK1 and talin1 R7R8 does not change when the S1589D mutant is introduced. The  $K_D$  for talin *WT* and CDK1 interaction was 20  $\mu\text{M}$  and the talin S1589D had a  $K_D$  of 24  $\mu\text{M}$ .



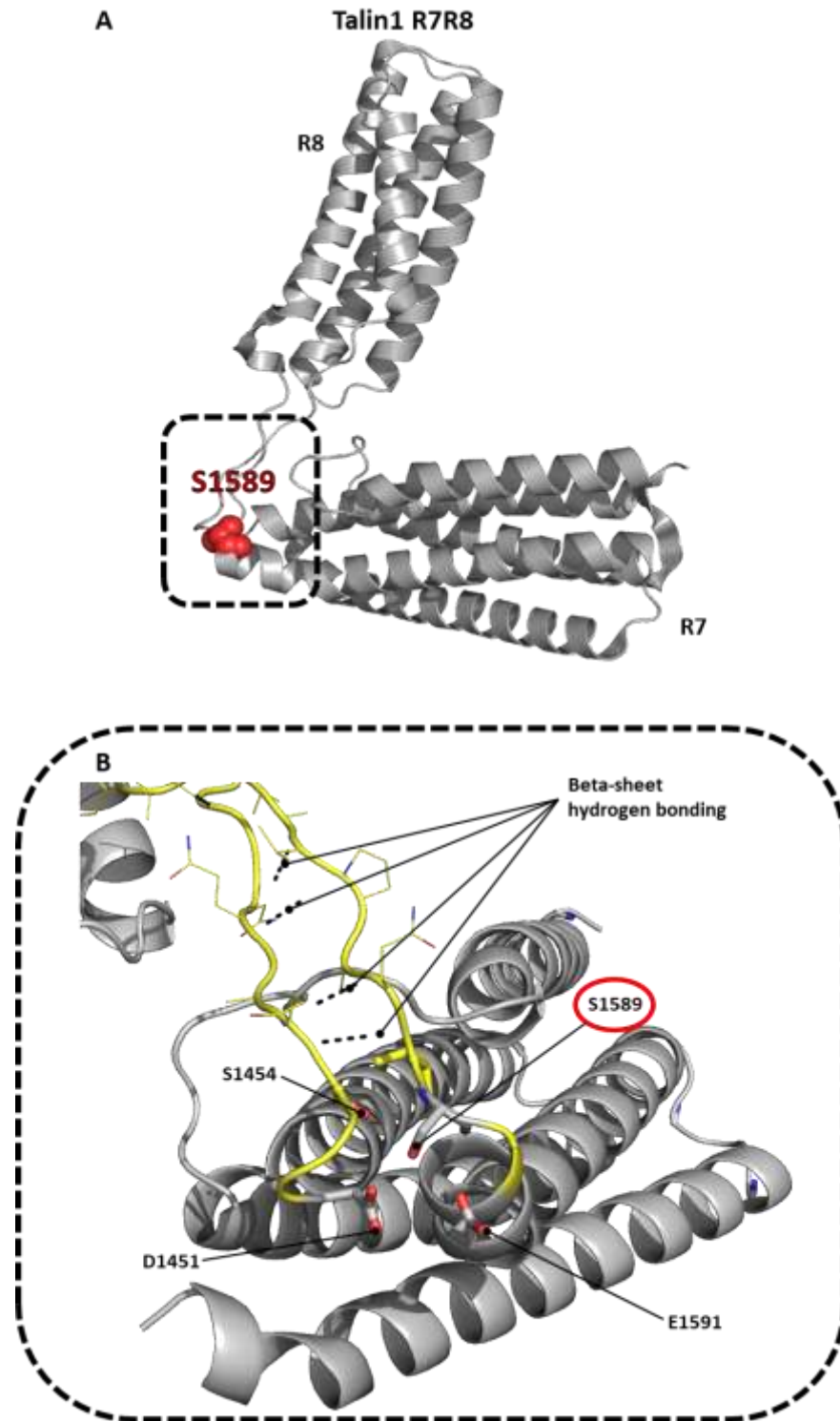


**FIGURE 6.32: TALIN1 CDK1 PHOSPHORYLATION SITE S1589**

(A) Talin1 R7R8 structure (PDB ID:5FZT) with CDK1 phosphorylation site (Ser1589) highlighted with a red sphere on the R7 domain. (B) talin1 R7 domain and R7R8 linker (yellow). Black dotted line showing hydrogen bonds across beta sheet.

To determine if the phosphomimetic effected the binding of other talin R7R8 ligands, FP was used to measure the affinity between talin S1589D and KANK30-60C and DLC1 465-489C. **FIGURE 6.33** shows that the phosphomimetic, S1589D, had no change on binding affinity to DLC1; DLC1 bound to the talin1 R7R8 S1589D with a  $K_D$  6  $\mu$ M and talin1 R7R8 *WT* 4  $\mu$ M. The R7 ligand KANK however, did bind more weakly to the S1589D mutant than talin R7R8 *WT* there was approximately a four-fold difference in  $K_D$  4  $\mu$ M and 1  $\mu$ M, respectively.

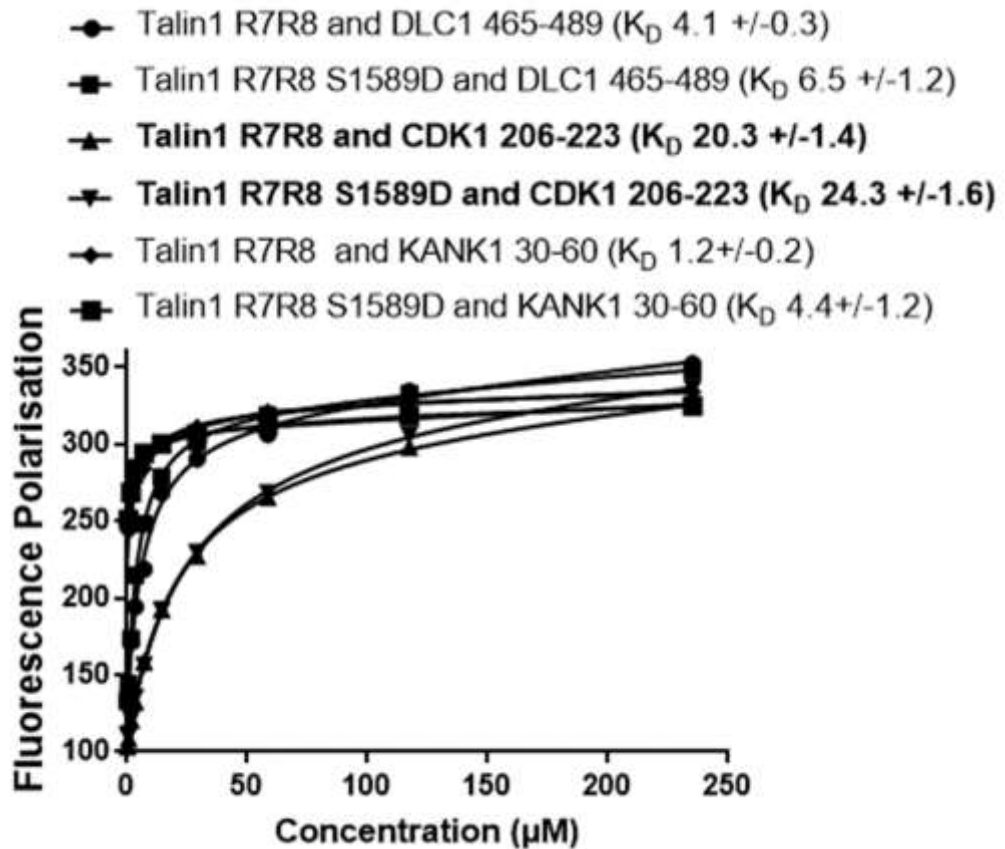


**FIGURE 6.33: TALIN1 SER1589 BINDING AFFINITY TO DLC1, KANK1 AND CDK1**

Binding of BODIPY-TMR labelled CDK1 206-223C, DLC1 465-489C and KANK1 30-60C peptides to talin1 R7R8 (1357–1653) and Talin1 R7R8 S1589D. Binding affinities were measured using a fluorescence polarization assay. Dissociation constants  $\pm$  SE ( $\mu$ M) for the interactions are indicated in the legend. All measurements were performed in triplicate. ND, not determined.

## 6.2.16 Biochemically characterising CDK1 phosphorylation site on talin2 R7R8

To determine the functional role of the talin2 CDK1 phosphorylation site Ser1489 we looked at its positioning on the talin2 structure. The talin2 R7R8 (Phyre2 (Kelley and Sternberg, 2009)) structure in **FIGURE 6.34** shows the Ser1489 residue is positioned on the talin R8 domain. The residue is positioned on helix 32 at the very top near the linker between helices 31 and 32. This talin helix makes up the binding surface for CDK1 and is also important for actin binding.

The R8 domain is one of five domains that make up the Actin Binding Site 2 (ABS2) region on talin. As previously mentioned ABS2 is important in focal adhesion maturation and generating traction force in the cell (Atherton *et al.*, 2015; Klapholz and Brown, 2017). The main actin binding surfaces on ABS2 are on the R4 and R8 domains. Both R4 and R8 talin domains have a higher isoelectric point (pI) values, compared to the other domains in the talin rod, causing the surface of R4 and R8 to be positively charged at physiological pH. The positive charge on the domains surface enables interactions with actin, which is negatively charged. A series of charge reversal mutants (Arg1500Glu, Arg1510Glu and Lys1522Glu) on the R8 domain, helices 31 and 32, have been shown to perturb the interaction between talin ABS2 and actin (Atherton *et al.*, 2015; Kumar *et al.*, 2016). When Ser1489 is phosphorylated by CDK1 a phosphate group addition will cause the residue to become negatively charged. Could phosphorylation of this residue reduce actin binding to the talin ABS2 site and, in turn, reduce the tension in the adhesion?



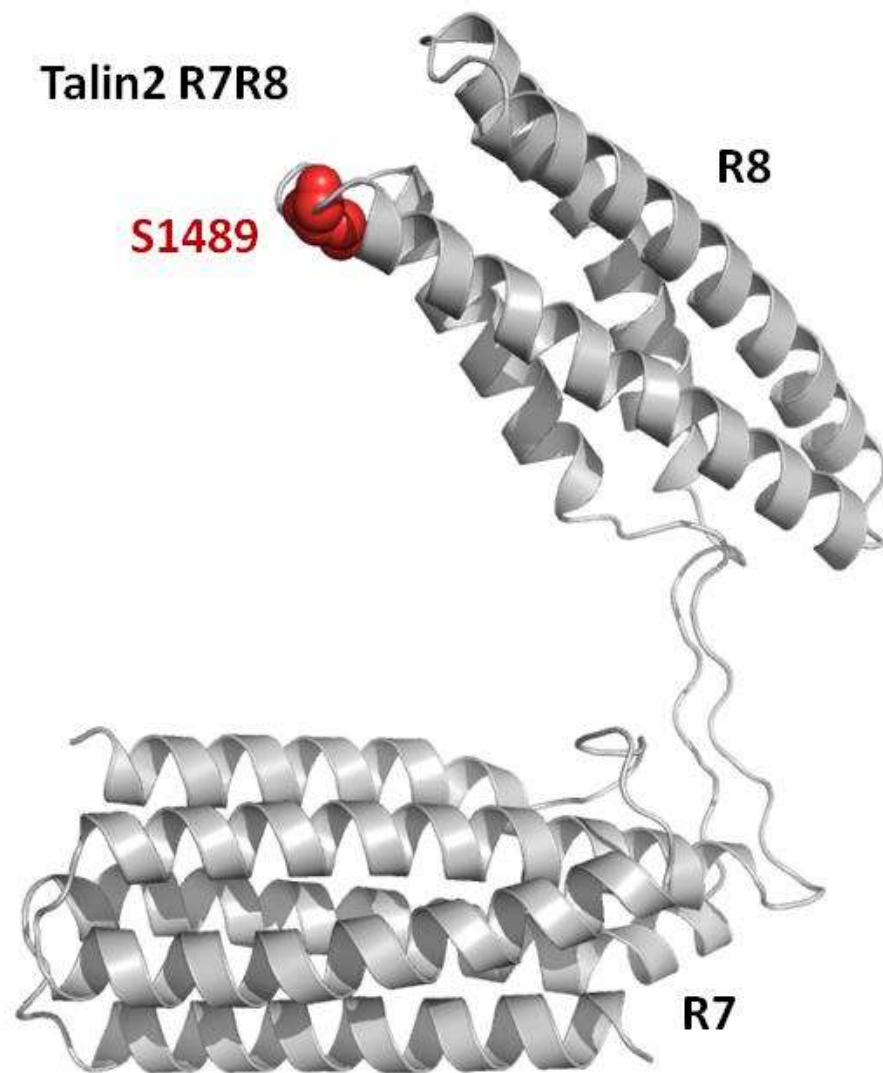


**FIGURE 6.34: TALIN2 CDK1 PHOSPHORYLATION SITE S1489**

Talin2 R7R8 structure prediction (Phyre2 (Kelley and Sternberg, 2009)) with CDK1 phosphorylation site (Ser1489) highlighted with a red sphere on the R8 domain.

### 6.2.17 Does CDK1 localise to adhesions

Having designed and biochemically characterised a successful CDK1 mutant (CDK1\_2A) capable of perturbing the talin:CDK1 interaction, the next step was to understand the significance this interaction in conjunction within the cellular context and determine its role in adhesion phenotype. In order to achieve this, our collaborator Martin Humphries, from the University of the Manchester, carried out cell biology experiments using our designed CDK1 mutant – CDK1\_2A.

Initially, we wanted to confirm the presence of CDK1 in cell adhesions. The Humphries' group transfected U2OS cells with GFP-CDK1 and stained the cells for the adhesion marker paxillin. **FIGURE 6.35A and B** show that CDK1 is distributed ubiquitously across the cell rather than uniquely localised to adhesions. However, it also shows that CDK1 is found at adhesions as it clusters around paxillin.

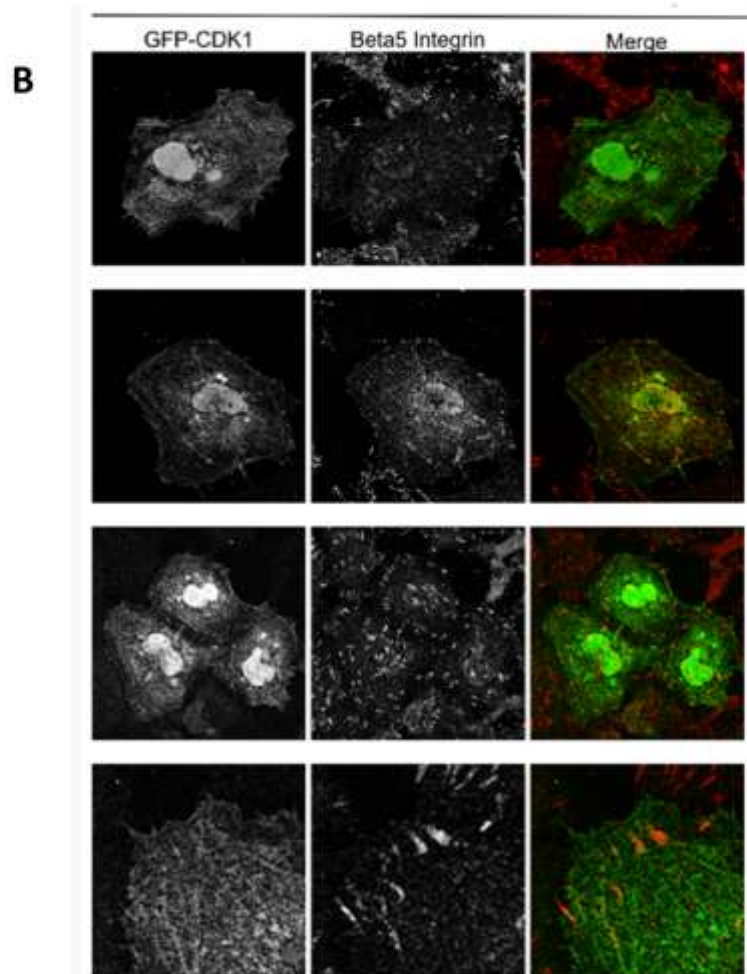
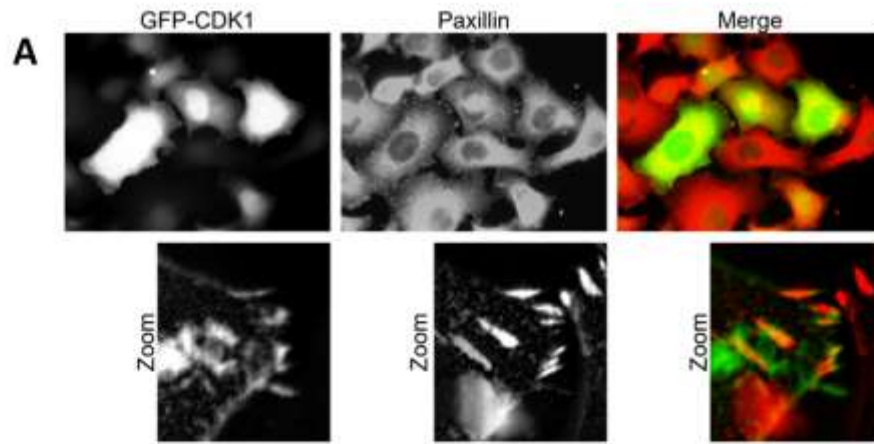


**FIGURE 6.35: LOCALISATION OF GFP-CDK1 IN THE CELL**

(A-B) Immunofluorescence images of U2OS cells plated on glass coverslips for 24 hours. (A) Cells co-expressed GFP-CDK1 and stained for paxillin. (B) Cells co-expressed GFP-CDK1 and stained for Beta5 integrin.

### 6.2.18 Characterisation of CDK1\_2A mutant in mammalian cells

Following this, to explore the importance of the talin:CDK1 interaction within the cell the Humphries' lab used a series of CDK1 and talin constructs: full-length HA-tagged CDK1; HA-tagged CDK1\_2A (our biochemically validated CDK1 mutant); GFP-talin1 and GFP-talin1 $\Delta$ R8 (a talin mutant that would perturb interaction).

To determine if the CDK1 and talin mutants perturbed the talin:CDK1 interaction, different combinations of CDK1 and talin constructs were transfected into U2OS cells. GFP-trap pulldown assays were performed, as shown in **FIGURE 6.36A**. These data show that the CDK1\_2A mutant reduced the interaction between talin and CDK1, corroborating my biochemical findings. Furthermore, the talin mutant GFP-talin $\Delta$ R8 also disrupted binding between talin and CDK1 indicating that the talin R8 domain is the main CDK1 binding site.

After confirming the existence of an *in vivo* interaction between CDK1 and talin, we set out to determine if the CDK1\_2A mutant affected adhesion size. **FIGURE 6.36B** shows CDK1 *knock-down* cells rescued with HA-CDK1 and the HA-CDK1\_2A. In cells with the HA-CDK1\_2A mutant the adhesion area was significantly reduced (**FIGURE 6.36C**) compared to the HA-CDK1 *WT*. This suggests that the talin:CDK1 interaction is involved in adhesion maturation and stability.

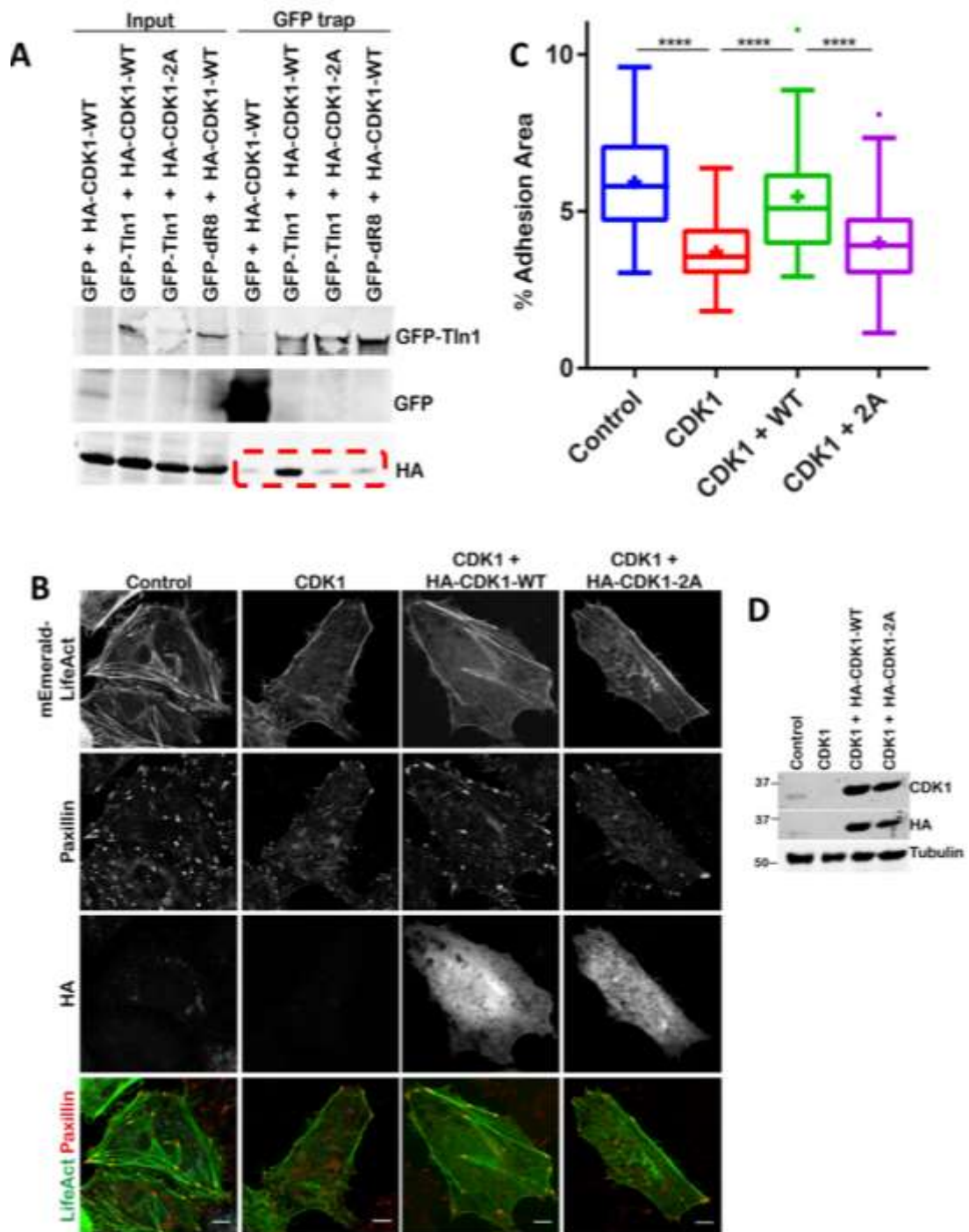


**FIGURE 6.36: CDK1\_2A MUTANT PREVENTS TALIN BINDING**

(A) Protein extracts of U2OS cells co-expressing GFP-talin1, GFP talin1 $\Delta$ R8 (or GFP control) and HA-tagged CDK1 or CDK1\_2A were subjected to GFP-pulldowns and analysed using western blots with an anti-HA antibody and an anti-GFP antibody. Due to the large amount of GFP-control, the signal was expanded to nearby lane. (B) Immunofluorescence images of U2OS cells transfected with LifeAct showing control with scrambled siRNA, CDK1-knock-down cells, and CDK1-knock-down cells expressing either HA-CDK1 or HA-CDK1\_2A. Cells were then stained against HA, as well as paxillin. (C) Quantification of adhesion area per cell after CDK1-knock-down and rescue with HA-tagged CDK1 and CDK1\_2A. (D) Western blot showing knock-down of endogenous CDK1 and expression of HA-tagged CDK1 and CDK1\_2A.

## 6.3 Conclusion

### 6.3.1 What is targeting CDK1 to adhesions?

Through the use of biochemical and biophysical techniques we have discovered an interaction between CDK1 and the talin R8 domain, and a CDK1 mutant (CDK1\_2A) capable of disrupting binding between the two proteins. Furthermore, the talin:CDK1 interaction has been confirmed *in vivo* and we show that the disruption of this interaction leads to a decrease in adhesion area in cells. Additionally, in U2OS cells, CDK1 localises to adhesions suggesting that the talin:CDK1 interaction is adhesion-specific. A question that still remains unanswered is: what is the mechanism that drives CDK1 to the adhesion at certain points in the cell cycle?

One hypothesis could be that talin actively recruits CDK1 from cytosol to the adhesion site. This scenario is, however, unlikely and, as discussed in **section 5.3.3.1**, talin can form homodimer complexes which are able to adopt a compact auto inhibited conformation in the cytosol (Goult, Xu, *et al.*, 2013). This auto-inhibited form would prevent talin from binding to CDK1 as the R8 domain is hidden. Additionally, the binding affinity between talin:CDK1 is in the micro molar range, meaning that a high concentration of either talin or CDK1 is needed to facilitate an interaction. It is unlikely that such high concentration is present in the cytosol, leading to the conclusion that such interaction is only occurs at adhesion sites.

In cells (**section 6.2.17**), CDK1 is well dispersed across the cytosol. It is also possible that CDK1 could be found in the vicinity of adhesions through non-directed signalling.

Alternatively, cyclins could play a large role in the regulation of CDK1 localisation to adhesions. The *in vitro* kinase assay demonstrated that the phosphorylation of talin was potentially cyclin specific (phosphorylation mainly occurred by the CDK1-cyclinA2 complex). This has also been described in the literature, with adhesion area growth occurring in the G<sub>1</sub> and predominantly S phase of the cell cycle through the association of CDK1 to cyclinA2. Adhesion area then dramatically decreases in G<sub>2</sub>, just before the cell enters mitosis. Adhesion size reduction correlates with elevated levels of CDK1 in complex with cyclinB1 (Jones *et al.*, 2018). The binding of cyclinA2 to CDK1 could increase the selectivity for CDK1 to adhesion substrates, drawing it to the adhesion area. When cyclinA2 activity is reduced the selectivity for adhesion targeting could be diminished and CDK1 is no longer recruited to adhesions.

Another potential way that CDK1 could be targeted to adhesions is via MTs. MT networks are constantly changing during the course of the cell cycle and, as discussed in **Chapter 4**, MTs are linked to FAs through the binding of KANK to talin. There is no evidence of the phosphorylation of

tubulin phosphorylated by CDK1 (Fourest-Lieuvin, 2005); however, a number of MT-binding proteins are phosphorylated by CDK1. This could be a possible mechanism to further explore in the future.

### 6.3.2 Why is talin phosphorylated by CDK1?

The *in vitro* kinase assays in **section 6.2.12**, revealed that talin R7R8 is phosphorylated by CDK1-cyclinA2. Further analysis using phosphoproteomics also identified two talin isoform-specific sites: talin1 Ser1589 and talin2 Ser1489. Phosphorylation of adhesion proteins by CDK1 has been found to be important in regulating cell-matrix adhesion complexes (Jones *et al.*, 2018) and, for this reason, understanding the functional role of the talin phosphorylation sites would contribute to the general knowledge on adhesion regulation by CDK1 through the cell cycle.

#### 6.3.2.1 Talin1

The talin 1 phosphorylation site is located in the R7 domain near to the flexible linker that joins the R7 and R8 talin domains. The talin1 Ser1589 is in an 'optimal consensus CDK1 phosphorylation sequence' (Ser/Thr-Pro-X-X-Arg/Lys) (Suzuki *et al.*, 2015). As described in the results, the sequence 'SPEGR' around Ser1589 is highly conserved across species suggesting that the sequence is of functional importance. In the results a phosphomimetic S1589D was used to determine if phosphorylation had any effect on the binding of CDK1 to talin. We hypothesised that the added phosphate group would destroy the hydrogen bonds in the linker region between R7 and R8 domains, affecting the binding of LD ligands on R8. However, we observed no difference in binding affinity of the CDK1 peptide to the phosphomimetic talin R7R8 compared to talin1 R7R8 *WT*, there was no difference in binding affinity with DLC1 either.

Interestingly, a four-fold difference in binding affinity was noted with the KANK1 30-60 peptide and Talin1 R7R8 S1589D compared to KANK1 30-60 and talin1 R7R8 *WT*. The KANK peptide still bound to talin S1589D but at a reduced affinity, which could affect the linkage between FA and the CMSC (see **section 4.3.4**). Future experiments could add the phosphomimetic mutant and a non-phosphorylatable mutant into cells to determine if there is a phenotype of talin phosphorylation. However, from our current data we think it would be unlikely that phosphorylation of this site is used as a mechanism to reduce or increase binding affinity for CDK1.

### 6.3.2.2 Talin2

The talin2 phosphorylation site is located on the R8 domain of talin at position Ser1489, the position is well conserved across talin 2 isoforms, which suggests a functional importance for the region. Unlike with the talin 1 phosphorylation site (Ser1589), the talin2 phosphorylation site Ser1489, does not fit the canonical CDK1 sequence. Instead, it fits the Ser/Thr-Pro sequence also known to be phosphorylated by CDK1.

This region on talin R8 is also conserved in talin1, not as a phosphorylation site but instead as a O-glycosylation site. O-glycosylation has been reported on talin1 Thr1487 (Hagmann, Grob and Burger, 1992). O-Glycosylation is a common PTM that attaches a sugar molecule to a Thr or Ser residue resulting in structural and functional changes of the protein. Talin1 has two reported O-glycosylation sites, one in R8 and one in R10, neither of which are conserved in talin2 (reviewed: Gough & Goult, 2018). Thus understanding the function of the Ser1489 phosphorylation site in talin2 could uncover a potential functional difference between the talin isoforms.

Unlike with the talin1 phosphorylation site, the talin2 site, Ser1489, is located on the same domain as the CDK1 binding site, at the top of helix 32 (see **FIGURE 6.34**). This is situated near the binding sites of all the R8 LD-motifs (RIAM, DLC1 and CDK1) and talin actin binding site 2 (ABS2). Could the addition of a phosphate group have an effect on the binding of CDK1 and of actin? **FIGURE 6.37** models talin2 R7R8 with an electrostatic surface. The surface of talin that binds to actin is negatively charged (shown in blue on **FIGURE 6.37**), mutations of this area (K1500E, K1522E and R1510E) have been found to disrupt binding of talin and actin by addition of a negatively charged residue (P Atherton *et al.*, 2015). The phosphate group addition to Ser1489 through phosphorylation would cause a negatively charged surface to be present on talin R8 and this could be enough to cause disruption between talin and actin. This dissociation between actin and talin would result in loss of force across the adhesion, it is unclear why this would be needed in talin2 and not in talin1. Further investigation to understand if this mutation does affect actin binding would need to be carried out. Future analysis and characterisation of this site could be an important step to gain a better understanding of role of talin2 at adhesions. A phosphomimetic and a non-phosphorylatable mutant of Ser1489 to search for a phenotype in cells could prove useful. Furthermore, it would be important to assess at which stages of the cell cycle phosphorylation occurs, and determine if it occurs in S-phase, thus aiding adhesion growth as it has been described for other adhesion proteins phosphorylated by CDK1 (Jones *et al.*, 2018). Biochemical characterisation of a phosphomimetic mutation would also answer binding to actin and LD motifs to talin R8 is affected.



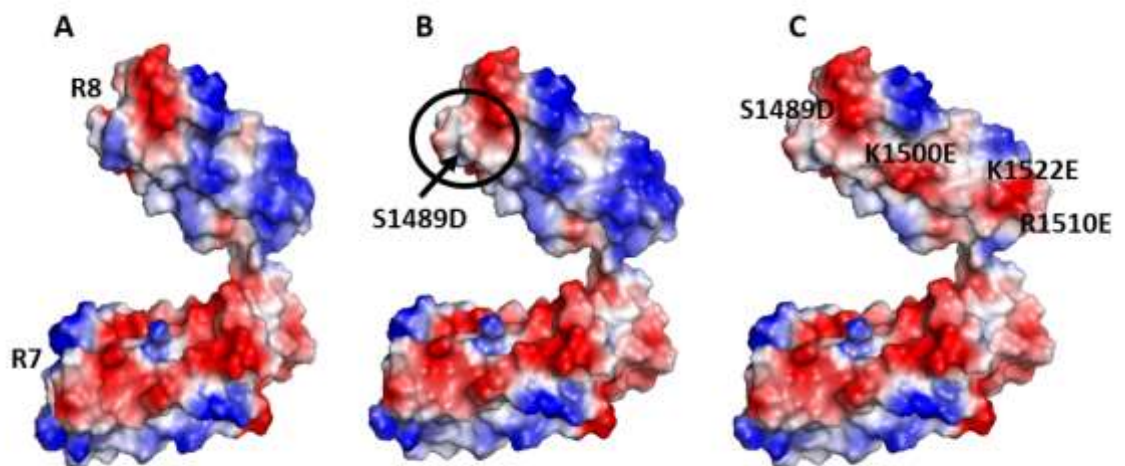


**FIGURE 6.37: TALIN2 PHOSHO MUTATION MAY PERTURB ACTIN BINDING**

(A-C) Structural prediction of talin2 R7R8 Phyre2 (Kelley and Sternberg, 2009)) modelled in PyMOL with electrostatic surfaces indicating the surface charge on the protein. Blue indicates positively charged and red indicated negatively charged. **B** modelled phosphomimetic S1489D, **C** known actin binding mutants K1500E, K1522E and R1510E.

#### 6.4 Does CKS1 binding talin regulate the talin:CDK1 interaction?

A CDK1 structure (PDB ID: 4YC6) shows CDK1 bound to a cyclin kinase substrate 1 (CKS1). CKS proteins are small cyclin-dependent kinase proteins frequently found overexpressed in cancers, especially breast cancer (Liberal *et al.*, 2011). However, a mechanistic link between overexpression of CKS proteins and oncogenesis is still not known. An increase in CKS proteins (CKS1 and CKS2) leads to an 'override' of the S-phase checkpoint. The S-phase checkpoint occurs between the S-phase and G<sub>2</sub>-phase and it controls DNA replication, preventing replication if the cell is under stress (Liberal *et al.*, 2011). Binding of CKS proteins to CDK2 overrides this checkpoint and allows the cells to continue to replicate DNA even under conditions of replicative stress.

Interestingly, CKS1 and CKS2 bind to CDK1 in the same place as talin R8 (shown in **FIGURE 6.38**). This overlap in binding area could provide a mechanism that determines when CDK1 binds to talin and when it is targeted to adhesions. CDK1 binds to talin via an LD motif through a predicted salt bridge between the CDK1's Asp211 and talin Lys1544 (as shown in **FIGURE 6.38B**). From structural analysis of the CKS1 and CDK1 structure it is apparent that the CDK1 Asp211 residue is involved in the interaction with CKS1 through the same mechanism, whereby there is the formation of a salt bridge with the CKS1 His21 residue (as shown in **FIGURE 6.38A**). This similar binding mechanism

means that the designed CDK1\_2A mutant could also perturb the CDK1:CKS1 interaction. To verify this, further experiments would have to be carried.

The binding of cyclins to CDKs regulates the latter's ability to phosphorylate substrates; in addition to cyclins, CKS can also influence the selection of substrates. Biochemical studies in *Xenopus* suggest that CKS proteins enhance the phosphorylation of selected CDK1 substrates in mitosis (Patra *et al.*, 1999). From this knowledge, we could suggest that talin might also have a similar effect when bound to CDK1 and help to enhance phosphorylation of selected substrates (potentially at adhesions). Furthermore, it would be interesting to explore if there is a connection between CKSs and talin binding to CDK1, to determine if CKS1/CKS2 acts as a regulatory mechanism that prevents talin binding to CDK1, until the correct time.

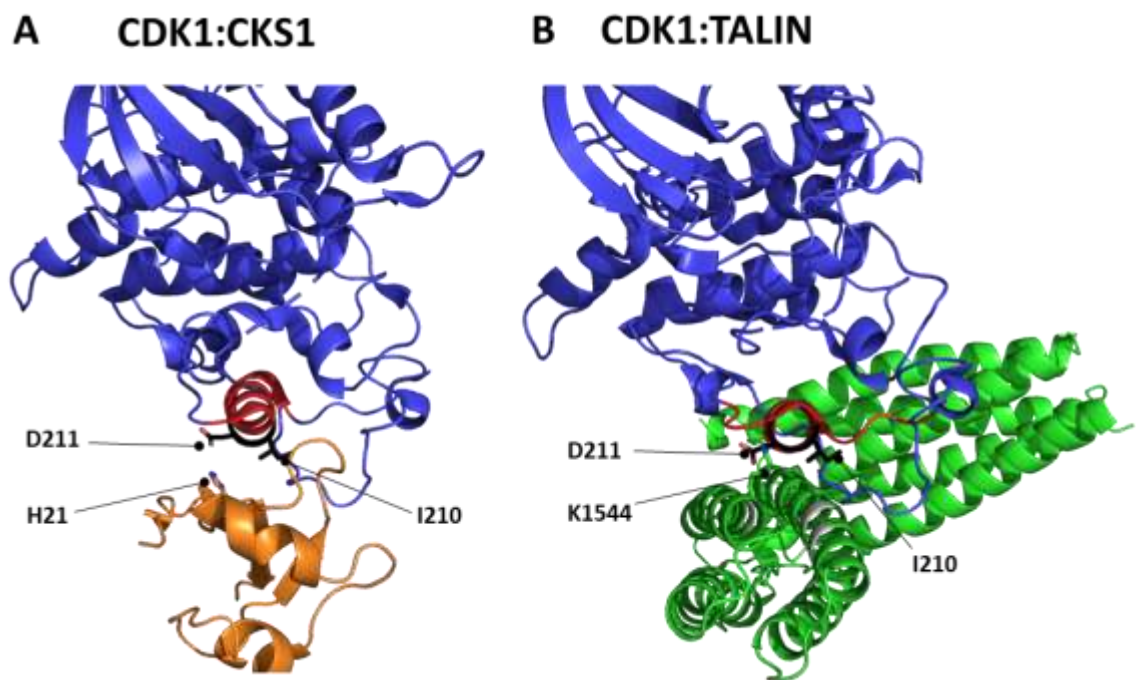


**FIGURE 6.38: TALIN AND CKS1 BINDING SITES ON CDK1**

(A) structure of CDK1 (blue) and CKS1 (orange) (PDB ID: 4YC6). (B) Predicted structure of CDK1 (blue) and talin R7R8 (green). Both A and B highlight the Ile Asp residues (black) on CDK1 required for talin binding, (A) shows a His residue on CKS1 that could form electrostatic interaction with CDK1 and (B) shows Lys residue on talin that forms electrostatic interaction with CDK1.

### 6.4.1 Could other members of the CDK family bind to talin?

As previously mentioned, humans have 20 different CDK genes that all encode for a different member of the CDK family (Egelhofer *et al.*, 2008). Intriguingly, our talin proteomics data only detected CDK1 as a binding partner for talin. What makes CDK1 different to the other CDKs, and does talin have the potential to bind to any of the other members?

To investigate this, the 20 human CDK isoforms were aligned using Clustal Omega, which immediately highlighted that some members of the CDK family are more similar in sequence than others. For example, CDK1 and CDK2 have very similar sequences sharing 65% sequence identity **FIGURE 6.39** shows the alignment of the LD-TBM across all the CDK family members. It appears that the sequence is well conserved in CDK1, CDK2 and CDK3 and that a similar sequence is also found in CDK11a and CDK11b. Although CDK4 and CDK6 (highlighted in red) are not deemed essential for cell cycle progression (Bockstaele *et al.*, 2006), both have become significant targets for breast cancer drug therapies (Lamb *et al.*, 2013).

**A**

```

CDK1_HUMAN STPVDIWSIGTIFAELAT-KKPLFHGDS-----EIDQLFRIFRALGTPNNEVWPEV 231
CDK2_HUMAN STAVDIWSLGCIFAEMVT-RRALFPGDS-----EIDQLFRIFRTLGTPEVWVPGV 230
CDK3_HUMAN TTAVDIWSIGCIFAEMVT-RKALFPGDS-----EIDQLFRIFRMLGTPSEDWPGV 230
CDK4_HUMAN ATPVDMWSVGCIFAEMFR-RKPLFCGNS-----EADQLGKIFDLIGLPPEDDWPRD 241
CDK5_HUMAN STSIDMWSAGCIFAELANAGRPLFPGND-----VDDQLKRIFRLLGTPTEEQWPSM 230
CDK6_HUMAN ATPVDLWSVGCIFAEMFR-RKPLFRGSS-----DVDQLGKILDVIGLPGGEDWPRD 246
CDK7_HUMAN GVGVDMWAVGCILAELL-LRVPFLPGDS-----DLQLTRIFETLGTPTTEEQWPD 240
CDK8_HUMAN TKAIIDIWAIGCIFAELLT-SEPIFHCQRQEDIKTSNPFHHDQLDRIFNVMGFADKDWEDI 270
CDK9_HUMAN GPPIDLWGAGCIMAEMWT-RSPIMQGNT-----EQHQLALISQLCGSITPEVWPNV 256
CDK10_HUMAN TTSIDMWAVGCILAELLA-HRPLLPGTS-----EIHQIDLIVQLLGTPESENIWPGF 266
CD11B_HUMAN STAVDMWSVGCIFGELLT-QKPLFPGKS-----EIDQINKVFKDLGTPSEKIWPGY 665
CD11A_HUMAN STAVDMWSVGCIFGELLT-QKPLFPGNS-----EIDQINKVFKELGTPSEKIWPGY 653
CDK12_HUMAN TPAIDVWSCGCILGELFT-KKPIFQANL-----ELAQLELISRLCGSPCAVWPDV 963
CDK13_HUMAN TPAIDVWSCGCILGELFT-KKPIFQANQ-----ELAQLELISRLCGSPCAVWPDV 941
CDK14_HUMAN STCLDMWGVGCVFVEMIQ-GVAAFPGMKD-----IQDQLERIFLVLGTPNEDTWPGV 360
CDK15_HUMAN SSELDIWGAGCIFIEMFQ-GQPLFPGVSN-----ILEQLEKIWEVLGVPTEDTWPGV 328
CDK16_HUMAN STQIDMWGVGCVFFEMAS-GRPLFPGST-----VEEQLHIFRILGTPTEETWPGI 389
CDK17_HUMAN STQIDMWGVGCVFFEMAS-GRPLFPGST-----VEDELHLIFRLLGTPSQETWPGI 416
CDK18_HUMAN STPIDMWGVGCVIHYEMAT-GRPLFPGST-----VKEELHLIFRLLGTPTEETWPGV 368
CDK19_HUMAN TKAIIDIWAIGCIFAELLT-SEPIFHCQRQEDIKTSNPFHHDQLDRIFNVMGFADKDWEDI 270
CDK20_HUMAN DQGVDLWSVGCIMGELLN-GSPLFPGKN-----DIEQLCYVLRILGTPNPQVWPEL 231

```

:\*: \* \* \* \* : : : \* \*

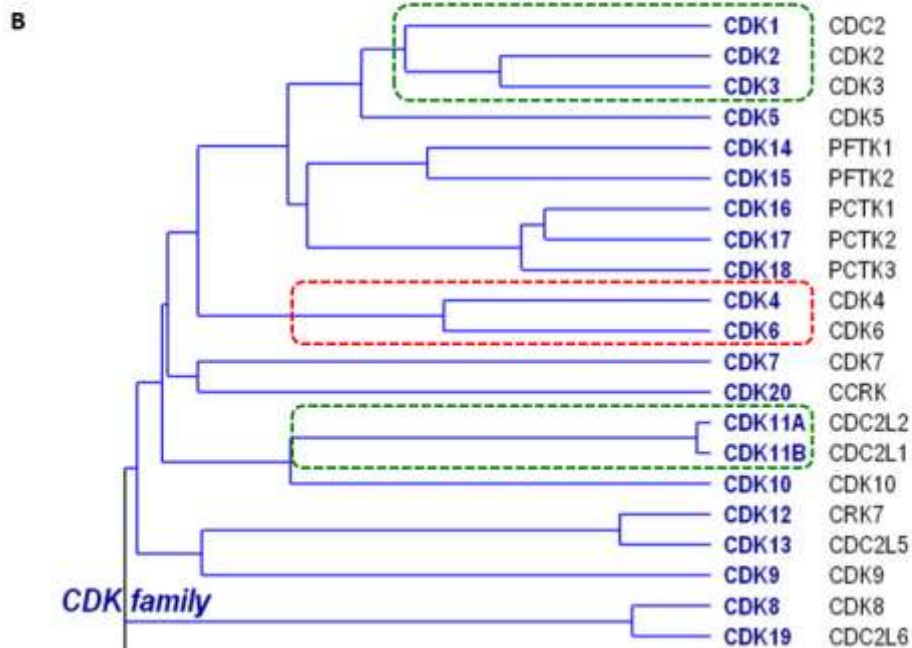


**FIGURE 6.39 SEQUENCE ALIGNMENT OF HUMAN CDK ISOFORMS**

The region of sequence containing the CDK1 206-223 peptide is shown and the CDK isoforms that contain an LD-motif are highlighted in green. (B) CDK family proteins with correct nomenclature the sequences have been aligned and analysed using Cluslal2 using the nearest neighbour method (Malumbres *et al.*, 2009). Human CDK1(P06493), CDK2(P24941), CDK3(Q00526), CDK4(P11802), CDK5(Q00535), CDK6(Q00534), CDK7(P50613), CDK8(P49336), CDK9(P50750), CDK10(Q15131), CDK11A (P21127), CDK11B(Q9UQ88), CDK12(Q9NYV4), CDK13(Q14004), CDK14(O94921), CDK15(Q96Q40), CDK16(Q00536), CDK17(Q00537), CDK18(Q07002), CDK19 (Q9BWU1), CDK20 (Q8IZL9) sequences aligned in Cluster Omega.

The conserved LD talin binding motif sequence found in CDK1 is absent in both CDK4 and CDK6, instead of an Ile residue at the start of the motif, they contain an Ala or Val residue, respectively. Ala and Val residues have shorter side chains than Ile that has not been identified in any LD-motif to date.

Closer inspection of the sequence alignment of CDK1, CDK2, CDK3, CDK11a and CDK11b revealed that the 206-223 region is well conserved (shown in **FIGURE 6.40**) and the 'Glu, Ile, Asp, Gln' residues can be found in all isoforms.

```

CDK1_HUMAN  VTLWYRSPEVLLGSARYSTPVDIWSIGTIFAELATKKPLFHGDSSEIDQLFRIFRALGTPN 224
CDK2_HUMAN  VTLWYRAPEILLGCKYYSTAVDIWSLGCIFAEMVTRRALFPGDSEIDQLFRIFRTLGTPD 223
CDK3_HUMAN  VTLWYRAPEILLGSKFYTTAVDIWSIGCIFAEMVTRKALFPGDSEIDQLFRIFRMLGTPS 223
CD11B_HUMAN VTLWYRAPELLLGAKEYSTAVDMWSVGCIFGELLTQKPLFPGKSEIDQINKVFKDLGTPS 658
CD11A_HUMAN VTQWYRAPELLLGAKEYSTAVDMWSVGCIFGELLTQKPLFPGNSEIDQINKVFKELGTPS 646
**  ***:***:***.  *: * **:*:* * *,*: *:: ** *,*****: :*: ****.

```

**FIGURE 6.40: SEQUENCE ALIGNMENT OF LD-TBM ACROSS THE CDK ISOFORMS**

Human CDK1 (P06493), CDK2 (P24941), CDK3 (Q00526), CDK11a (Q9UQ88) and CDK11b (P21127) sequences were aligned using Cluster Omega. (\*) indicates fully conserved residue, (:) indicates similar property residue. Green highlights the CDK1 peptide 206-223.

CDK11 is different to the other CDK proteins as the CDK11 gene is duplicated in humans giving rise to different but highly conserved isoforms: CDC2L1 (CDK11a) and CDC2L2 (CDK11b) (Zhou *et al.*, 2016). CDK11a and CDK11b have 98% sequence identity and while their role within the cell is not fully understood, it is thought that CDK11 kinases are essential for cell viability and early embryonic development (Li *et al.*, 2004). **Section 6.1.2** discussed that the CDK family was split into transcriptional CDKs and cell cycle CDKs unlike CDK2,3,4 and 6, CDK11 is a transcriptional CDK. CDK11 null mice result in early embryonic lethality due to apoptosis of blastocyst cells between days 3-4; cells from these embryos displayed proliferative defects, mitotic arrest and apoptosis (T. Li *et al.*, 2004). The CDK11 sequence between 641-655 is similar to that of CDK1 206-223, the only major difference being that instead of CDK1's Phe214, CDK11 has Asn648, which is not hydrophobic and, therefore, unlikely to bury itself into the groove of talin helices 32 and 33 in the same way as the Phe residue could. This could translate into a lower affinity to talin, compared to CDK1 or CDK2. Furthermore, when looking at the CDK11a structure (Phyre2 (Kelley *et al.*, 2015)) shown in **FIGURE 6.41**, the putative talin binding region (highlighted in red) does not have a predicted secondary structure like CDK1, CDK2 and CDK3. This, again suggests that there is a low possibility that CDK11 could bind to talin.

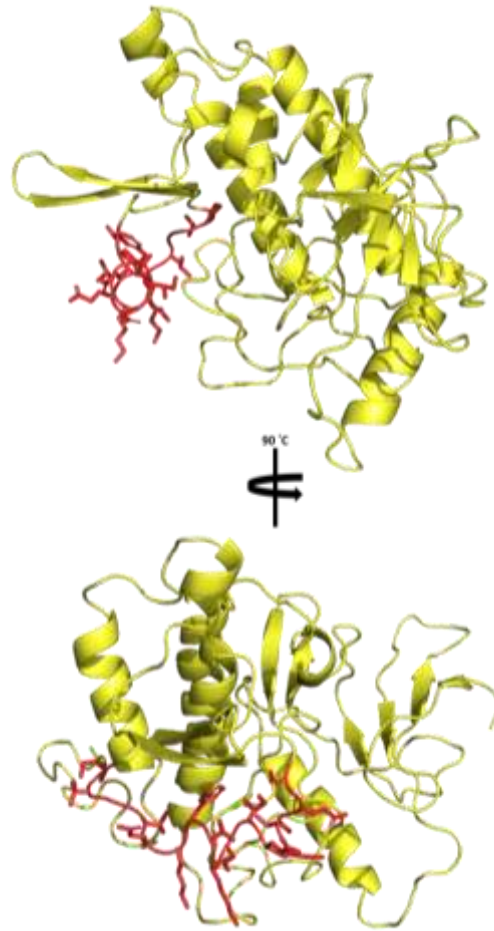


**FIGURE 6.41 STRUCTURAL OF HUMAN CDK11A**

Structure CDK11a (Phyre2 prediction) modelled in PyMOL with the CDK1:talín binding region highlighted on the structure in red.

It is, however likely that CDK2 and CDK3 could bind to talín based on the sequence of their LD-TBM.

**FIGURE 6.42** shows the alignment for the predicted structures of the motifs for CDK1, CDK2 and CDK3 (PDB ID: 4YC6, 4EK3, Phyre2 prediction (Kelley *et al.*, 2015) , respectively) using PyMOL. The LD-TBM region is highlighted by a black box and is predicted to be helical on all the structures. It would be interesting to identify if there is an interaction between talín and CDK2/CDK3 and determine if this interaction only occurs at specific points in the cell cycle. Furthermore, if there was an interaction between talín and the CDK2/CDK3 it would be interesting to determine if they can phosphorylate talín.



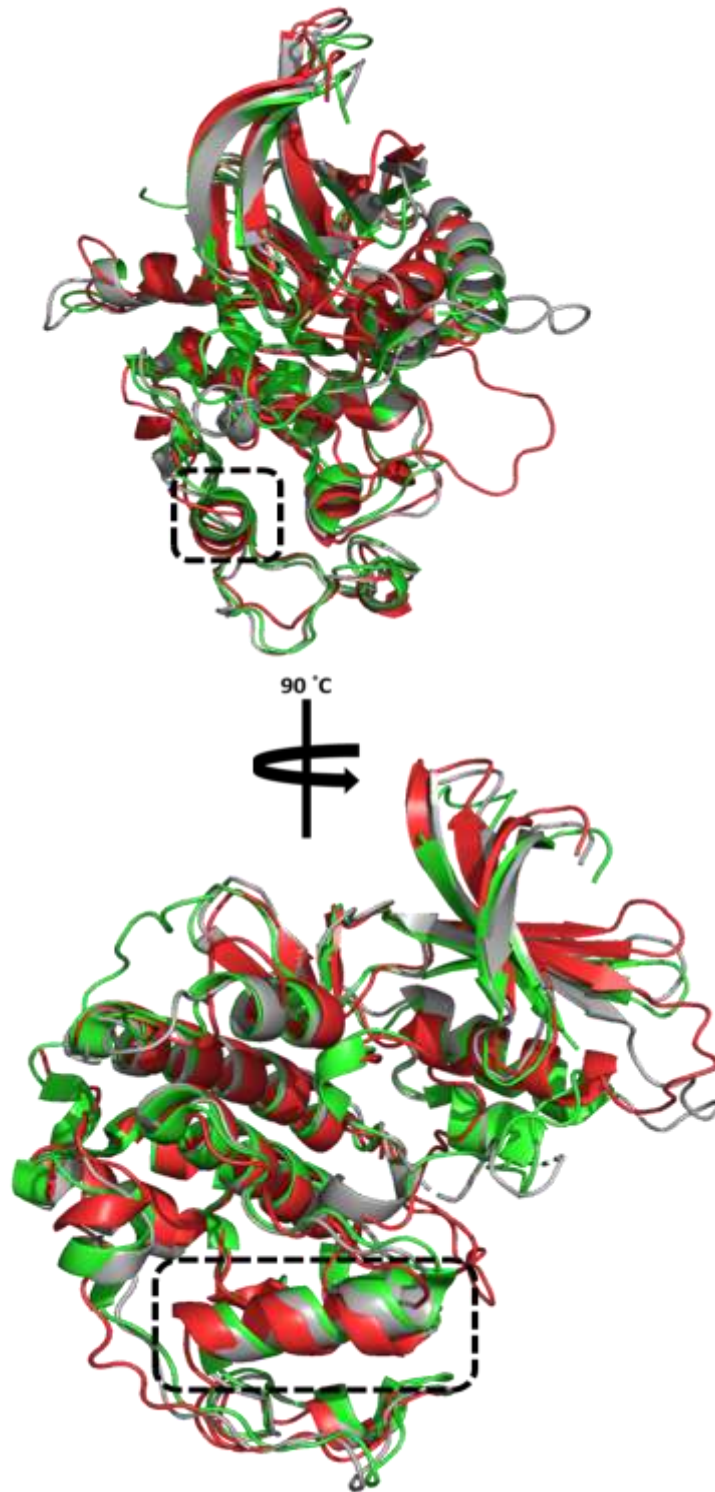


**FIGURE 6.42 STRUCTURAL ALIGNMENT OF HUMAN CDK1 AND CDK2 AND CDK3**

Structures CDK1 (PDB ID:4YC6), CDK2 (PDB ID: 4EK3), CDK3 (Phyre2 prediction) modelled in PyMOL and aligned. CDK1 (grey), CDK2 (green) and CDK3 (red) aligned closely together. With the CDK1:talin binding region highlighted on the structure with a black dashed box.

# Chapter 7. Conclusions

---



## 7.1 Summary

This thesis has focussed on the adapter protein talin, a crucial player in integrin-matrix adhesions. The investigation set out to identify novel binding partners for talin rod domains and explore the mechanism of LD-motifs binding to talin; with the view that identifying new talin interactors would lead to a deeper understanding of integrin-matrix adhesions.

The first novel binding partner we identified to bind talin, was the adapter protein KANK. Through biochemical characterisation it was determined that talin R7 could bind to the KANK KN domain via an LD-motif. Structural analysis of the interaction allowed a series of talin and KANK mutants to be designed that could perturb the interaction. Having designed and biochemically characterised both a successful KANK mutant (KANK\_4A) and a talin mutant (G1404L and W1630A) to perturb the talin:KANK interaction it allowed us to understand the significance the talin:KANK interaction in conjunction with the rest of the cell. These studies revealed that the talin:KANK interaction was the key link to associating focal adhesions (FAs) and the cortical microtubule stabilising complex (CMSC) and that abrogation of the interaction resulted in uncontrolled MT growth and loss of association of the MT complex with FAs.

Identifying this interaction has provided an answer to the long standing questions surrounding the mechanism that targeted microtubules to grow towards focal adhesions and regulate adhesion turnover.

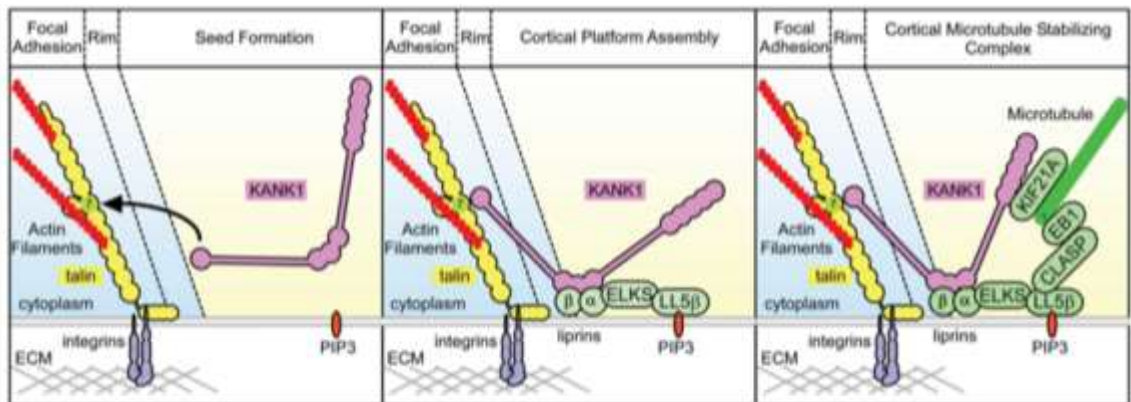


**FIGURE 7.1: THE TALIN KANK INTERACTION LINKS FA WITH CMSC**

Model of how talin1 directs the assembly of the cortical microtubule stabilizing complex in three stages. 1) KANK1 KN domain binds to talin R7, 2) KANK1 coiled-coil domain binds to liprin  $\beta$ 1, 3) this allows LL5 $\beta$  to bind and the final CMSC proteins to assemble including ELKS, CLASP and KIF21A.

Furthermore, the talin:KANK interaction revealed KANK to be a novel LD-motif that could bind to talin and gave new insight into the binding of LD-motifs to five-helix bundles. The structure of talin rod domains are highly conserved across evolution, providing compelling evidence that every domain within talin has an important functional role. Coupling this to the knowledge that LD-motifs can bind to both four and five-helix bundles it was hypothesised that every talin rod domain has the potential to bind an LD motif(s).

Literature described previous attempts at sequence searching for LD motifs to be unsuccessful due to the canonical LD motif sequence (LDxLLxxL) identifying many false positives results. To combat this problem, I compiled all the knowledge of known talin binding LD-motifs and designed a novel LD talin binding motif (LD-TBM) that could be used as a query search to interrogate a vast talin1 proteomics dataset. This sequence search was coupled with a structural evaluation of potential binding partners to reduce the chance of false positive hits being identified. The LD-TBM was successful at identifying potential talin binding partners and through the design of a novel pipeline the potential binding proteins were rapidly screened against talin to determine if binding occurred. From this initial screening the protein CDK1 was taken forward for biochemical characterisation.

Using a similar biochemical approach that was implemented to characterise the talin:KANK interaction, CDK1 was identified to bind to talin R8. NMR revealed the binding surface on which CDK1 binds to the talin R8, was the same site as other LD-motifs, DLC1 and RIAM. Structural analysis of the talin:CDK1 interaction allowed for the design and characterisation of a successful CDK1 (CDK1\_2A) mutant to perturb the talin:CDK1 interaction. This mutation was used to understand the significance of the interaction in conjunction with the rest of the cell and it revealed that disruption of the interaction reduced adhesion area in the cell.

Furthermore, biochemical data combined with phosphoproteomics shows that the CDK1-cyclinA complex phosphorylates talin1 and talin2 isoforms at two unique sites (Ser1589 in talin1 and Ser1489 in talin2). Interestingly, in talin2 this novel phosphorylation site is in the talin actin-binding site (ABS2). We postulate that this could be a mechanism to regulate the coupling/uncoupling of actin to talin. This interaction between talin and CDK1 gives an insight into how adhesions and the cell cycle are entwined and poses many questions regarding how adhesion formation and disassembly regulates or occurs within the cell cycle.

## 7.2 Potential Limitations

The cellular work presented in this thesis, studying both the talin:KANK and talin:CDK1 interactions has been carried out in a two dimensional (2D) environment, which allows for unrestricted movement of cells on a flat surface such as glass or plastic. The study of these mechanisms in 2D has provided us with the understanding of the mechanisms involved in linking FAs to the CMSC and linking adhesion regulation to the cell cycle. However, it is still not yet fully understood how migration in 2D relates to cellular migration in 3D. In 2D substrates the surface is typically homogenous so cells only have to adhere and generate force for a single environment however, in 3D the environment has a different topography, rigidity and uniformity. This requires the cell to recognize and respond to the different surrounding environments in order to migrate and proliferate. It is therefore unsurprising that the cell has adopted a number of different ways to migrate through a 3D environment. It would be intriguing to study the talin:KANK interaction in a 3D environment and to determine if perturbing the interaction between talin and KANK affects cells in the same way as a 2D environment. To study cells in a 3D environment a 3D matrix hydrogel or tissue environment could be used, this provides a different topography, rigidity and uniformity to the surface mimicking that of a 3D environment (Tibbitt and Anseth, 2009).

Large strides are being made in developing techniques to visualise and image complex 3D environments such as the development of high resolution light sheet microscopes (Gao *et al.*, 2012). However, there are many complexities that surround both visualising and quantifying cells in 3D environments and so there is still a necessity to study adhesion complexes in 2D.

## 7.3 Future Directions

The work presented here is some of the first evidence in the field that defines the link between FAs and MT assemblies. Furthermore, this is the first confirmation of an interaction between talin and CDK1 and it gives further evidence of adhesions being regulated by CDK1 in the cell cycle. These findings give great basis for future work and exploration for both the KANK and CDK1 interactions with talin.

An exciting avenue of exploration for future research will be to understand further the relationship between the cell cycle and regulation of adhesion assembly. Furthermore, it will be interesting to explore if the mechanism involving the cell cycle and integrin-matrix adhesions transposes across to cell-cell adhesions. The link between cell-matrix adhesions and cell-cell adhesions is often

thought of as spatially and functionally separate. However, both cell-cell and cell-matrix adhesions are intrinsically linked to each other through the actin cytoskeleton and they share many common signalling proteins as well as downstream effectors (Weber, Bjerke and DeSimone, 2011). It is thought that these two adhesion systems can form an integrated network that allows communication through biochemical signalling pathways and changes in the actin cytoskeleton (Weber, Bjerke and DeSimone, 2011). The CDK1-cyclinA complex has been identified to phosphorylate actin associated proteins such as FMNL2 within cell-matrix FAs (Jones *et al.*, 2018). It would be interesting to identify if any actin binding proteins involved in cell-cell junctions were too phosphorylated by CDK1. Then to explore if phosphorylation of these proteins lead to adhesion growth in S phase of the cell cycle. If this were the case, then this would reveal further evidence into cross-talk between cell matrix adhesions and cell-cell junctions and provide a bigger picture on how the cell cycle regulates adhesions.

Additionally, it would be interesting to look for cross-talk between MTs and CDK1 at adhesions and further explore the idea that CDK1 may be transported to adhesions via MTs which could suggest that CMSC regulation is also linked to the cell cycle. It would also be intriguing to examine at which points in the cell cycle FAs and CMSC complexes are most abundant, and to identify if this links to the finding that FA abundance largely increase in S phase.

# Chapter 8. References

---

Akhmanova, A. and Steinmetz, M. O. (2008) *Tracking the ends: A dynamic protein network controls the fate of microtubule tips*, *Nature Reviews Molecular Cell Biology*. Nature Publishing Group. doi: 10.1038/nrm2369.

Alam, T. *et al.* (2014) 'How to find a leucine in a haystack? Structure, ligand recognition and regulation of leucine-aspartic acid (LD) motifs.', *The Biochemical journal*. Portland Press Limited, 460(3), pp. 317–29. doi: 10.1042/BJ20140298.

Anderson, L. R., Owens, T. W. and Naylor, M. J. (2014) 'Structural and mechanical functions of integrins', *Biophysical Reviews*. doi: 10.1007/s12551-013-0124-0.

Anthis, N. J. *et al.* (2009) 'The structure of an integrin/talin complex reveals the basis of inside-out signal transduction.', *The EMBO journal*. European Molecular Biology Organization, 28(22), pp. 3623–32. doi: 10.1038/emboj.2009.287.

Ardito, F. *et al.* (2017) 'The crucial role of protein phosphorylation in cell signaling and its use as targeted therapy (Review).', *International journal of molecular medicine*. Spandidos Publications, 40(2), pp. 271–280. doi: 10.3892/ijmm.2017.3036.

Astro, V. and De Curtis, I. (2015) 'Plasma membrane-associated platforms: Dynamic scaffolds that organize membrane-associated events', *Science Signaling*. doi: 10.1126/scisignal.aaa3312.

Atherton, P. *et al.* (2015) 'Vinculin controls talin engagement with the actomyosin machinery', *Nature Communications*. doi: 10.1038/ncomms10038.

Atherton, P. *et al.* (2015) 'Vinculin controls talin engagement with the actomyosin machinery', *Nature Communications*. Nature Publishing Group, 6(1), p. 10038. doi: 10.1038/ncomms10038.

Ayed, A. *et al.* (2001) 'Latent and active p53 are identical in conformation', *Nature Structural Biology*. Nature Publishing Group, 8(9), pp. 756–760. doi: 10.1038/nsb0901-756.

Baines, A. J. (2010) 'Evolution of the spectrin-based membrane skeleton', *Transfusion Clinique et Biologique*, 17(3), pp. 95–103. doi: 10.1016/j.tracli.2010.06.008.

Bamford, S. *et al.* (2004) 'The COSMIC (Catalogue of Somatic Mutations in Cancer) database and

- website', *British Journal of Cancer*. Nature Publishing Group, 91(2), pp. 355–358. doi: 10.1038/sj.bjc.6601894.
- Banno, A. *et al.* (2012) 'Subcellular localization of talin is regulated by inter-domain interactions.', *The Journal of biological chemistry*. American Society for Biochemistry and Molecular Biology, 287(17), pp. 13799–812. doi: 10.1074/jbc.M112.341214.
- Banno, A. and Ginsberg, M. H. (2008) 'Integrin activation', *Biochemical Society Transactions*. doi: 10.1042/BST0360229.
- Bate, N. *et al.* (2012) 'Talin contains a C-terminal calpain2 cleavage site important in focal adhesion dynamics', *PLoS ONE*. Edited by M. Parsons, 7(4), p. e34461. doi: 10.1371/journal.pone.0034461.
- Beach, D., Durkacz, B. and Nurse, P. (1982) 'Functionally homologous cell cycle control genes in budding and fission yeast', *Nature*. doi: 10.1038/300706a0.
- Beaty, B. T. *et al.* (2014) 'Talin regulates moesin-NHE-1 recruitment to invadopodia and promotes mammary tumor metastasis.', *The Journal of cell biology*. The Rockefeller University Press, 205(5), pp. 737–51. doi: 10.1083/jcb.201312046.
- Bellis, S. L., Miller, J. T. and Turner, C. E. (1995) 'Characterization of tyrosine phosphorylation of paxillin in vitro by focal adhesion kinase', *Journal of Biological Chemistry*. doi: 10.1074/jbc.270.29.17437.
- Bivona, T. G. *et al.* (2004) 'Rap1 up-regulation and activation on plasma membrane regulates T cell adhesion', *Journal of Cell Biology*. doi: 10.1083/jcb.200311093.
- Bockstaele, L. *et al.* (2006) 'Regulation of CDK4', *Cell Division*. BioMed Central, 1(1), p. 25. doi: 10.1186/1747-1028-1-25.
- Bois, P. R. J. *et al.* (2006) 'The Vinculin Binding Sites of Talin and  $\alpha$ -Actinin Are Sufficient to Activate Vinculin', *Journal of Biological Chemistry*, 281(11), pp. 7228–7236. doi: 10.1074/jbc.M510397200.
- Bou-Gharios, G. and de Crombrughe, B. (2008) *Principles of Bone Biology, Principles of Bone Biology*. doi: 10.1016/B978-0-12-373884-4.00008-2.
- Bouaouina, M., Lad, Y. and Calderwood, D. A. (2008) 'The N-terminal domains of talin cooperate with the phosphotyrosine binding-like domain to activate beta1 and beta3 integrins.', *Journal of Biological Chemistry*, 283(10), pp. 6118–6125. doi: 10.1074/jbc.M709527200.

- Bouchet, B. P. *et al.* (2016) 'Talin-KANK1 interaction controls the recruitment of cortical microtubule stabilizing complexes to focal adhesions', *eLife*, 5(JULY), p. e18124. doi: 10.7554/eLife.18124.
- Bouvard, D. *et al.* (2013) 'Integrin inactivators: Balancing cellular functions in vitro and in vivo', *Nature Reviews Molecular Cell Biology*. doi: 10.1038/nrm3599.
- Brangwynne, C. P. *et al.* (2007) 'Bending dynamics of fluctuating biopolymers probed by automated high-resolution filament tracking', *Biophysical Journal*. doi: 10.1529/biophysj.106.096966.
- Bridgewater, R. E., Norman, J. C. and Caswell, P. T. (2012) 'Integrin trafficking at a glance.', *Journal of cell science*, 125(Pt 16), pp. 3695–701. doi: 10.1242/jcs.095810.
- Brown, M. C. (2004) 'Paxillin: Adapting to Change', *Physiological Reviews*. doi: 10.1152/physrev.00002.2004.
- Brown, M. C., Curtis, M. S. and Turner, C. E. (1998) 'Paxillin LD motifs may define a new family of protein recognition domains', *Nature Structural and Molecular Biology*, 5(8), pp. 677–678. doi: 10.1038/1370.
- Brown, M. C., Perrotta, J. A. and Turner, C. E. (1996) 'Identification of LIM3 as the principal determinant of paxillin focal adhesion localization and characterization of a novel motif on paxillin directing vinculin and focal adhesion kinase binding', *Journal of Cell Biology*. doi: 10.1083/jcb.135.4.1109.
- Burridge, K. and Connell, L. (1983) 'A new protein of adhesion plaques and ruffling membranes.', *The Journal of cell biology*, 97(2), pp. 359–67. Available at: <http://www.ncbi.nlm.nih.gov/pubmed/6684120> (Accessed: 23 January 2018).
- Calderwood, D. A. *et al.* (1999) 'The Talin head domain binds to integrin beta subunit cytoplasmic tails and regulates integrin activation.', *The Journal of biological chemistry*, 274(40), pp. 28071–4. Available at: <http://www.ncbi.nlm.nih.gov/pubmed/10497155> (Accessed: 4 March 2018).
- Calderwood, D. A. *et al.* (2002) 'The phosphotyrosine binding-like domain of talin activates integrins.', *The Journal of biological chemistry*, 277(24), pp. 21749–58. doi: 10.1074/jbc.M111996200.
- Calderwood, D. A. (2004) 'Talin controls integrin activation.', *Biochemical Society transactions*, 32(Pt3), pp. 434–7. doi: 10.1042/BST0320434.

Calderwood, D. a, Campbell, I. D. and Critchley, D. R. (2013) 'Talins and kindlins: partners in integrin-mediated adhesion.', *Nature reviews. Molecular cell biology*. Nature Publishing Group, 14(8), pp. 503–17. doi: 10.1038/nrm3624.

De Camilli, P., Takei, K. and McPherson, P. S. (1995) 'The function of dynamin in endocytosis', *Current Opinion in Neurobiology*. Elsevier Current Trends, 5(5), pp. 559–565. doi: 10.1016/0959-4388(95)80059-X.

Campanale, J. P., Sun, T. Y. and Montell, D. J. (2017) 'Development and dynamics of cell polarity at a glance', *Journal of Cell Science*. doi: 10.1242/jcs.188599.

Campbell, I. D. and Humphries, M. J. (2011) 'Integrin structure, activation, and interactions', *Cold Spring Harbor Perspectives in Biology*. doi: 10.1101/cshperspect.a004994.

Carisey, A. *et al.* (2013) 'Vinculin Regulates the Recruitment and Release of Core Focal Adhesion Proteins in a Force-Dependent Manner', *Current Biology*, 23(4), pp. 271–281. doi: 10.1016/j.cub.2013.01.009.

Carmona-Fontaine, C., Matthews, H. and Mayor, R. (2008) 'Directional cell migration in vivo: Wnt at the crest.', *Cell adhesion & migration*. Taylor & Francis, 2(4), pp. 240–2. Available at: <http://www.ncbi.nlm.nih.gov/pubmed/19262160> (Accessed: 8 August 2018).

Carreno, S. *et al.* (2008) 'Moesin and its activating kinase Slik are required for cortical stability and microtubule organization in mitotic cells', *Journal of Cell Biology*. doi: 10.1083/jcb.200709161.

Case, L. B. and Waterman, C. M. (2015) 'Integration of actin dynamics and cell adhesion by a three-dimensional, mechanosensitive molecular clutch', *Nature Cell Biology*. doi: 10.1038/ncb3191.

Caswell, P. T. *et al.* (2008) 'Rab-coupling protein coordinates recycling of alpha5beta1 integrin and EGFR1 to promote cell migration in 3D microenvironments.', *The Journal of cell biology*, 183(1), pp. 143–55. doi: 10.1083/jcb.200804140.

Chang, Y.-C. *et al.* (2014) 'Structural and mechanistic insights into the recruitment of talin by RIAM in integrin signaling.', *Structure (London, England: 1993)*, 22(12), pp. 1810–1820. doi: 10.1016/j.str.2014.09.020.

Changede, R. *et al.* (2015) 'Nascent Integrin Adhesions Form on All Matrix Rigidities after Integrin Activation', *Developmental Cell*, 35(5), pp. 614–621. doi: 10.1016/j.devcel.2015.11.001.

Choudhary, C. *et al.* (2009) 'Lysine acetylation targets protein complexes and co-regulates major



cellular functions', *Science*. doi: 10.1126/science.1175371.

Ciobanasiu, C. *et al.* (2018) 'Integrin-bound talin head inhibits actin filament barbed-end elongation', *Journal of Biological Chemistry*, 293(7), pp. 2586–2596. doi: 10.1074/jbc.M117.808204.

Cooper, G. M. (2000) 'The Cell: A Molecular Approach. 2nd edition - Intermediate Filaments', *Sinauer Associates*. doi: 10.1016/j.juro.2009.01.103.

Critchley, D. R. and Gingras, A. R. (2008) 'Talin at a glance.', *Journal of cell science*, 121(Pt 9), pp. 1345–7. doi: 10.1242/jcs.018085.

Debrand, E. *et al.* (2009) 'Talin 2 is a large and complex gene encoding multiple transcripts and protein isoforms', *FEBS Journal*. Blackwell Publishing Ltd, 276(6), pp. 1610–1628. doi: 10.1111/j.1742-4658.2009.06893.x.

Debrand, E. *et al.* (2012) 'Mice carrying a complete deletion of the talin2 coding sequence are viable and fertile', *Biochemical and Biophysical Research Communications*, 426(2), pp. 190–195. doi: 10.1016/j.bbrc.2012.08.061.

Deng, H. *et al.* (2016) 'Exome Sequencing of a Pedigree Reveals S339L Mutation in the TLN2 Gene as a Cause of Fifth Finger Camptodactyly', *PLOS ONE*. Edited by O. R. Bandapalli, 11(5), p. e0155180. doi: 10.1371/journal.pone.0155180.

Desiniotis, A. and Kyprianou, N. (2011) 'Significance of talin in cancer progression and metastasis', *International Review of Cell and Molecular Biology*. doi: 10.1016/B978-0-12-386039-2.00004-3.

Ding, M. (2003) 'C. elegans ankyrin repeat protein VAB-19 is a component of epidermal attachment structures and is essential for epidermal morphogenesis', *Development*. doi: 10.1242/dev.00791.

Drabek, K. *et al.* (2006) 'Role of CLASP2 in Microtubule Stabilization and the Regulation of Persistent Motility', *Current Biology*. doi: 10.1016/j.cub.2006.09.065.

Egelhofer, T. A. *et al.* (2008) 'The Septins Function in G1 Pathways that Influence the Pattern of Cell Growth in Budding Yeast', *PLoS ONE*. Edited by K. G. Hardwick. Public Library of Science, 3(4), p. e2022. doi: 10.1371/journal.pone.0002022.

Elliott, P. R. *et al.* (2010) 'The Structure of the Talin Head Reveals a Novel Extended Conformation of the FERM Domain', *Structure*, 18(10), pp. 1289–1299. doi: 10.1016/j.str.2010.07.011.

Ellis, S. J. *et al.* (2011) 'In vivo functional analysis reveals specific roles for the integrin-binding sites

of talin.', *Journal of cell science*. The Company of Biologists Ltd, 124(11), pp. 1844–56. doi: 10.1242/jcs.083337.

Emsley, P. *et al.* (no date) 'Biological Crystallography Features and development of Coot'. doi: 10.1107/S0907444910007493.

Enserink, J. M. and Kolodner, R. D. (2010) 'An overview of Cdk1-controlled targets and processes', *Cell Division*. BioMed Central, 5(1), p. 11. doi: 10.1186/1747-1028-5-11.

Ezratty, E. J. *et al.* (2009) 'Clathrin mediates integrin endocytosis for focal adhesion disassembly in migrating cells', *The Journal of Cell Biology*, 187(5), pp. 733–747. doi: 10.1083/jcb.200904054.

Ezratty, E. J., Partridge, M. A. and Gundersen, G. G. (2005) 'Microtubule-induced focal adhesion disassembly is mediated by dynamin and focal adhesion kinase', *Nature Cell Biology*. Nature Publishing Group, 7(6), pp. 581–590. doi: 10.1038/ncb1262.

Facey, G. (University of O. (2015) *No Title*, TROSY. Available at: <http://u-of-o-nmr-facility.blogspot.com/2015/05/trosy.html> (Accessed: 16 November 2018).

Fourest-Lieuvain, A. (2005) 'Microtubule Regulation in Mitosis: Tubulin Phosphorylation by the Cyclin-dependent Kinase Cdk1', *Molecular Biology of the Cell*. doi: 10.1091/mbc.E05-07-0621.

Franceschi, N. De *et al.* (2017) 'ProLIF: a quantitative assay for investigating integrin cytoplasmic protein interactions and synergistic membrane effects on proteoliposomes', *bioRxiv*. Cold Spring Harbor Laboratory, p. 209262. doi: 10.1101/209262.

Franco, S. J. *et al.* (2004) 'Calpain-mediated proteolysis of talin regulates adhesion dynamics', *Nature Cell Biology*, 6(10), pp. 977–983. doi: 10.1038/ncb1175.

Frantz, C., Stewart, K. M. and Weaver, V. M. (2010) 'The extracellular matrix at a glance.', *Journal of cell science*. Company of Biologists, 123(Pt 24), pp. 4195–200. doi: 10.1242/jcs.023820.

Fröbel, J. *et al.* (2013) 'Platelet Proteome Analysis Reveals Integrin-dependent Aggregation Defects in Patients with Myelodysplastic Syndromes', *Molecular & Cellular Proteomics*. doi: 10.1074/mcp.M112.023168.

Ganguly, K. K. *et al.* (2013) 'Integrins and metastasis', *Cell Adhesion and Migration*. doi: 10.4161/cam.23840.

Gao, L. *et al.* (2012) 'Noninvasive imaging beyond the diffraction limit of 3D dynamics in thickly

fluorescent specimens', *Cell*. doi: 10.1016/j.cell.2012.10.008.

Gasteiger, E. *et al.* (no date) *Protein Analysis Tools on the ExPASy Server 571 571 From: The Proteomics Protocols Handbook Protein Identification and Analysis Tools on the ExPASy Server*. Available at: <http://www.expasy.org/tools/>. (Accessed: 20 August 2018).

Gavet, O. and Pines, J. (2010) 'Progressive Activation of CyclinB1-Cdk1 Coordinates Entry to Mitosis', *Developmental Cell*. doi: 10.1016/j.devcel.2010.02.013.

Gee, H. Y. *et al.* (2015) 'KANK deficiency leads to podocyte dysfunction and nephrotic syndrome', *Journal of Clinical Investigation*, 125(6), pp. 2375–2384. doi: 10.1172/JCI79504.

Geiger, B. (1979) 'A 130K protein from chicken gizzard: its localization at the termini of microfilament bundles in cultured chicken cells.', *Cell*, 18(1), pp. 193–205. Available at: <http://www.ncbi.nlm.nih.gov/pubmed/574428> (Accessed: 10 March 2018).

Gibbs, R. A. *et al.* (2015) 'A global reference for human genetic variation', *Nature*. Nature Publishing Group, 526(7571), pp. 68–74. doi: 10.1038/nature15393.

Gilmore, A. P. *et al.* (1995) 'Localisation of the human gene encoding the cytoskeletal protein talin to chromosome 9p', *Human Genetics*. doi: 10.1007/BF00207384.

Gingras, A. R. *et al.* (2005) 'Mapping and consensus sequence identification for multiple vinculin binding sites within the talin rod.', *The Journal of biological chemistry*. American Society for Biochemistry and Molecular Biology, 280(44), pp. 37217–24. doi: 10.1074/jbc.M508060200.

Gingras, A. R. *et al.* (2006) 'The structure of the C-terminal actin binding domain of talin. Alexandre R. Gingras', pp. 1–21.

Gingras, A. R. *et al.* (2008) 'The structure of the C-terminal actin-binding domain of talin.', *The EMBO journal*, 27, pp. 458–69. doi: 10.1038/sj.emboj.7601965.

Gingras, A. R. *et al.* (2009) 'Structural determinants of integrin binding to the talin rod.', *The Journal of biological chemistry*. American Society for Biochemistry and Molecular Biology, 284(13), pp. 8866–76. doi: 10.1074/jbc.M805937200.

Gingras, A. R. *et al.* (2010) 'Central region of talin has a unique fold that binds vinculin and actin.', *The Journal of biological chemistry*. American Society for Biochemistry and Molecular Biology, 285(38), pp. 29577–87. doi: 10.1074/jbc.M109.095455.

Goksoy, E. *et al.* (2008) 'Structural Basis for the Autoinhibition of Talin in Regulating Integrin Activation', *Molecular Cell*, 31(1), pp. 124–133. doi: 10.1016/j.molcel.2008.06.011.

Gough, R. E. and Goult, B. T. (2018) 'The tale of two talins - two isoforms to fine-tune integrin signalling', *FEBS Letters*. doi: 10.1002/1873-3468.13081.

Gould, K. L. and Nurse, P. (1989) 'Tyrosine phosphorylation of the fission yeast cdc2+ protein kinase regulates entry into mitosis', *Nature*. doi: 10.1038/342039a0.

Goult, B. T. *et al.* (2009) 'The structure of an interdomain complex that regulates talin activity.', *The Journal of biological chemistry*. American Society for Biochemistry and Molecular Biology, 284(22), pp. 15097–106. doi: 10.1074/jbc.M900078200.

Goult, B. T. *et al.* (2010) 'The domain structure of talin: Residues 1815-1973 form a five-helix bundle containing a cryptic vinculin-binding site', *FEBS Letters*, 584(11), pp. 2237–2241. doi: 10.1016/j.febslet.2010.04.028.

Goult, B. T., Zacharchenko, T., *et al.* (2013) 'RIAM and vinculin binding to talin are mutually exclusive and regulate adhesion assembly and turnover.', *The Journal of biological chemistry*, 288(12), pp. 8238–49. doi: 10.1074/jbc.M112.438119.

Goult, B. T., Xu, X.-P., *et al.* (2013) 'Structural studies on full-length talin1 reveal a compact auto-inhibited dimer: Implications for talin activation', *Journal of Structural Biology*, 184(1), pp. 21–32. doi: 10.1016/j.jsb.2013.05.014.

Goult, B. T. B. T. *et al.* (2010) 'Structure of a double ubiquitin-like domain in the talin head: a role in integrin activation.', *The EMBO journal*, 29(6), pp. 1069–1080. doi: 10.1038/emboj.2010.4.

Goult, B. T., Yan, J. and Schwartz, M. A. (2018) 'Talin as a mechanosensitive signaling hub', *The Journal of Cell Biology*. doi: 10.1083/jcb.201808061.

Grikscheit, K. *et al.* (2015) 'Junctional actin assembly is mediated by Formin-like 2 downstream of Rac1.', *The Journal of cell biology*. The Rockefeller University Press, 209(3), pp. 367–76. doi: 10.1083/jcb.201412015.

Gunawan, M. *et al.* (2015) 'The methyltransferase Ezh2 controls cell adhesion and migration through direct methylation of the extranuclear regulatory protein talin', *Nature Immunology*. Nature Publishing Group, 16(5), pp. 505–516. doi: 10.1038/ni.3125.

Hagmann, J., Grob, M. and Burger, M. M. (1992) 'The cytoskeletal protein talin is O-glycosylated', 241

*Journal of Biological Chemistry.*

Hanahan, D., Jessee, J. and Bloom, F. R. (1991) 'Plasmid transformation of Escherichia coli and other bacteria', *Methods in Enzymology*. doi: 10.1016/0076-6879(91)04006-A.

Hartwell, L. H. *et al.* (1974) 'Genetic control of the cell division cycle in yeast', *Science*. doi: 10.1126/science.183.4120.46.

Helfrich, M. H. *et al.* (2008) 'Integrins and Other Cell Surface Attachment Molecules of Bone Cells', in *Principles of Bone Biology, Two-Volume Set*, pp. 385–424. doi: 10.1016/B978-0-12-373884-4.00039-2.

Hemmings, L. *et al.* (1996) 'Talin contains three actin-binding sites each of which is adjacent to a vinculin-binding site.', *Journal of cell science*, 109 ( Pt 11), pp. 2715–26. Available at: <http://www.ncbi.nlm.nih.gov/pubmed/8937989> (Accessed: 7 March 2018).

Higgins, D. G. *et al.* (1994) 'The evolution of titin and related giant muscle proteins.', *Journal of molecular evolution*, 38(4), pp. 395–404. Available at: <http://www.ncbi.nlm.nih.gov/pubmed/8007007> (Accessed: 4 March 2018).

Himmel, M. *et al.* (2009) 'Control of High Affinity Interactions in the Talin C Terminus', *Journal of Biological Chemistry*, 284(20), pp. 13832–13842. doi: 10.1074/jbc.M900266200.

Hochegger, H., Takeda, S. and Hunt, T. (2008) 'Cyclin-dependent kinases and cell-cycle transitions: Does one fit all?', *Nature Reviews Molecular Cell Biology*. doi: 10.1038/nrm2510.

Hoellerer, M. K. *et al.* (2003) 'Molecular Recognition of Paxillin LD Motifs by the Focal Adhesion Targeting Domain', *Structure*. Turner *et al.*, 11, pp. 1207–1217. doi: 10.1016/j.str.2003.08.010.

Hornbeck, P. V. *et al.* (2015) 'PhosphoSitePlus, 2014: Mutations, PTMs and recalibrations', *Nucleic Acids Research*. doi: 10.1093/nar/gku1267.

Horton, E. R. *et al.* (2016) 'The integrin adhesome network at a glance', *Journal of Cell Science*, 129(22), pp. 4159–4163. doi: 10.1242/jcs.192054.

Hotta, A. *et al.* (2010) 'Laminin-based cell adhesion anchors microtubule plus ends to the epithelial cell basal cortex through LL5 $\alpha/\beta$ ', *Journal of Cell Biology*. doi: 10.1083/jcb.200910095.

Howard, J. and Hyman, A. A. (2003) 'Dynamics and mechanics of the microtubule plus end', *Nature*. doi: 10.1038/nature01600.

- Hu, X. *et al.* (2012) 'Cell surface assembly of HIV gp41 six-helix bundles for facile, quantitative measurements of hetero-oligomeric interactions', *Journal of the American Chemical Society*. doi: 10.1021/ja301099s.
- Huang, C. *et al.* (2009) 'Talin phosphorylation by Cdk5 regulates Smurf1-mediated talin head ubiquitylation and cell migration', *Nature Cell Biology*, 11(5), pp. 624–630. doi: 10.1038/ncb1868.
- Huveneers, S. and Danen, E. H. J. (2009) 'Adhesion signaling - crosstalk between integrins, Src and Rho', *Journal of Cell Science*. doi: 10.1242/jcs.039446.
- Hynes, R. O. (2002) 'Integrins : Bidirectional , allosteric signaling machines in their roles as major adhesion receptors', *Cell*. doi: 10.1016/S0092-8674(02)00971-6.
- Jaka, O. *et al.* (2015) 'Costamere proteins and their involvement in myopathic processes', *Expert Reviews in Molecular Medicine*. doi: 10.1017/erm.2015.9.
- Jones, D. T. (1999) 'Protein secondary structure prediction based on position-specific scoring matrices 1 1Edited by G. Von Heijne', *Journal of Molecular Biology*, 292(2), pp. 195–202. doi: 10.1006/jmbi.1999.3091.
- Jones, M. C. *et al.* (2018) 'Cell adhesion is regulated by CDK1 during the cell cycle.', *The Journal of cell biology*. Rockefeller University Press, p. jcb.201802088. doi: 10.1083/jcb.201802088.
- Kakinuma, N. *et al.* (2009) 'Kank proteins: structure, functions and diseases', *Cellular and Molecular Life Sciences*, 66(16), pp. 2651–2659. doi: 10.1007/s00018-009-0038-y.
- Kakinuma, N. and Kiyama, R. (2009) 'A major mutation of KIF21A associated with congenital fibrosis of the extraocular muscles type 1 (CFEOM1) enhances translocation of Kank1 to the membrane', *Biochemical and Biophysical Research Communications*. Academic Press, 386(4), pp. 639–644. doi: 10.1016/j.bbrc.2009.06.109.
- Kelley, L. A. *et al.* (2015) 'The Phyre2 web portal for protein modeling, prediction and analysis', *Nature Protocols*. Nature Publishing Group, 10(6), pp. 845–858. doi: 10.1038/nprot.2015.053.
- Kelley, L. A. and Sternberg, M. J. E. (2009) 'Protein structure prediction on the Web: a case study using the Phyre server.', *Nature protocols*, 4, pp. 363–371. doi: 10.1038/nprot.2009.2.
- Kim, I. *et al.* (2018) 'A novel HIF1AN substrate KANK3 plays a tumor-suppressive role in hepatocellular carcinoma', *Cell Biology International*, 42(3), pp. 303–312. doi: 10.1002/cbin.10895.

- Kinsland, C. (2010) 'Bacterial Protein Overexpression Systems and Strategies', *Comprehensive Natural Products II*. Elsevier, pp. 695–721. doi: 10.1016/B978-008045382-8.00199-4.
- Klapholz, B. and Brown, N. H. (2017) 'Talin - the master of integrin adhesions.', *Journal of cell science*. The Company of Biologists Ltd, 130(15), pp. 2435–2446. doi: 10.1242/jcs.190991.
- Kopp, P. M. *et al.* (2010) 'Studies on the morphology and spreading of human endothelial cells define key inter- and intramolecular interactions for talin1', *European Journal of Cell Biology*. doi: 10.1016/j.ejcb.2010.05.003.
- Kumar, A. *et al.* (2016) 'Talin tension sensor reveals novel features of focal adhesion force transmission and mechanosensitivity.', *The Journal of cell biology*. Rockefeller University Press, 213(3), pp. 371–83. doi: 10.1083/jcb.201510012.
- Lagarrigue, F. *et al.* (2015) 'A RIAM/lamellipodin-talin-integrin complex forms the tip of sticky fingers that guide cell migration', *Nature Communications*, 6. doi: 10.1038/ncomms9492.
- Lahm, H.-W. and Langen, H. (2000) 'Mass spectrometry: A tool for the identification of proteins separated by gels', *Electrophoresis*. Wiley-Blackwell, 21(11), pp. 2105–2114. doi: 10.1002/1522-2683(20000601)21:11<2105::AID-ELPS2105>3.0.CO;2-M.
- Lal, H. (2009) 'Integrins and proximal signaling mechanisms in cardiovascular disease', *Frontiers in Bioscience*. doi: 10.2741/3381.
- Lamb, R. *et al.* (2013) 'Cell cycle regulators cyclin D1 and CDK4/6 have estrogen receptor-dependent divergent functions in breast cancer migration and stem cell-like activity', *Cell Cycle*. Taylor & Francis, 12(15), pp. 2384–2394. doi: 10.4161/cc.25403.
- Lansbergen, G. *et al.* (2006) 'CLASPs Attach Microtubule Plus Ends to the Cell Cortex through a Complex with LL5 $\beta$ ', *Developmental Cell*. doi: 10.1016/j.devcel.2006.05.012.
- Larkin, M. A. *et al.* (2007) 'Clustal W and Clustal X version 2.0', *Bioinformatics*. doi: 10.1093/bioinformatics/btm404.
- Lawson, C. *et al.* (2012) 'FAK promotes recruitment of talin to nascent adhesions to control cell motility.', *The Journal of cell biology*. Rockefeller University Press, 196(2), pp. 223–32. doi: 10.1083/jcb.201108078.
- Lecuit, T. and Yap, A. S. (2015) 'E-cadherin junctions as active mechanical integrators in tissue dynamics', *Nature Cell Biology*. doi: 10.1038/ncb3136.

- Lee, H.-S. *et al.* (2004) 'Characterization of an actin-binding site within the talin FERM domain.', *Journal of Molecular Biology*, 343(3), pp. 771–784. doi: 10.1016/j.jmb.2004.08.069.
- Lee, H.-S. *et al.* (2009) 'RIAM Activates Integrins by Linking Talin to Ras GTPase Membrane-targeting Sequences', *Journal of Biological Chemistry*, 284(8), pp. 5119–5127. doi: 10.1074/jbc.M807117200.
- Legate, K. R. *et al.* (2011) 'Integrin adhesion and force coupling are independently regulated by localized PtdIns(4,5)<sub>2</sub> synthesis', *The EMBO Journal*, 30(22), pp. 4539–4553. doi: 10.1038/emboj.2011.332.
- Lerer, I. *et al.* (2005) 'Deletion of the ANKRD15 gene at 9p24.3 causes parent-of-origin-dependent inheritance of familial cerebral palsy', *Human Molecular Genetics*. doi: 10.1093/hmg/ddi415.
- Ley, K. (2001) 'Functions of selectins', *Results Probl Cell Differ.*
- Li, A. *et al.* (2014) 'Integrin  $\alpha$ IIb tail distal of GFFKR participates in inside-out  $\alpha$ IIb $\beta$ 3 activation', *Journal of Thrombosis and Haemostasis*. doi: 10.1111/jth.12610.
- Li, G. *et al.* (2011) 'Full activity of the deleted in liver cancer 1 (DLC1) tumor suppressor depends on an LD-like motif that binds talin and focal adhesion kinase (FAK)', *Proceedings of the National Academy of Sciences*. doi: 10.1073/pnas.1112122108.
- Li, T. *et al.* (2004) 'Failure to proliferate and mitotic arrest of CDK11(p110/p58)-null mutant mice at the blastocyst stage of embryonic cell development.', *Molecular and cellular biology*, 24(8), pp. 3188–97. Available at: <http://www.ncbi.nlm.nih.gov/pubmed/15060143> (Accessed: 7 September 2018).
- Liberal, V. *et al.* (2011) 'Breast Cancer Special Feature: Cyclin-dependent kinase subunit (Cks) 1 or Cks2 overexpression overrides the DNA damage response barrier triggered by activated oncoproteins.', *Proceedings of the National Academy of Sciences of the United States of America*. doi: 10.1073/pnas.1102434108.
- Light, S. *et al.* (2012) 'The evolution of filamin – A protein domain repeat perspective', *Journal of Structural Biology*, 179(3), pp. 289–298. doi: 10.1016/j.jsb.2012.02.010.
- Lim, S. and Kaldis, P. (2013) 'Cdks, cyclins and CKIs: roles beyond cell cycle regulation', *Development*, 140(15), pp. 3079–3093. doi: 10.1242/dev.091744.
- Linder, S. and Kopp, P. (2005) 'Podosomes at a glance.', *Journal of cell science*, 118(Pt 10), pp. 2079–245



82. doi: 10.1242/jcs.02390.

Lodish, H. *et al.* (2000) 'The Dynamics of Actin Assembly'. W. H. Freeman.

Lodish Harvey, Berk Arnold, Kaiser Chris, K. M. (2016) *Molecular Cell Biology*. eighth. doi: 10.1016/S1470-8175(01)00023-6.

Lohka, M. J., Hayes, M. K. and Maller, J. L. (1988) 'Purification of maturation-promoting factor, an intracellular regulator of early mitotic events.', *Proceedings of the National Academy of Sciences*. doi: 10.1073/pnas.85.9.3009.

Lolli, G. and Johnson, L. N. (2005) 'CAK-Cyclin-dependent Activating Kinase: a key kinase in cell cycle control and a target for drugs?', *Cell cycle (Georgetown, Tex.)*, 4(4), pp. 572–7. Available at: <http://www.ncbi.nlm.nih.gov/pubmed/15876871> (Accessed: 14 May 2019).

Lu, P., Weaver, V. M. and Werb, Z. (2012) 'The extracellular matrix: A dynamic niche in cancer progression', *Journal of Cell Biology*. doi: 10.1083/jcb.201102147.

Luo, M. *et al.* (2016) 'Association of liprin  $\beta$ -1 with kank proteins in melanoma', *Experimental Dermatology*. doi: 10.1111/exd.12933.

Maekawa, M. *et al.* (1999) 'Signaling from Rho to the actin cytoskeleton through protein kinases ROCK and LIM-kinase', *Science*. doi: 10.1126/science.285.5429.895.

Malumbres, M. *et al.* (2009) 'Cyclin-dependent kinases: a family portrait.', *Nature cell biology*. NIH Public Access, 11(11), pp. 1275–6. doi: 10.1038/ncb1109-1275.

Malumbres, M. (2014a) 'Cyclin-dependent kinases.', *Genome biology*. BioMed Central, 15(6), p. 122. doi: 10.1186/GB4184.

Malumbres, M. (2014b) 'Cyclin-dependent kinases.', *Genome biology*. BioMed Central, 15(6), p. 122. doi: 10.1186/GB4184.

Manso, A. M. *et al.* (2013) 'Talin1 has unique expression versus talin 2 in the heart and modifies the hypertrophic response to pressure overload', *Journal of Biological Chemistry*, 288(6), pp. 4252–4264. doi: 10.1074/jbc.M112.427484.

Manso, A. M. *et al.* (2017) 'Loss of mouse cardiomyocyte talin-1 and talin-2 leads to  $\beta$ -1 integrin reduction, costameric instability, and dilated cardiomyopathy.', *Proceedings of the National Academy of Sciences of the United States of America*. National Academy of Sciences, 114(30), pp.

E6250–E6259. doi: 10.1073/pnas.1701416114.

Martin, L., Schwarz, S. and Breitsprecher, D. (2014) 'Analyzing Thermal Unfolding of Proteins: The Prometheus NT.48', *Nanotemper Technologies. Application Note NT-PR-001*, pp. 1–8.

McCann, R. O. and Craig, S. W. (1997) 'The I/LWEQ module: a conserved sequence that signifies F-actin binding in functionally diverse proteins from yeast to mammals.', *Proceedings of the National Academy of Sciences of the United States of America*. National Academy of Sciences, 94(11), pp. 5679–84. doi: 10.1073/pnas.94.11.5679.

McCoy, A. J. *et al.* (2007) 'Phaser crystallographic software', *Journal of Applied Crystallography*. doi: 10.1107/S0021889807021206.

Mimori-Kiyosue, Y. *et al.* (2005) 'CLASP1 and CLASP2 bind to EB1 and regulate microtubule plus-end dynamics at the cell cortex', *Journal of Cell Biology*. doi: 10.1083/jcb.200405094.

Mitra, S. K. and Schlaepfer, D. D. (2006) 'Integrin-regulated FAK–Src signaling in normal and cancer cells', *Current Opinion in Cell Biology*, 18(5), pp. 516–523. doi: 10.1016/j.ceb.2006.08.011.

Monkley, S. J. *et al.* (2000) 'Disruption of the talin gene arrests mouse development at the gastrulation stage', *Developmental Dynamics*, 219(4), pp. 560–574. doi: 10.1002/1097-0177(2000)9999:9999::AID-DVDY1079>3.0.CO;2-Y.

Monkley, S. J. *et al.* (2011) 'Endothelial cell talin1 is essential for embryonic angiogenesis', *Developmental Biology*, 349(2), pp. 494–502. doi: 10.1016/j.ydbio.2010.11.010.

Monkley, S. J., Pritchard, C. A. and Critchley, D. R. (2001) 'Analysis of the mammalian talin2 gene TLN2.', *Biochemical and Biophysical Research Communications*, 286(5), pp. 880–885. doi: 10.1006/bbrc.2001.5497.

Mori, S. *et al.* (1995) 'Improved Sensitivity of HSQC Spectra of Exchanging Protons at Short Interscan Delays Using a New Fast HSQC (FHSQC) Detection Scheme That Avoids Water Saturation', *Journal of Magnetic Resonance, Series B*. doi: 10.1006/jmrb.1995.1109.

Morishita, H. and Yagi, T. (2007) 'Protocadherin family: diversity, structure, and function', *Current Opinion in Cell Biology*, pp. 584–592. doi: 10.1016/j.ceb.2007.09.006.

Muca, R. *et al.* (2017) 'Effect of mass overloading on binding and elution of unstable proteins in hydrophobic interaction chromatography', *Journal of Chromatography A*. Elsevier, 1492, pp. 79–88. doi: 10.1016/J.CHROMA.2017.02.073.

- Murshudov, G. N., Vagin, A. A. and Dodson, E. J. (1997) 'Refinement of macromolecular structures by the maximum-likelihood method', *Acta Crystallographica Section D: Biological Crystallography*. doi: 10.1107/S0907444996012255.
- Neubauer, K. and Zieger, B. (2017) 'The Mammalian Septin Interactome.', *Frontiers in cell and developmental biology*. Frontiers Media SA, 5, p. 3. doi: 10.3389/fcell.2017.00003.
- Nikolopoulos, S. N. and Turner, C. E. (2000) 'Actopaxin, a new focal adhesion protein that binds paxillin LD motifs and actin and regulates cell adhesion', *Journal of Cell Biology*. doi: 10.1083/jcb.151.7.1435.
- Patra, D. *et al.* (1999) 'The Xenopus Suc1/Cks protein promotes the phosphorylation of G2/M regulators', *Journal of Biological Chemistry*. doi: 10.1074/jbc.274.52.36839.
- Pearson, M. A. *et al.* (2000) 'Structure of the ERM protein moesin reveals the FERM domain fold masked by an extended actin binding tail domain.', *Cell*. Elsevier, 101(3), pp. 259–70. doi: 10.1016/S0092-8674(00)80836-3.
- Peng, X. *et al.* (2011) 'New Insights into Vinculin Function and Regulation', *International Review of Cell and Molecular Biology*. Academic Press, 287, pp. 191–231. doi: 10.1016/B978-0-12-386043-9.00005-0.
- de Pereda, J. M. *et al.* (2005) 'Structural Basis for Phosphatidylinositol Phosphate Kinase Type I $\gamma$  Binding to Talin at Focal Adhesions', *Journal of Biological Chemistry*, 280(9), pp. 8381–8386. doi: 10.1074/jbc.M413180200.
- Perkins, D. N. *et al.* (1999) 'Probability-based protein identification by searching sequence databases using mass spectrometry data', *Electrophoresis*. Wiley-Blackwell, 20(18), pp. 3551–3567. doi: 10.1002/(SICI)1522-2683(19991201)20:18<3551::AID-ELPS3551>3.0.CO;2-2.
- Pervushin, K. V., Wider, G. and Wüthrich, K. (1998) 'Single transition-to-single transition polarization transfer (ST2-PT) in [15N,1H]-TROSY', *Journal of Biomolecular NMR*. doi: 10.1023/A:1008268930690.
- Pines, J. and Hunter, T. (1990) 'Human cyclin A is adenovirus E1A-associated protein p60 and behaves differently from cyclin B', *Nature*. doi: 10.1038/346760a0.
- Pollard, T. D. and Cooper, J. A. (2009) 'Actin, a central player in cell shape and movement', *Science*, pp. 1208–1212. doi: 10.1126/science.1175862.

- Qi, L. *et al.* (2016) 'Talin2-mediated traction force drives matrix degradation and cell invasion', *Journal of Cell Science*, 129(19), pp. 3661–3674. doi: 10.1242/jcs.185959.
- Ramkumar, N. and Baum, B. (2016) 'Coupling changes in cell shape to chromosome segregation', *Nature Reviews Molecular Cell Biology*. Nature Research, 17(8), pp. 511–521. doi: 10.1038/nrm.2016.75.
- Rantala, J. K. *et al.* (2011) 'SHARPIN is an endogenous inhibitor of  $\beta$ 1-integrin activation', *Nature Cell Biology*. doi: 10.1038/ncb2340.
- Ratnikov, B. *et al.* (2005) 'Talin phosphorylation sites mapped by mass spectrometry.', *Journal of cell science*. The Company of Biologists Ltd, 118(Pt 21), pp. 4921–3. doi: 10.1242/jcs.02682.
- Rhind, N. and Russell, P. (2012) 'Signaling pathways that regulate cell division.', *Cold Spring Harbor perspectives in biology*. Cold Spring Harbor Laboratory Press, 4(10). doi: 10.1101/cshperspect.a005942.
- Ridley, A. J. *et al.* (2003) 'Cell migration: integrating signals from front to back.', *Science (New York, N.Y.)*, 302, pp. 1704–1709. doi: 10.1126/science.1092053.
- Rinnerthaler, G., Geiger, B. and Small, J. V. (1988) 'Contact formation during fibroblast locomotion: Involvement of membrane ruffles and microtubules', *Journal of Cell Biology*. doi: 10.1083/jcb.106.3.747.
- del Rio, A. *et al.* (2009) 'Stretching Single Talin Rod Molecules Activates Vinculin Binding', *Science*, 323(5914), pp. 638–641. doi: 10.1126/science.1162912.
- Robertson, J. *et al.* (2015) 'Defining the phospho-adhesome through the phosphoproteomic analysis of integrin signalling', *Nature Communications*, 6(1), p. 6265. doi: 10.1038/ncomms7265.
- Rochlin, M. W., Dailey, M. E. and Bridgman, P. C. (1999) 'Polymerizing microtubules activate site-directed F-actin assembly in nerve growth cones.', *Molecular biology of the cell*. doi: 10.1091/mbc.10.7.2309.
- Rodius, S. *et al.* (2008) 'The Talin Rod IBS2  $\alpha$ -Helix Interacts with the  $\beta$ 3 Integrin Cytoplasmic Tail Membrane-proximal Helix by Establishing Charge Complementary Salt Bridges', *Journal of Biological Chemistry*, 283(35), pp. 24212–24223. doi: 10.1074/jbc.M709704200.
- Röttschke, O. *et al.* (2002) 'A pH-sensitive histidine residue as control element for ligand release from HLA-DR molecules', *Proceedings of the National Academy of Sciences of the United States of*

- America. National Academy of Sciences, 99(26), pp. 16946–50. doi: 10.1073/pnas.212643999.
- Rueden, C. T. *et al.* (2017) 'ImageJ2: ImageJ for the next generation of scientific image data', *BMC Bioinformatics*. doi: 10.1186/s12859-017-1934-z.
- Saltel, F. *et al.* (2009) 'New PI(4,5)P<sub>2</sub>- and membrane proximal integrin-binding motifs in the talin head control beta3-integrin clustering.', *The Journal of cell biology*. Rockefeller University Press, 187(5), pp. 715–31. doi: 10.1083/jcb.200908134.
- Santamaría, D. *et al.* (2007) 'Cdk1 is sufficient to drive the mammalian cell cycle', *Nature*. Nature Publishing Group, 448(7155), pp. 811–815. doi: 10.1038/nature06046.
- Santamaría D1, Barrière C, Cerqueira A, Hunt S, Tardy C, Newton K, Cáceres JF, Dubus P, Malumbres M, B. M. *et al.* (2007) 'Cdk1 is sufficient to drive the mammalian cell cycle.', *Nature*. doi: 10.1038/nature06046.
- Saxena, M. *et al.* (2017) 'Force-Induced Calpain Cleavage of Talin Is Critical for Growth, Adhesion Development, and Rigidity Sensing', *Nano Letters*, 17(12), pp. 7242–7251. doi: 10.1021/acs.nanolett.7b02476.
- Schaller, M. D. (2001) 'Paxillin: A focal adhesion-associated adaptor protein', *Oncogene*. doi: 10.1038/sj.onc.1204786.
- Schiemer, J. *et al.* (2016) 'Gα<sub>13</sub> Switch Region 2 Relieves Talin Autoinhibition to Activate αIIbβ3 Integrin', *Journal of Biological Chemistry*, 291(52), pp. 26598–26612. doi: 10.1074/jbc.M116.747279.
- Schmalzigaug, R. *et al.* (2007) 'GIT1 utilizes a focal adhesion targeting-homology domain to bind paxillin', *Cellular Signalling*. doi: 10.1016/j.cellsig.2007.03.010.
- Schönichen, A. *et al.* (2013) 'Considering Protonation as a Posttranslational Modification Regulating Protein Structure and Function', *Annual Review of Biophysics*, 42(1), pp. 289–314. doi: 10.1146/annurev-biophys-050511-102349.
- Senetar, M. A. and McCann, R. O. (2005) 'Gene duplication and functional divergence during evolution of the cytoskeletal linker protein talin', *Gene*, 362(1–2), pp. 141–152. doi: 10.1016/j.gene.2005.08.012.
- Senetar, M. A., Moncman, C. L. and McCann, R. O. (2007) 'Talin2 is induced during striated muscle differentiation and is targeted to stable adhesion complexes in mature muscle.', *Cell motility and*

*the cytoskeleton*. Wiley Subscription Services, Inc., A Wiley Company, 64(3), pp. 157–73. doi: 10.1002/cm.20173.

Senisterra, G., Chau, I. and Vedadi, M. (2012) 'Thermal Denaturation Assays in Chemical Biology', *ASSAY and Drug Development Technologies*. Mary Ann Liebert, Inc. 140 Huguenot Street, 3rd Floor New Rochelle, NY 10801 USA , 10(2), pp. 128–136. doi: 10.1089/adt.2011.0390.

Shattil, S. J., Kim, C. and Ginsberg, M. H. (2010) 'The final steps of integrin activation: The end game', *Nature Reviews Molecular Cell Biology*, 11(4), pp. 288–300. doi: 10.1038/nrm2871.

Sherr, C. J. and Bartek, J. (2017) 'Cell Cycle–Targeted Cancer Therapies', *Annual Review of Cancer Biology*. doi: 10.1146/annurev-cancerbio-040716-075628.

Sigrist, C. J. A. *et al.* (2002) 'PROSITE: a documented database using patterns and profiles as motif descriptors.', *Briefings in bioinformatics*, 3(3), pp. 265–74. Available at: <http://www.ncbi.nlm.nih.gov/pubmed/12230035> (Accessed: 7 October 2018).

Singh, P., Carraher, C. and Schwarzbauer, J. E. (2010) 'Assembly of fibronectin extracellular matrix.', *Annual review of cell and developmental biology*. NIH Public Access, 26, pp. 397–419. doi: 10.1146/annurev-cellbio-100109-104020.

Skinner, S. P. *et al.* (2015) 'Structure calculation, refinement and validation using CcpNmr Analysis', *Acta Crystallographica Section D: Biological Crystallography*, 71, pp. 154–161. doi: 10.1107/S1399004714026662.

Song, X. *et al.* (2012) 'A novel membrane-dependent on/off switch mechanism of talin FERM domain at sites of cell adhesion.', *Cell research*, 22(11), pp. 1533–45. doi: 10.1038/cr.2012.97.

Srivastava, J. *et al.* (2008) 'Structural model and functional significance of pH-dependent talin-actin binding for focal adhesion remodeling.', *Proceedings of the National Academy of Sciences of the United States of America*, 105(38), pp. 14436–14441. doi: 10.1073/pnas.0805163105.

Stebbens, S. and Wittmann, T. (2012) 'Targeting and transport: how microtubules control focal adhesion dynamics.', *The Journal of cell biology*, 198(4), pp. 481–9. doi: 10.1083/jcb.201206050.

Sun, N. *et al.* (2008) 'Identification of a repeated domain within mammalian  $\alpha$ -synemin that interacts directly with talin', *Experimental Cell Research*, 314(8), pp. 1839–1849. doi: 10.1016/j.yexcr.2008.01.034.

Sun, Z. *et al.* (2016) 'Kank2 activates talin, reduces force transduction across integrins and induces

central adhesion formation', *Nature Cell Biology*, 18(9), pp. 941–953. doi: 10.1038/ncb3402.

Suzuki, K. *et al.* (2015) 'Identification of non-Ser/Thr-Pro consensus motifs for Cdk1 and their roles in mitotic regulation of C2H2 zinc finger proteins and Ect2', *Scientific Reports*. Nature Publishing Group, 5(1), p. 7929. doi: 10.1038/srep07929.

Tamkun, J. W. *et al.* (1986) 'Structure of integrin, a glycoprotein involved in the transmembrane linkage between fibronectin and actin', *Cell*. doi: 10.1016/0092-8674(86)90744-0.

ThermoFisher (2018) *Phosphorylation, Protein Biology Resource Library*. Available at: <https://www.thermofisher.com/uk/en/home/life-science/protein-biology/protein-biology-learning-center/protein-biology-resource-library/pierce-protein-methods/phosphorylation.html>.

Thompson, J. D., Gibson, T. J. and Higgins, D. G. (2002) 'Multiple sequence alignment using ClustalW and ClustalX.', *Current protocols in bioinformatics*, Chapter 2(23), p. Unit 2.3. doi: 10.1002/0471250953.bi0203s00.

Tibbitt, M. W. and Anseth, K. S. (2009) 'Hydrogels as extracellular matrix mimics for 3D cell culture', *Biotechnology and Bioengineering*. doi: 10.1002/bit.22361.

Tsukita, S. and Yonemura, S. (1999) 'Cortical actin organization: Lessons from ERM (ezrin/radixin/moesin) proteins', *Journal of Biological Chemistry*. doi: 10.1074/jbc.274.49.34507.

Tumbarello, D. A., Brown, M. C. and Turner, C. E. (2002) 'The paxillin LD motifs.', *FEBS letters*, 513(1), pp. 114–8. Available at: <http://www.ncbi.nlm.nih.gov/pubmed/11911889> (Accessed: 14 August 2016).

Turner, C. E. *et al.* (1999) 'Paxillin LD4 motif binds PAK and PIX through a novel 95-kD ankyrin repeat, ARF-GAP protein: A role in cytoskeletal remodeling', *Journal of Cell Biology*. doi: 10.1083/jcb.145.4.851.

Uhlén, M. *et al.* (2015) 'Tissue-based map of the human proteome', *Science*. doi: 10.1126/science.1260419.

van der Vaart, B. *et al.* (2013) 'CFEOM1-Associated Kinesin KIF21A Is a Cortical Microtubule Growth Inhibitor', *Developmental Cell*. Cell Press, 27(2), pp. 145–160. Available at: <http://www.ncbi.nlm.nih.gov/pubmed/24120883> (Accessed: 18 February 2018).

Vasiliev, J. M. *et al.* (1970) 'Effect of colcemid on the locomotory behaviour of fibroblasts', *J Embryol Exp Morphol*.

- Vinci, G. *et al.* (2007) 'Association of deletion 9p, 46,XY gonadal dysgenesis and autistic spectrum disorder', *Molecular Human Reproduction*. doi: 10.1093/molehr/gam045.
- Vinogradova, O. *et al.* (2002) 'A structural mechanism of integrin  $\alpha$ IIb $\beta$ 3 "inside-out" activation as regulated by its cytoplasmic face', *Cell*. doi: 10.1016/S0092-8674(02)00906-6.
- Vitour, D. *et al.* (2004) 'RoXaN, a novel cellular protein containing TPR, LD, and zinc finger motifs, forms a ternary complex with eukaryotic initiation factor 4G and rotavirus NSP3', *Journal of virology*. doi: 10.1128/JVI.78.8.3851.
- Vranken, W. F. *et al.* (2005) 'The CCPN data model for NMR spectroscopy: Development of a software pipeline', *Proteins: Structure, Function and Genetics*. doi: 10.1002/prot.20449.
- Wade, R., Brimer, N. and Vande Pol, S. (2008) 'Transformation by bovine papillomavirus type 1 E6 requires paxillin.', *Journal of virology*. doi: 10.1128/JVI.02747-07.
- Wang, J. H. (2012) 'Pull and push: Talin activation for integrin signaling', *Cell Research*. doi: 10.1038/cr.2012.103.
- Wang, P., Ballestrem, C. and Streuli, C. H. (2011) 'The C terminus of talin links integrins to cell cycle progression', *The Journal of Cell Biology*, 195(3), pp. 499–513. doi: 10.1083/jcb.201104128.
- Wang, Q. *et al.* (2003) 'Regulation of the formation of osteoclastic actin rings by proline-rich tyrosine kinase 2 interacting with gelsolin', *Journal of Cell Biology*. doi: 10.1083/jcb.200207036.
- Wang, S. *et al.* (2012) 'Tiam1 interaction with the PAR complex promotes talin-mediated Rac1 activation during polarized cell migration.', *The Journal of cell biology*. Rockefeller University Press, 199(2), pp. 331–45. doi: 10.1083/jcb.201202041.
- Weber, G. F., Bjerke, M. A. and DeSimone, D. W. (2011) 'Integrins and cadherins join forces to form adhesive networks', *Journal of Cell Science*. doi: 10.1242/jcs.064618.
- Wegener, K. L. and Campbell, I. D. (2008) 'Transmembrane and cytoplasmic domains in integrin activation and protein-protein interactions (Review)', *Molecular Membrane Biology*. doi: 10.1080/09687680802269886.
- Wehrle-Haller, B. (2012) 'Assembly and disassembly of cell matrix adhesions', *Current Opinion in Cell Biology*. doi: 10.1016/j.ceb.2012.06.010.
- Willour, V. L. *et al.* (2004) 'Replication study supports evidence for linkage to 9p24 in obsessive-



compulsive disorder.', *American journal of human genetics*, 75(3), pp. 508–13. doi: 10.1086/423899.

Wood, D. J. and Endicott, J. A. (2018) 'Structural insights into the functional diversity of the CDK–cyclin family', *Open Biology*. doi: 10.1098/rsob.180112.

Xu, D. *et al.* (2018) 'Repression of Septin9 and Septin2 suppresses tumor growth of human glioblastoma cells', *Cell Death & Disease*. Nature Publishing Group, 9(5), p. 514. doi: 10.1038/s41419-018-0547-4.

Yan, J. *et al.* (2015) 'Talin Dependent Mechanosensitivity of Cell Focal Adhesions', *Cellular and molecular bioengineering*. Springer, 8(1), pp. 151–159. doi: 10.1007/s12195-014-0364-5.

Yang, J. *et al.* (2014) 'Conformational activation of talin by RIAM triggers integrin-mediated cell adhesion', *Nature Communications*. Nature Publishing Group, 5, p. 5880. doi: 10.1038/ncomms6880.

Yang, V. W. (2018) 'The Cell Cycle', in *Physiology of the Gastrointestinal Tract: Sixth Edition*. doi: 10.1016/B978-0-12-809954-4.00008-6.

Yao, M. *et al.* (2014) 'Mechanical activation of vinculin binding to talin locks talin in an unfolded conformation', *Scientific Reports*. Nature Publishing Group, 4(1), p. 4610. doi: 10.1038/srep04610.

Yao, M. *et al.* (2016) 'The mechanical response of talin', *Nature Communications*. Nature Publishing Group, 7, p. 11966. doi: 10.1038/ncomms11966.

Zacharchenko, T. *et al.* (2016) 'LD Motif Recognition by Talin: Structure of the Talin-DLC1 Complex.', *Structure (London, England : 1993)*. Elsevier, 24(7), pp. 1130–41. doi: 10.1016/j.str.2016.04.016.

Zaidel-Bar, R. *et al.* (2007) 'Functional atlas of the integrin adhesome', *Nature Cell Biology*, 9(8), pp. 858–867. doi: 10.1038/ncb0807-858.

Zamir, E. *et al.* (2000) 'Dynamics and segregation of cell-matrix adhesions in cultured fibroblasts', *Nature Cell Biology*. doi: 10.1038/35008607.

Zhang, F., Saha, S. and Kashina, A. (2012) 'Arginylation-dependent regulation of a proteolytic product of talin is essential for cell-cell adhesion.', *The Journal of cell biology*. The Rockefeller University Press, 197(6), pp. 819–36. doi: 10.1083/jcb.201112129.

Zhang, X. *et al.* (2008) 'Talin depletion reveals independence of initial cell spreading from integrin

activation and traction.', *Nature cell biology*. NIH Public Access, 10(9), pp. 1062–8. doi: 10.1038/ncb1765.


Zhou, Y. *et al.* (2016) 'The emerging roles and therapeutic potential of cyclin-dependent kinase 11 (CDK11) in human cancer.', *Oncotarget*. Impact Journals, LLC, 7(26), pp. 40846–40859. doi: 10.18632/oncotarget.8519.

Zhu, Y. *et al.* (2008) 'Kank proteins: a new family of ankyrin-repeat domain-containing proteins.', *Biochimica et biophysica acta*. Elsevier, 1780(2), pp. 128–33. doi: 10.1016/j.bbagen.2007.09.017.

# Chapter 9. Appendix

---

## The tale of two talins – two isoforms to fine-tune integrin signalling

Rosemarie E. Gough and Benjamin T. Goult 

School of Biosciences, University of Kent, Canterbury, UK

### Correspondence

B. T. Goult, School of Biosciences,  
University of Kent, Canterbury CT2 7NJ, UK  
Tel: +44 1227 816142  
E-mail: b.t.goult@kent.ac.uk

[Received 16 March 2018, revised 12 April  
2018, accepted 26 April 2018, available  
online 16 May 2018]

doi:10.1002/1873-3466.13061

Edited by Wilhelm Just

**Talins** are cytoplasmic adapter proteins essential for integrin-mediated cell adhesion to the extracellular matrix. Talins control the activation state of integrins, link integrins to cytoskeletal actin, recruit numerous signalling molecules that mediate integrin signalling and coordinate recruitment of microtubules to adhesion sites via interaction with KANK (kidney ankyrin repeat-containing) proteins. Vertebrates have two talin genes, *TLN1* and *TLN2*. Although talin1 and talin2 share 76% protein sequence identity (88% similarity), they are not functionally redundant, and the differences between the two isoforms are not fully understood. In this Review, we focus on the similarities and differences between the two talins in terms of structure, biochemistry and function, which hint at subtle differences in fine-tuning adhesion signalling.

**Keywords:** integrin; mechanobiology; talin

### Integrin adhesions: linking the cell to the extracellular matrix

Integrin-mediated adhesions to the extracellular matrix (ECM) are found in nearly all cell types and mediate a diverse range of functions. There are 24  $\alpha\beta$  heterodimeric integrins, which show distinct patterns of cell-type and tissue-specific expression, and support different forms of cell-ECM and cell-cell attachment. Integrins connect to the ECM via their large extracellular domains but, in contrast, the cytoplasmic domains, the 'integrin tails', are generally short (~40–60 amino acids). Despite this diminutive size, large multiprotein complexes assemble on the cytoplasmic face of integrins, providing linkages to the cell cytoskeleton and to numerous intracellular signalling pathways.

The complexity of cell-matrix adhesions has been highlighted by the analysis of the 'integrin adhesome' using mass spectrometry on multiple integrin adhesion complexes. This identified a network of > 240 proteins [1,2], and additional adhesome proteins are constantly being discovered, many of which are cytoplasmic

components that couple adhesions to numerous signalling cascades. These enable diverse intracellular responses, a process often referred to as 'outside-in' signalling. These signalling hubs regulate a multitude of cellular processes including cytoskeletal dynamics and cell motility, cell growth, survival and the cellular response to the local environment. Unsurprisingly, numerous diseases arise from the defects in components of the integrin adhesome [3]. Further analysis of integrin adhesome datasets collected under different conditions has revealed the dynamic nature of these complexes, and the functional diversity that can derive from the same building blocks. What emerges is a consensus adhesome of ~60 proteins centred around four axes comprising: ILK-PINCH-kindlin, FAK-paxillin, talin-vinculin and  $\alpha$ -actinin-zyxin-VASP, although it seems likely that all of these axes are linked to talin in some way. As well as 24 different integrins, vertebrates also have two major talin isoforms: talin1 and talin2.

Most of the attention on talin has focused on talin1, primarily due to its essential role in mediating cell

### Abbreviations

ABS, actin-binding site; DD, dimerisation domain; ECM, extracellular matrix; FA, focal adhesion; FERM, 4.1 protein, ezrin, radixin, moesin; IBS, integrin-binding site; IF, intermediate filament; PTM, post-translational modification; VBS, vinculin-binding site.

2108

FEBS Letters 592 (2018) 2108–2126 © 2018 Federation of European Biochemical Societies  
This is an open access article under the terms of the Creative Commons Attribution License, which permits use, distribution and reproduction in any medium, provided the original work is properly cited.

adhesion as shown by studies on talin1 knockout [4] and talin1-depleted cells [5–7]. Talin1 knockout is also embryonic lethal in mice due to arrested gastrulation, indicating a key role in early development [4]. In contrast talin2, which was only discovered following publication of the human genome sequence [8,9] has received less attention, and the fact that talin2 knockout mice are viable and fertile [10] suggests isoform redundancy. However, talin2 knockout mice display a mild dystrophic phenotype and the variability in the number of pups surviving to adulthood suggest underlying defects [10]. Therefore, it appears that talin2 plays important roles in development although many of its functions can be compensated for by talin1.

This Review aims to summarise what is currently known about the structural, biochemical and functional differences between the two talin isoforms. Evolutionary genomics has been used to study talin isoforms in the past, and here, we combine genetic analysis with the recent wealth of structural information to highlight the emerging functions of the two talins as signalling platforms.

### Integrin–talin–actin: the core of cell–matrix adhesions

Strikingly, despite the structural complexity of cell–ECM adhesions, the majority of these dynamic adhesion complexes comprise a simple and robust core of three proteins: talin which binds to and activates integrins and couples them to the actin cytoskeleton (Fig. 1). All of the other components can be assembled on to this framework to give rise to various types of adhesive structures. Once formed, the protein vinculin is recruited to the complex to stabilise the connection to actin, a process which is regulated by an elegant feedback mechanism. Thus, vinculin is only recruited when talin experiences mechanical force, and force will only be exerted when talin is successfully bound to an integrin *and* coupled to actin. If these conditions are not met, then nascent adhesions will not experience sufficient force to recruit vinculin and will disassemble. However, once vinculin is recruited to nascent adhesions, it crosslinks talin to actin, and the core, linkages are stabilised. How such complexes mature depends on multiple variables including cell type, ECM composition, matrix stiffness, integrin subtype, mechanical signals, etc. This leads to the development of a variety of adhesion complexes including nascent adhesions, focal adhesions (FAs), fibrillar adhesions, podosomes, invadopodia, etc., all of which have at their core the same integrin–talin–actin connection. In their recent Review, Klapholz and Brown eloquently describe the

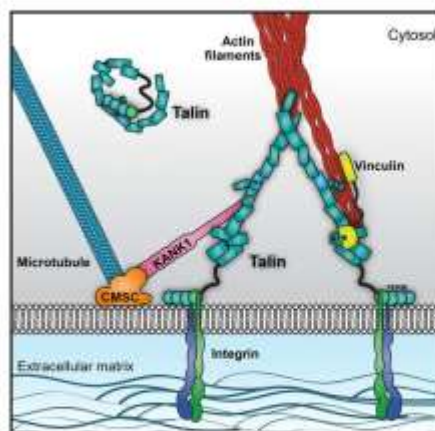


**Fig. 1.** Talin at the core of the adhesion. A cartoon of the core of integrin adhesions, highlighting talin's central role. Talin coordinates both the actin cytoskeleton, and through the interaction with KANK proteins, the microtubule cytoskeleton at adhesion sites. Once the adhesion core is assembled, talin serves as a scaffold to recruit many other proteins in order to form all the many different types of adhesive structures (focal adhesions, podosomes, invadopodia, etc.).

myriad of different roles that talin plays in adhesion, and provocatively call talin 'the master of integrin adhesions', a view we share [11].

### The talins

Talin is a large 270 kDa actin-binding protein that was first discovered in 1983 as a component of FAs and ruffling membranes [12]. Talin comprises an N-terminal FERM domain (the head) coupled to a flexible talin rod. Since then, it has been shown to be a key component of integrin adhesions with roles in integrin activation [13], the molecular clutch that couples integrins to cytoskeletal actin [14], FA assembly and the recruitment of numerous signalling molecules [15]. Talins also interact with the KANK family of adapter proteins [16,17] which target microtubules to adhesion sites, stimulating FA turnover [18]. As well as transmitting forces between integrins and the actin cytoskeleton, the length of talin has been shown to define the geometry of the adhesion [19], and talin plays a key role as a mechanosensitive adapter, undergoing force-dependent conformational transitions in its 13 rod domains [20–24] that modulate binding interactions with mechanosensitive ligands. Given the above, it is unsurprising that talin1 knockout in mice is embryonic lethal [4,25].



Tissue expression and cellular localisation vary considerably between the two isoforms; talin1 is expressed in all tissues. In contrast, talin2 expression is more variable, and it is absent entirely from some cell types, for example, no talin2 is present in endothelial cells possibly via silencing of the *Tln2* gene by promoter methylation [26,27]. The Human Protein Atlas [28] shows the near ubiquitous expression of talin1 in all cell types in all tissues, whereas the high levels of talin2 are found mainly in the brain, particularly the cerebral cortex, heart muscle and the kidney.

There is clear interplay in the expression of the two talin isoforms, although the mechanism for this is not known. Talin2 expression is rapidly upregulated following knockout of talin1, both transiently [26] and also in *Tln1*-knockout mouse embryonic fibroblasts [7] leading to rescue of many of the consequences of the loss of talin1. However, knockout of both talin isoforms completely ablates cell-ECM adhesion [5], confirming the essential role of talins in integrin biology.

In fibroblasts, both talins localise to FAs, and talin1 is recruited directly to the leading edge, via proteins like the Rap1 effector RIAM (Rap1-interacting adapter molecule) [29,30] and FAK (focal adhesion kinase) [31]. In contrast, less is known about talin2 recruitment. Although talin2 binds to RIAM, talin2-specific antibodies reveal that talin2 forms diffuse aggregates throughout the cell, which overtime coalesce to form larger complexes, either at focal or fibrillar adhesion sites [25]. For the most part, only talin2 is found at fibrillar adhesions in the centre of the cell [25]. This localisation positions talin2 at sites of fibronectin accretion and assembly [32] and also to formation of invadopodia [33]. Although much less is known about the role of talin2, it has recently been the subject of increased interest and isoform-specific functionalities have been reported. For example, talin2 has been reported to be indispensable for the generation of traction force and invadopodium-mediated matrix degradation required for invadopodia formation [33]. Furthermore, talin2 has been shown to be able to recruit vinculin in the absence of mechanical force suggesting different mechanical properties [34]. In summary, the relative roles of talin1 and talin2 remain to be fully elucidated.

## Structure of talin 1 and 2

### Gene structure and splice variation in talins

The two talins are encoded by separate genes, *Tln1* and *Tln2*, which have conserved intron-exon boundaries [9,35]. However, whereas talin1 has relatively

small introns resulting in a gene of ~30 kb, talin2 is much bigger (~190 kb), due to the presence of much larger introns. Moreover, initial studies suggest that multiple talin2 isoforms are generated via differential splicing [36]. While the function of these isoforms is currently unknown, the expression pattern of each is distinct. Testes, kidney and brain express short C-terminal proteins lacking the FERM domain [36] raising the possibility that such variants might function independent of integrins, although they do contain the integrin-binding site located in the rod domain. Intriguingly, expression of a C-terminal talin1 fragment resembling the testes-specific talin2 isoform was sufficient to rescue cell cycle progression in talin1-depleted cells suggesting a role in cellular signalling [37,38].

The ancestral *Tln* gene appears to have undergone duplication in chordates with the emergence of vertebrates to give rise to talin1 and talin2 [39]. Invertebrates and simple chordates have a single talin gene; vertebrates have two. Chordates can be divided into three major groups: Craniata (including the vertebrates), Cephalochordata (including the lancelets) and Tunicata (including sea squirts). Since the original publication on talin evolution [39], the genomes of *Petromyzon marinus* (one of the Cyclostomata, a jawless vertebrate) [40] and *Branchiostoma floridae* (a lancelet, one of the Cephalochordata) [41] have been published. Strikingly, the *Branchiostoma* has only a single talin, whereas the *Petromyzon* genome encodes two. This confirms and extends the original conclusions about talin evolution [9,39] and suggests that the genome duplication leading to present day talin1 and talin2 took place before the divergence of jawed and jawless vertebrates, but after (or with) the divergence of the craniates from other chordates. The acquisition of two different copies of talin appears to be beneficial to an organism; talin gene duplication has also occurred in Amboebozoa and in *Dictyostelium discoideum*. The *Dictyostelium* talin genes, *TalA* and *TalB*, encode proteins with distinct functions, with *TalA* required for cell-substrate adhesion, phagocytosis and cytokinesis, and *TalB* required for the force transmission required to support morphogenetic movements during differentiation [42].

### Talin domain structure

Remarkably, despite millions of years of evolutionary time since talin first appeared and since the two talins diverged, the length of both the major talin isoforms has remained almost identical (talin1: 2541aa; talin2: 2540aa). Furthermore, both major isoforms have

identical domain structure and contain 18 domains. This invariability is in stark contrast to many other multidomain proteins such as titin, spectrin and filamin – these have varied in length, increasing and decreasing in size through evolution until reaching the length we see today [43–45]. This unvarying domain arrangement in all available talin sequences suggests that each domain has a role that is universally required (it is worth mentioning that in some nonvertebrate organisms, including *Dictyostelium* and *Drosophila*, talin has acquired additional C-terminal residues that extend beyond the universal domain arrangement [39,46]). The following discussion of talin domain structure, therefore, applies to both talin1 and talin2.

### The talin head

Talins consists of an atypical N-terminal FERM (4.1 protein, ezrin, radixin, moesin) domain, known as the talin head containing four subdomains F0–F3 [47,48] rather than the three subdomains (F1–F3) found in most other FERM domain proteins. Moreover, the crystal structure of the talin1 FERM domain shows a linear domain structure [47] rather than the cloverleaf structure found in other FERM domain proteins. The structure of the talin2 FERM domain confirms this linear domain arrangement (our unpublished data). Extensive studies show that it is the talin F3 subdomain that directly engages the beta-integrin cytoplasmic tail via the first (membrane proximal) of two NPxY motifs in the tail [49]. The integrin-binding interfaces have been characterised in both the talin1 and talin2 F3 subdomains, and this has revealed that conserved residue changes in the binding surfaces tune the affinities of the two talins for different integrin tails [50]. For example, the ubiquitous beta1a-integrin was recently shown to bind preferentially to talin2 [51] whereas the muscle-specific beta1d-integrin has a threefold higher preference for talin2 over talin1 [33,52,53]. This provides selectivity for different talin and integrin complexes, and different couplings are likely to regulate different cellular functions [54].

However, whilst F3 is the only talin head subdomain that engages the integrin, F3 in isolation is not very effective at activating integrins and the other head subdomains are also required to make an effective 'integrin activation lock' and maintain the integrin in the active, high-affinity conformation [55]. The other head subdomains achieve this by interaction with phosphoinositides such as  $\text{PtdIns}(4,5)\text{P}_2$  (PIP2) in the plasma membrane; a basic surface on the F2 subdomain mediates interaction with the

plasma membrane, which applies torque on the integrin to stabilise the active conformation [52,56,57]. In addition, the F1 subdomain contains a large (~30aa) unstructured insertion, the F1-loop, which, via a cluster of positively charged residues, interacts with PIP2 and is essential for integrin activation [58]. The F0 subdomain has been shown to bind the membrane-tethered small GTPase, Rap1 [58–60] and this interaction has been implicated in membrane targeting of talin to the plasma membrane [59]. Interestingly, the additional F0 subdomain and the F1-loop elements of the talin FERM domain are also found in the kindlin family of proteins [58,61] which synergise with talin to activate integrins [62]. These features are not found in other FERM domain proteins and are unique to integrin-activating FERM domain proteins.

As well as binding to integrins, Rap1 and the membrane, the talin head (via the F3 subdomain) has been shown to bind to PIP kinase gamma [63], which is thought to generate the PIP2 required to support integrin activation [64]. Beyond this, the F3 subdomain has emerged as showing remarkable ligand-binding plasticity and has been linked to binding FAK [31], TIAM1 (T-cell lymphoma invasion and metastasis 1) [65], layilin [66], Gα13 (G-protein subunit *Gα13*) and RIAM [67] all via the same site. The hierarchy of these interactions, that are presumably mutually exclusive with integrin binding and each other, is not yet fully understood. Talin contains three actin-binding sites (ABS1–3) [68]. ABS1 is in F2–F3 in the talin head [69] and has recently been shown to be important for capping actin filaments to block actin polymerisation [70].

### The talin rod

The talin head is connected, via an 82-amino acid unstructured [71] calpain-sensitive linker [72,73] to the large 2000 residue talin rod that is made up of 62  $\alpha$ -helices. We have recently determined the boundaries and structures of the talin1 rod domains showing it contains 13 domains (R1–R13) [24] organised into two functionally distinct regions, a linear C-terminal rod-like region comprised of 5-helix bundles and a compact N-terminal region where three 4-helix bundles (R2–R4) are inserted into the series of 5-helix bundles (Fig. 2b).

Structural analysis of the talin rod was complicated as only two regions of the rod have sequence homology to other proteins: R13, which contains an I/LWEQ domain [8,74], and the central region of the rod (resolved to be R7–R8) which has homology to a

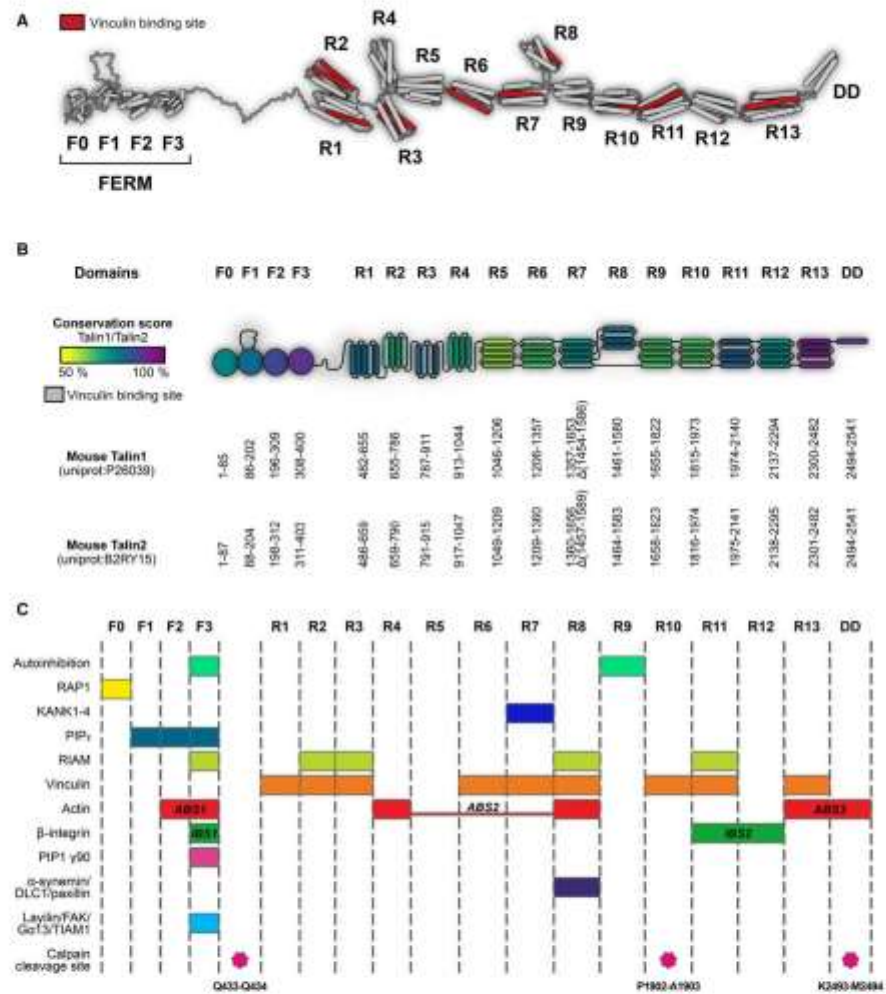


**Fig. 2.** Structure and domain map of the two talin isoforms. (A) Structural model of talin showing the domain arrangement of talin. Vinculin-binding sites are shown in red. The N-terminal talin head comprising F0-F3 and the talin rod domains R1-R13 are shown. (B) Schematic representation of the talin domain structures coloured by sequence-identity between the two isoforms. The domain boundaries are given for mouse talin1 (UniProt: P26039) and talin2 (UniProt: Q2RY15). Provided that these boundaries are used, it is possible to make any talin fragment or delete any talin domain while maintaining the structural integrity of the protein. (C) The locations of many of the talin ligand-binding sites are shown, as are the calpain cleavage sites.

protein of unknown function, MESDC1 [75]. The rest of the rod lacks homology to other proteins meaning prediction of the domain boundaries *a priori* was not

possible. Part of the reason for the lack of homology of the talin rod to other proteins turned out to be that 8 of the 13 talin rod domains – R1, R5–R7, R9–R12 –



contain a 5-helix bundle fold, the 'talin rod fold', that has so far only been recognised in talin.

#### The talin rod fold

Although 4-helix bundles are common in nature (the 4-helix up-down bundle present in R2, R3, R4 and R8 is a common fold (SCOP 47161 [76])), 5-helix bundles are unusual. At the core of the talin rod fold is a common 4-helix up-down, left-handed twist topology as seen in numerous 4-helix bundles. However, in the talin rod, this fold is augmented by an extra N-terminal helix, connected by a long (~9 residue) loop that allows the first helix to pack against helices 3 and 4 of the bundle (Fig. 2) to form a 5-helix bundle. This addition of an extra helix to the talin rod domains has profound effects on talin function, not least because 5-helix bundles, where the N- and C-termini are located at opposite ends of the bundle are optimal for forming a rod-like arrangement (Fig. 2). The linear rod-like region is perfectly designed to transmit forces, which act on the compact N-terminal region. Furthermore, the additional helix significantly enhances the thermal and mechanical stability of the domains [22,77], helping provide different mechanical responses for each domain [21] and restricting access to the cryptic vinculin-binding sites (VBS) buried inside many of the domains. As a result, each rod domain has its own unique properties, and this is central to talin's role as a mechanosensor (see next section). Unfolding 5-helix bundles by pulling on the termini positioned at opposite ends of the bundle is restricted by extensive contacts throughout the length of the helices and requires a gradual breaking of hydrogen bonds. In 4-helix bundles, the termini are at the same end, and applied force acts on the weak hydrophobic contacts, peeling helices away from the bundle [22].

#### Talin dimers

Full-length talin is dimeric, and helix 62 (dimerisation domain (DD)) forms an antiparallel dimer with another talin molecule [74]. In all our experiments to date, we see talin as a constitutive dimer when the DD is present; however, a calpain cleavage site immediately prior to the DD means it can be cleaved to yield monomeric talin [71]. Interestingly, the DD in talin2 is conserved with talin1, and structural predictions suggest it should be able to form heterodimers. However, to our knowledge, heterodimers have not been described in the literature. Dimeric full-length talin1 can adopt a compact autoinhibited conformation in the cytosol [78] where the two rod domains wrap around to form a 'double donut'

with the two talin heads buried inside. Activation of talin to a more open-active conformation requires a variety of activators.

#### Talin1 and talin2 rod interactions

To date, all the ligands that bind to talin1 have been shown to bind talin2 although the affinities for the different isoforms can be markedly different. Binding partners can interact with the talin rod domains via a number of different modes, that is, to the folded rod domains, to the unfolded rod domains or to some strained conformation between these two extremes. Mechanical force can drive transitions between these conformations and so dramatically alter the binding affinities of different ligands.

#### Ligand-binding sites in the talin rod

Elucidation of the domain structure of the talin rod has enabled the precise mapping of established ligand-binding sites, and the location of these sites is shown in Fig. 2.

#### Integrin

As well as interacting with the talin head, the beta-integrin tail also interacts with the R11-R12 domains of the talin rod [integrin binding site 2 (IBS2)] via a structurally undefined mechanism [79-81]. Unlike IBS1 where the integrin binds to the folded F3 subdomain, integrin binding to IBS2 appears to involve some intermediate conformation of the rod domains (integrin does not bind folded or unfolded R11-R12). The role of IBS2 in flies [79,82] has been well established, but its role in mammals is less clear, although it has been linked to nascent adhesion formation [83].

#### Actin

The talin rod contains two actin-binding sites, ABS2 (R4-R8) [68,84,85] and ABS3 (R13-DD) [8,86] which play different roles in adhesion. The current model of talin function envisages the C-terminal ABS3 [74] as responsible for the initial force exerted on talin that leads to unfolding of the mechanosensitive talin rod domain, R3. This triggers vinculin interactions and leads to adhesion maturation [23]. In contrast, ABS2, in the centre of the rod provides the tension-bearing actin connection [84,85]. As with the integrin connections, the actin-binding sites in talin2 bind more tightly to actin than the equivalent regions in talin1 ([35] and our unpublished data).

### Vinculin

Vinculin, discovered in 1979 [87], is another key talin interactor, and has been shown to bind to at least 11 of the 62 talin1 helices [88]. The vinculin-binding determinants lay on one side of each vinculin-binding helix [89]. However, the VBS are buried within the rod domains and are only exposed by mechanical force (Fig. 3), enabling vinculin to bind and strengthen the actin connection. It has been shown that exposed talin VBS can activate vinculin [90], and active vinculin has been shown to be able to activate talin [91]. The 11 VBS in talin2 are all conserved and so it is likely that the talin2 rod will also engage vinculin in a similar fashion.

### Other interactors

While the integrin-, actin- and vinculin-binding interactions define the primary adapter function of talin, there are an increasing number of additional ligands that bind to the talin rod that contribute to its mechanosignalling capabilities. These are summarised below.

### Talin binds LD-motif-containing proteins

A common mechanism for talin rod-binding proteins is via helix addition, whereby a helix from a ligand packs against the side of a talin rod domain. A number of talin ligands have now been identified that contain an 'LD-motif' [92] that mediates such helix addition. First identified in paxillin [93], amphipathic LD-motif helices bind via the aspartate (D) which forms an initial salt bridge with a basic residue at the beginning of the furrow between two adjacent helices of the interacting bundle. Specificity is then encoded by residues downstream of the 'LD' interaction site. This mode of binding to talin was initially identified from work on the tumour suppressor protein deleted in liver cancer 1 (DLC1) [94,95]. This led on to the identification of the talin-binding sequence in RIAM [24,29] as an LD-motif, and the identification of paxillin as a novel talin ligand [94]. More recently, the KANK (kidney ankyrin repeat-containing) proteins have been identified as LD-motif-containing ligands [16,17], binding to a conserved face on the R7 5-helix bundle. The ability of 5-helix bundles to bind

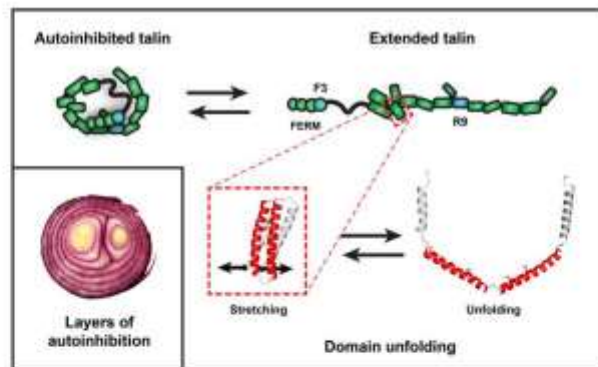


**Fig. 3.** Layers and layers of autoinhibition. A striking feature of talins is their remarkable conformational plasticity that enables different ligands to engage the same platform in different conditions; part of this flexibility emerges from autoinhibition. (Left) In the closed autoinhibited form, all of the domains are folded, and many of the ligand-binding sites for actin, integrin and vinculin are thought to be cryptic. Some binding sites may face outwards and remain accessible; for instance, RIAM is able to bind to the inactive conformation [127]. In the extended conformation in the absence of force, all the domains are still folded, and additional binding sites are exposed (BS1, BS2, ABS3, plus the sites for those ligands that require folded-rod domains) (Right). The exposure of BS1 and ABS3 facilitates adhesion formation, and by activating integrins and crosslinking them to the actin cytoskeleton, a nascent adhesion can form. As force is exerted on talin, another layer of autoinhibition is uncovered (Bottom). As talin domains unfold, starting with R3, the *in situ* mechanosensor in talin [21,23,24], vinculin-binding sites are exposed and talin/vinculin interactions can now occur. R3 unfolding also reveals the high affinity actin-binding site in talin, ABS2 that can then activate tension-bearing actin connections [84,85]. As domains unfold, the binding sites for ligands that engage the folded rod domains are destroyed, as is the case for RIAM binding to R3. A remarkable feature of talins conformational plasticity is that, in the absence of other factors, talin can readily refold to its default low-force state.

LD-motif proteins greatly expands the number of potential ligand-binding sites in talin.

#### The talin-moesin-NHE-1 complex and pH modulation of adhesion sites

The C-terminal part of the talin rod has also been shown to bind directly to the FERM domain of moesin, an interaction that is required to recruit the sodium/hydrogen exchanger (NHE-1) to adhesion sites [96]. This recruitment of a proton exchanger to adhesions and the resulting localised alterations of intracellular pH has a dramatic effect on adhesions. Small changes in local pH can result in protonation/deprotonation of side chains, particularly histidines, and this can directly alter interactions in a similar fashion to phosphorylation. In many ways, protonation can be considered a post-translational modification [97]. Many important protein:protein interactions have been shown to be regulated by pH in this way, including the interaction of talin ABS3 with actin [98], and it is likely that local fluctuations in pH will alter the protonation state of many other important interaction sites.

#### The talin- $\alpha$ -synemin connection – a link to intermediate filaments?

Another ligand that has been linked to talin which has the potential to have a significant impact on our view of adhesions is  $\alpha$ -synemin [99], an intermediate filament (IF) protein expressed in skeletal muscle. This suggests that talin has the potential to coordinate interactions between the actin, microtubule and IF networks.

#### The mechanical properties of talin

The mechanosensing abilities of talin rely on its force-dependent interactions with its binding partners. Some ligands (i.e. RIAM, KANK, DLC1, actin) bind only to folded talin domains, whereas vinculin is known to require domain unfolding and exposure of cryptic VBS. Force-induced talin domain unfolding will therefore release binding partners that bind to folded talin and stimulate binding of vinculin, triggering mechanosensing signals. *In vivo*, talin is initially extended by actin retrograde flow and then by actomyosin contractility and the resulting forces exerted on the talin rod drive structural transitions. Depending on the precise mechanical environment, individual talin molecules will experience different forces, and the different conformations may engage different ligands.

#### Mechanotransduction: force driving changes in biological signalling

The mutually exclusive interactions between talin and RIAM and talin and vinculin provide the perfect example of how talin can convert mechanical forces into biological signalling responses. The initial mechanosensitive domain in talin has been shown to be R3 [23,24], which binds RIAM but also contains two VBS. However, vinculin and RIAM have fundamentally different modes of binding. Talin VBS are buried within the talin rod domains and are only exposed when mechanical force unfolds that domain, allowing vinculin to bind. In contrast, the talin-binding sites in RIAM are single helices that interact only with folded talin rod domains (Fig. 2). The exquisite mechanosensitivity of R3 is due to the presence of a destabilising cluster of threonine residues buried in its hydrophobic core [24]. This means that the R3 domain is the first to unfold when talin experiences force, driving the transition between folded and unfolded R3 (this is one of the exciting aspects of structural mechanobiology in that the precise structural basis of a mechanosensitive event can be pinpointed to specific amino acids that encode the mechanosensitivity). This conformational change in R3 drives a change in biological signalling, displacing RIAM and thus the link to the Rap1 signalling pathways. Simultaneously, R3 unfolding leads to the recruitment of vinculin and strengthening of the connection to actin. This allows two different ligands to engage the same talin domain under different conditions and explains the different localisation of RIAM and vinculin in cells [100]. In the case of R3, a force of  $\sim 5$  pN is required for it to unfold, disrupting the RIAM-binding sites and recruiting vinculin, driving the maturation of nascent adhesions into FAs. This 5 pN force is roughly the force of a single actomyosin contraction, leading to an attractive hypothesis that talin only experiences this force threshold when it binds to an integrin and simultaneously connects to the actin cytoskeleton. Only when these two criteria are met will the R3 domain unfold and trigger adhesion maturation.

Expanding this to the rest of the talin rod, it seems likely that each of the talin rod domains can also serve as mechanochemical switches, and under different conditions, individual talin rod domains can adopt different conformations that support different signalling pathways. *In vivo* measurements of talin extension have shown that talin length is normally between 90 and 250 nm [101] (compared with a folded talin length of 50–60 nm *in vitro* [102]), suggesting that between two and eight talin rod domains are unfolded at any



time [21]. Using single molecule analysis with ultra-stable magnetic tweezers, we recently characterised the mechanical response of talin1 [21–23]. Stretching the whole talin rod revealed quantised mechanical responses with all 13 rod domains exhibiting switch-like behaviour at different force thresholds. These unfolding responses range from ~5 to 25 pN and are all rapidly reversible when force is removed. This reveals a spectrum of mechanosensitive switching events, turning on and off distinct effector functions in a force-dependent manner. This stochastic force-dependent folding and refolding of talin also make talin an effective force buffer protecting adhesions against excessive force [21].

The R8 domain is a hotspot for protein interactions, suggesting it represents a major signalling hub. R8 is a 4-helix bundle, uniquely protected from mechanical force by being inserted into the loop of a 5-helix bundle (R7), creating a novel 9-helix module, and a branch in the talin rod [21,75] (Fig. 2). By being positioned outside of the force-bearing region, R8 remains folded whilst talin is under force and maintains its ligand-binding surface.

A striking feature of the talin rod's response to force is that even after complete unfolding, the removal of force leads to refolding to the original native state, and this response is maintained through multiple cycles of extension and relaxation. The robustness of the mechanical response of the talin rod is perfectly suited to its role as a mechanosensor; when the mechanical force is relieved, the sensor reverts back to its original state.

Together, these features suggest that talins can sense and respond to mechanical forces with remarkable versatility. Depending on the applied force, different domains will unfold, and depending on the repertoire of expressed ligands, different signals will be generated. Depending on the mechanism of linkage to actin (e.g. via ABS2 vs. ABS3), or to microtubules via KANK, different regions of talin will be under tension. This network of protein interactions thus provides a mechanism for context and force-dependent regulation of multiple signalling pathways.

It will be important to characterise the mechanical response of talin2 as differences in mechanical responses of individual rod domains might help pinpoint sites of functional divergence. Recent work has shown that the two talins provide different mechanical linkages in cells [34], with talin2 able to engage vinculin in the absence of mechanical force, suggesting that the two proteins respond to forces differently. Talin2 is expressed at high levels in cardiac and skeletal muscle [103] where presumably its higher affinity

for integrin  $\beta$ tail and actin may serve to create more resilient adhesive connections.

#### Talin: layers and layers of autoinhibition

An interesting feature of talins is that the binding sites described above are not all accessible all of the time. Talin activity is regulated by multiple layers of autoinhibition where binding sites are masked, and only made available for binding in response to different signals. Talin autoinhibition mediated via the interaction between the integrin-binding site in F3 and the talin rod domain R9 maintains talin in a compact cytosolic form [104–107]. The F3-binding surface on talin2 R9 is highly conserved with only subtle conservative changes, and as such autoinhibition is likely common to both talins. Multiple factors (e.g. PIP2, FAK, Vinculin, RIAM, etc.) have been implicated in relieving talin autoinhibition, most recently, the G-protein Gz13 which binds F3, displacing the R9 rod domain, has emerged as an important talin regulator [108]. Once autoinhibition is relieved, it is likely that some of talin's functionalities are exposed, such as the integrin- and membrane-binding sites on the talin head [52,109], and the C-terminal actin-binding site ABS3 [8,74]. However, other functions are still autoinhibited; for example, the VBS remain inaccessible, buried in the hydrophobic core of the rod domains. As mechanical force is exerted on talin, its rod domains can unfold, exposing VBS and simultaneously destroying the binding sites for folded rod binders, enabling mechanochemical switching of binding. In this scenario, once RIAM has served its purpose and helped translocate talin to the plasma membrane, its binding to talin is no longer required and so these domains are repurposed for alternative functions. Furthermore, high affinity actin binding is mediated via the central actin-binding site (ABS2; R4–R8) which is maintained in an inactive conformation via the inhibitory effects of the adjacent R3 and R9 domains [84]. As a result of this stratified nature of talin autoinhibition, the same protein scaffold can coordinate many different processes. There are likely numerous other talin functions tightly regulated by talin conformation in a similar fashion.

#### Comparison of the talin1 and talin2 domains

Due to the high homology between talin1 and talin2, we used Modeller [110] to generate structural models of the talin2 domains using the talin1 structures as templates. Validation of the conserved hydrophobic cores of these domains and comparison of the

modelled F2F3 region of talin2 with the known structure [52] confirmed the reliability of this modelling approach. The domain boundaries of talin1 and talin2 are shown in Fig. 2. From this bioinformatics analysis, we have designed and validated expression constructs to express and purify each of the talin2 domains (deposited in Addgene [www.addgene.org/ben\\_goult](http://www.addgene.org/ben_goult)). We have recently solved the structures of a number of these talin2 rod domains and it is striking how structurally similar they are to the equivalent talin1 domains (our unpublished data).

#### Conserved differences between the two isoforms

The two talins are highly conserved (76% identical), and it is likely that identical regions between the two isoforms carry out equivalent functions. What has not been explored in detail is the 24% of the sequence that is not identical – it is here that differences in isoform function might be found. In particular, we sought to identify conserved differences between the isoforms in these divergent regions as these might provide the key to understand the differences in isoform function. We set out to look at differences in ligand specificity, affinity tuning, tertiary structure and the conservation of post-translational modification sites (PTMs).

We used BlastP to align the sequences of the corresponding domains from each isoform to establish the identity and similarity of each domain and to look for local variations. Interestingly, although the sequence identity between the two talins is 76%, sequence identity at the domain level shows much greater variation. The F2 (86%), F3 (89%) and R13 (92%) are highly conserved between isoforms, supporting their role in assembly of the core adhesion complex. In contrast, other regions of the talin rod show considerable variation in conservation between isoforms with R5 (60%) being the most divergent.

Using a sample set of vertebrates, we compared the conservation of each individual talin domain between species and between isoforms. Regions where sequence conservation is low within and between the individual isoforms likely represent regions of less functional importance. In contrast, regions that are highly conserved within an isoform but are less conserved between isoforms might indicate regions of functional divergence. This structure-oriented conservation analysis reveals that for some talin rod domains, the binding surfaces are completely conserved between isoforms. For example, talin rod domains, R7 and R8, both contain binding sites for LD-motif-containing proteins, and the R7- and R8-binding surfaces on both talin isoforms are identical. This is reflected by the

similar binding constants ( $K_d$ ) of these domains for their respective ligands; that is, the KANK 1 and KANK 2 binding site on R7 and the RIAM- and DLC1-binding site on R8. These proteins bind in the same manner and with the same affinity to both isoforms ([16] and our own unpublished data).

In contrast, the R5 domain, for which ligands have yet to be identified, has a highly conserved surface in talin2 with the characteristics of an LD-motif-binding domain, but this surface is markedly different in talin1. Based on this analysis, we suggest that regions of divergence between isoforms that are well conserved within each isoform likely encode regions that define the subtle differences in isoform functionalities.

#### Talin2 in disease and development

The roles of talin2 during embryogenesis and development are not fully understood, but studies of the two talin isoforms in the heart reveal that they are tightly regulated [5,111]. Both isoforms are highly expressed in cardiomyocytes, but during maturation, and in the mature heart, talin2 becomes the major isoform, localising to the costameres [111]. Indeed, cardiac-specific talin1 knockout mice show normal basal cardiac function. Interestingly, talin1 is upregulated in the failing human heart, and studies in mice show that an ablation of cardiac talin1 blunts the hypertrophic response and improves cardiac function [106]. The mechanisms behind isoform switching in heart remain to be elucidated, but the data clearly indicate that the two talin isoforms play distinct roles in cardiac muscle. Further evidence of the importance of talin2 in development comes from the exome sequencing-based identification of a mutation (S339L in F3) in the *Tln2* gene that causes fifth finger Camptodactyly [112]. Given that talin2 is not an essential gene, it seems likely that whole exome sequencing will reveal further disease-associated mutations in the *Tln2* gene, and these will provide further insights into its functions.

Interestingly, the *Tln2* gene also includes a highly conserved microRNA, miR-190, situated in intron 51 [10], which has been implicated as a modulator in multiple signalling pathways. Moreover, talin2 has appeared in a number of screens as a protein regulated by microRNAs whose expression is perturbed in cancer [53,113]. Thus, the humanised antibody trastuzumab, which recognises the extracellular domain of HER2, upregulates miR-194 expression in two HER2-positive breast cancer cell lines [113], and miR-194 suppresses cell migration reportedly via downregulation of talin2. Talin2 is also downregulated by miR-132, but miR-132 expression is itself suppressed by promoter methylation

in prostate cancer cells. This correlates with a worse prognosis, and the authors speculate that elevated talin2 levels may suppress cell death and increase metastasis [114]. Talin2 upregulation has also been implicated in breast cancer tumorigenesis and metastasis [33,53] driving more aggressive cell invasion.

### Post-translational modification of talins

Talin has been shown to be regulated by post-translational modification and the phosphorylation sites in platelet talin1 have been mapped [115]. Proteomics studies on the 'adhesome' also show phosphorylation of talin in adhesions [116], but there is much less data on talin2

PTMs. To explore this, we took all reported phosphorylation and acetylation sites for talin1 and found that the majority were conserved in talin2 (Table 1). Mass spectrometric analysis of calyculin-treated platelets identified numerous talin1 phosphorylation sites, with the three most abundant sites being T144 and T150 in the F1-loop (phosphorylation appears to negatively regulate integrin activation [58,115]) and S446 [115] in the linker between the head and rod domains. Phosphorylation of S446 is believed to be important in the regulation of the calpain cleavage between the head and the rod domain and is important for regulating FA turnover [71,117], a process that has recently been shown to be essential for adhesion development and rigidity sensing [118]. In addition, S425, which is also in the linker, is

**Table 1.** Post-translational modifications in talin1 and talin2. Summary of the identified talin phosphorylation [115,116], acetylation [128], arginylation [121], glycosylation [123] and methylation sites [122]. For each PTM, the modified residue, the domain it is located, and the conservation between isoforms are shown. Residue numbering is for mouse talin1 and talin2.

Talin1 phosphorylation					
Site	Domain of talin1	Site conserved in talin2	Talin1 phosphorylation site	Domain of talin1	Site conserved in talin2
S5	F0	Yes	S677	R2	No
Y26	F0	Yes	S729	R2	Yes
Y70	F0	Yes	S815	R3	Yes
T78	F0	No	S940	R4	No
T98	F1	No	S978/S981	R4	No/Yes
T114	F1	Yes	S1021	R4	Yes
Y127	F1	Yes	Y1118	R5	Yes
S128	F1	Yes	T1142	R5	Yes
T144	F1	Yes	S1201	R5	No
T150	F1	Yes	S1225	R6	No
T167	F1	Yes	T1263	R6	No
T190	F1	Yes	S1323	R6	Yes
S311	F3	Yes	S1508	R8	No
S405	LINKER	Yes	S1641	R7	Yes
S425	LINKER	Yes	S1694	R9	Yes
S429/T430	LINKER	Yes	S1849	R10	No
Y436	LINKER	No	T1855	R10	Yes
S446	LINKER	Yes	S1878	R10	No
S455/S468	LINKER	Yes	S2040	R11	No
S467	LINKER	Yes	S2127	R11	Yes
S620	R1	Yes	S2338	R12	No
			Y2530	DD	Yes
			S2535	DD	No

Talin2 phosphorylation					
Site	Domain of talin2	Site conserved in talin1	Talin1 PTM	Domain of talin1	Site conserved in talin2
Y1665	R9	No	K1544 (acetylation)	R8	Yes
T1843	R10	No	K2031 (acetylation)	R11	Yes
			K2119 (acetylation)	R11	Yes
			A1900 (arginylation)	R10	Yes
			T1467 (glycosylation)	R8	No
			T1690 (glycosylation)	R10	Yes
			K2404 (methylation)	R13	Yes



phosphorylated by CDK5, and this phosphorylation has been shown to enhance talin activity and increase integrin activation [119].

Calpain cleavage of talin is a permanent PTM, and three cleavage sites have been identified in talin1. The best characterised is that within the linker between the talin head and rod (between residues Q433 and Q434) [73], but there is a second site immediately prior to the DD (between residues K2493 and M2494) [71]. Both of these cleavage sites are present in talin2 [71]. Calpain cleavage of the neck exposes a recognition site for the E3 ligase SMURF1 that leads to ubiquitination of the liberated talin1 head [120]. A third force-dependent calpain cleavage site in the talin1 rod has also been identified [121]. This cleavage occurs between residue P1902 and A1903 (a site which is normally buried in the folded R10 domain) and is likely to only be accessible when talin is under force. This cleavage appears to be regulated by arginylation (a PTM that only occurs on the N-term residue of proteins [121]). It is not yet known whether this force-dependent cleavage site is also present in talin2, but the region is well conserved between both isoforms.

Finally, a number of additional PTMs have also been identified in talin1. For instance, the affinity of the talin:actin connection is controlled via the methyltransferase Ezh2 which methylates talin at lysine K2454 in ABS3 [122]. This PTM site is completely conserved in talin2. Talin1 is also modified by glycosylation [123] at sites in R8 and R10. Interestingly, the glycosylation sites are not conserved between talin1 and talin2, suggesting that if talin2 is glycosylated, then it is at different sites and linked to different functions.

## Conclusions and perspectives

Gene duplication is often viewed as an evolutionarily advantageous process, with duplicated genes giving rise to two proteins that can acquire distinct or completely new functions (subfunctionalisation or neofunctionalisation). Gene duplication may also allow more complex patterns of gene expression in different cell types and tissues [124]. Furthermore, differences in PTM sites as reported here for the two talins may enable new modes of regulation at the protein level. Although both talin isoforms have maintained their ancestral properties relating to cell adhesion, it seems likely that the two isoforms have undergone some neofunctionalisation to generate nuanced, isoform-specific regulation of signalling in cell adhesion. We imagine a scenario whereby talin2 plays a central role in some tissues, such as cardiac muscle, the brain and kidney, but then also a more global role in fine-tuning the adhesive response in many

other cell types. Recent work has shown that the two talins provide different mechanical linkages in cells [34], and the ability to measure talin mechanical response both at the single molecule level [21], in cells using genetically encoded tension sensors [34,85,125], and *in silico* with force extension molecular dynamics simulations [126] provide the tools to understand how talin signalling varies with mechanical forces. Detailed structural and biochemical characterisation of talin interactions is enabling targeted mutations to be designed that specifically disrupt individual talin functions, which in conjunction with the aforementioned technical advances should enable the study of talin function in unprecedented detail. It is likely that further novel talin-mediated cell functions will be identified as additional binding partners of the two talins are discovered.

Many different adhesive structures form on talins which signal in a highly reproducible manner. Precisely how talins' mechanosignalling capabilities are integrated with the more classical signalling pathways to give rise to these robust metastable cellular responses that facilitate all our cellular processes remain to be determined. The signalling pathways that regulate talin function, localisation, post-translational modifications, etc. coupled with the forces that define the conformational status of its rod domains, which cumulatively lead to the correct cellular responses are still poorly understood. For talin to generate robust, reproducible signalling responses and specialised adhesive structures in response to such diverse, multiple inputs suggest that there must be a code underpinning talins mechanotransductive response. Deciphering this 'talin code' is the next major challenge.

## Acknowledgements

We thank David Critchley for stimulating discussions and critical reading of the manuscript and for all his support over the years. We also thank Alex Carisey (Baylor College of Medicine) for the fantastic artwork. We thank the members of the Gout laboratory for discussions and reading of the manuscript. BTG is funded by BBSRC grant (BB/N007336/1) and HFSP grant (RGP00001/2016). REG is funded by a University of Kent studentship.

## References

- Horton ER, Humphries JD, James J, Jones MC, Askari JA and Humphries MJ (2016) The integrin adhesion network at a glance. *J Cell Sci* **129**, 4159–4163.

- 2 Zaidel-Bar R, Itzkovitz S, Ma'ayan A, Iyengar R and Geiger B (2007) Functional atlas of the integrin adhesome. *Nat Cell Biol* **9**, 858–867.
- 3 Winograd-Katz SE, Fässler R, Geiger B and Legate KR (2014) The integrin adhesome: from genes and proteins to human disease. *Nat Rev Mol Cell Biol* **15**, 273–288.
- 4 Monkley SJ, Zhou XH, Kinston SJ, Giblett SM, Hemmings L, Priddle H, Brown JE, Pritchard CA, Critchley DR and Fässler R (2000) Disruption of the talin gene arrests mouse development at the gastrulation stage. *Dev Dyn* **219**, 560–574.
- 5 Manso AM, Okada H, Sakamoto FM, Moreno E, Monkley SJ, Li R, Critchley DR and Ross RS (2017) Loss of mouse cardiomyocyte talin-1 and talin-2 leads to  $\beta$ -1 integrin reduction, costameric instability, and dilated cardiomyopathy. *Proc Natl Acad Sci U S A* **114**, E6250–E6259.
- 6 Nieswandt B, Moser M, Pleines I, Varga-Szabo D, Monkley S, Critchley D and Fässler R (2007) Loss of talin1 in platelets abrogates integrin activation, platelet aggregation, and thrombus formation in vitro and in vivo. *J Exp Med* **204**, 3113–3118.
- 7 Zhang X, Jiang G, Cai Y, Monkley SJ, Critchley DR and Sheetz MP (2008) Talin depletion reveals independence of initial cell spreading from integrin activation and traction. *Nat Cell Biol* **10**, 1062–1068.
- 8 McCann RO and Craig SW (1997) The I/LWEQ module: a conserved sequence that signifies F-actin binding in functionally diverse proteins from yeast to mammals. *Proc Natl Acad Sci U S A* **94**, 5679–5684.
- 9 Monkley SJ, Pritchard CA and Critchley DR (2001) Analysis of the mammalian Talin2 gene TLN2. *Biochem Biophys Res Commun* **286**, 880–885.
- 10 Debrand E, Cotti FJ, Bate N, Spence L, Mazzeo D, Pritchard CA, Monkley SJ and Critchley DR (2012) Mice carrying a complete deletion of the talin2 coding sequence are viable and fertile. *Biochem Biophys Res Commun* **426**, 190–195.
- 11 Klapholz B and Brown NH (2017) Talin – the master of integrin adhesions. *J Cell Sci* **130**, 2435–2446.
- 12 Burridge K and Connell L (1983) A new protein of adhesion plaques and ruffling membranes. *J Cell Biol* **97**, 359–367.
- 13 Shattil SJ, Kim C and Ginsberg MH (2010) The final steps of integrin activation: the end game. *Nat Rev Mol Cell Biol* **11**, 288–300.
- 14 Elsegui-Artola A, Oriá R, Chen Y, Kosmalska A, Pérez-González C, Castro N, Zhu C, Treppe X and Roca-Cusachs P (2016) Mechanical regulation of a molecular clutch defines force transmission and transduction in response to matrix rigidity. *Nat Cell Biol* **18**, 540–548.
- 15 Calderwood DA, Campbell ID and Critchley DR (2013) Talins and kindlins: partners in integrin-mediated adhesion. *Nat Rev Mol Cell Biol* **14**, 503–517.
- 16 Bouchet BP, Gough RE, Ammon YC, van de Willige D, Post H, Jacquemet G, Maarten Alteelaar AP, Heck AJR, Gout BT and Akhmanova A (2016) Talin-KANK1 interaction controls the recruitment of cortical microtubule stabilizing complexes to focal adhesions. *Elife* **5**, e18124.
- 17 Sun Z, Tseng H-Y, Tan S, Senger F, Kurzawa L, Dedden D, Mizuno N, Wasik AA, Thery M, Dunn AR *et al.* (2016) Kank2 activates talin, reduces force transduction across integrins and induces central adhesion formation. *Nat Cell Biol* **18**, 941–953.
- 18 Stehbens S and Wittmann T (2012) Targeting and transport: how microtubules control focal adhesion dynamics. *J Cell Biol* **198**, 481–489.
- 19 Liu J, Wang Y, Goh WI, Goh H, Baird MA, Ruchland S, Teo S, Bate N, Critchley DR, Davidson MW *et al.* (2015) Talin determines the nanoscale architecture of focal adhesions. *Proc Natl Acad Sci U S A* **112**, E4864–E4873.
- 20 del Rio A, Perez-Jimenez R, Liu R, Roca-Cusachs P, Fernandez JM and Sheetz MP (2009) Stretching single talin rod molecules activates vinculin binding. *Science* **323**, 638–641.
- 21 Yao M, Gout BT, Klapholz B, Hu X, Toseland CP, Guo Y, Cong P, Sheetz MP and Yan J (2016) The mechanical response of talin. *Nat Commun* **7**, 11966.
- 22 Yan J, Yao M, Gout BT and Sheetz MP (2015) Talin dependent mechanosensitivity of cell focal adhesions. *Cell Mol Bioeng* **8**, 151–159.
- 23 Yao M, Gout BT, Chen H, Cong P, Sheetz MP and Yan J (2014) Mechanical activation of vinculin binding to talin locks talin in an unfolded conformation. *Sci Rep* **4**, 4610.
- 24 Gout BT, Zacharchenko T, Bate N, Tsang R, Hey F, Gingras AR, Elliott PR, Roberts GCK, Ballestrem C, Critchley DR *et al.* (2013) RIAM and vinculin binding to talin are mutually exclusive and regulate adhesion assembly and turnover. *J Biol Chem* **288**, 8238–8249.
- 25 Praekelt U, Kopp PM, Rehm K, Linder S, Bate N, Patel B, Debrand E, Manso AM, Ross RS, Cotti F *et al.* (2012) New isoform-specific monoclonal antibodies reveal different sub-cellular localisations for talin1 and talin2. *Eur J Cell Biol* **91**, 180–191.
- 26 Kopp PM, Bate N, Hansen TM, Brindle NPJ, Praekelt U, Debrand E, Coleman S, Mazzeo D, Gout BT, Gingras AR *et al.* (2010) Studies on the morphology and spreading of human endothelial cells define key inter- and intramolecular interactions for talin1. *Eur J Cell Biol* **89**, 661–673.
- 27 Monkley SJ, Kostourou V, Spence L, Petrich B, Coleman S, Ginsberg MH, Pritchard CA and Critchley DR (2011) Endothelial cell talin1 is essential for embryonic angiogenesis. *Dev Biol* **349**, 494–502.



- 28 Thul PJ, Åkesson L, Wiking M, Mahdessian D, Geladaki A, Ait Blal H, Alm T, Asplund A, Björk L, Breckels LM *et al.* (2017) A subcellular map of the human proteome. *Science* **356**, eaa13321.
- 29 Lee H-S, Lim CJ, Puzon-McLaughlin W, Shattil SJ and Ginsberg MH (2009) RIAM activates integrins by linking talin to Ras GTPase membrane-targeting sequences. *J Biol Chem* **284**, 5119–5127.
- 30 Lagarrigue F, Vikas Anekal P, Lee HS, Bachir AI, Ablack JN, Horwitz AF and Ginsberg MH (2015) A RIAM/lamellipodin-talin-integrin complex forms the tip of sticky fingers that guide cell migration. *Nat Commun* **6**, 8492.
- 31 Lawson C, Lim ST, Uryu S, Chen XL, Calderwood DA and Schlaepfer DD (2012) FAK promotes recruitment of talin to nascent adhesions to control cell motility. *J Cell Biol* **196**, 223–232.
- 32 Singh P, Carráher C and Schwarzbauer JE (2010) Assembly of fibronectin extracellular matrix. *Annu Rev Cell Dev Biol* **26**, 397–419.
- 33 Qi L, Jafari N, Li X, Chen Z, Li L, Hytönen VP, Goult BT, Zhan C-G and Huang C (2016) Talin2-mediated traction force drives matrix degradation and cell invasion. *J Cell Sci* **129**, 3661–3674.
- 34 Austen K, Ringer P, Mehlich A, Chrostek-Grashoff A, Kluger C, Klingner C, Sabass B, Zent R, Rief M and Grashoff C (2015) Extracellular rigidity sensing by talin isoform-specific mechanical linkages. *Nat Cell Biol* **17**, 1597–1606.
- 35 Senetar MA, Moncman CL and McCann RO (2007) Talin2 is induced during striated muscle differentiation and is targeted to stable adhesion complexes in mature muscle. *Cell Motil Cytoskeleton* **64**, 157–173.
- 36 Debrand E, El Jai Y, Spence L, Bate N, Praekelt U, Pritchard CA, Monkley SJ and Critchley DR (2009) Talin 2 is a large and complex gene encoding multiple transcripts and protein isoforms. *FEBS J* **276**, 1610–1628.
- 37 Himmel M, Ritter A, Rothemann S, Pauling BV, Rottner K, Gingras AR and Ziegler WH (2009) Control of high affinity interactions in the talin C terminus. *J Biol Chem* **284**, 13832–13842.
- 38 Wang P, Ballestrem C and Steuli CH (2011) The C terminus of talin links integrins to cell cycle progression. *J Cell Biol* **195**, 499–513.
- 39 Senetar MA and McCann RO (2005) Gene duplication and functional divergence during evolution of the cytoskeletal linker protein talin. *Gene* **362**, 141–152.
- 40 Putnam NH, Butts T, Ferrier DEK, Furlong RF, Hellsten U, Kawashima T, Robinson-Rechavi M, Shoguchi E, Terry A, Yu J-K *et al.* (2008) The amphioxus genome and the evolution of the chordate karyotype. *Nature* **453**, 1064–1071.
- 41 Smith JJ, Kuraku S, Holt C, Sauka-Spengler T, Jiang N, Campbell MS, Yandell MD, Manoussaki T, Meyer A, Bloom OE *et al.* (2013) Sequencing of the sea lamprey (*Petromyzon marinus*) genome provides insights into vertebrate evolution. *Nat Genet* **45**, 415–421.
- 42 Tsujioka M, Yoshida K and Inouye K (2004) Talin B is required for force transmission in morphogenesis of *Dictyostelium*. *EMBO J* **23**, 2216–2225.
- 43 Higgins DG, Labelle S, Gautel M and Gibson TJ (1994) The evolution of titin and related giant muscle proteins. *J Mol Evol* **38**, 395–404.
- 44 Baines AJ (2010) Evolution of the spectrin-based membrane skeleton. *Transfus Clin Biol* **17**, 95–103.
- 45 Light S, Sagi R, Idhychanda SS, Qin J and Eklövsson A (2012) The evolution of filamin – a protein domain repeat perspective. *J Struct Biol* **179**, 289–298.
- 46 Tsujioka M, Machesky LM, Cole SL, Yahata K and Inouye K (1999) A unique talin homologue with a villin headpiece-like domain is required for multicellular morphogenesis in *Dictyostelium*. *Curr Biol* **9**, 389–392.
- 47 Elliott PR, Goult BT, Kopp PM, Bate N, Grossmann JG, Roberts GCK, Critchley DR and Barsukov IL (2010) The structure of the talin head reveals a novel extended conformation of the FERM domain. *Structure* **18**, 1289–1299.
- 48 Chishti AH, Kim AC, Marfatia SM, Lutchman M, Hanspal M, Jindal H, Liu SC, Low PS, Rouleau GA, Mohandas N *et al.* (1998) The FERM domain: a unique module involved in the linkage of cytoplasmic proteins to the membrane. *Trends Biochem Sci* **23**, 281–282.
- 49 Calderwood DA, Zent R, Grant R, Rees DJ, Hynes RO and Ginsberg MH (1999) The Talin head domain binds to integrin beta subunit cytoplasmic tails and regulates integrin activation. *J Biol Chem* **274**, 28071–28074.
- 50 Anthus NJ, Wegener KL, Critchley DR and Campbell ID (2010) Structural diversity in integrin/talin interactions. *Structure* **3**, 1654–1666.
- 51 Yuan Y, Li L, Zhu Y, Qi L, Azizi L, Hytönen VP, Zhan C-G and Huang C (2017) The molecular basis of talin2's high affinity toward  $\beta 1$ -integrin. *Sci Rep* **7**, 41989.
- 52 Anthus NJ, Wegener KL, Ye F, Kim C, Goult BT, Lowe ED, Vakonakis I, Bate N, Critchley DR, Ginsberg MH *et al.* (2009) The structure of an integrin/talin complex reveals the basis of inside-out signal transduction. *EMBO J* **28**, 3623–3632.
- 53 Li L, Li X, Qi L, Rychalshou P, Jafari N and Huang C (2017) The role of talin2 in breast cancer tumorigenesis and metastasis. *Oncotarget* **8**, 106876–106887.
- 54 Rossier O, Orcteau V, Sibarita J-B, Leduc C, Tessier B, Nair D, Gatterdam V, Destaing O, Albige-Rizo C, Tampé R *et al.* (2012) Integrins  $\beta 1$  and  $\beta 3$  exhibit

- distinct dynamic nanoscale organizations inside focal adhesions. *Nat Cell Biol* **14**, 1057–1067.
- 55 Bouaouina M, Lad Y and Calderwood DA (2008) The N-terminal domains of talin cooperate with the phosphotyrosine binding-like domain to activate beta1 and beta3 integrins. *J Biol Chem* **283**, 6118–6125.
- 56 Saltel F, Moertier E, Hytönen VP, Jacquier M-C, Zimmermann P, Vogel V, Liu W and Wehrle-Haller B (2009) New PI(4,5)P2- and membrane proximal integrin-binding motifs in the talin head control beta3-integrin clustering. *J Cell Biol* **187**, 715–731.
- 57 De Franceschi N, Mähkinen M, Hamidi H, Alanko J, Mai A, Picas L, Lévy D, Mattjus P, Goult BT, Goud B *et al.* (2017) ProLIF: a quantitative assay for investigating integrin cytoplasmic protein interactions and synergistic membrane effects on proteoliposomes. *bioRxiv*, 209262. [PREPRINT]
- 58 Goult BT, Bouaouina M, Elliott PR, Bate N, Patel B, Gingras AR, Grossmann JG, Roberts GCK, Calderwood DA, Critchley DR *et al.* (2010) Structure of a double ubiquitin-like domain in the talin head: a role in integrin activation. *EMBO J* **29**, 1069–1080.
- 59 Zhu L, Yang J, Bromberger T, Holly A, Lu F, Liu H, Sun K, Klapproth S, Hirbawi J, Byzova TV *et al.* (2017) Structure of Rap1b bound to talin reveals a pathway for triggering integrin activation. *Nat Commun* **8**, 1–11.
- 60 Plak K, Pots H, Van Haastert PJM and Korholt A (2016) Direct interaction between TalinB and Rap1 is necessary for adhesion of Dictyostelium cells. *BMC Cell Biol* **17**, 1.
- 61 Goult BT, Bouaouina M, Harburger DS, Bate N, Patel B, Anthis NJ, Campbell ID, Calderwood DA, Barsukov IL, Roberts GC *et al.* (2009) The structure of the N-Terminus of Kindlin-1: a domain important for alphaIIb beta3 integrin activation. *J Mol Biol* **394**, 944–956.
- 62 Kloecker S, Major MB, Calderwood DA, Ginsberg MH, Jones DA and Beckerle MC (2004) The Kindler Syndrome protein is regulated by transforming growth factor-beta and involved in integrin-mediated adhesion. *J Biol Chem* **279**, 6824–6833.
- 63 de Pereda JM, Wegener KL, Santelli E, Bate N, Ginsberg MH, Critchley DR, Campbell ID and Liddington RC (2005) Structural basis for phosphatidylinositol phosphate kinase type Igamma binding to talin at focal adhesions. *J Biol Chem* **280**, 8381–8386.
- 64 Legate KR, Takahashi S, Bonakdar N, Fabry B, Boettiger D, Zent R and Fassler R (2011) Integrin adhesion and force coupling are independently regulated by localized PtdIns(4,5)<sub>2</sub> synthesis. *EMBO J* **30**, 4539–4553.
- 65 Wang S, Watanabe T, Matsuzawa K, Katsumi A, Kakeno M, Matsui T, Ye F, Sato K, Murase K, Sugiyama I *et al.* (2012) Tiam1 interaction with the PAR complex promotes talin-mediated Rac1 activation during polarized cell migration. *J Cell Biol* **199**, 331–345.
- 66 Wegener KL, Basran J, Bagshaw CR, Campbell ID, Roberts GCK, Critchley DR and Barsukov IL (2008) Structural basis for the interaction between the cytoplasmic domain of the hyaluronate receptor layilin and the talin F3 subdomain. *J Mol Biol* **382**, 112–126.
- 67 Yang J, Zhu L, Zhang H, Hirbawi J, Fukuda K, Dwivedi P, Liu J, Byzova T, Plow EF, Wu J *et al.* (2014) Conformational activation of talin by RIAM triggers integrin-mediated cell adhesion. *Nat Commun* **5**, 5880.
- 68 Hemmings L, Rees DJ, Ohanian V, Bolton SJ, Gilmore AP, Patel B, Priddle H, Trevithick JE, Hynes RO and Critchley DR (1996) Talin contains three actin-binding sites each of which is adjacent to a vinculin-binding site. *J Cell Sci*, **109** (Pt 1), 2715–2726.
- 69 Lee H-S, Bellin RM, Walker DL, Patel B, Powers P, Liu H, Garcia-Alvarez B, de Pereda JM, Liddington RC, Volkmann N *et al.* (2004) Characterization of an actin-binding site within the talin FERM domain. *J Mol Biol* **343**, 771–784.
- 70 Ciobanaru C, Wang H, Henriot V, Mathieu C, Fente A, Csillag S, Vigouroux C, Fajvre B and Le Clainche C (2018) Integrin-bound talin head inhibits actin filament barbed-end elongation. *J Biol Chem* **293**, 2586–2596.
- 71 Bate N, Gingras AR, Bachir A, Horwitz R, Ye F, Patel B, Goult BT and Critchley DR (2012) Talin contains a C-terminal calpain2 cleavage site important in focal adhesion dynamics. *PLoS One* **7**, e34461.
- 72 O'Halloran T, Beckerle MC and Burridge K (1985) Identification of talin as a major cytoplasmic protein implicated in platelet activation. *Nature* **317**, 449–451.
- 73 Franco SJ, Rodgers MA, Perrin BJ, Han J, Bennin DA, Critchley DR and Huttenlocher A (2004) Calpain-mediated proteolysis of talin regulates adhesion dynamics. *Nat Cell Biol* **6**, 977–983.
- 74 Gingras AR, Bate N, Goult BT, Hazelwood L, Canestrelli I, Grossmann JG, Liu H, Putz NSM, Roberts GCK, Volkmann N *et al.* (2008) The structure of the C-terminal actin-binding domain of talin. *EMBO J* **27**, 458–469.
- 75 Gingras AR, Bate N, Goult BT, Patel B, Kopp PM, Emsley J, Barsukov IL, Roberts GCK and Critchley DR (2010) Central region of talin has a unique fold that binds vinculin and actin. *J Biol Chem* **285**, 29577–29587.
- 76 Murzin AG, Brenner SE, Hubbard T and Chothia C (1995) SCOP: a structural classification of proteins database for the investigation of sequences and structures. *J Mol Biol* **247**, 536–540.

- 77 Goult BT, Gingras AR, Bate N, Barsukov IL, Critchley DR and Roberts GCK (2010) The domain structure of talin: residues 1815-1973 form a five-helix bundle containing a cryptic vinculin-binding site. *FEBS Lett* **584**, 2237–2241.
- 78 Goult BT, Xu X-P, Gingras AR, Swift M, Patel B, Bate N, Kopp PM, Barsukov IL, Critchley DR, Volkman N *et al.* (2013) Structural studies on full-length talin1 reveal a compact auto-inhibited dimer: implications for talin activation. *J Struct Biol* **184**, 21–32.
- 79 Ellis SJ, Pines M, Fairchild MJ and Tanentzapf G (2011) In vivo functional analysis reveals specific roles for the integrin-binding sites of talin. *J Cell Sci* **124**, 1844–1856.
- 80 Gingras AR, Ziegler WH, Bobkov AA, Joyce MG, Fasci D, Himmel M, Rothemann S, Ritter A, Grossmann JG, Patel B *et al.* (2009) Structural determinants of integrin binding to the talin rod. *J Biol Chem* **284**, 8866–8876.
- 81 Rodius S, Chaloin O, Moes M, Schaffner-Reckinger E, Landrieu I, Lippens G, Lin M, Zhang J and Kieffer N (2008) The talin rod IBS2  $\alpha$ -helix interacts with the  $\beta$ 3 integrin cytoplasmic tail membrane-proximal helix by establishing charge complementary salt bridges. *J Biol Chem* **283**, 24212–24223.
- 82 Klapholz B, Herbert SL, Wellmann J, Johnson R, Parsons M and Brown NH (2015) Alternative mechanisms for talin to mediate integrin function. *Curr Biol* **25**, 847–857.
- 83 Changdele R, Xu X, Magadant F and Sheetz MP (2015) Nascent integrin adhesions form on all matrix rigidities after integrin activation. *Dev Cell* **35**, 614–621.
- 84 Atherton P, Stutchbury B, Wang D-Y, Jethwa D, Tsang R, Meier-Rodriguez E, Wang P, Bate N, Zent R, Barsukov IL *et al.* (2015) Vinculin controls talin engagement with the actomyosin machinery. *Nat Commun* **6**, 10038.
- 85 Kumar A, Ouyang M, Van den Dries K, McGhee EJ, Tanaka K, Anderson MD, Groisman A, Goult BT, Anderson KI and Schwartz MA (2016) Talin tension sensor reveals novel features of focal adhesion force transmission and mechanosensitivity. *J Cell Biol* **213**, 371–383.
- 86 Gingras AR, Bate N, Goult BT, Hazelwood L, Grossmann JG, Liu H, Putz NSM, Roberts CK, Volkman N, Haindl D *et al.* (2006) The structure of the C-terminal actin binding domain of talin. *EMBO J* **27**, 458–469.
- 87 Geiger B (1979) A 130K protein from chicken gizzard: its localization at the termini of microfilament bundles in cultured chicken cells. *Cell* **18**, 193–205.
- 88 Gingras AR, Ziegler WH, Frank R, Barsukov IL, Roberts GCK, Critchley DR and Emsley J (2005) Mapping and consensus sequence identification for multiple vinculin binding sites within the talin rod. *J Biol Chem* **280**, 37217–37224.
- 89 Papagrigoriou E, Gingras AR, Barsukov IL, Bate N, Fillingham IJ, Patel B, Frank R, Ziegler WH, Roberts GC, Critchley DR *et al.* (2004) Activation of a vinculin-binding site in the talin rod involves rearrangement of a five-helix bundle. *EMBO J* **23**, 2942–2951.
- 90 Bois PRJ, O'Hara BP, Niethspach D, Kirkpatrick J and Izard T (2006) The vinculin binding sites of talin and  $\alpha$ -actinin are sufficient to activate vinculin. *J Biol Chem* **281**, 7228–7236.
- 91 Carisey A, Tsang R, Greiner AM, Nijenhuis N, Heath N, Nazgiewicz A, Kemkemer R, Derby B, Spatz J and Ballestrem C (2015) Vinculin regulates the recruitment and release of core focal adhesion proteins in a force-dependent manner. *Curr Biol* **23**, 271–281.
- 92 Alam T, Alazmi M, Gao X and Arold ST (2014) How to find a leucine in a haystack? Structure, ligand recognition and regulation of leucine-aspartic acid (LD) motifs. *Biochem J* **460**, 317–329.
- 93 Brown MC, Perrotta JA and Turner CE (1996) Identification of LIM3 as the principal determinant of paxillin focal adhesion localization and characterization of a novel motif on paxillin directing vinculin and focal adhesion kinase binding. *J Cell Biol* **135**, 1109–1123.
- 94 Zacharchenko T, Qian X, Goult BT, Jethwa D, Almeida TB, Ballestrem C, Critchley DR, Lowy DR and Barsukov IL (2016) LD motif recognition by talin: structure of the talin-DLC1 complex. *Structure* **24**, 1130–1141.
- 95 Li G, Du X, Vass WC, Papageorge AG, Lowy DR and Qian X (2011) Full activity of the deleted in liver cancer 1 (DLC1) tumor suppressor depends on an LD-like motif that binds talin and focal adhesion kinase (FAK). *Proc Natl Acad Sci U S A* **108**, 17129–17134.
- 96 Beatty BT, Wang Y, Bravo-Cordero JJ, Sharma VP, Miskolci V, Hodgson L and Condeelis JS (2014) Talin regulates moesin-NHE-1 recruitment to invadopodia and promotes mammary tumor metastasis. *J Cell Biol* **205**, 737–751.
- 97 Schönichen A, Webb BA, Jacobson MP and Barber DL (2013) Considering protonation as a posttranslational modification regulating protein structure and function. *Annu Rev Biophys* **42**, 289–314.
- 98 Srivastava J, Barreiro G, Groscurth S, Gingras AR, Goult BT, Critchley DR, Kelly MJS, Jacobson MP and Barber DL (2008) Structural model and functional significance of pH-dependent talin-actin binding for focal adhesion remodeling. *Proc Natl Acad Sci U S A* **105**, 14436–14441.
- 99 Sun N, Critchley DR, Paulin D, Li Z and Robson RM (2008) Identification of a repeated domain within

- mammalian  $\alpha$ -synemin that interacts directly with talin. *Exp Cell Res* **314**, 1839–1849.
- 100 Lee H-S, Anekal P, Lim CJ, Liu C-C and Ginsberg MH (2013) Two modes of integrin activation form a binary molecular switch in adhesion maturation. *Mol Biol Cell* **24**, 1354–1362.
- 101 Margadant F, Chew LL, Hu X, Yu H, Bate N, Zhang X and Sheetz M (2011) Mechanotransduction in vivo by repeated talin stretch-relaxation events depends upon vinculin. *PLoS Biol* **9**, e1001223.
- 102 Goult BT, Zacharchenko T, Bate N, Tsang R, Gingras AR, Hey F, Elliott PR, Roberts GC, Ballestrin C, Critchley DR *et al.* (2013) RIAM and Vinculin binding to talin are mutually exclusive and regulate adhesion assembly and turnover. *J Biol Chem* **288**, 35–36.
- 103 Conti FJ, Monkley SJ, Wood MR, Critchley DR and Muller U (2009) Talin 1 and 2 are required for myoblast fusion, sarcomere assembly and the maintenance of myotendinous junctions. *Development* **136**, 3597–3606.
- 104 Goksoy E, Ma Y-Q, Wang X, Kong X, Perera D, Plow EF and Qin J (2008) Structural basis for the autoinhibition of talin in regulating integrin activation. *Mol Cell* **31**, 124–133.
- 105 Goult BT, Bate N, Anthis NJ, Wegener KL, Gingras AR, Patel B, Barsukov IL, Campbell ID, Roberts GC and Critchley DR (2009) The structure of an interdomain complex that regulates talin activity. *J Biol Chem* **284**, 15097–15106.
- 106 Banno A, Goult BT, Lee H, Bate N, Critchley DR and Ginsberg MH (2012) Subcellular localization of talin is regulated by inter-domain interactions. *J Biol Chem* **287**, 13799–13812.
- 107 Song X, Yang J, Hirbawi J, Ye S, Perera HD, Goksoy E, Dwivedi P, Plow EF, Zhang R and Qin J (2012) A novel membrane-dependent on/off switch mechanism of talin FERM domain at sites of cell adhesion. *Cell Res* **22**, 1533–1545.
- 108 Schiemer J, Bohm A, Lin L, Merrill-Skoloff G, Flaumenhaft R, Huang J-S, Le Breton GC and Chishti AH (2016)  $G_{12}$  switch region 2 relieves talin autoinhibition to activate  $\alpha$ IIb $\beta$ 3 integrin. *J Biol Chem* **291**, 26598–26612.
- 109 Tadokoro S (2003) Talin binding to integrin tails: a final common step in integrin activation. *Science* **302**, 103–106.
- 110 Šali A and Blundell TL (1993) Comparative protein modelling by satisfaction of spatial restraints. *J Mol Biol* **234**, 779–815.
- 111 Manso AM, Li R, Monkley SJ, Cruz NM, Ong S, Lao DH, Koshman YE, Gu Y, Peterson KL, Chen J *et al.* (2013) Talin1 has unique expression versus talin 2 in the heart and modifies the hypertrophic response to pressure overload. *J Biol Chem* **288**, 4252–4264.
- 112 Deng H, Deng S, Xu H, Deng H-X, Chen Y, Yuan L, Deng X, Yang S, Guan L, Zhang J *et al.* (2016) Exome sequencing of a pedigree reveals S339L mutation in the TLN2 Gene as a cause of fifth finger camptodactyly. *PLoS One* **11**, e0155180.
- 113 Le X-F, Almeida MI, Mao W, Spizzo R, Rossi S, Nicoloso MS, Zhang S, Wu Y, Calin GA and Bast RC (2012) Modulation of microRNA-194 and cell migration by HER2-targeting trastuzumab in breast cancer. *PLoS One* **7**, e41170.
- 114 Formosa A, Lena AM, Markert EK, Cortelli S, Miano R, Mauriello A, Croce N, Vandescampel J, Mestdagh P, Finazzi-Agrò E *et al.* (2013) DNA methylation silences miR-132 in prostate cancer. *Oncogene* **32**, 127–134.
- 115 Ratnikov B, Prak C, Han J, Shabanowitz J, Hunt DF and Ginsberg MH (2005) Talin phosphorylation sites mapped by mass spectrometry. *J Cell Sci* **118**, 4921–4923.
- 116 Robertson J, Jacquemet G, Byron A, Jones MC, Warwood S, Selley JN, Knight D, Humphries JD and Humphries MJ (2015) Defining the phospho-adhesome through the phosphoproteomic analysis of integrin signalling. *Nat Commun* **6**, 1–13.
- 117 Li Y, Luo X, Sun Y, Cui Z, Liu Y, Liu R and Guo X (2016) High stoichiometry phosphorylation of talin at T144/T150 or S446 produces contrasting effects on calpain-mediated talin cleavage and cell migration. *J Cancer* **7**, 1645–1652.
- 118 Saxena M, Chagede R, Hone JC, Wolfenson H and Sheetz MP (2017) Force induced calpain cleavage of talin is critical for growth, adhesion development and rigidity sensing. *Nano Lett*, **17**, 7242–7251.
- 119 Jin JK, Tien PC, Cheng CJ, Song JH, Huang C, Lin SH and Gallick GE (2015) Talin1 phosphorylation activates  $\beta$ 1 integrins: a novel mechanism to promote prostate cancer bone metastasis. *Oncogene* **34**, 1811–1821.
- 120 Huang C, Rajfur Z, Yousefi N, Chen Z, Jacobson K and Ginsberg MH (2009) Talin phosphorylation by Cdk5 regulates Smurf1-mediated talin head ubiquitylation and cell migration. *Nat Cell Biol* **11**, 624–630.
- 121 Zhang F, Saha S and Kashina A (2012) Arginylation-dependent regulation of a proteolytic product of talin is essential for cell-cell adhesion. *J Cell Biol* **197**, 819–836.
- 122 Gunawan M, Venkatesan N, Loh JT, Wong JF, Berger H, Neo WH, Li LYJ, La Win MK, Yau YH, Guo T *et al.* (2015) The methyltransferase Ezh2 controls cell adhesion and migration through direct methylation of the extranuclear regulatory protein talin. *Nat Immunol* **16**, 505–516.

- 123 Hagmann J, Grob M and Burger MM (1992) The cytoskeletal protein talin is O-glycosylated. *J Biol Chem* **267**, 14424–14428.
- 124 Lynch M and Conery JS (2000) The evolutionary fate and consequences of duplicate genes. *Science* **290**, 1151–1155.
- 125 Ringer P, Weißl A, Cost A-L, Frankamp A, Sabass B, Mehlisch A, Tramier M, Rief M and Grashoff C (2017) Multiplexing molecular tension sensors reveals piconewton force gradient across talin-1. *Nat Methods* **14**, 1090–1096.
- 126 Rahikainen R, Von Essen M, Schaefer M, Qi L, Azzi L, Kelly C, Ihalaainen TO, Wehrle-Haller B, Bastmeyer M, Huang C *et al.* (2017) Mechanical stability of talin rod controls cell migration and substrate sensing. *Sci Rep* **7**, 1–15.
- 127 Ellis SJ, Goult BT, Fairchild MJ, Harris NJ, Long J, Lobo P, Czerniecki S, Van Petegem F, Schöck F, Peifer M *et al.* (2015) Talin autoinhibition is required for morphogenesis. *Curr Biol* **23**, 1825–1833.
- 128 Choudhary C, Kumar C, Gnad F, Nielsen ML, Rehman M, Walther TC, Olsen JV and Mann M (2009) Lysine acetylation targets protein complexes and co-regulates major cellular functions. *Science* **325**, 834–840.

# Talin-KANK1 interaction controls the recruitment of cortical microtubule stabilizing complexes to focal adhesions

Benjamin P Bouchet<sup>1</sup>, Rosemarie E Gough<sup>2</sup>, York-Christoph Ammon<sup>1</sup>, Dieudonné van de Willige<sup>1</sup>, Harm Post<sup>3,4,5,6</sup>, Guillaume Jacquemet<sup>7</sup>, AF Maarten Altelaar<sup>3,4,5,6</sup>, Albert JR Heck<sup>3,4,5,6</sup>, Benjamin T Gout<sup>2\*</sup>, Anna Akhmanova<sup>1\*</sup>

<sup>1</sup>Cell Biology, Department of Biology, Faculty of Science, Utrecht University, Utrecht, The Netherlands; <sup>2</sup>School of Biosciences, University of Kent, Canterbury, United Kingdom; <sup>3</sup>Biomolecular Mass Spectrometry and Proteomics, Utrecht University, Utrecht, The Netherlands; <sup>4</sup>Bijvoet Center for Biomolecular Research, Utrecht University, Utrecht, The Netherlands; <sup>5</sup>Utrecht Institute for Pharmaceutical Sciences, Utrecht University, Utrecht, The Netherlands; <sup>6</sup>The Netherlands Proteomics Centre, Utrecht University, Utrecht, The Netherlands; <sup>7</sup>Turku Centre for Biotechnology, University of Turku, Turku, Finland

**Abstract** The cross-talk between dynamic microtubules and integrin-based adhesions to the extracellular matrix plays a crucial role in cell polarity and migration. Microtubules regulate the turnover of adhesion sites, and, in turn, focal adhesions promote the cortical microtubule capture and stabilization in their vicinity, but the underlying mechanism is unknown. Here, we show that cortical microtubule stabilization sites containing CLASPs, KIF21A, LLS $\beta$  and liprins are recruited to focal adhesions by the adaptor protein KANK1, which directly interacts with the major adhesion component, talin. Structural studies showed that the conserved KN domain in KANK1 binds to the talin rod domain R7. Perturbation of this interaction, including a single point mutation in talin, which disrupts KANK1 binding but not the talin function in adhesion, abrogates the association of microtubule-stabilizing complexes with focal adhesions. We propose that the talin-KANK1 interaction links the two macromolecular assemblies that control cortical attachment of actin fibers and microtubules.

DOI: 10.7554/eLife.18124.001

\*For correspondence: B.T.Gout@kent.ac.uk (BTG); a.akhmanova@uu.nl (AA)

Competing interest: See page 20

Funding: See page 20

Received: 24 May 2016

Accepted: 12 July 2016

Published: 13 July 2016

Reviewing editor: W James Nelson, Stanford University, United States

© Copyright Bouchet et al. This article is distributed under the terms of the [Creative Commons Attribution License](#), which permits unrestricted use and redistribution provided that the original author and source are credited.

## Introduction

Cell adhesions to the extracellular matrix support epithelial integrity and cell migration, and also provide signaling hubs that coordinate cell proliferation and survival (Hynes, 1992). Integrin-based adhesions (focal adhesions, FAs) are large macromolecular assemblies, in which the cytoplasmic tails of integrins are connected to the actin cytoskeleton. One of the major components of FAs is talin, a ~2500 amino acid dimeric protein, which plays a key role in adhesion formation by activating integrins (Anthis et al., 2009), coupling them to cytoskeletal actin (Atherton et al., 2015), regulating adhesion dynamics and recruiting different structural and signaling molecules (Calderwood et al., 2013; Gardel et al., 2010; Wehrle-Haller, 2012).

While the major cytoskeletal element associated with FAs is actin, microtubules also play an important role in adhesion by regulating the FA turnover (Akhmanova et al., 2009; Byron et al., 2015; Kaverina et al., 1999, 1998; Krylyshkina et al., 2003; Small and Kaverina, 2003; Stehbens and Wittmann, 2012; Yue et al., 2014). The recent proteomics work showed that



**eLife digest** Animal cells are organized into tissues and organs. A scaffold-like framework outside of the cells called the extracellular matrix provides support to the cells and helps to hold them in place. Cells attach to the extracellular matrix via structures called focal adhesions on the cell surface; these structures contain a protein called talin.

For a cell to be able to move, the existing focal adhesions must be broken down and new adhesions allowed to form. This process is regulated by the delivery and removal of different materials along fibers called microtubules. Microtubules can usually grow and shrink rapidly, but near focal adhesions they are captured at the surface of the cell and become more stable. However, it is not clear how focal adhesions promote microtubule capture and stability.

Bouchet et al. found that a protein called KANK1 binds to the focal adhesion protein talin in human cells grown in a culture dish. This allows KANK1 to recruit microtubules to the cell surface around the focal adhesions by binding to particular proteins that are associated with microtubules. Disrupting the interaction between KANK1 and talin by making small alterations in these two proteins blocked the ability of focal adhesions to capture surrounding microtubules. The next step following on from this work will be to find out whether this process also takes place in the cells within an animal's body, such as a fly or a mouse.

DOI: 10.7554/eLife.18124.002

microtubule-FA cross-talk strongly depends on the activation state of the integrins (Byron et al., 2015). Microtubules can affect adhesions by serving as tracks for delivery of exocytotic carriers (Stehbens et al., 2014), by controlling endocytosis required for adhesion disassembly (Ezratty et al., 2005; Theisen et al., 2012) and by regulating the local activity of signaling molecules such as Rho GTPases (for review, see [Kaverina and Straube, 2011; Stehbens and Wittmann, 2012]).

In contrast to actin, which is directly coupled to FAs, microtubules interact with the plasma membrane sites that surround FAs. A number of proteins have been implicated in microtubule attachment and stabilization in the vicinity of FAs. Among them are the microtubule plus end tracking proteins (+TIPs) CLASP1/2 and the spectraplakins MACF1/ACF7, which are targeted to microtubule tips by EB1, and a homologue of EB1, EB2, which binds to mitogen-activated protein kinase kinase kinase 4 (MAP4K4) (Drabek et al., 2006; Honnappa et al., 2009; Kodama et al., 2003; Mimori-Kiyosue et al., 2005). The interaction of CLASPs with the cell cortex depends on the phosphatidylinositol 3, 4, 5-trisphosphate (PIP3)-interacting protein LL5 $\beta$ , to which CLASPs bind directly, and is partly regulated by PI-3 kinase activity (Lansbergen et al., 2006). Other components of the same cortical assembly are the scaffolding proteins liprin- $\alpha$ 1 and  $\beta$ 1, a coiled-coil adaptor ELKS/ERC1, and the kinesin-4 KIF21A (Lansbergen et al., 2006; van der Vaart et al., 2013). Both liprins and ELKS are best known for their role in organizing presynaptic secretory sites (Hida and Ohtsuka, 2010; Spangler and Hoogenraad, 2007); in agreement with this function, ELKS is required for efficient constitutive exocytosis in HeLa cells (Grigoriev et al., 2007, 2011). LL5 $\beta$ , liprins and ELKS form micrometer-sized cortical patch-like structures, which will be termed here cortical microtubule stabilization complexes, or CMSCs. The CMSCs are strongly enriched at the leading cell edges, where they localize in close proximity of FAs but do not overlap with them ([Lansbergen et al., 2006; van der Vaart et al., 2013], reviewed in [Astro and de Curtis, 2015]). They represent a subclass of the previously defined plasma membrane-associated platforms (PMAPs) (Astro and de Curtis, 2015), which have overlapping components such as liprins, but may not be necessarily involved in microtubule regulation, as is the case for liprin-ELKS complexes in neurons, where they are part of cytomatrix at the active zone (Gundelfinger and Fejtova, 2012).

Several lines of evidence support the importance of the CMSC-FA cross-talk. In migrating keratinocytes, LL5 $\beta$  and CLASPs accumulate around FAs and promote their disassembly by targeting the exocytosis of matrix metalloproteases to FA vicinity (Stehbens et al., 2014). Furthermore, liprin- $\alpha$ 1, LL5 $\alpha/\beta$  and ELKS localize to protrusions of human breast cancer cells and are required for efficient cell migration and FA turnover (Astro et al., 2014). In polarized epithelial cells, LL5 $\beta$  and CLASPs are found in the proximity of the basal membrane, and this localization is controlled by the integrin

activation state (Hatta et al., 2010). CLASP and LL5-mediated anchoring of MTs to the basal cortex also plays a role during chicken embryonic development, where it prevents the epithelial-mesenchymal transition of epiblast cells (Nakaya et al., 2013). LL5 $\beta$ , CLASPs and ELKS were also shown to concentrate at podosomes, actin-rich structures, which can remodel the extracellular matrix (Proszynski and Sanes, 2013). Interestingly, LL5 $\beta$ -containing podosome-like structures are also formed at neuromuscular junctions (Kishi et al., 2005; Proszynski et al., 2009; Proszynski and Sanes, 2013), and the complexes of LL5 $\beta$  and CLASPs were shown to capture microtubule plus ends and promote delivery of acetylcholine receptors (Basu et al., 2015, 2014; Schmidt et al., 2012).

While the roles of CMSCs in migrating cells and in tissues are becoming increasingly clear, the mechanism underlying their specific targeting to integrin adhesion sites remains elusive. Recently, we found that liprin- $\beta$ 1 interacts with KANK1 (van der Vaart et al., 2013), one of the four members of the KANK family of proteins, which were proposed to act as tumor suppressors and regulators of cell polarity and migration through Rho GTPase signaling (Gee et al., 2015; Kakinuma et al., 2008, 2009; Li et al., 2011; Roy et al., 2009). KANK1 recruits the kinesin-4 KIF21A to CMSCs, which inhibits microtubule polymerization and prevents microtubule overgrowth at the cell edge (Kakinuma and Kiyama, 2009; van der Vaart et al., 2013). Furthermore, KANK1 participates in clustering of the other CMSC components (van der Vaart et al., 2013).

Here, we found that KANK1 is required for the association of the CMSCs with FAs. The association of KANK1 with FAs depends on the KN domain, a conserved 30 amino acid polypeptide sequence present in the N-termini of all KANK proteins. Biochemical and structural analysis showed that the KN domain interacts with the R7 region of the talin rod. Perturbation of this interaction both from the KANK1 and the talin1 side prevented the accumulation of CMSC complexes around focal adhesions and affected microtubule organization around FAs. We propose that KANK1 molecules, recruited by talin to the outer rims of FA, serve as 'seeds' for organizing other CMSC components in the FA vicinity through multivalent interactions between these components. This leads to co-organization of two distinct cortical assemblies, FAs and CMSCs, responsible for the attachment of actin and microtubules, respectively, and ensures effective cross-talk between the two types of cytoskeletal elements.

## Results

### Identification of talin1 as a KANK1 binding partner

Our previous work showed that the endogenous KANK1 colocalizes with LL5 $\beta$ , liprins and KIF21A in cortical patches that are closely apposed to, but do not overlap with FAs (van der Vaart et al., 2013). We confirmed these results both in HeLa cells and the HaCaT immortal keratinocyte cell line, in which CMSC components CLASPs and LL5 $\beta$  were previously shown to strongly cluster around FAs and regulate their turnover during cell migration (Stehbens et al., 2014) (Figure 1—figure supplement 1A,B). Inhibition of myosin-II with blebbistatin, which reduces tension on the actin fibers and affects the activation state of FA molecules, such as integrins and talin (Parsons et al., 2010), caused not only FA disassembly but also a strong reduction in clustering of CMSC components at the cell periphery (Figure 1—figure supplement 2A,B), as described previously (Stehbens et al., 2014). To investigate this effect in more detail, we partially inhibited contractility using a Rho-associated protein kinase 1 (ROCK1) inhibitor, Y-27632 (Oakes et al., 2012). In these conditions, the number of FAs was not affected although their size was reduced (Figure 1—figure supplement 2C–E). This treatment was sufficient to diminish CMSC clustering at the cell edge (Figure 1—figure supplement 2C,F). Interestingly, at the same time we observed a very significant increase in the overlap of KANK1 with FA adhesion markers (Figure 1—figure supplement 2C,G). Live imaging of KANK1 together with the FA marker paxillin showed a gradual redistribution of KANK1 into the areas occupied by FAs upon ROCK1 inhibitor-induced attenuation of contractility (Figure 1—figure supplement 2H, Video 1). These data indicate that the organization of CMSCs at the cell cortex might be controlled by interactions with tension-sensitive components of FAs.

To identify the domains of KANK1 required for cortical localization, we performed deletion mapping. KANK1 comprises an N-terminal KANK family-specific domain of unknown function, the KN domain (residues 30–68) (Kakinuma et al., 2009), a coiled coil region, the N-terminal part of which interacts with liprin- $\beta$ 1, and a C-terminal ankyrin repeat domain, which binds to KIF21A (van der



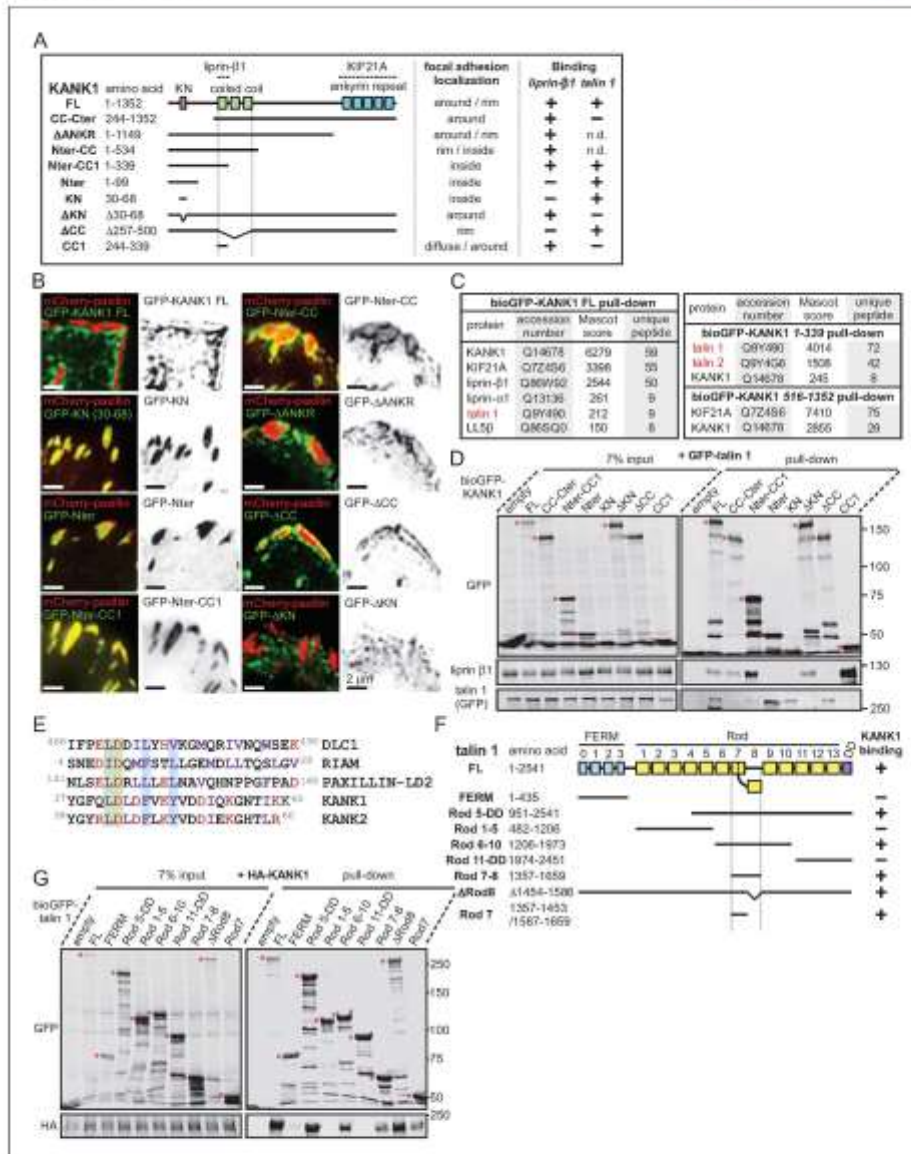


**Figure 1.** The KN motif of KANK1 interacts with the R7 domain of talin1. (A) Schematic representation of KANK1 and the deletion mutants used in this study, and the summary of their interactions and localization. N.d., not determined in this study. (B) TIRFM images of live HeLa cells transiently expressing the indicated GFP-tagged KANK1 deletion mutants together with the focal adhesion marker mCherry-paxillin. In these experiments, endogenous KANK1 and KANK2 were also expressed. (C) Identification of the binding partners of Bio-GFP-tagged KANK1 and its indicated deletion mutants. (D) Western blot analysis of 7% input and + GFP-talin 1 pull-down for bioGFP-KANK1. (E) Sequence alignment of the KN motif of KANK1 and KANK2 with other proteins. (F) Schematic representation of talin 1 and its rod domain mutants. (G) Western blot analysis of 7% input and + HA-KANK1 pull-down for bioGFP-talin 1.

## Figure 1 continued

mutants by using streptavidin pull down assays from HEK293T cells combined with mass spectrometry. (D) Streptavidin pull down assays with the BioGFP-tagged KANK1 or the indicated KANK1 mutants, co-expressed with GFP-talin1 in HEK293T cells, analyzed by Western blotting with the indicated antibodies. (E) Sequence alignment of KANK1 and KANK2 with the known talin-binding sites of DLC1, RIAM and Paxillin. The LD-motif and the interacting hydrophobic residues are highlighted green and blue respectively. (F) Schematic representation of talin1 and the deletion mutants used in this study, and their interaction with KANK1. (G) Streptavidin pull down assays with the BioGFP-tagged talin1 or the indicated talin1 mutants, co-expressed with HA-KANK1 in HEK293T cells, analyzed by Western blotting with the indicated antibodies.

DOI: 10.7554/eLife.18124.003

The following source data and figure supplements are available for figure 1:

**Figure supplement 1.** KANK1 colocalizes with CMSC components around FAs.

DOI: 10.7554/eLife.18124.004

**Figure supplement 2.** Role of myosin II activity in KANK1 localization to FA.

DOI: 10.7554/eLife.18124.005

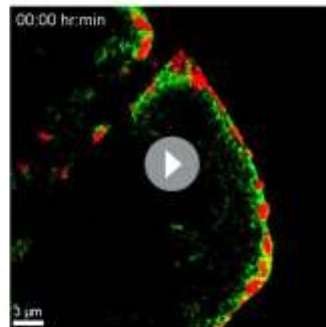
**Figure supplement 2—source data 1.** An Excel sheet with numerical data on the quantification of peripheral clustering of different markers, FA number and area and colocalization of KANK1 with talin represented as plots in Figure 1—figure supplement 2B,D–G.

DOI: 10.7554/eLife.18124.006

**Figure supplement 3.** FA localization of KN-bearing proteins.

DOI: 10.7554/eLife.18124.007

Vaart et al., 2013), while the rest of the protein is predicted to be unstructured (Figure 1A). Surprisingly, the KN domain alone strongly and specifically accumulated within FAs (Figure 1B). A similar localization was also seen with a somewhat larger N-terminal fragment of KANK1, Nter, as well as the Nter-CC1 deletion mutant, which contained the first, liprin- $\beta$ 1-binding coiled coil region of KANK1 (Figure 1A,B). However, an even larger N-terminal part of KANK1, encompassing the whole coiled coil domain (Nter-CC) showed a pronounced enrichment at the FA rim (Figure 1A,B). The KANK1 deletion mutant missing only the C-terminal ankyrin repeat domain ( $\Delta$ ANKR) was completely excluded from FAs but accumulated in their immediate vicinity, similar to the full-length KANK1 (Figure 1A,B). A tight ring-like localization at the outer rim of FAs was also observed with a KANK1 mutant, which completely missed the coiled coil region but contained the ankyrin repeat domain ( $\Delta$ CC), while the mutant which missed just the KN domain showed no accumulation around FAs (Figure 1A,B). To test whether the exclusion of larger KANK1 fragments from the FA core was simply due to the protein size, we fused GFP-tagged KN domain to the bacterial protein  $\beta$ -D-galactosidase (LacZ), but found that this fusion accumulated inside and not around FAs (Figure 1—figure supplement 3). Since GFP-KN-LacZ and GFP-KANK1- $\Delta$ ANKRD have a similar size (1336 and 1400 amino acids, respectively), but one accumulates inside FAs, while the other is excluded to their periphery, this result suggests that features other than the mere protein size determine the specific localization of KANK1 to the FA rim. We conclude that the KN domain of KANK1 has an affinity for FAs, but the presence of additional KANK1 sequences prevents the accumulation of the protein inside FAs and instead leads to the accumulation of KANK1 at the FA periphery.



**Video 1.** Effect of myosin II inhibition on KANK1 localization to FA. TIRFM-based time-lapse imaging of HeLa cells stably expressing GFP-KANK1 and TagRFP-paxillin and treated when indicated with 10  $\mu$ M ROCK1 inhibitor Y-27632. Both red and green fluorescence images were acquired at 1 min interval and displayed at 15 frames/second (accelerated 900 times).

DOI: 10.7554/eLife.18124.008

To identify the potential FA-associated partners of KANK1, we co-expressed either full-length KANK1 or its N-terminal and C-terminal fragments fused to GFP and a biotinylation (Bio) tag together with biotin ligase BirA in HEK293T cells and performed streptavidin pull down assays combined with mass spectrometry. In addition to

the already known binding partners of KANK1, such as KIF21A, liprins and LLS), we identified talin1 among the strongest hits (Figure 1C). Talin2 was also detected in a pull down with the KANK1 N-terminus though not with the full-length protein (Figure 1C). The interaction between KANK1 and talin1 was confirmed by Western blotting, and subsequent deletion mapping showed that the talin1-binding region of KANK1 encompasses the KN domain (Figure 1A,D), while liprin- $\beta$  binds to the N-terminal part of the coiled coil domain, as shown previously (van der Vaart *et al.*, 2013).

Sequence analysis of the KN domain showed that it is predicted to form a helix and contains a completely conserved leucine aspartic acid-motif (LD-motif) (Alam *et al.*, 2014; Zacharchenko *et al.*, 2016). The LD-motifs in RIAM (Goult *et al.*, 2013), DLC1 and Paxillin (Zacharchenko *et al.*, 2016) have recently been identified as talin-binding sites that all interact with talin via a helix addition mechanism. Alignment of the KN domain of KANK with the LD-motif of DLC1, RIAM and Paxillin (Zacharchenko *et al.*, 2016) revealed that the hydrophobic residues that mediate interaction with talin are present in the KN domain (Figure 1E).

Using deletion analysis, we mapped the KANK1-binding site of talin1 to the central region of the talin rod, comprising the R7-R8 domains (Figure 1F). This R7-R8 region of talin is unique (Gingras *et al.*, 2010), as the 4-helix bundle R8 is inserted into a loop of the 5-helix bundle R7, and thus protrudes from the linear chain of 5-helix bundles of the talin rod (Figures 1F, 2A). This R8 domain serves as a binding hub for numerous proteins including vinculin, synemin and actin (Calderwood *et al.*, 2013). R8 also contains a prototypic recognition site for LD-motif proteins, including DLC1 (Figure 2B), Paxillin and RIAM (Zacharchenko *et al.*, 2016). Based on the presence of the LD-binding site, we anticipated that KANK1 would also interact with R8. However, deletion mapping revealed that KANK1 in fact binds to the talin1 rod domain R7 (Figure 1F,G), suggesting that KANK1 interacts with a novel binding site on talin1.

### Structural characterization and mutational analysis of the KANK1-talin1 complex

To explore the interaction between talin1 and KANK1 in more detail, we used NMR chemical shift mapping using  $^{15}\text{N}$ -labeled talin1 R7-R8 (residues 1357–1653) and a synthetic KANK1 peptide of the KN domain, KANK1(30–60). The addition of the KANK1(30–60) peptide resulted in large spectral changes (Figure 2C), most of which were in the slow exchange regime on the NMR timescale indicative of a tight interaction. In agreement with the pull down data, the signals that shifted in slow exchange upon the addition of KANK1(30–60) mapped largely onto the R7 domain with only small progressive shift changes evident on R8. To validate R7 as the major KANK1-binding site on talin, we repeated the NMR experiments using the individual domains, R8 (residues 1461–1580) and R7 (residues 1359–1659  $\Delta$ 1454–1586). Addition of KANK1(30–60) induced small chemical shift changes on the R8 domain indicative of a weak interaction (most likely due to the interaction of LD with the LD-recognition box on R8). However, the addition of a 0.5 molar ratio of KANK1(30–60) to R7 induced large spectral changes with many of the peaks displaying two locations, corresponding to the free peak position and the bound peak position. This is indicative of slow-exchange and confirms a high affinity interaction between R7 and KANK1. The KN peptide is the first identified ligand for the R7 domain.

NMR chemical shifts also provide information on the residues involved in the interaction, as the peaks in the  $^{15}\text{N}$ -HSQC spectrum pertain to individual residues in the protein. To map these chemical shift changes onto the structure of R7-R8, it was first necessary to complete the backbone chemical shift assignments of the R7 domain. This was achieved using conventional triple resonance experiments as described previously (Banno *et al.*, 2012), using  $^{13}\text{C}$ ,  $^{15}\text{N}$  labeled R7. The chemical shift changes mapped predominantly onto one face of R7, comprised of helices 2 and 5 of the 5-helix bundle (talin rod helices 29 and 36), as shown in Figure 2D–E.

Our recent elucidation of the interaction between the LD-motif of DLC1 and talin R8 has generated insight into how LD-motifs are recognized by helical bundles (PDB ID: 5FZT, [Zacharchenko *et al.*, 2016]). In the DLC1:talin R8 complex the DLC1 peptide adopts a helical conformation that packs against two helices on the side of the helical bundle. It is becoming increasingly clear that other LD-motif proteins bind to talin through a similar interaction mode (Zacharchenko *et al.*, 2016). The surface of  $\alpha$ 2 and  $\alpha$ 5 on R7 forms a hydrophobic groove that the KANK1 helix docks into. A striking feature of this KANK1 binding surface is that the two helices are held apart by the conserved aromatic residues, W1630 at the end of  $\alpha$ 5 and Y1389 at the end of  $\alpha$ 2



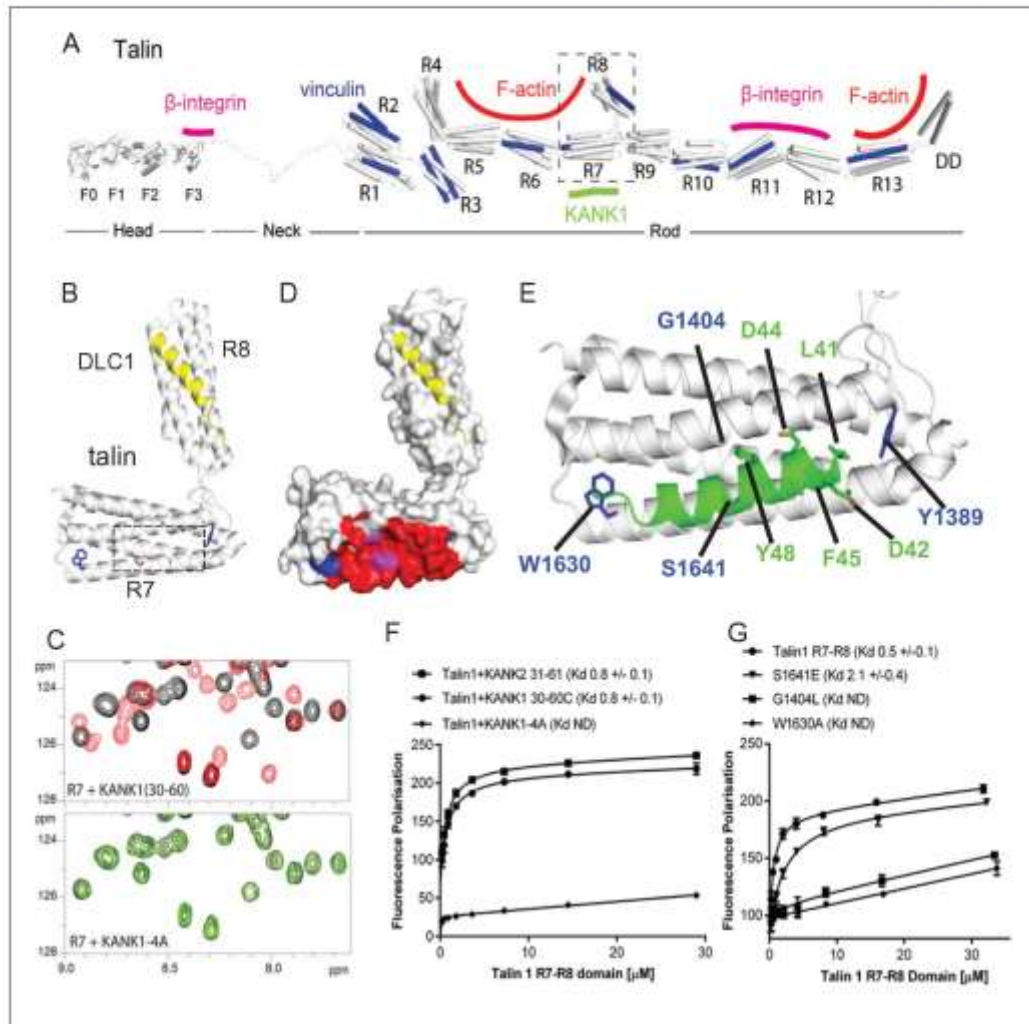


**Figure 2.** Biochemical and structural characterization of the Talin-KANK interaction. (A) Schematic representation of Talin1, with F-actin,  $\beta$ -integrin and vinculin binding sites highlighted. The KANK1 binding site on R7 is also shown. (B) The structure of the complex between talin1 R7-R8 (white) and the LD-motif of DLC1 (yellow) bound on the R8 subdomain (PDB ID: 5FZT, [Zacharchenko et al., 2016]). Residues W1630 and Y1389 (blue) and S1641 (magenta) are highlighted. (C-D) The KANK KN domain binds to a novel site on talin R7.  $^1\text{H}$ ,  $^{15}\text{N}$  HSQC spectra of  $150\ \mu\text{M}$   $^{15}\text{N}$ -labelled talin1 R7 (residues 1357–1659,  $\Delta$ 1454–1586) in the absence (black) or presence of KANK1(30–60C) peptide (red) (top panel) or KANK1-4A (green) (bottom panel) at a ratio of 1:3. (D) Mapping of the KANK1 binding site on R7 as detected by NMR using weighted chemical shift differences (red) – mapped onto the R7-R8 structure in (B). Residues W1630 and Y1389 (blue) and G1404 and S1641 (magenta) are highlighted. (E) Structural model of the talin1.KANK1 interface. Ribbon representation of the KANK1 binding site, comprised of the hydrophobic groove between helices 29 and 36 of R7. Two bulky conserved residues, W1630 and Y1389 (blue) hold these two helices apart forming the binding interface. A small glycine side chain (G1404) creates a pocket between the helices. S1641 (magenta) has been shown previously to be a phosphorylation site [Ratnikov et al., 2005]. The KN peptide (green) Figure 2 continued on next page

## Figure 2 continued

docked onto the KANK binding surface. (F–G) Biochemical characterization of the talin:KANK interaction. (F) Binding of BODIPY-labeled KANK1(30–60) C, KANK2(31–61)C and KANK1-4A peptides to Talin1 R7-R8 (1357–1659) was measured using a Fluorescence Polarization assay. (G) Binding of BODIPY-labeled KANK1(30–60)C to wild type R7-R8, R7-R8 S1641E, R7-R8 G1404L and R7-R8 W1630A. Dissociation constants  $\pm$  SE ( $\mu$ M) for the interactions are indicated in the legend. All measurements were performed in triplicate. ND, not determined.

DOI: 10.7554/eLife.18124.009

The following figure supplements are available for figure 2:

**Figure supplement 1.** NMR validation of the Talin1 R7-R8 mutants.

DOI: 10.7554/eLife.18124.010

**Figure supplement 2.** Biochemical characterization of the Talin2:KANK interaction.

DOI: 10.7554/eLife.18124.011

(Figure 2B,E). W1630 and Y1389 thus essentially serve as molecular rulers, separating helices  $\alpha$ 2 and  $\alpha$ 5 by  $\sim$ 8Å (compared with  $\sim$ 5–6Å for the other bundles in R7-R8). The spacing between the two helices is enhanced further as the residues on the inner helical faces, S1400, G1404, S1411 on  $\alpha$ 2 and S1637 and S1641 on  $\alpha$ 5, have small side chains which have the effect of creating two conserved pockets midway along the hydrophobic groove of the KANK1-binding site (Figure 2E).

The talin-binding site on KANK1 is unusual as it contains a double LD-motif, LDLD. The structure of R7 revealed a potential LD-recognition box with the positive charges, K1401 and R1652 positioned on either side to engage either one, or both, of the aspartic residues. Using the docking program HADDOCK (van Zundert et al., 2016), we sought to generate a structural model of the KANK1/R7 complex, using the chemical shift mapping on R7 and a model of KANK1(30–60) as a helix (created by threading the KANK1 sequence onto the DLC1 LD-motif helix). This analysis indicated that the KANK-LD helix can indeed pack against the sides of  $\alpha$ 2 and  $\alpha$ 5 (Figure 2E); interestingly, all of the models, irrespective of which way the KANK1 helix ran along the surface, positioned the bulky aromatic residue, Y48 in KANK1, in the hydrophobic pocket created by G1404. This raised the possibility that mutation of G1404 to a bulky hydrophobic residue might block KANK1 binding by preventing Y48 engagement. We also noticed that S1641, one of the small residues that create the pocket, has been shown to be phosphorylated *in vivo* (Ratnikov et al., 2005) and might have a regulatory function in the KANK1-talin1 interaction.

To test these hypotheses, we generated a series of point mutants in talin R7 and also in the KANK1 KN-domain, designed to disrupt the talinR7/KANK1 interaction. On the KANK1 side, we mutated the LDLD motif to AAAA, (the KANK1-4A mutant), while on the talin1 side, we generated a series of R7 mutants. These included G1404L, in which a bulky hydrophobic residue was introduced instead of glycine to occlude the hydrophobic pocket in R7, S1641E, a phosphomimetic mutant aimed to test the role of talin phosphorylation in regulating KANK1 binding, and W1630A, a substitution that would remove one of the molecular rulers holding  $\alpha$ 2 and  $\alpha$ 5 helices apart at a fixed distance. These mutants were introduced into talin1 R7-R8 and the structural integrity of the mutated proteins confirmed using NMR (Figure 2—figure supplement 1). The relative binding affinities were measured using an *in vitro* fluorescence polarization assay. In this assay, the KANK1(30–60) peptide is fluorescently labeled with BODIPY and titrated with an increasing concentration of talin R7-R8, and the binding between the two polypeptides results in an increase in the fluorescence polarization signal (Figure 2F). The KANK1-4A mutant abolished binding to talin (Figure 2C,F). The S1641E mutant had only a small effect on binding (Figure 2G), suggesting that either talin1 phosphorylation does not play a major role in modulating the interaction with KANK1 or that the S-E mutation is not a good phosphomimetic, possibly because phosphorylation might also affect helix formation integrity, an effect not mimicked by a single aspartate residue. However, strikingly, both the W1630A and the G1404L mutants abolished binding of KANK1 to talin R7 (Figure 2G), confirming the validity of our model. Finally, we also tested whether the KN-R7 interaction is conserved in talin2 and KANK2, and found that this was indeed the case (Figure 2—figure supplement 2). We conclude that the conserved KN domain of KANKs is a talin-binding site.

### Talin1-KANK1 interaction controls cortical organization of CMSC components

Next, we set out to test the importance of the identified interactions in a cellular context by using the KANK1-4A and the talin G1404L mutants. We chose the G1404L talin mutant over W1630A for our cellular studies, because removing the bulky tryptophan from the hydrophobic core of the R7 might have the off target effect of perturbing the mechanical stability of R7, and our recent studies showed that the mechanostability of R7 is important for protecting R8 from force-induced talin extension (Yao et al., 2016). As could be expected based on the binding experiments with purified protein fragments, the 4A mutation reduced the interaction of the full-length KANK1 with talin1 in a pull-down assay (Figure 3A). An even stronger reduction was observed when KANK1- $\Delta$ CC or the KN alone were tested (Figure 3A). Furthermore, the introduction of the G1404L mutation abrogated the interaction of full-length talin1 or its R7 fragment with full-length KANK1 (Figure 3B).

To investigate the localization of KANK1-4A, we used HeLa cells depleted of endogenous KANK1 and KANK2, the two KANK isoforms present in these cells based on our proteomics studies (van der Vaart et al., 2013) (Figure 3—figure supplement 1A), in order to exclude the potential oligomerization of the mutant KANK1 with the endogenous proteins. Rescue experiments were performed using GFP-KANK1, resistant for the used siRNAs due to several silent mutations (van der Vaart et al., 2013), or its 4A mutant. We also included in this analysis a KANK1 mutant lacking the liprin- $\beta$  1-binding coiled coil domain (the  $\Delta$ CC deletion mutant, Figure 1A), and the 4A-version of the KANK1- $\Delta$ CC deletion mutant. Total Internal Reflection Fluorescence Microscopy (TIRFM)-based live imaging showed that, consistent with our previous results, the GFP-tagged wild type KANK1 strongly accumulated in cortical patches that were tightly clustered around FAs (Figure 3C,D). The KANK1- $\Delta$ CC mutant, which lacked the liprin- $\beta$ 1-binding site but contained an intact KN motif, showed highly specific ring-like accumulations at the rims of FAs (Figure 3C,D). In contrast, KANK1-4A was not clustered anymore around FAs but was dispersed over the cell cortex (Figure 3C,D). The KANK1- $\Delta$ CC-4A mutant, lacking both the liprin- $\beta$ 1 and the talin-binding sites, and the KN-4A mutant were completely diffuse (Figure 3C,D).

To test the impact of the talin1-G1404L mutant, we depleted both talin1 and talin2, which are co-expressed in HeLa cells (Figure 3—figure supplement 1B), and rescued them by introducing mouse GFP-talin1, which was resistant to used siRNAs. The depletion of the two talin proteins resulted in a dramatic loss of FAs and cell detachment from coverslips (data not shown), in agreement with the well-established essential role of talin1 in FA formation (Calderwood et al., 2013; del Rio et al., 2009; Yan et al., 2015; Yao et al., 2014). Therefore, in this experiment only cells expressing GFP-talin1 displayed normal attachment and spreading (Figure 3—figure supplement 1C). The GFP-talin1-G1404L mutant could fully support cell attachment and spreading, although the cell area was slightly increased compared to cells rescued with the wild type GFP-talin1 (Figure 3—figure supplement 1C–E). The number and size of focal adhesions were not significantly different between the cells rescued with the wild type talin1 or its G1404L mutant (Figure 3—figure supplement 1F,G), indicating that the mutant is functional in supporting FA formation. Strikingly, while in cells expressing the wild-type talin1, KANK1 was prominently clustered around FAs, it was dispersed over the plasma membrane in cells expressing talin1-G1404L (Figure 3E,F, Figure 1—figure supplement 1). We conclude that perturbing the KANK1-talin interaction, including the use of a single point mutation in the ~2500 amino acid long talin1 protein, which does not interfere with the talin function in FA formation, abrogates KANK1 association with FAs.

We next tested whether mislocalization of KANK1 due to the perturbation of KANK1-talin1 binding affected other CMSC components. The localization of GFP-KANK1 and its mutants relative to FAs labeled with endogenous markers was very similar to that described above based on live imaging experiments (Figure 4A). Co-depletion of KANK1 and KANK2 abolished clustering of CMSC components, such as LLS $\beta$  and KIF21A at the cell edge (Figure 4B,C). Wild type GFP-KANK1 could rescue cortical clustering of these proteins in KANK1 and KANK2-depleted cells (Figure 4B,C). However, this was not the case for the KANK1-4A mutant, the KANK1- $\Delta$ CC mutant or the KANK1 version bearing both mutations (Figure 4B,C). Importantly, the dispersed puncta of the KANK1-4A mutant still colocalized with LLS $\beta$ , as the binding to liprin- $\beta$ 1 was intact in this mutant (Figure 3A, Figure 4B,C), while the FA-associated rings of KANK1- $\Delta$ CC, the mutant deficient in liprin- $\beta$ 1 binding, showed a mutually exclusive localization with LLS $\beta$  (Figure 4B). In contrast, KIF21A, which binds



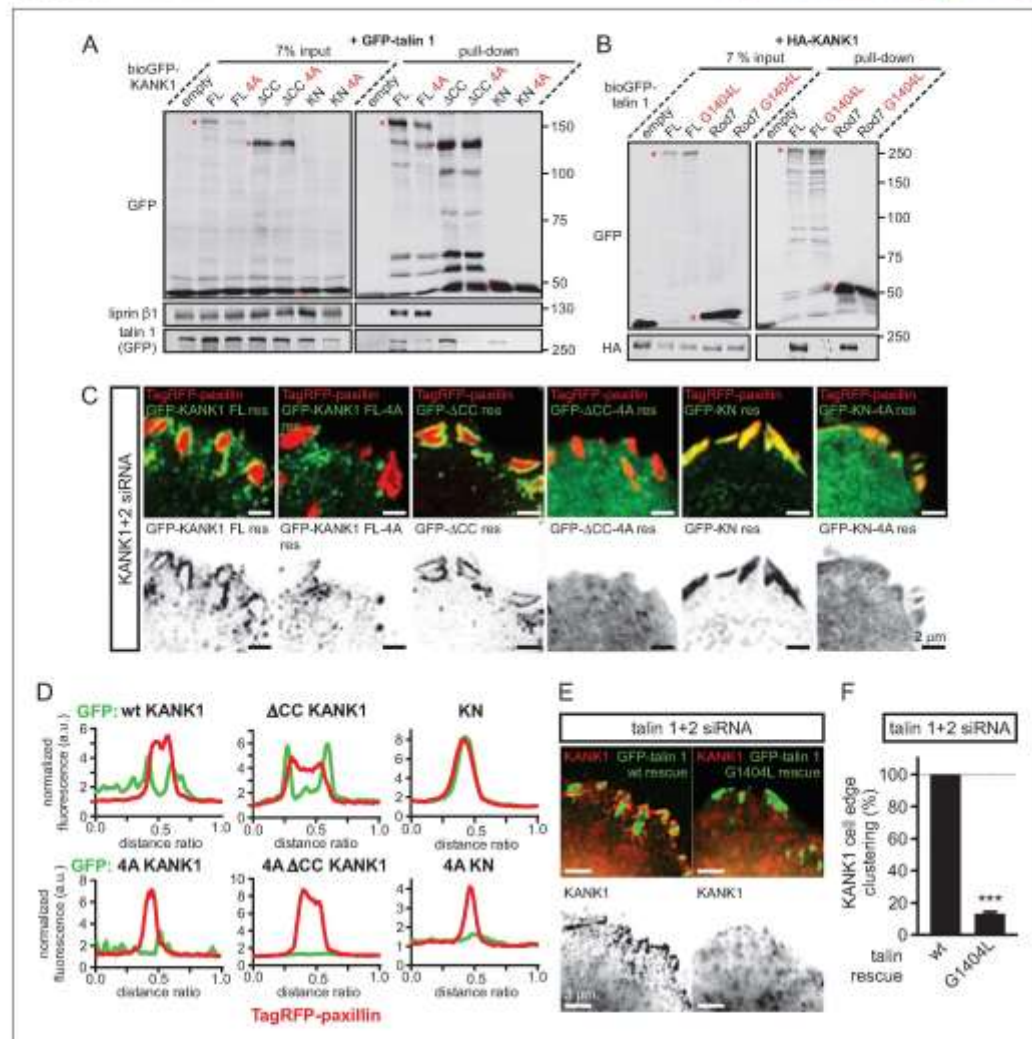


**Figure 3.** KANK1-talin interaction is required for recruiting KANK1 to FAs. (A) Streptavidin pull-down assays with the BioGFP-tagged KANK1 or the indicated KANK1 mutants, co-expressed with GFP-talin1 in HEK293T cells, analyzed by Western blotting with the indicated antibodies. (B) Streptavidin pull-down assays with the BioGFP-tagged talin1 or the indicated talin1 mutants, co-expressed with HA-KANK1 in HEK293T cells, analyzed by Western blotting with the indicated antibodies. (C) TIRFM images of live HeLa cells depleted of KANK1 and KANK2 and co-expressing the indicated siRNA-resistant GFP-KANK1 fusions and TagRFP-paxillin. (D) Fluorescence profile of GFP-tagged mutants and TagRFP-paxillin based on line scan measurement across the FA area in TIRFM images as in panel (C). (E) Widefield fluorescence images of HeLa cells depleted of endogenous talin1 and talin2, rescued by the expression of the wild type GFP-tagged mouse talin1 or its G1404L mutant and labeled for endogenous KANK1 by immunofluorescence staining. (F) Quantification of peripheral clustering of KANK1 in cells treated and analyzed as in (E) (n=12, 6 cells per condition). Error bar, SEM; \*\*\*p<0.001, Mann-Whitney U test.

Figure 3 continued on next page

Figure 3 continued

DOI: 10.7554/eLife.18124.012

The following source data and figure supplements are available for figure 3:

**Source data 1.** An Excel sheet with numerical data on the quantification of peripheral clustering of KANK1 represented as a plot in Figure 3F.

DOI: 10.7554/eLife.18124.013

**Figure supplement 1.** Validation of KANK1/2 and talin1/2 knockdown and effect of disrupted KANK/talin 1 binding in cell spreading and FA formation in HeLa cells.

DOI: 10.7554/eLife.18124.014

**Figure supplement 1—source data 1.** An Excel sheet with numerical data on the quantification of cell area, FA number and FA area represented as plots in Figure 3—figure supplement 1E–G.

DOI: 10.7554/eLife.18124.015

to the ankyrin repeat domain of KANK1, could still colocalize with KANK1- $\Delta$ CC at FA rims (Figure 4B). The overall accumulation of KIF21A at the cell periphery was, however, reduced, in line with the strongly reduced KANK1 peripheral clusters observed with the KANK1- $\Delta$ CC mutant. The diffuse localization of the KANK1-4A- $\Delta$ CC mutant led to the strongly dispersed distribution of the CMSC markers (Figure 4B,C). Furthermore, only the full-length wild type KANK1, but neither the 4A nor  $\Delta$ CC mutant could support efficient accumulation of CLASP2 at the peripheral cell cortex in KANK1 and KANK2-depleted cells (Figure 4D,E), in line with the fact that cortical recruitment of CLASPs depends on LLS $\beta$  (Lansbergen et al., 2006).

Next, we investigated whether disrupting the KANK1-talin1 interaction from the talin1 side would affect also CMSC localization and found that this was indeed the case: both LLS $\beta$  and KIF21A were clustered around FAs in talin1 and talin2-depleted cells rescued with the wild type GFP-talin1, but not in the cells expressing the GFP-talin1-G1404L mutant, deficient in KANK1 binding (Figure 4F,G).

Our data showed that KANK1- $\Delta$ CC could not support proper clustering of CMSC components at the cell edge in spite of its tight accumulation at the FA rims. These data indicate that in addition to binding to talin1, the localization of CMSC clusters depends on the KANK1-liprin- $\beta$ 1 connection. This notion is supported by the observation that the overexpressed coiled coil region of KANK1 (CC1), which can compete for liprin- $\beta$ 1 binding but cannot interact with talin1, acted as a very potent dominant negative, which suppressed accumulation of LLS $\beta$  at the cell periphery (Figure 4H,I). We conclude that the core CMSC protein LLS $\beta$  as well as the microtubule-binding CMSC components KIF21A and CLASP2 depend on the KANK1 interaction with both talin1 and liprin- $\beta$ 1 for their efficient clustering in the vicinity of focal adhesions at the cell periphery.

### Disruption of KANK1-talin1 binding perturbs microtubule plus end organization at the cell periphery

We next investigated the impact of the disruption of KANK1-talin1 interaction on microtubule organization. Due to their stereotypic round shape, HeLa cells represent a particularly convenient model for studying the impact of CMSCs on the distribution and dynamics of microtubule plus ends (Lansbergen et al., 2006; Mimori-Kiyosue et al., 2005; van der Vaart et al., 2013). In this cell line, microtubules grow rapidly in the central parts of the cell, while at the cell margin, where CMSCs cluster in the vicinity of peripheral FAs, microtubule plus ends are tethered to the cortex and display persistent but slow growth due to the combined action of several types of microtubule regulators, including CLASPs, spectraplakins and KIF21A (Drabek et al., 2006; Mimori-Kiyosue et al., 2005; van der Vaart et al., 2013). This type of regulation prevents microtubule overgrowth at the cell edge and results in an orderly arrangement of microtubule plus ends perpendicular to the cell margin (van der Vaart et al., 2013) (Figure 5A). In cells with perturbed CMSCs, microtubule plus ends at the cell periphery become disorganized: the velocity of their growth at the cell margin increases, and their orientation becomes parallel instead of being perpendicular to the cell edge (van der Vaart et al., 2013) (Figure 5A).

Using live cell imaging of the microtubule plus end marker EB3-mRFP in KANK1/2 depleted cells rescued with the wild-type GFP-KANK1, we could indeed show that microtubule plus end growth velocity was almost 2.5 times slower at the cell margin compared to the central part of the cell, and the majority of microtubules at the cell margin grew at a 60–80° angle to the cell edge (Figure 5B–E). In the KANK1/2 depleted cells expressing KANK1 mutants, the velocity of microtubule growth in



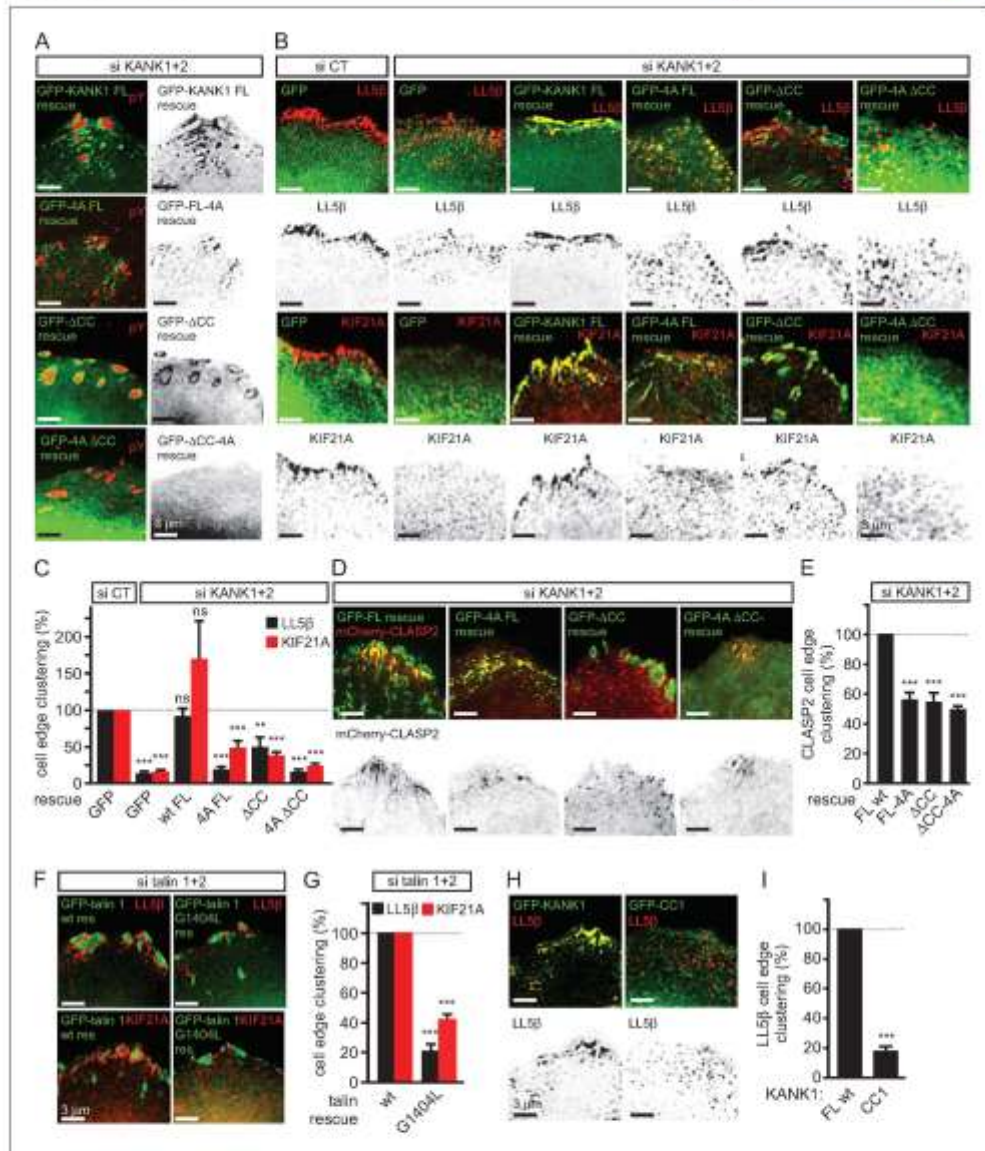


**Figure 4.** KANK1-talin interaction is required for recruiting CMSCs to FAs. (A) Widefield fluorescence images of HeLa cells depleted of KANK1 and KANK2 and expressing the indicated siRNA-resistant GFP-KANK1 fusions (rescue), stained for the FA marker phospho-tyrosine (pY). (B) Widefield fluorescence images of HeLa cells transfected with the control siRNA or siRNAs against KANK1 and KANK2, expressing GFP alone or the indicated siRNA-resistant GFP-KANK1 fusions and stained for LL5β or KIF21A. (C) Quantification of peripheral clustering of LL5β and KIF21A in cells treated as in Figure 4 continued on next page

## Figure 4 continued

panel (B) ( $n=12$ , 5–6 cells per condition). (D) TIRFM images of live HeLa cells depleted of KANK1 and KANK2 and co-expressing the indicated siRNA-resistant GFP-KANK1 fusions and mCherry-CLASP2. (E) Quantification of peripheral clustering of mCherry-CLASP2 in cells treated as in panel (D) ( $n=20$ , 8 cells per condition). (F) Widefield fluorescence images of HeLa cells transfected with the indicated GFP-KANK1 fusions and stained for endogenous LLS3. (G) Quantification of peripheral clustering of LLS3 in cells treated as in panel (F) ( $n=12$ , 6 cells per condition). (H) Widefield fluorescence images of HeLa cells transfected with GFP-tagged KANK1 or its CCT mutant and stained for LLS3. (I) Quantification of peripheral clustering of LLS3 cells treated as in panel (H) ( $n=12$ , 6 cells per condition). Error bars, SEM; ns, non-significant; \*\* $p<0.005$ ; \*\*\* $p<0.001$ , Mann-Whitney U test.

DOI: 10.7554/eLife.18124.016

The following source data is available for figure 4:

**Source data 1.** An Excel sheet with numerical data on the quantification of peripheral clustering of different markers represented as plots in Figure 4C, E, G, I.

DOI: 10.7554/eLife.18124.017

central cell regions was not affected, but the growth rate at the cell periphery increased, and microtubules were growing at oblique angles to the cell margin (Figure 5B–E). The increase of the microtubule growth rate observed with the GFP-KANK1- $\Delta$ CC mutant was less strong than with the two 4A mutants (Figure 5B–E). This can be explained by the fact that GFP-KANK1- $\Delta$ CC was strongly clustered at FA rims (Figure 3C, Figure 5B), and, through its ankyrin repeat domain, could still recruit some KIF21A, a potent microtubule polymerization inhibitor (van der Vaart et al., 2013).

The results with rescue of talin1 and talin2 co-depletion with GFP-talin1 or its G1404L mutant fully supported the conclusions obtained with the KANK1-4A mutant: while in GFP-talin1-expressing cells microtubule growth at the cell edge was three fold slower than in the cell center, only a 1.5 fold difference was observed in GFP-talin1-G1404L expressing cells, and the proportion of microtubules growing parallel rather than perpendicular to the cell edge greatly increased (Figure 5F–I). We conclude that a single point mutation in talin1, which does not interfere with FA formation, is sufficient to perturb CMSC clustering and, as a consequence, induce microtubule disorganization in the vicinity of peripheral FAs.

## Discussion

In this study, we have shown that the conserved KN motif of KANK1 represents an LD-type ligand of talin, which allows this adaptor protein to accumulate in the vicinity of integrin-based adhesions. This function is likely to be conserved in the animal kingdom, as the KANK orthologue in *C. elegans*, Vab-19, in conjunction with integrins, plays important roles in a dynamic cell-extracellular matrix adhesion developmental process (Ihara et al., 2011). The exact impact of KANK1-talin binding likely depends on the specific system, as the loss of KANK proteins was shown to reduce motility of HeLa cells and podocytes (Gee et al., 2015; Li et al., 2011), but promote insulin-dependent cell migration in HEK293 cells (Kakinuma et al., 2008).

An important question is how KANK-talin1 binding mediates the localization of KANK1 to the rim but not the core of FAs. One possibility, suggested by our deletion analysis of KANK1, is that while the KN peptide alone can penetrate into FAs, larger KN-containing protein fragments are sterically excluded from the dense actin-containing core of the FA. However, our experiment with the KN-LacZ fusion did not support this simple idea, indicating that the underlying mechanism is likely to be more complex and might involve specific disordered or ordered domains and additional partners of KANK1, or other regulatory mechanisms. Interestingly, we found that reducing contractility with a ROCK1 inhibitor caused an increase in overlap of KANK1 with FA markers, suggesting that the interaction between KANK1 and talin might be mechanosensitive. An exciting possibility is that full length KANK1 can efficiently interact only with talin molecules at the periphery of focal adhesions because they are not fully incorporated into the focal adhesion structure and are thus less stretched. The KANK1 binding site on talin R7 overlaps with the high affinity actin binding site in talin (which spans R4-R8) (Atherton et al., 2015) and it is possible that different conformational populations of talin exist within adhesions and link to different cytoskeletal components.

Another important question is how KANK1 binding to the rim of focal adhesions can promote CMSC accumulation around these structures, a spatial arrangement in which most of the CMSC molecules cannot be in a direct contact with FAs. Previous work on CMSC complexes showed that they

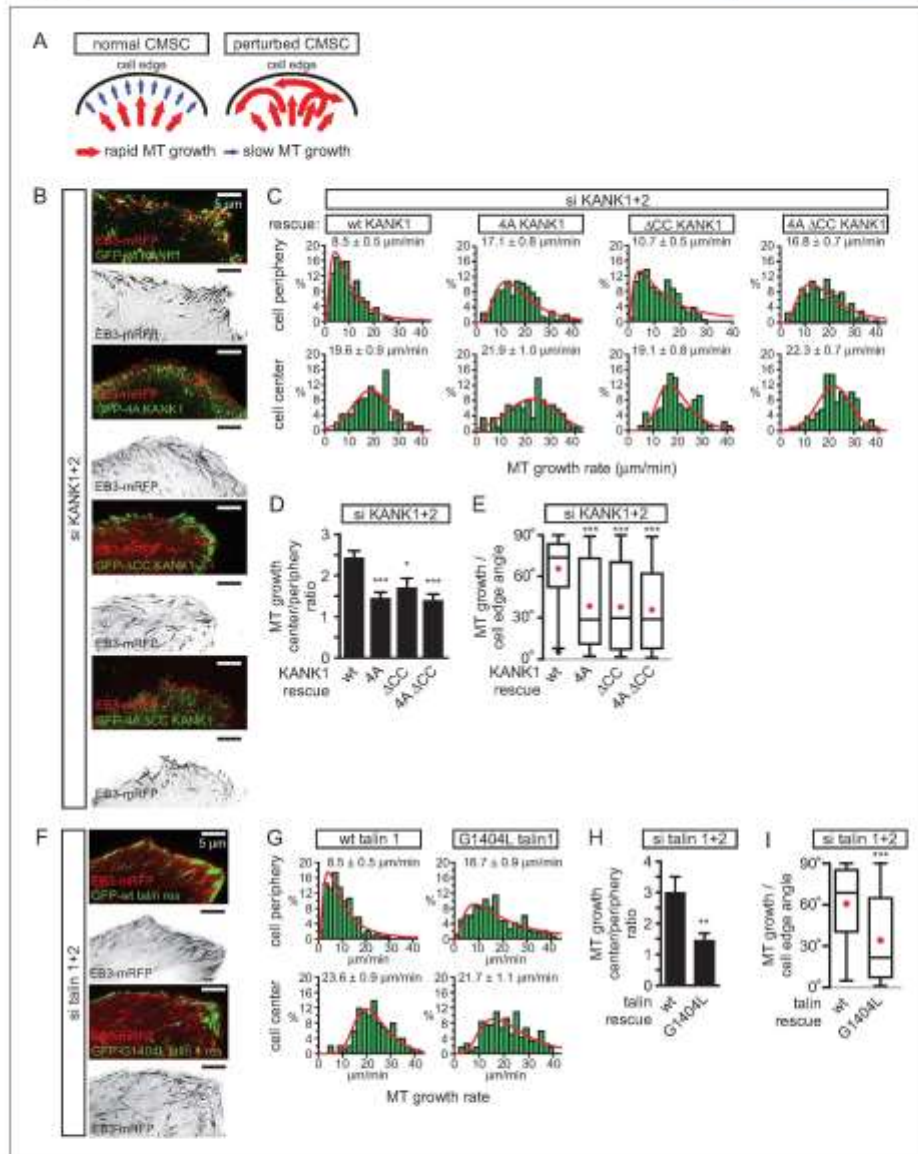


**Figure 5.** The role of talin-KANK1 interaction in regulating microtubule plus end dynamics around FAs. (A) Schematic representation of the pattern of microtubule growth in control HeLa cells and in cells with perturbed CMSCs, based on (van der Vaart et al., 2013). (B) TIRFM images of live HeLa cells depleted of KANK1 and KANK2 and co-expressing the indicated siRNA-resistant GFP-KANK1 fusions and EB3-mRFP. Images are maximum intensity projection of 241 images from time lapse recording of both fluorescence channels. (C) Distributions of microtubule growth rates at the 3 μm broad cell edge. Figure 5 continued on next page.



## Figure 5 continued

area adjacent to the cell edge, and in the central area of the ventral cortex for the cells treated as described in (B) ( $n=87-153$ , 7–8 cells). (D) Ratio of microtubule growth rate in the cell center and at the cell edge for the cells treated as described in B ( $n=7-8$  cells). (E) Angles of microtubule growth relative to the cell margin for the cells treated as described in B. Box plots indicate the 25th percentile (bottom boundary), median (middle line), mean (red dot), 75th percentile (top boundary), nearest observations within 1.5 times the interquartile range (whiskers) and outliers (black dots) ( $n=93-114$ , 7–8 cells). (F) TIRFM images of live HeLa cells depleted of talin1 and talin2 and co-expressing the indicated GFP-talin1 fusions and EB3-mRFP. Images are maximum intensity projection of 241 images from time lapse recordings of both fluorescence channels. (G) Distributions of microtubule growth rates at the 3  $\mu\text{m}$  broad cell area adjacent to the cell edge, and in the central area of the ventral cortex for the cells treated as described in F ( $n=88-154$ , 7 cells). (H) The ratio of microtubule growth rate in the cell center and at the cell edge for the cells treated as described in panel F ( $n=7$  cells). (I) Angles of microtubule growth relative to the cell margin for the cells treated as described in F. Box plots as in (E) ( $n=155-166$ , 10 cells). In all plots: error bars, SEM; ns, non-significant; \*\* $p<0.01$ ; \*\*\* $p<0.001$ , Mann-Whitney U test.

DOI: 10.7554/eLife.18124.019

The following source data is available for figure 5:

**Source data 1.** An Excel sheet with numerical data on the quantification of different aspects of microtubule organization and dynamics represented as plots in Figure 5C–E, G–I.

DOI: 10.7554/eLife.18124.019

are formed through an intricate network of interactions. The 'core' components of these complexes, which can be recruited to the plasma membrane independently of each other, are LL5 $\beta$  (and in some cells, its homologue LL5 $\alpha$ ), liprins and KANKs (of which KANK1 seems to predominate in HeLa cells) (Astro and de Curtis, 2015; Hotta et al., 2010; Lansbergen et al., 2006; van der Vaart et al., 2013) (Figure 6A). The clustering of CMSC components is mutually dependent and relies on homo- and heterodimerization of liprins  $\alpha 1$  and  $\beta 1$ , the association between KANK1 and liprin- $\beta 1$ , the scaffolding protein ELKS, which binds to both LL5 $\beta$  and liprin- $\alpha 1$ , and possibly additional interactions (Astro and de Curtis, 2015; Lansbergen et al., 2006; van der Vaart et al., 2013), while the microtubule-binding proteins, such as CLASPs and KIF21A, seem to associate as a second 'layer' with the membrane-bound CMSC-assemblies (Figure 6A). The CMSC 'patches' can remain relatively stable for tens of minutes, while their individual components are dynamic and exchange with different, characteristic turnover rates (van der Vaart et al., 2013).

The dynamic assemblies of CMSC components, which are spatially separate from other plasma membrane domains and which rely on multivalent protein-protein interactions, are reminiscent of cytoplasmic and nucleoplasmic membrane-unbound organelles such as P granules and stress granules, the assembly of which has been proposed to be driven by phase transitions (Astro and de Curtis, 2015; Brangwynne, 2013; Hyman and Simons, 2012). The formation of such structures, which can be compared to liquid droplets, can be triggered by local concentration of CMSC components. It is tempting to speculate that by concentrating KANK1 at the FA rims, talin1 helps to 'nucleate' CMSC assembly, which can then propagate to form large structures surrounding FAs (Figure 6B). Additional membrane-bound cues, such as the presence of PIP3, to which LL5 $\beta$  can bind (Paranavitane et al., 2003), can further promote CMSC coalescence by increasing concentration of CMSC players in specific areas of the plasma membrane. This model helps to explain why the CMSC accumulation at the cell periphery is reduced but not abolished when PI3 kinase is inhibited (Lansbergen et al., 2006), and why the clustering of all CMSC components is mutually dependent. Most importantly, this model accounts for the mysterious ability of the two large and spatially distinct macromolecular assemblies, FAs and CMSCs, to form in close proximity of each other.

To conclude, our study revealed that a mechanosensitive integrin-associated adaptor talin not only participates in organizing the actin cytoskeleton but also directly triggers formation of a cortical microtubule-stabilizing macromolecular assembly, which surrounds adhesion sites and controls their formation and dynamics by regulating microtubule-dependent signaling and trafficking.

## Materials and methods

### Cell culture and transfection

HeLa Kyoto cell line was described previously (Lansbergen et al., 2006; Mimori-Kiyosue et al., 2005). HEK293T cells were purchased from ATCC; culture and transfection of DNA and siRNA into these cell lines was performed as previously described (van der Vaart et al., 2013). HaCaT cells

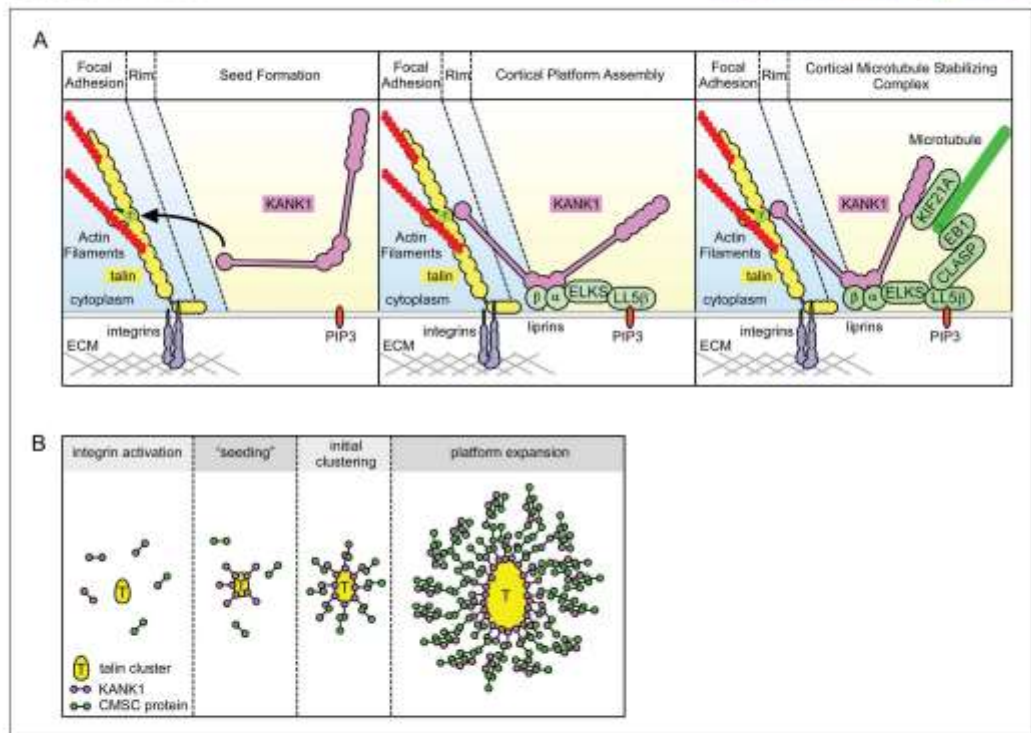


**Figure 6.** Model of talin-directed assembly of cortical microtubule stabilizing complex. (A) Three-step CMSC clustering around focal adhesion: 1) KANK1 binds talin rod domain R7 via the KN motif, 2) KANK1 initiates a cortical platform assembly by binding Iprins-β1 via its CC1 domain, 3) completion of CMSC assembly by further clustering of Iprins, ELKS, LLSβ, CLASP and KIF21A around FA. (B) KANK1 binding to nascent talin clusters acts as a 'seed' for macromolecular complex assembly and organization around a FA.

DOI: 10.7554/eLife.18124.020

were purchased at Cell Line Service (Eppelheim, Germany) and cultured according to manufacturer's instructions. The cell lines were routinely checked for mycoplasma contamination using LT07-518 Mycoalert assay (Lonza, Switzerland). The identity of the cell lines was monitored by immunofluorescence-staining-based analysis with multiple markers. Blebbistatin was purchased from Enzo Life Sciences and used at 50 μM. Serum starvation in HeLa cells was done for 48 hr and focal adhesion assembly was stimulated by incubation with fetal calf serum-containing medium with or without blebbistatin for 2 hr. ROCK1 inhibitor Y-27632 was purchased at Sigma-Aldrich and used at 1 or 10 μM. Double stable HeLa cell line expressing GFP-KANK1 and TagRFP-paxillin was made by viral infection. We used a pLVIN-TagRFP-paxillin-based lentivirus and a pQC-GFP-KANK1-based retrovirus packaged in HEK293T cells using respectively Lenti-X HTX packaging and pCL-Ampho vectors. Antibiotic selection was applied to cells 48 hr after infection using 500 μg/ml G418 (Geneticin, Life Technologies) and 1 μg/ml puromycin (InvivoGen).

#### DNA constructs and siRNAs

BioGFP-tagged KANK1 mutants were constructed using PCR and pBioGFP-C1 vector as previously described (van der Vaart et al., 2013). Rescue constructs for BioGFP-tagged KANK1 were either

based on the version previously described (van der Vaart et al., 2013) or a version obtained by PCR-based mutagenesis of the sequence AGTCAGCGTCTGCGAA to GGTGAGTGTGTGTGAG. mCherry-tagged paxillin construct was made by replacing GFP from pQC-GPXN (Bouchet et al., 2011) by mCherry (pmCherry-C1, Clontech). TagRFP-tagged paxillin construct was made by PCR-based amplification and cloning in pTagRFP-T-C1 (kind gift from Y. Mimori-Kiyosue, Riken Institute, Japan). HA-tagged KANK1 construct was generated by cloning KANK1 coding sequence into pMT2-5M-HA (gift of C. Hoogenraad, Utrecht University, The Netherlands). pLVX-IRES-Neo (pLVIN) vectors was constructed by cloning the IRES-neomycin resistance cassette from the pQCXIN plasmid (Clontech) into the pLVX-IRES-Puro plasmid (Clontech). The lentiviral Lenti-X HTX Packaging vector mix was purchased from Clontech. The retroviral packaging vector pCL-Ampho was kindly provided by E. Bindels, Erasmus MC, The Netherlands. The retroviral pQC-GFP-KANK1 vector was constructed by cloning GFP-KANK1 in pQCXIN and the lentiviral pLVIN-TagRFP-paxillin vector was constructed by cloning TagRFP-paxillin in pLVIN. BirA coding vector was described before (van der Vaart et al., 2013). GFP-tagged mouse talin 1 construct was a kind gift from Dr. A. Huttenlocher (Addgene plasmid # 26724) (Franco et al., 2004). GFP-tagged KN-LacZ fusion was made using PCR-based amplification of KN and LacZ (kind gift, C. Hoogenraad, Utrecht University, The Netherlands), pBioGFP-C1 vector and Gibson Assembly mix (New England Biolabs). Site directed mutagenesis of KANK1 and talin1 constructs was realized by overlapping PCR-based strategy and validated by sequencing. mCherry-tagged CLASP2 construct was a gift from A. Aher (Utrecht University, The Netherlands). Single siRNAs were ordered from Sigma-Aldrich or Ambion, used at 5–15 nM, validated by Western blot analysis and/or immunofluorescence, and target sequences were the following: human KANK1 #1, CAGAGAAGGACATGCGGAT; human KANK1#2, GAAGTCAGCGTCTGCGAAA, human KANK2#1, ATGTCAACGTGCAAGATGA; human KANK2 #2, TCGAGAATCTCAGCACATA; human talin 1 #1, TCTGTAAGTACTGAGTAATAGCCAT; human talin 1 #2, TGAATGTCTCTGCAACTGCTG; human talin 2 #1, TTTCTGTTTTCATCTACTCCTT; human talin 2 #2, TTCGTGTTTGGATTCTGTCGAC. The combination of siRNAs talin1 #2 and talin2#1 was the most efficient and was used for the experiments shown in the paper.

### Pull down assays and mass spectrometry

Streptavidin-based pull down assays of biotinylated proteins expressed using pBioGFP-C1 constructs transfected in HEK293T cells was performed and analyzed as previously described (van der Vaart et al., 2013). For mass spectrometry sample preparation, streptavidin beads resulting from pull-downs assays were run on a 12% Bis-Tris 1D SDS-PAGE gel (BioRad) for 1 cm and stained with colloidal coomassie dye G-250 (Gel Code Blue Stain Reagent, Thermo Scientific). The lane was cut and treated with 6.5 mM dithiothreitol (DTT) for 1 hr at 60°C for reduction and 54 mM iodoacetamide for 30 min for alkylation. The proteins were digested overnight with trypsin (Promega) at 37°C. The peptides were extracted with 100% acetonitrile (ACN) and dried in a vacuum concentrator. For RP-nanoLC-MS/MS, samples were resuspended in 10% formic acid (FA) / 5% DMSO and was analyzed using a Proxeon Easy-nLC100 (Thermo Scientific) connected to an Orbitrap Q-Exactive mass spectrometer. Samples were first trapped (Dr Maisch Reprosil C18, 3  $\mu$ m, 2 cm  $\times$  100  $\mu$ m) before being separated on an analytical column (Agilent Zorbax 1.8  $\mu$ m SB-C18, 40 cm  $\times$  50  $\mu$ m), using a gradient of 180 min at a column flow of 150 nl min<sup>-1</sup>. Trapping was performed at 8  $\mu$ L/min for 10 min in solvent A (0.1 M acetic acid in water) and the gradient was as follows: 15–40% solvent B (0.1 M acetic acid in acetonitrile) in 151 min, 40–100% in 3 min, 100% solvent B for 2 min, and 100% solvent A for 13 min. Nanospray was performed at 1.7 kV using a fused silica capillary that was pulled in-house and coated with gold (o.d. 360  $\mu$ m; i.d. 20  $\mu$ m; tip i.d. 10  $\mu$ m). The mass spectrometers were used in a data-dependent mode, which automatically switched between MS and MS/MS. Full scan MS spectra from m/z 350 – 1500 were acquired at a resolution of 35,000 at m/z 400 after the accumulation to a target value of 3E6. Up to 20 most intense precursor ions were selected for fragmentation. HCD fragmentation was performed at normalized collision energy of 25% after the accumulation to a target value of 5E4. MS2 was acquired at a resolution of 17,500 and dynamic exclusion was enabled. For data analysis, raw files were processed using Proteome Discoverer 1.4 (version 1.4.1.14, Thermo Scientific, Bremen, Germany). Database search was performed using the swiss-prot human database (version 29th of January 2015) and Mascot (version 2.5.1, Matrix Science, UK) as the search engine. Carbamidomethylation of cysteines was set as a fixed modification and oxidation of methionine was set as a variable modification. Trypsin was specified as enzyme and up to two



miss cleavages were allowed. Data filtering was performed using a percolator (Käll et al., 2007), resulting in 1% false discovery rate (FDR). Additional filter was ion score >20.

### Antibodies and immunofluorescence cell staining

Antibodies against HA and GFP tags, and liprin  $\beta$ 1 used for Western blot analysis were previously described (van der Vaart et al., 2013). Rabbit antibodies against KANK1 (HPA005539) and KANK2 (HPA015643) were purchased at Sigma-Aldrich. Western blot analysis of KANK1 was performed using rabbit polyclonal KANK1 antibody (A301-882A) purchased at Bethyl Laboratories. Talin immunofluorescence staining was performed using mouse monoclonal 8d4 antibody (Sigma-Aldrich). Western blot analysis of talin 1 and 2 expression was performed using respectively the isotype specific mouse monoclonal 97H6 (Sigma-Aldrich) and 68E7 (Abcam) antibodies. Ku80 (7/Ku80) antibody was purchased from BD Biosciences. Immunofluorescence staining of KANK1, LL5 $\beta$ , liprin  $\beta$ 1, KIF21A and CLASP2 in HeLa and HaCaT cells was performed using the antibodies and procedures previously described (Lansbergen et al., 2006; van der Vaart et al., 2013). F-actin was stained using Alexa Fluor 594-conjugated phalloidin (Life Technologies). Phospho-tyrosine mouse antibody (PT-66) was purchased from Sigma-Aldrich and rabbit FAK phospho-tyrosine 397 was purchased from Biosource.

### Microscopy and analysis

Fixed samples and corresponding immunofluorescence images were acquired using widefield fluorescence illumination on a Nikon Eclipse 80i or Ni upright microscope equipped with a CoolSNAP HQ2 CCD camera (Photometrics) or a DS-Qi2 camera (Nikon) an Intensilight C-HGF precentered fiber illuminator (Nikon), ET-DAPI, ET-EGFP and ET-mCherry filters (Chroma), Nikon NIS Br software, Plan Apo VC 100x NA 1.4 oil, Plan Apo Lambda 100X oil NA 1.45 and Plan Apo VC 60x NA 1.4 oil (Nikon) objectives. TIRFM-based live cell imaging was performed using the setup described before (van der Vaart et al., 2013) or a similar Nikon Ti microscope-based Ila<sup>2</sup> system (Roper Scientific, Evry, FRANCE) equipped with dual laser illuminator for azimuthal spinning TIRF (or Hilo) illumination, 150 mW 488 nm laser and 100 mW 561 nm laser, 49,002 and 49,008 Chroma filter sets, EMCCD Evolve mono FW DELTA 512x512 camera (Roper Scientific) with the intermediate lens 2.5X (Nikon C mount adapter 2.5X), CCD camera CoolSNAP MYO M-USB-14-AC (Roper Scientific) and controlled with MetaMorph 7.8.8 software (Molecular Devices). Simultaneous imaging of green TIRFM imaging was performed as described before (van der Vaart et al., 2013) or using the Optosplit III image splitter device (Andor) on the Ila<sup>2</sup> system.

For presentation, images were adjusted for brightness and processed by Gaussian blur and Unsharp mask filter using ImageJ 1.47v (NIH). Fluorescence profiles are values measured by line scan analysis in ImageJ, normalized by background average fluorescence, expressed as a factor of the baseline value obtained for individual channel and plotted as a function of maximum length factor of the selection line (distance ratio). Protein clustering at the cell edge is the ratio of the total fluorescence in the first 5  $\mu$ m from the cell edge to the next 5  $\mu$ m measured by line scan analysis in ImageJ after thresholding for cell outline marking and out-of-cell region value assigned to zero. The results were plotted as percentage of control condition average value. FA counting and area measurement was performed using Analyze Particles under ImageJ on focal adhesion binary mask obtained after Gaussian blur/threshold-based cell outline marking and background subtraction (rolling ball radius, 10 pixels). KANK1/talin colocalization was analyzed using Pearson R value provided by Colocalization Analysis plugin under Fiji-ImageJ and a 3  $\mu$ m diameter circular ROI centered on talin clusters detected by immunofluorescent staining.

nEB3-mRFP dynamics was recorded by 0.5 s interval time lapse TIRF imaging. Microtubule growth was measured using kymographs obtained from EB3-mRFP time lapse image series, plotted and presented as previously described (van der Vaart et al., 2013). Ratio of microtubule growth in cell center to periphery was obtained as values for individual cells. Microtubule growth trajectory angle to the cell edge was manually measured in ImageJ using tracks obtained by maximum intensity projection of EB3-mRFP image series.

### Expression of recombinant talin polypeptides

The cDNAs encoding murine talin1 residues 1357–1653 (R7-R8), 1357–1653  $\Delta$ 1454–1586 (R7) and 1461–1580 (R8) were synthesized by PCR using a mouse talin1 cDNA as template and cloned into

the expression vector pet151-TOPO (Invitrogen) (Gingras *et al.*, 2010). Talin mutants were synthesized by GeneArt. Talin polypeptides were expressed in *E. coli* BL21(DE3) cultured either in LB for unlabeled protein, or in M9 minimal medium for the preparation of isotopically labeled samples for NMR. Recombinant His-tagged talin polypeptides were purified by nickel-affinity chromatography following standard procedures. The His-tag was removed by cleavage with AcTEV protease (Invitrogen), and the proteins were further purified by anion-exchange. Protein concentrations were determined using their respective extinction coefficient at 280 nm.

### Fluorescence polarization assays

KANK peptides with a C-terminal cysteine residue were synthesized by Biomatik (USA):

KANK1(30–60)C - PYFVETPYGFQLDLDFVKYVDDIQKGNTIKKCC  
 KANK1(30–68)C - PYFVETPYGFQLDLDFVKYVDDIQKGNTIKKLNQKRRKCC  
 KANK1-4A - PYFVETPYGFQAAAAPVKYVDDIQKGNTIKKLNQKRRKCC  
 KANK2(31–61)C - PYSVETPYGYRLDLDFLYVDDIEKGHTLRRCC

Fluorescence Polarization was carried out on KANK peptides with a carboxy terminal cysteine. Peptide stock solutions were made in PBS (137 mM NaCl, 27 mM KCl, 100 mM Na<sub>2</sub>HPO<sub>4</sub>, 18 mM KH<sub>2</sub>PO<sub>4</sub>), 100 mg/ml TCEP and 0.05% Triton X-100, and coupled via the carboxy terminal cysteine to the Thiol reactive BIODIPY TMR dye (Invitrogen). Uncoupled dye was removed by gel filtration using a PD-10 column (GE Healthcare). The labeled peptide was concentrated to a final concentration of 1 mM using a centricon with 3K molecular weight cut off (Millipore).

The Fluorescence Polarization assay was carried out on a black 96well plate (Nunc). Titrations were performed in triplicate using a fixed 0.5 μM concentration of peptide and an increasing concentration of Talin R7-R8 protein within a final volume of 100 μl of assay buffer (PBS). Fluorescence Polarization measurements were recorded on a BMGLabTech CLARIOstar plate reader at room temperature and analyzed using GraphPad Prism (version 6.07). *K<sub>d</sub>* values were calculated with a non-linear curve fitting using a one site total and non-specific binding model.

### NMR spectroscopy

NMR experiments for the resonance assignment of talin1 R7, residues 1357–1653 Δ1454–1586 were carried out with 1 mM protein in 20 mM sodium phosphate, pH 6.5, 50 mM NaCl, 2 mM dithiothreitol, 10% (w/v) 2H<sub>2</sub>O. NMR spectra were obtained at 298 K using a Bruker AVANCE III spectrometer equipped with CryoProbe. Proton chemical shifts were referenced to external 2,2-dimethyl-2-silapentane-5-sulfonic acid, and <sup>15</sup>N and <sup>13</sup>C chemical shifts were referenced indirectly using recommended gyromagnetic ratios (Wisart *et al.*, 1995). The spectra were processed using Topspin and analyzed using CCPN Analysis (Skinner *et al.*, 2015). Three-dimensional HNCO, HN(CA)CO, HNCA, HN(CO)CA, HNCACB, and CBCA(CO)NH experiments were used for the sequential assignment of the backbone NH, N, CO, CA, and CB resonances.

The backbone resonance assignments of mouse talin1 R7 (1357–1653 Δ1454–1586) have been deposited in the BioMagResBank with the accession number 19139.

### Acknowledgements

We thank Y Mimori-Kiyosue (Riken Institute, Japan), A Huttenlocher (University of Wisconsin), A Aher and C Hoogenraad (Utrecht University, The Netherlands) for the gift of reagents. We thank M Geleijnse and A Floor for help with siRNA validation, cell culture and fluorescent staining. We are grateful to I Grigoriev (Utrecht University, The Netherlands) for assistance with microscopy and advice about microtubule dynamics analysis, and to JD Kaiser for advice about PowerPoint. This work was supported by the Netherlands organization for Scientific Research (NWO) ALW VICI grant 865.08.002 and a European Research Council (ERC) Synergy grant 609822 to AA, a BBSRC grant (BB/N007336/1) to BTG, Human Frontier Science Program RGP00001/2016 grant to AA and BTG, NWO VIDI grant (723.012.102) for AFMA and as part of the NWO National Roadmap Large-scale Research Facilities of the Netherlands (project number 184.032.201) for AFMA, AJRH and HP, and Fondation pour la Recherche Médicale and Marie Curie International Intra-European Fellowship to BPB Y-C A is supported by the MARIE SKŁODOWSKA-CURIE ACTIONS Innovative Training Network (ITN) 675407 PolarNet.



## Additional information

### Competing interests

AA: Reviewing editor, *eLife*. The other authors declare that no competing interests exist.

### Funding

Funder	Grant reference number	Author
Fondation pour la Recherche Médicale (FRM)	postdoctoral fellowship	Benjamin F Bouchet
Marie Curie International Intra-European Fellowship	postdoctoral fellowship	Benjamin F Bouchet
Nederlandse Organisatie voor Wetenschappelijk Onderzoek	National Roadmap for Large-Scale facilities Project 184.032.201	AF Maarten Altelaar Albert JR Heck
Nederlandse Organisatie voor Wetenschappelijk Onderzoek	VIDI 723.012.102	AF Maarten Altelaar
Biotechnology and Biological Sciences Research Council	Grant BB/N007336/1	Benjamin T Goult
Human Frontier Science Program	RGP00001/2016	Benjamin T Goult Anna Akhmanova
Nederlandse Organisatie voor Wetenschappelijk Onderzoek	ALW VICI 865.08.002	Anna Akhmanova
European Research Council	ERC Synergy 609622	Anna Akhmanova
Marie Curie Actions Innovative Training Network	ITN PolarNet 675407	Anna Akhmanova

The funders had no role in study design, data collection and interpretation, or the decision to submit the work for publication.

### Author contributions

BPB, BTG, Conception and design, Acquisition of data, Analysis and interpretation of data, Drafting or revising the article; REG, Y-CA, DvdW, HP, Acquisition of data, Analysis and interpretation of data, Drafting or revising the article; GJ, Conception and design, Drafting or revising the article, Contributed unpublished essential data or reagents; AFMA, Analysis and interpretation of data, Drafting or revising the article; AJRH, AA, Conception and design, Analysis and interpretation of data, Drafting or revising the article

### Author ORCIDs

Albert JR Heck, <http://orcid.org/0000-0002-2405-4404>

Benjamin T Goult, <http://orcid.org/0000-0002-3438-2807>

Anna Akhmanova, <http://orcid.org/0000-0002-9048-8614>

## References

- Akhmanova A, Stehbens SJ, Yap AS. 2009. Touch, grasp, deliver and control: functional cross-talk between microtubules and cell adhesions. *Traffic* **10**:268–274. doi: [10.1111/j.1600-0854.2008.00869.x](https://doi.org/10.1111/j.1600-0854.2008.00869.x)
- Alam T, Alazmi M, Gao X, Arnold ST. 2014. How to find a leucine in a haystack? Structure, ligand recognition and regulation of leucine-aspartic acid (LD) motifs. *Biochemical Journal* **460**:317–329. doi: [10.1042/BJ20140298](https://doi.org/10.1042/BJ20140298)
- Arthurs NJ, Wegener KL, Ye F, Kim C, Goult BT, Lowe ED, Vakonakis I, Bate N, Critchley DR, Gieseberg MH, Campbell ID. 2009. The structure of an integrin/talin complex reveals the basis of inside-out signal transduction. *The EMBO Journal* **28**:3623–3632. doi: [10.1038/emboj.2009.287](https://doi.org/10.1038/emboj.2009.287)
- Astro V, Chiarelli S, Magistrati E, Fivaz M, de Curtis I. 2014. Lpfr $\alpha$ 1, ERC1 and LLS define polarized and dynamic structures that are implicated in cell migration. *Journal of Cell Science* **127**:3862–3876. doi: [10.1242/jcs.155663](https://doi.org/10.1242/jcs.155663)
- Astro V, de Curtis I. 2015. Plasma membrane-associated platforms: dynamic scaffolds that organize membrane-associated events. *Science Signaling* **8**:re1. doi: [10.1126/scisignal.1253312](https://doi.org/10.1126/scisignal.1253312)
- Atherton P, Stutchbury B, Wang D-Y, Jethwa D, Tsang R, Meiler-Rodríguez E, Wang P, Bate N, Zent R, Barsukov IL, Goult BT, Critchley DR, Ballastrém C. 2015. Vinculin controls talin engagement with the actomyosin machinery. *Nature Communications* **6**:10038. doi: [10.1038/ncomms10038](https://doi.org/10.1038/ncomms10038)

- Banno A, Goult BT, Lee H, Bate N, Critchley DR, Ginsberg MH. 2012. Subcellular localization of talin is regulated by inter-domain interactions. *Journal of Biological Chemistry* **287**:13799–13812. doi: 10.1074/jbc.M112.341214
- Basu S, Sladeczek S, Martínez de la Peña y Valenzuela I, Akaaboune M, Smal I, Martin K, Galjart N, Brenner HR. 2015. CLASP2-dependent microtubule capture at the neuromuscular junction membrane requires LLS3 and actin for focal delivery of acetylcholine receptor vesicles. *Molecular Biology of the Cell* **26**:938–951. doi: 10.1091/mbc.E14-06-1158
- Basu S, Sladeczek S, Pemble H, Witmann T, Slotman JA, van Cappellen W, Brenner HR, Galjart N. 2014. Acetylcholine receptor (AChR) clustering is regulated both by glycogen synthase kinase 3 $\beta$  (GSK3 $\beta$ ) dependent phosphorylation and the level of CLIP-associated protein 2 (CLASP2) mediating the capture of microtubule plus-ends. *Journal of Biological Chemistry* **289**:30857–30867. doi: 10.1074/jbc.M114.589457
- Bouchet BP, Fauzet F, Gröller G, Galmarini CM, Puisieux A. 2011. p21(Cip1) regulates cell-substrate adhesion and interphase microtubule dynamics in untransformed human mammary epithelial cells. *European Journal of Cell Biology* **90**:631–641. doi: 10.1016/j.ejcb.2011.03.002
- Brangwynne CP. 2013. Phase transitions and size scaling of membrane-less organelles. *Journal of Cell Biology* **203**:875–881. doi: 10.1083/jcb.201308087
- Byron A, Askari JA, Humphries JD, Jacquemet G, Koper EJ, Warwood S, Choi CK, Stroud MJ, Chen CS, Knight D, Humphries MJ. 2015. A proteomic approach reveals integrin activation state-dependent control of microtubule cortical targeting. *Nature Communications* **6**:6135. doi: 10.1038/ncomms7135
- Caldenwood DA, Campbell ID, Critchley DR. 2013. Talins and kindlins: partners in integrin-mediated adhesion. *Nature Reviews Molecular Cell Biology* **14**:503–517. doi: 10.1038/nrm3424
- del Río A, Perez-Jimenez R, Liu R, Roca-Cusachs P, Fernandez JM, Sheetz MP. 2009. Stretching single talin rod molecules activates vinculin binding. *Science* **323**:638–641. doi: 10.1126/science.1162912
- Drabek K, van Ham M, Stepanova T, Draegsteiner K, van Hoesen R, Sayas CL, Akhmanova A, Ten Hagen T, Smits R, Fodde R, Grosveld F, Galjart N. 2006. Role of CLASP2 in microtubule stabilization and the regulation of persistent motility. *Current Biology* **16**:2259–2264. doi: 10.1016/j.cub.2006.09.065
- Earratty EJ, Partridge MA, Gundersen GG. 2005. Microtubule-induced focal adhesion disassembly is mediated by dynamin and focal adhesion kinase. *Nature Cell Biology* **7**:581–590. doi: 10.1038/ncb1262
- Franco SJ, Rodgers MA, Perrin BJ, Han J, Bennis DA, Critchley DR, Huttenlocher A. 2004. Calpain-mediated proteolysis of talin regulates adhesion dynamics. *Nature Cell Biology* **6**:977–983. doi: 10.1038/ncb1175
- Gardel ML, Schneider IC, Aratyn-Schaus Y, Waterman CM. 2010. Mechanical integration of actin and adhesion dynamics in cell migration. *Annual Review of Cell and Developmental Biology* **26**:315–333. doi: 10.1146/annurev.cellbio.011209.122036
- Gee HY, Zhang F, Ashraf S, Kohl S, Sadowski CE, Vega-Warner V, Zhou W, Lovric S, Fang H, Nettleton M, Zhu Jun-yi, Hoefele J, Weber LT, Podracka L, Boor A, Fehrenbach H, Innis JW, Washburn J, Levy S, Liften RP, et al. 2015. KANK deficiency leads to podocyte dysfunction and nephrotic syndrome. *Journal of Clinical Investigation* **125**:2375–2384. doi: 10.1172/JCI79504
- Gingras AR, Bate N, Goult BT, Patel B, Koop PM, Emsley J, Barsukov IL, Roberts GC, Critchley DR. 2010. Central region of talin has a unique fold that binds vinculin and actin. *Journal of Biological Chemistry* **285**:29577–29587. doi: 10.1074/jbc.M109.095455
- Goult BT, Zacharchenko T, Bate N, Tsang R, Hay F, Gingras AR, Elliott PR, Roberts GC, Ballestrem C, Critchley DR, Barsukov IL. 2013. RIAM and vinculin binding to talin are mutually exclusive and regulate adhesion assembly and turnover. *Journal of Biological Chemistry* **288**:8238–8249. doi: 10.1074/jbc.M112.438119
- Grigoriev I, Splinter D, Keijzer N, Wolf PS, Demmers J, Ohtsuka T, Modesti M, Maly IV, Grosveld F, Hoogenraad CC, Akhmanova A. 2007. Rab6 regulates transport and targeting of exocytotic carriers. *Developmental Cell* **13**:305–314. doi: 10.1016/j.devcel.2007.06.010
- Grigoriev I, Yu KL, Martínez-Sánchez E, Serra Marques A, Smal I, Meijering E, Demmers J, Peränen J, Pasterkamp RJ, van der Sluis P, Hoogenraad CC, Akhmanova A. 2011. Rab6, Rab8, and MICAL3 cooperate in controlling docking and fusion of exocytotic carriers. *Current Biology* **21**:967–974. doi: 10.1016/j.cub.2011.04.030
- Gundelfinger ED, Fajtova A. 2012. Molecular organization and plasticity of the cytomatrix at the active zone. *Current Opinion in Neurobiology* **22**:423–430. doi: 10.1016/j.conb.2011.10.005
- Hida Y, Ohtsuka T. 2010. CAST and ELKS proteins: structural and functional determinants of the presynaptic active zone. *Journal of Biochemistry* **148**:131–137. doi: 10.1093/jb/mvq065
- Honnappa S, Gouveia SM, Weisbrich A, Damberger FF, Bhavesh NS, Jawhari H, Grigoriev I, van Rijssel FJ, Buey RM, Lawera A, Jelasarov I, Winkler FK, Wüthrich K, Akhmanova A, Steinmetz MO. 2009. An EB1-binding motif acts as a microtubule tip localization signal. *Cell* **138**:366–376. doi: 10.1016/j.cell.2009.04.065
- Hotta A, Kawakatsu T, Nakazani T, Sato T, Matsui C, Sukezane T, Akagi T, Hamaji T, Grigoriev I, Akhmanova A, Takai Y, Mimori-Kiyosue Y. 2010. Laminin-based cell adhesion anchors microtubule plus ends to the epithelial cell basal cortex through LLSa/3. *Journal of Cell Biology* **189**:901–917. doi: 10.1083/jcb.200910595
- Hyman AA, Simons K. 2012. Cell biology. Beyond oil and water—phase transitions in cells. *Science* **337**:1047–1049. doi: 10.1126/science.1223728
- Hynes RO. 1992. Integrins: versatility, modulation, and signaling in cell adhesion. *Cell* **69**:11–25. doi: 10.1016/0092-8674(92)90115-5
- Ihara S, Hagedorn EJ, Morrissey MA, Chi Q, Motegi F, Kramer JM, Sherwood DR. 2011. Basement membrane sliding and targeted adhesion remodels tissue boundaries during uterine-vulval attachment in *Caenorhabditis elegans*. *Nature Cell Biology* **13**:641–651. doi: 10.1038/ncb2233

- Kakinuma N, Kiyama R. 2009. A major mutation of KIF21A associated with congenital fibrosis of the extraocular muscles type 1 (CFEOM1) enhances translocation of Kank1 to the membrane. *Biochemical and Biophysical Research Communications* **386**:639–644. doi: [10.1016/j.bbrc.2009.06.109](https://doi.org/10.1016/j.bbrc.2009.06.109)
- Kakinuma N, Roy BC, Zhu Y, Wang Y, Kiyama R. 2008. Kank regulates RhoA-dependent formation of actin stress fibers and cell migration via 14-3-3 in PI3K-Akt signaling. *The Journal of Cell Biology* **181**:537–549. doi: [10.1083/jcb.200707022](https://doi.org/10.1083/jcb.200707022)
- Kakinuma N, Zhu Y, Wang Y, Roy BC, Kiyama R. 2009. Kank proteins: structure, functions and diseases. *Cellular and Molecular Life Sciences* **66**:2651–2659. doi: [10.1007/s00016-009-0038-y](https://doi.org/10.1007/s00016-009-0038-y)
- Käll L, Canterbury JD, Weston J, Noble WS, MacCoss MJ. 2007. Semi-supervised learning for peptide identification from shotgun proteomics datasets. *Nature Methods* **4**:923–925. doi: [10.1038/nmeth1113](https://doi.org/10.1038/nmeth1113)
- Kaverina I, Krylyshkina O, Small JV. 1999. Microtubule targeting of substrate contacts promotes their relaxation and dissociation. *The Journal of Cell Biology* **146**:1033–1044. doi: [10.1083/jcb.146.5.1033](https://doi.org/10.1083/jcb.146.5.1033)
- Kaverina I, Rottner K, Small JV. 1998. Targeting, capture, and stabilization of microtubules at early focal adhesions. *The Journal of Cell Biology* **142**:181–190. doi: [10.1083/jcb.142.1.181](https://doi.org/10.1083/jcb.142.1.181)
- Kaverina I, Straube A. 2011. Regulation of cell migration by dynamic microtubules. *Seminars in Cell & Developmental Biology* **22**:968–974. doi: [10.1016/j.semcdb.2011.09.017](https://doi.org/10.1016/j.semcdb.2011.09.017)
- Kishi M, Künmer TT, Eglen SJ, Sanes JR. 2005. LL5beta: a regulator of postsynaptic differentiation identified in a screen for synaptically enriched transcripts at the neuromuscular junction. *The Journal of Cell Biology* **169**:355–366. doi: [10.1083/jcb.200411012](https://doi.org/10.1083/jcb.200411012)
- Kodama A, Karakesisoglou I, Wong E, Vaezi A, Fuchs E. 2003. ACF7: an essential integrator of microtubule dynamics. *Cell* **115**:343–354. doi: [10.1016/S0092-8674\(03\)00813-4](https://doi.org/10.1016/S0092-8674(03)00813-4)
- Krylyshkina O, Anderson KL, Kaverina I, Upmann I, Manstein DJ, Small JV, Toomre DK. 2003. Nanometer targeting of microtubules to focal adhesions. *The Journal of Cell Biology* **161**:853–859. doi: [10.1083/jcb.200301102](https://doi.org/10.1083/jcb.200301102)
- Lansbergen G, Grigoriev I, Mimori-Kiyosue Y, Ohtsuka T, Higa S, Kitajima I, Demmers J, Galjart N, Houtsmuller AB, Grosveld F, Akhmanova A. 2006. CLASPs attach microtubule plus ends to the cell cortex through a complex with LL5beta. *Developmental Cell* **11**:21–32. doi: [10.1016/j.devcel.2006.05.012](https://doi.org/10.1016/j.devcel.2006.05.012)
- Li C-C, Kuo J-C, Waterman CM, Kiyama R, Moss J, Vaughan M. 2011. Effects of brefeldin A-inhibited guanine nucleotide-exchange (BIG) 1 and KANK1 proteins on cell polarity and directed migration during wound healing. *PNAS* **108**:19228–19233. doi: [10.1073/pnas.1117051108](https://doi.org/10.1073/pnas.1117051108)
- Mimori-Kiyosue Y, Grigoriev I, Lansbergen G, Sasai H, Matsui C, Severin F, Galjart N, Grosveld F, Vorobjev I, Taubka S, Akhmanova A. 2005. CLASP1 and CLASP2 bind to EB1 and regulate microtubule plus-end dynamics at the cell cortex. *The Journal of Cell Biology* **168**:141–153. doi: [10.1083/jcb.200405094](https://doi.org/10.1083/jcb.200405094)
- Nakaya Y, Sukowati EW, Sheng G. 2013. Epiblast integrity requires CLASP and Dystroglycan-mediated microtubule anchoring to the basal cortex. *The Journal of Cell Biology* **202**:637–651. doi: [10.1083/jcb.201302075](https://doi.org/10.1083/jcb.201302075)
- Oakes PW, Beckham Y, Stricker J, Gardel ML. 2012. Tension is required but not sufficient for focal adhesion maturation without a stress fiber template. *The Journal of Cell Biology* **196**:363–374. doi: [10.1083/jcb.201107042](https://doi.org/10.1083/jcb.201107042)
- Paranavittane V, Coadwell WJ, Eguinoa A, Hawkins PT, Stephens L. 2003. LL5beta is a phosphatidylinositol (3,4,5)-trisphosphate sensor that can bind the cytoskeletal adaptor, gamma-filamin. *Journal of Biological Chemistry* **278**:1328–1335. doi: [10.1074/jbc.M208352000](https://doi.org/10.1074/jbc.M208352000)
- Parsons JT, Horwitz AR, Schwartz MA. 2010. Cell adhesion: integrating cytoskeletal dynamics and cellular tension. *Nature Reviews Molecular Cell Biology* **11**:633–643. doi: [10.1038/nrm2957](https://doi.org/10.1038/nrm2957)
- Prasaynkil TJ, Gingras J, Valdez G, Krzewski K, Sanes JR. 2009. Podosomes are present in a postsynaptic apparatus and participate in its maturation. *PNAS* **106**:18373–18378. doi: [10.1073/pnas.0910391106](https://doi.org/10.1073/pnas.0910391106)
- Prasaynkil TJ, Sanes JR. 2013. Amotl2 interacts with LL5, localizes to podosomes and regulates postsynaptic differentiation in muscle. *Journal of Cell Science* **126**:2225–2235. doi: [10.1242/jcs.121327](https://doi.org/10.1242/jcs.121327)
- Ratnikov B, Ptak C, Han J, Shabanowitz J, Hunt DF, Ginsberg MH. 2005. Talin phosphorylation sites mapped by mass spectrometry. *Journal of Cell Science* **118**:4921–4923. doi: [10.1242/jcs.02682](https://doi.org/10.1242/jcs.02682)
- Roy BC, Kakinuma N, Kiyama R. 2009. Kank attenuates actin remodeling by preventing interaction between IRSp53 and Rac1. *The Journal of Cell Biology* **184**:253–267. doi: [10.1083/jcb.200805147](https://doi.org/10.1083/jcb.200805147)
- Schmidt N, Basu S, Sladeczek S, Gatti S, van Haren J, Treves S, Pielage J, Galjart N, Brenner HR. 2012. Agrin regulates CLASP2-mediated capture of microtubules at the neuromuscular junction synaptic membrane. *The Journal of Cell Biology* **198**:421–437. doi: [10.1083/jcb.201111130](https://doi.org/10.1083/jcb.201111130)
- Sklerner SP, Gault BT, Fogh RH, Boucher W, Stevens TJ, Laue ED, Vuister GW. 2015. Structure calculation, refinement and validation using CcpNmr Analysis. *Acta Crystallographica Section D Biological Crystallography* **71**:154–161. doi: [10.1107/51399004714026662](https://doi.org/10.1107/51399004714026662)
- Small JV, Kaverina I. 2003. Microtubules meet substrate adhesions to arrange cell polarity. *Current Opinion in Cell Biology* **15**:40–47. doi: [10.1016/S0955-0674\(02\)00008-X](https://doi.org/10.1016/S0955-0674(02)00008-X)
- Spangler SA, Hoogenraad CC. 2007. Liprin-alpha proteins: scaffold molecules for synapse maturation. *Biochemical Society Transactions* **35**:1278–1282. doi: [10.1042/BST0351278](https://doi.org/10.1042/BST0351278)
- Stehbens S, Wittmann T. 2012. Targeting and transport: how microtubules control focal adhesion dynamics. *The Journal of Cell Biology* **198**:481–489. doi: [10.1083/jcb.201206050](https://doi.org/10.1083/jcb.201206050)
- Stehbens SJ, Paszek M, Pemble H, Ettinger A, Gierke S, Wittmann T. 2014. CLASPs link focal-adhesion-associated microtubule capture to localized exocytosis and adhesion site turnover. *Nature Cell Biology* **16**:561–573. doi: [10.1038/ncb2975](https://doi.org/10.1038/ncb2975)



- Thelsen U, Straube E, Straube A. 2012. Directional persistence of migrating cells requires KIF1C-mediated stabilization of trailing adhesions. *Developmental Cell* **23**:1153–1166. doi: [10.1016/j.devcel.2012.11.005](https://doi.org/10.1016/j.devcel.2012.11.005)
- van der Vaart B, van Riel WE, Doodhi H, Kevenaar JT, Kasrukha EA, Gumy L, Bouchet BP, Grigoriev I, Spangler SA, Yu KL, Wulf PS, Wu J, Lansbergen G, van Battum EY, Pasterkamp RJ, Mimori-Kiyosue Y, Demmers J, Olieric N, Maly IV, Hoogenraad CC, et al. 2013. CFEOM1-associated kinesin KIF21A is a cortical microtubule growth inhibitor. *Developmental Cell* **27**:145–160. doi: [10.1016/j.devcel.2013.09.010](https://doi.org/10.1016/j.devcel.2013.09.010)
- van Zundert GC, Rodrigues JP, Trellet M, Schmitz C, Kastiris PL, Karaca E, Melquiond AS, van Dijk M, de Vries SJ, Bonvin AM. 2016. The HADDOCK2.2 web server: user-friendly integrative modeling of biomolecular complexes. *Journal of Molecular Biology* **428**:720–725. doi: [10.1016/j.jmb.2015.09.014](https://doi.org/10.1016/j.jmb.2015.09.014)
- Wehrle-Haller B. 2012. Assembly and disassembly of cell matrix adhesions. *Current Opinion in Cell Biology* **24**:569–581. doi: [10.1016/j.cob.2012.06.010](https://doi.org/10.1016/j.cob.2012.06.010)
- Wishart DS, Bigam CG, Yao J, Abildgaard F, Dyson HJ, Oldfield E, Markley JL, Sykes BD. 1995. 1H, 13C and 15N chemical shift referencing in biomolecular NMR. *Journal of Biomolecular NMR* **6**:135–140. doi: [10.1007/BF00211777](https://doi.org/10.1007/BF00211777)
- Yan J, Yao M, Goult BT, Sheetz MP. 2015. Talin dependent mechanosensitivity of cell focal adhesions. *Cellular and Molecular Bioengineering* **8**:151–159. doi: [10.1007/s12195-014-0364-5](https://doi.org/10.1007/s12195-014-0364-5)
- Yao M, Goult BT, Chen H, Cong P, Sheetz MP, Yan J. 2014. Mechanical activation of vinculin binding to talin locks talin in an unfolded conformation. *Scientific Reports* **4**:4610. doi: [10.1038/srep04610](https://doi.org/10.1038/srep04610)
- Yao M, Goult BT, Klepzig B, Hu X, Toseland CP, Guo Y, Cong P, Sheetz MP, Yan J. 2016. The mechanical response of talin. *Nature Communications* **7**:11966. doi: [10.1038/ncomms11966](https://doi.org/10.1038/ncomms11966)
- Yue J, Xie M, Gou X, Lee P, Schneider MD, Wu X. 2014. Microtubules regulate focal adhesion dynamics through MAP4K4. *Developmental Cell* **31**:572–585. doi: [10.1016/j.devcel.2014.10.025](https://doi.org/10.1016/j.devcel.2014.10.025)
- Zacharchenko T, Qian X, Goult BT, Jethwa D, Almeida TB, Balkestrem C, Critchley DR, Lowy DR, Barasikov IL. 2016. LD motif recognition by talin: structure of the talin-DLC1 complex. *Structure* **24**:1130–1141. doi: [10.1016/j.str.2016.04.016](https://doi.org/10.1016/j.str.2016.04.016)